

# The Failure-Mode-Concept FMC

*– a physical and theoretical Material Symmetry-driven basis  
to generate Strength Criteria, giving a reason to look after  
a more closed Strength Mechanics Building –  
and much More* including Cuntze Life data

Material Symmetry seems to tell the author:

*In the case of ideally homogeneous materials a generic number is inherent.  
This is valid for elastic entities, yield modes and fracture modes, for yield strengths  
 $R_{0.2}$  and fracture strengths  $R$ , fracture toughness entities  $K_c$ ,  
and for the invariants used to generate strength criteria.*

This generic number is

2 for isotropic and 5 for transversely–isotropic materials,

One might think:

*“Mother Nature gives Strength Mechanics a mathematical order?”*

The many FMC applications are intended to underpin above imaginable Building.

***A ‘little’ older now but  
STRENGTH is still his Life !***

“Anyone who stops learning is old,  
whether at twenty or at eighty.  
Anyone who keeps learning stays young.  
The greatest thing in life is to keep your mind young”

[Henry Ford]



***Ralf Cuntze, engineer and hobby material modeler*** [Ralf\\_Cuntze@t-online.de](mailto:Ralf_Cuntze@t-online.de)

Hope to be a bridge builder between mechanical engineering and construction.

This paper comprises results of the author’s non-funded, non-supported research work.  
The paper basically addresses the author’s strength-dedicated work with numerical results found over the past decades.

*“As single author - due to my age - I am quite forced to publish this work as quickly as possible. Peers could not be found. I therefore ask the readers to deal generously with the shortcomings to be found. ”  
This wide-spread work shall be an invitation for discussion.*

**Prof. Dr.-Ing. habil. Ralf Cuntze VDI**

1964: Dipl.-Ing. Civil Engineering CE (construction, TU Hannover)

1968: Dr.-Ing. in Structural Dynamics (CE)

1978: Dr.-Ing. habil. Venia Legendi in Mechanics of Lightweight Structures (TU-M, CE)

1980-1983 Lecturer at Universität der Bundeswehr München: on 'Fracture Mechanics' in construction faculty and 1990 - 2002 on 'Composite Lightweight Design' in aerospace faculty

1987: C3-full professorship 'Lightweight Construction', not started in favor of industry

1998: Honorary professorship at Universität der Bundeswehr München

1968-1970: FEA-programming (DLR-Essen/Mühlheim);

1970-2004: MAN-Technologie (München and Augsburg). Headed the Main Department 'Structural and Thermal Analysis'. 50 years of life with fibers CF, AF,GF, BF,BsF

Theoretical fields of work: structural dynamics, finite element analysis, rotor dynamics, structural reliability, partial/deterministic safety concepts, material modeling and model validation, fatigue, fracture mechanics, design development 'philosophy' & design verification

Mechanical Engineering applications at MAN: ARIANE 1-5 launcher family (design of different parts of the launcher stages inclusively Booster) Cryogenic Tanks, High Pressure Vessels, Heat Exchanger in Solar Towers (GAST Almeria) and Solar Field, Wind Energy Rotors (GROWIAN Ø103 m, WKA 60, AEROMAN. Probably the first world-wide wind energy conference organized in 1979), Space Antennas, Automated Transfer Vehicle (Jules Verne, supplying the space station ISS), Crew Rescue Vehicle (CMC application) for ISS, Carbon and Steel Gas-Ultra-Centrifuges for Uranium enrichment. Material Databank etc.

Civil Engineering applications: Supermarkets, armoring plans, pile foundation, 5th German climbing garden (1980 designed, concreted and natural stone bricked)

1971-2010: Co-author of ESA/ESTEC-Structural Materials Handbook, Co-author and first convener of the ESA-Buckling Handbook and co-author in Working Groups WGs for ESA-Standards 'Structural Analysis', 'High Pressure Vessels' (metal and composites), 'Safety Factors'

1972–2015, IASB: Luftfahrt-Technisches Handbuch HSB 'Fundamentals and Methods for Aeronautical Design and Analyses'. Author / Co-author of numerous HSB sheets, co-transfer with co-translation of the HSB aerospace structural handbook into its present English version.

1980-2011: Surveyor/Advisor for German BMFT (MATFO, MATEC), BMBF (LuFo), DFG

1980-2006: VDI Guideline 2014, co-author of Parts 1 and 2, Beuth Verlag '*Development of Fiber-reinforced Plastic Components, Part 3 Analysis*', editor/convener/co-author

1986 and 1889: One week lecture on composite design in Pretoria

2019: GLOSSAR "Fachbegriffe für Kompositbauteile - *technical terms for composite parts*". Springerverlag 2019. Edited at the suggestion of carbon concrete colleagues to help to better understand each other in the co-working disciplines

World-Wide-Failure-Exercise WWFE (2000-2013) on UD materials strength: WWFE-I (2D stress states) non-funded winner against the institutes of the world, WWFE-II (3D states) top-ranked

2009-2021 linked to Carbon Composites e.V. at Augsburg, later Composites United CU e.V and to TUDALIT Dresden. Since 2011 working on the light weight material Fiber-reinforced (polymer) Carbon Concrete. Founded and headed the CU working groups: (1) 2009: 'Engineering' linked to the WG Non-Destructive Testing and the WG Connection Technologies, mechanical engineering. (2) 2010: 'Composite Fatigue'. In 2010 the author held an event that was excellently attended by international speakers. (3) 2011: 'Design Dimensioning (Auslegung, Bemessung) and Design Verification (Nachweis)' mainly for carbon concrete. This working group was the foundation stone for the later specialist network CU Construction, aim "*Fiber-based lightweight construction*". (4) 2017: 'Automated fabrication in construction including serial production' (3D-Prin). (5) 2020, 2021: Forum 'Carbon concrete for practice' at 'Ulm Concrete Days'.

## Keywords:

Structural strength mechanics building, material modelling, failure criteria, multiple failure modes, brittle

## **Abstract**

Novel simulation-driven product development shifts the role of physical testing to virtual testing, to simulation respectively. This requires High Fidelity concerning the material models used. First and usual assumption for the material models is an ideally homogeneous material. Deviations are specifically taken into account.

Material resistance must be generally demonstrated by a positive Margin of Safety  $MoS$  or a Reserve Factor  $RF = MoS - 1 > 1$  in order to achieve Structural Integrity for the envisaged Limit State! For the 3D-Demonstration of Strength - *nowadays a must regarding the usual 3D FEA stress output* - principally so-called 3D strength criteria or 3D failure bodies are required to firstly perform Design Dimensioning and to finally achieve Design Verification. In the case of brittle materials it is a fracture (failure) body. The surface of such a failure body is determined by the points of all those stress states that lead to failure. It is mathematically defined by a Failure function  $F$  which becomes 1 at Onset-of-Failure. Usually these  $F$ s are written as Strength Failure Conditions (SFC)  $F = 1$ . SFCs used in this paper are those which have been generated of the author's Failure-Mode-Concept (FMC). The FMC incorporates a rigorous thinking in failure modes and can be briefly described by the features: Failure mode-wise mapping, stress invariant-based formulation, equivalent stress generation, each failure mode is governed by just one strength  $R^{mode}$  and all SFC model parameters are measurable entities. This involves a direct use of the friction value  $\mu$  in the case of compressed brittle materials where the model parameter for friction in the SFC is replaced by the measured  $\mu$ . Therefore, the very challenging task to transform an SFC in structural stresses into a SFC in Mohr stresses had to be performed.

The difference between a so-called 'global fitting' and a '(failure mode-linked) modal fitting', such as with 'Mises Yielding', of failure test data is pointed out. Further, terms such as mixed failure mode (mode interaction), multiple failure mode action and multi-axial strength are presented and discussed.

During the derivation of the FMC a closer look at material symmetry facts was taken whereby the question arose: "Does a material symmetry-linked Generic Number exist with a number 2 for isotropic and 5 for UD materials? This looks to be proven by the investigation of Normal Yielding NY of plexiglass and a compressive fracture toughness  $K_{cr}$  for an ideally brittle material.

The SFC approaches consider - following Beltrami and Mohr-Coulomb - that the solid material element may experience, generated from different energy portions, a shape change (HMH), a volume change and friction. The derivation of the SFCs is based on specific FMC ideas and partly builds up on the hypotheses of Beltrami, Hencky-Mises-Huber (HMH) and Mohr-Coulomb.

FMC-based SFCs, nowadays most often termed Strength Criteria are enlisted for a large variety of isotropic brittle structural materials such as porous Concrete Stone, Normal Concrete, UHPC sandstone, monolithic ceramics and for the transversely-isotropic fiber-reinforced polymers Lamina (ply, lamella) and Fabrics. Orthotropic fabrics inclusively fabric ceramics are further included. Available multi-axial fracture test data were mapped to validate the SFCs chosen for the description of the envisaged fracture failure model. For a large variety of materials the course of test data was mapped and the associated fracture bodies displayed with distinct cross-sections of them: Principal stress plane, octahedral stress plane and tensile and meridian planes. Various links or interrelationships between the materials are outlined. Different but similar behaving materials can be basically treated with the same SFC.

If several failure modes are activated by the stress state then the application of the *material stressing effort*  $Eff$  (Werkstoffanstrengung) is very helpful because the full  $Eff$  consists of the mode portions  $Eff^{mode}$ . The contribution of each single  $Eff^{mode}$  informs the designing engineer about the importance of the single portions in the SFC and thereby about the critical failure driving mode. Whereas the structural engineer is more familiar with the equivalent stress the material engineer prefers above 'material stressing effort'  $Eff$  (Werkstoffanstrengung). These terms are linked by  $\sigma_{eq}^{mode} = Eff^{mode} \cdot R^{mode}$ .

Special attention is paid not only to the porous materials grey cast iron, concrete, foam which possess a *convex* fracture failure surface, but also to the normal yielding experiencing plexiglass PMMA which possesses a *concave* fracture failure surface part in the principal tension stress domain.

Of further intensive concern was to automatically generate Constant Fatigue Life curves on basis of just a few tested Master S-N curves together with a physically based model, namely Kawai's 'Modified fatigue strength ratio'  $\Psi$ . This procedure is a novelty and applicable for materials like UD plies and isotropic concrete as well.

An automatic insertion of the 3D stress state FE output was numerically foreseen in order to obtain a problem-free strength assessment by a Reserve Factor  $RF$ .

## Two typical Bavarian peculiarities addressing Strength and Composites

Demut *humility* (results may be not O. K.)

stressman & his work = stubborn donkey

**STRENGTH organ compartment**

self respect (you can do it)

hope (PC will run)

Sorgfalt *carefulness* (check of input + output)

ambitiousness Ehrgeiz (solve the problem)

- **Strength** is a very essential thing.  
Human beings possess strength not just in muscles!

- This attribute was located by the so-called *Phrenological Society of Munich* as an organ at the top of the head (1860 !)

The Wolperdinger,  
most famous  
Bavarian Composite



*Fiber-reinforced Composites in the various technical disciplines are the main topic in this work. In this context the author tries to more inform about composite applications in construction. These are less known in engineering.*

|      |  |    |
|------|--|----|
| 1    | Introduction .....   | 8  |
| 1.1  | General on Design .....  | 8  |
| 1.2  | Scheme of Strength Failure Conditions (SFCs) with potential Missing Links .....                        | 14 |
| 1.3  | Material properties, tables and international designations .....                                       | 16 |
| 2    | Theoretical Background of Cuntze's Failure-Mode-Concept (FMC) .....                                    | 21 |
| 2.1  | Basic knowledge from former investigators.....   | 21 |
| 2.2  | Beltrami hypothesis for generation of isotropic and of UD materials.....                               | 22 |
| 2.3  | Stresses and invariants of isotropic and UD materials .....  | 24 |
| 2.4  | Material symmetry-based assumptions of the author .....  | 27 |
| 2.5  | Effects to be considered with isotropic and transversely-isotropic materials .....                     | 28 |
| 2.6  | Fracture behavior of the Various Materials .....   | 31 |
| 2.7  | Fiber-reinforced semi-finished products in construction.....   | 37 |
| 2.8  | Visualization of an Isotropic Failure Body consisting of Mode Domains SF and NF .....                  | 38 |
| 3    | Collection of FMC-based SFCs formulated in Structural Stresses .....                                   | 40 |
| 3.1  | Introduction with comparison of so-called 'Global' and 'Modal' SFCs .....                              | 40 |
| 3.2  | Basic features of the Failure-Mode-Concept FMC (1996).....   | 42 |
| 3.3  | Modal equivalent stress $\sigma_{eq}$ and Modal material stressing effort $Eff$ .....                  | 44 |
| 3.4  | History of FMC with Search of a 'More Closed Strength Mechanics Building' .....                        | 45 |
| 3.5  | SFCs for 'dense' and 'porous' Isotropic Material.....  | 46 |
| 3.6  | SFCs for 'dense' and 'porous' transversely-isotropic materials (UD lamina, lamella).....               | 49 |
| 3.7  | SFCs for differently porous, fabric pattern-dependent orthotropic materials (fabrics).....             | 53 |
| 3.8  | SFCs for the differently porous Structural Ceramic Materials.....                                      | 57 |
| 3.9  | Validity limits for SFC applications and Automatic Insertion of 3D Stress States.....                  | 58 |
| 3.10 | UD-material, stress-strain curve parts Strain-hardening and Strain-softening .....                     | 61 |
| 3.11 | A closer Look at Materials addressing Shear Stress and Multi-fold Failure .....                        | 63 |
| 3.12 | Note on Polymer Matrix Reinforcement by Fiber Patch work.....  | 65 |
| 4    | Construction Applications and Modelling of 'open' and 'closed' FRP and FRC Structural Components ..... | 66 |
| 4.1  | Some semi-finished products in construction.....   | 66 |
| 4.2  | Applications with Fiber-Reinforced Polymer (FRP) matrices .....  | 67 |
| 4.3  | Applications with Fiber-Reinforced Mineral (FRM) matrices.....   | 70 |
| 4.4  | Some Freshly arrived Applications.....   | 76 |
| 4.5  | Influence of Production Process on the Damage of Filaments and roving Fiber Strands .....              | 79 |

|       |  |     |
|-------|--|-----|
| 5     | Two Missing Links filling the Strength Mechanics ‘Building’ of Isotropic Materials.....                      | 86  |
| 5.1   | Experimental Proof and Description of Normal Yielding NY of Isotropic Materials.....                         | 86  |
| 5.2   | , Some Proof of the 2 <sup>nd</sup> ‘Basic’ Stress Intensity Factor $K_{IIcr}^c$ .....                       | 91  |
| 5.3   | Transversely-isotropic UD lamina materials, 5 fracture toughness properties.....                             | 97  |
| 5.3.1 | <i>Number of Fracture Mechanics (FM) modes</i> .....   | 97  |
| 5.3.2 | <i>Determination of the microcrack-linked softening curve by FM-testing</i> .....                            | 101 |
| 6     | Validation by 3D-Applications of the FMC-SFCs to 3 Material Families.....                                    | 104 |
| 6.1   | Isotropic Grey Cast Iron.....  | 104 |
| 6.2   | Isotropic Glass C 90 (window pane of ISS).....   | 105 |
| 6.3   | Isotropic porous Foam Rohacell (SFC is applicable for Concrete Stone material, too).....                     | 105 |
| 6.4   | ‘Isotropic’ Normal Concrete (slightly porous).....   | 108 |
| 6.5   | ‘Isotropic’ UHPC (relatively dense).....   | 111 |
| 6.6   | Rock Material, example Sandstones.....   | 116 |
| 6.7   | Bi-axial strength of Solid Clay Brick Masonry.....   | 125 |
| 7     | Transversely-isotropic UD-materials (GFRP, CFRP).....  | 127 |
| 7.1   | General Transversely-isotropic UD applications (partly very old figure collection of the author).....        | 127 |
| 7.2   | Transversely-isotropic UD-materials, WWFE-I and WWFE-II applications.....                                    | 131 |
| 7.3   | 2D-Application to (Technical) Ceramics isotropic, UD and orthotropic fabrics.....                            | 150 |
| 8     | Mohr Stress Transformation to obtain the dependence Friction Parameter from Friction Value<br>.....          | 155 |
| 8.1   | Dependence of isotropic friction model parameter on friction value $\mu$ .....                               | 155 |
| 8.2   | Dependence of transversely-isotr. friction model parameters on friction values $\mu_{LL}$ , $\mu_{II}$ ..... | 170 |
| 9     | Miscellaneous.....   | 180 |
| 9.1   | Bridging Shear Fracture $F^{SF}$ and Yield Failure $F^{Mises}$ with view at failure ‘planes’.....            | 180 |
| 9.2   | Influence of 2D- and 3D-compression stress states on the strength capacity.....                              | 182 |
| 9.3   | Application of Safety Concepts with Determination of a Reserve Factor.....                                   | 183 |
| 9.4   | Failure Index $ F $ versus Material Stressing Effort $Eff$ , Example UD 3D-stress state.....                 | 188 |
| 9.5   | Classical Laminate Theory CLT.....   | 189 |
| 9.6   | Material Modelling in Additive Fabrication AF, construction-linked (Bauwesen).....                           | 197 |
| 9.7   | Average Properties and Average Stress-strain Curve.....  | 200 |
| 10    | FMC-based Fatigue Life Models, basically displayed for the brittle UD material.....                          | 204 |
| 10.1  | General and Terms.....   | 204 |
| 10.2  | S-N curve (Woehlerkurve) and Haigh-Diagram.....  | 208 |
| 10.3  | FMC-based Fatigue Life Estimation Model.....   | 212 |

|      |  |     |
|------|--|-----|
| 10.4 | Some examples of S-N curves ‘feeding’ Haigh-Diagrams, FF and IFF.....        | 219 |
| 10.5 | Procedure for deriving CFL curve estimates and associated Steps .....        | 222 |
| 10.6 | Check of the FMC-driven Idea to Split the Operational Loading mode-wise..... | 224 |
| 10.7 | Estimation of the Amplitude and Comparison with the Measured Value.....      | 227 |
| 10.8 | Steps of the FMC-based Fatigue Life Estimation Procedure .....               | 227 |
| 11   | Conclusions, Literature and Terms .....                                      | 230 |
| 11.1 | Conclusions .....  | 230 |
| 11.2 | Literature .....   | 236 |
| 11.3 | Basic Terms and Definitions.....   | 247 |

Depending on stress state and environment a material may behave ductile and brittle.  
 Here, brittle shall be engineering-like defined as:  $R^c > \approx 3 \cdot R^t$  (uni-axial, ambient)



**Ductile Fracture =**  
 type of failure in a material or  
 a structure generally  
 preceded by a large amount  
 of plastic deformation

*One feels good until  
 sudden fracture occurs*

[Courtesy: Prof. C. Mattheck]



**Lessons Learned:**

When using brittle materials, more care must therefore be taken  
 on the fracture verification under Design Ultimate Load.

In the sense of lightweight construction and sustainability, this deficiency should not lead to the choice  
 of increased design safety factors  $j, \gamma$  in design dimensioning but by an  
 increased knowledge of the material failure behavior.

The delivery of such a better knowledge on fracture failure behavior is the essential intention of this  
 work.

# 1 Introduction

## 1.1 General on Design

The variety of new materials in engineering requires the knowledge of the failure state in order to enable verification of the designed structural part. And this much more since lightweight design requires a higher exertion of the material and thereby contributes to sustainable engineering.

Design Verification demands for reliable reserve factors  $RF$  or Margins of Safety  $MoS$  and these – besides a reliable structural analysis - demand for reliable Strength Failure Conditions (SFCs). Such a condition is the mathematical formulation  $F = 1$  of a failure curve or of a failure surface (body). Generally required are a yield strength condition and a fracture strength condition. A load-driven growing yield failure surface is terminated by the fracture failure surface.

A yield SFC usually describes just one mode, namely for isotropic materials the classical ‘Mises’ shear yielding SY. For PMMA, however, there are two yield modes SY in the compression domain and normal yielding NY in the tension domain.

Fracture SFCs usually describe two independent fracture modes, shear fracture SF and normal fracture NF.

*Fig.1-1* displays the structural engineer’s tasks he is involved when designing a structural part. It is to demonstrate that as well the static Dimensioning Load Cases as the dynamic and cyclic ones, considering lifetime, and others are fulfilled. Addressed are Design Dimensioning (Auslegung, Bemessung) and Design Verification (Nachweis), respectively Proof. Of special focus thereby is the strength verification of non-cracked (regime micro-cracking) components and the fracture mechanics verification of cracked structural (macro-cracking) components.

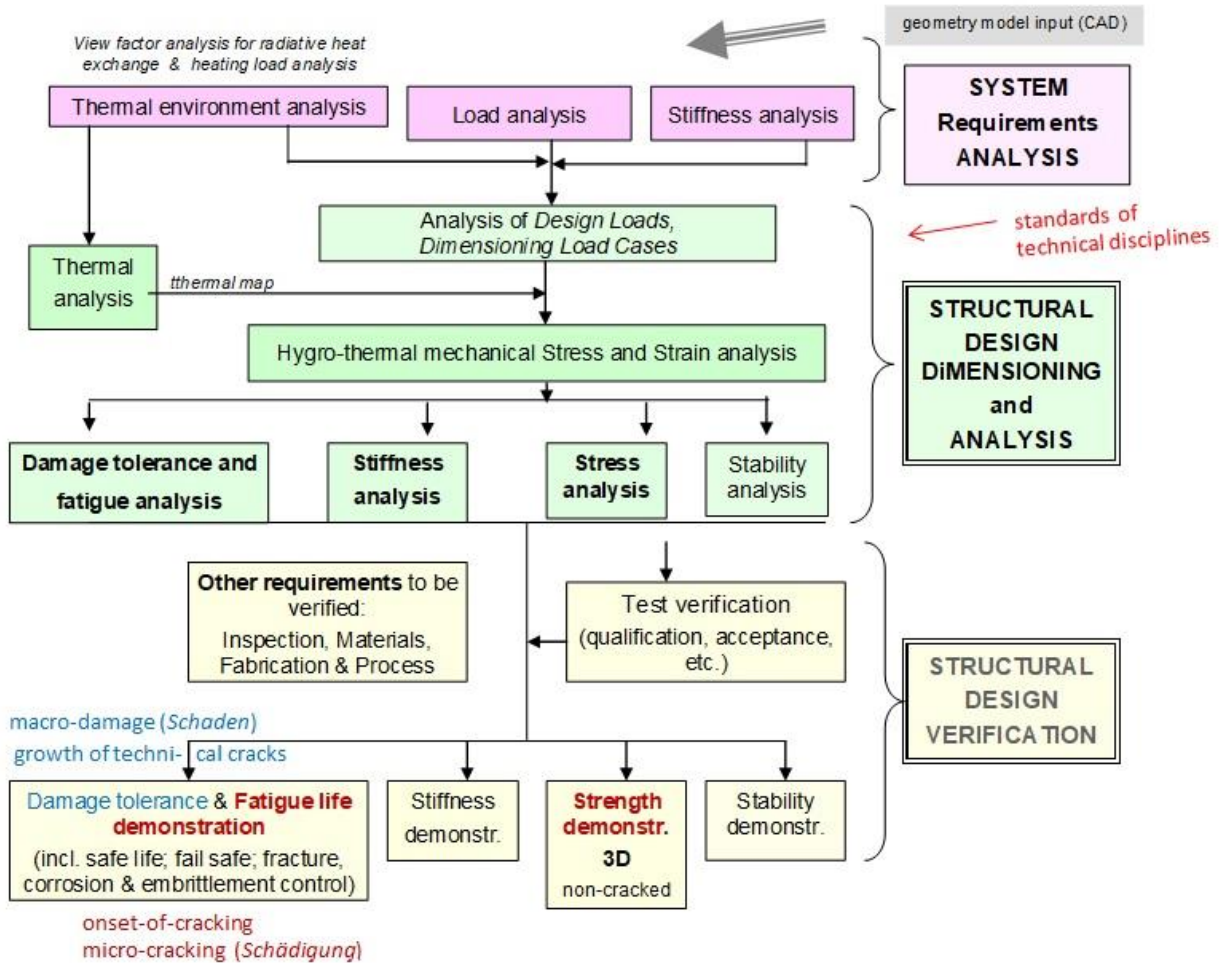
Strength verification of non-cracked structural components is demonstrated through SFCs by  
“No relevant limit failure state is met considering all dimensioning load cases”.

The size of the (macro-)damage decides whether it is to apply a Strength Failure Condition SFC  $F = 1$  (now most often termed strength criterion, which originally means  $F = < = > 1$ ) for the verification of onset-of-fracture of the un-cracked structural part or a mechanics-based Damage Tolerance Condition in case of a technical crack.

*Fig.1-2* gives hints where which verification procedure is to apply or in other words: When must be fracture mechanics used and when strength mechanics? The figure refers to: (a) Strength Mechanics versus Linear Elastic Fracture Mechanics (LEFM) analysis; (b) Crack-free and crack-driven fracture through  $a_0$  being an initial flaw size (surface flaw, delamination) or a developed crack. Further, *Fig.1-2* depicts in b where the different technical failure types Normal Fracture NF, Shear Fracture SF and Shear Yielding SY are located.

In order to understand the mechanisms of crack growth itself, it is necessary to consider the phenomena at the tip of a crack on a microscopic level. On the modelling-desired macroscopic structural level, however, such an approach is not practical. Therefore, Fracture Mechanics FM works on a macroscopic scale, and tries to determine parameters from structural response results.





**Resistances, to be demonstrated by proof of a Reserve Factor  $RF > 1$  or a positive Margin of Safety ( $MoS = RF - 1$ ) to achieve Structural Integrity for Certification Process**

- Mechanical Engineering, proof of: \*Design Ultimate Load (limit state) DUL, \* Design Limit Load (limit state) DLL
- Civil Engineering, proof of: \*Ultimate Limit State (ULS, GZT), \* Serviceability Limit State (SLS, GZG)

Fig.1-1: Structural engineer's tasks and complete work flow in structural design

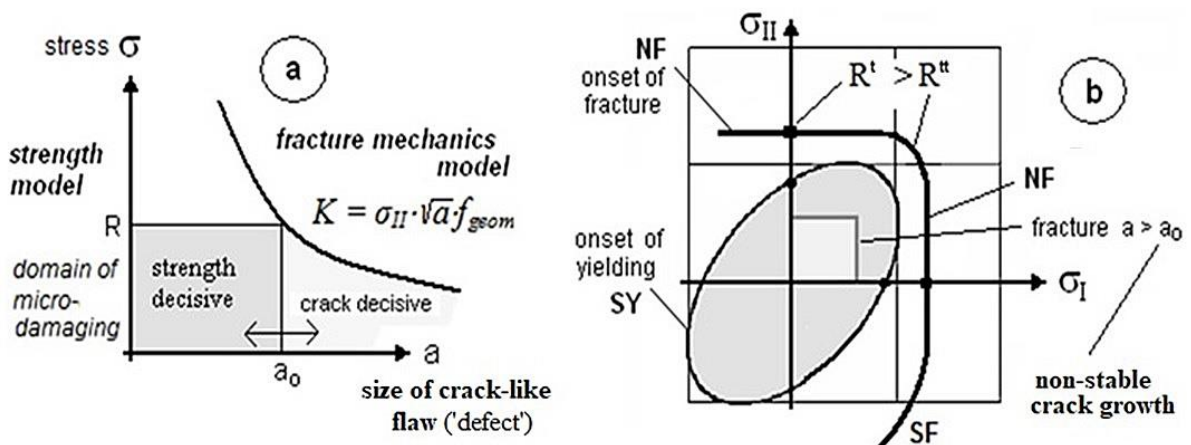


Fig.1-2: (a) Continuum mechanics strength analysis versus fracture mechanics analysis. (b) Crack free fracture onset and crack-driven fracture through a crack geometry factor,  $a_0$  the initial flaw size (surface flaw, delamination, ..),  $K$  is stress intensity factor,  $a$  is crack size, NF Normal Fracture, SF Shear Fracture,  $R$  is strength value,  $^t$  means tensile.  $\sigma_{II}$  is principal stress

‘Unclearness’ or Fuzziness (Unschärfe) is inherent in loadings, strengths, and other design variables such as geometrical parameters, applied engineering models, etc. All these uncertainty sources in design contribute to the overall Structural Risk defined here arbitrarily as Amount of Costs - incurred in the case of Later Failure - times the Probability that the distinct Failure occurs in the structural part. Risk drives the designer to follow Table 1-1.

Hence, reliable structural components are searched in design.

*Table 1-1: Design objectives and process*

Objective: Reliable Structural Components

Design = compromise of *Design-to-Cost* and *Design-to-Quality*. Robust design helps to accept smaller design changes and to ‘survive’ manufacturing flaws, and it saves money and trouble! Optimisation to manufacturing is mandatory considering (as-built, effects-of-flaws (‘defects’)).

Functional Integration is a basic driver especially with composites when viewing costs. Thereby the two essential requirements have to be fulfilled:

- Functional Requirements (tasks to let the developers know what to build, to let the testers know what tests to run, to let stakeholders know what they are getting [Wikipedia]) and
- Operational Requirements (needed performance capabilities, lifetime etc.)

Vehicle: Reduction of design uncertainties

Means: Sort out the weakest links in the development process which involve the highest uncertainties. Most often the loadings are the most uncertain design parameters.

The next tables present a short survey on loading conditions and Load Cases LC. To consider are media, temperature, creeping, aging, relaxing.

*Table 1-2: Loading conditions for the design of  $\lambda\lambda$*

Static loading: *strength*

Validated 3D strength failure conditions for isotropic (foam, concrete, PMMA,...), transversely-isotropic UD materials, and orthotropic materials (e.g. textiles) to determine ‘Onset-of-fracture’ and ‘Final fracture’ in case of benign failure behavior (quasi-ductile).

Standardisation of material test procedures, test specimens, test rigs, and test data evaluation for a comparably good structural analysis input.

Consideration of manufacturing imperfections (tolerance width of uncertain design variables) in order to achieve a production cost minimum by „Design-to-Imperfections“, which includes flaws (avoid the term defect) .

Dynamic loading: *hazards, impact, crash loading, blast*

Cyclic loading: *fatigue and crack growth*

Concern is the development of practical, physically-based lifetime-prediction methods and the generation of S-N curve test data for the validation of the prediction models, crack growth models, delamination growth models if laminates.

Table 1-3: Design load analysis, loadings, combinations of loadings & Load Cases LC  
- Mechanical Engineering and Civil Engineering

Design Loadings:

Estimation of all external + internal loadings of the structural component :

- mechanical (static, cyclic, and dynamic) and hygro-thermal,
- acoustical environment as well as of the
- corresponding lifetime requirements (duration, number of cycles)

Loadings are specified by

- a Technical Specification from the customer, or an authority or
- a common standard (EC codes, DIN, EN, FAA, ESA, Automotive, ...)

Otherwise a load(ings) analysis is required = Establishment of load events the structure is likely to experience (= load history). Dynamic structural system analysis performed to estimate the loadings. *Examples: launcher in aerospace, 'old' bridge refurbishment in construction*

Combinations of Loadings: → structural specifications

Involve usually a Worst Case scenario w.r.t. combinations of loadings, temperature and moisture, and undetected damage.

- Set of Combinations of Loadings termed Load Cases (LCs). From this usually vast number of Load Cases - if possible - a minimum
- Set of (*design driving*) Dimensional Load Cases (DLCs) should be extracted for fast decisions in the case of input changes, to by-pass an FEA output evaluation death and to automatically provide the engineer with a better understanding of the structure's behavior.



*The caiman mother Maria observes the limit "No trespassing (No pase!)". That was very good for the personal health of my friend Eddi (he fell in front of her snout while running away).*

We learn: Structural engineers should always observe the limits set by the structural specifications. That is very good for structural health [Cuntze 2013]

Design Dimensioning and Design Verification are performed on different structural levels, see Table I-4 . The bold letters show the focus viewed here.

Table 1-4: Levels of Design Verification with respect to Static Strength

- Structure level : forces & moments (resistance of a truss element *strut*)
- Cross-section level : section forces (stress resultants) & section moments (resistance of a *shell wall*)
- **Material level** : **stresses** (strength at a material point, *envisaged most often and here*).

Structural load-carrying capacity is mainly *locally* determined by the stress state in the critical material locations, such as in:

- \* **undisturbed areas** (uniform material areas, membrane areas etc.),
- \* **disturbed areas** (discontinuities such as joints, notches etc. ).

Assessment of stress states at critical locations is to be performed for the material families:

- \* **isotropic material** (concrete, glass, etc.)
- \* **transversely-isotropic material** (UD := uni-directional material)
- \* **orthotropic (rhombically-isotropic) material** (textiles etc.)

In Fig.1-3 a simple static strength verification procedure is visualized for completeness and added are the levels of possible design verification.

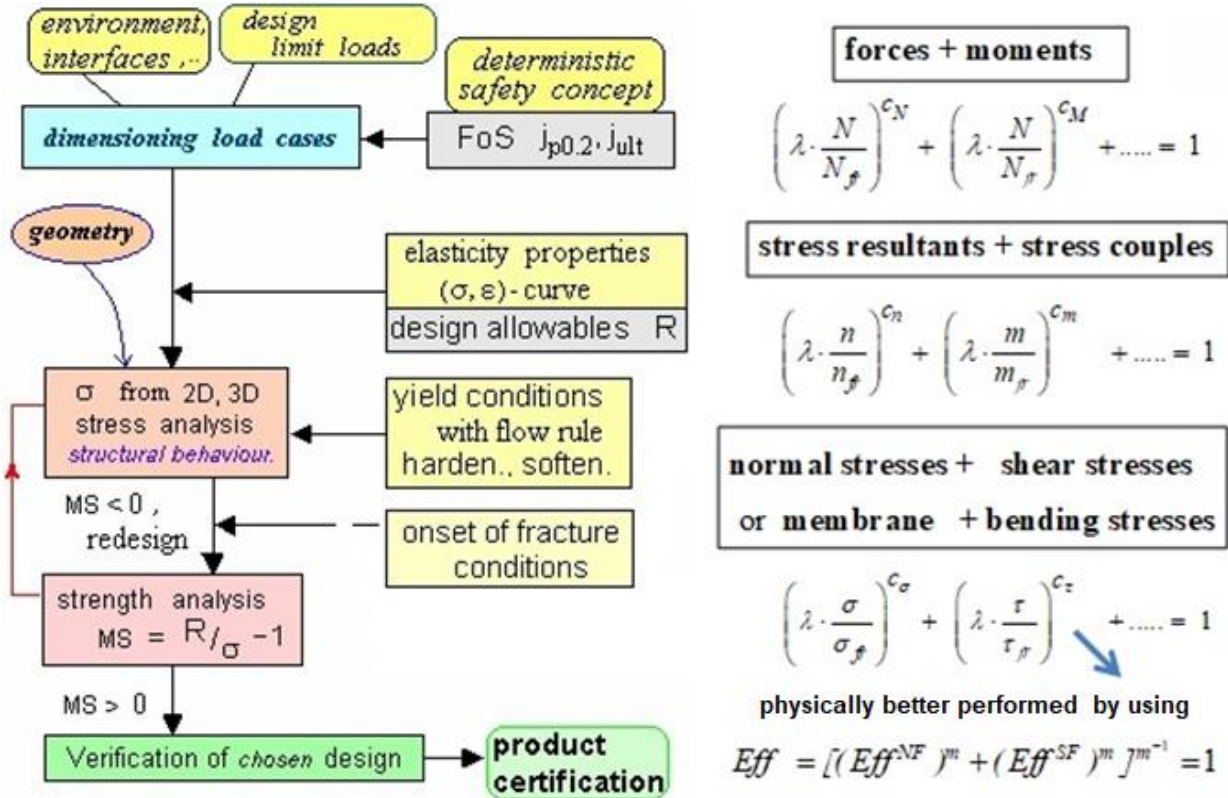


Fig.1-3: Static strength verification procedure. (design) Factor of Safety  $j$ , strength  $R$ , stress  $\sigma$ . Exponents  $c$  from tests, handbooks.  $\lambda$  is a loading multiplier, which corresponds to some extent to  $RF$

Design Dimensioning and Design Verification are to perform considering different stress situations, see Table 1-5.

Table 1-5: Analysis Levels of the structural component – static & cyclic

- **Stress**, locally at a critical material location ('point'): *using strength mechanics*. Micro-damage. Verification by uni-axial ('basic') strengths and multi-axial strength criteria. Applied stresses are local stresses (continuum mechanics, regarding cyclic growth of initially most often diffuse and later localized micro-damage)
- **Stress concentration** at a **notch** (joint): *using notch mechanics*. Verification by a notch strength (usually 'Neuber-like', Nuismer, etc.). Applied stress peaks. Mind: S-N curves of plain material narrow 'notched' S-N curves
- **Stress 'intensity' (stress intensity factor)** at a crack tip: *using fracture mechanics*. Macro-damage. Verification by fracture toughness  $K_{cr}$  or a critical energy release rate  $G_{cr}$  (energy-related). Applied stresses are 'far'-field stresses (far from the crack-tip). Task: Cyclic growth of a detected 'technical damage' (i.e. interlaminar delamination).

Each failure mode contributes to the experienced micro-damage or macro-damage activated by the 3D-stress state:

**Strength Mechanics:**

If all strength failure modes are activated then the failure condition beyond which onset-of-failure will occur reads  $Eff = f(Eff^{modes}) = 1 = 100\%$  with  $Eff$  the so-called material stressing effort (*Werkstoffanstrengung*).

### Fracture Mechanics:

If all fracture mechanics failure modes are activated then the failure condition beyond which the crack will begin to propagate reads  $\mathcal{G} / \mathcal{G}_{cr} = 1$  with  $\mathcal{G} = \mathcal{G}_I + \mathcal{G}_{II} + \mathcal{G}_{III}$  with  $\mathcal{G}_{cr}$  the critical energy release rate. For a general stress state the (linear elastic) fracture mechanics situation is fully similar to strength mechanics.

### **Need for a 3D strength assessment:**

There is an urgent need to move to 3D failure analysis.

FEA output delivers 3D stress states if required and these are then to assess. Such stress states are encountered in submarine hulls, bolted and screwed joints, in bearings, in the foot of a hoop-reinforced concrete strut, after impact and ballistics, hazards and in applications like composite high pressure vessels. However in the past, mainly specific and effortful experimental investigations have been performed including 2D and 3D compression (such as hydrostatic pressure loading  $p_{hyd}$ ) and not so much effort was put on analytical investigations. In consequence, there is a strong need to validate failure conditions in the compression domain.

2D models are not sufficient to describe the fracture progress of brittle behaving isotropic materials such as grey cast iron, rock material, concrete, UD-material etc. 3D failure theory and experimental evidence are needed. For instance an example from tests on Ultra-High-Performance-Concrete proofs that the consideration of a realistic 3D stress state promises advantages: A failure stress state in MPa (-160, 0, 0) fully corresponds to (-224 -6, -6, -6). In both the cases is  $F = 1$  or is 'Onset-of-Fracture' Failure met.

Linear and non-linear structural analyses are to perform considering all (D)LCs and design limit states  $\mathcal{G}$  which represent all failure modes, Table 1-6. Often the aim of non-linear analysis is just: „Save a structural design or a still produced structure” by making the hidden load carrying reserves visible. Hidden, practically means, if linear analysis was only used in design.

Mind in non-linear analysis: Standard survival probabilities shall be kept as usually applied in the linear case.

*Table 1-6: Linear and nonlinear structural analyses*

Linear Analysis: action  $S$  (stress level) < material resistance  $R$  (strength) for each LC

*Design Dimensioning 3D or*

*with section quantities which depend on the distribution of the structure's stiffness.*

Non-linear Analysis: action  $E$  (Einwirkung, load level) < structural resistance  $W$  (Widerstand)

for each LC.

### LL:

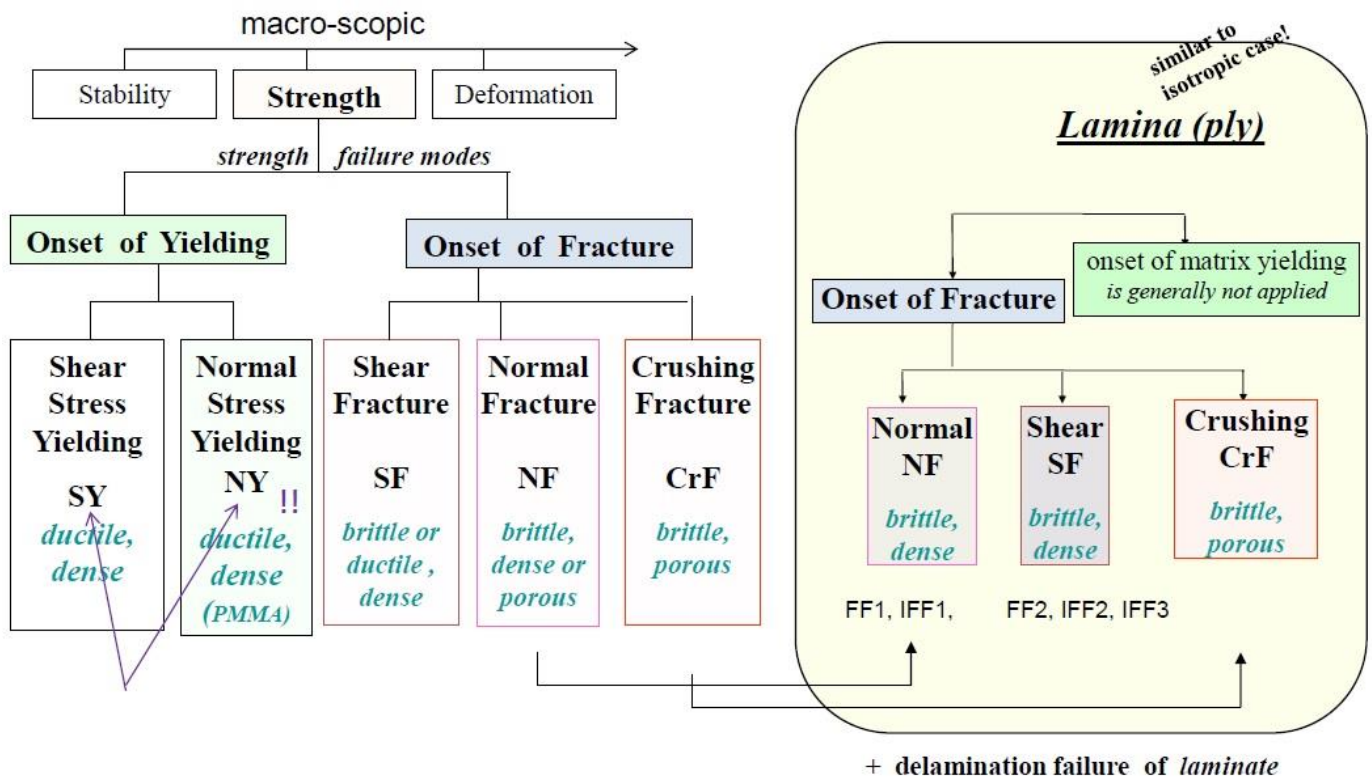
- *Statically in-determinate structures are redundant and must be treated differently to the statically determinate ones (one load path). Principally, in order to avoid either to be too conservative or too un-conservative, a separation of the always needed analysis of the average structural behavior in Design Dimensioning from the finally following Design Verification is required.*
- *It must be applied: (1) An average  $\sigma$ - $\varepsilon$  curve and characteristic (= typical, average) design parameters (Example statically indeterminate continuous beam: Determination for Design Dimensioning of the most realistic section quantities with 50% probability of expectation for the following local cross-section proofs (However, exemplarily, but not only: EuroCode2 reduces the Young's modulus of the compressive stress-strain curve of the concrete. No physical reason given?). (2) Design values: Consideration of minimum values for strength and min, mean or max as task-required for other properties.*

## 1.2 Scheme of Strength Failure Conditions (SFCs) with potential Missing Links

In the development of structural components the application of 3D-validated strength failure conditions SFCs ('criteria') is one essential pre-condition for achieving the required fidelity for the user. This includes Yield Failure Conditions (ductile behavior) for the non-linear analysis of the material and the Onset-of-Yield limit verification. It further includes conditions to verify that Onset-of-Fracture does not occur, in the case of brittle and ductile behavior.

Since two decades the author believes in a macroscopically-phenomenological 'complete classification' system, where all strength failure types are included, see *Fig.1-4*. In his assumed system several relationships may be recognized: (1) shear stress yielding SY, followed by shear fracture SF viewing 'dense' materials. For porous materials under compression, the SF for dense materials is replaced by crushing fracture CrF. (2) However, to complete a system beside SY also NY should exist. The right side of the scheme shows that a similarity of isotropic materials with UD materials exists. The strength failure modes involve a variety of failure types such as SY, NF, IFF2.

Usual light-weight materials exhibit SY ('Mises'), whereas polymers may further show NY due to crazing! For instance PMMA (plexiglass) with its chain-based texture shows NY.



*Fig.1-4: Author-proposed scheme to outline interrelations of isotropic and UD materials. Lamina (ply)= lamella in construction.*

Capturing all kinds of possible types of failure in a uniform classification scheme is challenging, because the classification can be carried out according to different ways. The author thinks that a material behavior-overarching system delivers a good classification scheme for a 'macro-mechanics building of all materials'. This scheme should be clear and as simple as possible for the dimensioning structural engineer without violating any material-typical facts.

In consequence, the author concludes:

*If one knows from a similar behaving material some material facts  
that can be transferred to the behavior of the ‘new’ material,  
then pre-dimensioning with the new material becomes easier and more trusting!*

**LL:**

- There are coincidences between brittle UD laminæ and brittle isotropic materials
- With composites: After an initial matrix yielding of the ductile polymer matrix follows ‘Quasi-Yielding’ due to diffuse micro-cracking. Increased degradation occurs in the laminate beyond onset of the first Inter-Fiber-Failure IFF
- What may be learned from Fig.1-4 and from studying the associated failure conditions? If the shear stress yielding mechanism is still active until fracture its yield failure function remains at least part of the formulation of the fracture failure function  $F$ . The same mathematical form of a failure condition (means interaction of stresses within one mode) may be valid from Onset-of-Yielding  $SY$  to Onset-of-Fracture  $SF$  if the physical mechanism remains, such as with shear yielding in case of ductile steels (‘Mises’  $J_2$  part + volume change part in the ultimate strain regime before the ‘Gurson’ domain)
- Today’s FEA gives 3D FE stress results as output. The evaluation of these 3D stress states therefore requires 3D conditions that predict the onset-of-failure. Unfortunately, due to a lack of 3D test results, the known standard ‘global’ SFCs – even for isotropic materials – are usually not sufficiently well 3D-validated.

From above follows an advantage when material symmetry knowledge is applied: Presuming, homogeneity is a valid assessment for the project task-determined model, just a minimum number of properties must be measured, only. These offers significant benefits in cost and time.

The author sees two missing links or empty rooms in the Strength Mechanics Building of Fig.1-4: Why are there not also 2 yield modes and 2 ‘basic’ critical stress intensity factors (fracture toughness entities), only?’

**Strength Mechanics**

**SY**

known

**Normal Yielding NY**

**Fracture Mechanics**

$K_{Icr}^t \equiv K_{Ic}, K_{IIc}, K_{IIIc}$  (tension, shear)

$K_{IIcr}^c$  (compression)

Fig.1-5: Isotropic material, the two searched ‘rooms’ or missing links **NY**,  $K_{IIcr}^c$

(1) **NY:** Is there Normal Yielding?

NY is known for a long time, but not in structural mechanics design. An explanation for the ‘Not known’ is that a describing yield failure condition  $F^{NY}$  was missing. For establishing this missing link in his ‘complete system’ the author found applicable test data which he evaluated and visualized in chapter 5. → Proof is given.

(2)  $K_{IIcr}^c$ : Is there a Critical Stress Intensity Factor (SIF) under compression or a fracture toughness under a compression-induced shear, respectively?

Here, the author remembers a two decades old citation of A. Carpinteri that approximately reads:” With homogeneous isotropic brittle materials there are 2 real energy release rates  $\mathcal{G}_{Icr}, \mathcal{G}_{IIcr}$ , one in tension and one in compression. These two  $\mathcal{G}_s = K^2 \cdot (1-\nu^2) / E$  (formally, plane strain case) possess the attribute that the crack plane does not turn and are therefore real (or ‘basic’) material properties”. This forced the author at that time to intensively search  $K_{IIcr}^c$  as the basic pendant to

$K_{Icr}^t$ , officially indexed  $K_{Ic}$  in fracture mechanics FM, and to postulate in the sense of Carpinteri: “*Only a stable crack growth plane-associated (self-similar crack growth) SIF is a ‘basic’ FM property*”.

This is valid in the tension domain for the SIF  $K_{Ic} \equiv K_{Icr}^t$  above and not for the *model-necessary*  $K_{IIc}$  and  $K_{IIIc}$ . It should be valid in the compression domain, too, that means shear, for  $K_{IIcr}^c$ .

This missing link will be presented by the author in chapter 6. The author admits at this point that this SIF is not relevant for the treatment of common fracture-mechanical tasks in the compression range because it requires an ideal homogeneous crack-tip situation. However, he believes that the proof of  $K_{IIcr}^c$  is an important theoretical task for achieving a ‘complete system’.

### 1.3 Material properties, tables and international designations

Before treating properties some definitions are presented in order to distinguish all addressed topics accurately. Structural composites can be metallic, non-metallic or a hybrid combination thereof. One distinguishes two structural composite types: Material Composite (*Werkstoffverbund*) and Composite Material (*Verbundwerkstoff*). In this context: Structural Material is usually the model of a homogenized more complex solid (*on the considered scale or level the homogenized model of the envisaged complex solid is modelled as a smeared solid. The objective usually is a macro-model*).

Material Composite is structural-mechanically a composite ‘construction of different materials (*a not smearable ‘conglomerate’ such as i.e. carbon fiber grid-reinforced concrete which is not a ‘composite material’ despite it is usually termed so.*

Composite Material is a combination of constituent materials, different in composition (*constituents retain their identities in the composite; that is, they do not dissolve or otherwise merge completely into each other although they act in concert. Normally the constituents can be physically identified, and there is an interface between them to consider regarding its interphase material*). This type is hopefully homogenizable to a smeared material such as UD-ply, lamella, short fiber-reinforced concrete, foam etc.

Essential for this paper are the fiber-reinforced lightweight materials with its various combinations including polymer matrix and mineral matrix, see Fig.1-5.

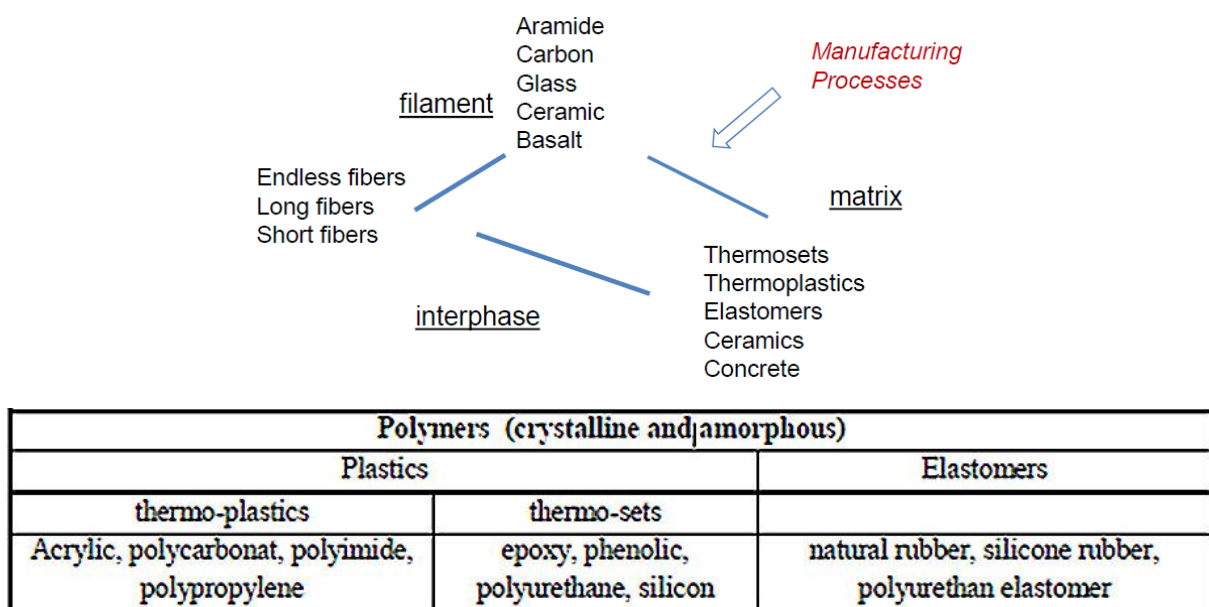


Fig.1-5: Possible combinations of different constituents with various polymers used



Traditional epoxy resin systems deliver rigid thermoset structures after curing, excellent properties but recycling of the FRP-composite is pretty difficult. Residual stresses from curing are inherent and can merely be lowered by a heat treatment process. Thermo-plastics can be further deformed after curing are recycling-friendly and suffer not from residual stresses. Both, these traditional polymers might be topped by the new VITRIMAX (US company Mallinda), that allows bonding across the interface of prepreg-layers even after curing, and this ‘endless’. Recycling and residual stresses then would be no problem.

In the context of Fig.1-5, various combinations of different constituents building up the final homogenized (hopefully ‘smearing’ is possible) material are possible and to model.

In the following Tables 1-2a through 1-2c, on basis of investigations for the VDI-2014 and the formerly planned novel ESA Materials Handbook, Cuntze proposed internationally not confusing notations for strength properties and for the physical properties.

Table 1-2a: Self-explaining symbolic notations for strength properties

|                    |                     | Fracture <b>Strength Properties</b> |                     |                     |   |                     |                     |                     |                        |                     |                                       |
|--------------------|---------------------|-------------------------------------|---------------------|---------------------|---|---------------------|---------------------|---------------------|------------------------|---------------------|---------------------------------------|
|                    |                     | tension                             |                     |                     | compression   |                     |                     | shear               |                        |                     |                                       |
| loading            |                     |                                     |                     |                     |   |                     |                     |                     |                        |                     |                                       |
| direction or plane |                     | 1                                   | 2                   | 3                   | 1   | 2                   | 3                   | 12                  | 23                     | 13                  |                                       |
| 9                  | general orthotropic | $R_1^t$                             | $R_2^t$             | $R_3^t$             | $R_1^c$   | $R_2^c$             | $R_3^c$             | $R_{12}$            | $R_{23}$               | $R_{13}$            | friction properties                   |
| 5                  | UD                  | $R_{  }^t$<br>NF                    | $R_{\perp}^t$<br>NF | $R_{\perp}^t$<br>NF | $R_{  }^c$<br>SF  | $R_{\perp}^c$<br>SF | $R_{\perp}^c$<br>SF | $R_{  \perp}$<br>SF | $R_{\perp\perp}$<br>NF | $R_{  \perp}$<br>SF | $\mu_{\perp\perp}, \mu_{  \perp}$     |
| 6                  | fabrics             | $R_W^t$                             | $R_F^t$             | $R_3^t$             | $R_W^c$   | $R_F^c$             | $R_3^c$             | $R_{WF}$            | $R_{F3}$               | $R_{W3}$            | Warp = Fill                           |
| 9                  | fabrics general     | $R_W^t$                             | $R_F^t$             | $R_3^t$             | $R_W^c$   | $R_F^c$             | $R_3^c$             | $R_{WF}$            | $R_{F3}$               | $R_{W3}$            | $\mu_{W3}, \mu_{F3}, \mu_{WF}$        |
| 5                  | mat                 | $R^t$                               | $R^t$               | $R_3^t$             | $R^c$   | $R^c$               | $R_3^c$             | $R^\tau$            | $R^\tau$               | $R^\tau$            | (≡ UD material with turned direction) |
| 2                  | isotropic matrix    | $R^t$<br>SF                         | $R^t$<br>SF         | $R^t$<br>SF         | deformation-limited, cylindrical test specimen bulges: What is then $R^c$ ? |                     |                     | $R^\tau$            | $R^\tau$               | $R^\tau$            | $\mu$                                 |
|                    |                     | $R^t$<br>NF                         | $R^t$<br>NF         | $R^t$<br>NF         | $R^c$<br>SF   | $R^c$<br>SF         | $R^c$<br>SF         | $R^\tau$<br>NF!     | $R^\tau$<br>NF         | $R^\tau$<br>NF      | $\mu$                                 |

number of independent properties due to material symmetry of isotropic materials

Notes: \*As a consequence to isotropic materials (European standardization) the letter  $R$  ( $\equiv f$  in construction) has to be used for strength. US notations for UD material with letters X (direction 1) and Y (direction 2) confuse with the structure axes’ descriptions X and Y. \*Effect of curing-based residual stresses and environment is dependent on hygro-thermal stresses. \*Effect of the difference of stress-strain curves of e.g. the usually isolated UD test specimen and the embedded (redundancy, strain-softening part too) UD lamina.  $R_m$  := ‘resistance maximale’ (French) = tensile fracture strength (superscript  $t$  is usually skipped because design runs in tensile domain),  $R$  is basic strength. Composites are most often brittle and only slightly porous! SF is shear fracture, NF Normal Fracture.

Isotropic:  $\{R\} = (R^t, R^c)^T$  with  $\mu$

Transversely-isotropic:  $\{R\} = (R_{||}^t, R_{||}^c, R_{\perp}^t, R_{\perp}^c, R_{\perp\perp})^T$  with  $\mu_{\perp\perp}, \mu_{||\perp}$

Orthotropic:  $\{R\} = (R_W^t, R_W^c, R_F^t, R_F^c, R_{WF}, R_3^t, R_3^c, R_{3F}, R_{3W})^T$  with  $\mu_{WF}, \mu_{3W}, \mu_{3F}$

Mind: Lamina properties used as input for the analysis are test results from *isolated* UD lamina specimens such as a tensile coupon. They are load-controlled derived and the results are of weakest link type whereas the in-situ behaviour of an *embedded* UD lamina is deformation-controlled and therefore of redundant type. This fact shows up that a good mapping of the course (strain-hardening) of ‘isolated UD test data’ does not involve the full information (also strain-softening) necessary for a qualified analysis of laminates which consist of a stack of embedded laminas.

Table 1-1b: Self-explaining symbolic notations for elasticity properties

|                    |                               | Elasticity Properties |             |             |               |                  |               |                 |                    |                 |   |
|--------------------|-------------------------------|-----------------------|-------------|-------------|---------------|------------------|---------------|-----------------|--------------------|-----------------|---|
| direction or plane |                               | 1                     | 2           | 3           | 1             | 2                | 3             | 12              | 23                 | 13              |   |
| 9                  | general orthotropic           | $E_1$                 | $E_2$       | $E_3$       | $G_{12}$      | $G_{23}$         | $G_{13}$      | $\nu_{12}$      | $\nu_{23}$         | $\nu_{13}$      | comments  |
| 5                  | UD, $\cong$ non-crimp fabrics | $E_{  }$              | $E_{\perp}$ | $E_{\perp}$ | $G_{  \perp}$ | $G_{\perp\perp}$ | $G_{  \perp}$ | $\nu_{  \perp}$ | $\nu_{\perp\perp}$ | $\nu_{  \perp}$ | $G_{\perp\perp} = E_{\perp} / (2 + 2\nu_{\perp\perp})$<br>$\nu_{\perp  } = \nu_{  \perp} \cdot E_{\perp} / E_{  }$<br>3 is perpendicular to quasi-isotropic 2-3-plane |
| 6                  | fabrics                       | $E_W$                 | $E_F$       | $E_3$       | $G_{WF}$      | $G_{W3}$         | $G_{WF}$      | $\nu_{WF}$      | $\nu_{W3}$         | $\nu_{W3}$      | Warp = Fill   |
| 9                  | fabrics general               | $E_W$                 | $E_F$       | $E_3$       | $G_{WF}$      | $G_{W3}$         | $G_{F3}$      | $\nu_{WF}$      | $\nu_{F3}$         | $\nu_{W3}$      | Warp $\neq$ Fill  |
| 5                  | mat                           | $E$                   | $E$         | $E_3$       | $G$           | $G_3$            | $G_3$         | $\nu$           | $\nu_3$            | $\nu_3$         | $G = E / (2 + 2\nu)$<br>1 is perpendicular to quasi-isotropic mat plane   |
| 2                  | isotropic for comparison      | $E$                   | $E$         | $E$         | $G$           | $G$              | $G$           | $\nu$           | $\nu$              | $\nu$           | $G = E / (2 + 2\nu)$  |

Table 1-1c: Self-explaining symbolic notations for hygro-thermal properties

| Hygro-thermal properties      |                |                   |                   |                |                   |                   |                  |
|-------------------------------|----------------|-------------------|-------------------|----------------|-------------------|-------------------|------------------|
| direction, or plane           | 1              | 2                 | 3                 | 1              | 2                 | 3                 |                  |
| general orthotropic           | $\alpha_{T1}$  | $\alpha_{T2}$     | $\alpha_{T3}$     | $\alpha_{M1}$  | $\alpha_{M2}$     | $\alpha_{M3}$     | comments         |
| UD, $\cong$ non-crimp fabrics | $\alpha_{T  }$ | $\alpha_{T\perp}$ | $\alpha_{T\perp}$ | $\alpha_{M  }$ | $\alpha_{M\perp}$ | $\alpha_{M\perp}$ |                  |
| fabrics                       | $\alpha_{TW}$  | $\alpha_{TW}$     | $\alpha_{T3}$     | $\alpha_{MW}$  | $\alpha_{MW}$     | $\alpha_{M3}$     | Warp = Fill      |
| fabrics general               | $\alpha_{TW}$  | $\alpha_{TF}$     | $\alpha_{F3}$     | $\alpha_{MW}$  | $\alpha_{MF}$     | $\alpha_{M3}$     | Warp $\neq$ Fill |
| mat                           | $\alpha_T$     | $\alpha_T$        | $\alpha_{T3}$     | $\alpha_M$     | $\alpha_M$        | $\alpha_{M3}$     |                  |
| isotropic                     | $\alpha_T$     | $\alpha_T$        | $\alpha_T$        | $\alpha_M$     | $\alpha_M$        | $\alpha_M$        |                  |

Comments on properties to be used in analysis:

- Properties are ‘agreed’ values to achieve a common and comparable design basis
- Properties must be provided with average value and coefficient of variation CoV
- Sources of uncertainty should be investigated. In this context: changing a certified material is economically seldom possible)
- Model parameters should be measurable unambiguously properties and physically self-explaining
- Variety of Composites: Many properties for design and manufacturing are not yet available
- Generally valid for materials: A multi-axial stress assessment is not possible on basis of uni-axial strength values alone. Knowledge of material internal friction values, following Mohr-Coulomb, is mandatory in the compression domain.

For a better understanding of the body text the stress-strain relations of the investigated 3 material families are added here:

Table 1-2: Compliance matrices for test data evaluation

$\{\varepsilon\} = [S] \cdot \{\sigma\}$  with  $[S]$  compliance matrix,  $\{\sigma\} = [C] \cdot \{\varepsilon\}$  with  $[C]$  stiffness matrix

Generalized Hooke's law, tensorial format

$$\begin{Bmatrix} \varepsilon_{11} \\ \varepsilon_{22} \\ \varepsilon_{33} \\ 2\varepsilon_{23} \\ 2\varepsilon_{13} \\ 2\varepsilon_{12} \end{Bmatrix} = \begin{bmatrix} S_{1111} & S_{1122} & S_{1133} & 2S_{1123} & 2S_{1113} & 2S_{1112} \\ S_{1122} & S_{2222} & S_{2233} & 2S_{2223} & 2S_{2213} & 2S_{2212} \\ S_{1133} & S_{2233} & S_{3333} & 2S_{3323} & 2S_{3313} & 2S_{3312} \\ 2S_{1123} & 2S_{2223} & 2S_{3323} & 4S_{2323} & 4S_{2313} & 4S_{2312} \\ 2S_{1113} & 2S_{2213} & 2S_{3313} & 4S_{2313} & 4S_{1313} & 4S_{1312} \\ 2S_{1112} & 2S_{2212} & 2S_{3312} & 4S_{2312} & 4S_{1312} & 4S_{1212} \end{bmatrix} \begin{Bmatrix} \sigma_{11} \\ \sigma_{22} \\ \sigma_{33} \\ \sigma_{23} \\ \sigma_{13} \\ \sigma_{12} \end{Bmatrix}$$

$$\begin{Bmatrix} \sigma_{11} \\ \sigma_{22} \\ \sigma_{33} \\ \sigma_{23} \\ \sigma_{13} \\ \sigma_{12} \end{Bmatrix} = \begin{bmatrix} C_{1111} & C_{1122} & C_{1133} & C_{1123} & C_{1113} & C_{1112} \\ C_{1122} & C_{2222} & C_{2233} & C_{2223} & C_{2213} & C_{2212} \\ C_{1133} & C_{2233} & C_{3333} & C_{3323} & C_{3313} & C_{3312} \\ C_{1123} & C_{2223} & C_{3323} & C_{2323} & C_{2313} & C_{2312} \\ C_{1113} & C_{2213} & C_{3313} & C_{2313} & C_{1313} & C_{1312} \\ C_{1112} & C_{2212} & C_{3312} & C_{2312} & C_{1312} & C_{1212} \end{bmatrix} \begin{Bmatrix} \varepsilon_{11} \\ \varepsilon_{22} \\ \varepsilon_{33} \\ 2\varepsilon_{23} \\ 2\varepsilon_{13} \\ 2\varepsilon_{12} \end{Bmatrix}$$

Generalized Hooke's law, engineering format

$$\begin{Bmatrix} \varepsilon_x \\ \varepsilon_y \\ \varepsilon_z \\ \gamma_{yz} \\ \gamma_{xz} \\ \gamma_{xy} \end{Bmatrix} = \begin{bmatrix} \frac{1}{E} & -\nu & -\nu & 0 & 0 & 0 \\ -\nu & \frac{1}{E} & -\nu & 0 & 0 & 0 \\ -\nu & -\nu & \frac{1}{E} & 0 & 0 & 0 \\ & & & \frac{1}{G} & 0 & 0 \\ & & & & \frac{1}{G} & 0 \\ & & & & & \frac{1}{G} \end{bmatrix} \begin{Bmatrix} \sigma_x \\ \sigma_y \\ \sigma_z \\ \tau_{yz} \\ \tau_{xz} \\ \tau_{xy} \end{Bmatrix} \quad \begin{Bmatrix} \varepsilon_I \\ \varepsilon_{II} \\ \varepsilon_{III} \end{Bmatrix} = \begin{bmatrix} \frac{1}{E} & -\nu & -\nu \\ -\nu & \frac{1}{E} & -\nu \\ -\nu & -\nu & \frac{1}{E} \end{bmatrix} \begin{Bmatrix} \sigma_I \\ \sigma_{II} \\ \sigma_{III} \end{Bmatrix}$$

(symm.)

from which follows  $E \cdot (\varepsilon_x + \varepsilon_y + \varepsilon_z) = -3 \cdot p_{hyd} \cdot (1 - 2 \cdot \nu)$  or  $E \cdot \Delta V / V = p_{hyd} \cdot (3 - 6 \cdot \nu)$ . It can be recognized that the bulk modulus  $K = E / (3 - 6\nu)$  is activated.

$$\begin{Bmatrix} \varepsilon_1 \\ \varepsilon_2 \\ \varepsilon_3 \\ \gamma_{23} \\ \gamma_{13} \\ \gamma_{12} \end{Bmatrix} = \begin{bmatrix} \frac{1}{E_{\parallel}} & -\frac{\nu_{\parallel\perp}}{E_{\perp}} & -\frac{\nu_{\parallel\perp}}{E_{\perp}} & 0 & 0 & 0 \\ -\frac{\nu_{\perp\parallel}}{E_{\parallel}} & \frac{1}{E_{\perp}} & -\frac{\nu_{\perp\perp}}{E_{\perp}} & 0 & 0 & 0 \\ -\frac{\nu_{\perp\parallel}}{E_{\parallel}} & -\frac{\nu_{\perp\perp}}{E_{\perp}} & \frac{1}{E_{\perp}} & 0 & 0 & 0 \\ & & & \frac{1}{G_{\perp\perp}} & 0 & 0 \\ & & & & \frac{1}{G_{\parallel\perp}} & 0 \\ & & & & & \frac{1}{G_{\parallel\perp}} \end{bmatrix} \begin{Bmatrix} \sigma_1 \\ \sigma_2 \\ \sigma_3 \\ \tau_{23} \\ \tau_{13} \\ \tau_{12} \end{Bmatrix}$$

(symm.)

$$\begin{Bmatrix} \sigma_x \\ \sigma_y \\ \sigma_z \\ \tau_{yz} \\ \tau_{zy} \\ \tau_{xy} \end{Bmatrix} = \begin{bmatrix} 1-\nu & C_{12} & C_{13} & 0 & 0 & 0 \\ C_{21} & 1-\nu & C_{13} & 0 & 0 & 0 \\ C_{31} & C_{32} & 1-\nu & 0 & 0 & 0 \\ 0 & 0 & 0 & 0.5 \cdot (1-2\nu) & 0 & 0 \\ 0 & \text{symm.} & 0 & 0 & 0.5 \cdot (1-2\nu) & 0 \\ 0 & 0 & 0 & 0 & 0 & 0.5 \cdot (1-2\nu) \end{bmatrix} \begin{Bmatrix} \varepsilon_x \\ \varepsilon_y \\ \varepsilon_z \\ \gamma_{yz} \\ \gamma_{zy} \\ \gamma_{xy} \end{Bmatrix}$$

$$[S] = \begin{bmatrix} \frac{1}{E_{\parallel}} & -\frac{\nu_{\parallel\perp}}{E_{\perp}} & -\frac{\nu_{\parallel\perp}}{E_{\perp}} & 0 & 0 & 0 \\ -\frac{\nu_{\perp\parallel}}{E_{\parallel}} & \frac{1}{E_{\perp}} & -\frac{\nu_{\perp\perp}}{E_{\perp}} & 0 & 0 & 0 \\ -\frac{\nu_{\perp\parallel}}{E_{\parallel}} & -\frac{\nu_{\perp\perp}}{E_{\perp}} & \frac{1}{E_{\perp}} & 0 & 0 & 0 \\ & & & \frac{1}{G_{\perp\perp}} & 0 & 0 \\ & & & & \frac{1}{G_{\perp\parallel}} & 0 \\ & & & & & \frac{1}{G_{\perp\parallel}} \end{bmatrix}$$

(symm.)

transversely isotropic

$$[S] = \begin{bmatrix} \frac{1}{E_W} & -\frac{\nu_{WF}}{E_F} & -\frac{\nu_{W3}}{E_F} & 0 & 0 & 0 \\ \frac{1}{E_F} & -\frac{\nu_{F3}}{E_F} & 0 & 0 & 0 & 0 \\ & \frac{1}{E_3} & 0 & 0 & 0 & 0 \\ & & & \frac{1}{G_{F3}} & 0 & 0 \\ & & & & \frac{1}{G_{W3}} & 0 \\ & & & & & \frac{1}{G_{WF}} \end{bmatrix}$$

(symm.)

orthotropic (also called rhombically anisotropic)

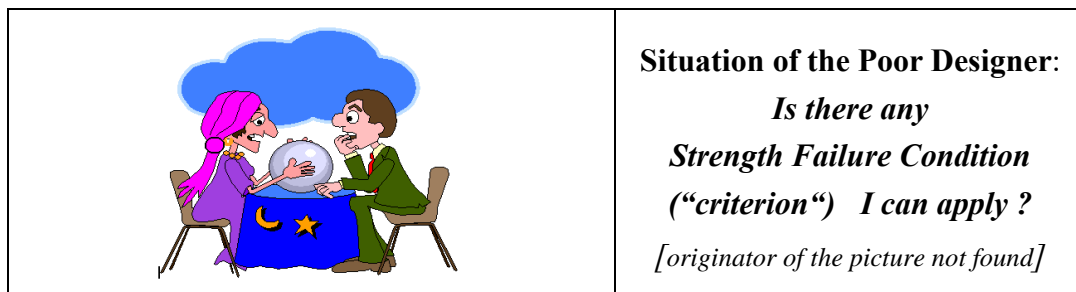
## 2 Theoretical Background of Cuntze's Failure-Mode-Concept (FMC)

### 2.1 Basic knowledge from former investigators

The Hypothesis of Beltrami for isotropic materials states: “At onset-of-failure (*Beltrami said yielding*) the strain energy density  $W$  in a solid material element consists of two portions, one describes the strain energy due to a change in volume (= dilatation or dilation in US) and the other the strain energy due to a change in shape (distortion)”. Hence, following Beltrami above and Hencky-Mises-Huber HMM (see *Fig.2-1*), each invariant term or a multiple of it in the strength failure function  $F$ , may be dedicated to one physical mechanism in the solid or cubic material element, respectively.

Further, these mechanisms are linked to energies, namely  $I_1^2 \sim$  dilatational energy from a volume change,  $J_2 \sim$  distortional energy from a shape change caused by shear distortion under volume consistency. Invariants are a combination of stresses – powered or not powered – the value of which does not change when altering the coordinate system CoS. This attribute is used when looking for an optimum formulation of a usually desired scalar SFC.

What is missing in the case of compression-loaded materials is the Mohr-Coulomb-linked friction energy which is mandatory for investigations of so-called pressure-sensitive materials and which is captured by  $I_1$ .



Hencky-Mises-Huber (HMH)



Henri Tresca  
1814-1885  
*Engineer*



Richard von Mises  
1883-1953  
*Mathematician*



Eugenio Beltrami  
1835-1900  
*Mathematician*



Otto Mohr  
1835-1918  
*Civil Engineer*



Charles de Coulomb  
1736-1806  
*Physician*

‘Onset of Yielding‘

‘Onset of Cracking (fracture)‘

*Fig.2-1: Some pioneers which set up strength failure hypotheses.*

\*The SFC models of Drucker-Prager and of Ottosen, often used in civil engineering, are shortly treated in *Sub-chapter 9.3.2*.

\*The consequent FMC thinking in failure modes comes from the discussions with my friend Prof. Rüdiger Rackwitz at the institute of concrete construction (*head at that time Prof. Herbert Kupfer*) on SFCs like Drucker-Prager and the partial safety concept.

Creating SFCs, Beltrami's statement guarantees an advantageous use of the 'physics-based' invariants  $I_1$  and  $J_2$  for very different materials such as grey-cast iron, concrete, plexiglass PMMA and more structural materials.

A rounding-off or smoothing-out procedure, by employing an interaction equation in mode interaction zones of adjacent mode failure curves (2D) or of partial failure surfaces is leading again to a *pseudo-global* failure curve or surface. In other words, a so-called '*single surface failure description*' is achieved such as with Tsai/Wu [Tsa71] for UD materials, however, without the well-known shortcomings, that are later described.

Material symmetry demands gave reason that the FMC strictly describes just single independent failure modes by its failure mode-wise concept. This will make the derivation of equivalent stresses possible despite of the fact whether the material is isotropic, transversely-isotropic or orthotropic (*is practically still a structure*).

- 1 If a material element can be homogenized to an ideal crystal (= *frictionless*), material symmetry requires for the isotropic and the transversely-isotropic UD material a distinct number of properties (*witnessed*)
- 2 A real solid material model is represented by a description of the ideal crystal (*frictionless*) + a description of its friction behavior. Mohr-Coulomb requires for the real crystal another physical parameter, namely the inherent material friction value  $\mu$  (*1 value for isotropic and 2 for UD materials*)
- 3 Fracture morphology finally gives evidence: Each strength corresponds to a distinct *strength failure mode* and to a distinct *strength fracture type*, to Normal Fracture (NF) or Shear Fracture (SF)
- 4 Note: Densely packed frictional material experiences dilatation when sheared.

In order to only use experimentally derivable material quantities, the author directly introduced in his 3D-SFCs for the compression domain, internal friction  $\mu$  as a formula parameter. Friction is a well-known physical property in engineering. One does not yet find a direct use of  $\mu$  in the textbooks! Why using Mohr's friction angle  $\varphi$  if  $\mu$  ( $\varphi$ ) exists? How to derive  $\mu$  will be shown in chapter 6. Mohr stresses are needed to determine the friction values  $\mu$ . The mathematically challenging topic thereby is the derivation of the fracture plane angles  $\Theta_{fp}^\circ$ . The angle is of high interest for understanding the physics behind the desired transformation from structural stress formulations into Mohr stress-based ones. The determination of the Mohr-Coulomb fracture curve is required which often is seen to capture the tensile-compressive interaction domain or transition zone between its uni-axial limit points compressive strength  $R^c$  and tensile strength  $R^t$ . Its friction-related part ends at the cohesive point  $R^t$ . Practically it means, regarding structural stresses: It captures the transition zone between the two interacting modes SF and NF. The two required SFCs to determine Onset-of-Fracture in this transition zone will be generated on basis of Cuntze's successful Failure-Mode-Concept FMC.

*It should be noted: The author could not find any investigation where the effortful SFC transformation from structural stresses into Mohr stresses has been performed as in Chapter 6.*

## 2.2 Beltrami hypothesis for generation of isotropic and of UD materials

Beltrami, Schleicher et al. assume at initiation of yield that the strain energy (denoted by  $W$ ) in a cubic element (*Fig.2-5*) of a material will consist of two portions:

$$W = \int \{\sigma\} \{\varepsilon\} d\{\varepsilon\} = W_{Vol} + W_{shape} \quad \text{with} \quad \{\sigma\} = (\sigma_1, \sigma_2, \sigma_3, \tau_{23}, \tau_{13}, \tau_{12})^T.$$

Including Hooke's law in the case of a *transversely-isotropic* (UD solid) the expression will take the form, using  $s_{ik} :=$  compliance coefficients,  $E :=$  elasticity modulus,  $\nu :=$  Poisson's ratio,

$$W = [s_{11} \cdot \sigma_1^2 + s_{22} \cdot \sigma_2^2 + s_{33} \cdot \sigma_3^2 + s_{44} \cdot \tau_{23}^2 + s_{55} \cdot (\tau_{12}^2 + \tau_{13}^2)] / 2 + s_{12} \cdot (\sigma_1 \sigma_2 + \sigma_1 \sigma_3) + s_{23} \cdot \sigma_2 \sigma_3 = \frac{I_1^2}{2E_{\parallel}} + \frac{I_2^2(1-\nu_{\perp\perp})}{4E_{\perp}} - \frac{\nu_{\perp\parallel} I_1 I_2}{E_{\parallel}} + \frac{I_3}{2G_{\perp\parallel}} + \frac{I_4(1+\nu_{\perp\perp})}{4E_{\perp}} .$$

volume    volume    volume    shape    shape

with the invariants  $I_1 = \sigma_1$ ,  $I_2 = \sigma_2 + \sigma_3$  ;  $I_3 = \tau_{31}^2 + \tau_{21}^2$  ;  $I_4 = (\sigma_2 - \sigma_3)^2 + 4\tau_{23}^2$  ;  
 $I_5 = (\sigma_2 - \sigma_3) (\tau_{31}^2 - \tau_{21}^2) - 4\tau_{23} \tau_{31} \tau_{21}$  .

In the *isotropic* case analogously follows, however simpler,

$$W = \left[ \frac{1-2\nu}{3} I_1^{iso2} + \frac{2+2\nu}{3} 3J_2^{iso} \right] / 2E$$

volume                      shape

with  $I_1^{iso} = \underline{f(\underline{\sigma})} = \sigma_I + \sigma_{II} + \sigma_{III}$ ,  $6 \cdot J_2^{iso} = \underline{f(\underline{\tau})} = (\sigma_I - \sigma_{II})^2 + (\sigma_{II} - \sigma_{III})^2 + (\sigma_{III} - \sigma_I)^2$ ,

It is known, both portions in the bracket above are used to formulate a failure function

$$F = c_1 \cdot \frac{(1-2\nu) \cdot I_1^{iso2}}{3\bar{R}^2} + c_2 \cdot \frac{(2+2\nu) \cdot 3J_2^{iso}}{3\bar{R}^2} .$$

volume                      shape

Fig. 2-2 displays for the 2 material families above the physically-based choice of invariants.

From **Beltrami**, **Mises (HMH)**, and **Mohr / Coulomb (friction)** can be concluded:

Below invariant terms - used in a FMC-based *failure function F* - can be dedicated to a **physical mechanism** in the solid = cubic material element:

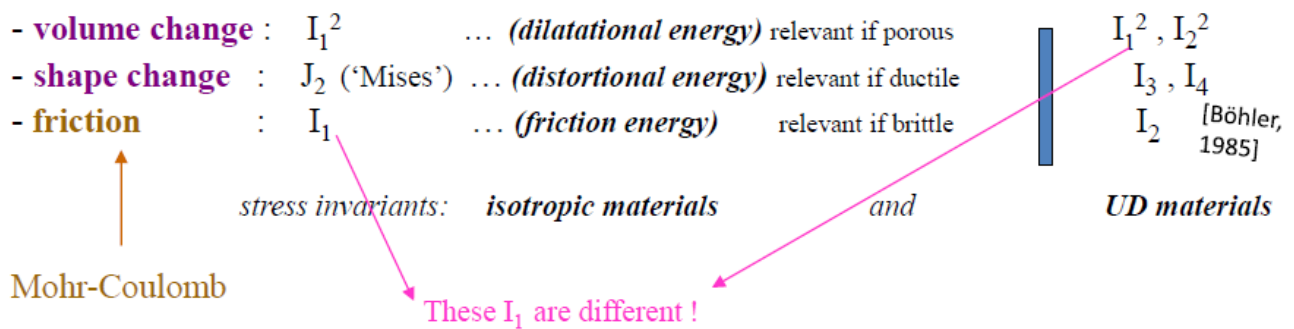


Fig.2-2: Reasons for choosing invariants in the generation of SFCs

Above invariants can be formulated in 3D structural component stresses, principal stresses and Mohr stresses An application is depicted in [Fig.2-3](#), representing an isotropic schematic example for the use of the invariants in the case  $I_1 < 0$  considering their physical meaning.

$$F^{SF} = \begin{array}{ccc} \text{shape change} & \text{friction} & \text{volume change} \\ c_1^{SF} \cdot \frac{3J_2 \cdot \Theta^{SF}}{(\bar{R}^c)^2} & + c_2^{SF}(\mu) \cdot \frac{I_1}{\bar{R}^c} & + c_3^{SF} \cdot \left(\frac{I_1}{\bar{R}^c}\right)^2 = 1 \end{array}$$

'Mises Cylinder' formula

Above *general* SFC is normalized by the compressive strength  $\bar{R}^c$

Two-fold failure danger can be modelled by using the well known invariant  $J_3$ .

The non-circularity function  $\Theta^{SF}$  includes  $d^{SF}$  as non-circularity parameter.

It represents the 120°-rotational symmetry of isotropic materials, caused by the equivalency of the 3 principal stresses and directions (see the fracture bodies, following ).

$$\Theta^{SF}(J_3, J_2) = \sqrt[3]{1 + d^{SF} \cdot \sin(3\vartheta)} = \sqrt[3]{1 + d^{SF} \cdot 1.5 \cdot \sqrt{3} \cdot J_3 \cdot J_2^{-1.5}}$$

$$\text{Compressive Meridian: } \Theta^{SF} = \sqrt[3]{1 - d^{SF}}, \quad \text{Tensile Meridian: } \Theta^{SF} = \sqrt[3]{1 + d^{SF}},$$

$$\text{Neutral Meridian: } \Theta^{SF} = 1.$$

*Fig.2-3: Schematic example for the use of invariants for isotropic, slightly porous materials*

$J_3$  is only required when the same 'strength fracture mode' multiply occurs, which practically means for brittle isotropic materials that a 120° rotational symmetry of the fracture body is to face. The author was able to use these material symmetry specifications successfully in strength mechanics, using his failure mode concept for homogenized isotropic and for UD materials in many test data sets (see applications in [Chapter 5](#)).

### 2.3 Stresses and invariants of isotropic and UD materials

At first in [Fig.2-4](#) the different stresses applied in structural mechanics are depicted. Secondly for the three material families the associated stresses and invariants are displayed. The suffixes I, II, III denote principal stresses, ||, ⊥ lamina stresses, W (warp), F (fill, weft) fabric stresses. The stresses in the different CoS can be transferred into each other.

Residual stresses are taken into account by adding their values to the load stresses due to  $\{\sigma\} = \{\sigma_L\} + \{\sigma_R\}$ .

Some relationships follow:

$$I_1 = (\sigma_I + \sigma_{II} + \sigma_{III}) = f(\sigma), \quad 6J_2 = (\sigma_I - \sigma_{II})^2 + (\sigma_{II} - \sigma_{III})^2 + (\sigma_{III} - \sigma_I)^2 = f(\tau) \text{ 'Mises' invariant}$$

$$27J_3 = (2\sigma_I - \sigma_{II} - \sigma_{III}) \cdot (2\sigma_{II} - \sigma_I - \sigma_{III}) \cdot (2\sigma_{III} - \sigma_I - \sigma_{II}),$$

$$3 \cdot \sigma_{oct} = \sigma_I + \sigma_{II} + \sigma_{III} = \sigma_\ell + \sigma_n + \sigma_t; \quad 9 \cdot \tau_{oct}^2 = 6J_2 = 4 \cdot (\tau_{III}^2 + \tau_I^2 + \tau_{II}^2), \quad \tau_{II} = \max \tau(\text{mathem.})$$

$\sigma_I, \sigma_{II}, \sigma_{III}$  are principal stresses,  $\sigma_I > \sigma_{II} > \sigma_{III}$  are mathematical stresses (> means more positive)



The *Figs 2-4* through *2-7* present the invariants and the associated structural (component) stresses, principal stresses and the Mohr (fracture plane) stresses necessary to derive the friction value (see *Chapter 6*).

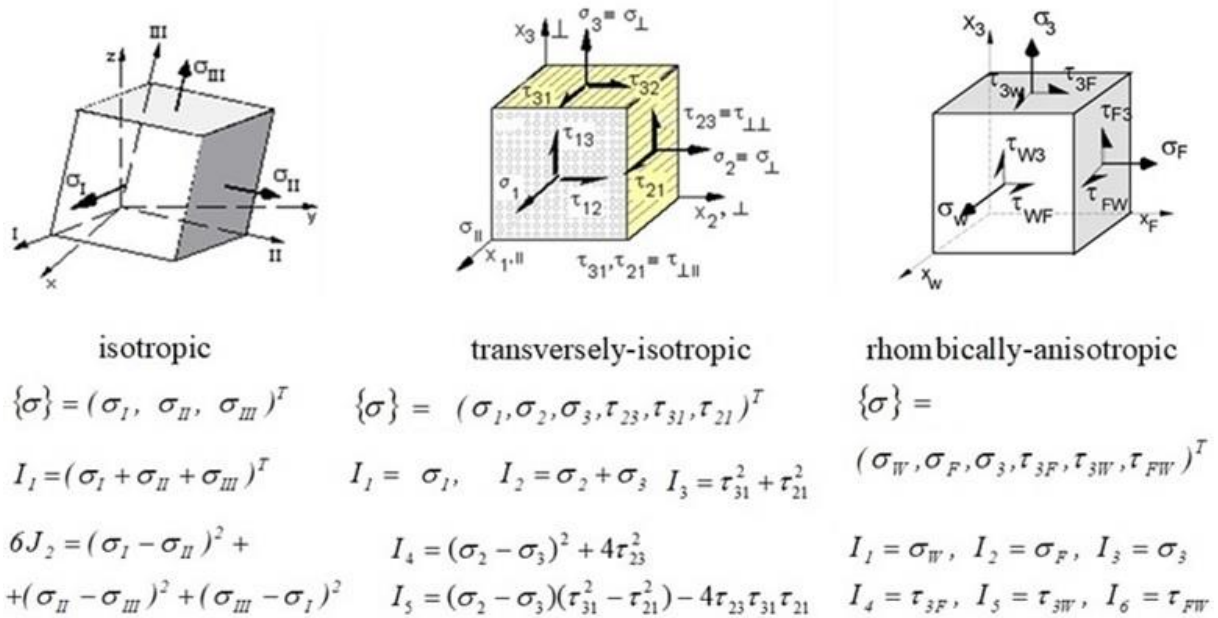


Fig.2-4: Stresses & invariants of isotropic, transversely-isotropic and orthotropic materials

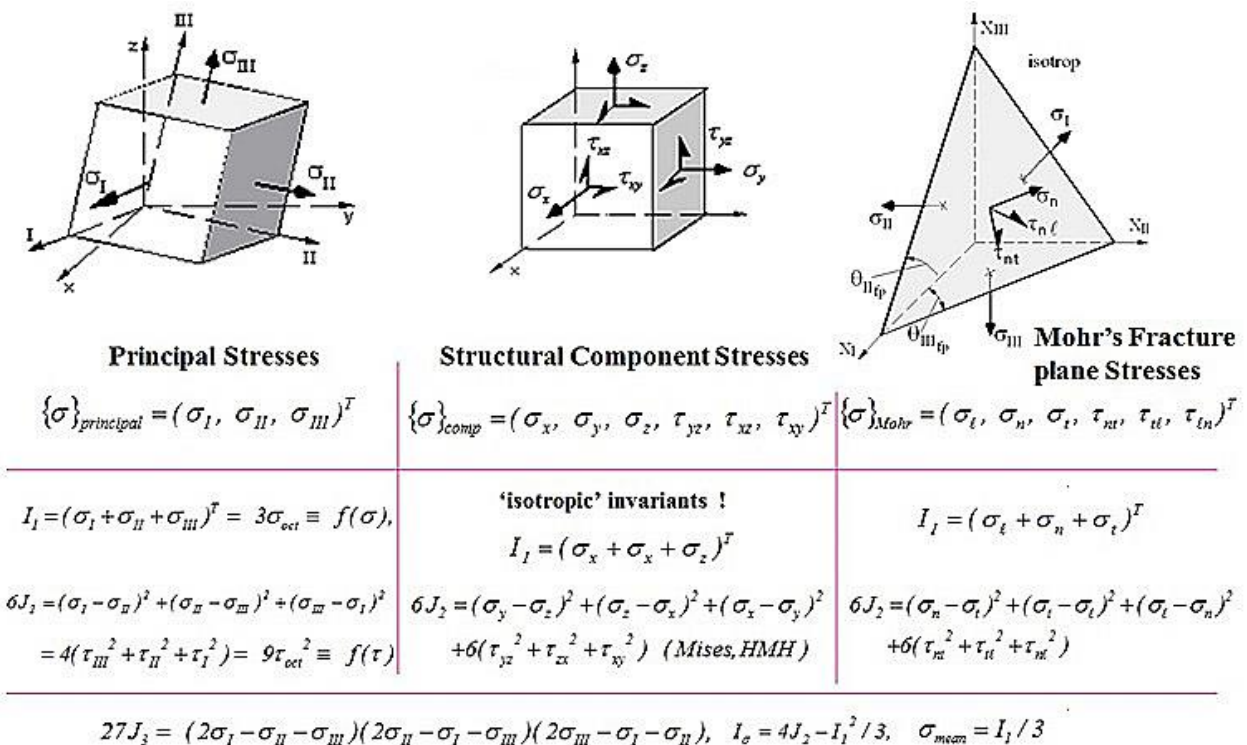


Fig.2-5: Applicable stresses and invariants of isotropic materials. Principal stresses (left) on the material cube's surfaces, (center) structural (component) stresses, and (right) Mohr stresses acting at the associated fracture plane

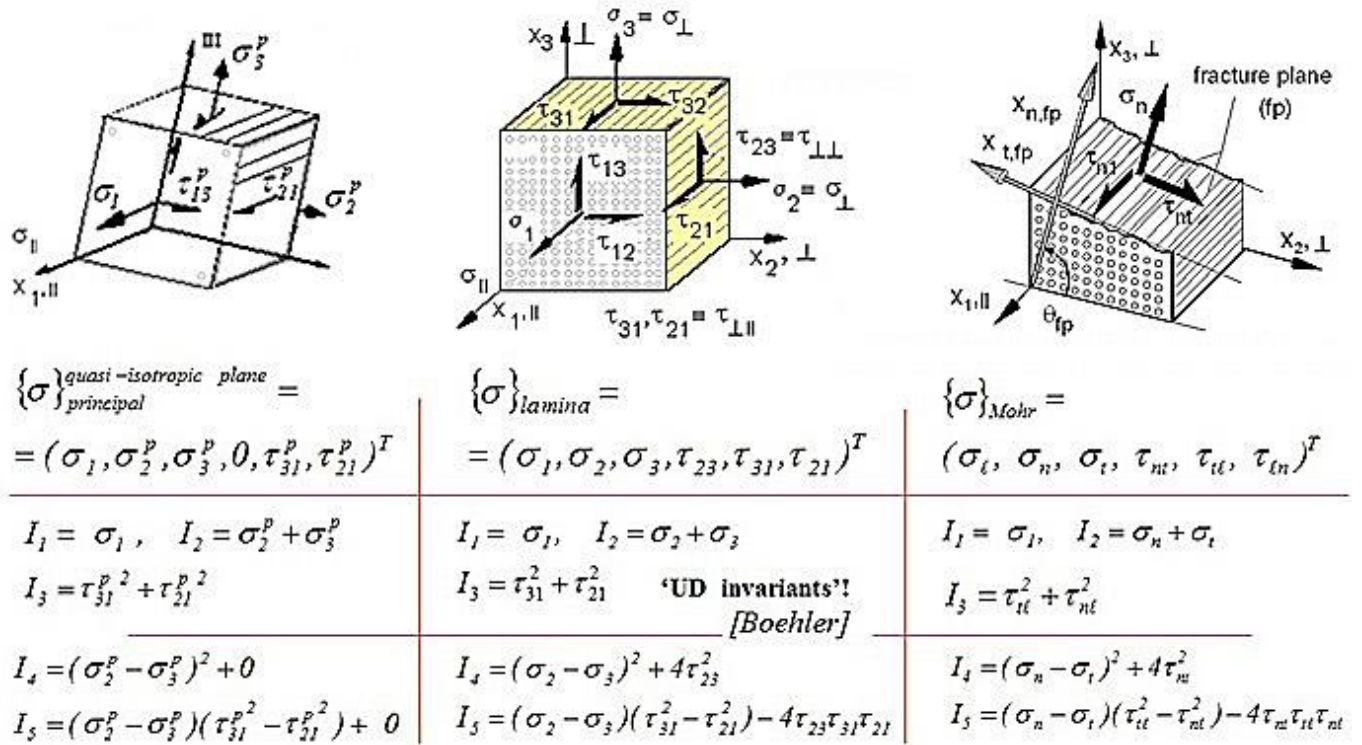


Fig.2-6: Applicable stresses and invariants of transversely-isotropic UD materials

In the case of (rhombically-anisotropic) orthotropic materials much more modes and strengths are present, however simple invariants are to apply.

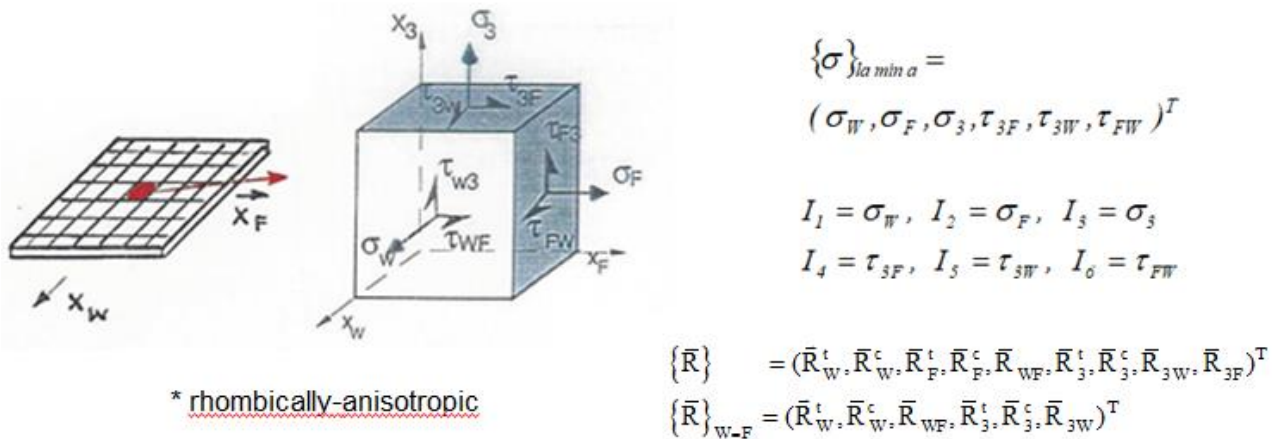


Fig.2-7: Applicable stresses, strengths and invariants of orthotropic materials

The FMC was at first intensively applied to UD materials in the World-Wide-Failure-Exercise. In this context it makes sense to add here all the hypotheses used for establishing SFCs, describing Inter-Fiber-Failure IFF of the UD- material family. Table 2-1 shows the basic UD hypotheses.

Table 2-1: Hypotheses used to predict Inter-Fiber-Failure IFF of UD materials

Mohr's Statement for isotropic materials:

“The strengths of a material are determined by the stresses  $\sigma_n, \tau_{nt}$  on the fracture plane” (the fracture plane is usually inclined with respect to the action of the external stresses)

Paul's modification of the Mohr-Coulomb Hypothesis:

“Brittle (behaving) material will fracture in either that plane where the shear stress  $\tau_{nt}$  reaches a critical value which is given by the shear resistance of a fiber-parallel plane increased by a certain amount of friction caused by the simultaneously acting compressive stress  $\sigma_n$  on that plane. Or, it will fracture in that plane, where the maximum principal (tensile) stress reaches the transverse tensile strength  $R_{\perp}^t$  (in the quasi-isotropic plane)”

Hashin [Has80]:

Proposed a modified Mohr-Coulomb IFF approach but did not pursue this idea due to numerical difficulties (Puck succeeded on this way). Also into this paper he included an invariant-based global quadratic approach (Cuntze's invariant way)

Puck's Action Plane IFF Conditions:

Based his IFF conditions on Mohr-Coulomb and Hashin, Puck interacts the 3 Mohr stresses  $\sigma_n, \tau_{nt}, \tau_{nl}$  on the IFF fracture plane. He uses simple polynomials (*parabolic or elliptic*) to formulate a so-called master fracture body in the  $(\sigma_n, \tau_{nt}, \tau_{nl})$  space. A compressive  $\sigma_n$  cannot cause fracture on its action plane

Cuntze Failure-Mode-Concept – based IFF conditions:

Used 3 different invariant IFF conditions, based on his idea that each fracture condition is governed by 1 strength.

## 2.4 Material symmetry-based assumptions of the author

Under the presumption “homogeneity is an acceptable assessment for the material concerned”, and regarding the respective tensors, it follows from material symmetry: *The Number of strengths  $\equiv$  number of elasticity properties!* This means, a characteristic number of quantities is fixed: 2 for isotropic material and 5 for the transversely-isotropic UD lamina ( $\equiv$  lamellas, sheets in civil engineering). Hence, the applicability of material symmetry involves that a *minimum number of properties needs to be measured only* (cost + time benefits)! Therefore, material symmetry requirements are helpful when setting up strength criteria and test programs. See the literature of Christensen [Chr98]

Again the experience of the author shows when comparing material behavior: Similarly behaving materials possess the same shape of a fracture body.

Table 2-2 collects the basic conclusions drawn from witnessed material symmetry knowledge. There might be a material ‘generic’ inherent number (*term was chosen by the author*).

For the theoretical case of homogeneity in Table 2-3 the author adds additional assumptions of the author assuming that generic numbers really exist, 2 for isotropic and 5 for UD material.

‘Basic’ fracture toughness properties means, that the crack plane under tension or under compression remains the same after up-loading.

Table 2-2: Assumed Generic Numbers of isotropic and transversely-isotropic materials

Material symmetry demand for the Isotropic Material: generic number 2

- 2 elastic ‘constants’, 2 strengths, 2 strength failure modes fracture (NF, SF)
- 1 physical parameter (such as coefficient of thermal expansion CTE, coefficient of moisture expansion CME, friction value  $\mu$ , etc.)

Material symmetry demand for the Transversely-Isotropic Material: generic number 5

Basic knowledge: for brittle materials

- 5 elastic ‘constants’, 5 strengths, 5 strength failure modes fracture (NF, SF)
- 2 physical parameters (CTE, CME,  $\mu_{\perp\perp}$ ,  $\mu_{\parallel}$  etc.)

Table 2-3: Cuntze’s full set of material symmetry-based assumptions.  
Extension of Table 2-2 by assumed additional assumptions

|   |
|---|
| <p><b>Material symmetry demands for the Isotropic Material: assumed as generic number 2</b></p> <p>Basic knowledge:</p> <ul style="list-style-type: none"> <li>- 2 elastic ‘constants’, 2 strengths, 2 strength failure modes fracture (NF, SF)</li> <li>- 1 physical parameter CTE, CME, <math>\mu</math>, etc.)</li> </ul> <p>Author’s additional assumptions:</p> <p>2 ‘basic’ fracture toughness properties, 2 invariants* <math>I_1, J_2</math>, 2 modes yielding (NY,SY)<br/>(* valid as long as a one-fold acting failure mode is to describe by the distinct SFC and not a multi-fold one. Presumed it is an ideal homogeneous material [Cun17,19a], 2 Master S-N curves (<math>R = 0.1</math> for 0, tension; 10 for <math>\infty</math>, compression)</p> <p><b>Material symmetry demands for the Transversely-Isotropic Material: generic number 5</b></p> <p>Basic knowledge from these at most quasi- brittle materials</p> <ul style="list-style-type: none"> <li>- 5 elastic ‘constants’, 5 strengths, 5 strength failure modes fracture (NF, SF)</li> <li>- 2 physical parameters (CTE, CME, <math>\mu_{\perp\perp}</math>, <math>\mu_{\parallel}</math> etc.)</li> </ul> <p>Author’s additional assumption</p> <ul style="list-style-type: none"> <li>- 5 ‘basic’ fracture toughness properties, 5 invariants*, 5 Master S-N curves</li> </ul> |
|---|

Material symmetry shows that the number of strengths is identical to the number of elasticity properties! Using material symmetry in material modelling requires that homogeneity is a prerequisite. Then however, the application of material symmetry beneficially fixes the number of material properties that are to measure to a minimum one.

Further should be mentioned: “The choice of the material model always depends on the efficiency a structural task must be and can be solved and on the required quality of the answer.”

## 2.5 Effects to be considered with isotropic and transversely-isotropic materials

### Pores and crack-like flaws (‘defects’):

Fig.2-8 completes the understanding of the effect of crack-like flaws, notches, pores and inclusions. It very well characterizes the different effects of ‘round’ void flaws and crack-like flaws (from legal reasons avoid the term defect, please). Under uniaxial tensile stresses, micro-damaging depends on the orientation of the crack-like flaws due to the generated different stress intensity at the crack tips. In the case of round micro-pores the micro-damaging effect is pretty similar in both the direction due to similar stress concentrations.

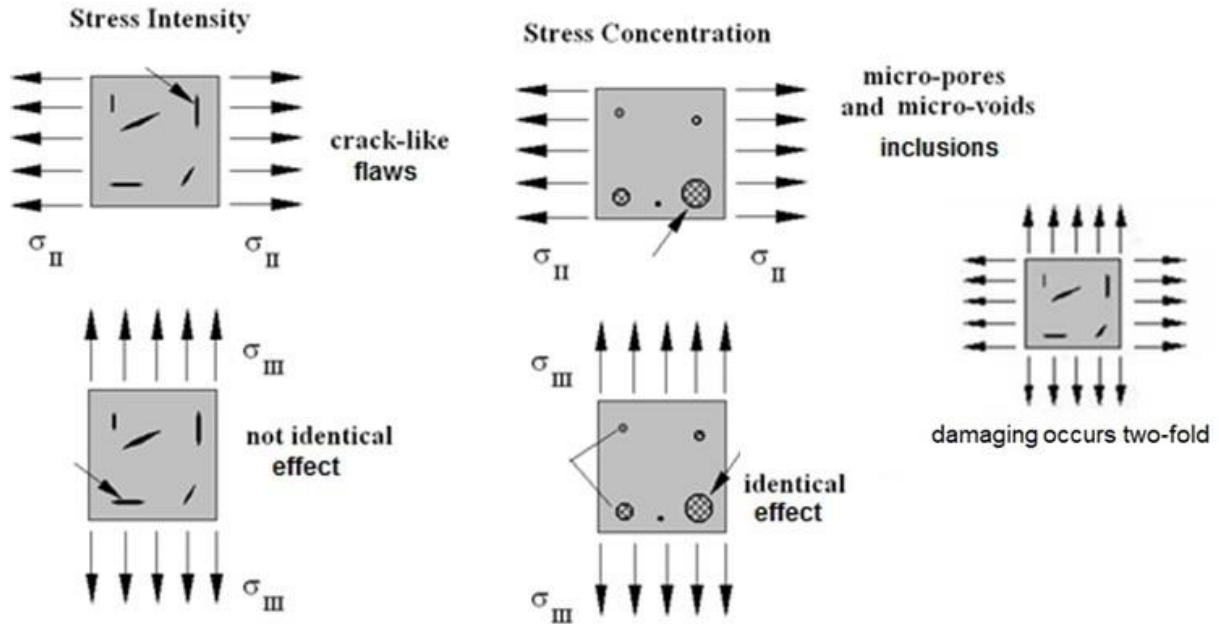


Fig.2-8: Effect of cracks, notches and inclusions as originators of fracture. Influence of flaw type, size and orientation

It is to conclude: Failure causing effects are different for round pores and crack-like flaws.

This effect usually increases with the grade of the tri-axiality factor, defined as  $TrF = p_{hyd} / \sigma_{eq}^{Mises} = (I_1/3) / \sqrt{3J_2}$ .

Remind: The decision, whether a strength design verification must be performed in a critical material location as strength demonstration or as a fracture mechanics design verification in the structural component, depends on the size of the flaw. If the size becomes a technical crack, then fracture mechanics must demonstrate structural integrity.

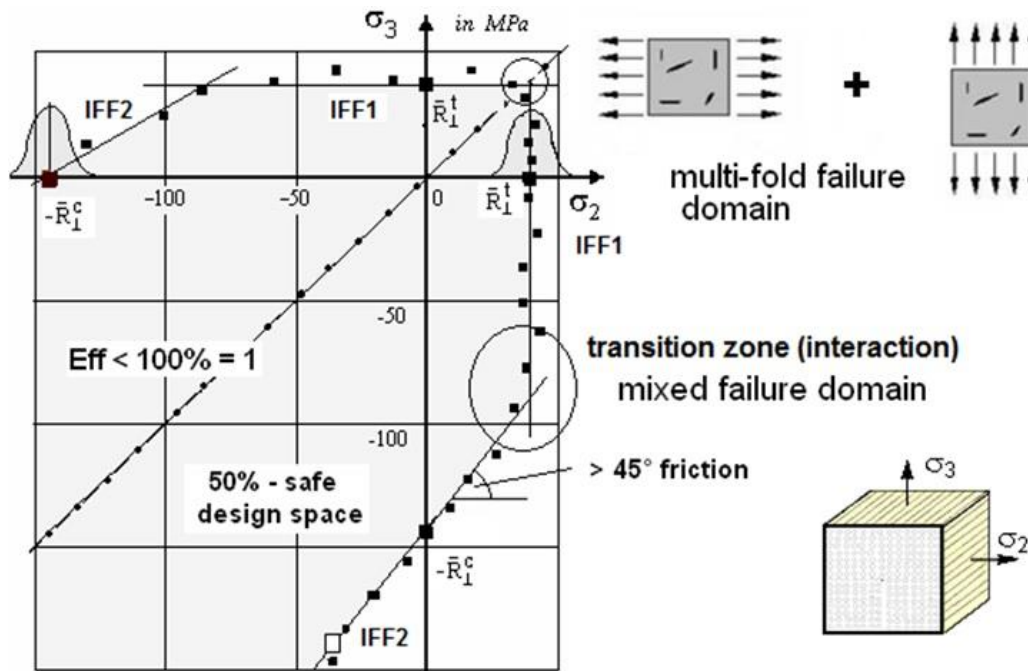


Fig.2-9: Schematic example for a two-fold failure domain and a mixed-failure domain (UD material)

### ***Mixed (fracture) Failure and Multi-fold Failure, isotropic and UD:***

Fig.2-9 displays the difference between Mixed Failure and Multi-fold Failure which can be recognized in the associated domains indicated in the figure. Due to the small tensile strength  $R^t$  of many brittle materials the bi-axial tensile strength  $R^{tt}$  of them - for instance of concrete - is not of interest but its bi-axial compressive strength as will be demonstrated later.

### ***Multi-fold failure effects:***

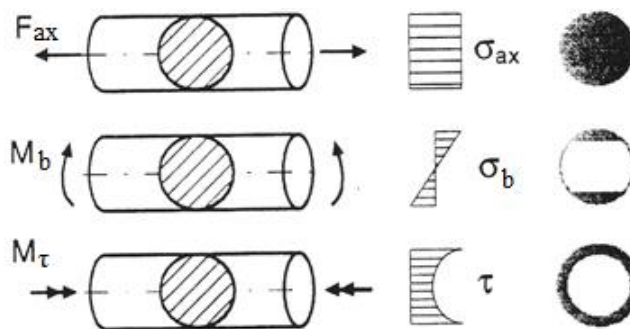
The existence of twofold and threefold failure effects must be considered: *example isotropic*

- A usual SFC just describes a 1-fold occurring failure mode or mechanism
- A multi-fold occurrence of a failure with its joint probabilistic effects must be additionally considered in the formulas as follows: 2-fold  $\sigma_{II} = \sigma_I$  tension or compression is elegantly captured by using the invariant  $J_3$  ; 3-fold  $\sigma_{II} = \sigma_I = \sigma_{III}$  hydrostatic compression, by a closing bottom formula part in the case of porous materials.

The 120°-located dents of the failure body, as the probabilistic result of the 2-fold acting of the same failure mode, are described by replacing  $J_2$  by  $J_2 \cdot \theta (J_3, J_2)$ . It describes the non-circularity of the 120° rotationally-symmetric isotropic fracture body.

### ***Effect of High Failure Probability Domains, isotropic material:***

This effect comes to act where differently large domains of ultimately stressed material parts are given. In the axial load case each material volume is stressed equally high, Fig.2-10.



*Fig.2-10: Domains of different fracture probabilities for the simple example rod*

Weibull volume effect and Weibull surface effect are used to estimate the value of a measured strength especially under tension.

### **Redundancy effects (healing, benign behavior):**

Such effects occur in hydro-static pressure cases. Examples are the materials UHPC and UD. In the UD-case the failure curve consists of the most often weakest-link part and a redundant part under  $p_{hyd}$ . This requires a different mapping of the course of test data in the  $p_{hyd}$ -dominated IFF2 domain and the IFF3 domain. (see *WWFE-II, Test Case, marked later*). Such redundancy effects are also given for UHPC viewing  $R^{cc} > R^c$ . Amount, size and orientation of flaws determine whether the generated crack ‘plane’ becomes in-plane or out-of-plane.

Hydrostatic pressure seems to ‘heal’ the adverse effect of flaws (such as micro-cracks, micro-voids) and delamination by compressing the flaws and increasing the amount of fracture energy necessary for crack growth. However, when fracture then begins to act this will happen faster and hence more

‘catastrophically’ which means fracture occurs in this compressed state in a more brittle manner. Thus, hydrostatic compression and in a minor manner through-thickness compression alone improve both static strength capacity and cyclic strength capacity. This issue is of high importance, e.g. at bearings and joints.

In this context mind, please: Opposite to *redundancy* the material may experience *weakest link* behaviour. In the case of brittle material is valid  $R'' < R^t$  because flaws are activated by stresses in two orthogonal directions.

### **Residual stresses (Eigenspannungen) and pre-stresses (Vorspannungen):**

In a lamina of a laminate the curing process generates wall thickness-dependent residual stresses. These stresses are decaying with decreasing stiffness caused by the degradation which accompanies an increasing non-linearity. In other words: In parallel to the decay of the stiffness the non-linear analysis releases matrix-dominated stresses.

Pre-stresses are used to lower for instance the stress state in the low tensile strength polymer matrix at the cost of the fiber [Cun93]. The same is standard in construction with pretension the mineral matrix concrete at the cost of the steel or of the carbon fiber reinforcement.

### **Thickness effect, example UD:**

Due to being strain-controlled, the material flaws in a *thin* lamina cannot grow freely up to micro-crack size in the thickness direction (*this is sometimes called thin layer effect*), because the neighboring laminae act as micro-crack-stoppers. Considering fracture mechanics, the strain energy release rate, responsible for the development of damage in the 90° plies from flaws into micro-cracks and larger, increases with increasing ply thickness. Therefore, the actual absolute thickness of a lamina in a laminate is a driving parameter for initiation or onset of micro-cracks, i.e. [Fla82].

### **Viewing the material’s behavior:**

Based on his experience the author looks at the material’s behavior not whether it is a concrete or a grey cast iron etc. If such a view is permitted, then the mathematical description of a fracture failure body model of a similarly behaving, still multi-axially tested material in the past can be used. This transferability was stressed for an isotropic example: Given was a good Foam test data basis which was transferred to a Concrete Stone, due to the lack of multi-axial failure stress test data for the concrete stone.

**LL:** *Presumption “SHAPE of the fracture failure body model is known”. Then, just the SIZE of the body needs to be further determined. This can be always performed by the necessarily known (uni-axial) different tensile and compressive strengths.*

## **2.6 Fracture behavior of the Various Materials**

### **General:**

According to the macroscopic load deformation curve, one can distinguish between deformation-poor and deformation-rich fracture processes. Here, too, the real material plays only a minor role. A mineral material can exhibit the same macroscopic behavior as a carbon fiber material, as a cast material or as a ferritic steel in the low-temperature range. And, a metal and a polymer can show

large irreversible deformations up to fracture, although the micro-mechanical deformation mechanisms may be different.

The micromechanical failure mechanisms of fracture are material-specific and therefore arbitrarily diverse. This is where (micro-)damage models come in. Some of what appears "similar" at the macro level (e.g. "brittle" behavior) may turn out to be completely different on the micro level. Examples are: A cleavage fracture in ferritic steels is for instance preceded by local *plastic deformations*. A fracture failure of concrete for instance implies small deformations from *damage mechanisms* on different length scales, micro-damage and macro-damage due to the complex microstructure,

Macroscopic fractures can be classified spanning deformation-rich and deformation-poor (grey casting, concrete) fractures, respectively. In tension and compression, the deformation-rich material experiences sliding failure under the influence of the failure-driving shear stress. In the deformation-poor case, the material is plastically non-deformable and at first micro-fractures and then macro-fractures under tension perpendicular to the tensile stress as soon as the normal stress reaches the separation (tensile) strength  $R^t$ . This is accompanied by cleavage fracture designated here as Normal Fracture NF.

Compression of brittle materials causes shear failure, because the shear stress is decisive. This includes as well sliding failure of ductile materials in the tensile and the compressive range as friction-sliding fracture failure of brittle materials in the compressive range, see [Fig.2-10](#).

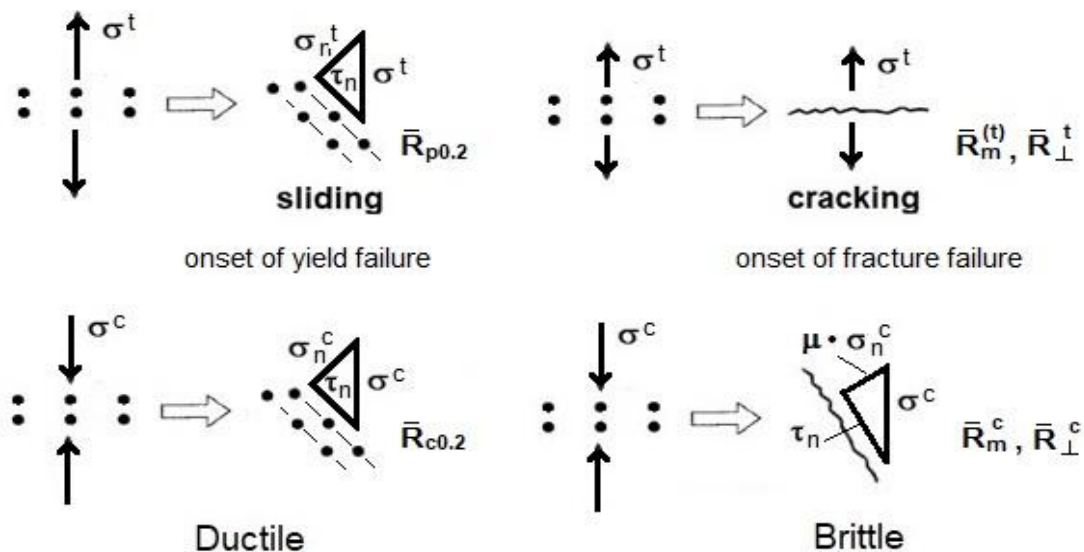


Fig.2-10: Rendering Sliding (micro)Cracking, ductile and brittle and the effect of  $p_{hyd}$

### Isotropic dense materials:

If brittle, then failure is fracture failure. The normative suffix  $_m$  in  $R_{(m)} = R^t$  should and can be dropped in [Fig.2-11](#) to [2-12](#) in order to achieve a simpler and clearer general designation system.

### LL:

\*Brittle: failure is fracture failure, 2 failure modes, 2 strengths to be measured.

\*Ductile: failure is yield failure, 1 failure mode, 1 strength  $\bar{R}^t$  to be measured (= load-controlled value),  $\bar{R}^c$  is neither really existing due to barreling of the cylindrical test specimen nor necessary for design  $\rightarrow R_{0.2}$  is the design driving 'strength'.



In Fig.2-11 (left) Load situations with associated fracture plane sketches and shear fracture pictures, and (right) of tensioned, differently brittle isotropic materials are depicted.

Before tensile rupture ('Gurson domain') firstly a diffuse and later a local *necking* with *void growth* occurs associated by a volume change before rupture starts. Dimples are generated under tension.

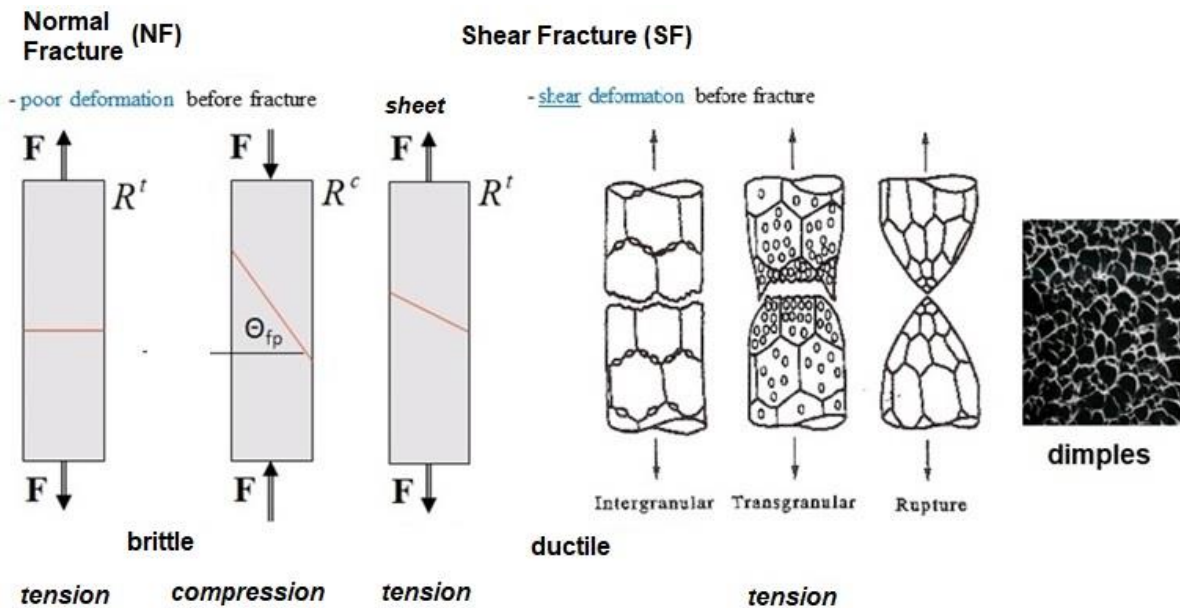
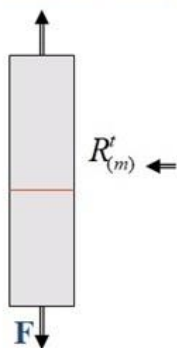


Fig.2-11: Fracture 'plane' sketches of different isotropic tensile test specimens

In the case of isotropic brittle porous materials two failure modes are faced, NF and CrF:

**Normal Fracture (NF)** (Spaltbruch, Trennbruch):

- volumetric change before fracture

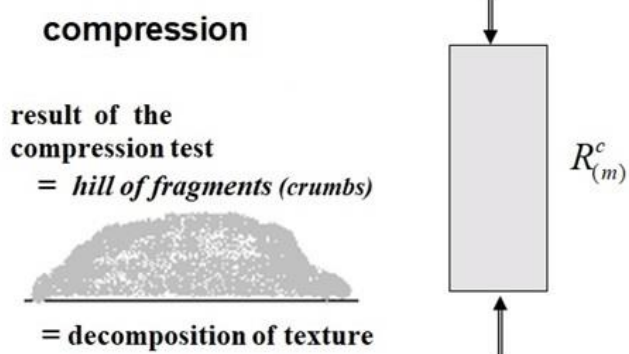


tension

**Crushing Fracture (CrF):**

- volumetric change before fracture

helpful knowledge for the choice of invariants



compression

Fig.2-12: Normal Fracture NF and Crushing Fracture CrF of isotropic materials

This leads over to grain materials.

**Mineral grain material:**

In the case of cracks, in contrast to the strength of intact solid materials, a uni-axial compressive stress causes a tensile stress at the crack tip of an inclined crack. This generates a secondary crack, termed wing (kink) crack, that turns into the direction of the acting compressive stress which may lead to splitting (*principally, this is similar to what happens in the fracture mechanics tension*

domain to an oblique macro-crack. Under multi-axial stress states the original crack may become instable and kink with an altering direction of the fracture plane (strain rate is influencing this behavior). This problem has attracted much attention and shall be here considered by using a strength failure view, see Fig.2-13.

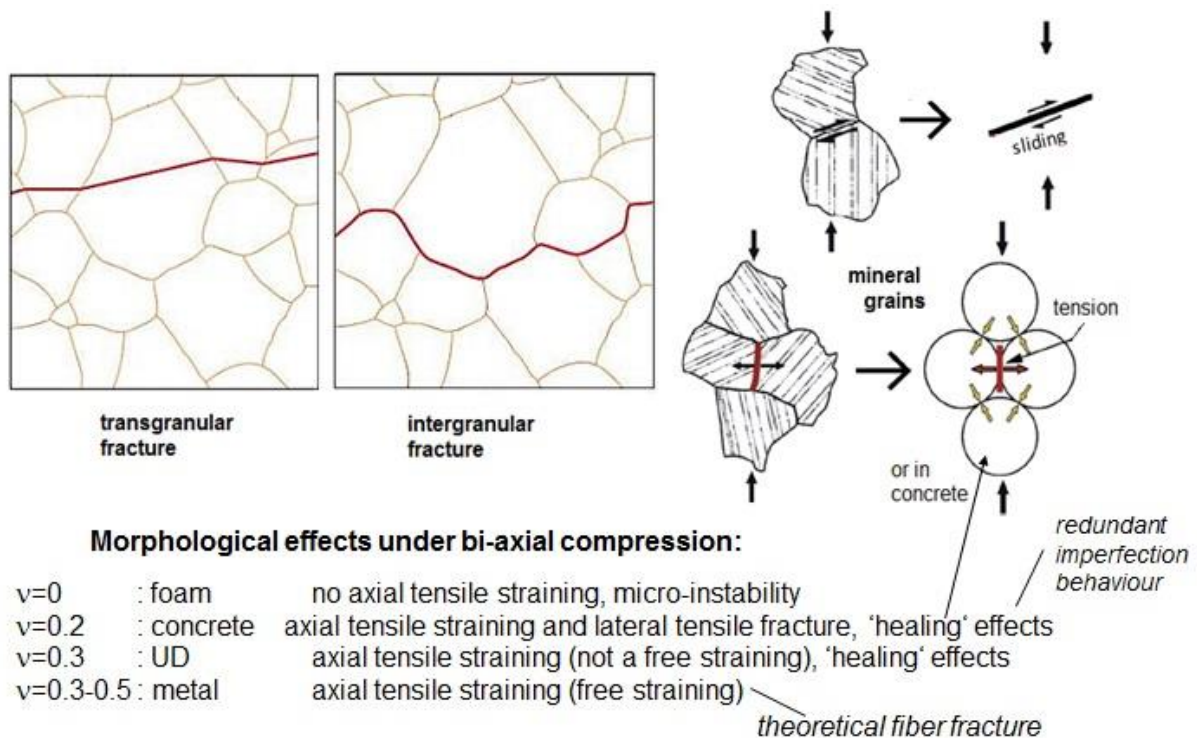


Fig.2-13: Texture influence considering inter-granular and trans-granular fracture under tension; (right) fracture between the mineral grains under compression due to 3D-tensile stress states

In the 2D compression case one wing branches off from each end of the initial crack, Fig.2-14 [Ger94]. These wings are generated dynamically. Then the further wing growth proceeds continuously. In the 3D compression case the generation of the wings causes an additional volume (cavitation) which is suppressed under multi-axial compression.

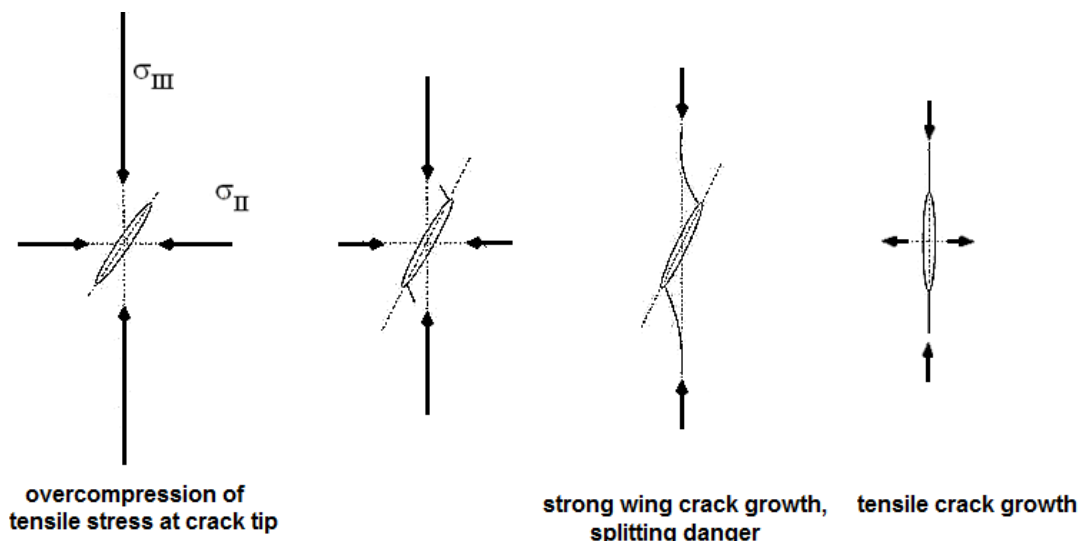


Fig.2-14: Initiation and attenuation of wing cracks (see [Ger94])

**LL:** 2D-models are not sufficient to describe progress of fracture in brittle behaving isotropic [Ger 94] materials such as grey cast iron, rock material, concrete, UD-material etc. 3D-theory and 3D experimental proofs are principally needed.

Under operational loading open-through crack and closed-through crack situations are to treat.

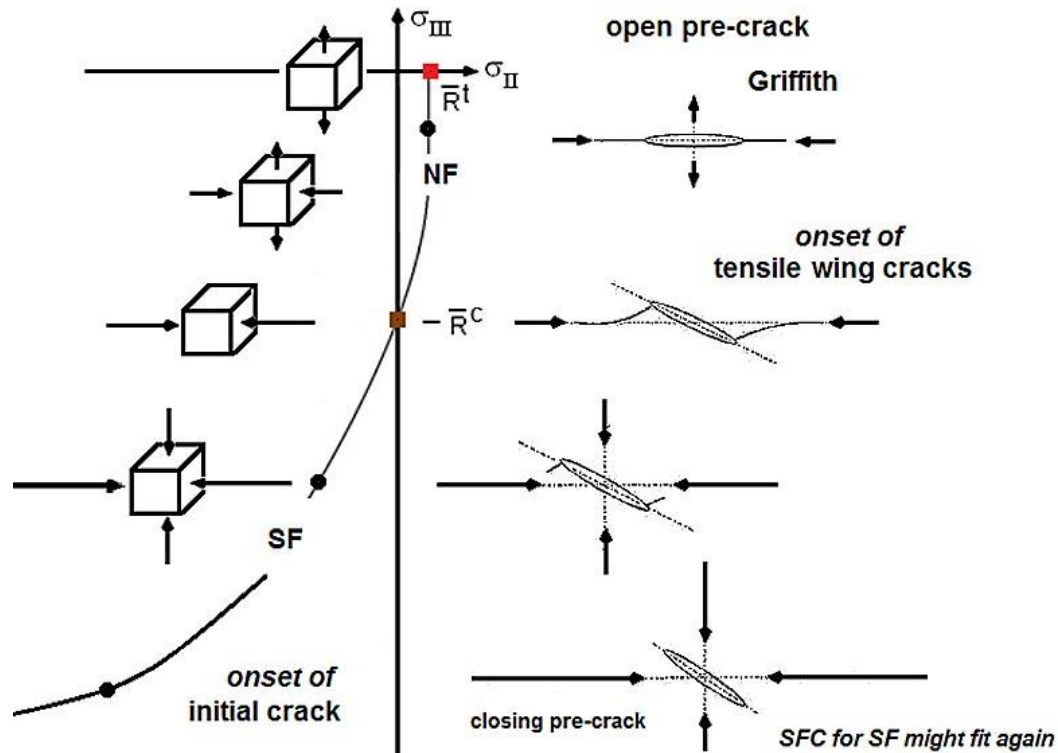


Fig.2-15, Mixed-Mode Compression, isotropic: 2D stress states, Observations w.r.t. failure modes NF and SF and fracture 'planes' in the case of initially crack-free (intact), open-through crack and closed-through crack situations

In the context of this subchapter it makes sense to talk a little about the influence of porosity.

Porosity is composed of all the cavities that are connected to each other and to the environment (open porosity) and the unconnected cavities. A highly open-pored material is a honeycomb for instance, closed porosity one finds with foams, see [Dr. J. Macht, Univ.-Doz., Dr. P. Nischer, Forschungsinstitut der VÖZ, Wien].

Porous materials, such as foams, porous laminates, porous polymer and concrete matrices, mortar and brick, geo-materials have stress-strain curves, which can be divided into 3 sections: (1) pressure low: the material behaves elastically, pores are preserved, (2) pressure increased: pores are compressed, (3) pressure exceeds a certain limit: finally complete compaction with pulverization of the crushed material. Collapse of the pores during crushing drives the compaction behavior of porous materials.

The Fig.2-16 presents micro-mechanical fracture.

The observed fracture types of Fig.2-17 depict failure modes which can be dedicated to the well-known 5 UD fracture failure modes.

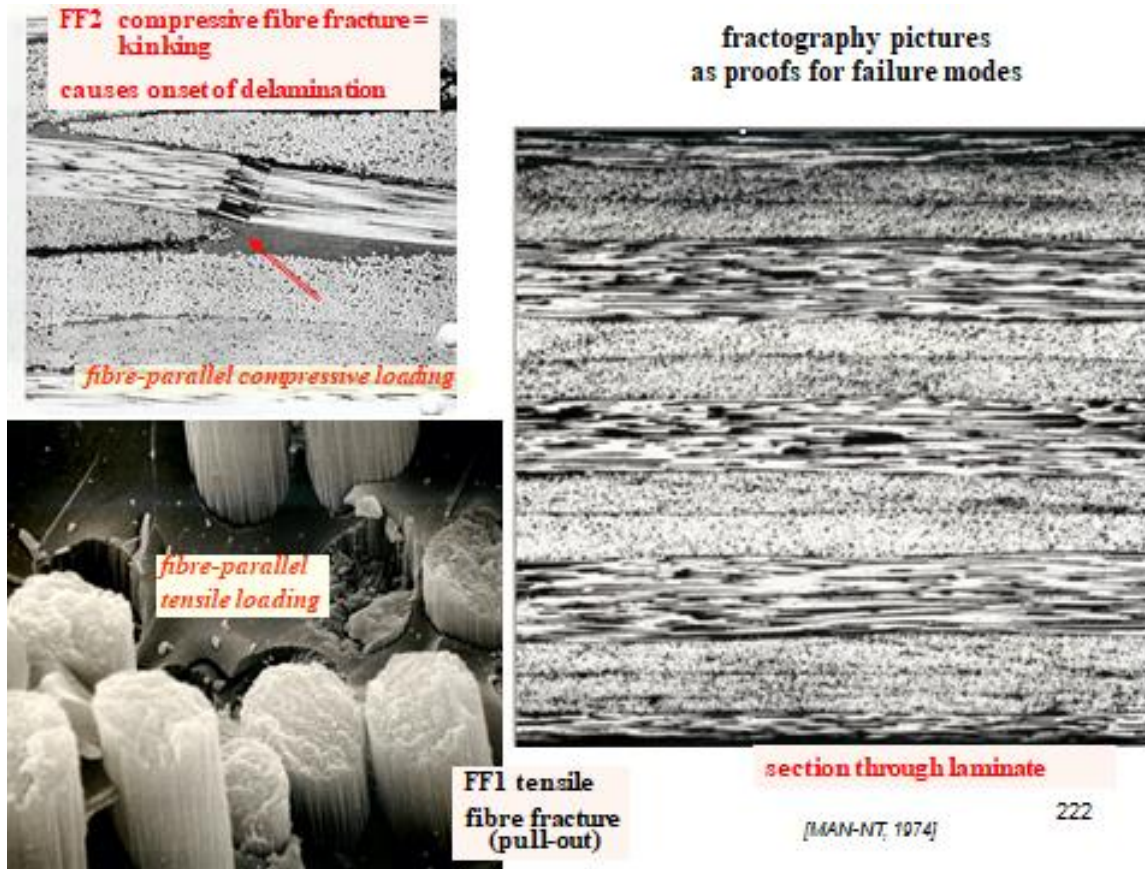


Fig.2-16: Fracture of UD material on microlevel

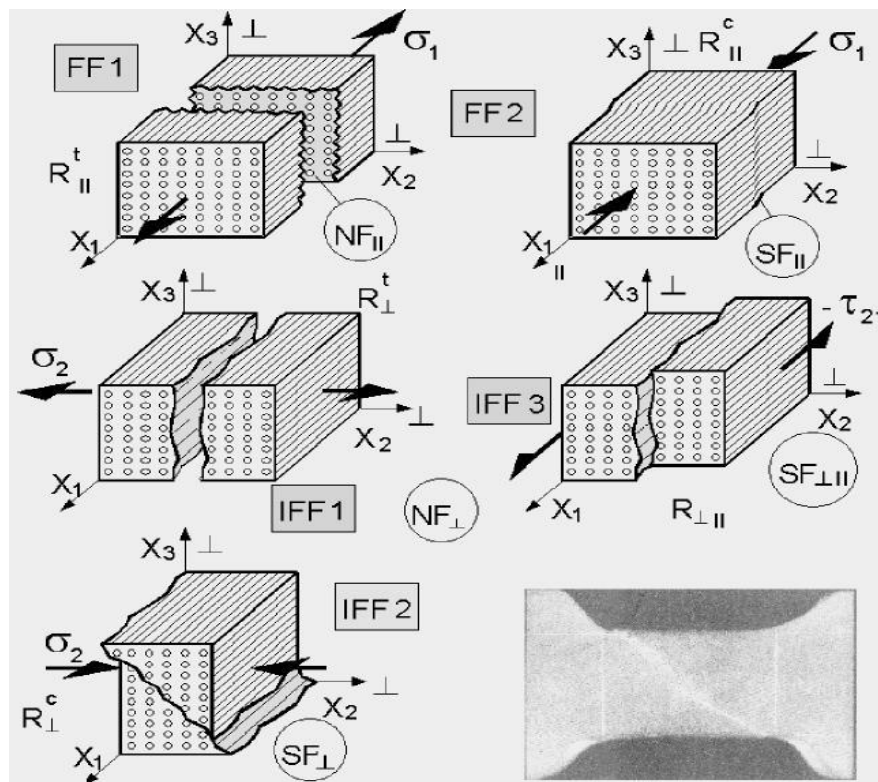


Fig.2-17: Test-observed UD Failure modes

## 2.7 Fiber-reinforced semi-finished products in construction

In construction so-called ‘open reinforcing’ such as fiber grids and so-called ‘closed reinforcing’ semi-finished products are to discriminate, see Table 2-18, Fig.2-18 and the definitions in the textile book of Chokri Cherif [Che11].

Table 2-4: Strength designations for fiber-reinforcements of the mineral matrix (concrete) and the polymer matrix

**Pultruded rod, bar**, transversely-isotropic material, composed of usually heavy tows: cured polymer matrix:  $R_{\parallel}^c$ ,  $R_{\parallel}^t$  ( $R_f$  is just fiber strength! [VDI 2014]). For the ‘fiber strand tensile test specimen’ (Faserstrang), cut out of the textile fiber grid, above designations can be used

**Lamella, UD-lamina**, transversely-isotropic material, polymer matrix, ‘closed reinforcing’: 2D and 3D stress states. Longtime used strength designations  $R_{\parallel}^c$ ,  $R_{\parallel}^t$ ,  $R_{\perp\parallel}$

**Fabrics**, orthotropic material (if homogenized, smearable), ‘closed reinforcing’: 2D and 3D materials (not to be confused with 3D *Directional* fabrics = 2D material). Strength designations longtime used for polymer matrix Warp and Fill (weft).  $F = W \rightarrow$  the number of strengths reduces from 9 to 6, in the fabric plane under 2D stress states from 5 to 3

**Textile Fiber grids**, orthotropic, 2D ‘open reinforcing’: 2D semi-finished product: if ‘smearable’ it is a composite material (Verbundwerkstoff) other ways a material composite (Werkstoffverbund). According to the textile process the indexing of the fiber grids R-mat and Q-mat (if both directions are equally reinforced then suffix  $_F$  is equal to  $_W$  (2m x 6m  $\rightarrow$  3m x 8m is available) can follow Warp and Fill (weft) of fabrics and according to the usual 2D loadings, basically to be employed in dimensioning. Is the spacing of the tows dense enough to permit ‘smearing’ in the analysis model then above fabric designations can be used for the composite material.  $R_{WF}$  is then to be determined on top of the fiber parallel strengths. the number of strengths is like for fabrics.

**Bar-grids of pultruded bars**, orthotropic, 2D - ‘open reinforcing’:

Strength designations, see bar. Smearable? Load-bearing width comes in for slabs.



Fig.2-18: Lamella, fiber grid, pultruded bars (CF, GF, AF, BsF) and bar grid

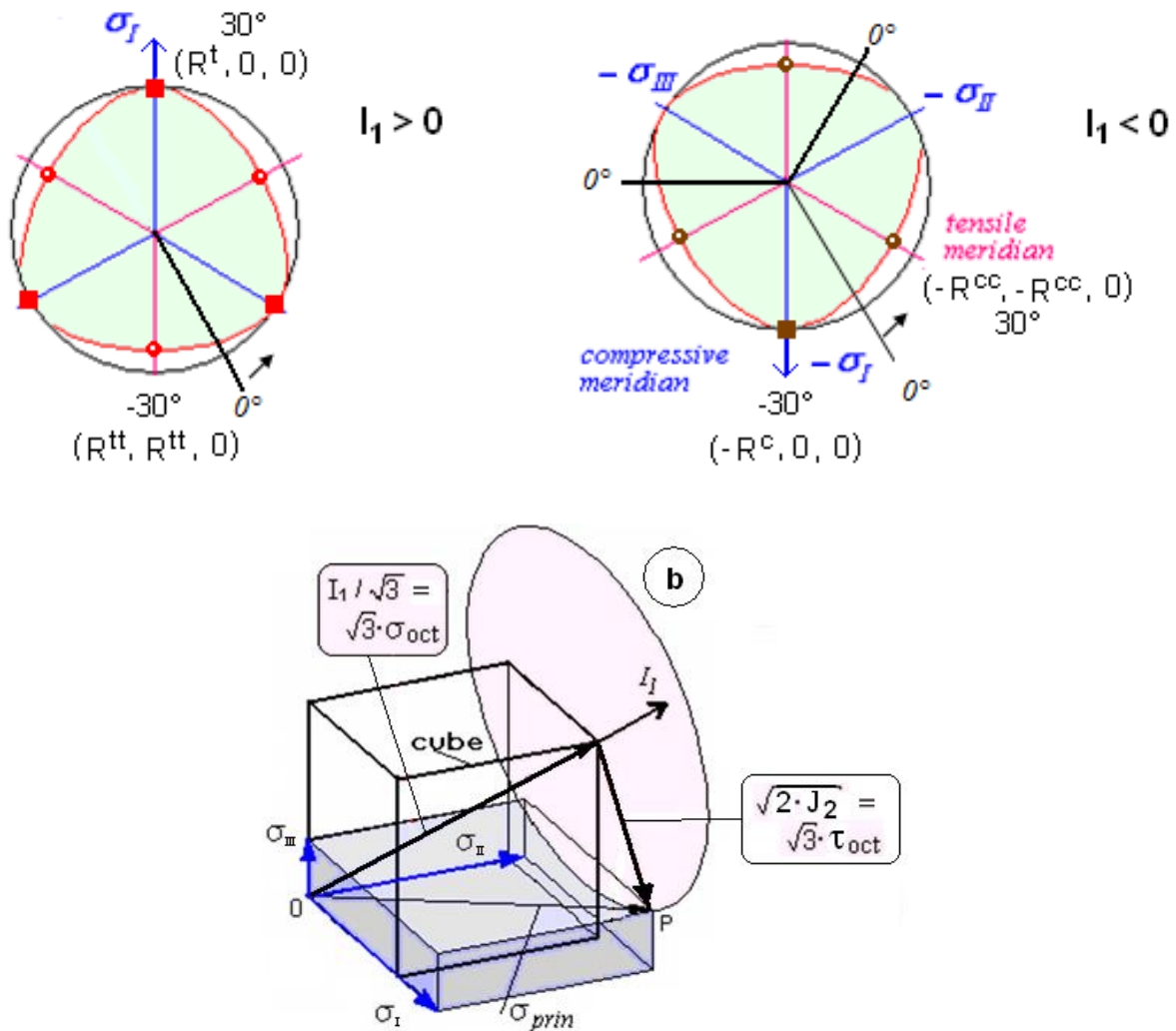
### LL:

- \* Decisive is a straight orientation of the fibers in the tows. Therefore, of essential influence on the strength are the tow crossings.
- \*  $R_{\parallel}^c < R_{\parallel}^t$  because there is usually not enough lateral support in the compression test for the fiber strand to buckle (not become in-stable). It is usually an instability-linked structural property which we use in design and not a strength material property. H. Schürmann and H. Bansemir proved for CFRP by effortful UD tests that  $R_{\parallel}^c \cong R_{\parallel}^t$  with a test rig of high lateral support, impeding micro-buckling .
- \* With the improved production of ideally aligned pultruded bars the possibility is given to mass-optimize the reinforcement of a serial part, if a dominant load case is ruling the design.

## 2.8 Visualization of an Isotropic Failure Body consisting of Mode Domains SF and NF

Engineers better learn from meaningful figures than from formulas. Therefore, numerically very effortful visualizations of the generated SFC failure bodies are a strong need, because a failure body shows the designing engineer the ‘multiaxial strength capacity’ of a material. This task will be exemplarily performed for an isotropic Normal Concrete material where a test data set was available.

A failure body is the location of all 1D-, 2D- and 3D-failure stress states. These are all points on the failure surface. As still mentioned,  $F = 1$  or  $Eff = 100\%$  mathematically defines the surface of the failure body. Such an isotropic failure body is rendered here using the Haigh-Westergaard-Lode coordinates with  $I_1/\sqrt{3}$  as y-coordinate (axial) and  $\sqrt{2 \cdot J_2}$  as x-coordinate (hoop), see [Fig.2-19](#).



*Fig.2-19: Mises cylinder shape, meridians, dents, Lode angle  $\vartheta^\circ$  around the  $120^\circ$ -hoop. Ansatz:  $\sin(3\vartheta)$  with  $\vartheta=0^\circ$  at shear meridian was taken; right figure: visualization of Lode coordinates*

In [Fig.2-20](#) the upper left part figure confirms, that above coordinate choice physically makes sense. The part figure, left down, depicts the stress states belonging to a tensile meridian and to a compressive meridian. These are those axial cross-sections of the failure body (right) along most of the compression tests are run. On the fracture failure body the 3 main meridians are outlined. For the tensile meridian the Lode angle is  $\vartheta = +30^\circ$  and for the compressive meridian  $-30^\circ$ . The shear

meridian was chosen here as neutral meridian with a Lode angle  $\vartheta = 0$ . Some 3D-failure stress states are indicated as fracture body points. Finally, for three essential design quantities the formulas are presented at the right side down.

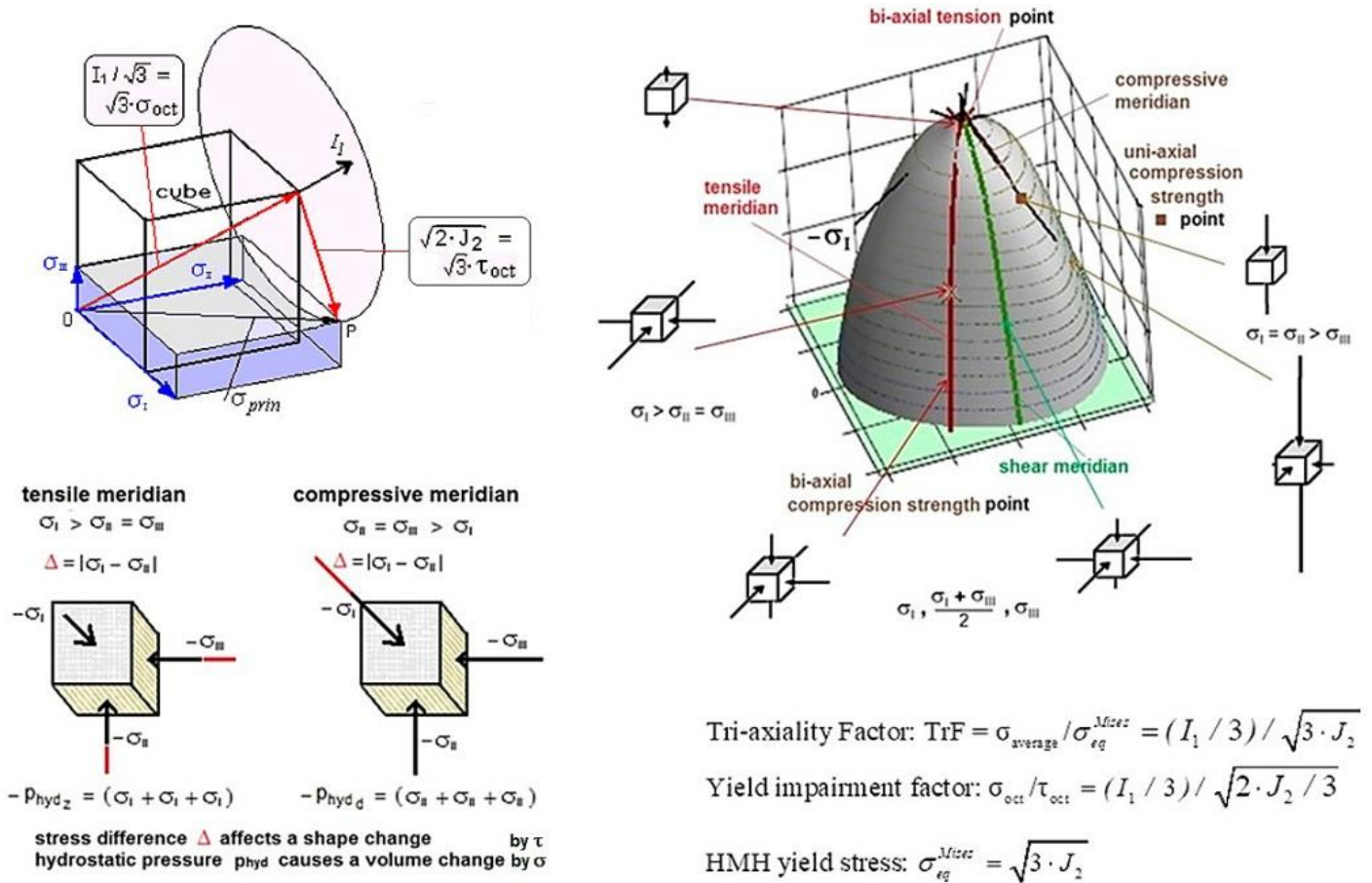


Fig.2-20: Visualization of the main meridians using Haigh-Westergaard Lode-coordinates  $I_1 / \sqrt{3}$ ,  $\sqrt{2 \cdot J_2}$  and various multi-axial stress states. Squares  $\blacksquare$   $\blacklozenge$  indicate strength values (strengths are defined as uni-axial failure stresses) and crosses mark bi-axial points (bi-axial failure stresses)

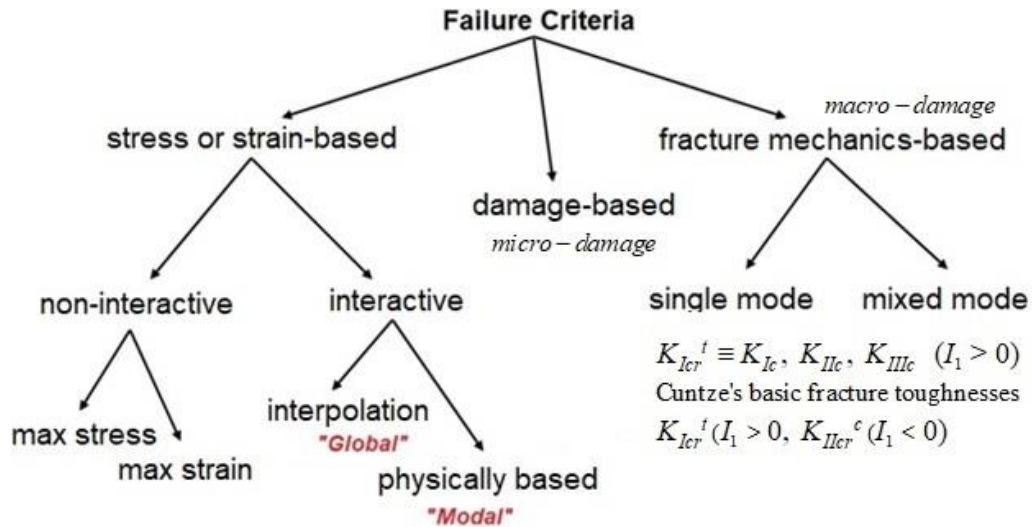
Mind, please:

The technical strength  $R$  or 1D-failure stress, respectively, is defined by standards and cannot be increased considering the same material. Its value is fixed!

### 3 Collection of FMC-based SFCs formulated in Structural Stresses

#### 3.1 Introduction with comparison of so-called ‘Global’ and ‘Modal’ SFCs

There are a lot of possibilities to generate SFCs. *Fig.3-1* gives a survey about this variety.



*Fig.3-1: Possibilities to generate SFCs following Klaus Rohwer [Roh1?]*

Stress-based SFCs have the advantage that residual stresses can be simply captured in the analysis.

Interactive SFCs can be discriminated. To do that the author choose the term “Global“ as a ‘play on words’ to “modal” and both the terms as being self-explaining names. Here, global and modal have a similar level of abstraction, as in the case of stability the terms ‘global’ and ‘local’.

*Fig.3-2* presents the main features of global and modal SFCs.

Drucker-Prager, Ottosen, Willam-Warnke, Tsai –Wu, Altenbach/Bolchun/Kolupaev , Yu, etc.

All modes are married in a Global Formulation. Any change hits all mode areas NF, SF of the fracture body surface !

**1 Global strength failure condition :  $F(\{\sigma\}, \{R\}) = 1$  (usual formulation)**

**Set of Modal strength failure conditions:  $F(\{\sigma\}, R^{mode}) = 1$  (addressed in FMC)**

$R \equiv f$

(Mises), Puck, Cuntze

All modes are separately formulated. Any change hits only the relevant mode area of the fracture body surface !

... and more precisely, considering Mohr-Coulomb for brittle materials under compression

$$F(\{\sigma\}, (R^{mode}, \mu^{mode})) = 1$$

direct introduction of the friction value  $\mu$

UD:  $\{\sigma\} = (\sigma_1, \sigma_2, \sigma_3, \tau_{23}, \tau_{31}, \tau_{21})^T$ ,  $\{\bar{R}\} = (\bar{R}_{||}^t, \bar{R}_{||}^c, \bar{R}_{\perp}^t, \bar{R}_{\perp}^c, \mu_{\perp\perp}, \bar{R}_{\perp\perp})^T$   
 vector of 6 stresses (general)      vector of 5 strengths with 2 friction values

Isotrop:  $\{\sigma\} = (\sigma_x, \sigma_y, \sigma_z, \tau_{yz}, \tau_{zx}, \tau_{xy})^T = (\sigma_I, \sigma_{II}, \sigma_{III})^T$ ,  $\{\bar{R}\} = (\bar{R}^t, \bar{R}^c, \mu)^T$

Needs an **Interaction of Failure Modes**: This is performed by a probabilistics-based ‘rounding-off’ approach (series failure system) in the transition zones between the neighbour mode domains NF and SF, directly delivering the reserve factor in linear analysis.

Test data mapping :  $\bar{R}$  average strength value (statistical mean)  
 Design Verification :  $R$  strength design allowable

*Fig.3-2: ‘Global’ and ‘Modal’ SFCs (in construction  $R \rightarrow f = \text{Festigkeit}$ )*



Global SFCs describe the full failure surface by one single equation capturing all existing failure modes such as Normal (NF, under tension or shear) or Shear Fracture (SF, under compression). A specific name used for global is ‘Single Failure Surface Description. Modal SFCs describe each failure mode-associated part of the full failure surface by an equation.

Example for the derivation of an isotropic Global SFC: Formulation of shape functions for the failure body describing (1) the hoop cross-section ( $\pi$ -plane  $\equiv I_1 = \text{constant}$  plane regarding the Lode angle  $\vartheta$ ), (2) the axial cross-section = meridian along  $I_1$ .

*Table 3-1: Pros and Cons of ‘global‘ and ‘modal‘ SFCs*

### Global SFCs

- (+) Describe the full failure surface by one single mathematical equation
- (-) Usual global SFCs do not capture a multi-fold acting failure mode, i.e.  $\sigma_1 = \sigma_{II}$  or  $\sigma_2 = \sigma_3$  or a 3-fold acting failure mode under  $\sigma_{\text{hyd}}$  with tension or compression
- (-) Re-calculation: In the case of a test data change in a distinct mode domain re-calculation of model parameters is mandatory. Any change in one of the ‘forcibly married’ modes requires a new global mapping which also changes the failure curve in a physically independent failure domain, see [Fig.3-3](#). In consequence, the material reserve factor has to be determined again
- (-) The determination of *RF* for multi-axial stress states seems to be questionable for the simple Drucker-Prage model (conical failure body) still often used in civil engineering, see *Sub-chapter 9.3.2*.

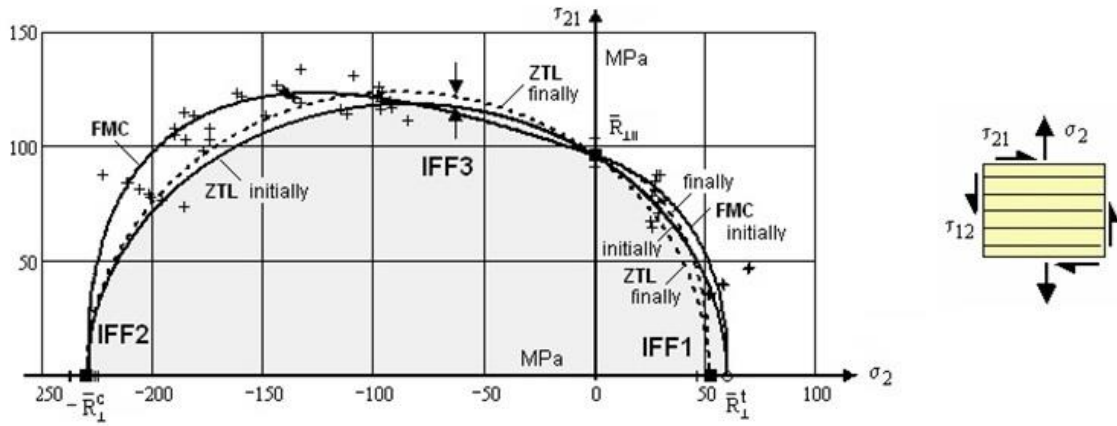
### Modal SFCs

- (+) Describes each failure mode-associated part of the full failure surface by a single equation. Therefore, modal SFCs are more physically-based than global SFCs
- (+) A change within one mode just hits this mode, see [Fig.3-3](#). *RF* is just to re-determine in the affected failure mode domain !
- (+) Equivalent stresses  $\sigma_{\text{eq}}$  are always determinable for isotropic UD materials
- (+) Cuntze’s SFCs capture multi-fold occurring failure modes by an additional term
- (+) Cuntze’s SFCs directly use the well to estimate parameter friction value  $\mu$
- (-) Affords an interaction of the FMC-based SFCs for the activated failure modes.

*Fig.3-3* visualizes for a distinct global SFC, used in a German guideline, how dramatically a change of the tensile strength  $\bar{R}_t$  affects the failure curve in the compression domain, where no physical impact can be!

Mind, please: Often, SFCs employ just strengths. This is physically not accurate: Mohr-Coulomb acts in the case of compressed brittle materials! Consequence: The computed *RF* may not be on the safe side.

In order to only use experimentally derivable material quantities, the author directly introduced in his 3D-SFCs for the compression domain, internal friction  $\mu$  as a SFC formula or model parameter. Friction is a well-known physical property in engineering. One does not yet find a direct use of  $\mu$  in the textbooks! Why using Mohr's friction angle  $\varphi$  if  $\mu$  ( $\varphi$ ) exists? The direct introduction of the measurable friction value is possible for modal SFCs. This possibility was achieved after the performance of an effortful transition of the SFC formulated in structural stresses into a Mohr stresses formulated one (see *Chapter 6*)



$$\begin{array}{cc}
 \text{ZTL: global} & \text{FMC: modal} \\
 \frac{\sigma_2^2}{R_{\perp}^t \cdot R_{\perp}^c} + \sigma_2 \cdot \left( \frac{1}{R_{\perp}^t} - \frac{1}{R_{\perp}^c} \right) + \frac{\tau_{21}^2}{R_{\perp\parallel}} = 1 & \left( \frac{\sigma_2}{R_{\perp}^t} \right)^m + \left( \frac{-\sigma_2}{R_{\perp}^c} \right)^m + \left( \frac{|\tau_{21}|}{R_{\perp\parallel} - \mu_{\perp\parallel} \cdot \sigma_2} \right)^m = 1
 \end{array}$$

Fig.3-3: Effect of global modelling

Considering the shortcomings of Global UD SFCs, my friend John Hart-Smith cited in [Har93]:

***“It is scientifically incorrect to employ polynomial interaction failure models (‘global’), whenever the mechanism of failure changes?”***

### 3.2 Basic features of the Failure-Mode-Concept FMC (1996)

From above can the basic features of the FMC derived

- Each failure mode represents 1 independent failure mechanism and thereby represents 1 piece of the complete (*is global again*) failure surface
- Each failure mechanism is governed by 1 basic strength (this is witnessed)
- Each failure mode can be represented by 1 failure condition SFC [Cun04,12,15a]

Therefore, equivalent stresses can be computed for each mode. This is of advantage when deriving S-N curves and Haigh diagrams in fatigue with minimum test effort, see [Cun17]

- Consequently, the FMC-approach requires an interaction of all modes!

$$Eff = \sqrt[m]{(Eff^{\text{mode } 1})^m + (Eff^{\text{mode } 2})^m + \dots} = 1 = 100\% \quad \text{for Onset-of-Failure.}$$

This interaction of adjacent failure modes is modelled by the spring model ‘series failure system’. That permits to formulate the total material stressing effort from all activated failure modes as the ‘accumulation’ of Effs  $\equiv$  sum of all the failure danger proportions. Eff = 1 represents the mathematical description of the surface of a failure body!

From engineering reasons, Cuntze takes the same interaction exponent  $m$  for each transition zone between failure mode domains. The value of  $m$  depends on the ratio  $R^c / R^t$ . For brittle dense materials with about  $R^c / R^t > 3$  the value is about  $m = 2.6$ , from mapping experience in the transition zone of the two modes. A smaller  $m$  is always ‘design verification conservative’.

Failure at the lower microscopic level shall be considered in the applied macroscopic SFC.

LL:

- Failure condition is a condition on which a failure becomes effective
- Criterion is a distinctive feature as a condition for a state  $F < = >$ . And SFC means  $F = 1$
- Decisive for a High Fidelity SFC application is: Is the used SFC validated by multi-axial fracture stress states or not really? To be not 3D-validated is an essential bottleneck. How sure can the designer be with the 3D validation performed for the used classical strength criterion? Check.
- High values of  $m (> 4)$  have to be taken if there is just a very low mutual triggering of the failure effects of the affected modes.

The knowledge about the materials - collected above - lead in the FMC to consider: a

1. Rigorous postulation of a number of failure modes = number of strengths
2. Application of a failure mode-wise concept for the generation of SFCs
3. Direct use of the friction value  $\mu$  in the SFC.

Ideas/desires, formed over the years, became pre-requisites of the author for the ‘Creation of the Failure–Mode–Concept FMC’ and shall be collected in Table 3-1:

*Table 3-1: Desires for generation of effective High Fidelity (Genauigkeit, Verlässlichkeit) SFCs*

- applicable for all material families
- rigorous independent treatment of each single failure mode NF, SF, CrF, FF, IFF, ..
- physically convincing mapping method (*then just a minimum test information is needed*)
- numerically robust, unique solutions, simple, as much as physics allows it
- stress invariant-based (*like ‘Mises’ for the single mode yielding,  $J_2$* )
- application of the hypothesis of Beltrami (isotropic invariants stand for a deformation change  $J_2$  for the shape of the material element and  $I_1^2$  for a volume change. Similarly for UD)
- application of the hypothesis of Mohr-Coulomb, considering internal material friction by use of  $I_1$  in isotropic case
- delivery of equivalent stresses  $\sigma_{eq}$  (*very helpful for a failure mode-based turning of the ‘design screw’*)
- using a material behavior-linked thinking and not a material-linked one
- an approach, where all model parameters can be measured (*model parameters are to determine separately in each mode domain*)
- viewing the Strength Mechanics ‘Building’: More physically-based it should become simpler
- shall allow for a simple determination of  $RF$  or of the so-called *material stressing effort*  $Eff$  which is best understood from engineers in stress state assessment of a material. The link is  $\sigma_{eq} = Eff \cdot R$ ,
- use of so-called ‘proportional loading’ in order to derive  $Eff$  in case of *mathematically non-homogeneous SFCs*, however, fulfilling the requirement that with a zero failure driving stress  $\sigma$  or  $\tau$  the  $Eff$ -value becomes zero, too.

LL:

- (1) Three energy terms – represented by two invariants, only - are required to establish ‘isotropic SFCs’. Hence, the FMC approach is not without any energy basis as some other ‘stress-based criteria.’
- (2) Material symmetry seems to have told the author: In the case of isotropic materials, for the quantities a generic (basic) number of 2 is inherent. This is valid for modes, invariants, yield

- strengths, fracture strengths, fracture mechanical SIFs [Cun20] and more entities. And this also affects the test effort considering ‘What is the minimum test effort to be necessarily measured?’
- (3) The 120°-rotational symmetry could be mapped by employing  $J_3$  (only reason for a third invariant)
- (4) A brittle slightly porous concrete in the compression domain ( $p_{hyd}$ ) can be SFC-described by the same SFC formula as a metal in the ductile rupture or ‘Gurson tension domain’, respectively due to similarly describable effects of the material element.

### 3.3 Modal equivalent stress $\sigma_{eq}$ and Modal material stressing effort $Eff$

For the failure mode ‘yielding’ the HMM hypothesis (in short ‘Mises’) delivers an equivalent stress and this for all stress situations (normal stress, shear stress, torsion stress) when the mode yielding comes to act, Fig.3-4. Fully analogously to the (modal) HMM equivalent yield stress the equivalent fracture stress is related to the material stressing effort

$$Eff^{Mises} = \sigma_{eq}^{Mises} / R_{po,2} \Rightarrow Eff^{fracture\ mode} = \sigma_{eq}^{fracture\ mode} / R_m, Eff^{mode\ \varepsilon} = \sigma_{eq}^{mode\ \varepsilon} / \bar{R}^{mode}$$

Above possibility to formulate equivalent stresses caused Cuntze to differentiate Global from Modal strength criteria types. About more details and the Pros and Cons, see [Cun16c].

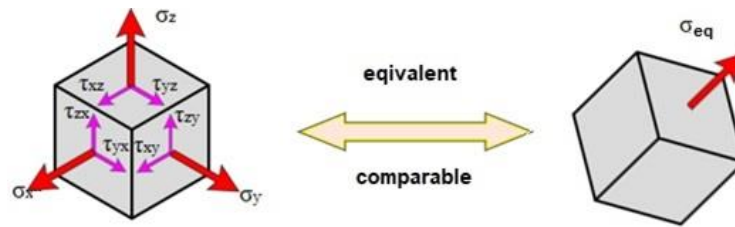


Fig.3-4: multi-axial structural stress state with its representing equivalent stress

The next figure shows the definition of the material stressing effort.  $Eff$  is an artificial term, created with the WWFE orinators in the UK, because an equivalent term does not exist in English. It is derived in analogy to Mises.

**modal material stressing effort  $Eff$**  (in German “Werkstoffanstrengung”)

$$Eff^{mode} = \sigma_{eq}^{mode} / \bar{R}^{mode}$$

mode equivalent stress

mode associated average strength  
(in test data-mapping with bar over, as  $\bar{R}$ )

analogy to ‘Mises’

$$Eff^{yielding\ mode} = \sigma_{eq}^{Mises} / \bar{R}_{0,2}$$

$$Eff^{fracture\ mode} = \sigma_{eq}^{fracture\ mode} / \bar{R}$$

Interaction of adjacent failure modes is modelled with the model ‘Series failure system”, that permits to formulate the total material stressing effort from all activated failure modes

$$Eff = \sqrt[m]{(Eff^{mode\ 1})^m + (Eff^{mode\ 2})^m + \dots} = 1 = 100\%, \text{ if Onset of Failure}$$

= ‘Accumulation’ of Effs  
≡ sum of the failure danger risk proportions

Fig.3-5: Definition of material stressing effort

### 3.4 History of FMC with Search of a ‘More Closed Strength Mechanics Building’

After 1985 the author co-worked in several structural reliability groups and projects. Aim in structural reliability is to prove that a distinct limit state is not yet met. In the group of structural limit states the material’s strength limit states play a very essential role. The author experienced the advantage to ‘think in strength failure modes’, which led him to a rigorous thinking in strength failure mode limit states and that later paved the way for the development of the FMC.

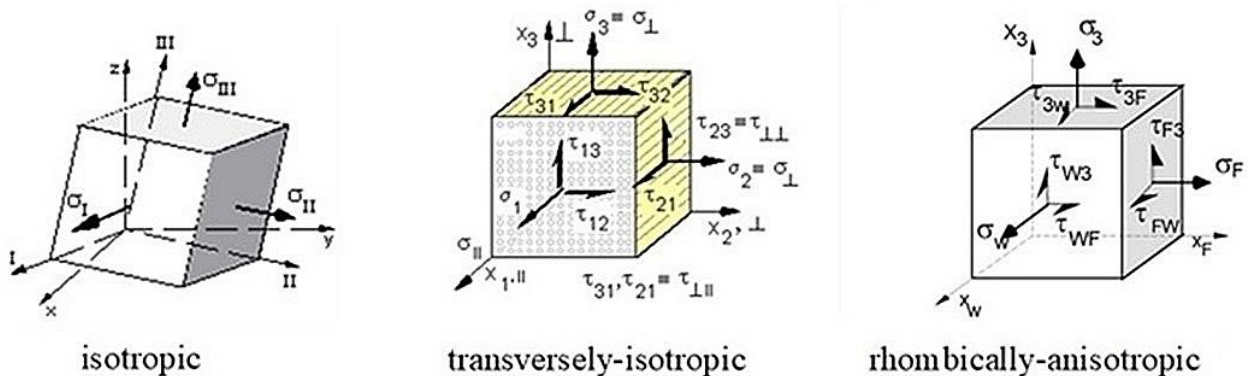
In industry the author headed the department ‘Structural and Thermal Analysis’. Therefore, he had to take care of material modelling because he faced a not sufficient ‘feeling’ in structural engineering considering the strength of non-cracked materials. This experience is valid for the three material families used isotropic materials, transversely-isotropic (UD fiber reinforced matrices) materials and orthotropic (fabrics etc.) materials, where design verification for the fabricated structural parts had to be performed. Thereby brittle materials were the main focus.

This situation firstly caused the author to think about SFCs for a variety of structural materials and secondly – after being successful with the SFCs – to think about a strength mechanics building that includes the previously assumed missing links as ‘rooms’.

This building includes the assumed full set of strength failure modes for the intact, non-cracked material and also regarded the fracture mechanics modes. The task involved isotropic and transversely-isotropic materials where clear SFCs can be found as long as ‘conglomerate materials’ can be homogenized (‘smeared’) to a model material. Orthotropic materials are usually still structures where a separation of fracture failure modes is not simple.

The FMC-derived SFCs, applied in tensile and compression domain, are presented in the following Tables. A SFC is a model that should be as simple as possible but should well describe physics macro-mechanically and as far as possible capture the associated micro-mechanically failure events.  $F = 1$  or  $Eff = 100\%$  mathematically defines the surface of the fracture failure body. For each mode, the SFC model parameters are just to determine in each associated ‘pure’ failure mode domain.

As reminder, before the presentation of the SFCs, all stress state figures of the 3 material families:



$$\{\sigma\} = (\sigma_x, \sigma_y, \sigma_z, \tau_{yz}, \tau_{xz}, \tau_{xy})^T$$

$$\{\sigma\} = (\sigma_1, \sigma_2, \sigma_3, \tau_{23}, \tau_{13}, \tau_{21})^T$$

$$\{\sigma\} = (\sigma_W, \sigma_F, \sigma_3, \tau_{3F}, \tau_{3W}, \tau_{FW})^T$$

Mapping requirements: Before presenting all the SFCs should be noted: 2D test data sets must be mapped by the 3D failure function  $F$  broken down to a 2D one in the 2D principal plane. 3D test data sets are directly mapped by the 3D SFC defining the 3D failure body or surface.

Meridional shape functions (cross section of the failure body) should be not the result of a separate 2D meridional mapping of the associated isotropic test data, but the result of the desired meridian angle  $\vartheta$  inserted into the 3D SFC.

### 3.5 SFCs for ‘dense’ and ‘porous’ Isotropic Material

Table 3-2 collects all information necessary to design dimension a dense isotropic material.

Table 3-2 ‘Dense’ materials: SFC formulations for **NF** and **SF**, 120°-rotational symmetry

**Normal Fracture NF** for  $I_1 > 0$   $\leftrightarrow$  **Shear Fracture SF** for  $I_1 < 0$

$$F^{NF} = c^{NF} \cdot \Theta^{NF} \cdot \frac{\sqrt{4J_2 \cdot \Theta^{NF} - I_1^2 / 3 + I_1}}{2 \cdot \bar{R}^t} = 1 \quad \leftrightarrow \quad F^{SF} = c_{1\Theta}^{SF} \cdot \frac{3J_2 \cdot \Theta^{SF}}{\bar{R}^{c2}} + c_{2\Theta}^{SF} \cdot \frac{I_1}{\bar{R}^c} = 1$$

$$Eff^{NF} = c^{NF} \cdot \frac{\sqrt{4J_2 \cdot \Theta^{NF} - I_1^2 / 3 + I_1}}{2 \cdot \bar{R}^t} = \frac{\sigma_{eq}^{NF}}{\bar{R}^t} \quad \leftrightarrow \quad Eff^{SF} = \frac{c_{2\Theta}^{SF} \cdot I_1 + \sqrt{(c_{2\Theta}^{SF} \cdot I_1)^2 + 12 \cdot c_{1\Theta}^{SF} \cdot 3J_2 \cdot \Theta^{SF}}}{2 \cdot \bar{R}^c} = \frac{\sigma_{eq}^{SF}}{\bar{R}^c}$$

If a failure body is rotationally symmetric, then  $\Theta = 1$  like for the neutral or shear meridian.

A two-fold acting mode makes the rotationally symmetric fracture body 120°-symmetric and is modelled by  $\Theta(J_3)$  using the invariant  $J_3$  and  $\Theta$  as non-circularity function with  $d$  as non-circularity parameter

$$\Theta^{NF} = \sqrt[3]{1 + d^{NF} \cdot \sin(3\vartheta)} = \sqrt[3]{1 + d^{NF} \cdot 1.5 \cdot \sqrt{3} \cdot J_3 \cdot J_2^{-1.5}}, \quad \Theta^{SF} = \sqrt[3]{1 + d^{SF} \cdot 1.5 \cdot \sqrt{3} \cdot J_3 \cdot J_2^{-1.5}}$$

Lode angle  $\vartheta$ , here set as  $\sin(3 \cdot \vartheta)$  with ‘neutral’ shear meridian angle set  $\vartheta = 0^\circ$ ;

tensile meridian angle  $30^\circ \rightarrow \Theta^{NF} = \sqrt[3]{1 + d^{SF} \cdot (+1)}$ ; compr. merid. angle  $-30^\circ \rightarrow \Theta^{SF} = \sqrt[3]{1 + d^{SF} \cdot (-1)}$ .

Equation of the fracture failure body:  $Eff = [(Eff^{NF})^m + (Eff^{SF})^m]^{m^{-1}} = 1 = 100\%$  total effort

$$Eff = \sqrt[m]{\left(c^{NF} \cdot \frac{\sqrt{4J_2 \cdot \Theta^{NF} - I_1^2 / 3 + I_1}}{2 \cdot \bar{R}^t}\right)^m + \left(\frac{c_{2\Theta}^{SF} \cdot I_1 + \sqrt{(c_{2\Theta}^{SF} \cdot I_1)^2 + 12 \cdot c_{1\Theta}^{SF} \cdot 3J_2 \cdot \Theta^{SF}}}{2 \cdot \bar{R}^c}\right)^m} = 1.$$

Curve parameter relationships obtained by inserting the compressive strength point  $(0, -\bar{R}^c, 0)$ :

\* Rotationally symmetric:  $c_1^{SF} = 1 + c_2^{SF}$ ,  $d^{SF} = 0$ , friction parameters are equal  $c_2^{SF} \equiv c_{2\Theta}^{SF}$   
 $c_2^{SF} = c_{2\Theta}^{SF} \approx (1 + 3 \cdot \mu) / (1 - 3 \cdot \mu)$  from  $\mu = \cos(2 \cdot \theta_{fp}^c \cdot \pi / 180)$  and for  $50^\circ \rightarrow \mu = 0.174$ .

\* 120°-rotationally symmetric:  $c_{1\Theta}^{SF} = 1 + c_{2\Theta}^{SF} \cdot \sqrt[3]{1 + d^{SF} \cdot (-1)}$  with

$c^{NF}, \Theta^{NF}$  from the two points  $(\bar{R}^t, 0, 0)$  and  $(\bar{R}^{tt}, \bar{R}^{tt}, 0)$  or by a minimum error fit, if data,

$c^{SF}, \Theta^{SF}$  from the two points  $(-\bar{R}^c, 0, 0)$  and  $(-\bar{R}^{cc}, -\bar{R}^{cc}, 0)$  or by minimum error fit.

A paraboloid serves as closing cap  $\frac{I_1}{\sqrt{3} \cdot \bar{R}_t} = s^{cap} \cdot \left(\frac{\sqrt{2J_2 \cdot \Theta^{NF}}}{\bar{R}_t}\right)^2 + \frac{\max I_1}{\sqrt{3} \cdot \bar{R}_t}$ .

$$I_1 = (\sigma_I + \sigma_{II} + \sigma_{III}) = f(\boldsymbol{\sigma}), \quad 6J_2 = (\sigma_I - \sigma_{II})^2 + (\sigma_{II} - \sigma_{III})^2 + (\sigma_{III} - \sigma_I)^2 = f(\boldsymbol{\tau})$$

$$27J_3 = (2\sigma_I - \sigma_{II} - \sigma_{III}) \cdot (2\sigma_{II} - \sigma_I - \sigma_{III}) \cdot (2\sigma_{III} - \sigma_I - \sigma_{II}).$$

\* Friction value  $0 < \mu < 0.2$

\* From mapping experience the interaction exponent is in the range of  $2.5 < m < 2.9$ .

\* Failure surface is closed at the top. As closing cap the paraboloid in Table 3-3 is to apply.

The NF-approach  $\sqrt{4J_2 \cdot 1 - I_1^2 / 3} + I_1 = 2 \cdot \bar{R}^t$  is for the rotationally symmetric failure body. It was constructed by connecting uni-axial strength point and bi-axial strength point by a straight line in the principal stress plane.

LL: \* A failure surface is the result of optimally mapping the course of multi-axial test data and, therefore, has the attribute 50% survival probability. \* Bi-axial tensile stressing: In [Lem08] the author found for intermediate ratios of stresses  $\sigma_1/\sigma_{II}$  in Normal Concrete that the combined fracture stress is a little higher than the uni-axial strength! This has been never observed by the author with any brittle material. Might there have been a problem with testing or test data evaluation? From physical interpretation a multi-axial tensile stress state activates more fracture-driving flaws and danger to fracture increases.

Table 3-3 collects all information necessary to design dimension a porous isotropic material like a foam or a concrete stone. These materials experience 120°-rotational symmetry.

Table 3-3 'Porous' isotropic material: SFC formulations for NF and CrF, 120°-rotational symmetry

**Normal Fracture NF** for  $I_1 > 0$

↔

**Crushing Fracture CrF** for  $I_1 < 0$

$$F^{NF} = c^{NF} \cdot \Theta^{NF} \cdot \frac{\sqrt{4J_2 \cdot \Theta^{NF} - I_1^2 / 3} + I_1}{2 \cdot \bar{R}^t} = 1 \leftrightarrow F^{CrF} = c^{CrF} \cdot \Theta^{CrF} \cdot \frac{\sqrt{4J_2 \cdot \Theta^{CrF} - I_1^2 / 3} + I_1}{2 \cdot \bar{R}^c} = 1$$

$$Eff^{NF} = c^{NF} \cdot \frac{\sqrt{4J_2 \cdot \Theta^{NF} - I_1^2 / 3} + I_1}{2 \cdot \bar{R}^t} = \frac{\sigma_{eq}^{NF}}{\bar{R}^t} \leftrightarrow Eff^{CrF} = c^{CrF} \cdot \frac{\sqrt{4J_2 \cdot \Theta^{CrF} - I_1^2 / 3} + I_1}{2 \cdot \bar{R}^c} = \frac{\sigma_{eq}^{CrF}}{\bar{R}^c}$$

If a failure body is rotationally symmetric, then  $\Theta = 1$  like for the neutral or shear meridian, respectively . A 2-fold acting mode makes the rotationally symmetric fracture body 120°-symmetric and is modelled by using the invariant  $J_3$  and  $\Theta$  as non-circularity function with  $d$  as non-circularity parameter

$$\Theta^{NF} = \sqrt[3]{1 + d^{NF} \cdot \sin(3\vartheta)} = \sqrt[3]{1 + d^{NF} \cdot 1.5 \cdot \sqrt{3} \cdot J_3 \cdot J_2^{-1.5}} \leftrightarrow \Theta^{CrF} = \sqrt[3]{1 + d^{CrF} \cdot 1.5 \cdot \sqrt{3} \cdot J_3 \cdot J_2^{-1.5}}$$

Lode angle  $\vartheta$ , here set as  $\sin(3 \cdot \vartheta)$  with 'neutral' (shear meridian) angle  $\vartheta = 0^\circ$  ( $\rightarrow \Theta = 1$ );

tensile meridian angle  $30^\circ \rightarrow \Theta^{NF} = \sqrt[3]{1 + d^{NF} \cdot (+1)}$ ; compr. mer. angle  $-30^\circ \rightarrow \Theta^{CrF} = \sqrt[3]{1 + d^{CrF} \cdot (-1)}$ .

Mode interaction  $\rightarrow$  Equation of the fracture body:  $Eff = [(Eff^{NF})^m + (Eff^{CrF})^m]^{m^{-1}} = 1 = 100\%$

$$Eff = \sqrt[m]{\left(c^{NF} \cdot \frac{\sqrt{4J_2 \cdot \Theta^{NF} - I_1^2 / 3} + I_1}{2 \cdot \bar{R}^t}\right)^m + \left(c^{CrF} \cdot \frac{\sqrt{4J_2 \cdot \Theta^{CrF} - I_1^2 / 3} + I_1}{2 \cdot \bar{R}^c}\right)^m} = 1$$

Curve parameter relationships obtained by inserting the compressive strength point  $(0, -\bar{R}^c, 0)$ :

\* Rotationally symmetric  $\Theta = 1$ :  $d^{SF} = 0$ ,  $c_{1\Theta}^{SF} = 1 + c_{2\Theta}^{SF}$

\* 120°-rotat. symmetric  $\Theta \neq 1$ :  $c_{1\Theta}^{SF} = 1 + c_{2\Theta}^{SF} \cdot \sqrt[3]{1 + d^{SF} \cdot (-1)}$ , with

$c^{NF}$ ,  $\Theta^{NF}$  from the two points  $(\bar{R}^t, 0, 0)$  and  $(\bar{R}^t, \bar{R}^t, 0)$  or by a minimum error fit, if data available,

$c^{CrF}$ ,  $\Theta^{CrF}$  from the two points  $(-\bar{R}^c, 0, 0)$  and  $(-\bar{R}^c, -\bar{R}^c, 0)$  or by minimum error fit.

The failure surface is closed at both the ends: A paraboloid serves as closing cap and bottom

$$\frac{I_1}{\sqrt{3} \cdot \bar{R}_t} = s^{cap} \cdot \left(\frac{\sqrt{2J_2 \cdot \Theta^{NF}}}{\bar{R}_t}\right)^2 + \frac{\max I_1}{\sqrt{3} \cdot \bar{R}_t} \quad \frac{I_1}{\sqrt{3} \cdot \bar{R}_t} = s^{bot} \cdot \left(\frac{\sqrt{2J_2 \cdot \Theta^{CrF}}}{\bar{R}_t}\right)^2 + \frac{\min I_1}{\sqrt{3} \cdot \bar{R}_t}$$

Slope parameters  $s$  are determined connecting the respective hydrostatic strength point with the associated point on the tensile and compressive meridian,  $\max I_1$  must be assessed whereas  $\min I_1$  can be measured.

### Mapping the Decay of the Bi-axial Stress 'Perturbation' of the isotropic failure body

In the hoop direction the bi-axiality-affected zone is automatically mapped and thereby confined by the  $J_3$ -120°-symmetry. However, what is the situation in the axial direction of the fracture body. Is it to be handled along the axis as a decaying perturbation (Störung) or is the decay practically enough

well mapped by the increasing negative  $I_1$ , which for large values finally leads to a circle? The author believed that the inward and outward dents of the fracture body should be mapped as a perturbation (Störung) that can be described by a decay function along the meridian. This affects the non-circularity functions  $\Theta$  and shall be depicted for

$$\Theta^{NF} = \sqrt[3]{1 + d^{NF} \cdot \sin(3\vartheta)} \Rightarrow \sqrt[3]{1 + D\sigma(y) \cdot \sin(3\vartheta)} \quad \text{with } D\sigma(y) = \alpha\sigma \cdot \beta\sigma \cdot y^{\beta\sigma-1} \cdot \exp[-\alpha\sigma \cdot y^{\beta\sigma}] \cdot D\sigma_{tt}$$

$$\Theta^{SF} = \sqrt[3]{1 + d^{SF} \cdot \sin(3\vartheta)} \Rightarrow \sqrt[3]{1 + D\tau(y) \cdot \sin(3\vartheta)}, \quad D\tau(y) = \alpha\tau \cdot \beta\tau \cdot (-y)^{\beta\tau-1} \cdot \exp[-\alpha\tau \cdot (-y)^{\beta\tau}] \cdot D\tau_{cc}$$

Below is the Mathcad-derivation of  $D\sigma(y)$  and  $D\tau(y)$  with  $y$ , a normalized function across meridian.

abbreviation       $y_t := \frac{I_{1t}}{\sqrt{3} \cdot R_t}$        $y_{tt} := \frac{I_{1tt}}{\sqrt{3} \cdot R_t}$        $y_c := \frac{I_{1c}}{\sqrt{3} \cdot R_t}$        $y_{cc} := \frac{I_{1cc}}{\sqrt{3} \cdot R_t}$   
 Lode-coordinate

Approach NF decay function :  $D\sigma(y) = \alpha\sigma \cdot \beta\sigma \cdot (y)^{\beta\sigma-1} \cdot \exp[-\alpha\sigma \cdot (y)^{\beta\sigma}] \cdot D\sigma_{tt}$

derivation in the bi-axial stress point:

$$\frac{d}{dy} [\alpha\sigma \cdot \beta\sigma \cdot (y)^{\beta\sigma-1} \cdot \exp[-\alpha\sigma \cdot (y)^{\beta\sigma}] \cdot D\sigma_{tt}] \rightarrow$$

horizontal tangent required:

$$[\beta \cdot \alpha \cdot D\sigma_{tt} \cdot \alpha \cdot (y)^{\beta} \cdot (y)^{\beta-2} \cdot (\beta-1) - \beta^2 \cdot \alpha^2 \cdot D\sigma_{tt} \cdot \alpha \cdot (y)^{\beta} \cdot (y)^{2 \cdot \beta-2}] \cdot D\sigma_{tt} = 0$$

$$\begin{cases} 0 \\ \beta-1 \\ \beta \cdot y^{\beta} \end{cases} \quad \text{if } 0 \leq \text{Re}(\beta) \vee \text{Re}(\beta) < 0 \wedge y = 0$$

undefined otherwise

after insertion of  $y = y_{tt}$  :  $\alpha\sigma = \frac{\beta\sigma - 1}{\beta\sigma \cdot (y_{tt})^{\beta\sigma}}$

Vorgabe  $\beta\sigma := 1.1$

$$\frac{\frac{\beta\sigma - 1}{\beta\sigma \cdot (y_{tt})^{\beta\sigma}} \cdot \beta\sigma \cdot (2y_{tt})^{\beta\sigma-1} \cdot \exp\left[-\frac{\beta\sigma - 1}{\beta\sigma \cdot (y_{tt})^{\beta\sigma}} \cdot (2y_{tt})^{\beta\sigma}\right]}{\frac{\beta\sigma - 1}{\beta\sigma \cdot (y_{tt})^{\beta\sigma}} \cdot \beta\sigma \cdot (y_{tt})^{\beta\sigma-1} \cdot \exp\left[-\frac{\beta\sigma - 1}{\beta\sigma \cdot (y_{tt})^{\beta\sigma}} \cdot (y_{tt})^{\beta\sigma}\right]} = 0.5$$

Aim: 50% decay at uni-axial strength.

D $\sigma_{tt}$  vanishes!

$A\sigma := \text{Suchen}(\beta\sigma)$

$A\sigma = \blacksquare$        $\beta\sigma := A\sigma$        $\beta\sigma = \blacksquare$

$$\alpha\sigma := \frac{\beta\sigma - 1}{\beta\sigma \cdot (y_{tt})^{\beta\sigma}} \quad \alpha\sigma = \blacksquare$$

Approach SF decay function :  $D\tau(y) = \alpha\tau \cdot \beta\tau \cdot (-y)^{\beta\tau-1} \cdot \exp[-\alpha\tau \cdot (-y)^{\beta\tau}] \cdot D\tau_{cc}$

analogous

$$\beta\tau := 1.918$$

$$\alpha\tau := \frac{\beta\tau - 1}{\beta\tau \cdot (-y_{cc})^{\beta\tau}} \quad \alpha\tau = \blacksquare$$

Resulting function:

$$\Theta_{\tau}(y) = \sqrt[3]{1 + D\tau(y) \cdot \sin(3\vartheta)} = \sqrt[3]{1 + \alpha\tau \cdot \beta\tau \cdot (-y)^{\beta\tau-1} \cdot \exp[-\alpha\tau \cdot (-y)^{\beta\tau}] \cdot D\tau_{cc} \cdot \sin(3\vartheta)}$$

Whether the application of above decay function is practically necessary must be cleared by more multi-axial measurements on the tensile and compressive meridians.

Investigating tensile meridian test data from Dr. Scheerer, IfM TU Dresden, on Normal Concrete with and without the perturbation sub-model delivered the result: With the perturbation model mapping was only slightly better. Drawing a conclusion for practice: **As it is just one example it is recommended - viewing the scatter of test data - to not presently use the more sophisticated perturbation sub-model.** See also the calculation of the Reserve Factor in *Sub-chapter 9.3.2*.



### 3.6 SFCs for ‘dense’ and ‘porous’ transversely-isotropic materials (UD lamina, lamella)

#### 3.6.1 Derivation of the SFCs

A SFC should be numerically-optimally formulated on the usual engineering working level, the macro-mechanical level. However, a SFC formulation should also capture micro-mechanical failure that triggers macro-mechanical failure, i.e. UD will filament-break under a bi-axial stress state  $\sigma_2^c = \sigma_3^c$  due to  $\varepsilon_{\parallel} = -\nu_{\perp\parallel} \cdot (\sigma_2^c + \sigma_3^c) / E_{\parallel}$ .

At the beginning of WWFE Cuntze’s numerically non-optimal set of 5 invariant-based failure functions F was

$$FF1: F_{\parallel}^{\sigma} = \frac{I_1}{\bar{R}_{\parallel}^t}, \quad FF2: F_{\parallel}^{\tau} = \frac{-I_1}{\bar{R}_{\parallel}^c},$$

$$IFF1: F_{\perp}^{\sigma} = \frac{I_2 + \sqrt{I_4}}{2\bar{R}_{\perp}^t}, \quad IFF2: F_{\perp}^{\tau} = a_{\perp\perp} \frac{I_2}{\bar{R}_{\perp}^c} + \frac{b_{\perp\perp} \sqrt{I_4}}{\bar{R}_{\perp}^c}, \quad IFF3: F_{\perp\parallel} = \frac{I_3^{3/2}}{\bar{R}_{\perp\parallel}^3} + b_{\perp\parallel} \frac{I_2 \cdot I_3 - I_5}{\bar{R}_{\perp\parallel}^3}.$$

$$I_1 = \sigma_1, \quad I_2 = \sigma_2 + \sigma, \quad I_3 = \tau_{31}^2 + \tau_{21}^2, \quad I_4 = (\sigma_2 - \sigma_3)^2 + 4 \cdot \tau_{23}^2,$$

$$I_5 = (\sigma_2 - \sigma_3) \cdot (\tau_{31}^2 - \tau_{21}^2) - 4\tau_{23}\tau_{31}\tau_{21}, \quad I_2 \cdot I_3 - I_5 \rightarrow I_{23-5} = 2\sigma_2 \cdot \tau_{21}^2 + 2\sigma_3 \cdot \tau_{31}^2 + 4\tau_{23}\tau_{31}\tau_{21}.$$

with  $a_{\perp\perp}(\mu_{\perp\perp})$ ,  $b_{\perp\perp}(a_{\perp\perp})$ ,  $b_{\perp\parallel}(\mu_{\perp\parallel})$  see *Table 3-4*

and had to be improved - regarding IFF3 – for numerical reasons.

#### Numerically necessary modification of IFF3:

Above single portions are to interact by the interaction equation, and this requires *Effs*. However, after deriving  $Eff^{\perp\parallel}$  (see below) the solution of a numerically unpleasant third order equation is

faced:

$$\frac{I_3^{3/2}}{\bar{R}_{\perp\parallel}^3 \cdot Eff^{\perp\parallel 3}} + b_{\perp\parallel} \frac{(I_2 \cdot I_3 - I_5)}{\bar{R}_{\perp\parallel}^3 \cdot Eff^{\perp\parallel 3}}.$$

The numerical problem can be bypassed if for  $F_{\perp\parallel}$  the usual *principle of proportional stressing* (all stresses of the actually given state of stress or vector are equally factored) is not applied. It interprets so-called mode reserve factors as mode stretch factors of the actual stress vector, where the stretching ends when the associated mode failure curve or surface is met. Now, instead of factoring the full state of stress, that means factoring each single stress, just the mode driving shear stresses  $\tau_{21}, \tau_{31}$  are factored and not the transversal normal stresses and shear stress  $\tau_{23}$  (has a normal stress effect). Unfortunately, with this approach the failure condition includes a reserve factor with power <sup>2</sup> and <sup>3</sup>.

$$\rightarrow \frac{I_3^{3/2}}{\bar{R}_{\perp\parallel}^3 \cdot Eff^{\perp\parallel 3}} + b_{\perp\parallel} \frac{(I_2 \cdot I_3 - I_5)}{\bar{R}_{\perp\parallel}^3 \cdot Eff^{\perp\parallel 2}}.$$

Therefore, the approach for establishing the interaction domain will be modified in order to the numerically advantageous powers 4 and 2

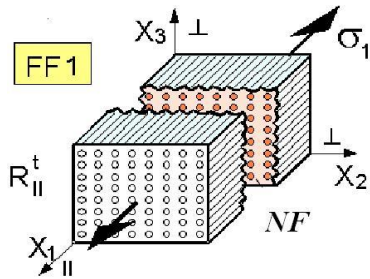
$$\Rightarrow \frac{I_3^2}{\bar{R}_{\perp\parallel}^4 \cdot Eff^{\perp\parallel 4}} + b_{\perp\parallel} \frac{(I_2 \cdot I_3 - I_5)}{\bar{R}_{\perp\parallel}^3 \cdot Eff^{\perp\parallel 2}}.$$

Just a quadratic equation needs to be solved anymore. Of course, the parameter  $b_{\perp\parallel}$  is now slightly different to the former one. But this procedure practically has no effect because this condition is

used as the new mapping or curve fitting function of IFF3.

Limit of macro-homogenization FFs: (micro-mechanical fiber fractures)

There exist limits of the macro-mechanical fibre failure SFCs for FF1 and FF2. In general, the fibre failure mode FF cannot be described by a homogenized (smeared) macro-mechanical stress value  $\sigma_1$ , Fig.3-6. Due to Poisson the filaments may fracture under bi-axial compression without any  $\sigma_1$ . Thus, the engineering-like macro-mechanical modelling has to be exchanged by an accurate micro-mechanical failure capturing one. Praiseworthy, this can be approximately well formulated by a macro-mechanical entity which is the FEA-computed output, the macro-mechanical strain  $\varepsilon_1$ . Reminding reference [Cun04], it follows  $\sigma_1 \rightarrow \check{\sigma}_1$ .



$$I_1 = \sigma_1 \cong \nu_f \cdot \sigma_f = \nu_f \cdot \varepsilon_1 \cdot E_f = \varepsilon_1 \cdot E_{||}$$

Fig.3-6: Capturing micro-mechanical fracture in a macro-mechanical formulation

$\sigma_f$  is the filament (fibre) stress which is proportional to the strain and responsible for fracture.

Here it is to mention in order to correct a citation of the WWFE-peers: *Within the FMC, applied to UD material, no fiber properties are required!*

**3.6.2 Final set of brittle UD SFCs**

Employing the mode strength  $\bar{R}^{\text{mode}}$  and its equivalent mode stress  $\sigma_{eq}^{\text{mode}}$ , according to the general equation  $Eff^{\text{mode}} = \sigma_{eq}^{\text{mode}} / \bar{R}^{\text{mode}}$ , the following set of formulas for the material stressing effort of each of the 5 modes can be provided and its relationship to the associated equivalent stress.

An equivalent stress  $\sigma_{eq}$  is always positive such as the strength. It includes all actual load stresses and the residual stresses (from curing etc.) that are acting together in a given mode. The vector of the modes' equivalent stresses reads

$$\left\{ \sigma_{eq}^{\text{mode}} \right\} = \left( \sigma_{eq}^{\parallel\sigma}, \sigma_{eq}^{\parallel\tau}, \sigma_{eq}^{\perp\sigma}, \sigma_{eq}^{\perp\tau}, \sigma_{eq}^{\parallel\perp} \right)^T$$

Table 3-4 presents the final set of UD SFCs.

As abbreviation,  $I_2 \cdot I_3 - I_5 = I_{23-5}$  is used. In the equations above,  $\bar{R}$  denotes an average = typical strength value that is to be used in stress and deformation analysis. The superscripts <sup>t</sup>, <sup>c</sup> stand for tensile, compressive. The superscripts  $\sigma$  and  $\tau$  mark the type of fracture failure whether it is caused by a tensile stress (Normal Fracture, NF, 'cleavage') or a shear stress (Shear Fracture, SF), e.g. due to a compressive normal stress  $\sigma_{||}^c$  or a transverse normal stress  $\sigma_{\perp}^c$ . Whether a failure may be called a SF or a NF depends on the envisaged size scale.

Table 3-4 'Dense' UD materials: SFC formulations for FF1, FF2 and IFF1, IFF2, IFF3

$$\text{FF1: } Eff^{\parallel\sigma} = \check{\sigma}_1 / \bar{R}_{\parallel}^t = \sigma_{eq}^{\parallel\sigma} / \bar{R}_{\parallel}^t \quad \text{with} \quad \check{\sigma}_1 \cong \varepsilon_1^t \cdot E_{\parallel} \quad (\text{matrix neglected})$$

$$\text{FF2: } Eff^{\parallel\tau} = -\check{\sigma}_1 / \bar{R}_{\parallel}^c = +\sigma_{eq}^{\parallel\tau} / \bar{R}_{\parallel}^c \quad \text{with} \quad \check{\sigma}_1 \cong \varepsilon_1^c \cdot E_{\parallel}$$

$$\text{IFF1: } Eff^{\perp\sigma} = [(\sigma_2 + \sigma_3) + \sqrt{\sigma_2^2 - 2\sigma_2 \cdot \sigma_3 + \sigma_3^2 + 4\tau_{23}^2}] / 2\bar{R}_{\perp}^t = \sigma_{eq}^{\perp\sigma} / \bar{R}_{\perp}^t$$

$$\text{IFF2: } Eff^{\perp\tau} = [a_{\perp\perp} \cdot (\sigma_2 + \sigma_3) + b_{\perp\perp} \sqrt{\sigma_2^2 - 2\sigma_2 \sigma_3 + \sigma_3^2 + 4\tau_{23}^2}] / \bar{R}_{\perp}^c = \sigma_{eq}^{\perp\tau} / \bar{R}_{\perp}^c$$

$$\text{IFF3: } Eff^{\perp\parallel} = \{[b_{\perp\parallel} \cdot I_{23-5} + (\sqrt{b_{\perp\parallel}^2 \cdot I_{23-5}^2 + 4 \cdot \bar{R}_{\perp\parallel}^2 \cdot (\tau_{31}^2 + \tau_{21}^2)^2}] / (2 \cdot \bar{R}_{\perp\parallel}^3)\}^{0.5} = \sigma_{eq}^{\perp\parallel} / \bar{R}_{\perp\parallel}$$

$$\{\sigma_{eq}^{\text{mode}}\} = (\sigma_{eq}^{\parallel\sigma}, \sigma_{eq}^{\parallel\tau}, \sigma_{eq}^{\perp\sigma}, \sigma_{eq}^{\perp\tau}, \sigma_{eq}^{\perp\parallel})^T, \quad I_{23-5} = 2\sigma_2 \cdot \tau_{21}^2 + 2\sigma_3 \cdot \tau_{31}^2 + 4\tau_{23}\tau_{31}\tau_{21}$$

Inserting the compressive strength point  $(0, -\bar{R}_{\perp}^c)$ : delivers  $b_{\perp\perp} = a_{\perp\perp} + 1 = 1 / (1 - \mu_{\perp\perp})$

$a_{\perp\perp} \cong \mu_{\perp\perp} / (1 - \mu_{\perp\perp})$  from  $\mu_{\perp\perp} = \cos(2 \cdot \theta_{fp}^{\circ} \cdot \pi / 180)$  and for  $50^{\circ} \rightarrow \mu = 0.174$

$b_{\perp\perp} \cong 2 \cdot \mu_{\perp\perp}$  (derivation of the curve parameter relations  $a_{\perp\perp}(\mu_{\perp\perp})$ ,  $b_{\perp\perp}(\mu_{\perp\perp})$ , Chapter 8.2).

From mapping experience obtained typical ranges: at least for CFRP

friction values  $0 < \mu_{\perp\parallel} < 0.3$ ,  $0 < \mu_{\perp\perp} < 0.2$ , interaction exponent  $2.5 < m < 2.9$ .

Failure surface and failure body are to derive from interaction equation:

$$Eff^m = (Eff^{\parallel\tau})^m + (Eff^{\parallel\sigma})^m + (Eff^{\perp\sigma})^m + (Eff^{\perp\tau})^m + (Eff^{\perp\parallel})^m = 100\% \quad \text{if failure}$$

Two-fold failure danger in the  $\sigma_2$ - $\sigma_3$ -domain stands for a failure surface closing, modelled by

$$Eff^m = (Eff^{\parallel\tau})^m + (Eff^{\parallel\sigma})^m + (Eff^{\perp\sigma})^m + (Eff^{\perp\tau})^m + (Eff^{\perp\parallel})^m + (Eff_{\perp}^{\text{MfFd}})^m = 1$$

with  $Eff_{\perp}^{\text{MfFd}} = (\sigma_2^t + \sigma_3^t) / 2\bar{R}_{\perp}^t$ , and  $\bar{R}_{\perp}^t \approx \bar{R}_{\perp}^c / \sqrt[m]{2}$  after [Awa78]

considering  $\sigma_2^t = \sigma_3^t$  and  $\sigma_2^c = \sigma_3^c$ ;  $\bar{R}_{\perp}^t \leq \bar{R}_{\perp}^c$ ,  $\bar{R}_{\perp}^c \geq \bar{R}_{\perp}^t$  if dense and not porous.

Above interaction equation includes all mode material stressing efforts, and each of them represents a portion of load-carrying capacity of the material.

In practice in thin laminas, at maximum, 3 modes of the 5 modes will physically interact. Considering 3D-loaded thick laminas, there, all 3 IFF modes might interact.

Usually, the value of  $m$  is obtained by curve fitting of test data in the transition zone. The mode interaction exponent  $m$  is also termed rounding-off exponent, the size of which is high in case of low scatter and vice versa. A lower value chosen for the interaction exponent is more on the 'safe' side. From engineering reasons the interaction exponent  $m$  is chosen the same in the transition zones of all adjacent domains.

Of interest is not only the interaction of the fracture surface parts in the discussed mixed failure domains or interaction zones of adjacent failure modes, respectively, but further failure in a multi-fold failure domain (superscript <sup>MfFd</sup>) such as in the  $(\sigma_2^t, \sigma_3^t)$ -domain. There the associated mode stress effort acts twofold. It activates failure in two directions which may be considered by adding a

multi-fold failure term, proposed in [Awa78] for isotropic materials. It can be applied to brittle UD material in the transversal (quasi-isotropic) plane as well

Notes:

- If formulations in the quasi-isotropic plane of the UD material will be used, then the stresses reduce from 6 lamina (ply) stresses to 5 principal stresses

$$\{\sigma^{pr}\} = (\sigma_1, \sigma_2^{pr}, \sigma_3^{pr}, 0, \tau_{31}^{pr}, \tau_{21}^{pr})^T$$

- In IFF3 the shear stress  $\tau_{21}$  is taken and not  $\tau_{12}$  because  $\tau_{21}$  causes the failure, which is macroscopically SF however microscopically NF, an NF like for IFF1. This makes ‘rounding’ in the interaction zone physically-based.

### Delamination conditions:

These SFCs are just a *subset* of the 5 SFCs above. They are intentionally given here in a separate manner because other researchers present special delamination conditions. With regard to the 3D nature of the IFF conditions, both, IFF1 ( $F_{\perp}^{\sigma}$  transverse tensile failure; inter-laminar stresses  $\sigma_3^t, \tau_{32}, \tau_{31}$  may cause cracking) and IFF2 ( $F_{\perp}^{\tau}$  wedge failure; intra-laminar stresses such as  $\sigma_2^c, \tau_{21}$  cause cracking and may initiate a local 3D state of stress, including  $\sigma_3$ ) can also serve as conditions for the assessment of ‘onset of delamination’ which practically is a *laminar* failure type. One or two modes will be the design driving ones in the critical local material location of a composite lay-up. These are activated by the delamination-critical stress state  $\{\sigma\}_{lamina} = (0, \sigma_2, \sigma_3, \tau_{23}, \tau_{31}, \tau_{21})^T$  which includes all inter-laminar stresses. Introducing the two relevant combinations of the delamination-active stress vector above delivers:

Tension/shear stressing

$$(Eff^{\perp\sigma})^m + (Eff^{\perp\parallel})^m = 1 \quad \text{with} \quad \{\sigma\}_{lamina} = (0, \sigma_2^t, \sigma_3^t, \tau_{23}, \tau_{31}, \tau_{21})^T$$

Compression-shear stressing

$$(Eff^{\perp\tau})^m + (Eff^{\perp\parallel})^m = 1 \quad \text{with} \quad \{\sigma\}_{lamina} = (0, \sigma_2^c, \sigma_3^t, \tau_{23}, \tau_{31}, \tau_{21})^T .$$

### **3.6.2 IFF2 SFC for ‘porous’ UD material**

UD materials may be pretty porous. This mainly affects IFF2 where a porosity-capturing SFC shall be provided in the following Table.

\* IFF2 Failure Function for the dense UD material (for comparison)

$$\begin{aligned}
 F^{SF} &= [a_{\perp\perp} \cdot I_2 + b_{\perp\perp} \cdot \sqrt{I_4}] / \bar{R}_{\perp}^c = 1 \text{ with } a_{\perp\perp} = b_{\perp\perp} - 1 \text{ after inserting } \bar{R}_{\perp}^c = 104 \text{ MPa} \\
 &= [a_{\perp\perp} \cdot (\sigma_2 + \sigma_3) + b_{\perp\perp} \cdot \sqrt{(\sigma_2 - \sigma_3)^2 + 4\tau_{23}^2}] / \bar{R}_{\perp}^c = 1 \\
 &= [a_{\perp\perp} \cdot (\sigma_2^{pr} + \sigma_3^{pr}) + b_{\perp\perp} \cdot \sqrt{(\sigma_2^{pr} - \sigma_3^{pr})^2 + 0^2}] / \bar{R}_{\perp}^c = 1 \leftarrow 2 \text{ structural stresses}
 \end{aligned}$$

\* IFF2 Failure Function for the porous UD material (index por, author's simple approach)

$$F_{porosity}^{SF} = \sqrt{a_{\perp\perp por}^2 \cdot I_2^2 + b_{\perp\perp por}^2 \cdot I_4 - a_{\perp\perp por} \cdot I_2} / 2\bar{R}_{\perp}^c = 1 .$$

The two curve parameters are determined - as before performed - from insertion of the compressive strength point and from the bi-axial fracture stress point.

### 3.7 SFCs for differently porous, fabric pattern-dependent orthotropic materials (fabrics)

#### 3.7.1 2D Fabrics

Fig.3-7 depicts the stresses and strengths faced with general orthotropic fabrics

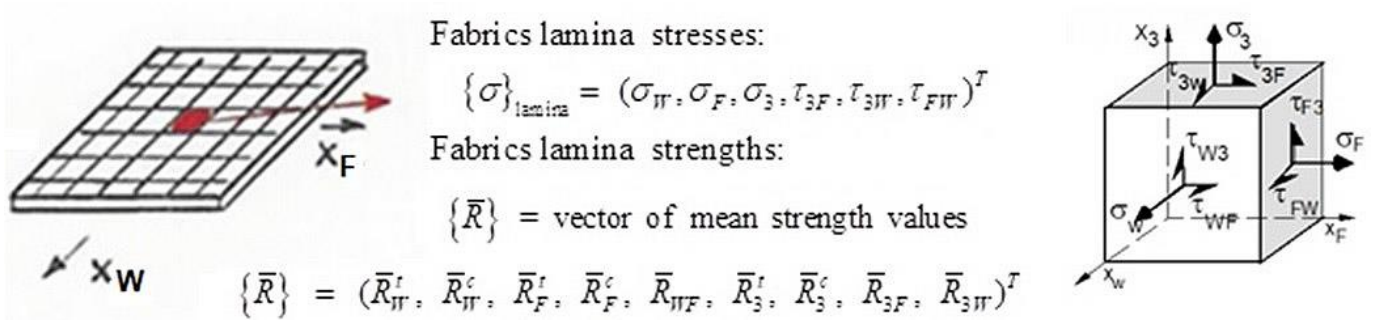


Fig.3-7: Stresses and strength properties of fabrics

Orthotropic (rhombically-anisotropic) material is that material family of the highest structural rank. It is already a structural element. Table 3-6 presents the mode-SFCs directly included in the interaction equation. According to the existing undulations that cause bending, material homogenization is merely possible. In this case of orthotropic material just a formulation in fabric's lamina stresses makes sense. Now, one has to deal with simpler invariants. An UD-FF analogous Poisson- regarding strain-formulation is not necessary.

Porosity is found within all the textiles where the 2D fabric material type (plain) are most often used in structural engineering (Fig.3-8).

LL:

\*A good exploitation of fibers is only given if they are fully straight built in. Therefore the undulation of fabrics is a big shortcoming especially under cyclic loading.

\*The use of short fibers in fabrics increase this unpleasant situation.

Table 3-6 'Porous' fabric materials: SFC formulations

Fabrics invariants, privately obtained from J.F. Boehler, 1995

$$I_1 = \sigma_W, I_2 = \sigma_F, I_3 = \sigma_3, I_4 = \tau_{3F}^2, I_5 = \tau_{3W}^2, I_6 = \tau_{WF}^2, I_7 = \tau_{3F} \cdot \tau_{3W} \cdot \tau_{WF}$$

Invariant SFC formulations

$$F_W^t = I_1 / R_W^t, F_F^t = I_1 / R_F^t, F_3^t = I_3 / R_3^t, F_W^c = I_1 / R_W^c, F_F^c = I_1 / R_F^c, F_3^c = I_3 / R_3^c,$$

$$F_{WF} = I_6 / (R_{WF} - \mu_{WF}(\sigma_W + \sigma_F)), F_{3F}^c = \sqrt{I_4} / (R_{3F} - \mu_3 \cdot \sigma_3), F_{3W}^c = \sqrt{I_4} / (R_{3W} - \mu_3 \cdot \sigma_W)$$

For the insertion into the interaction equation  $Eff = 1$  the  $Eff^{modes}$  must be provided:  
 Replacing the invariants by the associated stresses and solving for the  $Eff^{modes}$  it reads  
 The 3D-SFCs are engineering-like simplified to just capture the main physics in the interaction equation :

$$\left( \frac{\sigma_W + |\sigma_W|}{2 \cdot \bar{R}_W^t} \right)^m + \left( \frac{-\sigma_W + |\sigma_W|}{2 \cdot \bar{R}_W^c} \right)^m + \left( \frac{\sigma_F + |\sigma_F|}{2 \cdot \bar{R}_F^t} \right)^m + \left( \frac{-\sigma_F + |\sigma_F|}{2 \cdot \bar{R}_F^c} \right)^m + \left( \frac{|\tau_{WF}|}{\bar{R}_{WF} - \mu_{WF} \cdot \sigma_W} \right)^m$$

$$+ \left( \frac{\sigma_3 + |\sigma_3|}{2 \cdot \bar{R}_3^t} \right)^m + \left( \frac{-\sigma_3 + |\sigma_3|}{2 \cdot \bar{R}_3^c} \right)^m + \left( \frac{|\tau_{3W}|}{\bar{R}_{3W} - \mu_{3W} \sigma_3} \right)^m + \left( \frac{|\tau_{3F}|}{\bar{R}_{3F} - \mu_{3F} \sigma_3} \right)^m = 1$$

For a cross-ply fabric, Warp = Fill with  $\bar{R}_W^t = \bar{R}_F^t, \bar{R}_W^c = \bar{R}_F^c$ , the inter-laminar  $Effs$  go and just the intra-laminar  $Effs$  remain.

The range of parameters is  $2.5 < m < 2.9, 0 < \mu_{WF} < 0.15, 0 < \mu_3 < 0.1?$  (no tests).

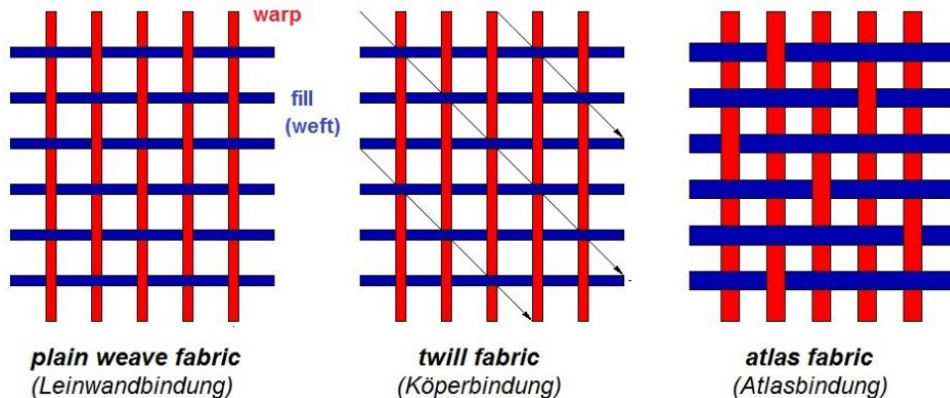
If  $\sigma_F$  is also active, this double mode contributes by additional term  $\left( \frac{|\tau_{WF}|}{\bar{R}_{WF} - \mu_{WF} \cdot \sigma_F} \right)^m$ .

Layers of a laminate show increasing complexity [Cun19] from

*UD-layer* → *Non-crimp fabric layer* → *Plain weave layer* → *spatial (3D) textile layer*.

The chosen textile is firstly to model and secondly the associate SFC is to provide for analysis. Fig.3-8 together with Fig.3-9 point out that the atlas fabric > 1:4 could be modelled by two UD-laminas (Fig.3-8).

A SFC choice is directly to link to the possible model choice.



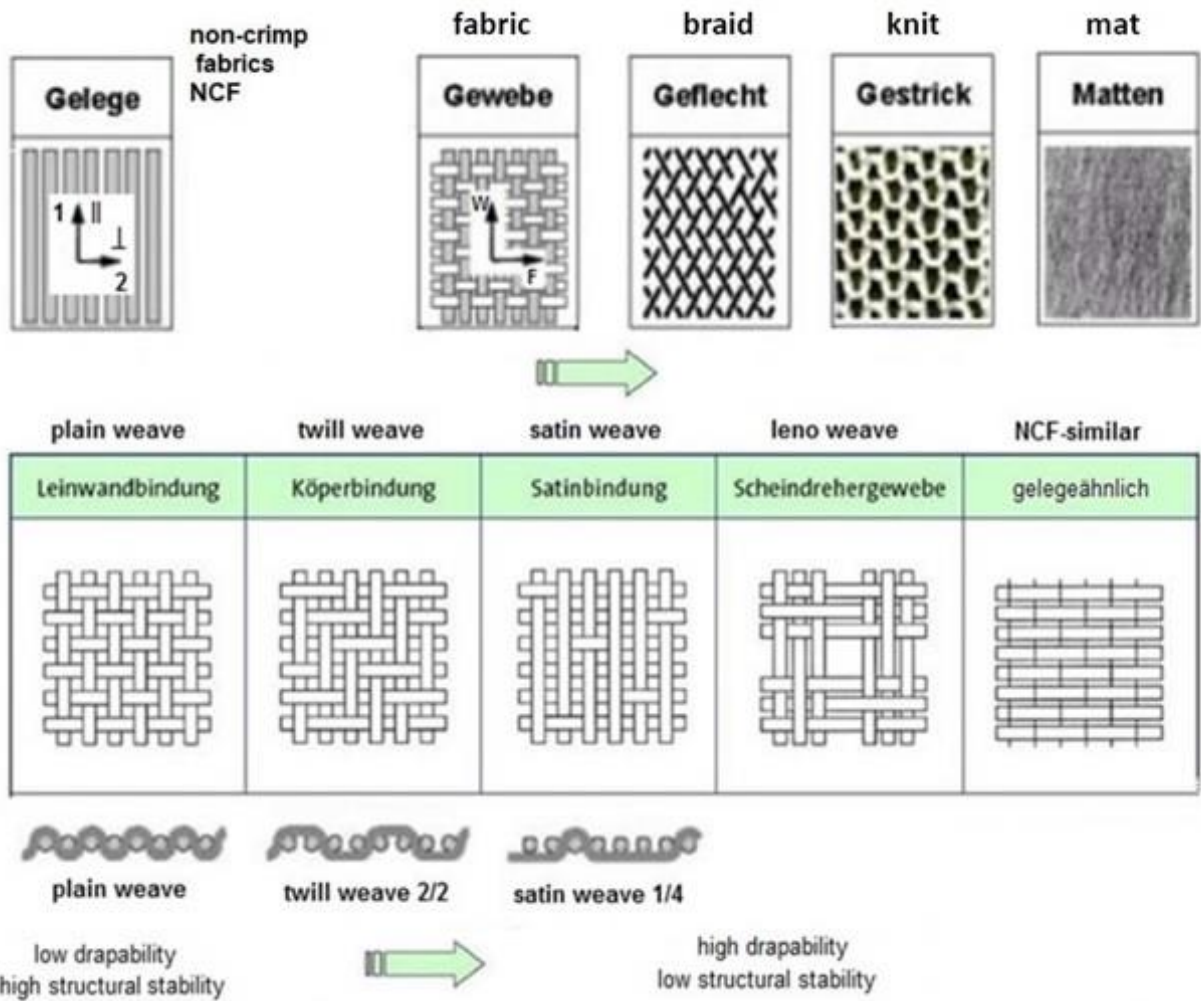


Fig.3-8: (up) Three essential 2D fabrics, (down) Semi-finished plane fabric products

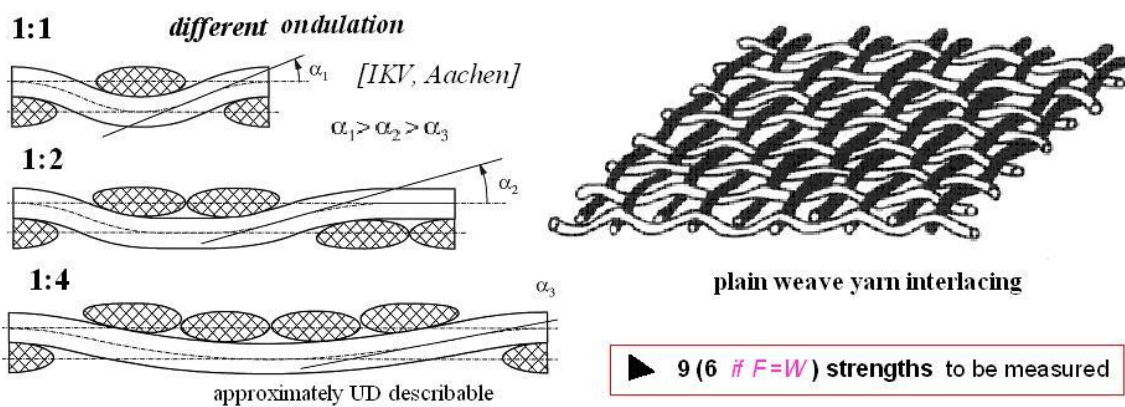


Fig. 3-9: Woven fabric material modelling

LL: For woven fabrics

➤ Fabrics are still structural elements and no smeared materials anymore. It is to check when the microscopic failure is to consider and to map because the macro-scopic model cannot capture a realistic

mapping of the full failure behaviour. 'Maximum stress-SFCs' play an essential role, friction must be considered in-plane and under lateral pressure in thickness direction.

➤ Enough information from acceptable spatial (3D)-tests for a real validation is not yet available!

In contrast to the UD lamina a strain formulation of tension FF – due to 2D-compression, in order to capture fiber straining without an acting stress  $\sigma_1$  - seems to be not necessary w.r.t. to the undulation effect of the fibres in woven fabrics

➤ The meaning of 3D- textile is different

- Most often this term is used for a spatial shape of a textile pre-form
- 3D 'flat' semi-finished product with 3 fiber directions (tri-axial fabric)
- The material modeller uses it, if the textile is to model like an orthotropic 3D-solid.

➤ Interaction has to manage the transition from a micro-mechanical failure of the matrix to the macro-mechanical Warp or Fill fiber failure of the fabric structure. Thereby, the activated strength can be engineering-like applied by increasing the matrix tensile strength  $\bar{R}_m^t$  continuously up to the fabric's tensile Warp strength  $\bar{R}_W^t > \bar{R}_m^t$  according to - for instance - the stress ratio  $\tau_{WF} / \sigma_W^t$  in the tension domain,  $\bar{R} = \bar{R}_m^t \cdot (1 - a \cdot e^{-\beta \cdot x})$ . Applied later however, for a ceramic fabric in [Fig.7.3-7](#), are physically decay functions for both the modes which become zero at the other mode domain.

### 3.7.2 3D Fabrics (Textiles)

3D textiles are 3D semi-finished products made with fabrication methods such as weaving, knitting, braiding, or nonwoven. Real 3D textiles are produced with spatial geometry, opposed to 2D textiles that are made in planes. The yarn in 2D textiles is fed along length axis and width axis, while 3D textiles also have an upright weave, using an extra yarn which creates thickness.

3D weaves are orthogonal weave structures, multilayer structures, and possess angle interlocks.

Mechanically 3D textiles are - after curing - orthotropic solids, which have a large number of properties that are to be provided before dimensioning.

Viewing [Fig. 3-10](#), for the modeler at first essential is, what is the meaning of the distinct 3D. Is it a real 3D fabric or is it a 3D 'flat' semi-finished product with 3 fiber directions (tri-axial fabric) or in construction a curved spatial armoring cage, for instance.

3D textiles of continuous fibers add a 3<sup>rd</sup> direction of reinforcement by the yarns interlacing through the thickness, which improves damage tolerance behavior.

From literature some characteristics could be derived [*Bil11*]:

-Stacked 2D fabrics: stapled on top of another and in z-direction stitched together. In-plane properties good, out-of-plane very low

-3D woven fabrics: See figure above. In-plane properties good, out-of-plane very low

-3D braided fabrics: Multiple layers. Damage tolerance high. Transverse properties low

-3D knitted fabrics: Fabricated to create near net shape, curved structures such as cone and sphere

-3D non-woven fabrics: usually a short fiber-preform. In z-direction reinforced by stitching, low mechanical properties.



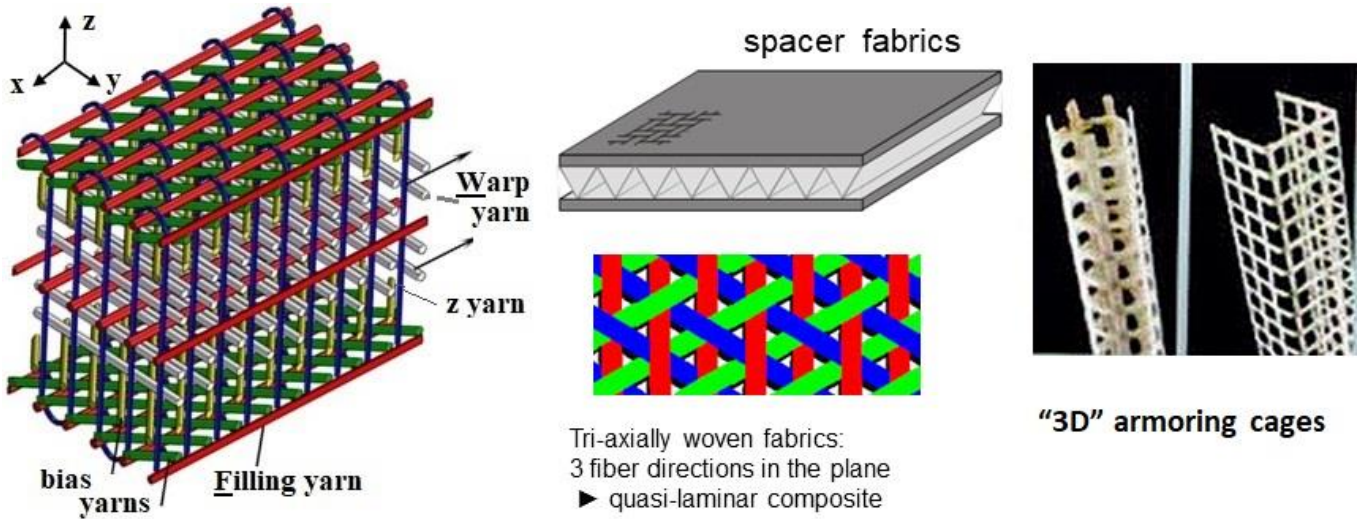


Fig.3-10: Pre-forms termed "3D" ('left' scheme)

[www.iccm-central.org/Proceedings/ICCM21proceedings/papers/4198.pdf](http://www.iccm-central.org/Proceedings/ICCM21proceedings/papers/4198.pdf)

However, this opportunity of adding a 3<sup>rd</sup> dimension to the weave pattern creates stiffness but adds distinct failure and thermo-mechanical behavior. Effective Properties of 3D Woven Cosites are to determine for design. This will be usually performed by employing representative volume element (RVE) procedures..

### 3.8 SFCs for the differently porous Structural Ceramic Materials

#### 3.8.1 Isotropic ceramics

This sub-chapter is dedicated to the more or less porous structural ceramic materials from an isotropic monotonic, via a transversely-isotropic UD material to an orthotropic fabric ceramic material.

In some applications task-associated porosity is intended in order to obtain for instance some quasi-ductile behavior after micro-damaging occurred.

SFCs for NF and CrF from Table 3-3 'Porous' isotropic material:

$$Eff^{NF} = c^{NF} \cdot \frac{\sqrt{4J_2 \cdot \Theta^{NF} - I_1^2 / 3 + I_1}}{2 \cdot \bar{R}^t} = \frac{\sigma_{eq}^{NF}}{\bar{R}^t} \leftrightarrow Eff^{CrF} = c^{CrF} \cdot \frac{\sqrt{4J_2 \cdot \Theta^{CrF} - I_1^2 / 3 + I_1}}{2 \cdot \bar{R}^c} = \frac{\sigma_{eq}^{CrF}}{\bar{R}^c}.$$

#### 3.8.1 UD ceramics

Here, IFF2 has to be replaced by the porous variant.

$$FF1: Eff^{\parallel\sigma} = \check{\sigma}_1 / \bar{R}_{\parallel}^t = \sigma_{eq}^{\parallel\sigma} / \bar{R}_{\parallel}^t \quad \text{with} \quad \check{\sigma}_1 \cong \varepsilon_1^t \cdot E_{\parallel} \quad (\text{matrix neglected})$$

$$FF2: Eff^{\parallel\tau} = -\check{\sigma}_1 / \bar{R}_{\parallel}^c = +\sigma_{eq}^{\parallel\tau} / \bar{R}_{\parallel}^c \quad \text{with} \quad \check{\sigma}_1 \cong \varepsilon_1^c \cdot E_{\parallel}$$

$$IFF1: Eff^{\perp\sigma} = [(\sigma_2 + \sigma_3) + \sqrt{\sigma_2^2 - 2\sigma_2 \cdot \sigma_3 + \sigma_3^2 + 4\tau_{23}^2}] / 2\bar{R}_{\perp}^t = \sigma_{eq}^{\perp\sigma} / \bar{R}_{\perp}^t$$

$$IFF2: F_{porosity}^{SF} = \sqrt{a_{\perp\perp por}^2 \cdot I_2^2 + b_{\perp\perp por}^2 \cdot I_4 - a_{\perp\perp por} \cdot I_2} / 2\bar{R}_{\perp}^c = 1$$

$$FF3: Eff^{\perp\parallel} = \{ [b_{\perp\parallel} \cdot I_{23-5} + (\sqrt{b_{\perp\parallel}^2 \cdot I_{23-5}^2 + 4 \cdot \bar{R}_{\perp\parallel}^2 \cdot (\tau_{31}^2 + \tau_{21}^2)}) / (2 \cdot \bar{R}_{\perp\parallel}^3) ] \}^{0.5}.$$

### 3.8.3 Orthotropic fabric ceramics

See SFC formulations in *Table 3-6* and the interaction equation capturing all modes.

$$\left(\frac{\sigma_w + |\sigma_w|}{2 \cdot \bar{R}_w^t}\right)^m + \left(\frac{-\sigma_w + |\sigma_w|}{2 \cdot \bar{R}_w^c}\right)^m + \left(\frac{\sigma_F + |\sigma_F|}{2 \cdot \bar{R}_F^t}\right)^m + \left(\frac{-\sigma_F + |\sigma_F|}{2 \cdot \bar{R}_F^c}\right)^m + \left(\frac{|\tau_{wF}|}{\bar{R}_{wF} - \mu_{wF} \cdot \sigma_w^c}\right)^m$$

$$\left(\frac{\sigma_3 + |\sigma_3|}{2 \cdot \bar{R}_3^t}\right)^m + \left(\frac{-\sigma_3 + |\sigma_3|}{2 \cdot \bar{R}_3^c}\right)^m + \left(\frac{|\tau_{3W}|}{\bar{R}_{3W} - \mu_{3W} \sigma_3^c}\right)^m + \left(\frac{|\tau_{3F}|}{\bar{R}_{3F} - \mu_{3F} \sigma_3^c}\right)^m = 1 .$$



Feeling of the author after generating the various sets of FMC-based SFCs.

(left) After so much effort, the pain will be soon over? The top seems to be reached?  
 (right) No, the view of the SFC-climber widens: FMC-based SFC applications will require many long-lasting difficult numerical visualizations

## 3.9 Validity limits for SFC applications and Automatic Insertion of 3D Stress States

### 3.9.1 Validity limits for SFC applications

The next table lists comments about SFC applicability limits.

*Table 3-5: Comments on Validity Limits for the Applicability of a SFC (mainly given for UD)*

- As a SFC is a necessary but not a sufficient condition to predict failure [Leguillon, W. Becker] a fracture mechanics-based energy condition must be fulfilled, too.
- Even in plain (smooth) stress regions a SFC can be only a necessary condition which may be not sufficient for the prediction of ‘onset of fracture’, i.e. the in-situ lateral strength in an embedded lamina. Example: thick layers fail earlier than thin ones under the same 2D stress state see e.g. [Flaggs-Kural 1982].
- Attempts to link ‘onset-of-fracture’ combined with ‘cracking prediction’ methods for structural components are under-gone, see e.g. [Leg02]. In his finite fracture mechanics Leguillon assumes a crack as one more unknown but one can solve the equation system by one more equation from fracture mechanics (see later sub-chapter)

- In case of discontinuities such as notches with steep stress decays only a *toughness + characteristic length-based energy balance condition* may form a sufficient set of two fracture conditions
- When applying test data from ‘isolated lamina’ test specimens (like tensile coupons) to an embedded lamina of a laminate one should consider that coupon test deliver tests results of ‘weakest link’ type. An embedded or even an only one-sided constrained lamina, however, possesses redundant behaviour, see Fig.3-11
- A SFC usually describes only a one-fold occurrence of a mode or of a failure mechanism, respectively! A multiple occurrence of a mode, such as for  $\sigma_1 = \sigma_{II}$  or for  $\sigma_2 = \sigma_3$  is to map by an additional term in  $Eff = 1$ , see for instance in *Table 3-6*.

Experience led to the following notes:

Each failure stress state belongs to  $Eff = 100\%$  and represents one point on the surface of the failure body. This is valid for 1D- (these are the strength values), for 2D- and for 3D-stress states. In the case of a multiaxial compressive stress state the strength does not increase but the risk to fracture may become smaller, indicated by  $Eff$  which becomes lower than 100 % !

- 1) Each failure mechanism is affected by an associated typical state of stress. The failure mechanism with the highest material stressing effort will dominate the UD failure. The mode effort has to become zero if the mode driving stress is zero.
- 2) Due to IFF the curing stresses decay in parallel to the degradation.
- 3) The not design-driving stresses of a mode might increase or decrease the material stressing effort  $Eff$  which is basically caused by the design driving one. This influence is considered in the equivalent mode stress  $\sigma_{eq}^{mode}$ . Note that the Mises equivalent stress for the mode yielding is not the only equivalent stress.
- 4) The 5 strength and 2 friction parameters can be measured and therefore fulfil a basic design verification requirement: Strength properties shall be statistically-based, material friction properties  $\mu$  are so-called physical quantities which shall be average (typical) values in order to best meet the optimum being the maximum expectation value of 50% probability.
- 6) The FFs are special fiber strain failure equations to capture filament fracture under bi-axial compression.
- 7) The NF-function chosen for isotropic and UD materials enables to map a straight line of test data in the principle stress plane
- 8) If the failure body is fully rotational symmetric then  $c^{NF} (\Theta^{NF} = 1 \text{ or } d^{NF} = 0) = 1$ . Above NF can manage inward and outward dents by  $c^{NF} (\Theta^{NF}) < 1$  which renders the 120°-rotational symmetry
- 9) The friction effect decreases with increasing porosity. Ideal dense materials possess no porosity. A fully porous material may be defined by  $R^{cc} \cong R^c$ . This case is modelled like the porous foam material [Cun16a]
- 10) When mapping, then  $\bar{R}$  must be used, because the average behavior or value is required
- 11) Only  $Eff = 100\%$  is equal to the SFC  $F = 1$ , see further *chapter 9.2* and sub-chapter 9.3.2
- 12) If any plane in a 3D stress state is a plane of maximum danger, being possible to become a fracture plane, then that plane with the most unfavorable flaw situation becomes the fracture plane.

### 3.9.2 Enabling an Automatic Insertion of 3D stress states into the SFCs, example UD

When automatically inserting the FEA stress output  $\{\sigma\} = (\sigma_1, \sigma_2, \sigma_3, \tau_{23}, \tau_{13}, \tau_{12})^T$  into all 5 effort equations some efforts may become negative which mechanically means zero  $Eff$ . In order to make an automatic use of the FMC-based fracture SFCs also in a 3D state of stresses possible and to avoid complicate queries in the computer program some specifics are to consider:

- 1) FF, IFF: By the automatic insertion of a 3D state of stress physically incorrect negative efforts and negative equivalent stresses may occur. These are bypassed by using absolute values

$$Eff^{\parallel\sigma} = (\varepsilon_1 + |\varepsilon_1|) \cdot E_{\parallel} / (2 \cdot R_{\parallel}^t), \quad Eff^{\parallel\tau} = (-\varepsilon_1 + |\varepsilon_1|) \cdot E_{\parallel} / (2 \cdot R_{\parallel}^c),$$

$$\sigma_{eq}^{\perp\sigma} = (+\sigma_{eq}^{\perp\sigma} + |\sigma_{eq}^{\perp\sigma}|) / 2, \quad \sigma_{eq}^{\perp\tau} = (-\sigma_{eq}^{\perp\tau} + |\sigma_{eq}^{\perp\tau}|) / 2.$$

or formalistically by taking the Macaulay brackets ( $\equiv$  Föppl symbols  $\{\}$ ). They describe a discontinuous function and are defined here by

$$\{Eff^{mode}\} = \begin{cases} 0, & Eff^{mode} < 0 \\ Eff^{mode}, & Eff^{mode} \geq 0 \end{cases}.$$

Numerical Use of the Equation of the fracture body:

$$Eff^m = (\{Eff^{\parallel\sigma}\})^m + (\{Eff^{\parallel\tau}\})^m + (\{Eff^{\perp\sigma}\})^m + (\{Eff^{\perp\parallel}\})^m + (\{Eff^{\perp\tau}\})^m$$

Deleting the woven brackets the total efforts reads:

$$Eff = \sqrt[m]{(Eff^{\parallel\sigma})^m + (Eff^{\parallel\tau})^m + (Eff^{\perp\sigma})^m + (Eff^{\perp\parallel})^m + (Eff^{\perp\tau})^m}$$

However, in Mathcad to be formulated for solving as

$$Eff = [(Eff^{\parallel\sigma})^m + (Eff^{\parallel\tau})^m + (Eff^{\perp\sigma})^m + (Eff^{\perp\parallel})^m + (Eff^{\perp\tau})^m]^{m^{-1}}$$

If an  $Eff$  becomes negative, caused by the numerically advantageous automatic insertion of the FEM stress output into all 5 failure conditions (example UD), then a value of 0 shall replace the negative value. A negative  $\sigma_{eq}^{\perp\tau}$  may occur in the case of a combination of a high friction parameter  $a_{\perp\perp}$  with a certain state of bi-axial stressing.

- 2) IFF1, IFF2: A problem is originated by the fact that a shear stress  $\tau_{23}$  can be composed of a normal tensile stress and a normal compressive stress (only a shear stress can be substituted by (shear) *stress components*!) which affects two failure modes but just one is significant in the case of the actual, brittle behaving UD material. Due to this, naturally as tensile driving effort in case of a brittle behaving material  $Eff^{\perp\sigma}$  is caused and a compressive effort  $Eff^{\perp\tau}$  as well. The compressive effort incorporates a smaller additional failure danger. This is simply outlined via the principal stresses in the quasi-isotropic domain (advantage: reduction to the two principal stresses)

$$\sigma_I = 0.5 \cdot (\sigma_2 + \sigma_3) + \sqrt{(0.5 \cdot (\sigma_2 - \sigma_3))^2 + \tau_{23}^2}, \quad \sigma_{II} = 0.5 \cdot (\sigma_2 + \sigma_3) - \sqrt{(0.5 \cdot (\sigma_2 - \sigma_3))^2 + \tau_{23}^2},$$

$$\text{with } \sigma_I : 0 \text{ if } \sigma_I \geq 0, \sigma_I \text{ otherwise and } \sigma_{II} : 0 \text{ if } \sigma_{II} \geq 0, \sigma_{II} \text{ otherwise.}$$

$$\text{Then it holds } Eff^{\perp\tau} = [ b_{\perp\perp} \cdot \sqrt{\sigma_I^2 - 2 \cdot \sigma_I \cdot \sigma_{II} + \sigma_{II}^2 + 4 \cdot 0^2} + a_{\perp\perp} \cdot (\sigma_I + \sigma_{II}) ] / \bar{R}_{\perp}^c.$$

$Eff^{\perp\tau} = 1$  delivers for  $\sigma_2(\sigma_3)$  two roots and therefore two branches as can be seen in [Section 7.2](#) of WWFE-II, (Test Case) TC 5, for instance.

Reminder for numerics:

$$\text{Determination of Eff} \neq 1: \quad Eff = [\sum (Eff^{modes})^m]^{m^{-1}}$$

$$\text{Determination of failure curve Eff} = 1: \quad 1 = \sum (Eff^{modes})^m.$$



### Strain-softening:

The full stress-strain curve consists of a hardening part which can be load-controlled measured and a softening part which is deformation-controlled by the structural vicinity. The associate two separate formulae are linked in the strength point.

The softening formula has to be assumed. This is due to the fact that the designer is generally lacking of experimental information for the degradation of the embedded lamina. An engineering modelling of this softening part or the post initial failure behaviour of a laminate requires that assumptions have to be made regarding the decaying properties of the actually degrading lamina or laminae.

The author's approach is based on the idea that the softening function is factorizing the Ramberg-Osgood hardening function. A simple function was used to map this softening in order to then derive the secant modulus for the full non-linear analysis. The equations for this effective curve (*smearred over the micro-cracks*) read:

$$\sigma_{soft} = \bar{R}_m / (1 + \exp[(a_{soft} + \varepsilon) / b_{soft}]) = \bar{R}_m \cdot \eta \quad \text{using} \quad \exp[z] = e^z$$

where  $\eta$  is a degradation function and equals 1 in the hardening domain. The two curve parameters  $a_{soft}$ ,  $b_{soft}$  are determined from two calibration points at least

$$(0.995 \cdot \bar{R}_m, \varepsilon(\bar{R}_m)) \quad \text{and} \quad (0.1 \cdot \bar{R}_m, \varepsilon(0.1 \cdot \bar{R}_m))$$

or from curve fitting if enough test data is available in the softening domain. Applying  $1.0 \cdot \bar{R}_m$ ,  $\varepsilon(\bar{R}_m)$  as input is numerically not permitted.

The moduli required for the non-linear analysis in the isotropic case read

$$E_{sec}^{hard} = \frac{\sigma}{\varepsilon} = \frac{\sigma}{\frac{\sigma}{E_0} + 0.002 \cdot \left(\frac{\sigma}{R_{0.2}}\right)^{\bar{n}}} = \frac{E_0}{1 + 0.002 \cdot \frac{E_0}{R_{0.2}} \cdot \left(\frac{\sigma}{R_{0.2}}\right)^{\bar{n}-1}},$$
$$E_{sec}^{soft} = \frac{E_0}{1 + 0.002 \cdot \frac{E_0}{R_{0.2}} \cdot \left(\frac{\sigma \cdot \eta}{R_{0.2}}\right)^{\bar{n}-1}} \quad \text{with} \quad \eta = \frac{1}{1 + \exp\left(\frac{a_{soft} + \varepsilon}{b_{soft}}\right)}.$$

By employing the equivalent stress reached in each failure mode the associated secant modulus of each mode can be determined for the hardening and the softening regime. For the various modes the same formula is valid, however, the mode parameters are different. Considering a consistent stress concept for all  $\sigma_{eq}^{modes}$  an *explicit* dependency for  $E_{sec}(\sigma_{eq}^{modes})$  is provided.

For UD material above the *Onset-of-Failure* or *Initial Failure* level of, respectively, an appropriate progressive failure analysis method has to be employed (or a *Successive Degradation Model* for the description of Post Initial failure) by using a failure mode condition that indicates failure type and damage danger (level of Eff  $\leq$  100%). Final Failure occurs after the laminate (and thereby the structural part) has experienced a stiffness reduction and has degraded to a level where it is no longer capable of carrying additional load.

Strain controlled testing requires a very high frame stiffness.

Note, please: If R-O-material data sets are not provided for the hardening domain then instead of the R-O-approach a more mathematical formulation can be applied which shall include both hardening and softening.

One formula, that includes both, reads  $\sigma = c1 \cdot c2 \cdot \varepsilon^{c1-1} \cdot \exp(-c1 \cdot \varepsilon^{c2})$  [Mathcad manual].

Another formula from [Mat??) reads  $\sigma(\varepsilon) = \bar{R} \cdot \exp\left[\frac{1}{c1 \cdot e} \cdot \left(\frac{\varepsilon}{\varepsilon_{fracture}}\right)^{c1}\right] \cdot \frac{\varepsilon}{\varepsilon_{fracture}}$ .

Table 3-7: Comparison of shear stress and normal stress acting in the SFCs

\* Isotropic, ductile: 1 yield failure mode is failure driving and activated (no friction)

$$I_1 = \sigma_x + \sigma_y + \sigma_z, \quad 6 \cdot J_2 = (\sigma_x - \sigma_y)^2 + (\sigma_y - \sigma_z)^2 + (\sigma_z - \sigma_x)^2 + 6 \cdot (\tau_{xy}^2 + \tau_{yz}^2 + \tau_{xz}^2)$$

$$Eff^{Mises} = \frac{\sqrt{3J_2}}{(\bar{R}_{0.2})^2} = \frac{\sigma_{eq}^{Mises}}{\bar{R}_{0.2}} : \text{just } \tau_{xy} \neq 0 \rightarrow \sigma_{eq}^{Mises} = \sqrt{3} \cdot \tau_{xy}; \sigma_x \neq 0 \rightarrow \sigma_{eq}^{Mises} = \sigma_x$$

\* Isotropic, brittle, rot. symm. fracture body  $\Theta = 1$ :  $\tau_{xy} \rightarrow$  activates 2 fracture failure modes

$$Eff^{fr} = \sigma_{eq}^{fr} / \bar{R}^t : \tau_{xy} \rightarrow I_1 = 0, J_2 = \tau_{xy}^2; \sigma_x \rightarrow I_1 = \sigma_x, J_2 = \sigma_x^2 / 3. \quad c_1^{SF} = 1 + c_2^{SF}$$

$$\sigma_{eq}^{NF} = 1 \cdot (\sqrt{4J_2 \cdot 1 - I_1^2 / 3} + I_1) / 2; \quad \sigma_{eq}^{SF} = (c_2^{SF} \cdot I_1 + \sqrt{(c_2^{SF} \cdot I_1)^2 + 12 \cdot c_1^{SF} \cdot J_2 \cdot 1}) / 2$$

$$\tau_{xy} \rightarrow \sigma_{eq}^{NF} = 1 \cdot \tau_{xy}, \quad \sigma_{eq}^{SF} = \sqrt{3} \cdot \tau_{xy}; \quad \sigma_x \rightarrow \sigma_{eq}^{NF} = 1 \cdot \sigma_x, \quad \sigma_{eq}^{SF} = 0.5 \cdot \sigma_x \cdot \sqrt{c_2^{SF2} + 4 \cdot (1 + c_2^{SF}) \cdot 1}$$

\* Transversely-isotropic UD, brittle: 5 fracture failure modes;  $\tau_{23}$  acts

out-of-plane shear stress activates 2 modes  $\{\sigma\}_L = (0, 0, 0, \tau_{23}, 0, 0)^T = (0, \tau_{23}, -\tau_{23}, 0, 0, 0)^T$

principal stresses replacement:  $\sigma_2^{pr} = 0.5 \cdot (\sigma_2 + \sigma_3) + \sqrt{[0.5 \cdot (\sigma_2 + \sigma_3)]^2 + \tau_{23}^2} = \tau_{23}, \sigma_3^{pr} = -\tau_{23}$

$$Eff^{\perp\sigma} = [(\sigma_2 + \sigma_3) + \sqrt{(\sigma_2 - \sigma_3)^2 + 4\tau_{23}^2}] / 2\bar{R}_\perp^t = \tau_{23} / \bar{R}_\perp^t$$

$$Eff^{\perp\tau} = \left[ \left( \frac{\mu_{\perp\perp}}{1 - \mu_{\perp\perp}} \right) \cdot (\sigma_2 + \sigma_3) + \frac{1}{1 - \mu_{\perp\perp}} \sqrt{(\sigma_2 - \sigma_3)^2 + 4\tau_{23}^2} \right] / \bar{R}_\perp^c = \frac{2\tau_{23}}{\bar{R}_\perp^c \cdot (1 - \mu_{\perp\perp})}$$

$\rightarrow$  same results for shear stress or replacing principal stresses  $\equiv$  shear stress components.

### 3.11 A closer Look at Materials addressing Shear Stress and Multi-fold Failure

Keep in mind, please, for this subchapter:

SFCs are principally set up for strength failures which occur only one-fold !

Principally shear tests are not uni-axial tests but can be seen to be bi-axial and can be performed bi-axially. In the isotropic and a quasi-isotropic plane  $\tau$  can be replaced by  $\sigma_i^{pr} = \tau$ ,  $\sigma_i^{pr} = -\tau$ . Inserting  $\tau$  or the two principal stresses =  $\tau$ -stress components does give the same result.

Friction micro-damage is caused by shear stress  $\tau$  with compression stress  $\sigma^c$ . For instance, for a fabric - experiencing  $\sigma_W$  and  $\sigma_F$  - an additional term must consider this additional failure danger.

For the UD-material the double tensile mode  $\sigma_2^t + \sigma_3^t$  could be considered by the other form of the invariant  $I_3$ , namely  $I_3 = \tau_{23}^2 - \sigma_2^t \cdot \sigma_3^t$  or  $I_3 = -\sigma_2^{pr} \cdot \sigma_3^{pr}$  from [Mul], by  $Eff = I_3 / (R^u)^2$ , similarly to  $J_3$  for the isotropic case.

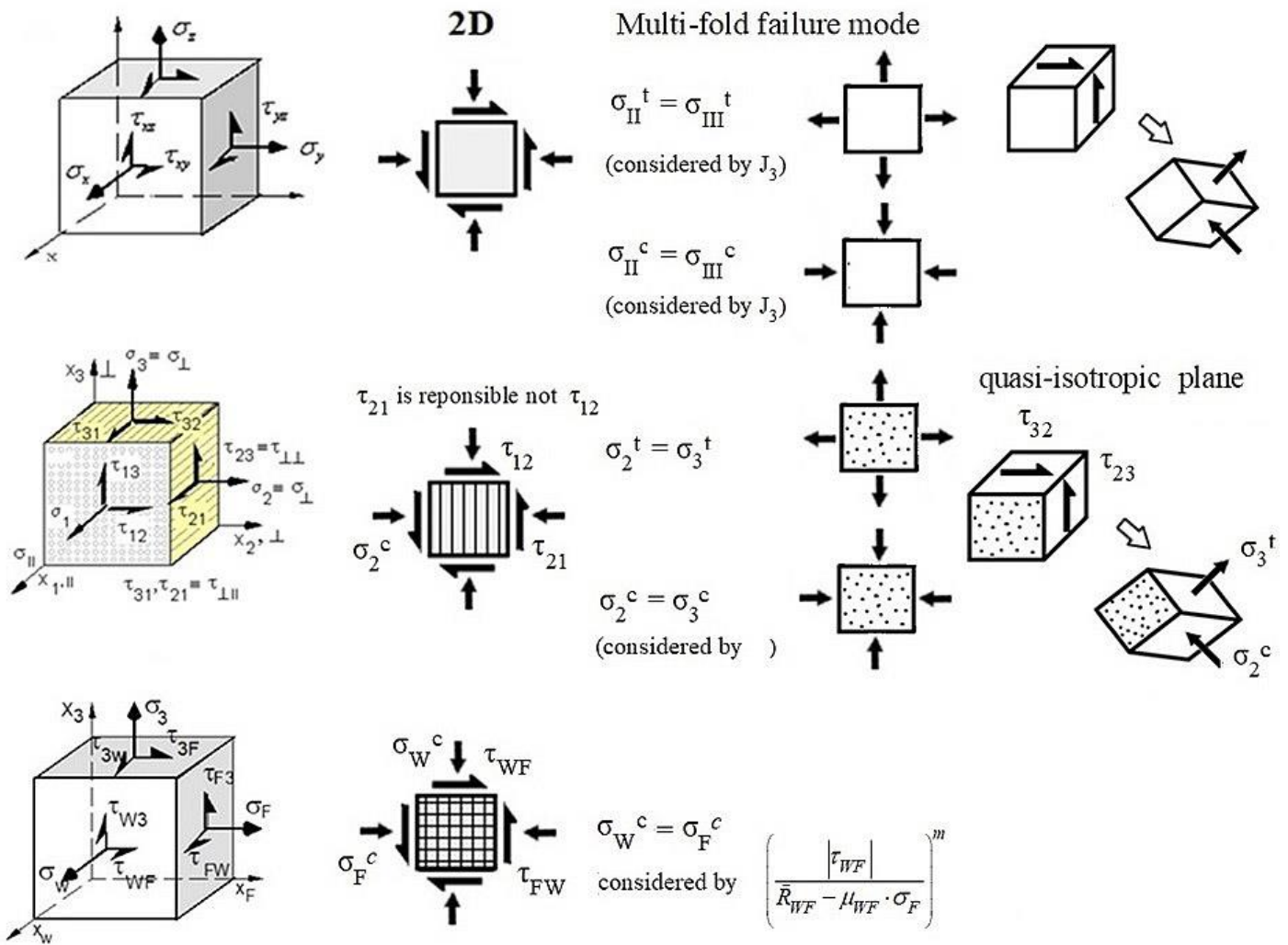


Fig.3-12: Consideration of multi-fold failures

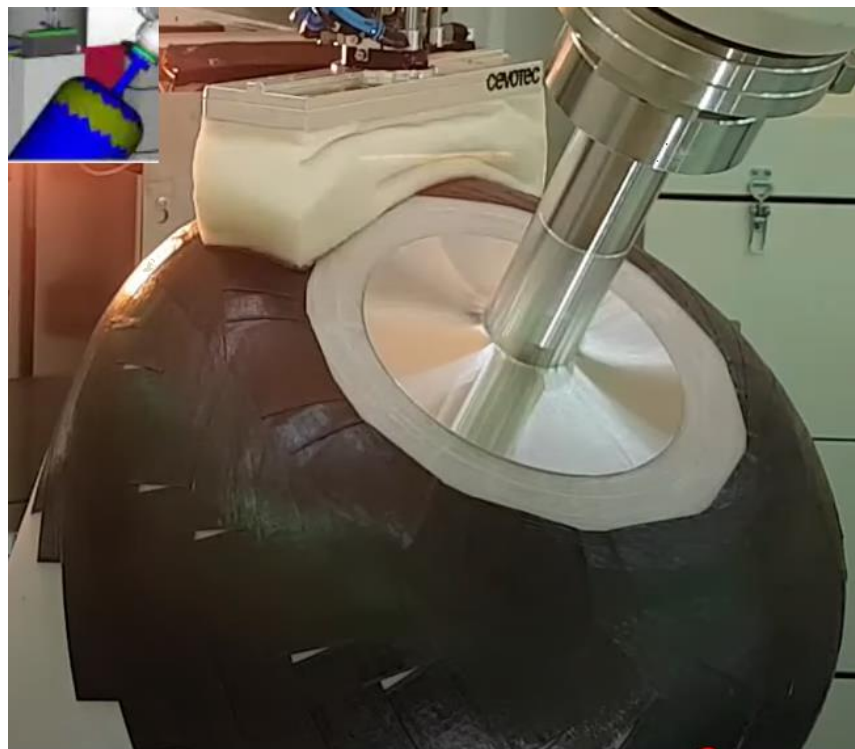


### 3.12 Note on Polymer Matrix Reinforcement by Fiber Patch work

Modern automated production methods allow to place the reinforcement there where it is needed thus reducing waste. To mention are the methods AFP (Automated Fiber Placement) and AFPP (Automated Fiber Patch Placement). UD and fabric tapes are cut into a required patch size in order to accurately place the locally required strength and stiffness to build up the multi-stacked laminate wall.

This process is also applied to pressure vessels where the development was: filament winding → tape winding → patch placing. *See Fig.3-13.*

For design dimensioning essential are the steps of the single patches over the thickness and the interfaces (with gaps, because of a better draping, or without gaps) between the patches. Do these location harm the cyclic and less the static behaviour? This is to consider when modelling and assessing the distinct structural component.



*Fig.3-13: AFPP-fabricated dome-reinforcement of a pressure vessel. (CEVETEC).*

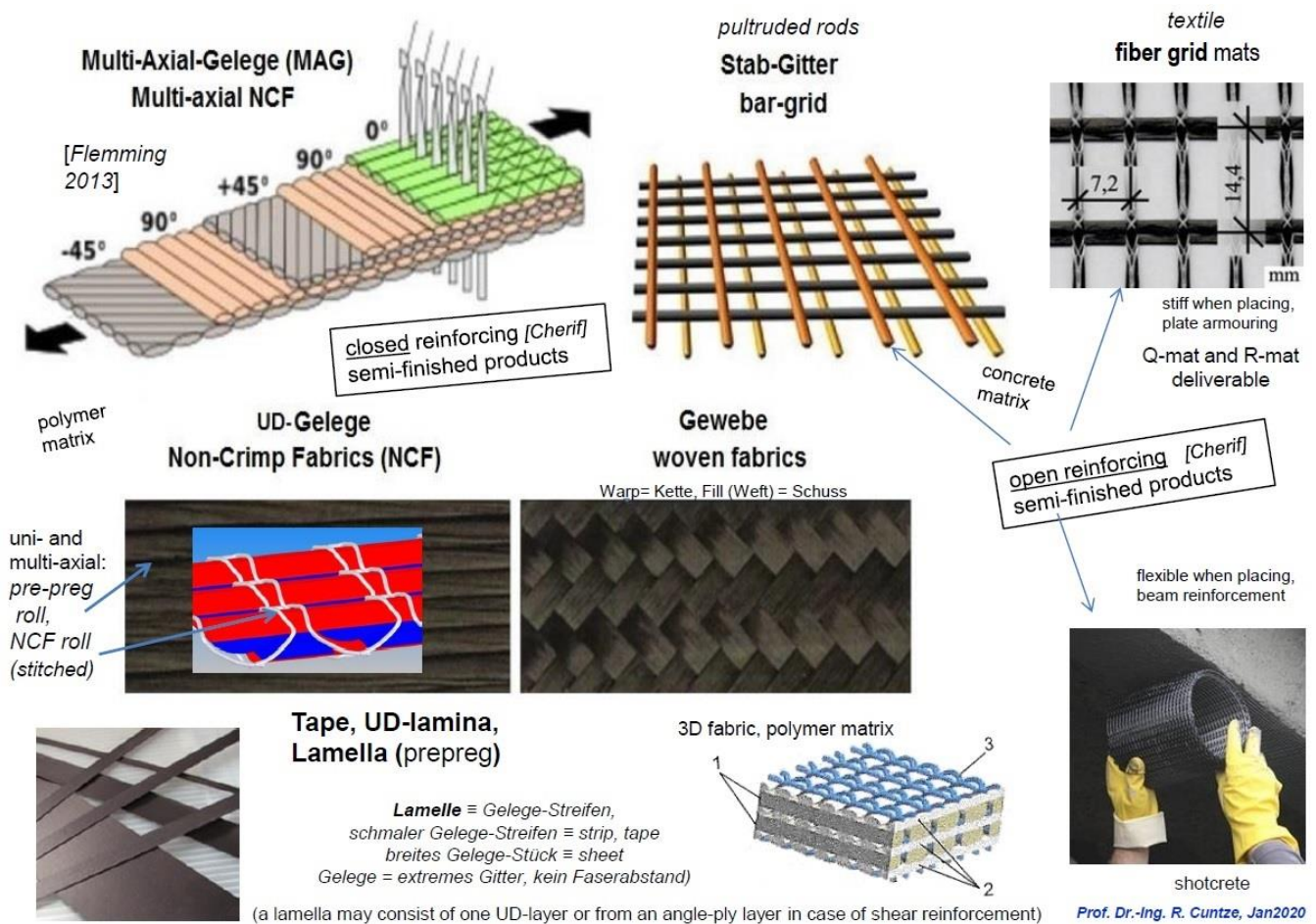
*[www.cevotec.com/verbesserung-der-speichereffizienz-von-verbundtanks/](http://www.cevotec.com/verbesserung-der-speichereffizienz-von-verbundtanks/)*

## 4 Construction Applications and Modelling of ‘open’ and ‘closed’ FRP and FRC Structural Components

### 4.1 Some semi-finished products in construction

Before referring to specific SFCs it is helpful to take a look at the variety of upcoming reinforcements in civil engineering especially for concrete reinforcements.

The main semi-finished products are depicted in *Fig.4-1*.



*Fig.4-1: Fiber-reinforced semi-finished products in civil engineering [Che11]*

There are semi-finished products spanning from pultruded 1D-rods via 2D-non-crimped fabrics up to fiber grids. They are designed as practiced taking the different stress-strain behavior into account.

In construction, FRP is used for structural rehabilitation (retrofitting) and new structures. The range is from the huge GFRP tanks and chimneys, profiles and tubes, cables, girders and slabs, bonded stripes, external strengthening by tendons through direct reinforcement of beams, slabs and columns. In this chapter some examples of the construction industry are presented. Additional applications can be found in the Springer-published Glossar\* of the author.

## 4.2 Applications with Fiber-Reinforced Polymer (FRP) matrices

In polymer matrix *CFRP* a large variety of applications are *known* such as core wires for the Chinese ultrahigh-voltage power transmission line, constructions in Saudi-Arabia, below. Much more applications are presented on the next pages

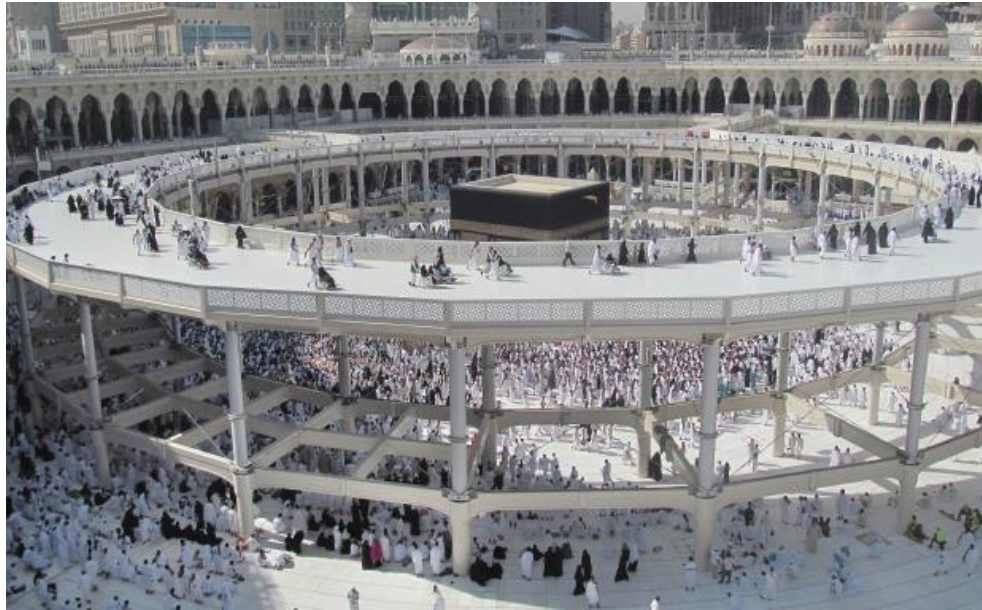


Fig.4-2: Mekka, CFRP- Pilgrim path construction around the Kaaba. Inner -  $\Phi$  80 m, 400 t CFRP  
[Premier Composite Technology PCT, Dubai, Vancouver.sun.com]

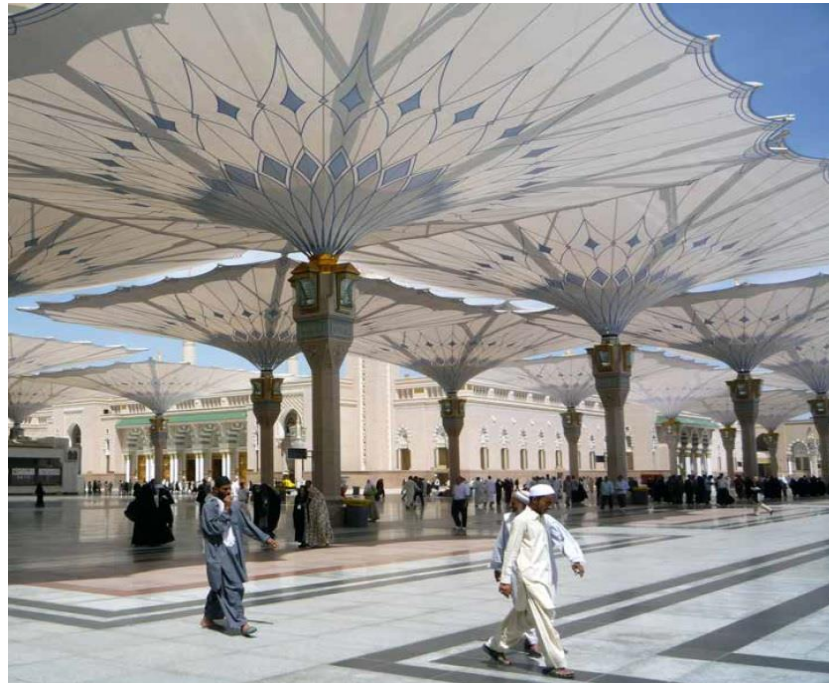


Fig.4-3: (left) Test tower [Jahn/Sobek] transverse vibration-avoiding GF fabric cover of the Thyssen-Krupp test tower for high-speed elevators Rottweil, 245m. (right) Mosque Masjid an Nabawi, Medina, sun protection 'umbrellas', Medina SA, 2010 [ILEK in cooperation with SL-Rasch]



*Fig.4-4: Special automated fabrication process with endless fiber strands ‘wound’ over the fixed 'truss' nodes as strand turning points. Lightweight 'fiber pavilion' made of 60 CFRP/GRP components, BUGA Heilbronn 2020. Art structure meets load-carrying structure [Knippers, Koslowski, ITKE Stuttgart; Menges, CD].*



*Fig.4-5: CFRP truss work production using a special strand placement (winding) technique and the fabricated bridge [BaltiCo GmbH, July 2020]. Thanks Dirk  
25 m bicycle and pedestrian bridge made of CFRP in Sassnitz was installed, which was easier than usual due to the weight of just 1.4 tons of a single segment and took place within a single day.  
BaliCo Portfolio: Lattice masts, functionalized modular cabin plate elements, bridges, girders, lattice masts, telescopic towers, rotor blades.*



*Fig.4-6: The Stuttgart Stadtbahn bridge, installed over the A8 motorway on May 3 in Germany, is the world's first network arch railway bridge (127 m) that hangs entirely on tension elements made of carbon fiber-reinforced plastic (CFRP). The 72 hangers are produced by Carbo-Link AG (Fehrltorf, Switzerland) supported by EMPA (Urs Meier), with Teijin carbon fibers (Wuppertal, Germany), Tenax. The bridge meets installation, mass and sustainability goal*



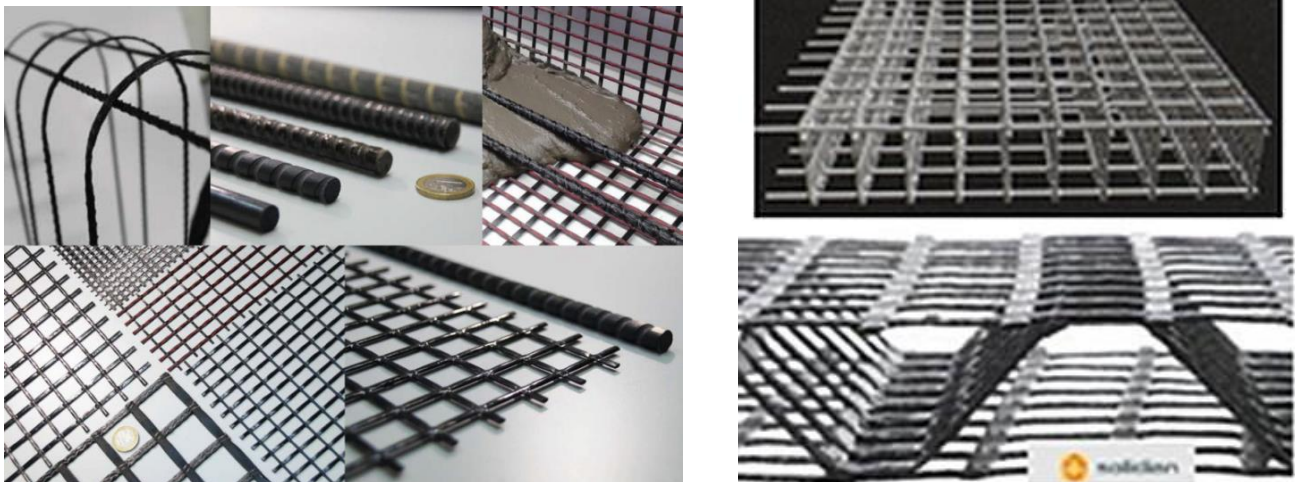
*Fig. 4-7: CFRP tension members made of continuous loops for cranes, since 2003 [Liebherr with with the EMPA Spin-Off Company Carbo-Link]*



*Fig.4-8: Fiber composites in building construction [Sorry. Originator not found in web].  
The GFRP profiles of the cooling towers in the combined cycle power plant in Herne received approval on a case-by-case basis (Zustimmung im Einzelfall). In addition, the project-related type approval (Bauartgenehmigung) was granted for a cell cooling tower made of these GFRP profiles*

### 4.3 Applications with Fiber-Reinforced Mineral (FRM) matrices

The usual mineral matrix is concrete which leads to the technical term for carbon-fiber reinforced concrete namely CFRC. Additional applications are in the Glossar of the author [Cun19].



*Fig.4-9: (left) Several reinforcements [Frank Jesse],  
(right) armoring cages for a sandwich [Fraas] and an  $\Omega$ -shaped reinforcement [Solidian].*

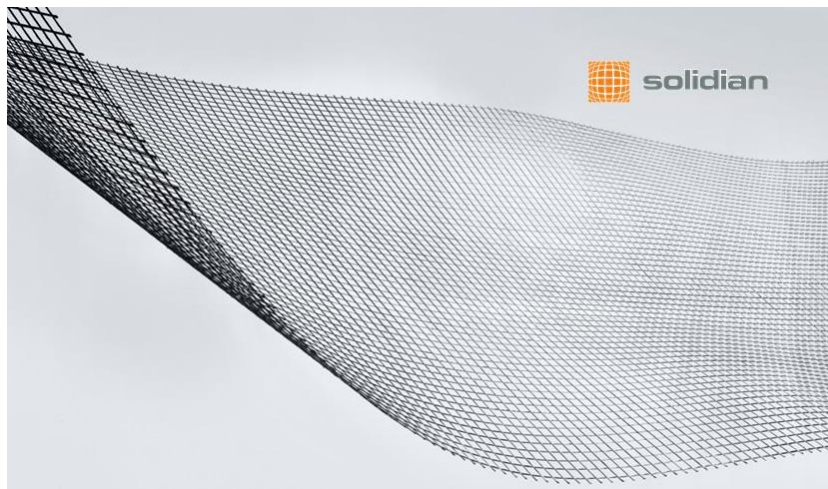


Fig. 4-10: 'solidian GRID\_free shape-1' made of carbon fibers with epoxy resin impregnation; characteristic tensile strength  $> 2.800 \text{ N/mm}^2$ , standard dimension  $6,0 \times 2,30 \text{ m}$ , on request up to  $8 \times 3 \text{ m}$  as well as roll material up to  $80 \text{ m} \times 3 \text{ m}$

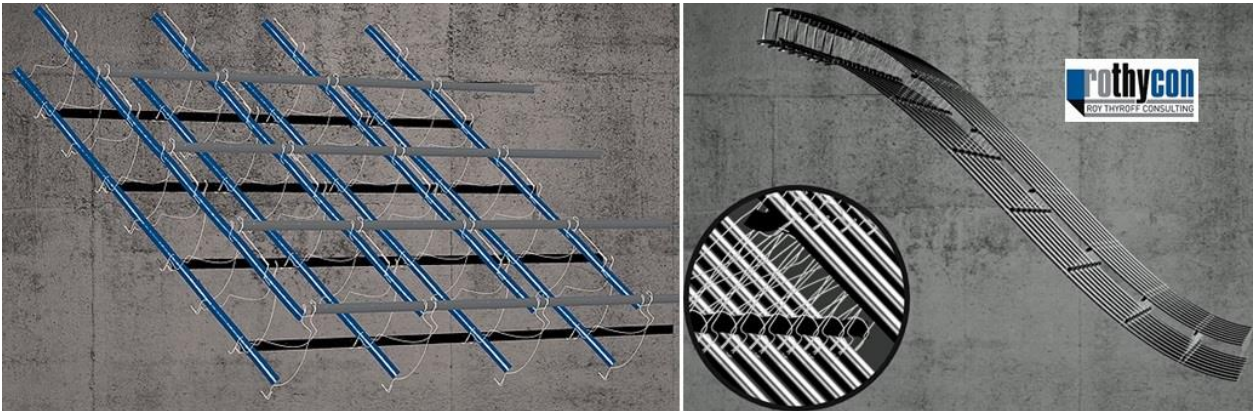
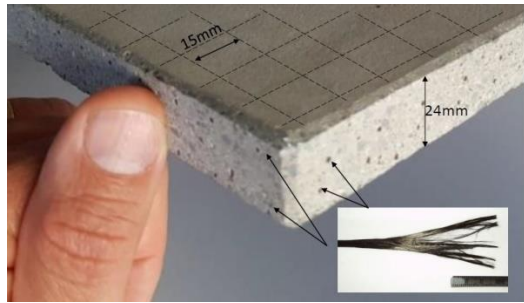


Fig. 3-11: (up) 3D bi-axial spacer fabrics [rothycon], (below) 3D cage



200g Carbon  
und 55kg Beton  
pro m<sup>2</sup> Platte



CPC 24mm

during test

after test

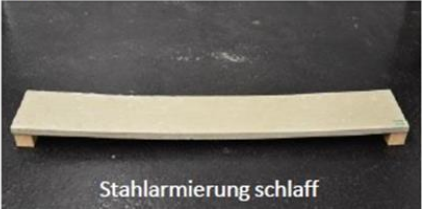
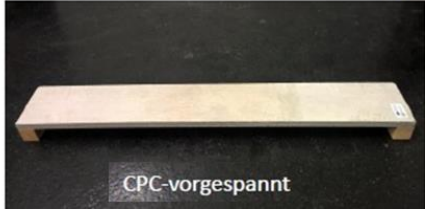


Fig.4-12: Application of pre-tension. The concrete is compression-activated, which massively increases the stiffness of the component, carbon fiber strength can be fully utilized. (center) Stiffness for service loads remains for CPC pre-stressed. (right) Permanent deformation for the slack reinforcement (Stahlarmierung, schlaff) due to the stretched steel reinforcement

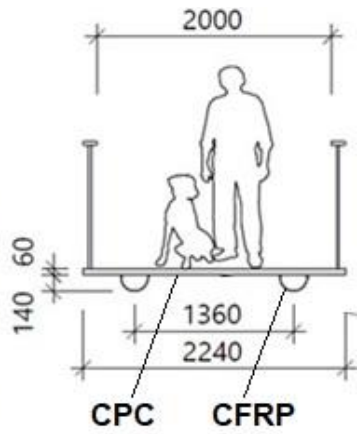


Fig.4-13: Hybrid bridge in Turbenthal made of pretensioned CPC slabs and CFRP beam supports. CPC-plate size: 2-7 cm thick, length 3.5 – 17 m [ZHAW, with J. Kurath]. Thanks Sepp



Fig.4-14: Multi-curved textile carbon concrete shell structure. Thanks © Ingelore Gatzsch





*Fig.4-15: (up) a solidian GRID Q95-CCE-38 fiber grid (mat) [christian.kulas@solidian.com, [www.solidian.com](http://www.solidian.com)] Thanks Christian  
(down) First, purely CF-reinforced concrete bridge in the world. Albstadt-Ebingen. 2015.  
According to (Construction) Mayor of Albstadt, Udo Hollauer, "The bridge pays off, and is sustainable"*

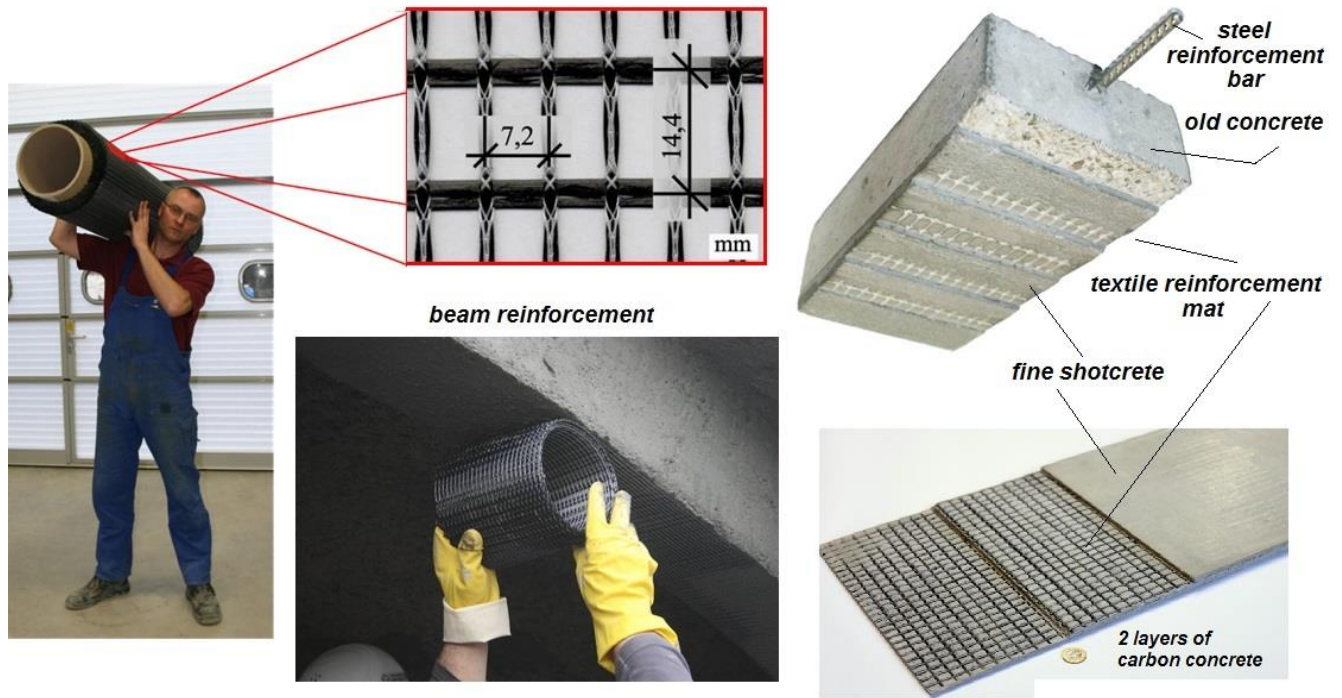
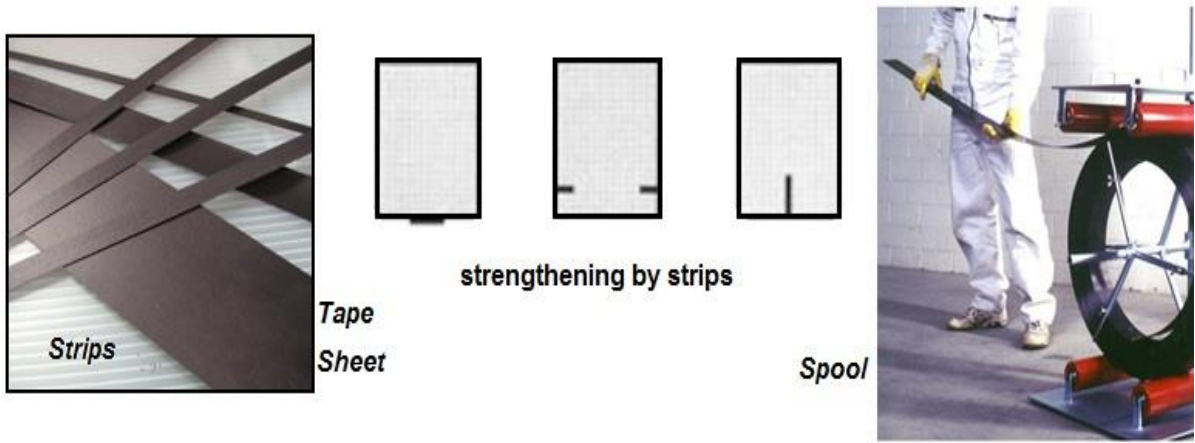


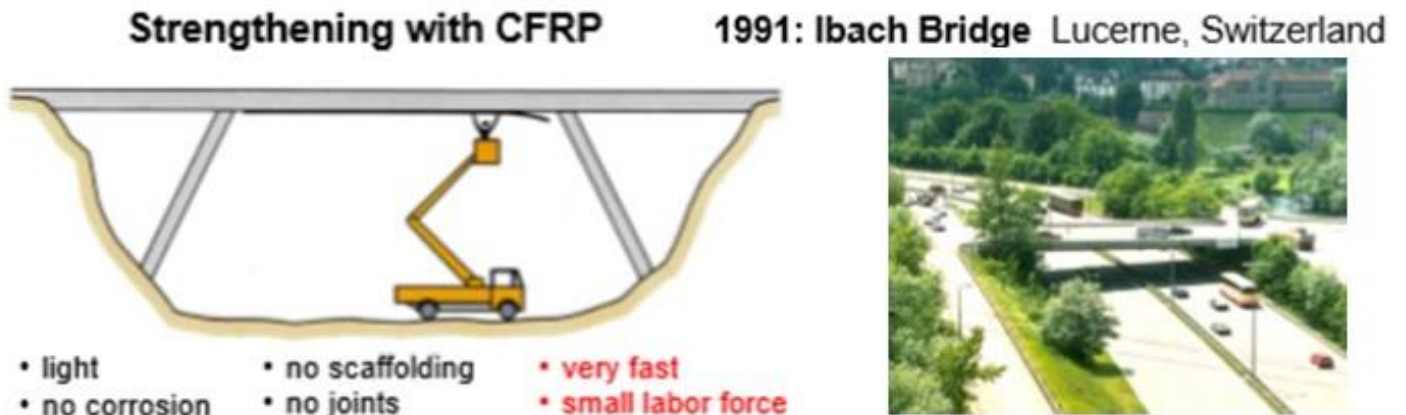
Fig.4-16: for Rehabilitation, retrofitting of a slab. Fiber grid in detail and wrapped on a on roll during application. As an example 2 applied fiber grid lattice layers of CF yarns. [IfM Dresden]



Fig.4-17: light CF-reinforced concrete elements (left) amphibian guidance facility © informbeton GmbH, (right) NTRC – Nonwoven Textile Reinforced Concrete (feinbetonetränkter Vliesstoff , 4.50 m length, 60 cm width, 12 mm thick © Bendl HTS GmbH.



*Fig.4-18 Rehabilitation of existing buildings:  
 (up) Possibilities to strengthen by strip, pre-tensioned or slack.  
 (down) Reinforcement of slabs because of increased moments by CFRP-lamellas, hydrostatic pressure from ground, applying External Reinforced Bonding ERB. Mineralbad "Berg", Stuttgart, 2018, [HPTL]. And for post-reinforcement of slab break-throughs to capture the local stress concentrations  
 Refurbishment by reinforcement of Beam and slabs*



*Fig.4-19: Construction Applications of FRM (Urs Meier, EMPA. Thanks Urs)*



*Fig.4-20: Staircase-Reinforcement with long steel fibers.*  
 [Faserbeton im Bauwesen, Springer, Bernhard Wietek. Thanks Bernhard].  
 What about long C-fibers?



It is very rarely good to be late! If we had been half of an hour earlier, I would probably lie down in the ravine. In this context my plea is  
 “Use the new fantastic build possibilities. It is not beneficial to wait and to become too late!”

#### **4.4 Some Freshly arrived Applications**

From Gabi Boehm, principal architect at PCT, PREMIER COMPOSITE TECHNOLOGIES LLC. Dubai.  
*Pictures, copyright ENOC. Thanks Gabi.*



*Fig.4.4-1 UAE Pavilion: FRP wings (built from a hybrid carbon and glass fibre build-up) and the claddings (built in glass fibre) resulted in an impressive 40% mass saving. The reduced mass was also beneficial during installation and allowed the entire wings to be hoisted in one piece. The wings were produced at PCT facilities to a maximum transportable size. Most wings were transported to the site already assembled – the larger ones arrived in two halves which were bolted together on-site and finished with a seamless joint. The repetitive nature of the FRP panels was critical for the effective use of tooling and cost-effective serial production of the wings and claddings. Furthermore, lamination schedule with curing procedure were optimized for each wing and for each zone to meet the structural requirements with a cost-effective approach*



*Fig.4.4-2 E-Trees Sustainability Pavilion: Light and stiff CFRP 'steering wheels' keep the load manageable for the mechanical rotation system that allows the E-trees to track the sun as the days progress to ensure that the up to 14 t of PV panels are always ideally positioned to maximize their efficiency.*



*Fig.4.4-3 ENOC Petrol Station : CFRP was used to construct the entire structure of a service station canopy (roof) . It consists of 133 diamond shaped CFRP frames housing ETFE inflated cushions and photovoltaic panels. The entire structure is supported by an exoskeleton consisting of 9 slender molded CFRP Ghaf trees ( the tubes are built using filament winding with molded nodes manufactured from the same carbonfibre fabric).*

*Awarded the LEED (Energy and Environmental Design) platinum certification. LEED is a classification system for ecological building, the most widely used green building rating system (in Germany: Deutsches Gütesiegel Nachhaltiges Bauen)*

#### 4.5 Influence of Production Process on the Damage of Filaments and roving Fiber Strands

The structural engineer should keep in mind what production ‘makes’ with the filament and with the roving. The author was confronted several times in his life with these problems.

The following information shall improve the knowledge nad is written for a filament (CF =7μm ϕ) and is partly directly transferable to a 4k roving or a 49k heavy tow thread used in order to increase the material feed. It is valid for wrapping, tape storage and braiding. These production simulation ideas can be transferred to static and cyclic operational loading. Basic terms are presented in the

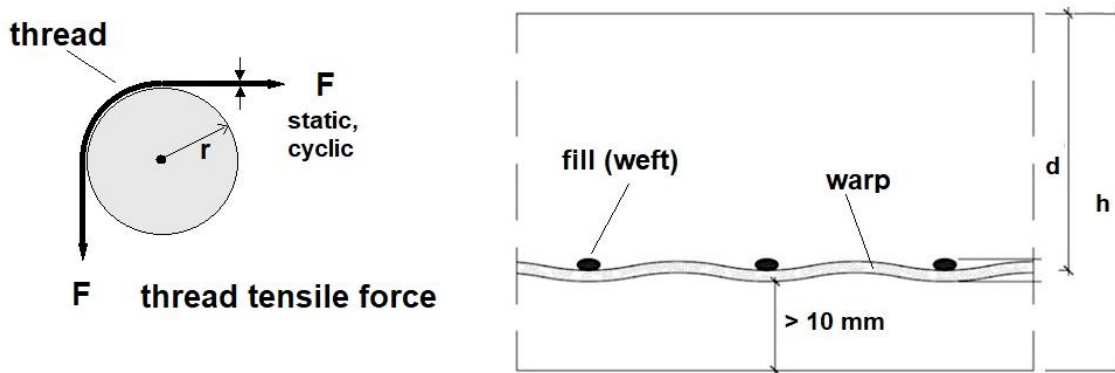


Fig.4-19: (left) Sketch of the deflection situation at a thread curvature location. (right) visualization of the waviness of a fiber grid layer within the concrete matrix of a plate. Determination of the static usable height separated for warp and weft direction

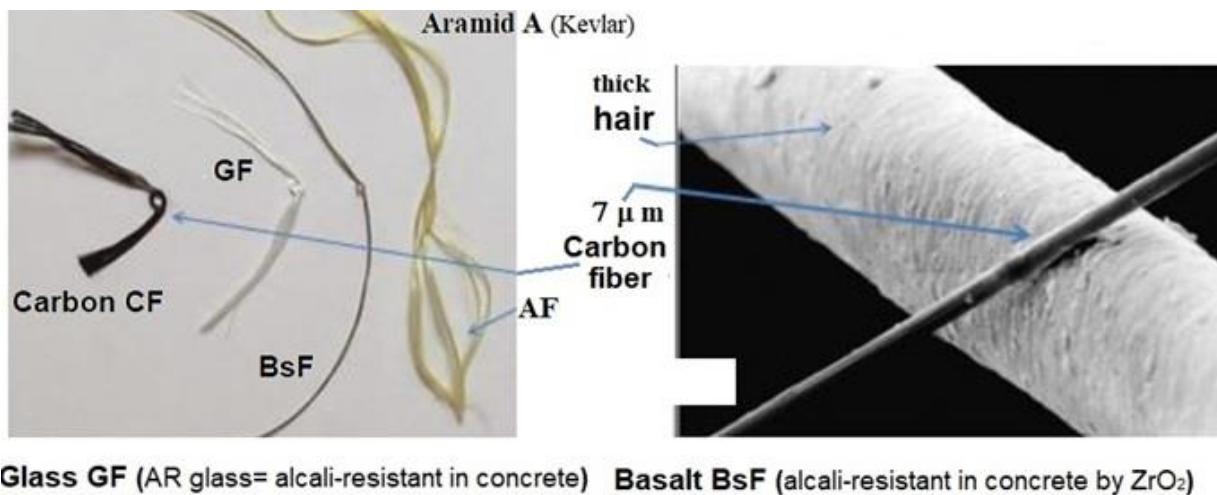


Fig.4-20: Different strengthening fibers and comparison CF with human hair

#### Radius of curvature ρ:

The high stiffness and, above all, brittleness determine the degree of curvature and bending of the filaments during deflection. A simple calculation delivers a thumb value which is of high interest when bending armoring cages:

Single Carbon fiber:

$$d = 7 \mu\text{m}, \text{ fracture strain } \varepsilon_{fr} = 1.5 \%, E_f = 240000 \text{ N/mm}^2, \text{ fracture stress } \sigma_{fr} = \varepsilon_{fr} \cdot E_f.$$

$$\text{From this follows } \rho \approx E \cdot I / M = 0.5 \cdot E \cdot d / \sigma_{fr} \rightarrow 0.2\text{mm.} \quad \text{Mind } \rho_{crit} < 1 \text{ mm.}$$

Roving fiber bundle, cured stiff: bent outer filament of the bundle

$$\text{assumed } d = 1 \text{ mm}, \rho \approx 0.5 \cdot E \cdot d / \sigma_{fr} \quad \text{Mind } \rho_{crit} \approx 20\text{mm.}$$

Angle of re-direction (Umlenkwinkel)  $90^\circ > \alpha > 90^\circ$ : [Kun04]

The contact length of fiber and thread guide roller impacts the stress distribution in the contact area. Thereby, the radius of curvature has much an effect.

Surface structure and roughness of the thread guide roller (Fadenführungsrolle): The friction behavior between filament and thread guide roller influences the damage of the filaments. Glazed porcelain is recommended in [Kun04].

Thread tensile force  $F$ : Due to tensile load of the thread during the production process a stress distribution over the cross-section is caused. This also depends on the shape of the thread guide roller

Thread speed: Determines production rate and is to optimize with  $F$

Filament arrangement in the thread: Thread guide roller change the arrangement of the filaments in the cross-section of the roving feed, so that the very important fiber parallelism may be disturbed, especially when braiding.

Winding: The author was several times confronted in his professional life with the strength problems addressed in the two following figures, when winding layers were built up to the required laminate wall thickness.

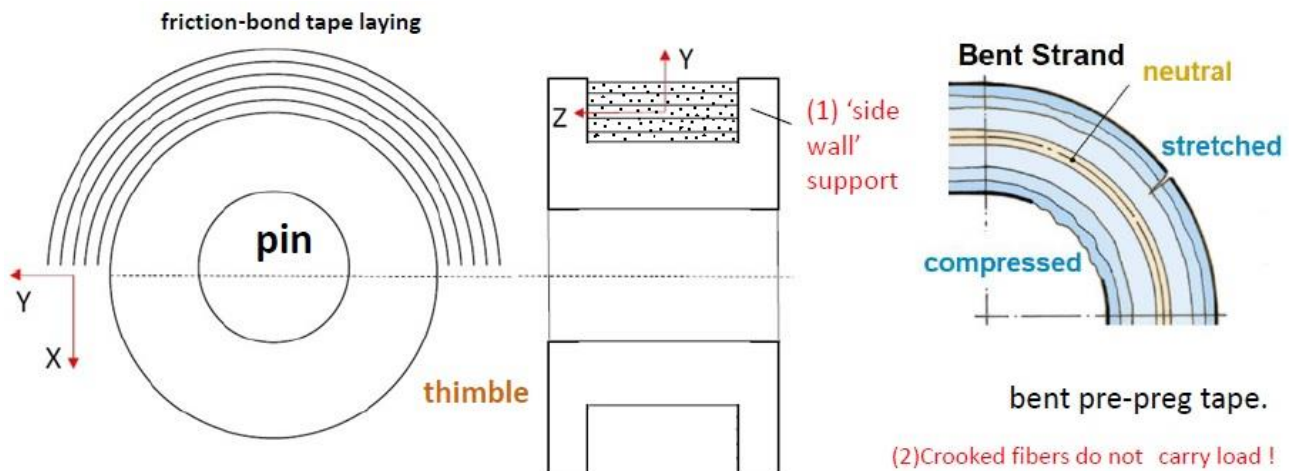


Fig.4-21: Benefit of semi-cured layer placing and of a side wall supported layer stack

Some points to consider regarding the design challenge 'Fiber Stress Concentration along the strand loop':

- \* Crooked fibers or tapes practically do not carry the desired tensile loading. Fibers or tapes losing some stretch, caused by the winding or tape-laying process, carry much less tensile loading and are not efficiently used (*less exploitation of fiber capacity*).
- \* Reducing the bond between the layers increases the strength capacity of the loop, see CarboLink idea → Good Design ideas 'make' structural Strength!
- \* Side walls: A 1D-compressive radial stress state in the groove of the thimble would lead to IFF2-caused wedge failure of the laterally compression-loaded UD loop strand. On the other side, in the case of side walls the radial compression generates a positively acting lateral 2D-compressive stress state. Hence, side walls of the groove are mandatory despite of the fact that the fibers experience a little higher tensile stress.
- \* Thin tapes (layers) help to exploit the capacity of the fibers.



- \* The contact roving (filament) ↔ thimble principally causes some wear under cyclic loading.
- \* Critical location is at the ‘cheek’, where a stress and strain concentration is generated. This causes a changing contact situation with sliding friction and wear. This is important for the fatigue life.

High secondary stresses occur in the bolt area when loading laminated strand loops.

The more rigid the fibre and the “thicker” the loop is, the higher the secondary stresses are that will be generated.

Non-laminated strand loops solve this problem. Such a strand loop is made of a very thin UD tape of only 0.12 mm thickness. This tape is continuously laid in the desired number of layers around corresponding deflection bodies (bolts, pins) by an ‘endless tape lay-up device’. There is no full bond between the individual layers, just friction bond. The last layer is laminated with the penultimate layer on a length of about 10 cm and anchored with it. [Winistörfer, A.; Mottram, T.: *Finite Element Analysis of Non-Laminated Composite Pin-Loaded Straps for Civil Engineering*, Journal of Composite Materials, Vol. 35, 2001. Carbo-Link and EMPA Dübendorf, Prof. Urs Meier].

When loading the strand loop, a relatively even stress distribution is achieved due to relative shifts possible between the adjacent tape layers. The load transmission between the layers is carried out by friction. This is also more cost-effective because no consolidation of the shifts is required.

Lateral supports increase the load-bearing capacity of strand loops made of carbon fibre. This indicates that in dimensioning of loops it is necessary to apply a 3D-strength analysis (VDI 2014 Part 3, editor: R. Cuntze).

**Production experience: full bond**

When putting layer upon layer the ‘winding tension force’ will compress the former layer and reduce the efficiency of the former layer. This situation is improved by an optimal choice of the ‘winding tension force’ in the process together with intermediate consolidation.

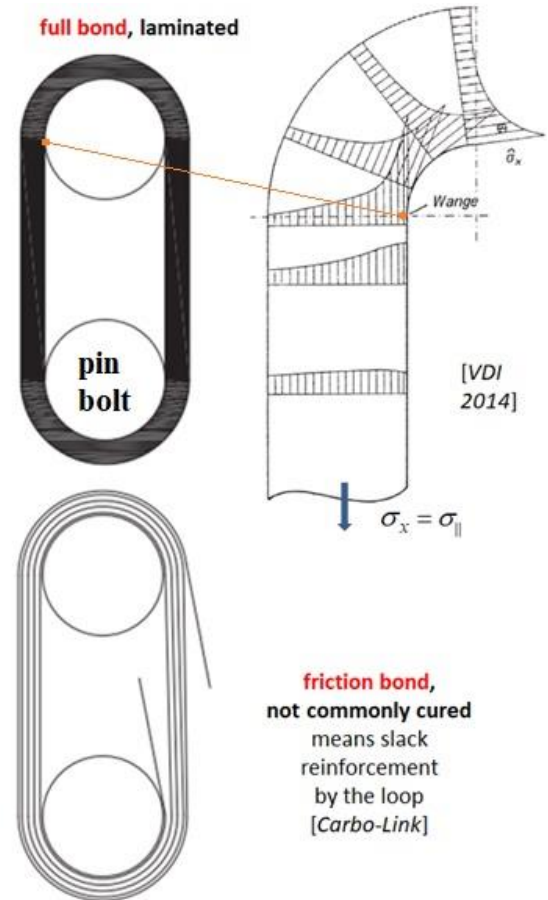


Fig.4-22: CarboLink Idea of a flexible construction of the strand loop (Strangschlaufe) to obtain equally stressed layers by friction bonding instead of a full bond solution together with winding intermediate curing

Friction bonding production leads to a higher fatigue life.

#### 4.5 On Material Modelling of some of the Semi-finished Products

**Pultruded Rod:** uni-axial loading, usually 1D tensile design dimensioning. Reference cross-section is the fiber cross-sectional area for the strands cut out of the fiber grids and the cross-sectional area resulting from the nominal diameter for pultruded rods. Necessary properties to provide are  $E_{||}, R_{||}^t \equiv f_{||}^t, R_{||}^c$  for bending, obtained from tension test specimens.

**Lamella:** (‘closed’ reinforcing tape for structural habilitation): Uni-axial and bi-axial reinforcement of beams and slabs (Fig.4-1): The application is inserting the lamella into cut slits with bonding or external bonding on the surface of the beam or slab. In construction the name lamella is used for the polymer-impregnated lamina layer (not just surface coated). If a lamella is multi-axially stressed then the stress state assessment follows sub-chapter 3.6.

GFRP-fabrics: (‘closed’ reinforcing sheet, sun protection ‘umbrellas’, 2D stress state). If multi-axially stressed, the stress state assessment follows Sub-chapter 3.7. Then the lateral properties come in, required for the proof of ULS and SLS.

Fiber-grids (‘open’ reinforcing grid, mat): Uni-axial and bi-axial reinforcement of plates and shells: Modelling depends on the grid width and the ratio of the orthogonal reinforcements. The necessary fiber cross-section of the orthogonal directions is separately determined according to the bi-axial loading. In the case of a large grid width the concrete matrix might shear fracture between the reinforcement under compression.

(short) Fiber-Reinforced Concrete (s)FRC: According to the intended production process sFRC a variety between directed  $\leftrightarrow$  quasi-isotropic short fiber distributions is to model.

“3D-print” processes: and extrusion head-placed mortar strands: *with/without fiber-reinforcement*

There are basically two types of so-called ‘3D-print processes in construction’.

- (1) Powderbed process (*Pulverbettverfahren*): A real 3D print process unreinforced or reinforced by using short filaments (single fibers) from cut rovings which may be intentionally pretty directed up or which shall approach a quasi-isotropic distribution.
- (2) Path-oriented, extrusion head-placed mortar strand process using short, or long or endless filaments (*pfad-orientierte Mörtelraupen-Extrusion*). Endless filaments within the tows are inserted in the mortar strand similar to the (*not fiber-reinforced*) so-called ‘polymer filament’ process.

#### **4.6 Structural Modelling and Dimensioning, *cross-section level in construction***

Upcoming standards are finalized for:

- polymer matrix: BÜV 10 update
- mineral matrix: novel DAfStb-Richtlinie “Betonbauteile mit nicht-metallischer Bewehrung“.

The DAfStb guideline “Concrete components with non-metallic reinforcement” is intended for fiber-reinforced components with concrete matrix. For engineers it is confusing not to clearly say which material group the guideline is for. Then the suffix <sub>nm</sub> could be replaced by the indices of the polymer matrix world namely for the pure fiber <sub>f</sub> and the cured fiber strand <sub>||</sub>. Why sticking further to *f* (strength). Still at the GruSiBau time (*about 1985, development of the excellent partial safety factor concept*) the author used the international letter *R* for the resistance entity strength. Using *R* makes life of engineers simpler, internationally at least.

*Author’s comment: From above follows that these two upcoming standards are not harmonized regarding the designations amongst themselves and w.r.t. terms half a century used internationally in timber construction and with polymer matrices. This is all the sadder for the author, because he edited the VDI 2014 guideline, initiated by civil engineers but not used in construction. The European Codes hopefully will improve this unfortunate situation.*

In the context above it seems to be necessary to cite here again two long-time used terms in the composite domain:

Material composite (Werkstoffverbund) structural-mechanically a composed ‘construction of different materials. Note: A not smearable ‘conglomerate’ is usually the Fiber-grid-Reinforced-Concrete.

Composite material (Verbundwerkstoff) combination of constituent materials, different in composition. Notes: (1) The constituents retain their identities in the composite; that is, they do not dissolve or otherwise merge completely into each other although they act in concert. Composite materials provide improved characteristics not obtainable by any of the original constituents acting alone. (2) Normally the constituents can be physically identified, and there is an interface between them. (3) Composites include fibrous materials, fabrics, laminated (layers of materials), and combinations of any of the above. (4) Composite materials can be metallic, non-metallic or a hybrid combination thereof, and carbon concrete is a further example. (5) Probably homogenizable to a smeared material such as FRC, SMC, UD-ply and lamella. The lamella is smearable and therefore it can be modelled as a ‘composite material’ (Verbundwerkstoff). (6) Layered materials and foam materials are also forms of composite materials. (7) Cement-based mortar is a ‘smearable’ composite material (RILEM has a problem here, because they do not discriminate material composite from composite material)

**BÜV-Empfehlung**

Überarbeitung 2019

**Tragende  
Kunststoffbauteile  
im Bauwesen [TKB]**

- Entwurf, Bemessung  
und Konstruktion -

Stand 08 / 2010

Zwanzig20 - Verbundvorhaben Carbon Concrete Composite C<sup>3</sup>  
V1.2: Nachweis- und Prüfkonzepte für Normen und Zulassungen

C3 V1.2 PG3  
DAFStb D 109

C3 V1.2 PG1/2  
DAFStb D 161

Arbeitspapier Bewehrung

Carbonbewehrung; Sorten, Eigenschaften, Kennzeichnung, Prüfkonzepte

Schlussfassung V1.2 (16.07.2019)

Ansprechpartner:

DAFStb  
FTA Albstadt  
Glassoiden GmbH Oschatz  
ILK TU Dresden  
IMB TU Dresden  
ITM TU Dresden

**Warnhinweis:**

Dieses Dokument stellt keine DIN-Norm oder Richtlinie dar.

Es handelt sich um ein Arbeitsdokument, welches im Rahmen des Projekts C3 V1.2 als möglicher Vorschlag für eine Richtlinie erarbeitet wurde und im Rahmen des Projekts C3 L9 weiterentwickelt wird.

DEUTSCHER AUSSCHUSS FÜR STAHLBETON

D 36 DAFStb UA  
Nichtmetallische Bewehrung

DAFStb-Richtlinie

Betonbauteile mit nichtmetallischer Bewehrung

Entwurf 19. August 2019  
Cyan – Änderungen und Ergänzungen gegenüber D 29

---

Teil 1: Bemessung und Konstruktion  
Teil 2: Bewehrungsprodukte  
Teil 3: Hinweise zur Ausführung  
Teil 4: Prüfverfahren

Notifiziert gemäß der Richtlinie (EU) 2015/1535 des Europäischen Parlaments und des Rates vom 9. September 2015 über ein Informationsverfahren auf dem Gebiet der technischen Vorschriften und der Vorschriften für die Dienste der Informationsgesellschaft (kodifizierter Text) (ABl. L 241/1 vom 17.09.2015).

Bezüglich der in dieser Richtlinie genannten Normen, anderen Unterlagen und technischen Anforderungen, die sich auf Produkte oder Prüfverfahren beziehen, gilt, dass auch Produkte bzw. Prüfverfahren angewandt werden dürfen, die Normen oder sonstigen Bestimmungen und/oder technischen Vorschriften anderer Mitgliedstaaten der Europäischen Union oder der Türkei oder einem EFTA-Staat, der Vertragspartei des EVR-Abkommens ist, entsprechen, sofern das geforderte Schutzniveau in Bezug auf Sicherheit, Gesundheit und Gebrauchstauglichkeit gleichermaßen dauerhaft erreicht wird.

Herausgeber:  
Deutscher Ausschuss für Stahlbeton e. V. – DAFStb  
Budapester Straße 31  
D-10757 Berlin  
Telefon: 030 2693-1320  
info@dafstb.de

Der Deutsche Ausschuss für Stahlbeton (DAFStb) beansprucht alle Rechte, auch das der Übersetzung in fremde Sprachen. Ohne ausdrückliche Genehmigung des DAFStb ist es nicht gestattet, diese Veröffentlichung oder Teile daraus auf fotomechanischem Wege oder auf andere Art zu vervielfältigen.

Guideline work ahead! In Germany

Verkauf durch den Beuth Verlag GmbH, Berlin, Vertriebs-Nummer 653006

Other standard works on fiber-reinforced materials are :  
wind energy GL re-work, Deutsche Bundesbahn

Fig.4-23: Guideline work ahead in Germany, BÜV10 update and D 36 novel

Basically in construction, design dimensioning is performed on cross-section level:

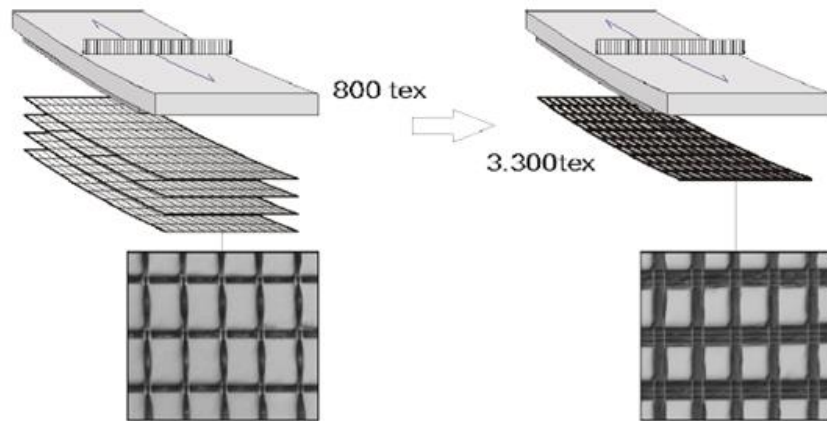
Beams:  $N$ ,  $M$ ,  $Q$ ,  $T$  internal cross-section loading

For fiber-reinforced beams the same models can be applied as with steel reinforcement. This is valid for pre-tensioned beams and for beams with slack reinforcement (*schlaffe Bewehrung*).

*Plate and shell elements: n, m, q, t, width-related internal cross-section loading*

Smearability depends on the grid width. If smearable then the so-called ‘layer-wise failure analysis’ can be employed using the Classical-Laminate-Theory CLT (*applied since 1970 by the author to polymer-matrix laminates, see [VDI06] and the short description in Annex 7.5*). The CLT may serve as analysis model for a layered plate or a layered shallow shell. Design dimensioning is to perform in Germany by application of the novel standards above. In the D36, dated August 2019, just the *procedure* of the CLT is addressed.

There are very different grid widths of the available fiber grids to be considered in modelling. S. Rittner shows in *Fig.4-24* the intention to replace several small ‘k roving layers’ by a 48 k Heavy Tow layer fiber grid. This increases the anchor length and impacts the shear load transfer problematic in the interface fiber strand-concrete matrix.



*Fig.4-24: Difference of 8k-roving and 48k-heavy tow application in fiber grids (armouring mats)  
(fineness of a roving, tow: 1 tex = 1 g/km length)*

In order to capture stress concentrations at a notch et cetera– instead of manually arming these spots – at distinct load introduction locations a quasi-isotropic, short fiber–reinforced high performance mortar could help to industrially solve this task. An armoring grade of  $V_f < 0.5\%$  C-fiber volume content is aimed at. The dispersion of the cut rovings into filament pieces (cut to a length  $< 8$  mm) could be performed direction optimal or is quasi-isotropic as required.

Often in discussions the question arises how much base material is needed for the Zirkonoxide added production of the fiber ARglass GF and the alkal-resistant carbon CF.

If basalt fibers BsF will reach a general approval from sustainability reasons they would be much better ecologically and economically due to the fact that enough base material is available. Added  $ZrO_2$  too provide alkali resistance is foreseen.

Fig.4-25 shall give a survey about the portions of the structural materials in the market. This is of high interest and helpful for many discussions.

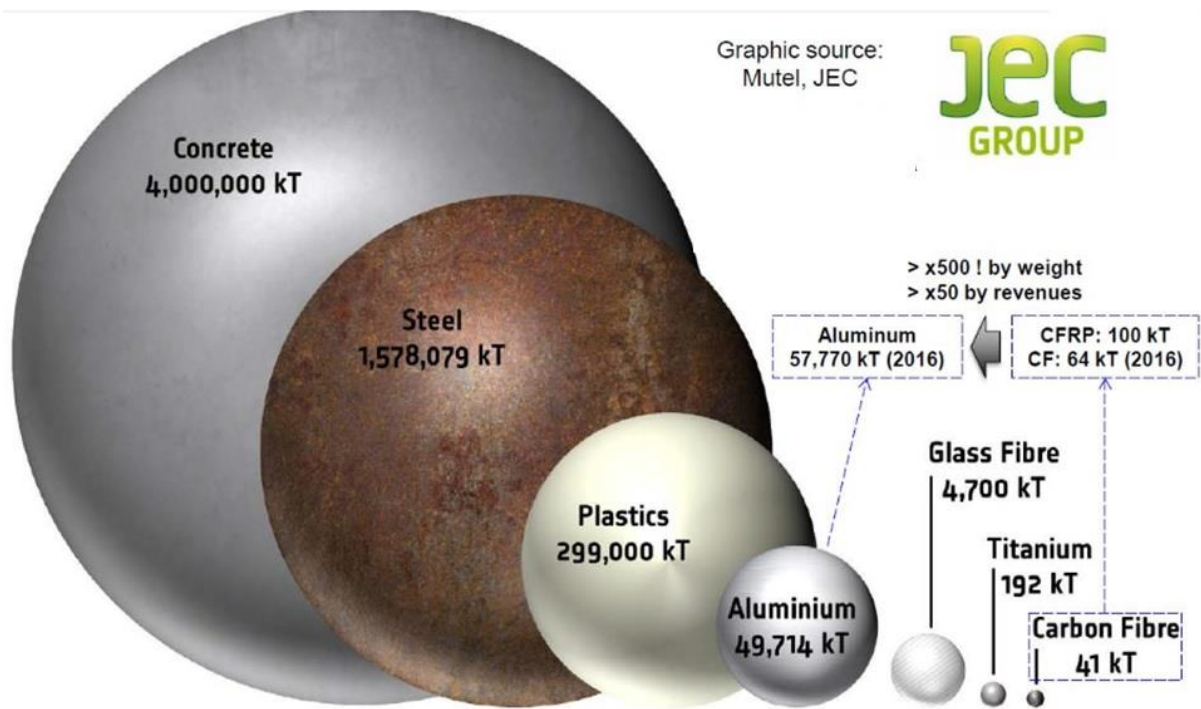


Fig.4-25: Weight ratios of structural materials, year 2016

CF total / Steel = 1/10000  
 In Germany it is CF total / concrete reinforcing steel  $\approx$  0.1%  
 Concrete / crude oil = 1, GF / CF = 100. Car consumes about 1 t oil / year

## 5 Two Missing Links filling the Strength Mechanics ‘Building’ of Isotropic Materials

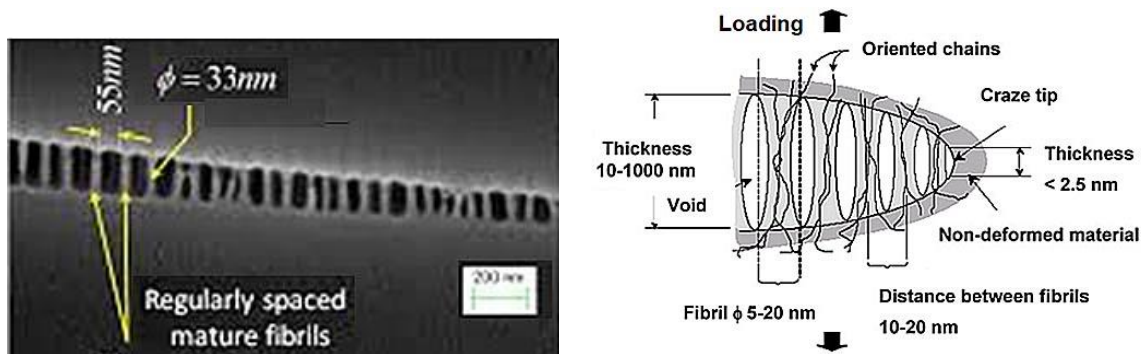
### 5.1 Experimental Proof and Description of Normal Yielding NY of Isotropic Materials

#### 5.1.1 General

Glassy (amorphous, brittle) polymers like polystyrene (PS), polycarbonate (PC) and PolyMethylMethacrylate (PMMA, plexiglass) are often used structural materials. They experience two different yield failure types, namely crazing and shear stress yielding that is often termed shear-banding, too. Crazing may be linked to Normal Yielding (NY) which precedes crazing-following fracture. Crazing occurs with an increase in volume and shear banding does not. Therefore, the dilatational  $I_1^2$  must be employed in the approach for tension  $I_1 > 0$ . Under compression, brittle amorphous polymers usually shear-band (SY) and with it they experience friction. Therefore,  $I_1$  must be employed in the approach for  $I_1 < 0$  in order to consider material internal friction. For obtaining the complete yield failure body its parts NY and SY are to interact in the transition zone, as still performed for concrete before.

Reminder on HMH-linked ‘Mises-cylinder’ for ‘Onset-of-Shear Stress Yielding SY: *There is no friction acting and therefore the yield strengths for compression and tension are the same  $R_{0.2}^c = R_{0.2}^t$  ( $\equiv R_{p0.2}$ , in which the superfluous suffix  $p$  practically has nothing to do with proportional). HMH means frictionless yielding and therefore it forms a cylinder.*

Crazing involves the formation of fibrils bridging two neighboring layers of the un-deformed polymer. These subsequently elongate and locally fail which leads to a formation or an elongation of an existing micro-crack, *Fig.5-1*. This micro-crack can be simulated under Fracture Mode-I loading conditions, using  $K_{Ic}$  (later necessarily to be termed  $K_{Icr}^t$ ).



*Fig.5-1: PMMA, SEM image of a craze in Polystyrene Image (created by Y. Arunkumar)*

The failure type crazing shows a curiosity under tensile stress states: A non-convex shape exists for Onset-of-Crazing ( $\bar{R}_{NY}^t$ ). NY is followed by the crazing-driven fracture NF for which - due to the similar shape - the NY-SFC can be used too. Under compressive stress states the usual shear band yielding SY occurs and later final shear fracture SF occurs. For both, SY and SF, the same SFC can be applied. *Due to the fact, that the Onset-of-Crazing and the Onset-of-Shear yielding associated failure stresses (“strengths”) are not yet accurately described, the designations  $\bar{R}_{NY}^t$  and  $\bar{R}_{0.2}^c$  are used. This has no influence on the logic followed here.*

**Available test data sets for PMMA:**

For the validation of the FMC-based SFC for PMMA two data sets were available, one NY-2D-data set from Sternstein-Myers [Ste73] and a SY-3D-data set from Matsushige [Mat73]. These two sets, depicted in Fig.5-2, are unfortunately of different origin: (1) Sternstein-Myers performed bi-axial experiments on craze initiation on the surface of thin-walled cylinders (tubes). The loadings were axial tension + internal pressure and tension + torsion. Test temperature was 60° C. Therefore, following literature, to match with Matsushige’s ambient test temperature 23°C data, from consistency reasons the value of  $\bar{R}_{NY}^t$  is to increase to become comparable with Matsushige. (2) Matsushige performed tri-axial experiments on sealed (surface crazing is hindered) solid rods at 23° C, under axial tension +  $p_{hyd}$ . The test specimen was pressurized within a chamber. This series along the tensile meridian, characterized by  $\sigma_I > \sigma_{II} = \sigma_{III}$ , contains the bi-axial point  $(-\bar{R}_{0.2}^{cc}, -\bar{R}_{0.2}^{cc}, 0)$ . In comparison to the thin tube the solid rod experiences more bulk crazing than the more dangerous surface crazing. This is essential for test data evaluation.

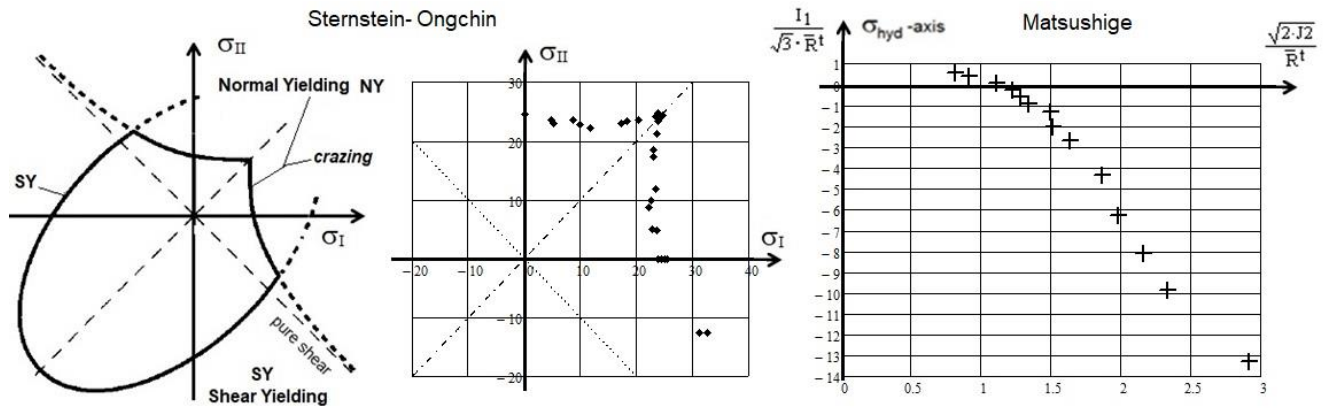


Fig.5-2 PMMA: (left) Sternstein’s mapping idea with his 2D test data set (center) in the principal stress plane, (right) Matsushige 3D-PMMA test data set rendered in Haigh-Westergaard-Lode coordinates.

Of special interest for the demonstration of a qualified mapping by SY-SFC and NY-SFC is the mapping of tensile meridian and compressive meridian as the essential cross-sections of the yield failure body. The definitions of the meridians are given below, associated test stress states are formulated in principal stresses and in mathematical stresses:

tensile meridian

compressive meridian

$$(\sigma_{ax}^t - p_{hyd}, -p_{hyd}, -p_{hyd}) = (\sigma_I, \sigma_{II}, \sigma_{III}) \rightarrow \sigma_I > \sigma_{II} = \sigma_{III} \Leftrightarrow (-p_{hyd}, -p_{hyd}, \sigma_{ax}^c - p_{hyd}) = (\sigma_I, \sigma_{II}, \sigma_{III}) \rightarrow \sigma_I = \sigma_{II} > \sigma_{III}$$

A 2D-data set and a 3D-data set can be displayed together in the Lode-Haigh-Westergaard diagram. There, the two data sets clearly outline crazing NY (Sternstein) and shear banding SY (Matsushige) and therefore can serve for mapping. However, the still mentioned harmonization of the two data sets is necessary: After transferring into MPa, the Matsushige fracture stress values were much higher than the Sternstein ones. Following Sternstein et al the threshold stress value required for crazing (ten minutes hold-time) is about 3900 psi (1000 psi = 6.89 MPa) and for ambient temperature about 5500 psi is guessed, extrapolating his curve approximately. This has the consequence to increase the Sternstein test data by a correction factor of  $f \approx 5500/3900$ . The choice finally was  $f = 1.3$ .

Fig.5-3 clearly outlines, that the course of test data needs to be differently mapped for the convex-shaped SY and the concave-shaped NY.

In the interaction zone from crazing to shearing a brittle-to-ductile transition occurs,  $p_{hyd}$  induces the transition from NY to SY by suppressing crazing.

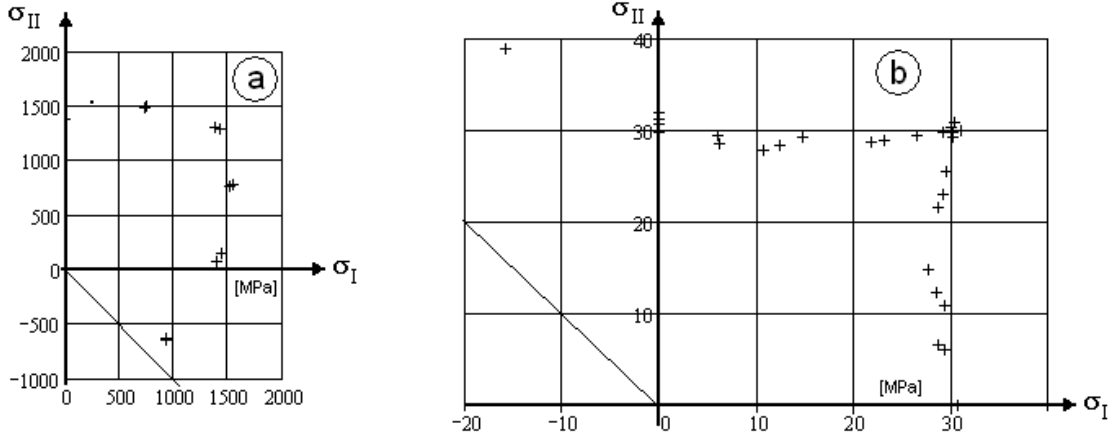


Fig.5-3: Tension domain with (a) Onset-of-Shear Yielding test data for a steel, SY, for comparison; (b) PMMA, Onset-of-Crazing NY. Strength points:  $(\bar{R}_{NY}^t, 0, 0)$ ,  $(\bar{R}_{NY}^{tt}, -\bar{R}_{NY}^{tt}, 0)$ ,  $(\bar{R}_{0.2}^c, 0, 0)$

**Formulas and visualization Onset of Yielding NY with SY: isotropic, dense material:**

Traditional SFCs describing yielding are related to Hencky-Mises-Huber (HMH hypothesis (*Mises, in short*) or to the ‘corner-suffering’ Tresca hypothesis. Tresca was preferred in the past due to its less computational effort and is still often mistakenly used as strength fracture failure condition seduced by its failure surface shape in tension in the principal stress plane. HMH delivers an ellipse as the cylinder’s cross-section, whereas Tresca leads to a hexagon, see Fig.5-4.

Table 5-1 PMMA: SFCs for normal yielding and shear yielding

Normal Yielding NY (hyperboloid)  $I_1 > 0$

Shear Yielding SY (paraboloid)  $I_1 < 0$

$$F^{NY} = \frac{x^2}{(c_2^{NY})^2} - \frac{(y - c_1^{NY})^2}{c_3^{NY2}} = 1 \text{ with } x = \frac{\sqrt{2 \cdot J_2 \cdot \Theta^{NY}}}{\bar{R}_{NY}^t}, y = \frac{I_1}{\sqrt{3} \cdot \bar{R}_{NY}^t} \Leftrightarrow F^{SY} = c_1^{SY} \cdot \frac{3J_2 \cdot \Theta^{SY}}{\bar{R}_{0.2}^{c2}} + c_2^{SY} \cdot \frac{I_1}{\bar{R}_{0.2}^c} = 1$$

Considering bi-axial strength (failure mode occurs twice,  $\Theta \neq 1$ ). In Effs now, index  $\Theta$  dropped.

$$Eff^{NY} = \frac{c_3^{NY} \cdot \sqrt{-c_2^{NY2} \cdot y^2 + (\Theta^{NY})^2 \cdot (c_3^{NY2} + c_1^{NY2}) \cdot x^2 + c_2^{NY} \cdot c_1^{NY} \cdot y}}{c_2^{NY} \cdot (c_3^{NY2} + c_1^{NY2})}, \quad Eff^{SY} = \frac{c_2^{SY} \cdot I_1 + \sqrt{(c_2^{SY} \cdot I_1)^2 + 12 \cdot c_1^{SY} \cdot 3J_2 \cdot \Theta^{SY}}}{2 \cdot \bar{R}_{0.2}^c}$$

Onset of Crazing = Normal Yielding NY (for fracture similar)

$c^{NY}$ ,  $d^{NY}$  from the two points  $(\bar{R}_{NY}^t, 0, 0)$  and  $(\bar{R}_{NY}^{tt}, \bar{R}_{NY}^{tt}, 0)$

$d^{SY}$  from the point  $(-\bar{R}_{0.2}^{cc}, -\bar{R}_{0.2}^{cc}, 0)$

Two-fold failure danger can be modelled by using the well known invariant  $J_3$  including  $d$  = non-circularity parameter

$$\Theta^{NY} = \sqrt[3]{1 + d^{NY} \cdot \sin(3\vartheta)} = \sqrt[3]{1 + d^{NY} \cdot 1.5 \cdot \sqrt{3} \cdot J_3 \cdot J_2^{-1.5}} \text{ and } \Theta^{SY} = \sqrt[3]{1 + d^{SY} \cdot \sin(3\vartheta)} = \sqrt[3]{1 + d^{SY} \cdot 1.5 \cdot \sqrt{3} \cdot J_3 \cdot J_2^{-1.5}}$$

Lode angle  $\vartheta$ , here set as  $\sin(3 \cdot \vartheta)$  with ‘neutral’ ‘shear meridian angle  $0^\circ$ ; compressive meridian angle  $-30^\circ$ .

A failure body is rotationally-symmetric if  $\Theta = 1$

Equation of the yield failure body:  $Eff = [(Eff^{NY})^m + (Eff^{SY})^m]^{m-1} = 1 = 100\%$  total effort, interaction

$0 < d^{NY} < 0.5$ ,  $0 < d^{SY} < 0.5$ , meridian angles  $\vartheta$ :  $\bar{R}_{0.2}^t, 30^\circ$ ;  $\bar{R}_{0.2}^{tt}, -30^\circ$ ;  $\bar{R}_{0.2}^c, -30^\circ$ ;  $\bar{R}_{0.2}^{cc}, 30^\circ$



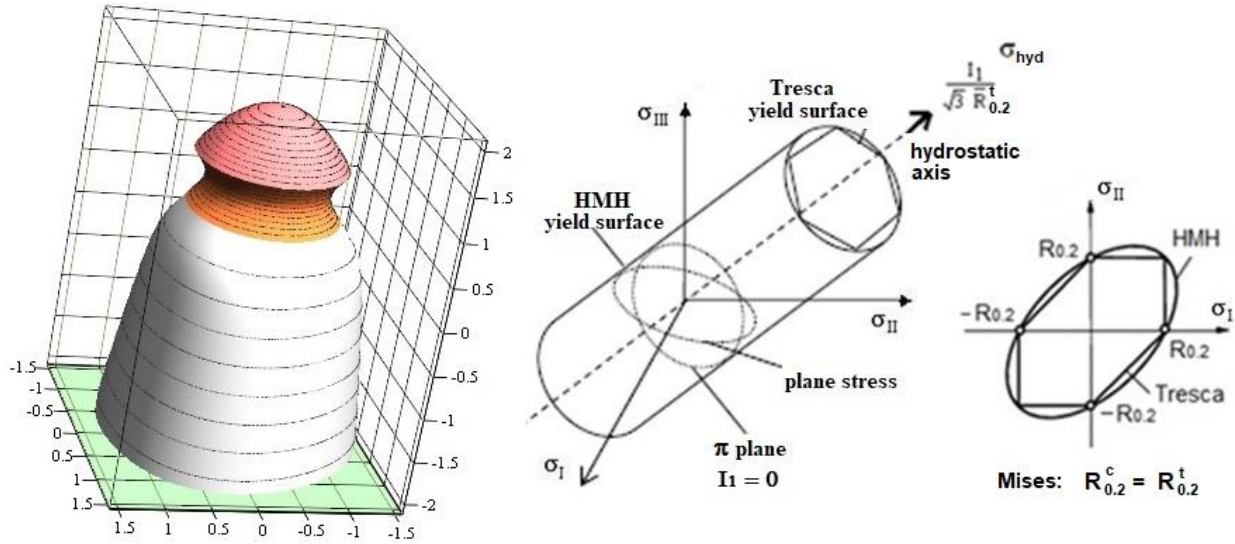


Fig.5-4 PMMA: (left) Onset-of-Yield surface (NY with SY) and for comparison Hencky-Mises-Huber with the Tresca yield surface (engineering yield strengths are used)

$$\bar{R}^I = 37; \bar{R}^{II} = 36; \bar{R}^{III} = 42; \bar{R}^c = 60; \bar{R}^{cc} = 69; \sigma_{I_{lm}} = 34, \sigma_{II_{lm}} = 18, \sigma_{I_{t0}} = 48, \\ \sigma_{III_{t0}} = -19. c_1^{NY} = 0.83, c_2^{NY} = 0.66, c_3^{NY} = 0.41, c_1^{SY} = 1.21, c_2^{SY} = 0.24, s^{cap} = -0.81, \\ d^{NF} = -0.26; d^{SF} = -0.08; m = 2.6, \text{ set } \max I_1 = 3 \cdot \bar{R}^{III} = 8.43; \min I_1 = -4.58.$$

Check of identical hoop curve at the Cap-NF contact  $I_1$  performed.

The NY yield failure body is a  $120^\circ$ -symmetric one in the deviator plane. This is captured by  $\Theta(J_3)$ , again.  $I_1^2$  stands for the experienced volume change. Above formula for the failure body is new.

In Fig.5-5 the two main meridians as axial-parallel cross-sections of the failure body are presented (upper part) and further the  $I_1 = \text{constant}$  yield failure curves (lower part).

- In the upper part, the plain failure curves are shown and the magenta coloured curves in the transition zone after interaction.  $\bar{R}_{SY}^c$  is not clearly defined by Sternstein and Matsushige, but this is not essential, because NY-mapping is the objective. So, instead of the not defined  $\bar{R}_{NY}^t$ ,  $\bar{R}_{SY}^c$  the usual denominations for strengths are kept.
- In the lower part, the ' $I_1 = \text{constant}$  yield failure curves' are displayed for the tensile and the uni-axial compressive strength and the bi-axial strength capacity. In addition the most inner ring of the hyperboloid is included (orange).

Fig.5-5 also shows that the Matsushige tests were run along the tensile meridian. On the hoop plane, due to the  $120^\circ$ -symmetry the inserted test points are three times present. For the derivation of the tensile fracture failure body – due to the similar shape – the NY-SFC can be employed too, viewing yield curve and fracture curve presented in [Bre79]. For the compression part is similarly valid, SY  $\rightarrow$  SF.

*Note:* Many years ago the author constructed a hyperboloid function that could map straight test data courses in the principal stress plane for NF-SFC (see the examples before). This NY-SFC enables to manage outward and inward dents in the hoop plane., see Fig.4-5 and 4-6 (principal stress plane).

Fig.5-6 demonstrates, that probably for the first time 3D mapping of the NY yield surface and the combined NY.SY-surface and its 3D visualization was successfully performed. A high interaction

exponent  $m = 5.2$  was applied due to the fact that the two different yield modes do not occur that mixed in the interaction zone as experienced otherwise.

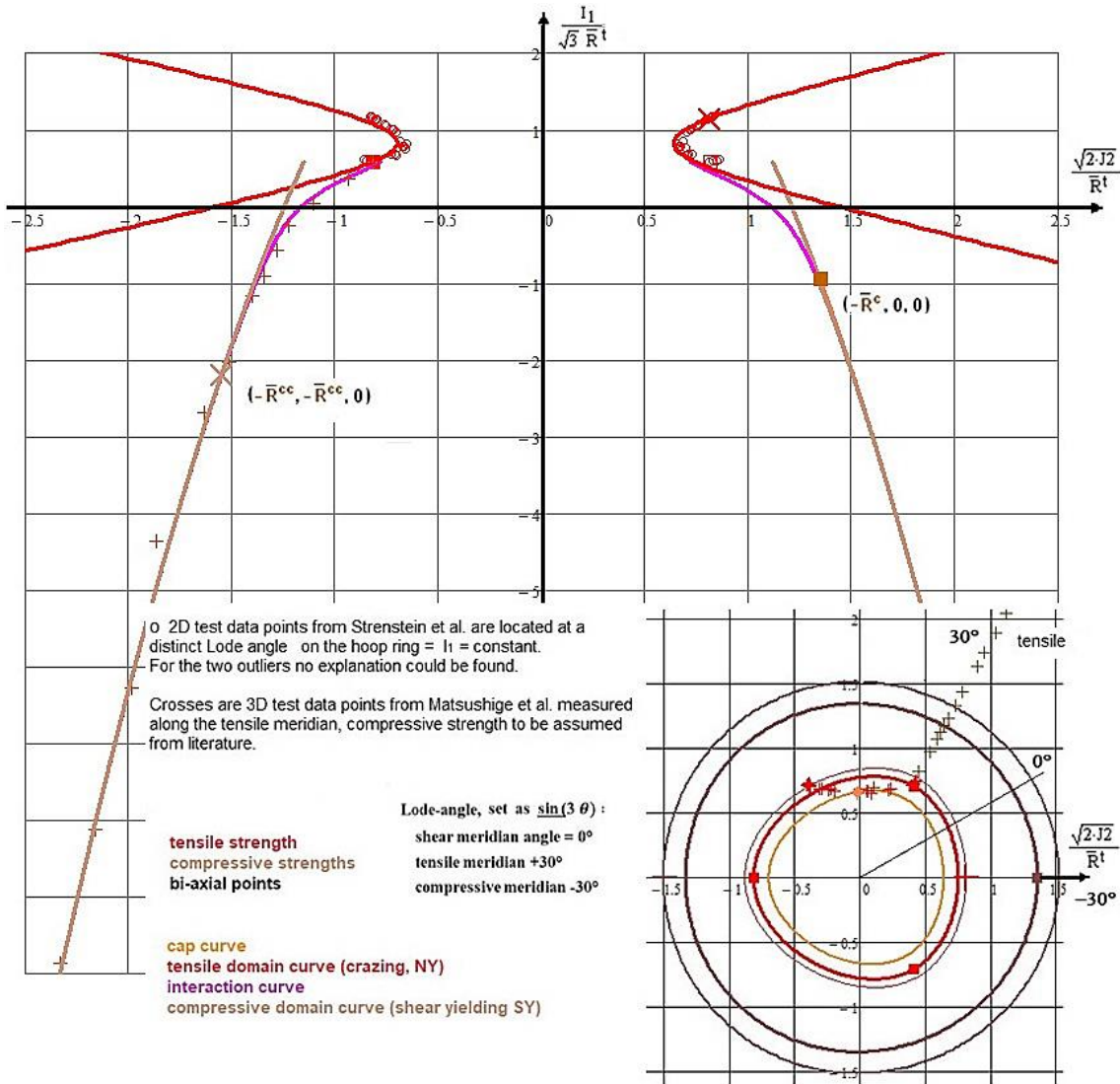


Fig.5-5 PMMA: Tensile (left) and compressive (right) meridians of the fracture body (not optimized, the most negative test points are not shown in the figure); (below)  $I_1$  = cross-sections of the NY-SY-body.

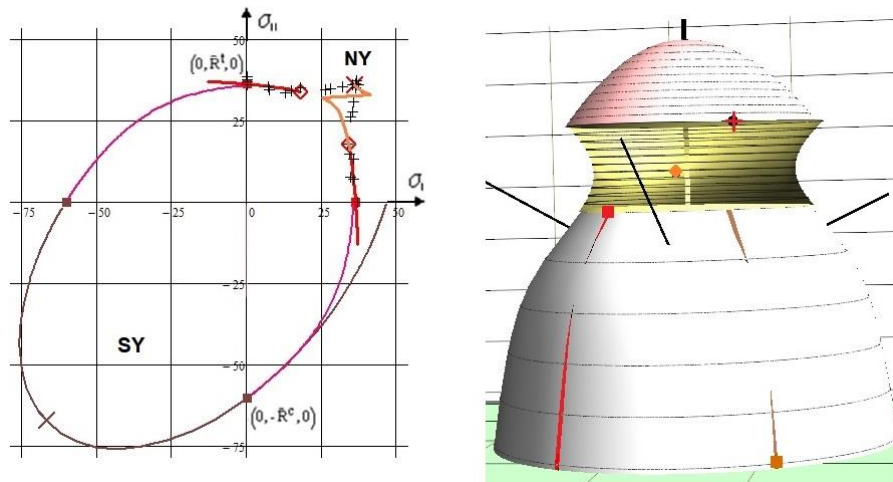


Fig.5-6 PMMA: (left) Mapping test data in tension and compression principal stress domain with and without interaction; (right) depiction of the fracture body shape with some representative points

The visualization of the NY failure surface using Mathcad 15 code (*a 35 DIN A4-pages application*) was very challenging considering the solver that has to face a concave 2D principal stress plane situation instead of a usual convex one. Regarding the successful 3D visualization, the success in the principal stress plane was clouded. Also after a huge effort, the author unfortunately could not obtain a mapping of the upper test data in the first quadrant with the used Mathcad 15 code. The computed mapping curve remains a zig-zag even after several different computational approaches as for example from the outer bi-axial point **X** to the more inner points! Question: Why does the solver in the lower tensile part of the yellow colored failure surface work and captures such a concave situation and in the upper not (**zig-zag** curve in *Fig. 5-6*)? The accurate points on the 3D body surface of the right figure in *Fig.5-6* do not give an answer.

## 5.2 , Some Proof of the 2<sup>nd</sup> ‘Basic’ Stress Intensity Factor $K_{IIcr}^c$

### 5.2.1 General about the 2 basic fracture toughness quantities of isotropic materials

Presumption: An ideally homogeneous isotropic material in front of the flaw, viewed as cracktip.

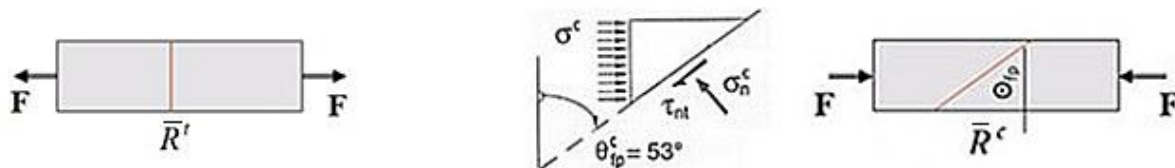
The following investigation is only for the ideal structural mechanics building of importance, In practice, there are usually no ideal homogeneous conditions at the cracktip.

Fracture Mechanics FM is the field of mechanics concerned with the study of the propagation of cracks. These cracks might have been there from the beginning or are formed under loading. Final fracture occurs when cracks propagate up to a defined limit defined by a critical stress intensity factor SIF or fracture toughness  $K_{cr}$ , respectively. The critical SIF  $K_{Ic}$  (later necessarily to be termed  $K_{Icr}^t$ ) is found in a plane strain condition, and is accepted as the defining (basic) property in Linear Elastic Fracture Mechanics, considering tension.

Comparing strength mechanics and fracture mechanics a question of the author is: “*Are there any links between them?*”

Normal fracture NF acts perpendicular to the mathematically highest stress (‘most positive’)  $\sigma_I$ . If a centrally cracked test specimen is loaded up to a certain level, the crack theoretically well grows in the given fracture ‘plane’.  $\bar{R}^t$  and  $\bar{K}_{Icr}^t$  correspond, *Fig.5-7*.

Shear Fracture SF occurs under a compressive stress, that causes a critical combination of the Mohr stresses  $\sigma_n, \tau_n$ , leading to a fracture plane angle  $\theta_{fp}^c$ . If a cracked test specimen is loaded up to a certain level the question arises: Does the crack keep its original plane? "Is there a crack plane-linked ‘transition’ from 'Without crack' (strength mechanics) to 'With crack' (fracture mechanics) also in the compression domain  $I_1 < 0$  ? ”



*Fig.5-7: Fracture angles of brittle material under tension and compression; (left) NF with tensile strength, (right) SF with compressive strength*

*Note: In order to cope with the generally in structural engineering used indexing, one has to keep <sup>c</sup> for compression and <sup>t</sup> for tension and set critical <sub>cr</sub> for all fracture-mechanical quantities instead of the suffix <sub>c</sub>*

A first response is:

From material symmetry information one could conclude that the number of fracture toughness quantities or crack resistances, which are equivalent to the (basic) critical SIFs, is the same as the number of strength fracture resistances, namely  $R^I$  and  $R^C$ . The number of the (basic) critical SIFs may be also two, namely  $K_{Icr}^I \equiv K_{Ic}$  and  $K_{IIcr}^C$ .

Focusing tension: According to the multi-dimensional stress state present cracks in materials usually do not propagate along their original crack plane but under so-called ‘mixed mode loading’ on curved paths in which the specific singularity situation at the crack tip is decisive.

The decomposition of a loading state into the three basic deformation modes, the fracture mechanics Modes-I, -II, -III, was introduced by Irwin and the different deformations he indicated by arrows, see *Table 4-3*. These deformation states are usually linked in literature, however, to crack driving loadings and then further to stresses: Mode I – Opening mode (a tensile stress normal to the plane of the crack), Mode II – Sliding mode (a shear stress acting parallel to the plane of the crack and perpendicular to the crack front), and Mode III – Tearing mode (out-of-plane shear loading).

Structural engineers, who apply FM tools for predicting lifetime by damage tolerance means, are used to think in stresses. Therefore they claim "*The fracture mechanics modes FM II and III are not in local equilibrium*". Bouquet’s faces clearly depict this in *Table 5-3*. Of course, the consequence of being not in equilibrium is a turning of the original crack-plane into a direction normal to the principal *tensile* stress  $\sigma_1$ . And this happens to be. The crack runs out of the original ligament plane.

Focusing compression: There is another engineering domain, namely geo-engineering and rock fracture mechanics, that is pretty decoupled from the tension domain in mechanical engineering, but where FM plays a big role. The cracks to be faced here under compression loads are many meters long and more. Here,  $K_{IIcr}^C$  is the focus but usually prevented by the secondary wing-cracking accompanied by splitting! Therefore, the situation to detect it and to measure it is complicated.

At the crack tip a local perturbation caused by for instance a stiff or a too large grain can change the local stress singularity situation by not generating a desired ‘fine grained, homogeneous micro-structure’. Then the modelling-desired ideal homogenization state is violated and splitting of the brittle test specimen will occur.

Author’s postulate employing crack path stability:

**Only an angle-stable, self-similar crack growth plane-associated SIF is a ‘basic’ FM property.**

#### Notes

- (1) *FM Mode I delivers a real (‘basic’) fracture resistance property generated under a tensile stress. Both the Modes II  $K_{IIc}$ , and III  $K_{IIIc}$  do not show a stable crack plane situation but are nevertheless essential FM model parameters to capture ‘mixed mode loading’ for performing a multi-axial assessment of the far-field stress state.*
- (2) *With the Mode-II compressive fracture toughness  $K_{IIcr}^C$  it is like with strength. One says compressive failure, but actually shear (stress) failure is meant, compressive stress is ‘only’ the descriptive term. The index II is to take.*

Literature seems to support the author who assumes that there are two basic critical SIFs, only. His more detailed definition of such a basic SIF is: *The direction of the crack progress remains in the*

distinct plane if the stress situation remains the same and the singularity situation at the crack tip is not changed by for instance a large grain (then it is not a theoretically ideal situation anymore). In other words, the crack increases in its original plane, if the stress state remains in the crack case as in the formerly (non-cracked) strength case. This should be valid in the compression domain, too.

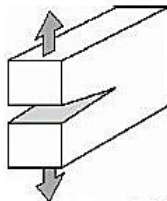
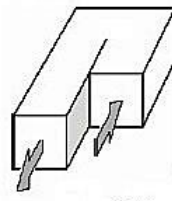
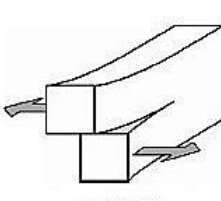
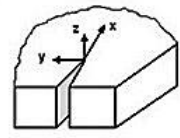

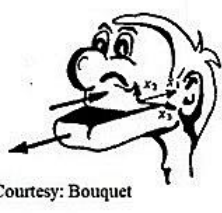

- Tension domain: One knows from  $K_{Icr}^I$  (tension), that – viewing the angle - it corresponds to  $R^I$ .
- Compression domain: The not generally known second basic SIF  $K_{IIcr}^c$  seems to exist under ideal conditions. It corresponds to shear fracture SF happening under compressive stress and leading to the angle  $\Theta_{fp}^c$ . The crack surfaces are closed for  $K_{IIcr}^c$ , friction sliding occurs.

The author’s postulate “ $K_{IIcr}^c$  exists” is firstly supported by an experiment with cracked test specimens under compression and secondly by a still available  $K_{IIcr}^c$  formula substantiated by the maximum value of the material stressing effort  $Eff$  for  $\alpha = 90 - \Theta_{fp}^c$ .

### 5.2.2 Some experimental proofing of $K_{IIcr}^c$

A first proof of the author’s postulate could be: There is a minimum value of the compressive loading at a certain fracture angle. This means that the  $K_{IIcr}^c$  becomes a minimum, too. Liu et al performed in [Liu14] tests using a cement mortar material. They describe the test investigations as “The specimens were square plates of 180mm×180mm×50mm, with three collinear artificial and penetrated cracks, which measure 20 mm in length. The ratio of cement, sand, and water was 1 : 1 : 0.35 by weight. The cracks were made by using a 0.1 mm film, placed during casting. Curing period was 28 days. Under controlled temperature 130°C for 2hrs, the films can be easily pulled out. The crack length and their interval distance are the same and equal 1.0 cm. The test specimens were loaded by a tri-axial loading device: The vertical loading is the major principal stress  $\sigma_1$  and the two horizontal confining stresses are kept as constants during the process of vertical loading.

Table 5-2: Fracture mechanics modes, stress states

|  |   |   |   |
|--|---|---|---|
|  <p>mode I</p>          |  <p>mode II</p>        |  <p>mode III</p>         |    |
|  <p>tensile opening</p> |  <p>in-plane shear</p> |  <p>anti-plane shear</p> | <p>structural stresses <math>\{\sigma\} =</math></p> $(\sigma_x, \sigma_x, \sigma_x, \tau_{yz}, \tau_{xz}, \tau_{xz})^T$ <p>principal stresses <math>\{\sigma\}_{prin} =</math></p> $(\sigma_I, \sigma_{II}, \sigma_{III})^T$ <p>Mohr stresses <math>\{\sigma\}_{Mohr} =</math></p> $(\sigma_t, \sigma_n, \sigma_n, \tau_{nt}, \tau_{tl}, \tau_{nt})^T$ |

Courtesy: Bouquet

Table 5-3: Considerations about stress states, possible fracture angle plane and fracture toughness ( $\alpha$  = inclination angle, angle  $\Theta_{fp}^c$  is measured in compression test, differently defined)

Tension:

$$\text{Full 3D-stress state } \{\sigma\} = (\sigma_x, \sigma_y, \sigma_z, \tau_{yz}, \tau_{zx}, \tau_{xy})^T \equiv (\sigma_I, \sigma_{II}, \sigma_{III})^T$$

with mathematical stresses  $\sigma_I >$  (more positive)  $\sigma_{II} > \sigma_{III}$

$$\{\sigma\} = (0, \sigma_y, 0, 0, 0, 0)^T \equiv (\sigma_I, 0, 0)^T \Rightarrow K_{Ic} = K_{Icr}^t \text{ (stable crack angle)}$$

$$\Theta_{fp} = 0^\circ \quad \leftrightarrow \text{ strength: } (\sigma_n^t, 0)^T \text{ with } \Theta_{fp} = 0^\circ \text{ (fracture angle, NF)}$$

$$\{\sigma\} = (0, 0, 0, 0, 0, \tau_{xy})^T \equiv (\sigma_I, 0, \sigma_{III})^T \Rightarrow K_{IIcr} \leftarrow \text{ (no stable crack angle)}$$

$$\{\sigma\} = (0, 0, 0, \tau_{yz}, 0, 0)^T \equiv (\sigma_I, 0, \sigma_{III})^T \Rightarrow K_{IIIcr} \leftarrow \text{ (no stable crack angle)}$$

if fully ductile, dense:  $\rightarrow \Theta_{fp} = 45^\circ$  inclined yield plane

Full farfield stress states: Superposition possible, if linear problem is applicable,

Mixed Fracture Mode condition: altering angle  $\Theta_{fp}$  turns into the transversal plane of principal tensile stress

$$\{\sigma\} = (0, \sigma_y, 0, \tau_{yz}, 0, \tau_{xy})^T \equiv (\sigma_I, \sigma_{II}, \sigma_{III})^T \leftrightarrow 3D : (\sigma_n^t, \tau_{nt}, \tau_{nl})^T, \Theta_{fp}(x,y,z)$$

The fracture mechanics modes II and III cause a turning of the original crackplane.

Compression:

$$\{\sigma\} = (\sigma_x, \sigma_y, \sigma_z, \tau_{yz}, \tau_{zx}, \tau_{xy})^T \equiv (\sigma_I, \sigma_{II}, \sigma_{III})^T$$

with mathematical stresses  $\sigma_I > \sigma_{II} > \sigma_{III}$

$$\{\sigma\} = (\sigma_x, 0, 0, 0, 0, 0)^T \equiv (0, 0, \sigma_{III})^T \Rightarrow K_{IIcr}^c \text{ (stable crack angle is assumed)}$$

$$\Theta_{fp}^c \text{ ideal crack tip situation presumed } \leftrightarrow \text{ strength: } (\sigma_{ncr}^t, \tau_{ncr})^T \text{ with } \Theta_{fp}^c \text{ (SF fracture angle)}$$

$$\alpha \neq \Theta_{fp}^c \quad \leftrightarrow \text{ strength: } (\sigma_n^t, \tau_{nt})^T \text{ (no stable crack angle, wing cracks created)}$$

Full farfield stress states: Superposition possible, if linear problem is given.

Different stress states lead to different Mohr stress states and different failure planes  $\Theta_{fp}$

$$\{\sigma\} = (\sigma_x, 0, 0, \tau_{yz}, 0, \tau_{xy})^T \equiv (\sigma_I, \sigma_{II}, \sigma_{III})^T \leftrightarrow 3D : (\sigma_n^c, \tau_{nt}, \tau_{nl})^T, \Theta_{fp}(x,y,z)$$

$$\{\sigma\} = (\sigma_x, \sigma_y, 0, 0, 0, 0)^T \equiv (\sigma_I, 0, \sigma_{III})^T \leftrightarrow 3D : (\sigma_n^c, 0, \tau_{nl})^T, \Theta_{fp}(x,y,z)$$

$$\{\sigma\} = (\sigma_x, \sigma_y, \sigma_z, \tau_{yz}, \tau_{zx}, \tau_{xy})^T \equiv (\sigma_I, \sigma_{II}, \sigma_{III})^T \leftrightarrow 3D : (\sigma_n^c, \tau_{nt}, \tau_{nl})^T, \Theta_{fp}.$$

One of the horizontal stresses is denoted  $\sigma_3$ , and the other one  $\sigma_2$ , as shown in [Fig.5-9](#). In order to avoid the effect of the friction between the specimen and the loading device, the specimen surfaces were smeared with oil before testing”.

$\rightarrow$  The significant result of this test series is: A minimum value is located at about  $\alpha = \Theta_{fp}^c \approx 45^\circ$ . That fits relatively well. Of course there is some difference between three collinear cracks and a single crack.

The validity of the results, to use them as a proof, would have been improved if the angle  $\alpha = 50^\circ$  had been tested, too.

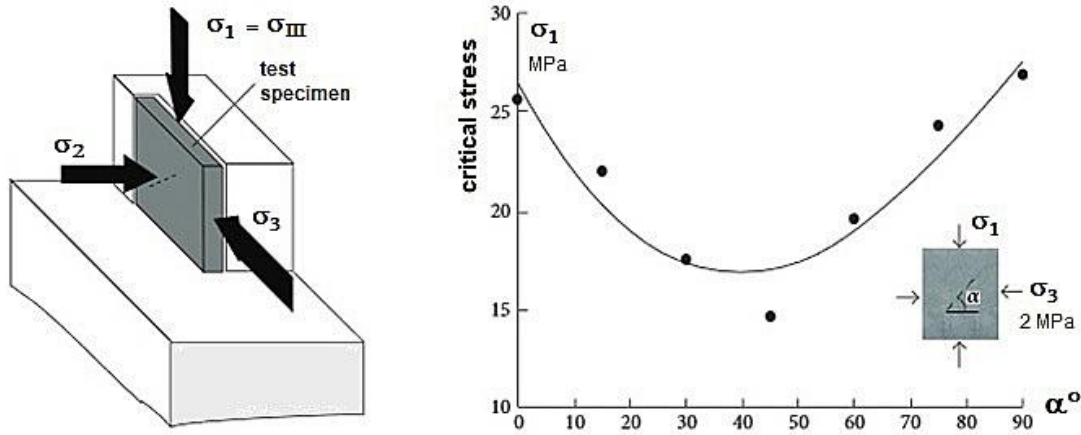


Fig.5-9: Scheme of the test set-up and of the test points obtained for cement mortar [Liu14],  $\sigma_1$  represents the mathematical stress  $\sigma_{III}$  (largest compressive stress value). Here, literature defines  $\Theta_{fp}^c = \alpha$

Formulation and course of the SIF  $K_{IIcr}^c$  :

The author believes – as a second proof for the existence of the fracture toughness  $K_{IIcr}^c$  - that a formula is still available. PH Melville published in [Mel77] (in literature not available, information from [Pha03])

$$K_{IIcr}^c = \sigma \cdot \sqrt{\pi \cdot a} \cdot \sin(\alpha) \cdot [\cos(\alpha) - \tan(\varphi) \cdot \sin(\alpha)] \quad \text{with}$$

$\sigma$  = far field stress,  $a$  = half crack size,  $\alpha$  = flaw (crack) angle and  $\tan(\varphi) \cong \mu$  .

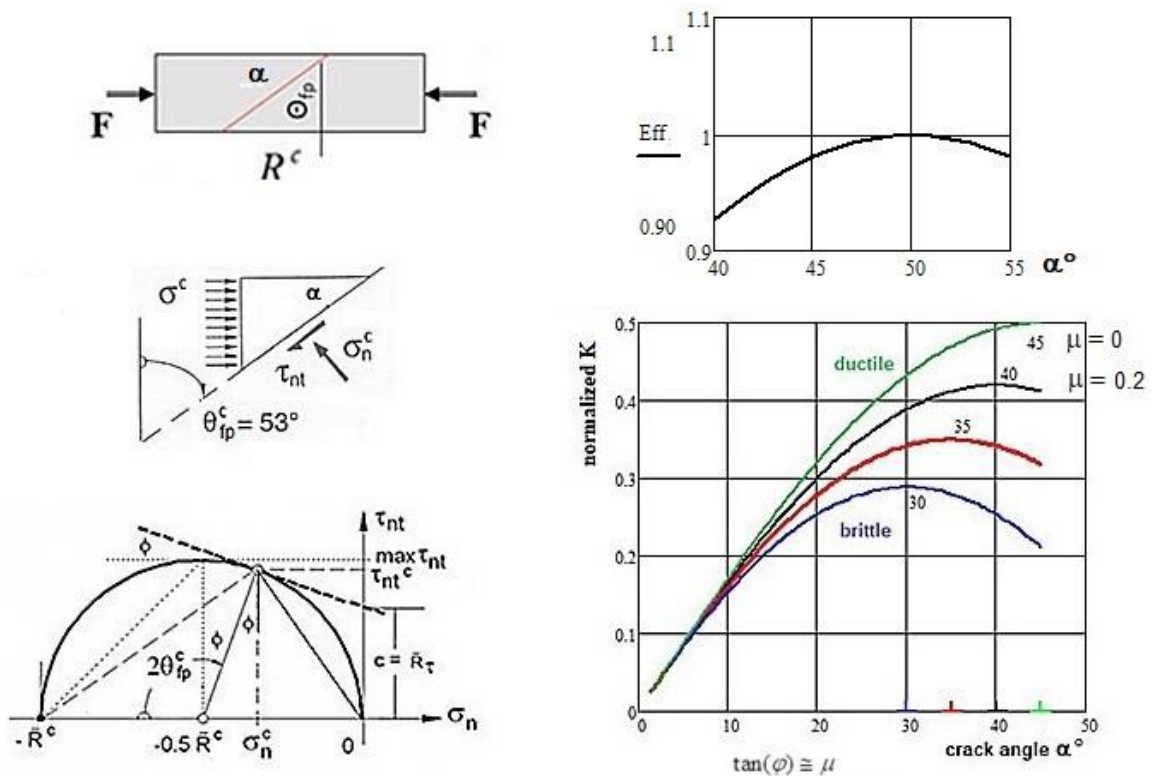


Fig.5-10: (left) the different angles in strength, Mohr-Coulomb; (right up) dependence of the material stressing effort  $Eff$  on the inclination angle  $\alpha$ , (right down)  $K_{IIcr}^c$  versus inclination crack  $\alpha$  considering the friction value  $\mu$  (here  $\Theta_{fp}^c = 90^\circ - \alpha$  is valid in literature [Mel77])

The SIF depends on the size of the friction value  $\mu$ . It is the highest, if  $\Theta_{fp}^c = 90 - \alpha$  (as defined here) Fig.5-10.

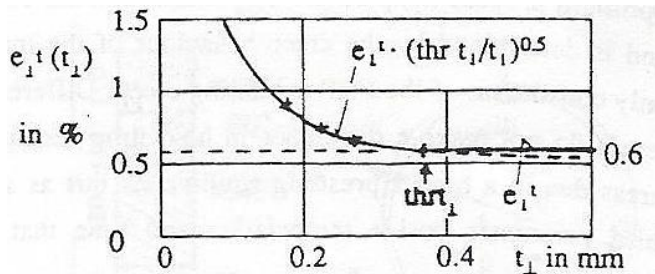
The number on the curves in the right figure marks the maximum value of each ‘friction’ curve.

Exemplarily assuming the usual linear Mohr-Coulomb  $\tan(\varphi) = \mu = 0.2$  means that  $\Theta_{fp}^c = 50^\circ$ . A check of the special case “ductile” with  $\mu = 0$  works as the angle  $\alpha$  then correctly becomes the frictionless shear sliding angle or yield angle  $45^\circ$ .

Finding:  $\rightarrow$  For a brittle material with its associated friction the SIF  $K_{II}^c$  becomes highest when  $\alpha = 90 - \Theta_{fp}^c$ . This means this is the friction-dependent critical situation and that it will lead to further crack growth in this plane.

### 5.2.3 When does flaw size-driven Onset-of-Failure occur?

From fiber-reinforced laminates is known that a strength failure condition SFC as well as an energy condition must be met at onset-of-failure. For thin layers the strength failure conditions used in Classical Laminate Theory are sufficient, for thicker layers a linear elastic fracture mechanics condition (by a SIF) is



Thin-layer effect: Corrective means.  
M40 with MY750/HY917/DY070.  
[Fla82], tube test results

to apply in order to predict failure of the transverse stresses in the ‘90°- layers’. This is a complicate task. An old investigation of [Fla82] gives insight how the layer thickness effect acts. The author simply described it by  $R_{\perp}^t (t_{\perp} < t_{thr}) = R_{\perp}^t \sqrt{t_{thr} / t_{\perp}}$ . It is generally to note: The application of a SFC must be checked whether it is ‘Necessary’ and ‘Sufficient’. Principally it is to check whether any one energy-based condition is on top to take into account, like a LEFM one. Is the energy a minimum one or is  $K$  a maximum one?

This means – in the case of isotropic materials - when linking Strength Mechanics and LEFM to investigate the crack growth angle:

\* Domain  $I_1 > 0$  (tension, classical fracture mechanics):

The maximum hoop stress in front of the crack-tip rules - after Erdogan-Sih - the growth direction of the crack. This practically means that a SFC for NF is employed when investigating the turning of the crack in front of the crack-tip under multi-axial far field stress states.  $K_{Icr}^t (= K_{Ic})$  rules.

\* Domain  $I_1 < 0$  (compression, civil engineering, rock mechanics):

Could it not be that under compression also a SFC for SF can be employed? This SFC considers the energy at fracture failure. At which fracture angle becomes the SF-SFC a minimum? This can be performed by using the material stressing effort  $Eff$  in combination with a minimum necessary energy amount  $G = K^2 \cdot (1 - \nu^2) / E$ . One can pose the questions:



- At which angle does  $Eff$  have a maximum? Applying linear Mohr-Coulomb the material stressing effort follows  $Eff = \tau_n / (R^t - \mu \cdot \sigma_n)$
- At which angle takes the stress intensity  $K$  a maximum?

This is elaborated in the various pictures in *Fig.5-10*, right side, with the response:

*If the inclination angle corresponds to the fracture angle  $\Theta_{fp}^c$ , then a critical state is generated.*

LL:

*A crack  $a$ , inclined the same as a compression-induced fracture shear angle  $\Theta_{fp}$  of the formerly intact isotropic material is linked to minimum energy and to a maximum SIF. Both these values are critical quantities for further crack growth of the solid material element*

### 5.3 Transversely-isotropic UD lamina materials, 5 fracture toughness properties

#### 5.3.1 Number of Fracture Mechanics (FM) modes

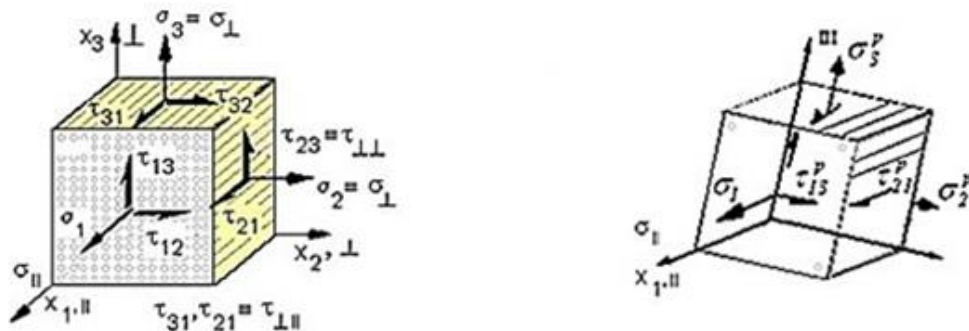
FM is applied micromechanically to investigate the de-bonding of filament-matrix, macro-mechanically to the UD lamina material (*ply or layer as physical lamina*) and to investigate the delamination crack of the laminate. In order to assess the associated stress states the corresponding critical stress intensity factors (*fracture toughness properties*)  $K_{cr}$  are to determine. Beside this, it is intended to give another proof that the ‘generic’ number for the transversely-isotropic UD material is 5.

Before planning an FM test program the probable number of fracture mechanics modes should be derived. After transformation into the quasi-isotropic plane  $\sigma_2 - \sigma_3$  from the former 6 lamina stresses 5 stresses remain. Due to the material symmetry and after switching to the unambiguously symbolic indices it is valid (see *Fig.5-11*):

$$\{\sigma\} = (\sigma_1, \sigma_2, \sigma_3, \tau_{23}, \tau_{31}, \tau_{21})^T \rightarrow$$

$$\{\sigma^{pr}\} = (\sigma_1, \sigma_2^{pr}, \sigma_3^{pr}, 0, \tau_{31}^{pr}, \tau_{21}^{pr})^T \rightarrow \{\sigma^{pr}\} = (\sigma_{\parallel}, \sigma_{\perp}^{pr}, \sigma_{\perp}^{pr}, 0, \tau_{\parallel\parallel}^{pr}, \tau_{\perp\parallel}^{pr})^T.$$

$\sigma_{\parallel}, \sigma_{\perp}^{pr}, \tau_{\perp\parallel}^{pr}$ , neglecting the index  $^{pr}$  leads to  $\sigma_{\parallel}, \sigma_{\perp}, \tau_{\perp\parallel}$  and 5 SFC and 5 FM modes.



*Fig.5-11: Derivation of the number of fracture mechanical modes*

In FM of isotropic materials structural stresses are used. The crack plane may be arbitrary which means a reduction to the principal stress treatment is not possible.

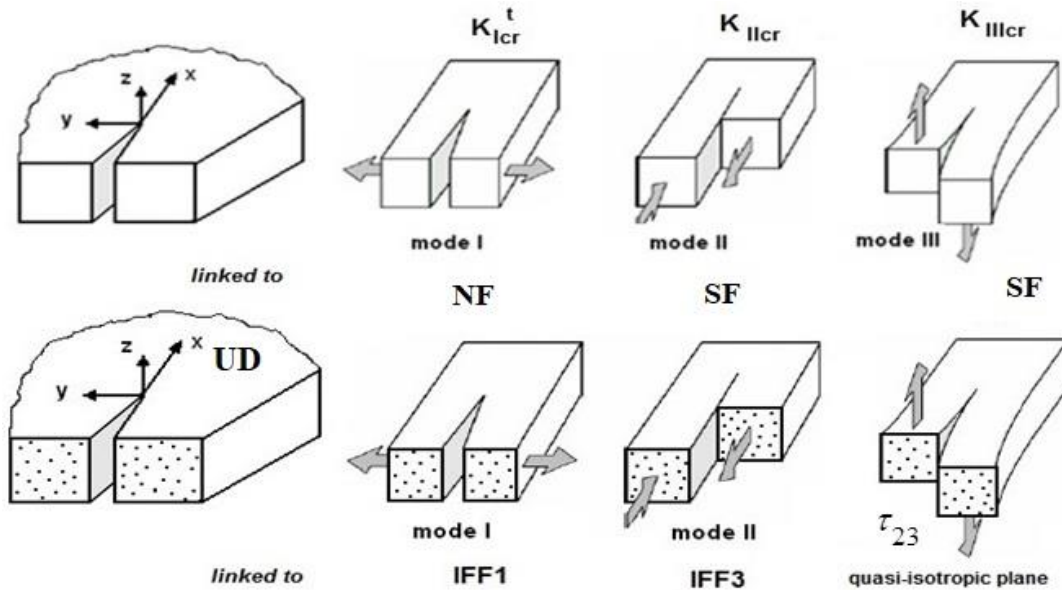
$$\{\sigma\} = (\sigma_x, \sigma_y, \sigma_z, \tau_{yz}, \tau_{zx}, \tau_{xy})^T \equiv (\sigma_I, \sigma_{II}, \sigma_{III})^T$$

In FM of UD materials the crack plane is practically known in case of relatively thin layers and therefore the isotropic FM shear modes II and III are not to consider. The investigation uses principal lamina stresses and by doing that it reduces to 5 UD FM modes, a reduction to the principal stresses is possible.

*Fig.5-12* visualizes the mode differences between isotropic and UD materials.

For UD material, Mode I corresponds to  $\sigma_{\parallel}^t$  ( $\sigma_y \equiv \sigma_n$ ) or  $\sigma_{\perp}^t$ , mode II to  $\tau_{21}$  ( $= \tau_{12}$ ) and mode III to  $\tau_{23}$ . In the case of a UD-lamina  $K_{IIcr}$  ( $\tau_{21}$ ) can be seen – in contradiction to the isotropic  $K_{II}$  ( $\tau_{xy}$ ) – as a real macro-mechanical material property because the fracture plane remains stable under crack growth, due to constraints from the fibre direction. The macro-mechanical stresses are dedicated to single, remote stresses.

The failure condition beyond which the crack will begin to propagate reads  $K/K_{cr} = 1$ . In practical design dimensioning  $K_{cr}$  is reduced to a feasible statistically-based value  $K_{feasible}$ .



*Fig.5-12: Standard fracture mechanics modes for isotropic material and corresponding modes for UD (dots represent the filaments). Mode I opening mode (tension driven), II sliding mode (shear), III tearing mode (scissoring shear), 2D-plate*

Analogous to the SFCs – the following matrix-related and fiber-related stress intensity factors SIFs are to consider. The so-called matrix modes, linked to  $\sigma_{\perp}$ ,  $\tau_{\perp\parallel}$  are pretty clear regarding the crack growth, but there is still some un-clearness about the SIFs K of the 2 fiber modes.

\*  $K_{\parallel}^t$ : Knowledge about this stress intensity factor is necessary, because an assessment of the crack growth is essential for the final stage of fatigue life. From fatigue investigations at the DTU Bent F. Soerensen sorted out for the tensile mode (see the figure below) that, see *Fig.5-13*: (1) Fiber failure is not random, (2) All fibers are broken behind the damage front and intact ahead of the damage front, (3) Failure is row-wise step-by-step, (4) Splitting along the fibers is generated [Soerensen, *Comp. Techn.* 2019], (5) There are stress concentrations at the broken fiber end and at the end of the de-bonded zone which moves along the fiber after further cycling.

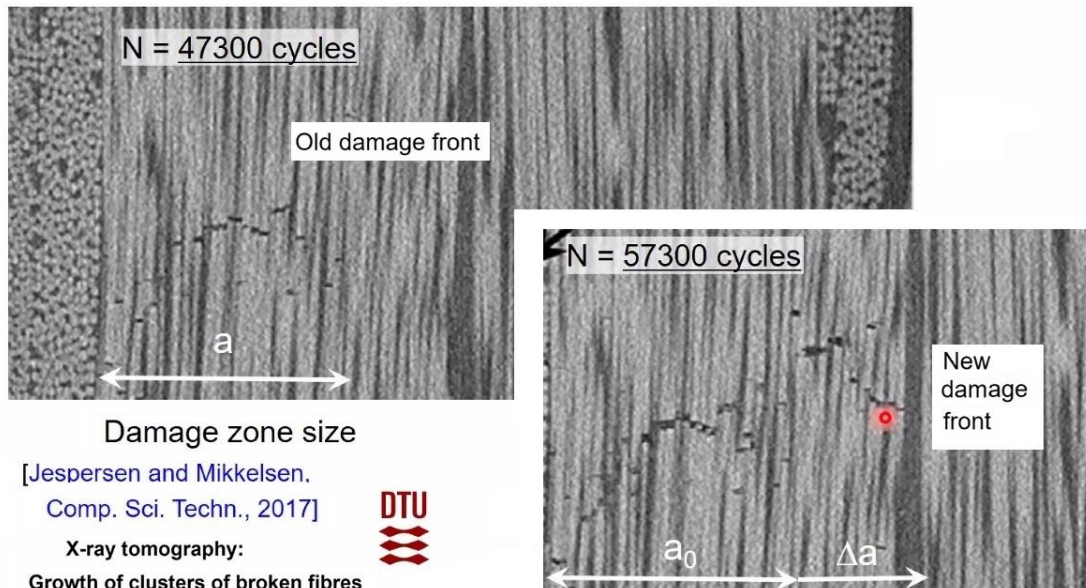


Fig.5-13: Increase of 'crack front'. Presentation B. Soerensen at CU eV.

Fiber/matrix debond growth along the broken filament interface is Mode II-related and described by the strain energy release rate  $\mathcal{G}$ , reading in the very brittle isotropic case  $\mathcal{G} = K^2 \cdot (1 - \nu^2) / E$ . For a long debonding length the interface crack growth is self-similar which means remains in its crack 'plane'. For a short de-bonding length the interface crack interacts with the fiber break and its stress concentration.

\*  $K_{\parallel}^c$ : From practical reasons this property is not of that interest because critical static kinking must be avoided in design.

\*  $K_{\perp}^t, K_{\perp}^c, K_{\perp\parallel}$ : SIFs for cracks within a layer (lamina) or between the layers within a laminate (multilayered tape, sheet). They may be referred to as matrix-linked fracture mechanics modes. UD energy release rates measured, formally follow  $\mathcal{G} = K^2 \cdot (1 - \nu^2) / E$ .

Finally *Fig.5-14* presents a comparing scheme of FM Modes involving isotropic and UD material. The main difference comes whether the crack plane remains in the case of a self-similar crack growth ('thin' layered laminate) or not as for the isotropic materials. Considering the SIF  $K_{II}^c$  the reader is referred to the previous chapter.

Fracture toughness quantities  $\mathcal{G}_i$  for the 3 modes may be determined by standardized tests helping to assess the danger of failure for an onset-of-static crack growth or delamination growth and to assess the cyclic crack growth. Employing again material symmetry reflections for the transversely-isotropic UD-material 5 fracture mechanics modes should correspond to 5 strength failure modes. *Fig.5-15* indicates how 4 of the 5 test specimens look like.

At the ILK/ZLS at Dresden University 4 of the 5 principally necessary UD energy release rates  $\mathcal{G}$  were measured. Problematic for the quality of the test results is that the test specimens (see literature of [Pin06]) may out-of-plane buckle, due to the fact that they are too thin to approximately respect the plane strain condition in order to obtain a real material property.

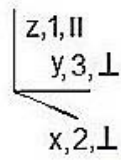
**isotropic material**

**transversely-isotropic material (UD)**

$$\begin{pmatrix} \sigma_x, \sigma_y, \sigma_z, \tau_{yz}, \tau_{zx}, \tau_{yx} \\ \sigma_I, \sigma_{II}, \sigma_{III} \\ \sigma_n, \tau_{nt} \end{pmatrix}^T$$

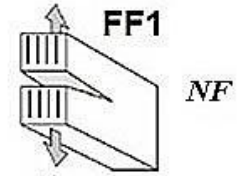
structural stresses  
principal stresses  
Mohr stresses

$$\begin{pmatrix} \sigma_1, \sigma_2, \sigma_3, \tau_{23}, \tau_{31}, \tau_{21} \\ \sigma_1^p, \sigma_2^p, \sigma_3^p, 0, \tau_{31}^p, \tau_{21}^p \\ \sigma_n, \tau_{nb}, \tau_{n1} \end{pmatrix}^T$$



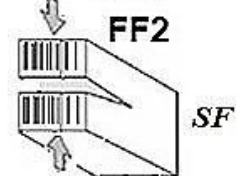
$$\{\sigma\} = (\sigma_1^t, 0, 0, 0, 0, 0)^T$$

$$K_1^t$$



$$\{\sigma\} = (\sigma_1^c, 0, 0, 0, 0, 0)^T$$

$$K_1^c$$



$$\{\sigma\} = (0, \sigma_y^t, 0, 0, 0, 0)^T$$

$$= (\sigma_I, \sigma_{II}, \sigma_{III})^T K_{II}^t$$

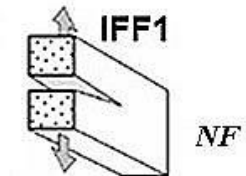
opening mode  
mode I  
crack plane remains

opening mode  
mode I

$$\{\sigma\} = (0, \sigma_2^t, 0, 0, 0, 0)^T$$

$$K_2^t$$

crack plane remains

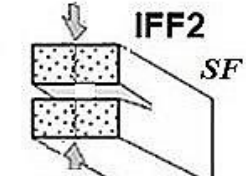


$$\{\sigma\} = (0, \sigma_y^c, 0, 0, 0, 0)^T$$

$$= (\sigma_I, \sigma_{II}, \sigma_{III})^T K_{II}^c$$

$$\{\sigma\} = (0, \sigma_2^c, 0, 0, 0, 0)^T$$

$$K_2^c$$



$$\{\sigma\} = (0, 0, 0, 0, 0, \tau_{xy})^T$$

$$= (\sigma_I, \sigma_{II}, \sigma_{III})^T K_{II}$$

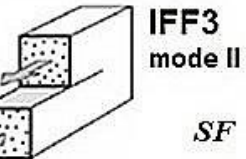
sliding shear  
mode II  
crack plane turns

sliding shear  
mode II

$$\{\sigma\} = (0, 0, 0, 0, 0, \tau_{21})^T$$

$$K_{12}$$

crack plane remains



$$\{\sigma\} = (0, 0, 0, 0, \tau_{xz}, 0)^T$$

$$(\sigma_I, \sigma_{II}, \sigma_{III})^T K_{III}$$

scissoring shear  
mode III  
crack plane turns

scissoring shear  
mode III

$\tau_{23}$   
not given

**Interaction Mixed Mode**

**Strength Failure Modes**

Interaction of all micro-damage contributing stresses by the interaction equation

$$Eff = \sqrt[m]{(Eff^{mode\ 1})^m + (Eff^{mode\ 2})^m + \dots} = 1$$

**Fracture Mechanics Failure Modes**

Interaction of three contributing stresses by the Mixed Mode equation

$$\{\sigma\} = (0, \sigma_y^t, 0, 0, \tau_{zx}, \tau_{xy})^T$$

energy release rate  $G = \sum G_i$   
to be inserted into  $G / G_{feasible} = 1$

$$\{\sigma\} = (0, \sigma_2^t, 0, 0, \tau_{31}, \tau_{12})^T$$

Fig.5-14: Scheme of fracture mechanics modes, stress intensity factors  $K$  (inherent and model-associated ones) of brittle isotropic and brittle transversely-isotropic UD materials.

NF = Normal Fracture, SF = Shear Fracture

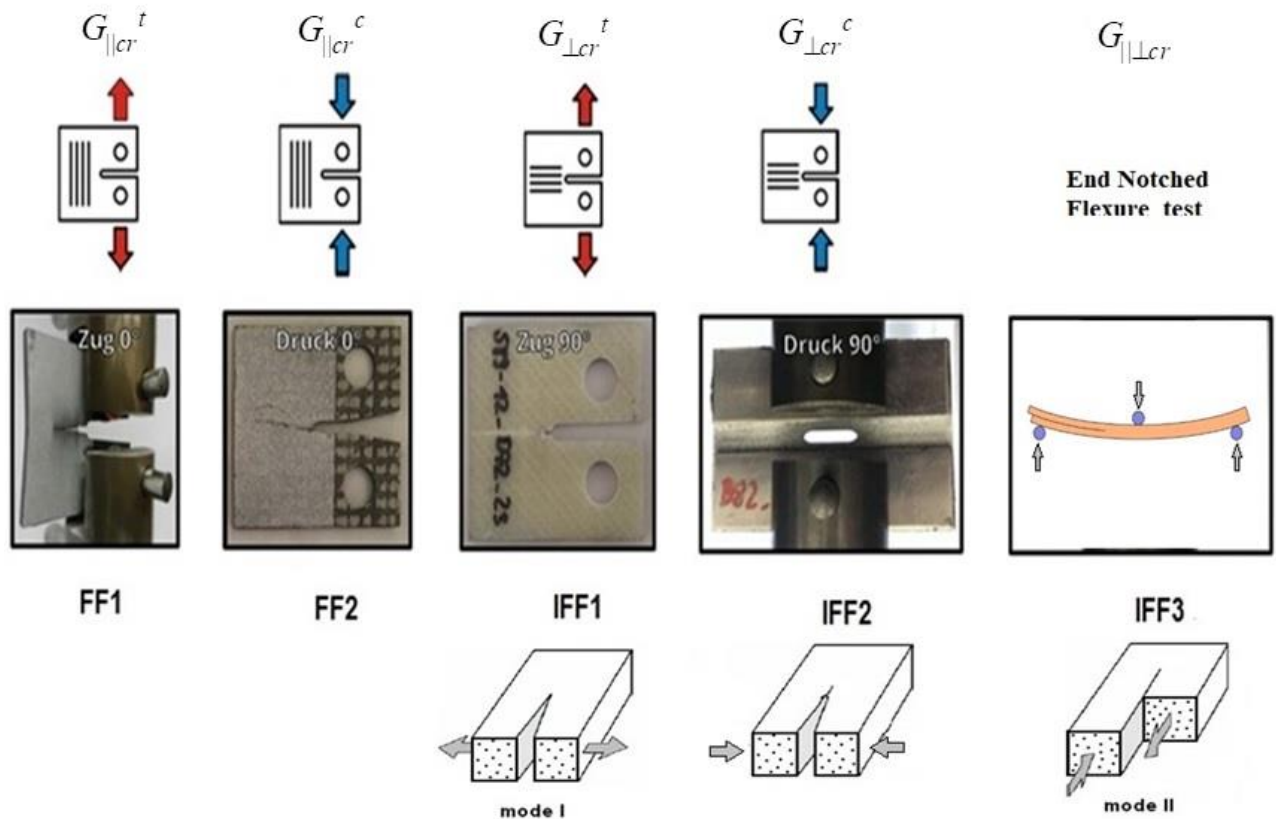


Fig.5-15: Specimens tested under tension in 0°-direction, 90°-direction, and under Compression in 0°-direction, 90°-direction, [ILK, ZLS Dresden].  $G = \mathcal{G}$

**LL:**

\*Confirmation of the author's assumption, that - according to material symmetry - the number of real strength or FM-related material properties is 2 for isotropic and 5 for transversely-isotropic materials !

\*The continuum mechanics approach 'captures' the fracture mechanics approach if the fracture plane remains the same (self-similar) after onset-of-cracking at Initial Failure and further loading.

**5.3.2 Determination of the microcrack-linked softening curve by FM-testing**

Fig.5-15 was a guide to the basic idea of this paragraph, namely the estimation of a softening curve. The shape of this curve is differently described, for instance as a falling straight line. From physical reflections the softening function in *Sub-chapter 3.10* was chosen for a lamina embedded in a laminate and this is also valid for reinforced concrete. Nature usually behaves smooth in strain-controlled situations. A lamina embedded (*strain-controlled by the material vicinity and deformation-controlled by the test rig*) in a laminate or a reinforced concrete matrix (*strain-controlled*) behave similarly and keep a decaying capacity after onset-of-failure (*cracking at 'post peak'*). This is very advantageously in limit load cases. After onset-of-cracking embedded lamina and reinforced concrete contribute to stiffness and load carrying capacity of the designed structural element.

Beyond initial failure or cracking one might assume that FM may be approximately used. Therefore, the assumption of setting the work under the softening curve and under the FM crack progress curve equal  $\mathcal{G}_{cr}$ , offers a comparison to estimate the area content under the softening curve. In the following formula  $\max \delta = \delta_{\text{fracture}}$  and  $\max \gamma \approx 3 \cdot \gamma(\bar{R}_{\perp\parallel})$ .

$$\int_{\gamma \text{ at Onset-of-Fracture}}^{\max \gamma} \sigma_{soft} \cdot \gamma_{soft} \cdot d\gamma = \int_0^{\max \delta} F(\delta) d\delta = \mathcal{G}_{cr}.$$

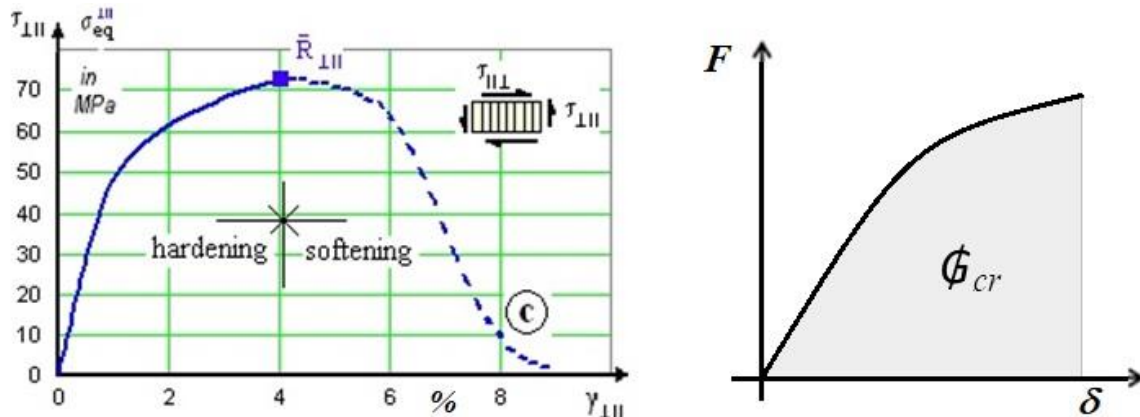


Fig.5-16: Assessment of the area size under the softening curve (example IFF3).  $F$  is force and  $\delta$  deformation or crack opening displacement

Design dimensioning: *laminare deformation-controlled lamina*

Crack growth is initiated when the energy release rate over comes a critical value  $\mathcal{G}_{cr}$  which is a material property that considers material inherent friction.

The associated FM failure condition reads  $\mathcal{G} / \mathcal{G}_{cr} = 1$ .

For an arbitrary combination of all loading modes, the  $\mathcal{G}$ s are superposed.

For the laminate Test Cases, beyond initial failure an appropriate progressive failure analysis method has to be employed (a successive degradation model for the description of post initial failure) by using a failure condition that indicates failure mode and measure for the stress effort and damage. Final failure occurs after the laminate structure has degraded to a level where it is no longer capable of carrying additional load.

The altering micro-crack density has to be regarded up to the characteristic damage state (CDS) where the number of micro-cracks reaches its maximum value and beyond where the initiated micro-cracks just increase their size. The softening curve may therefore termed an 'effective' curve. For the quasi-brittle FRP it can be concluded that so-called cohesive forces still exist at IFF in the fracture process zone at the micro-crack tips in the laminae.

### 5.3.3 Link Continuum Mechanics - Fracture Mechanics

As still mentioned: A SFC is necessary but might not be sufficient for prediction of the initiation of failure (Onset-of-Failure). Examples are locations of stress singularities like the stress concentrations:

- at notches, where the notch stress causes failure even for relatively low far-field stresses
- the influence of the size of a bore has an effect
- the thickness of the in-situ behavior of an embedded layer in a laminate has an effect.

These are typical deformation-controlled stress situations.

When applying SFCs ideal solids are viewed at which are assumed to be free of micro-voids or microcrack-like flaws. When applying FM the solid is considered to contain macro-voids or macro-

cracks. There are usually three approaches treating these states: Strength conditions (SFC), Continuum Damage mechanics (CDM) conditions and Conditions of crack fracture mechanics (FM) employing crack growth models.

A bridge must be built from strength failure conditions to fracture mechanics failure conditions. Neglecting CDM, attempts to link ‘onset of fracture’ prediction methods for structural components are actually undergone. Best known is the Hypothesis of Leguillon [Leg02] :

*“A crack is critical when and only when both the released energy and the local stress reach critical values along an assumed finite crack”.*

While the application to combined stresses is very common in the instance of SFCs it is not at all common to apply crack fracture conditions to 3D states of stress. Based on physical reasons such a bridge should provide a more unified perspective, because - ahead of the crack tip - both approaches are linked together. Such a bridging approach should respect a 3D-farfield state of stress and a full mixed-mode crack situation.

For the stress concentration examples above an energy-based FM failure condition delivers the second condition to check whether failure occurs or whether failure does not occur. After Leguillon Linear Elastic Fracture Mechanics (LEFM) delivers the missing failure condition which is an *energetic failure condition* formulated by the above still used

energy release rate  $\mathcal{G} = \Sigma \mathcal{G}_i$  to be inserted into  $\mathcal{G} / \mathcal{G}_{feasible} = 1$  .

This so-called coupled criterion SFC  $Eff = 1$  together with  $\mathcal{G} / \mathcal{G}_{feasible} = 1$  has a pro-nounced macroscopic nature. In the case of delamination between plies under normal and/or shear stresses, the determination of the critical energy release rate  $\mathcal{G}_{cr}$  is crucial to analyze designs.

Typical methods of determining the critical energy release rate are through experiments, such as the double-cantilever beam (DCB) for mode I, end-notched flexure (ENF) for mode II, and mixed-mode flexure (MMF).

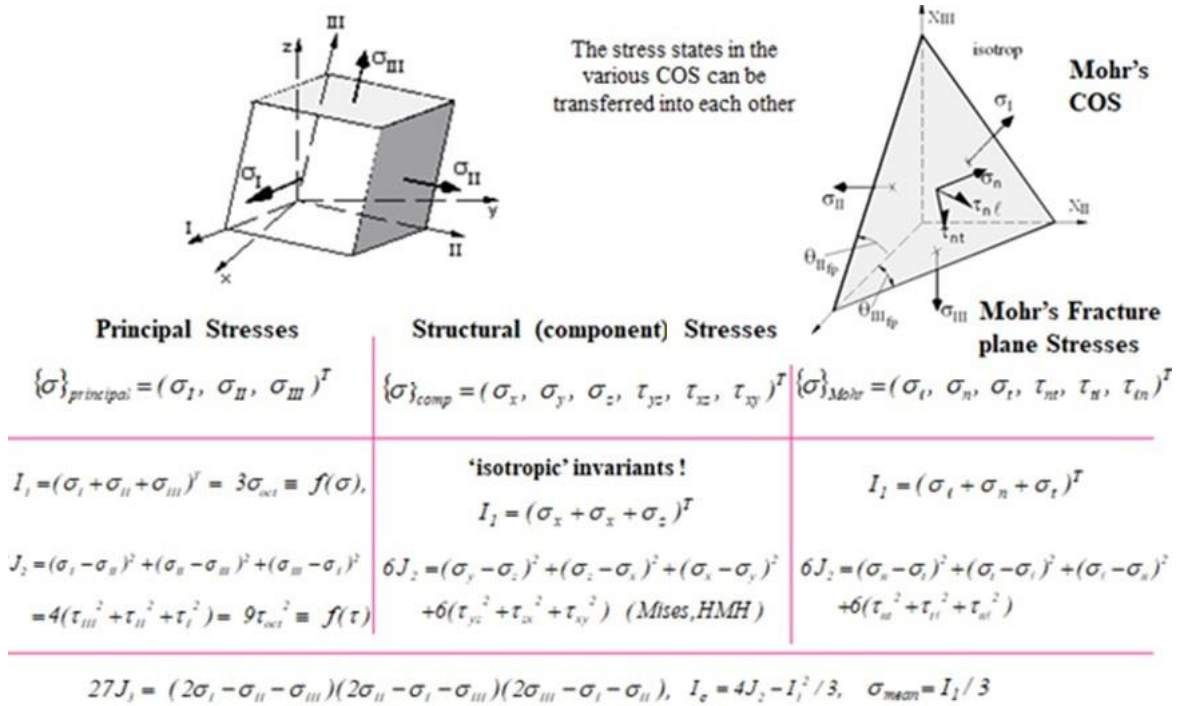
The concept of Finite Fracture Mechanics (FFM) fills a gap in FM, since it is able to offer a framework and criteria for predicting the crack initiation in brittle materials. Classical FM is restricted to the analysis of stability and growth of existing cracks. Instead of the consideration of infinitesimal cracks, as in FM, cracks of finite length are considered within FFM.

*Reminder:*

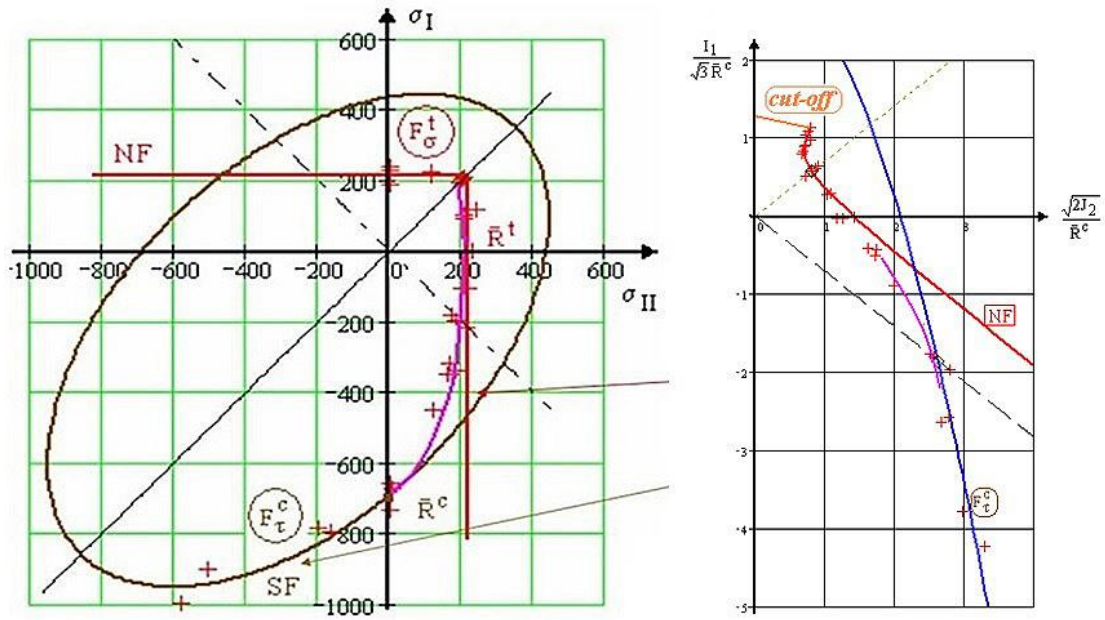
*The FMC is originally energy-based, however, the modified forms may not have sufficiently well kept this previously intended characteristic.*

## 6 Validation by 3D-Applications of the FMC-SFCs to 3 Material Families

At first a repetition of the different stress formulations. (*Sorry for some old figures*)



### 6.1 Isotropic Grey Cast Iron



$$Eff^{NF} = 1 \cdot \frac{\sqrt{4J_2 \cdot (1) - I_1^2/3 + I_1}}{2 \cdot \bar{R}^t} = \sigma_{eq}^{NF} / \bar{R}^t \quad \text{deformation-poor mode}$$

$$Eff^{SF} = \frac{c_2^{SF} \cdot I_1 + \sqrt{(c_2^{SF} \cdot I_1)^2 + 12 \cdot c_1^{SF} \cdot 3J_2 \cdot (1)}}{2 \cdot \bar{R}^c} = \sigma_{eq}^{SF} / \bar{R}^c \quad \text{considers shear deformation and friction}$$

$$\rightarrow Eff = [(Eff^{NF})^m + (Eff^{SF})^m]^{m^{-1}} = 1 = 100\%$$

$$\bar{R}^t = 215 \text{ MPa}, \bar{R}^c = 690 \text{ MPa}$$

$$c_1^{SF} = 1.58, c_2^{SF} = c_1^{SF} - 1 \quad m = 2.6$$

Fig.6-1: 2D-application to Grey-cast Iron [Coffin]. Principal stress plane and meridional cross section



## 6.2 Isotropic Glass C 90 (window pane of ISS)

A glass fiber SiO<sub>2</sub> (E, S, R, AR) is made by blending raw materials, melting them at 1720°C in a three-stage furnace, extruding the molten glass through a bushing in the bottom of the forehearth, cooling the filaments with water (*to prevent the crystallization to quartz and obtain a amorphous, randomly ordered atomic structure we know as glass*) and then applying a chemical sizing. The filaments then are gathered to rovings and wound on spools. Commercial glass fiber can be made from silica alone, other ingredients are added to reduce the working temperature and impart other properties that are useful in specific applications such as making alkali-reistant (by ZrO<sub>2</sub>) for use in concrete. [Source | OCV].

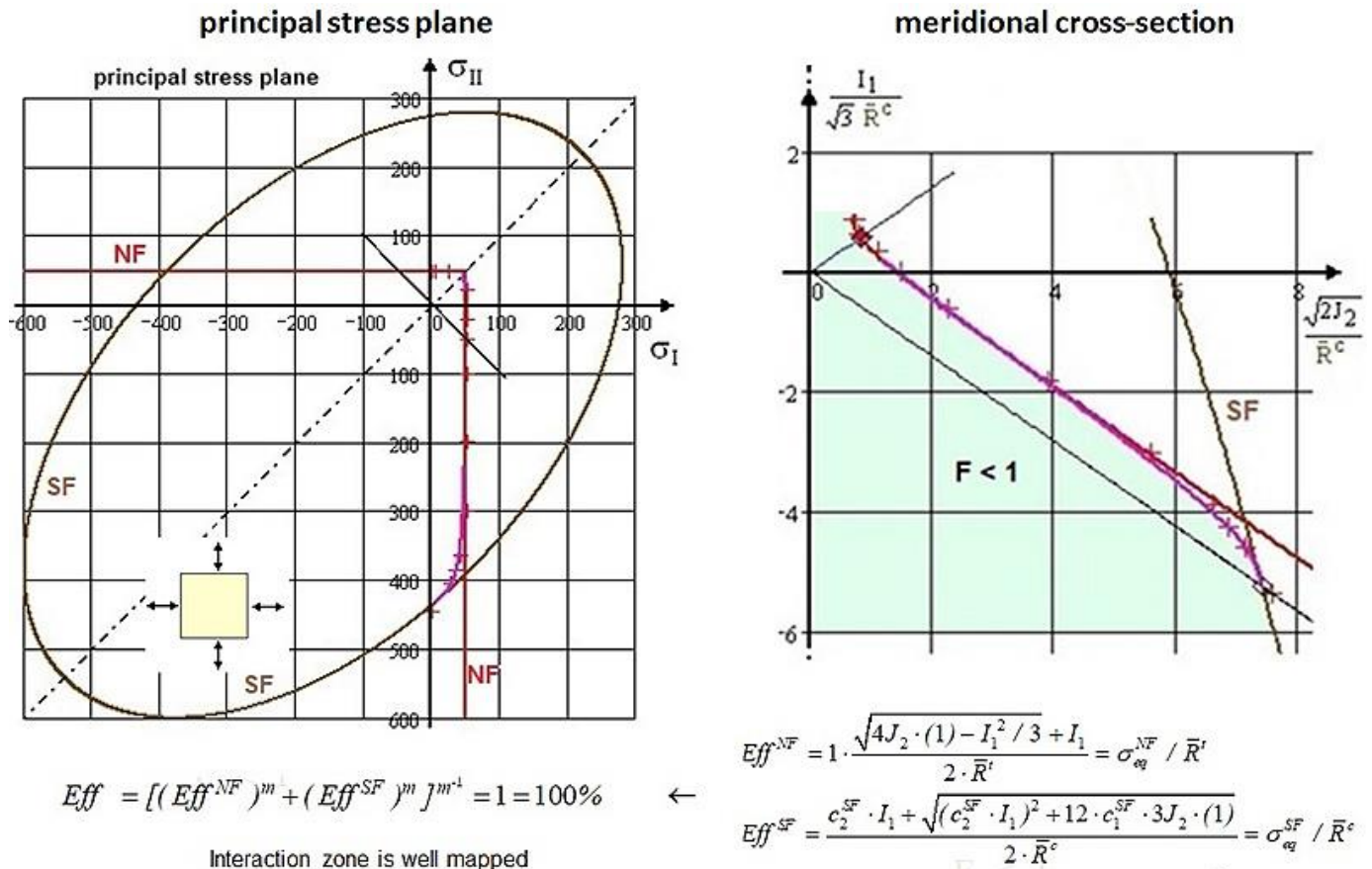


Fig.6-2: Glass C 90 [Kow83]

## 6.3 Isotropic porous Foam Rohacell (SFC is applicable for Concrete Stone material, too)

Usually, for structural parts of high stiffness, honeycombs are used. With the new Rohacell Hero (Evonik) a PMI (Poly-Methacryl-Imide) structural foam of an increased tensile fracture strain is available which may replace the expensive honeycombs. In order to apply this material in structural parts Structural Integrity must be proven. This requires reliable multi-axial strength test data as well as reliable Strength Failure Conditions SFCs (criteria) for an optimal Design Development process. Given is 'only' a 2D - Test Data Set and therefore just a realistic mapping in the Principal Stress Plane is possible. To apply is the 2D subversion of the 3D SFC. → From this follows: Validation of the 3D SFC is 'just' 2D-based.

The data set used reads: (*thanks to Dr. Kolupaev for the test data*)

$\bar{R}^t = 1.8$ ;  $\bar{R}^u = 1.25$ ;  $\bar{R}^{tt} = 1.01$ ;  $\bar{R}^c = 1.65$ ;  $\bar{R}^{cc} = 1.4$ ;  $\bar{R}^{ccc} = 1.53$ ,  $\max I_1 = 3.03$ ;  
 $\min I_1 = -4.58$ ,  $d^{NF} = -0.71$ ;  $d^{CrF} = 0.21$ ;  $c^{CrF} = 1.03$ ,  $s^{cap} = -0.27$ ;  $s^{bot} = 0.87$ ,  
 $g^{NF} = -0.57$ ;  $g^{CrF} = 0.52$ ;  $\Theta^{NF} = 1.2$ ;  $\Theta^{CrF} = 1.07$ ,  $m = 2.5$ .

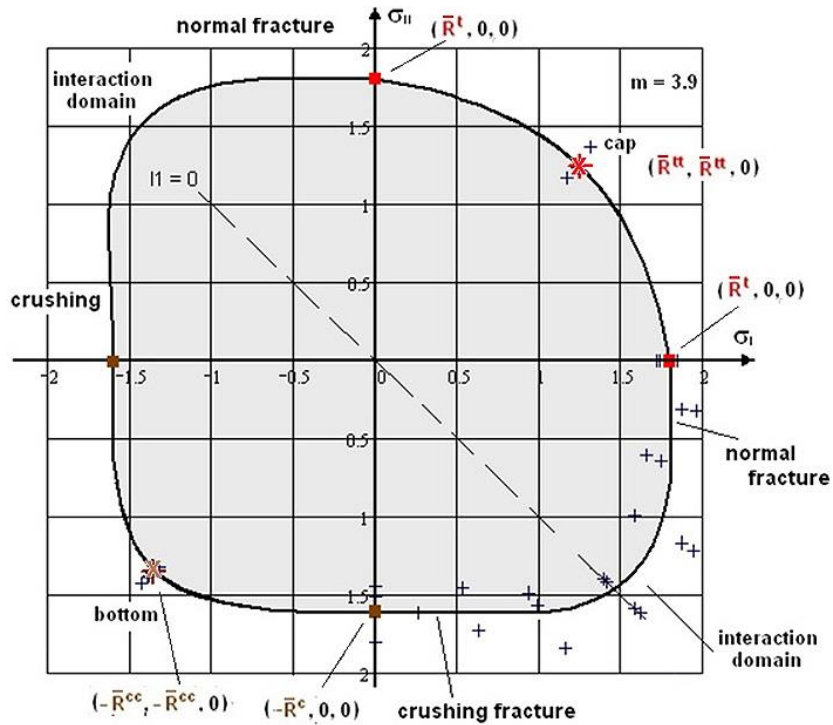


Fig.6-3: Foam Rohacell 71 IG, mapping of 2D-test data in the Principal Stress Plane.  
 MathCad plot [test data: courtesy V. Kolupaev, LBF Darmstadt]

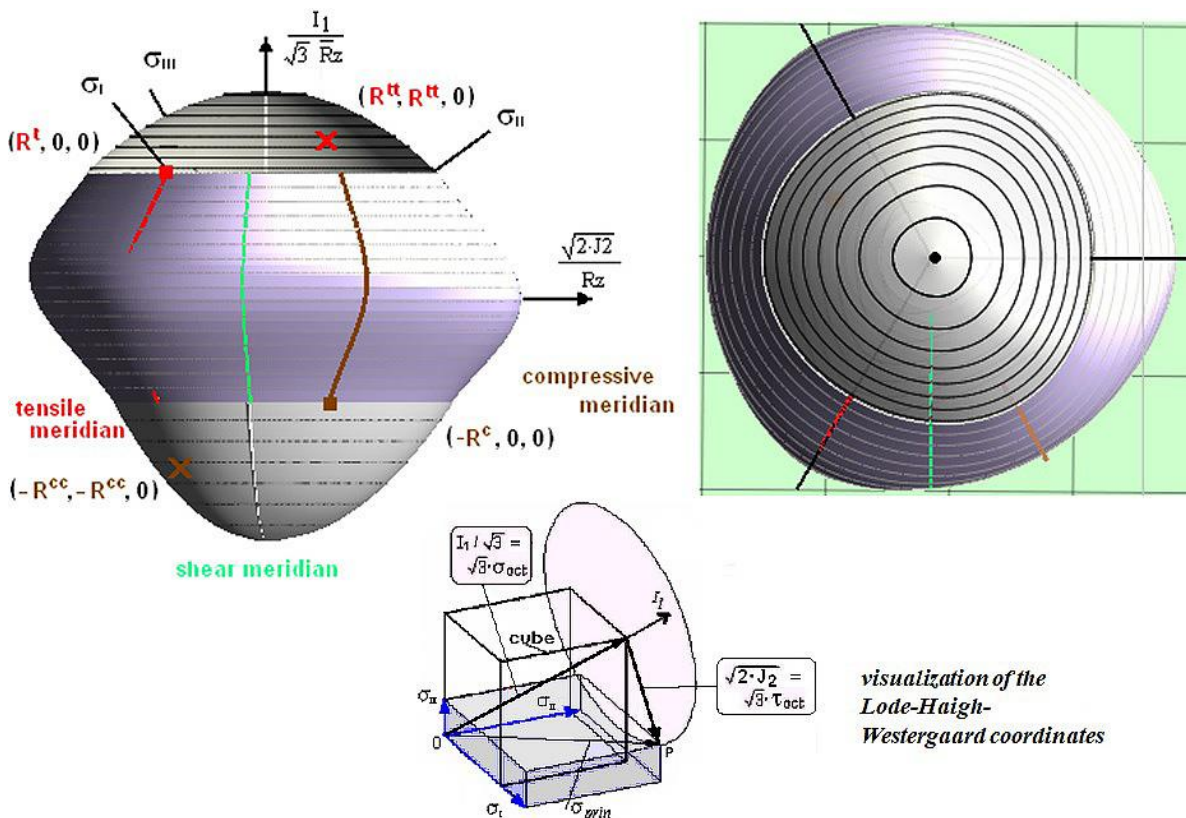
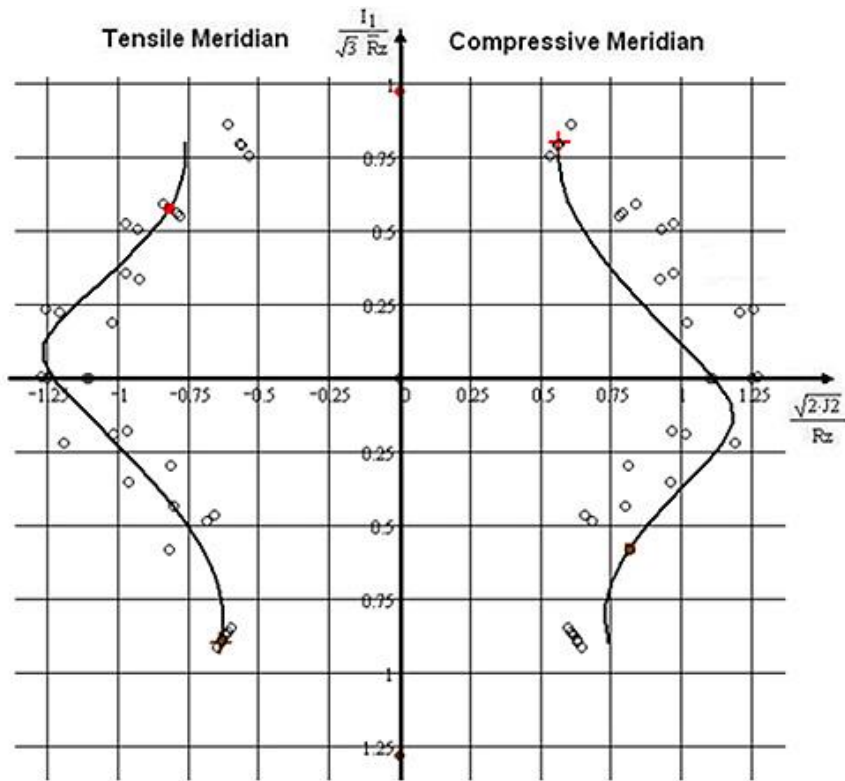


Fig.6-4: Rohacell 71 IG Fracture body with its different meridians (left) and view from top (right).



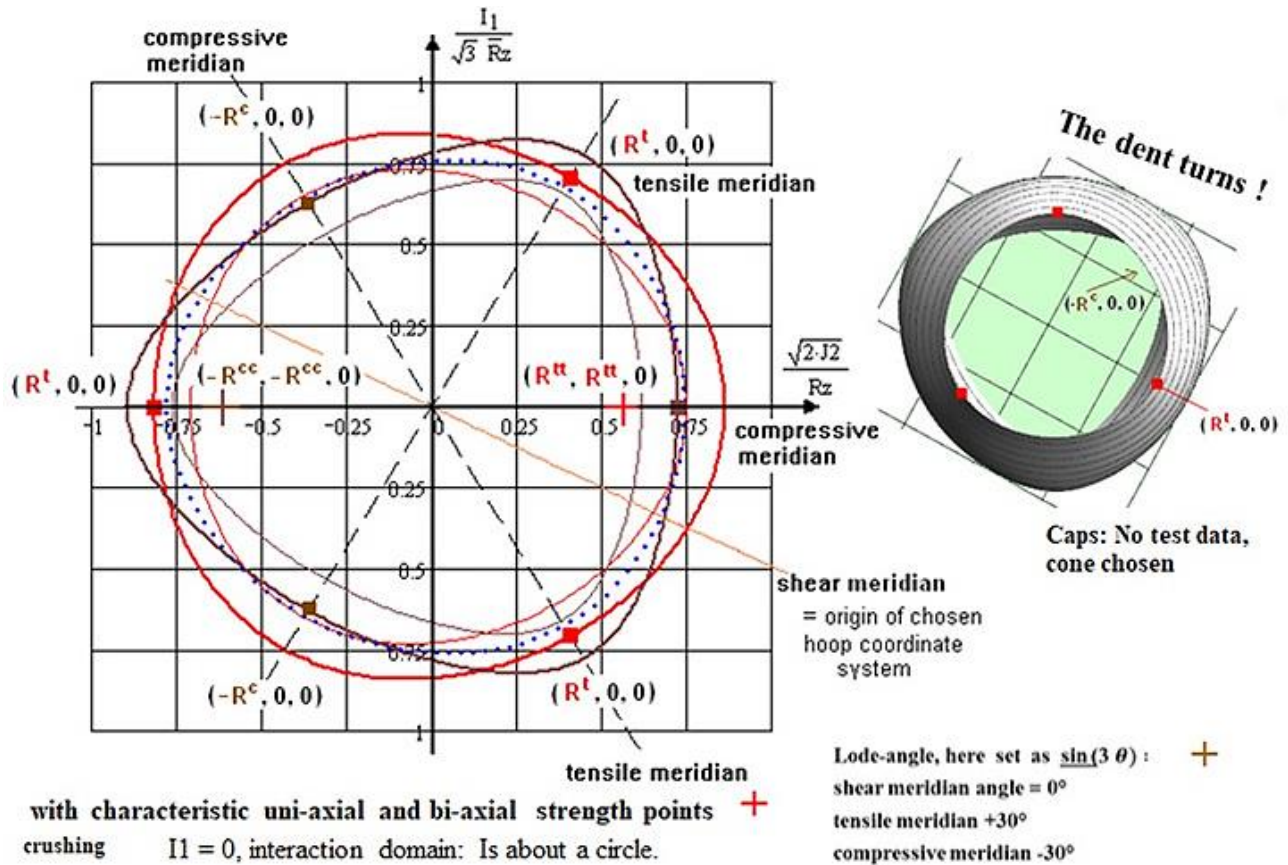
**Meridional cross-section of the Fracture Body**

in Lode-Haigh-Westergaard coordinates

bi-axial = +

consideration of a 'twofold mode' by above well-known approach

Fig.6-5: The test points are located at a distinct Lode angle of its associated ring  $\sigma$ ,  $120^\circ$ -symmetry. Cap and bottom are closed by a cone shape, a shape being on the conservative side



with characteristic uni-axial and bi-axial strength points +  
crushing  $I_1 = 0$ , interaction domain: Is about a circle.

Lode-angle, here set as  $\sin(3\theta)$ : +  
shear meridian angle =  $0^\circ$   
tensile meridian  $+30^\circ$   
compressive meridian  $-30^\circ$

Fig.6-6: 2D Test Data and Mapping in the Orthogonal Stress Plane (brittle, porous) Caps were taken away to better visualize that the dent turns for this material along the hydrostatic axis. Bar over not set

As still mentioned,  $F = 1$  or  $Eff = 100\%$  mathematically defines the surface of the fracture failure body. Such a body is rendered here using the Haigh-Westergaard-Lode coordinates with  $I_1 / \sqrt{3}$  as y-coordinate and  $\sqrt{2 \cdot J_2}$  as x-coordinate. Fig.6-4 depicted the stress states belonging to a tensile meridian and to a compressive meridian. These are those axial cross-sections of the failure body (right) along most of the two above compression tests are run.

Mechanical strength behavior shows up: Different structural materials

- can possess similar material behavior or
- can belong to the same class of material symmetry.

Welcomed Consequence is: The same strength failure function SFC can be used for different materials. The Foam SFC is exemplarily applicable to Concrete Stone. → More information is available for pre-dimensioning + modelling in the case of a newly applied material from the experimental results of a still being tested similarly behaving material.

### 6.4 'Isotropic' Normal Concrete (slightly porous)

On the fracture failure body figure below the 3 main meridians are outlined. For the tensile meridian the Lode angle  $\vartheta = +30^\circ$  is valid and for the compressive meridian  $-30^\circ$ . The shear meridian was chosen by the author as neutral meridian with a Lode angle  $\vartheta = 0$ . For each mode, the SFC model parameters must be determined in each associated 'pure' failure mode domain. To remember is:

*bi-axial tension* = 'weakest link failure behavior' (schwächstes Glied'-Versagen)

*bi-axial compression* = redundant (benign) failure behavior (Stützwirkung)

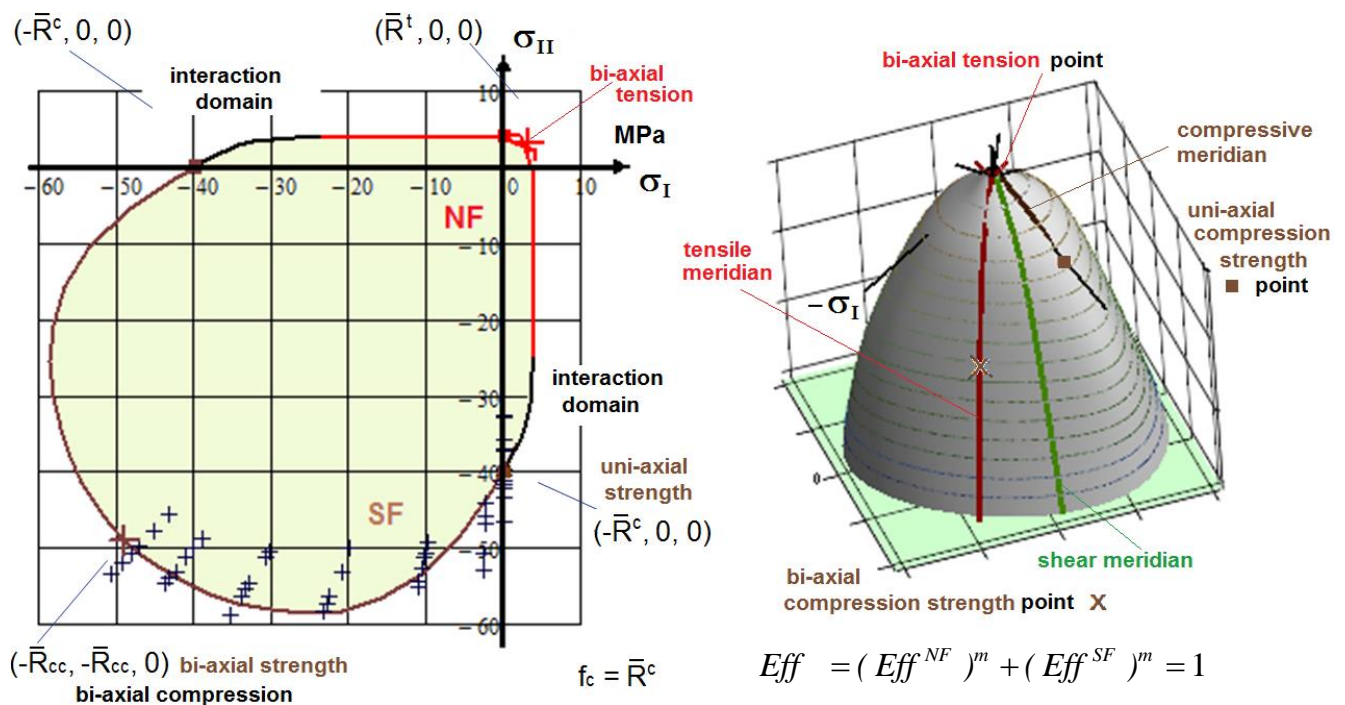


Fig.6-7: Normal Concrete, mapping of 2D-test data in the Principal Stress Plane (bias cross-section of fracture body).  $R$ := strength  $\equiv f$ ;  $t$ :=tensile,  $c$ :=compressive; bar over means mean value.  $\mu = 0.2$ . (test data, courtesy Dr. S. Scheerer, IfM Dresden).

$\bar{R}^t = 4 \text{ MPa}$ ,  $\bar{R}^c = 40 \text{ MPa}$ ,  $\bar{R}^t = 0.8 \cdot \bar{R}^c$  (assumed) = 3.2,  $\bar{R}^{III} = 2.81$ ,  $\bar{R}^{cc} = 49 \text{ MPa}$ ,  
 $\bar{R}^{ccc} = 1000 \text{ MPa}$  (set, necessary for computation),  $\max I_1 = 8.43$ ;  $\min I_1 = -4.58$ ,  $m = 2.5$   
 120°-rotationally-symmetry parameter:  $c_{1\Theta}^{SF} \cdot \Theta^{SF} = 1 + c_{2\Theta}^{SF}$  with  $c_{2\Theta}^{SF}$  as friction parameter  
 $c^{NF} = 0.86$ ,  $d^{NF} = 0.86$ ,  $c_{2\Theta}^{SF} = 0.26$ ,  $c_{1\Theta}^{SF} = 1.04$ ,  $d^{SF} = 0.13$ ,  $\Theta^{SF} = 0.51$ ,  $s^{cap} = -1.31$ .

Conclusion:

Pretty large scatter of the compressive strength data. Mapping of the course of test data in Fig.6-7 worked with the SFCs.

Fig.6.8 through 6.10 present a hoop cross-section ( $\pi$  plane) and two axial cross-sections (meridians) of the failure body. One recognizes that with increasing neagitive  $I_1$  the hoop shape becomes more and more circular.

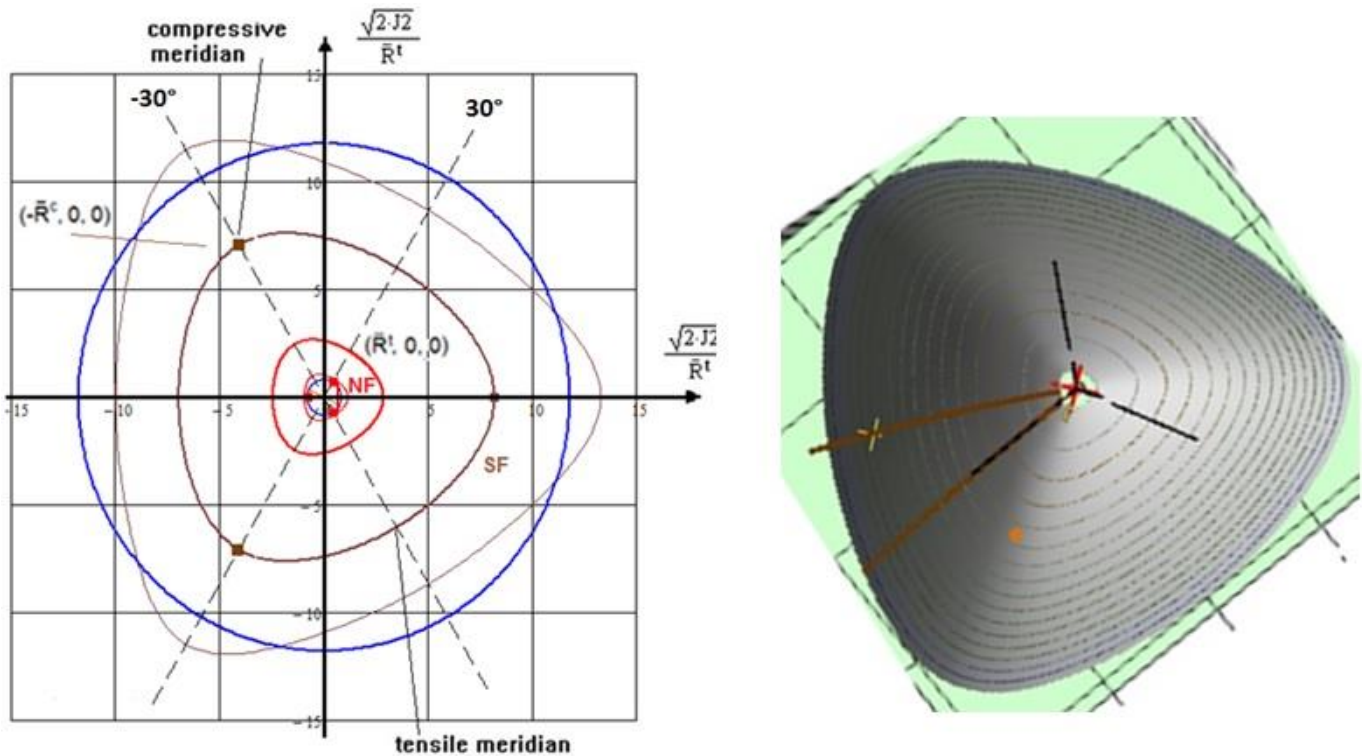


Fig.6-8: Octahedral stress plane or  $\pi$ -plane and view from top  
(blue means plane  $I_1=0$ )

In Fig.6.9 the modeling of cap, normal and shear fracture domain is depicted.

Modelling of the cap is performed by the function  $y_{cap} = \frac{I_1}{\sqrt{3} \cdot \bar{R}^t} = s^{cap} \cdot \left( \frac{\sqrt{2J_2} \cdot \Theta^{NF}}{\bar{R}^t} \right)^2 + \frac{\max I_1}{\sqrt{3} \cdot \bar{R}^t}$ .

Fig.6-10 informs about the test data scatter of the 3D fracture states experienced under hydrostatic pressure when running test on the tensile meridian and on the compressive meridian (-30°).

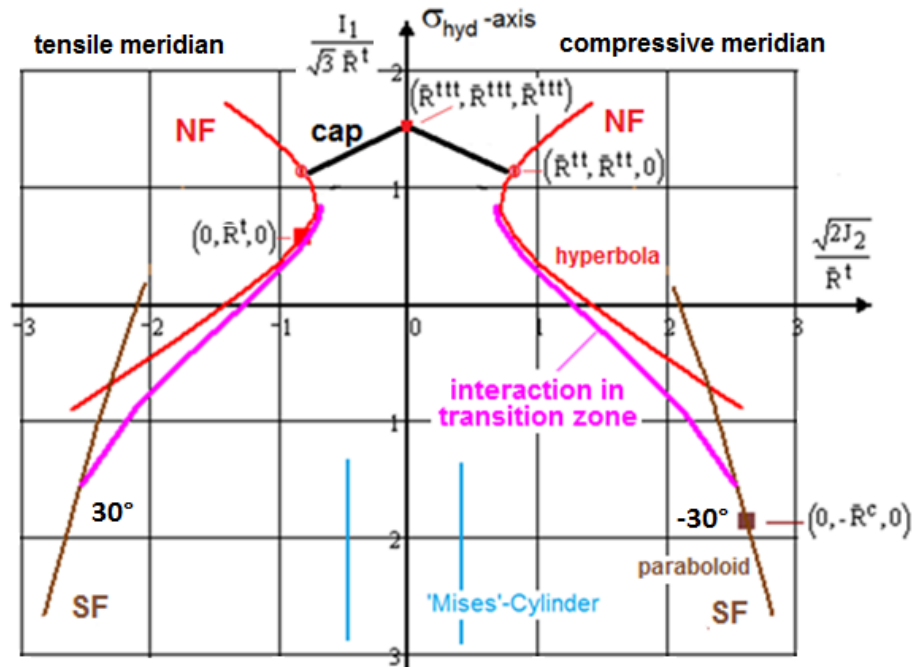


Fig. 6-9: Visualization of the courses of the 2 mode mapping functions for *NF* and *SF* along the meridian cross sections of the fracture body and after *interaction*

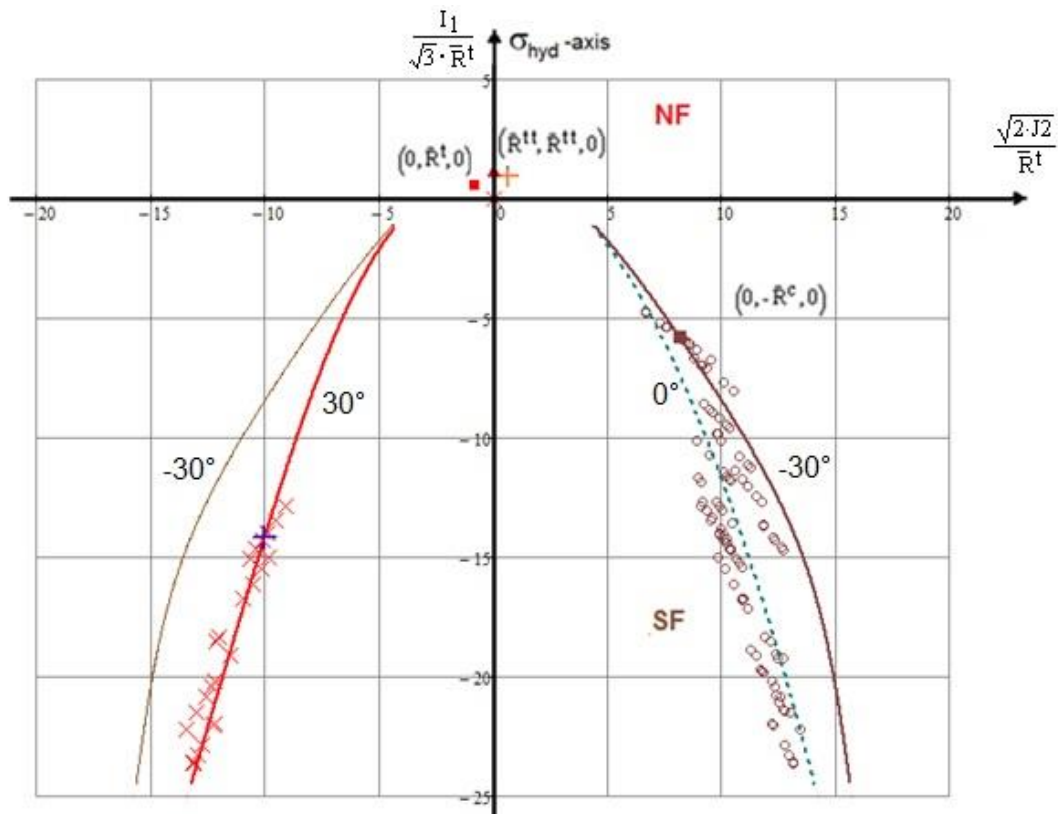


Fig.6-10.: Tensile meridian curve and test data ( $x$ ,  $30^\circ$ ), compressive meridian ( $-30^\circ$ ) curve and test data on the respective hoop ring  $o$  (these circles  $o$  are located at different meridian angles  $\theta$ )

The failure body possesses inward dents for  $I_1 > 0$  and outward dents for  $I_1 < 0$  in contrast to porous concrete stone. These dents become smaller with increasing  $|I_1|$ . Due to the Poisson effect it should be checked whether the material may tensile fracture (NF) under biaxial compression,  $\epsilon_{axial} > \max \epsilon$ .

## 6.5 ‘Isotropic’ UHPC (relatively dense)

Ultra-High-Performance-Concrete principally behaves similarly to Normal Concrete unless the normalized hydrostatic compression does not become larger than  $|I_1 / R_t \cdot \sqrt{3}| \approx 10$  ( $> 300$  MPa), see [Fig.6-10](#). From about this stress state on a different failure behavior takes places, which can be substantiated best by the following test result: Just a slight hydrostatic pressure of 6 MPa or N/mm<sup>2</sup> increases the uniaxial strength capacity from 160 MPa up to 230MPa - 6 MPa = 224 MPa!

$$\sigma_{fracture} = (\sigma_I, \sigma_{II}, \sigma_{III})_{fracture}^T : (-160, 0, 0)^T \Rightarrow (-224 - 6, -6, -6)^T$$

This explains why for the less ‘dense’ Normal Concrete  $R^{cc}/R^c$  is higher.

The author dedicates this to the still mentioned ‘healing’ of the flaw effects. If in addition to shear a **volume** change happens, then  $F^{SF}$  is to replace by  $F^{SFV}$  to capture all effects engineering-like

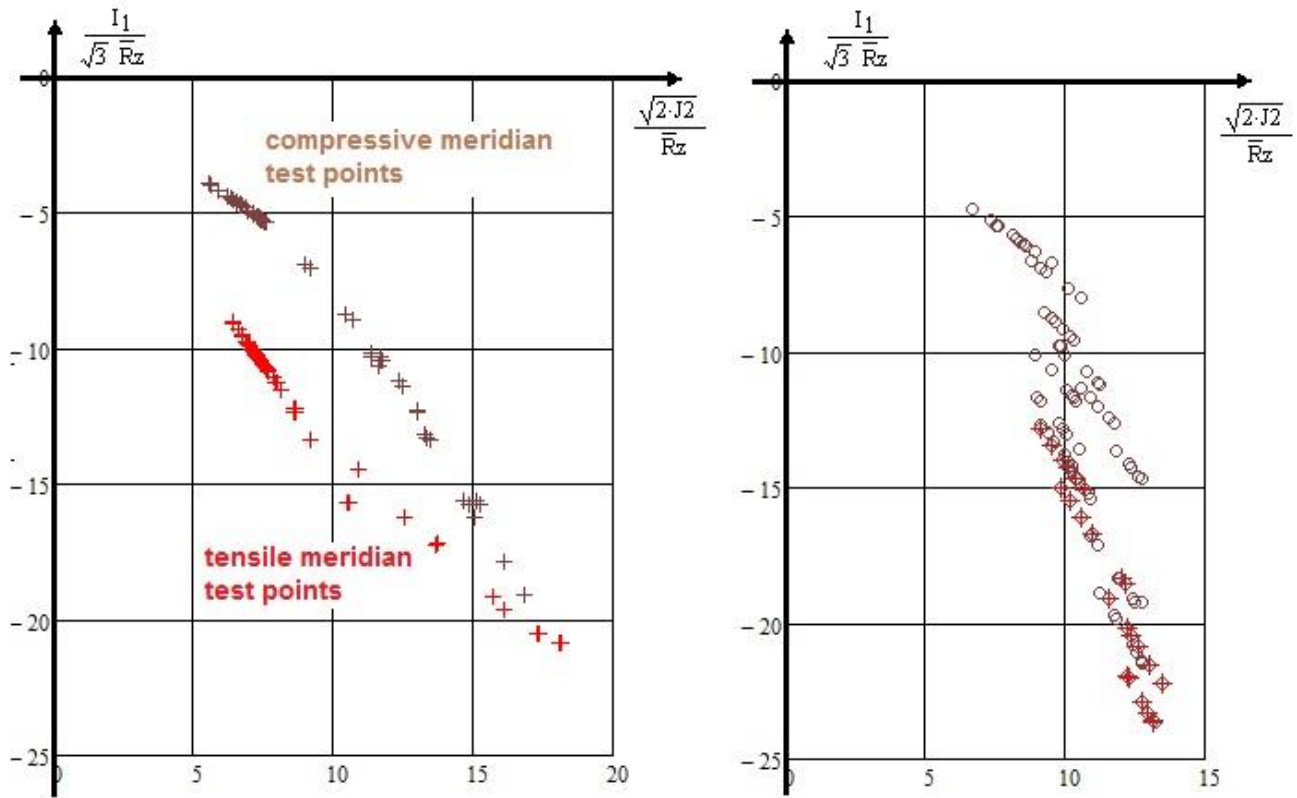
$$F^{SF} = c_{1\Theta}^{SFV} \cdot \frac{3J_2 \cdot \Theta^{SF}}{R^{c2}} + c_{2\Theta}^{SFV} \cdot \frac{I_1}{R^c} \Rightarrow F^{SFV} = c_{1\Theta}^{SFV} \cdot \frac{3J_2 \cdot \Theta^{SF}}{R^{c2}} + c_{2\Theta}^{SFV} \cdot \frac{I_1}{R^c} + c_{3\Theta}^{SFV} \cdot \frac{I_1^2}{R^{c2}}$$

Points for the determination of the SFV curve are indicated in [Fig.6-12](#). By the way, for fiber-reinforced plastics a similar redundant behaviour occurs, see [[Cun13](#), [14](#)]. Again, mind the Poisson effect. The effortful calculation of the fracture body is in progress.

[Fig.6-11](#) provides a mapping of those test data which are lying on the tensile meridian and on the compressive meridian. In contrast to Normal Concrete with usually relatively low hydrostatic pressure loadings UHPC experiences a hydrostatically activated effect, ‘densification with volume shrinkage’. Therefore, the volume change must be considered by  $I_1^2$  in the extended formula, see [Fig.6-12](#).

The fracture body of a theoretically dense concrete (matrix) possesses in the high hydrostatic compressive domain ( $I_1 < 0$ ) an open fracture surface. Practically however, the fracture body is closed due to impacting flaws, i.e. porosities. Further, the bi-axial compressive strength  $R_{cc} \equiv f_{cc}$  may be not only determined by SF but also by NF due to the Poisson’s ratio activated tensile strain in the axial direction despite  $\sigma_{ax} = 0$

When searching the data set for the tensile meridian and the compressive meridian out of the full bunch of 3D test data the Lode angle or meridian angle  $\vartheta$ , respectively, must be computed. It documents by the values which test point belongs more to the tensile meridian  $\sin(3\vartheta) = 1$  or to the compressive meridian  $\sin(3\vartheta) = -1$ . The shear meridian means  $\sin(3\vartheta) = \vartheta = 0$ .



UHPC test points: (left) tensile meridian + and compressive meridian +;  
 (right) all 3D test points are marked by o (hoop ring), visualizing to be located at different meridians

Fig.6-11 UHPC:Compressive and tensile meridian points

$$\bar{R}^t = 16 \text{ MPa}, \bar{R}^c = 160 \text{ MPa}, \bar{R}^u = 0.89 \cdot \bar{R}^t = 14 \text{ MPa (assumed)}, \bar{R}^{cc} = 175 \text{ MPa}$$



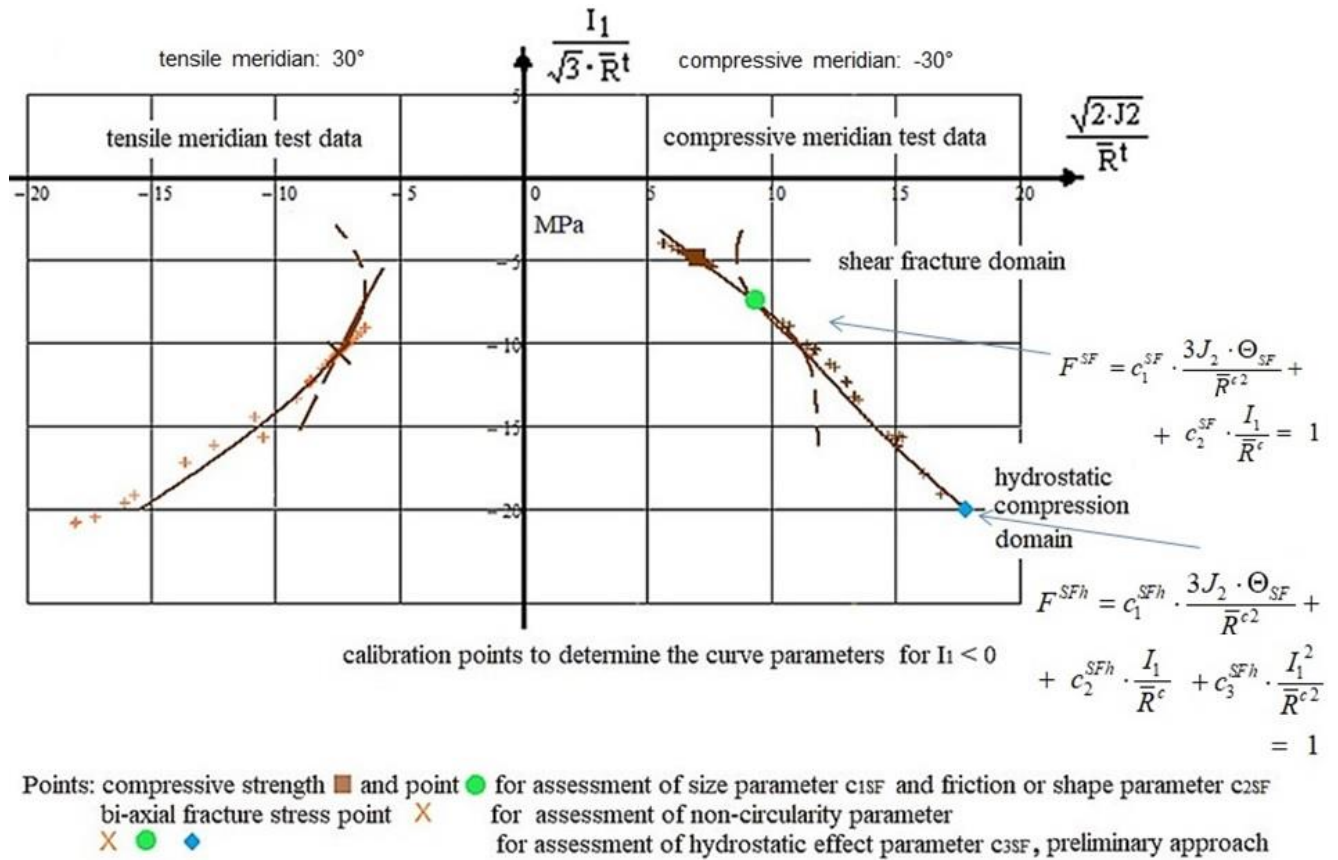


Fig.6-12 Ultra-High-Performance-Concrete (UHPC):

[Test data: Dr. Speck, IfM, TU-Dresden]. From this general data set as sub-sets the meridian data sets (constant Lode angles) have been extracted by the author

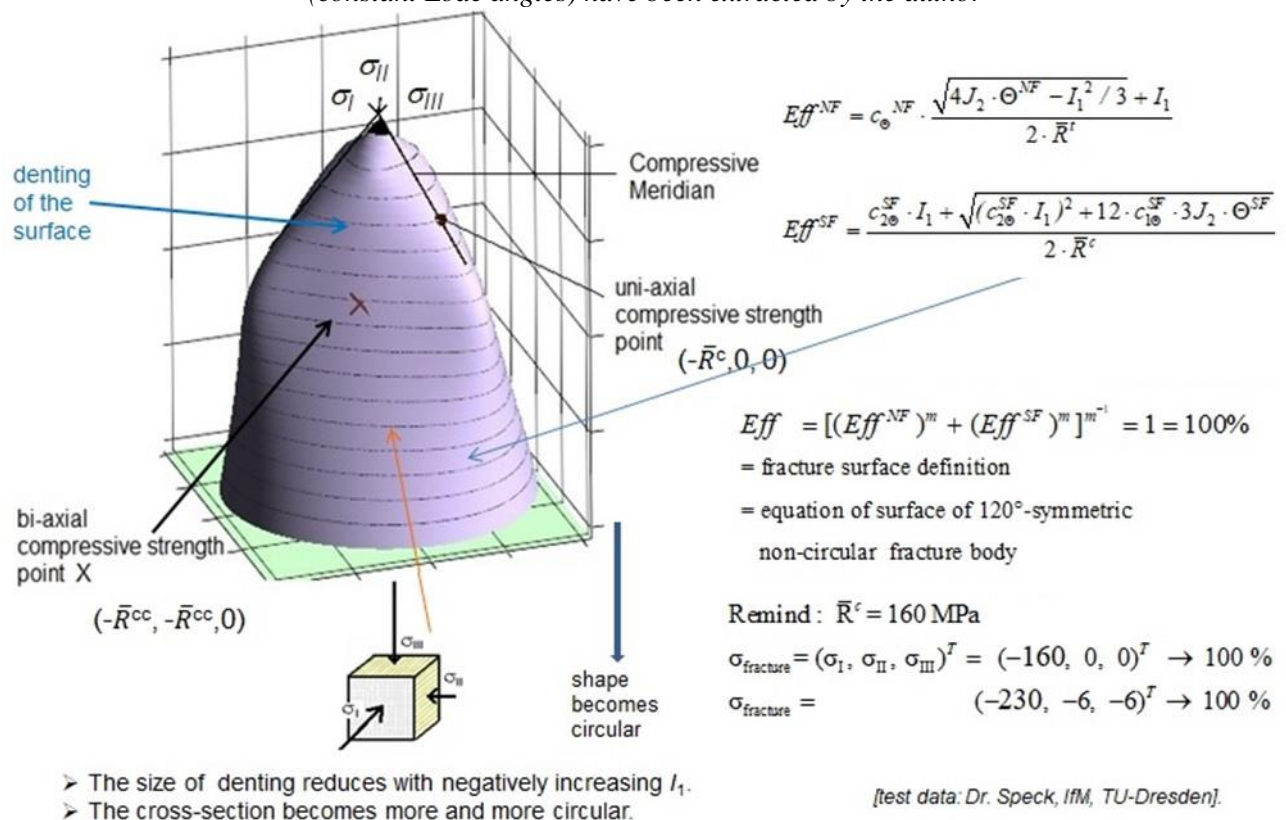


Fig.6-13 UHPC: Fracture body

Fig.6-14 shows a graph bi-axial compressive strength over uni-axial compressive strength. It turns out that with increasing uni-axial strength the ration approximates one.

The author tries to explain this:

The effect of redundancy under hydrostatic loading can be interpreted as an out-smoothing of stress concentrations. In the case of Normal Concrete this effect becomes more chances according to being more roughly grained than UHPC. This explains why the bi-axial strength capacity increase of a roughly grained Normal Concrete is higher than for UHPC.

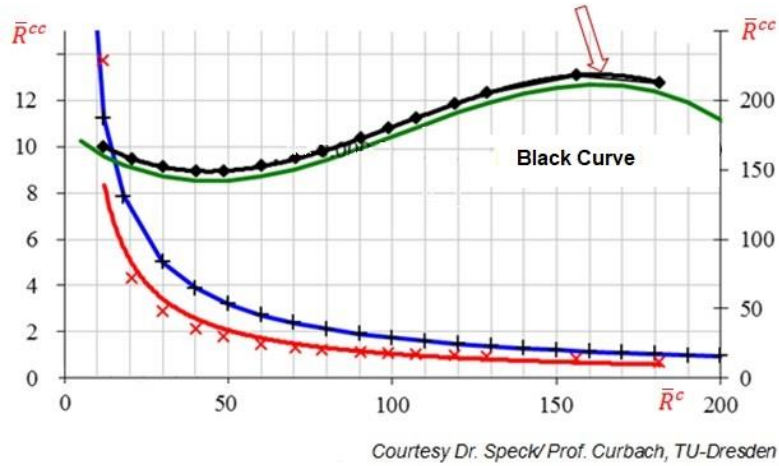


Fig.6-14: compressive strength capacity ratio of concrete  $\bar{R}^{cc} / \bar{R}^c$  ( $R = f$ ),  
 $\bar{R}^{cc} / \bar{R}^c$  (Normal Concrete) >  $\bar{R}^{cc} / \bar{R}^c$  (UHPC)

In Fig.6-15 shown are mode domains and transition zone obtained with the interaction formula.

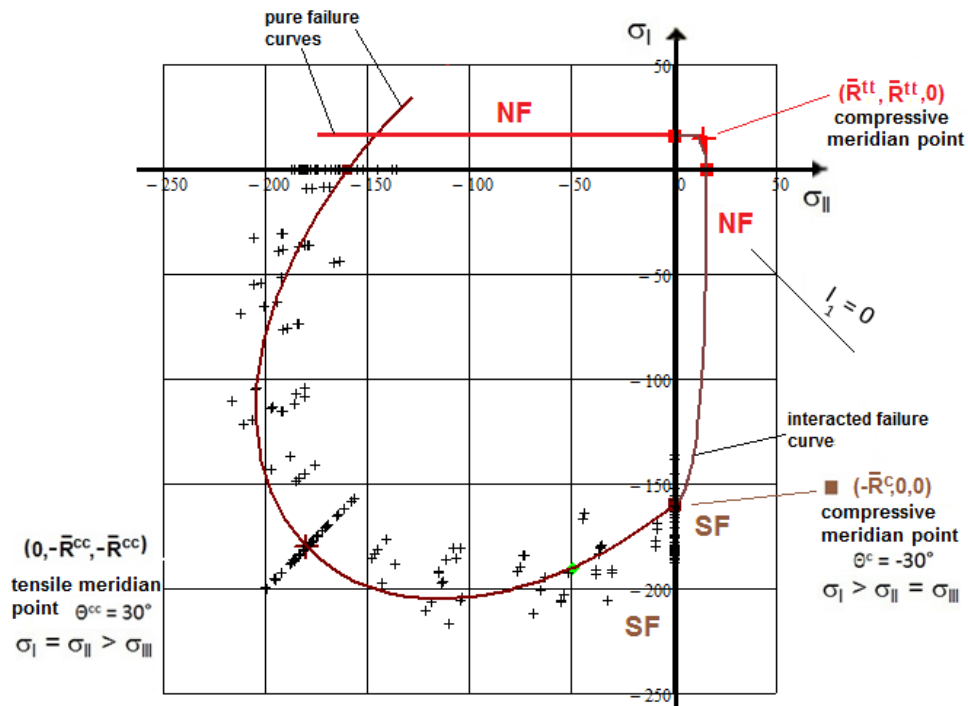


Fig.6-15, UHPC: principal stress plane with measured test data and evaluated strength points

Table 6-2: Characteristic material data when evaluating UHPC fracture tests.  $E = 20000 \text{ MPa}$ ,  $\nu = 0.2$ ,

$$\tau_{max} = \sigma_I - \sigma_{III} \text{ ), } \sigma_{II} = \sigma_{III} \text{ ; } \varepsilon_{ax} = -2 \cdot \nu / E \text{ .}$$

|              | Stress state<br>in MPa        | $I_1/\sqrt{3}$<br>/ $R^t$ | $\sqrt{2 \cdot J_2}$<br>/ $R^t$ | $\tau_{max}$<br>in MPa | $(\sigma_{hyd}; \sigma_{ax})$<br>in MPa | $\theta^\circ$ | $\epsilon_{ax}^{el}$<br>in $10^{-3}$ | remarks               |
|--------------|-------------------------------|---------------------------|---------------------------------|------------------------|---|----------------|--------------------------------------|-----------------------|
| $R^{tt}$     | (14, 14, 0)                   | 1                         | 0.7                             | -                      | -                                       | -30            | 0.6                                  | two-fold NF           |
| $R^c$        | (0, 0, -160)                  | -5.8                      | 8.2                             | 80                     | (-0; -160)                              | -30            | -8                                   | $Eff_{SF}$            |
| Compressive  | (-6, -6, -230)                | -8.7                      | 11.4                            | 111                    | (-6; -224)                              | -30            | -11                                  |                       |
|              | (-16, -16, -272)              | -11.0                     | 13.1                            | 128                    | (-16; -256)                             | -30            | -13                                  |                       |
|              | (-35, -35, -350)              | -15.2                     | 16.1                            | 157                    | (-35; -315)                             | -30            | -17                                  |                       |
|              | (-83, -83, -490)              | -23.7                     | 20.8                            | 204                    | (-83; -407)                             | -30            | -23                                  |                       |
|              | comput.<br>$(-23, -23, -305)$ | -12.6                     | 14.4                            | 141                    | (-23; -282)                             | -30            | -15                                  |                       |
| Tensile      | $R^{cc}$<br>(0, -175, -175)   | -12.6                     | 8.9                             | 88                     | (0; -)                                  | +30            | 3.5                                  | two-fold SF           |
|              | (-2, -210, -210)              | -15.2                     | 10.6                            | 104                    | (-2; -)                                 | +30            | 4.1                                  |                       |
|              | (-24, -310, -310)             | -23.2                     | 14.6                            | 143                    | (-24; -)                                | +30            | 5.0                                  |                       |
|              | $R^t$<br>(-54, -388, -388)    | -30                       | 17                              | 167                    | (-54; -)                                | +30            | 5.1                                  |                       |
| shear change | (16, 0, 0)                    | 0.6                       | 0.8                             | -                      | -                                       | +30            | 0.8                                  | $Eff_{NF}$            |
|              | (9, -9, 0)                    | 0                         | 0.8                             | 9                      | -                                       | 0              | 0.5                                  | $Eff_{NF} > Eff_{SF}$ |
|              | (0, -52, -193)                | -8.8                      | 8.8                             | 97                     | -                                       | -15            | -9.1                                 |                       |

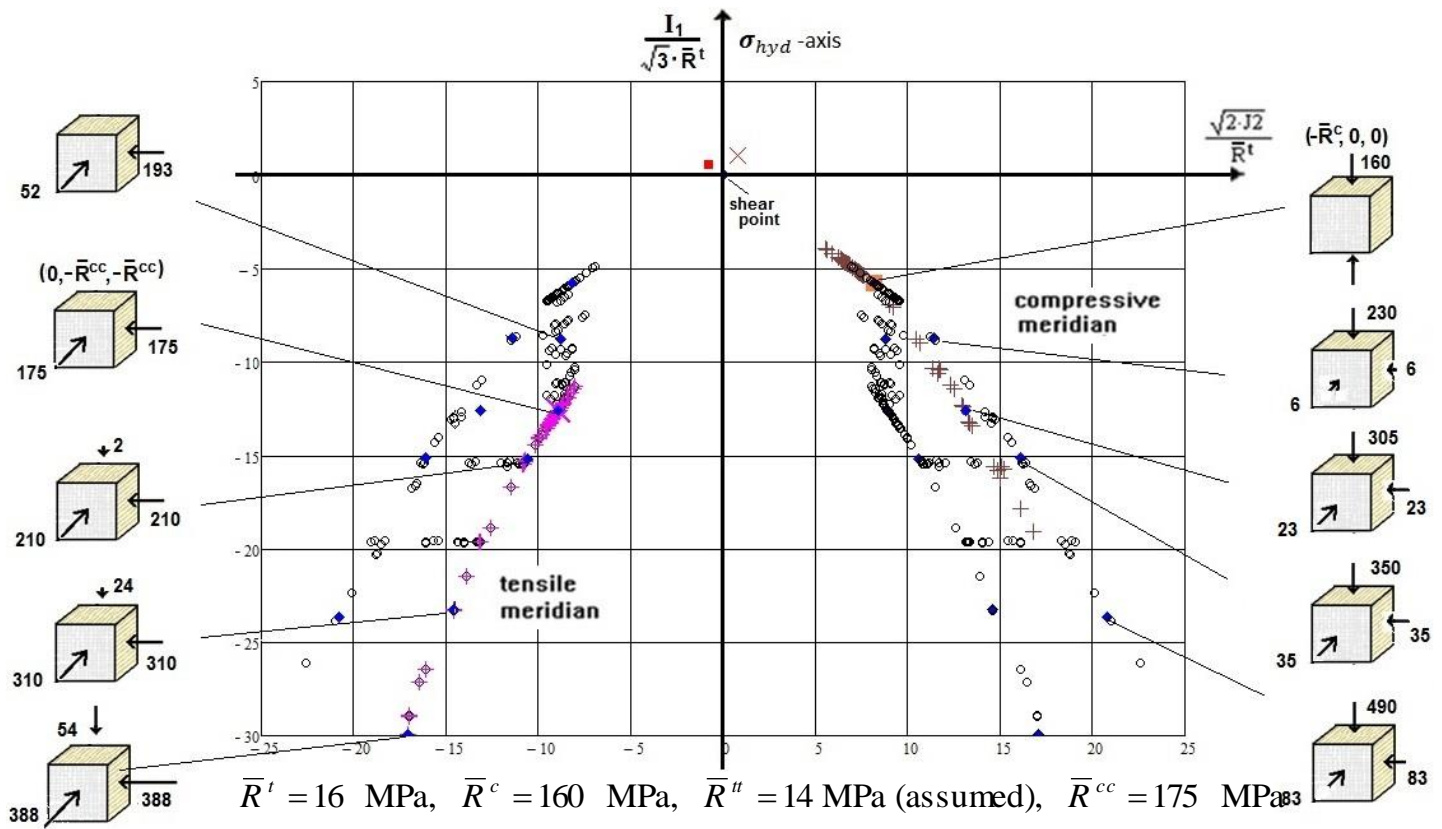


Fig.6-16: Compressive and tensile meridian of the UHPC fracture body with associated stress states

On basis of redundancy effects it may be concluded that with increasing hydrostatic pressure both the meridians run into a common scatter band → circle shape of the hoop. Then, the effect of flaws generating micro-damaging in this heterogeneous material reduces. Thereby, the fracture body (has an open bottom fracture surface) becomes more and more cylindrical.

## 6.6 Rock Material, example Sandstones

### 6.6.1 Required properties for underground rock failure stress analysis

Tension domain:

Also in rock materials in the vicinity of excavations and boreholes tensile stresses will occur. An undesirable brittle sudden failure is to prevent when a bore-hole is drilled.

Therefore, the tensile strength proof requires a tensile strength  $\bar{R}^t$  for the distinct rock material. An estimation for the tensile strength value delivers the Brazilian splitting test (*indirect* tensile strength test) because a usual tensile test specimen is seldom to obtain. Solid cylinder or disk (short cylinder) test specimens are used for the initially crack-free (intact) material, see Fig.6.6-1. The evaluation is performed via the formula

$$f_{sp} = \bar{R}^t = 2 \cdot q / (\pi \cdot d \cdot \ell) \quad [The\ constructor.org].$$

This difficulty caused researchers to predict a value by using a Mohr-Coulomb-based SFC but the determined value is doubtful. In this context the author fully supports Mingqing You [You15] that a tensile strength  $R^t$  is a separate parameter and cannot be estimated by models working in the tensile-compressive transition zone. Chapter 8.1 investigates the Mohr-Coulomb model (*physically just a friction-related compression domain model which runs into the tensile domain but is not representative for the tensile domain*) and clearly derives that the Mohr-Coulomb model is applied in the transition zone between the Normal Fracture mode under tension and the Shear Fracture mode under compression.

The result in chapter 8.1 is:

- (1) A real value for  $\bar{R}^t$  is to obtain by a uni-axial tensile stress test  $\{\sigma\} = (\sigma_{ax}^t = F^t/A, 0, 0)^T$
- (2) Even the computation of a cohesive strength value  $\bar{R}^t$  is doubtful.

Compression domain:

Usual test series for concrete material (see the concrete applications in Chapter 6.4) are performed along the compressive meridian and not so often along the tensile meridian. For the demonstration of concrete strength, however, the full fracture failure body is required because all mixed 3D-compressive stress states are principally possible. In rock mechanics the stress situation is linked to stress states on the compressive meridian. This explains why no bi-axial strength  $\bar{R}^{cc}$  is provided in literature those entity which enables to describe the 120°-symmetric fracture failure body. It simplifies the task: Just the functional description of the compressive curve remains of interest.

A stress state in a material, formulated in Mohr's *mathematical* stresses, reads

$$\{\sigma\} = (\sigma_I, \sigma_{II}, \sigma_{III})^T \text{ with } \sigma_I \text{ becoming the smallest failure stress (most positive)}$$

$$\sigma_I > \sigma_{II} > \sigma_{III} \text{ mathematically and } \sigma_{III} \text{ the largest compressive failure stress (most negative).}$$

Tensile stresses must be signed positive in this context, otherwise confusion becomes extreme!

$$\text{For the tensile meridian follows } \{\sigma\} = (\sigma_I, \sigma_{II}, \sigma_{III} = \sigma_{II})^T \text{ with } \sigma_I = \sigma_{ax}^t - p_{hyd}$$

$$\text{and the compressive meridian } \{\sigma\} = (\sigma_I = \sigma_{II}, \sigma_{II}, \sigma_{III})^T \text{ with } \sigma_{III} = \sigma_{ax}^c - p_{hyd}.$$

The tensile meridian captures  $\bar{R}^{cc}$  (and  $\bar{R}^t$ , in the domain of the Normal Fracture mode) and the compressive meridian captures  $\bar{R}^c$  (and  $\bar{R}^t$ , in the domain of the Normal Fracture mode).

In rock mechanics the term hydrostatic pressure, used when testing concrete and UD material, is to replace by the Confining Pressure CP. This makes to introduce some definitions of rock mechanics terms: *Here, tensile stress is still negative, but not always anymore which make an interpretation difficult!*

- (3D) Rock compressive strength (capacity) [You15]  
(the stress-sketch in Figure 1 of [Lan19] must be corrected. It does not fit to the provided failure stress states. In Fig.6.6-1 corrected)

$$\sigma_{III} \equiv \sigma_s \equiv \sigma_1 \text{ termed here } \textit{minor} \text{ principal stress}$$

- 1D uni-axial strengths: UTS =  $\bar{R}^t$ , UCS =  $\bar{R}^c$

Unfortunately the author found different meanings: In engineering design dimensioning UTS means Ultimate Tensile Strength and not Uni-axial Tensile Strength and UCS ultimate compressive strength (still also applied in 'geo engineer'! Why it is not generally used in rock mechanics?) and not for instance Unconfirmed Compressive Strength [Wikipedia]. UCS stands for the maximum axial compressive stress that a specimen can bear under zero confining stress CP, which means it is nothing else than the usual simple standardized technical compression strength  $\bar{R}^c$  in engineering

- ✓ Confining pressure CP: maximum level of hydrostatic compression applied in a tri-axial compression test of a concrete, a rock material or a neat resin test specimen defined by  $\{\sigma\} = (\sigma_{ax}^t - CP, -CP, -CP)$  or with  $\sigma_{ax}^c$  (induced by test rig brushes in case of concrete).
- ✓ Confining lithostatic pressure: CP =  $p_{hyd} + \text{overlying weight}$ . (T is amount of confinement. What for in addition?).

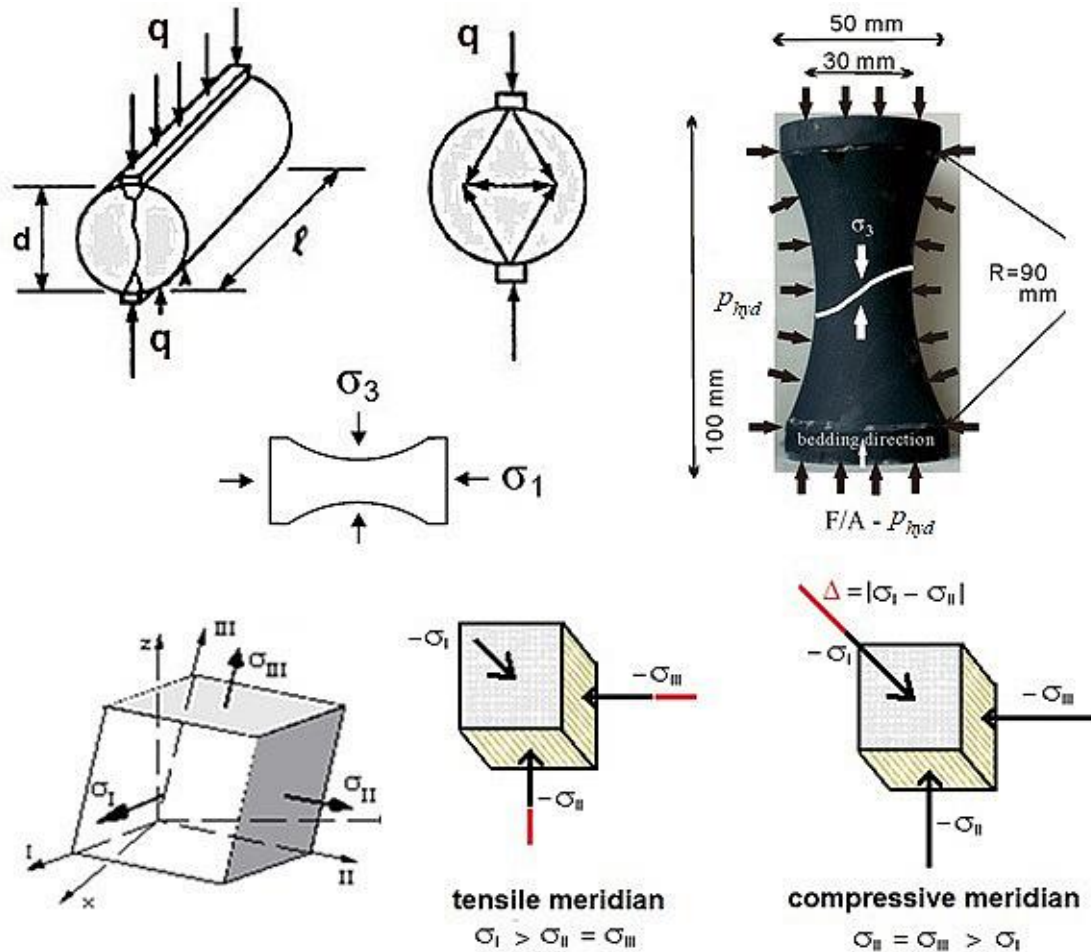


Fig. 6.6-1: Brazilian cylinder or disk (short length) for an indirect estimation of  $\bar{R}^t$  and dog-bone (sealed, highest preparation effort, grinding from solid block with axial bedding layers) test specimen for direct measurement of tri-axial fracture stress states along compressive meridian including the tension-compression domain.

( $\Delta$  depicts the differential stress entity causing shear stress with shear deformation)

The author would like to conclude: *using usual mathematical stresses and taking a look at Fig.6-16*

- Sealed, polished dog-bone test specimens deliver the failure stress points  $(-\bar{R}^{ccc}, -\bar{R}^{ccc}, -\bar{R}^{ccc})$  no pore pressure,  $(-\bar{R}^c, 0, 0)$ ,  $(\bar{R}^t, 0, 0)$  and further multi-axial compressive failure stresses on the compressive meridian.
- A bi-axial compressive failure stress  $(-\bar{R}^{cc}, -\bar{R}^{cc}, 0)$  is obtainable by the dog-bone test specimen for  $\sigma_1=0$  or  $\sigma_{ax}^t = -CP$ . However, the author did not find a bi-axial strength value in the papers ?
- A bi-axial tensile failure stress  $(\bar{R}^{tt}, \bar{R}^{tt}, 0)$  can be obtained by cube test specimens prepared by a good gluing in order to load the needed bi-axial tensile stresses.

Test procedure: The confining pressure CP is achieved and then kept constant during the test. The axial stress  $\sigma_1$  is increased at a certain rate until the test specimen fails at  $\max\sigma_1$ . It is to consider whether the porosity of the rock or the soil material and the saturation plays a role.

Fig.6.6-2 presents fracture pictures of the investigated Berea sandstone. Essential is that the fracture angle increases with CP.



*Fig.6.6-2 Sandstone: Fracture pictures of Berea sandstone from [Lan19].*

The author's definition of the center of the transition zone between the tensile domain and the compressive domain is: The first invariant becomes zero

$$I_1 = \sigma_1 + \sigma_2 + \sigma_3 = 0, \text{ means pure shear. For } \sigma_2^c = \sigma_3^c \rightarrow \sigma_1^t = 2 \cdot \sigma_3^c.$$

The ability for mobilizing friction processes depends on active compression stresses that cause via the friction value  $\mu$  the necessary shear.

Keep in mind, please:

Unfortunately, engineers in other disciplines become pretty stressed because we civil engineers use construction design tools which still call tensile stresses negative stresses, so as depicted in the Fig.6.6-3. This completely disturbs the logic of the 'civil engineer' Mohr in context with the definition of mathematical stresses !

### **6.6.2 Test data for three sandstone materials**

Some test data sets from tests, running along the compressive meridian, were available for the foreseen modelling and further investigation. The graphs in Fig.6.6-3 are formulated in rock

mechanics terms. For general purpose, these graphs at first have to be transformed from the usual rock-mechanics depiction into the standard mechanical one in Lode coordinates. For this the usual rock mechanics letters will be used (*unfortunately these letters fully confuse with the standard fiber-reinforced UD composite indices*)

$$\{\sigma\} = (\sigma_1, \sigma_2, \sigma_3 = \sigma_2)^T \quad \text{with} \quad \sigma_1 \equiv \sigma_{III} = \sigma_{ax}^c - CP, \quad \sigma_2 = -CP.$$

As long as  $(\sigma_1^t, \sigma_2^c, \sigma_3^c = \sigma_2^c)$  is given, due to the confinement in this so-called “*confined, direct tensile test on intact rock*”, friction processes still act which influence the combined failure stress state in this transition zone before tension cut-off. It is not mentioned i.e. in [Lan15], how the bi-axial tensile stresses are applied to the test specimen. Test results show in the transition zone: Frictional processes diminish when passing  $(\bar{R}^{tt}, \bar{R}^{tt}, 0)$  and failure becomes dominated by tensile strength  $\bar{R}^t$  and the bond between grains.

The graphs unfortunately use different scales. Therefore, for a better comparison *Fig.6.6-4* was generated.

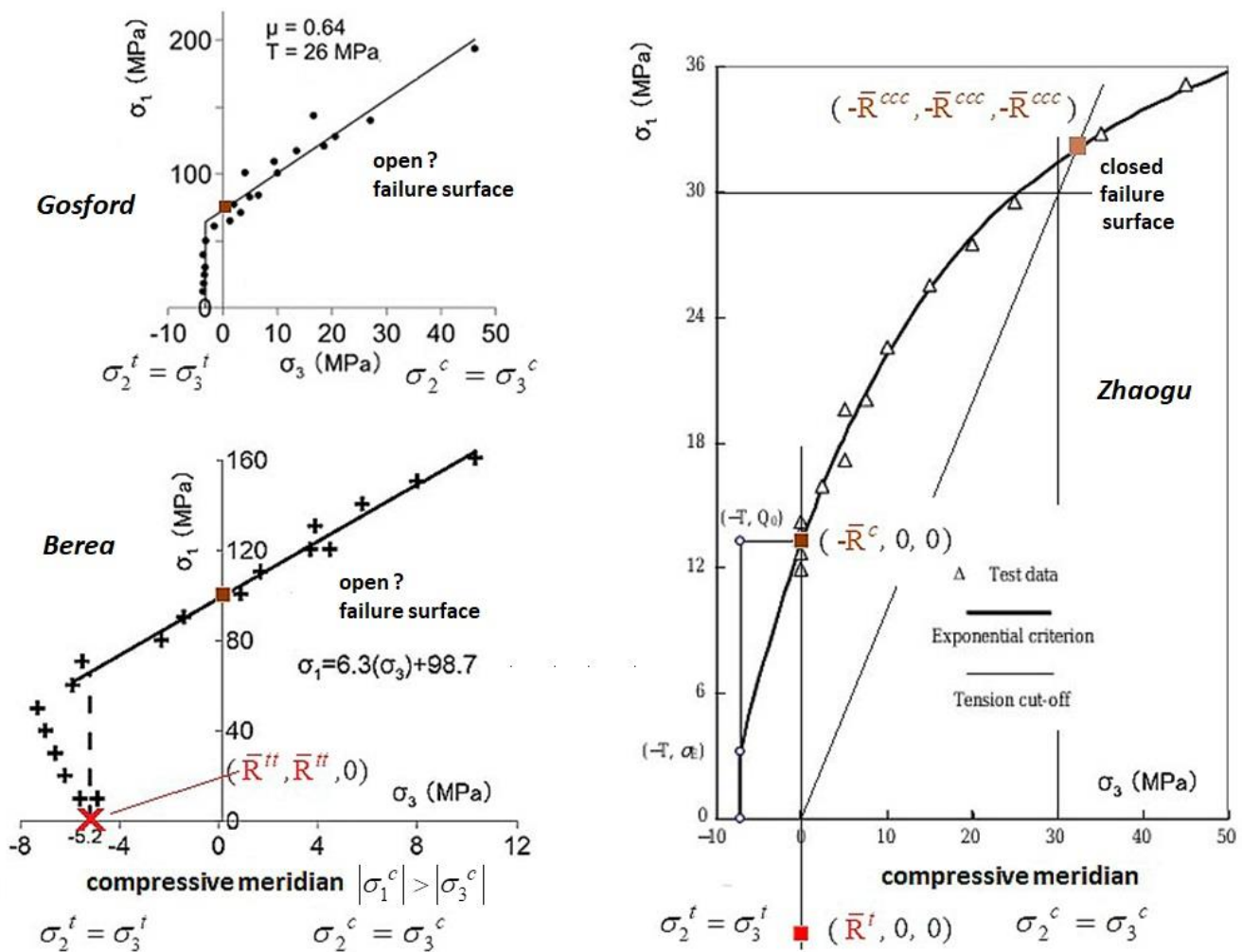


Fig. 6.6-3: Three sandstone materials with depiction of the failure stress points = ‘strength’. (left down) Berea sandstone [Lan19]; (left up Gosford sandstone [Lan19]); (right) Zhaogu sandstone [You15].

The courses of test data in *Fig.6.6-3* are presented for the different sandstones and different scaling. Only a presentation with the same scaling enables to draw comparative conclusions, *Fig.6.6-4*.

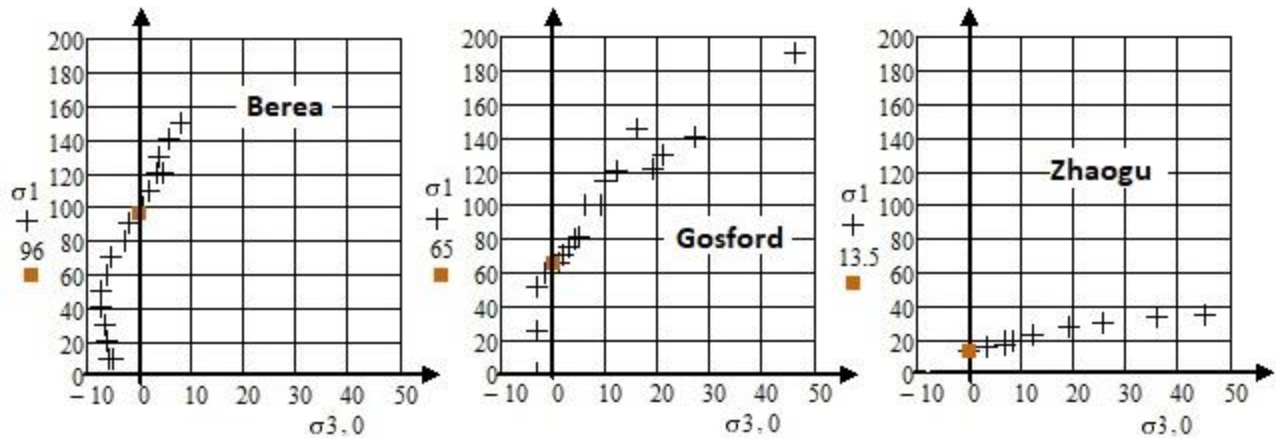


Fig. 6.6-4: Comparison for Berea, Gosford and Zhaogu sandstones, same scale.(tensile stress is positive in order to keep the convention in civil engineering)

From interpretation of the given test data sets depicted in the equally scaled Fig.6.6-5 the author likes to conclude:

(a) Berea sandstone, Figure 2 in [Lan19]:  $\mu \approx 0.76$  (computation), failure surface seems to be open.

From the course of given test data can be derived  $\bar{R}^t \cong 6$  MPa,  $\bar{R}^c = 96$  MPa . No bi-axial compressive strength  $\bar{R}^{cc}$  is provided for this sandstone material. Missing  $\bar{R}^{cc}$  means: The fracture failure body cannot be computed like for the concrete materials. Bi-axial strength is to know to sort out whether a 120°-symmetrical failure body or a fully rotational one is to face. Tensile meridian and compressive meridian are the opposite axial cross-sections of the failure body (see concrete material pictures before).

Discussion Berea sandstone from [You15]: Was taken by the author as a challenge for the author's SFC application

- The author could not find how the bi-axial tensile stresses are introduced into the test specimen (gluing devices)
- The Berea sandstone shows no typical tension cut-off. Does this come from gluing in context with a suppression of the flaw impact on the failure by the axial compression?
- From experience with brittle materials the author was just one time confronted with such a huge friction value of a structural material, namely within WWFE-I, TC1, UD lamina, GFRP. The author could sort out that the responsible test points were not right. This makes insecure for the Berea sandstone when mapping the course of test data. The friction value  $\mu$  is very high compared to a usual concrete value a little above 0.2. This needs to be checked.
- The reason for the increase of the fracture angle (see Fig.6.6-2 and Chapter ??) with CP needs to be discussed.
- The axial compression head plate causes friction under the plate and usually disturbs the 3D stress state.

(b) Gosford sandstone, Figure 5 in [Lan19]:  $\mu \approx 0.39$ , failure surface seems to be open

From the course of given test data can be derived,

$$\bar{R}^{tt} \cong 3.5 \text{ MPa}, \bar{R}^t \cong 4 \text{ MPa (assumed)}, \bar{R}^c = 65 \text{ MPa} .$$

Discussion Gosford sandstone from [Lan15]:



- The comparison with Berea shows a less steep increase  $\sigma_1(\sigma_3)$
- Cuntze computed  $\mu = (c2\tau - 1) / (3 \cdot c2\tau + 3) = 0.39$  and in [Lan19]  $\mu \approx 0.64$  is given. The given friction value  $\mu = 0.64$  is very which needs to be checked.

(c) Zhaogu sandstone, Fig.4 in [You15]:  $\mu \approx -0.46$ , *failure surface seems to be closed*

From the course of given test data can be derived  $\bar{R}^{ccc} \cong 32$  MPa and  $\bar{R}^c = 13.5$  MPa.  $\bar{R}^t \cong 7.2$  MPa (measured). No bi-axial compressive strength  $\bar{R}^{cc}$  is provided for this sandstone material. Because the failure surface seems to be closed the closing bottom point on the axis is to determine applying the previously used Awaji-formula

$$I_1 = -3 \cdot \bar{R}^{ccc}, J_2 = 0 : I_1 / (\bar{R}^t \cdot \sqrt{3}) = -20, \sqrt{2 \cdot J_2} / \bar{R}^t = 0$$

A closed fracture surface can be described by

$$F^{SF} = c_{1\Theta}^{SF} \cdot \frac{3J_2 \cdot \Theta^{SF}}{\bar{R}^{c2}} + c_{2\Theta}^{SF} \cdot \frac{I_1}{\bar{R}^c} = 1 \Rightarrow c_{1\Theta}^{SF} \cdot \frac{3J_2 \cdot \Theta^{SF}}{\bar{R}^{c2}} + c_{2\Theta}^{SF} \cdot \frac{I_1}{\bar{R}^c} + c_{3\Theta}^{SF} \cdot \left(\frac{I_1}{\bar{R}^c}\right)^2 = 1.$$

Discussion of [You15]:

- In Fig.1 and 2 (halite) of [You15] the increase of the axial compressive stress, termed there  $\sigma_s$  (*Why not  $\sigma_1$ ?*), under CP =  $\sigma_3$  increases as experienced. However in Fig.4 (Zhaogu sandstone)  $\sigma_1(\sigma_3)$  is depicted with a never experienced low increase. Is this accurate? Is there a conversion error to be seen in context with the next point?
- Table 1 in [You15] should present  $\bar{R}^c = 13.5$  MPa  $\equiv$  UCS but gives  $\sigma_1 = 132$  MPa at CP = 45 MPa !?
- The last 2 test points *beyond* the tri-axial compression strength are to investigate. Mind in this context: Confirmed by fracture pictures found in literature the fracture usually shows a wide scatter and different fracture patterns, crushing with shearing acts
- The computed negative friction value underpins the question marks
- Cuntze computed a physically negative friction value that is not accurate for this material.

In advance of applying the author's FMC-based SFCs (criteria) a view at Fig.6.6-5 will show the differences of the mapping approaches due to the failure criteria of Mohr-Coulomb (M-C) and Hoek-Brown (H-B). The Hoek-Brown parameters defined as  $\sigma_{ci}$  is the uniaxial compressive strength  $\bar{R}^c$ ,  $m_i$  is a steep parameter based on the rock type,  $\sigma_1$  the maximum absolute compressive stress and  $\sigma_3$  the minimum compressive stress (Why does it not read 'negative CP'?).

'Universal confined tensile strength' of intact rock. Available from:

[https://www.researchgate.net/publication/332447674\\_Universal\\_confined\\_tensile\\_strength\\_of\\_intact\\_rock](https://www.researchgate.net/publication/332447674_Universal_confined_tensile_strength_of_intact_rock)

The linear M-C (*Mohr assumed: mean stress is of no influence*) – due to its logic – practically just linearly maps by employing the friction angle  $\varphi$ . H-B maps non-linearly. However, why do both the approaches not run through the fix point 'compression strength' at  $\sigma_1(\sigma_3 = 0) \rightarrow (\bar{R}^c, 0, 0)$  ?

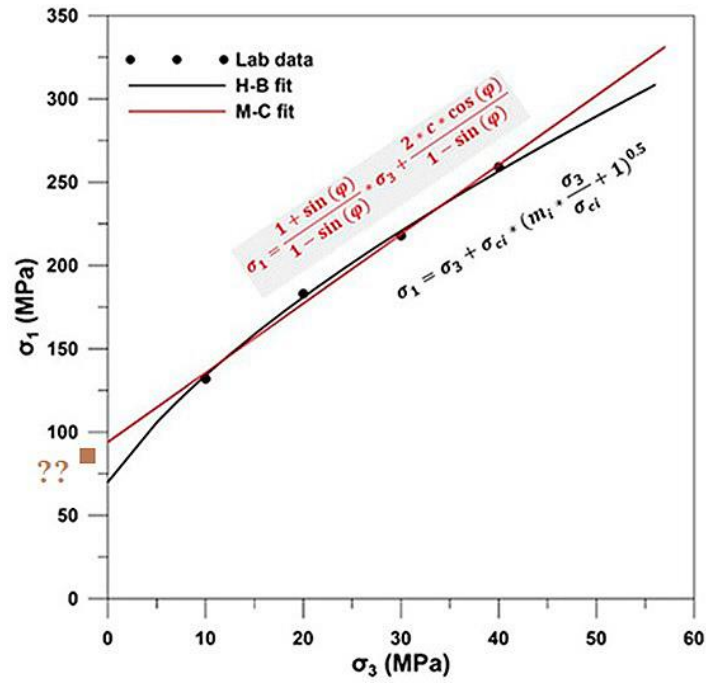


Fig.6.6-5: Geo Engineer, tri-axial compression test, Rock Laboratory, Testing Rock Mechanics. (compression stress here positive)

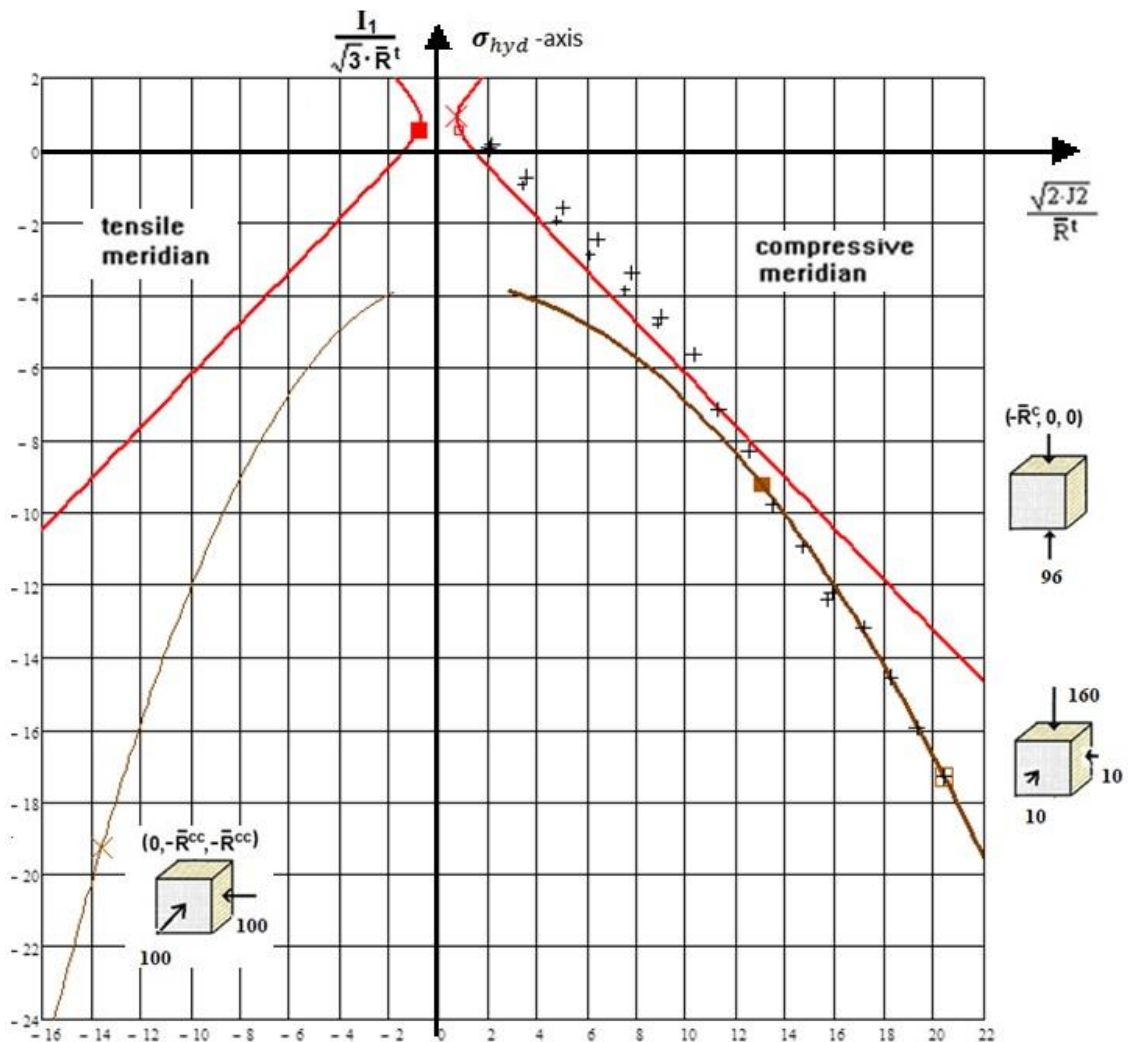


Fig.6.6-6 Berea Sandstone: Compressive meridian test data sets, not delivering  $\bar{R}^{cc}$ , X. Squares are uni-

axial *tensile* and uni-axial *compressive* strength.

transition zone on compressive meridian between the modes, mapped by the interaction equation.  
(here: tensile stresses are positive stresses due to the general convention in engineering).

$$\bar{R}^t = 6; \bar{R}^n = 5.2; \bar{R}^c = 96; \bar{R}^{cc} = 100; d^{SF} = 1.06; c_{1\Theta}^{SF} = -3.21, c_{2\Theta}^{SF} = -2.54,$$

$$g^{SF^\circ} = -30^\circ, g^{SF} = 0.5; m = 2.5.$$

Fig.6.6-6 displays the course of data in the classical diagram using the physically-based Lode-Haigh-Westergaard coordinates. Tensile and compressive meridian belong to an axial cross-section of the fracture failure body (see Fig.6.8). The two meridians outline a 120°-symmetric failure body. The brown curve maps the course of test data in the negative domain experiencing Shear Fracture SF. From the compression meridian strength test point  $(-\bar{R}^c, 0, 0)$ , tensile stress now positive, on the transition zone follows with an end at the tensile strength point  $(\bar{R}^n, \bar{R}^n, 0)$ . In the transition zone the contributions to failure come from NF and SF failure events. This is due to a statistical and probabilistic flaw situation behavior that usually is captured by the interaction equation.

Intentionally, there was no fitting procedure for a better mapping of the course of test points employed just the two SFCs with the associate parameters were used with the compressive strength as fix point.

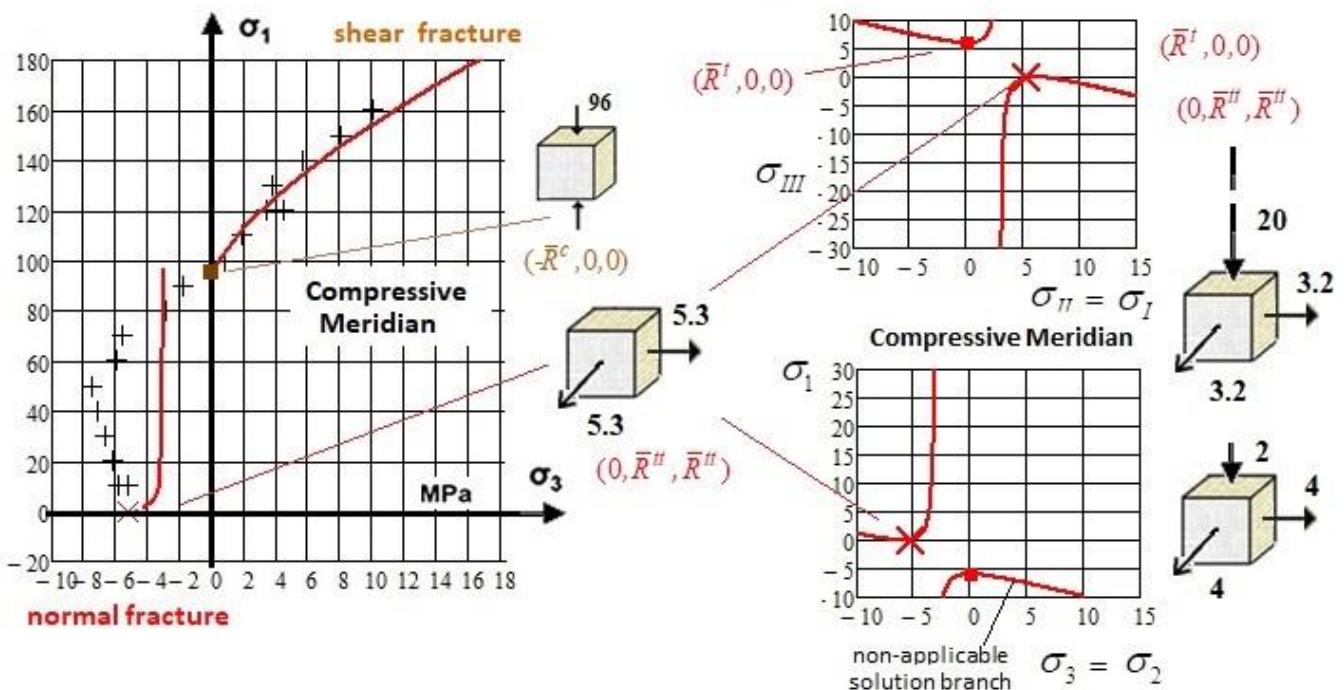


Fig.6.6-7 Berea Sandstone: (left) Simple mapping of the course of test data. X bi-axial tensile strength, square uni-axial tensile strength. (right) details in normal mode domain

General conclusions and specifically on Berea sandstone:

Author's experience after mapping the 3D-fracture stress dates of various isotropic and of transversely-isotropic (faced in layered rock materials, too!) materials:

- Each domain has to be mapped separately in order to optimally fulfill physical conditions. In this context M-C is right to just map the compression domain with its shear fracture failure mechanism (SF)

- The tensile domain belongs to another failure mechanism, namely normal fracture (NF), and therefore needs another SFC
- The transition zone between these domains can be mapped by an adequate interaction condition – if necessary in the special material case - as performed by the author
- In the case of Berea sandstone the ‘transition’ test points directly follow the test points of the compression domain. Therefore no interaction equation is applicable and is to apply. Un-usually high friction values and (here combined) high ratios  $\bar{R}^c / \bar{R}^t$  require different mapping in the transition zone
- In the full transition zone the test data points lie outside of the **NF** failure envelope. The author tried to improve the situation by taking a constant value of  $\bar{R}^{tt} = 5.3$ , indicated by the small crosses. It did not solve the (physical) problem
- Tension cut-off:
  - \* In the 3D-Lode diagram, example Normal Concrete, this limit is defined by  $I_1 / (\sqrt{3} \cdot \bar{R}^t = 1 / \sqrt{3}$ .
  - \* In the 3D-principal stress space this limit is defined by  $\sigma_I$  and  $\sigma_{II}$  and  $\sigma_{III} \leq \bar{R}^t$ . In order to be conservative it is recommended to use the NF-SFC for smaller values than  $I_1^c / (\sqrt{3} \cdot \bar{R}^t$ .

### Computing procedure

Following Mohr and mathematical stress formulations it reads

$$I_1 = (\sigma_I + \sigma_{II} + \sigma_{III}) = f(\boldsymbol{\sigma}), \quad 6J_2 = (\sigma_I - \sigma_{II})^2 + (\sigma_{II} - \sigma_{III})^2 + (\sigma_{III} - \sigma_I)^2 = f(\boldsymbol{\tau})$$

$$27J_3 = (2\sigma_I - \sigma_{II} - \sigma_{III}) \cdot (2\sigma_{II} - \sigma_I - \sigma_{III}) \cdot (2\sigma_{III} - \sigma_I - \sigma_{II}),$$

$\sigma_I, \sigma_{II}, \sigma_{III}$  principal stresses,  $\sigma_I > \sigma_{II} > \sigma_{III}$  mathematical stresses (> means more positive).

With the traditional rock mechanics letters the stresses read: regarding  $\sigma_2 = \sigma_3 = CP$

$$I_1 = (\sigma_1 + \sigma_2 + \sigma_3), \quad 6J_2 = (\sigma_1 - \sigma_2)^2 + (\sigma_2 - \sigma_3)^2 + (\sigma_3 - \sigma_1)^2 = (\sigma_1 - \sigma_2)^2 + (\sigma_3 - \sigma_1)^2$$

$$27J_3 = (2\sigma_1 - \sigma_2 - \sigma_3) \cdot (2\sigma_2 - \sigma_1 - \sigma_3) \cdot (2\sigma_3 - \sigma_1 - \sigma_2) = 2(\sigma_1 - \sigma_3) \cdot (\sigma_2 - \sigma_1) \cdot (\sigma_3 - \sigma_1).$$

For the determination of the failure curve in the transition domain the use of the *Effs* is mandatory

$$Eff^{NF} = \frac{\sqrt{4J_2 - I_1^2 / 3} + I_1}{2 \cdot \bar{R}^t} = \frac{\sigma_{eq}^{NF}}{\bar{R}^t} \leftrightarrow Eff^{SF} = \frac{c_{2\Theta}^{SF} \cdot I_1 + \sqrt{(c_{2\Theta}^{SF} \cdot I_1)^2 + 12 \cdot c_{1\Theta}^{SF} \cdot 3J_2 \cdot \Theta^{SF}}}{2 \cdot \bar{R}^c} = \frac{\sigma_{eq}^{SF}}{\bar{R}^c}.$$

$$\text{with } \Theta^{SF} = \sqrt[3]{1 + d^{SF} \cdot \sin(3\vartheta)} = \sqrt[3]{1 + d^{SF} \cdot 1.5 \cdot \sqrt{3} \cdot J_3 \cdot J_2^{-1.5}}$$

tensile meridian angle  $30^\circ \rightarrow \Theta^{NF} = \sqrt[3]{1 + d^{SF} \cdot (+1)}$ ; compr. meridian angle  $-30^\circ \rightarrow \Theta^{SF} = \sqrt[3]{1 + d^{SF} \cdot (-1)}$ .

The tension-compression transition zone between the modes NF and SF - analogous to concrete - is mapped by the interaction equation that determines the surface of the fracture failure body:

$$Eff = [(Eff^{NF})^m + (Eff^{SF})^m]^{m^{-1}} = 1 = 100\% \quad \text{total material stressing effort,}$$

$$Eff = \sqrt[m]{\left(\frac{\sqrt{4J_2 - I_1^2 / 3} + I_1}{2 \cdot \bar{R}^t}\right)^m + \left(\frac{c_{2\Theta}^{SF} \cdot I_1 + \sqrt{(c_{2\Theta}^{SF} \cdot I_1)^2 + 12 \cdot c_{1\Theta}^{SF} \cdot 3J_2 \cdot \Theta^{SF}}}{2 \cdot \bar{R}^c}\right)^m} = 1.$$

It also determines the transition from the tension part  $I_1 > 0$  of the compressive meridian to its compression part  $I_1 < 0$ .

Curve parameter relationships obtained by inserting the compressive strength point  $(0, -\bar{R}^c, 0)$ :

\* Rotationally symmetric:  $c_1^{SF} = 1 + c_2^{SF}$ ,  $d^{SF} = 0$ , friction parameters are equal  $c_2^{SF} \equiv c_{2\Theta}^{SF}$

\* 120°-rotationally symmetric:  $c_{1\Theta}^{SF} = 1 + c_{2\Theta}^{SF} \cdot \sqrt[3]{1 + d^{SF} \cdot (-1)}$  with  $c_{2\Theta}^{SF}$  friction parameter .  
 $c^{SF}, d^{SF}$  from the two points  $(-\bar{R}^c, 0, 0)$  and  $(-\bar{R}^{cc}, -\bar{R}^{cc}, 0)$  or by minimum error fit .

The function for the compressive meridian curve - of interest is the pure compression domain - is derived by implicitly solving for  $\sigma_1$ ,  $CP = \sigma_3$  (explicitly is not possible here) with the

compressive meridian Lode angle  $\delta = -30^\circ \rightarrow \Theta^{SF} = \sqrt[3]{1 + d^{SF} \cdot (-1)}$

$$\frac{c_{2\Theta}^{SF} \cdot I_1 + \sqrt{(c_{2\Theta}^{SF} \cdot I_1)^2 + 12 \cdot c_{1\Theta}^{SF} \cdot 3J_2 \cdot \Theta^{SF}}}{2 \cdot \bar{R}^c} = 1.$$

## 6.7 Bi-axial strength of Solid Clay Brick Masonry

Here without any discussion, just three pictures of loadings in the principal stress plane shall be shown. For information see [Pag81, Pag83, Pap96].

E. Papa considers masonry as a composite material. Its mechanical properties are obtained by taking into account the properties of the components brick and mortar through a homogenization technique. To describe the behavior of the material components a unilateral damage model is proposed by him that is based on three damage variables. The model was applied to the simulation of tests on masonry panels and miniaturized walls [Pap96]. Numerical results are discussed and successfully compared with experimental data.

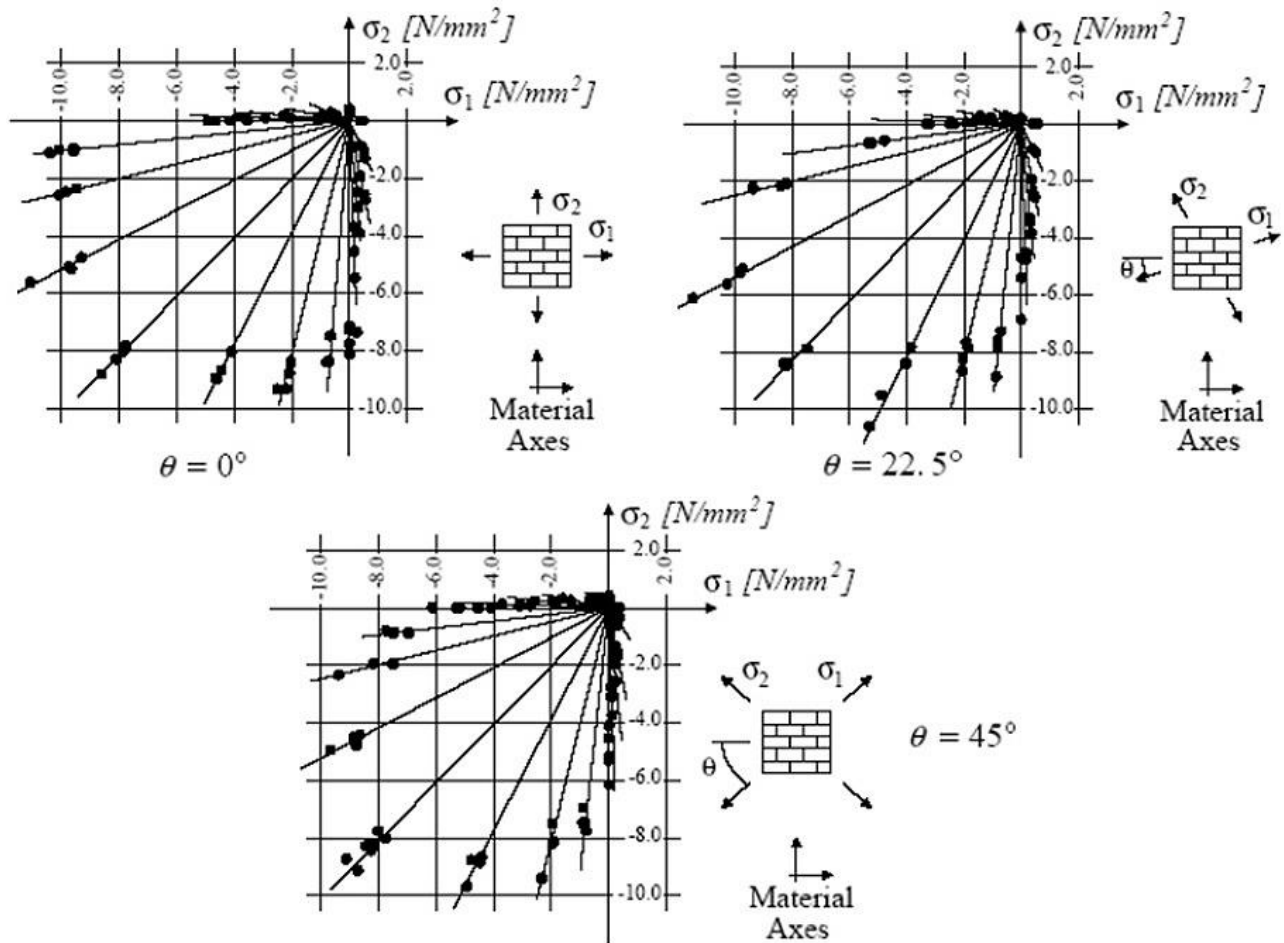


Fig.6.7 -1: Bi-axial strength of solid clay units Masonry, [Pag81,83].

$\sigma_2(\sigma_1)$ , numbers in construction ←  $\sigma_{II}(\sigma_I)$ , general indexing

## 7 Transversely-isotropic UD-materials (GFRP, CFRP)

### 7.1 General Transversely-isotropic UD applications (partly very old figure collection of the author)

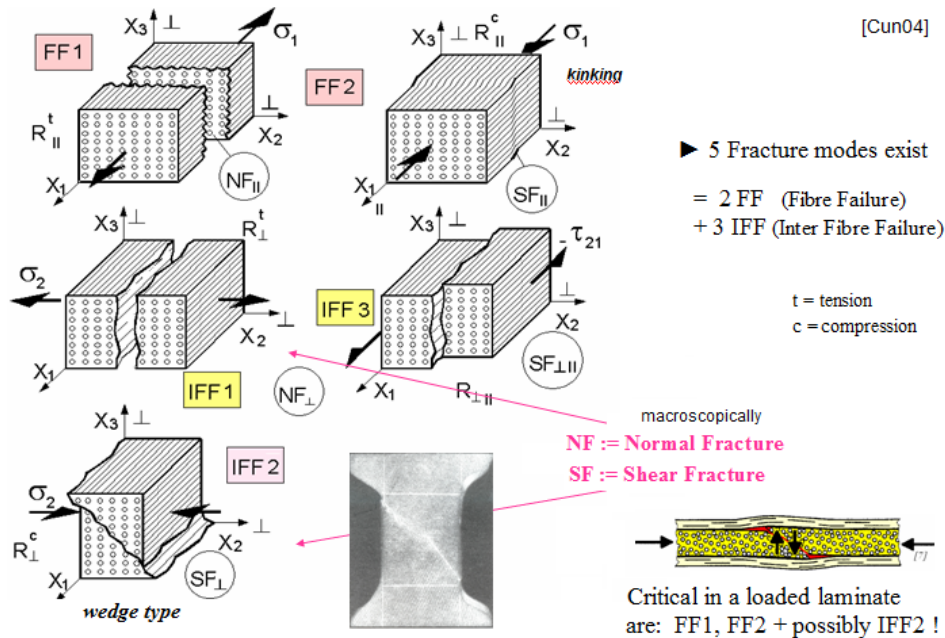


Fig. 7-1: Reminder Fracture failure modes of UD material, NF = Normal fracture, SF = Shear fracture

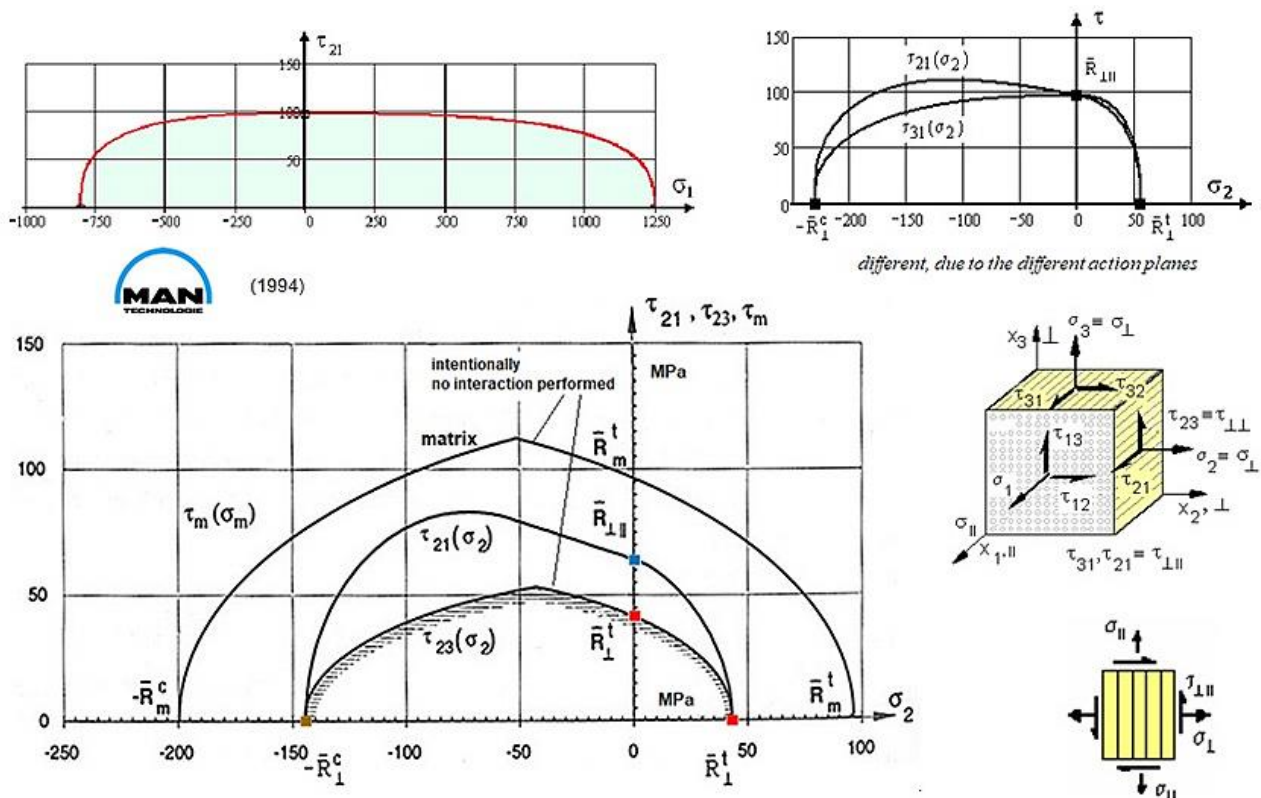
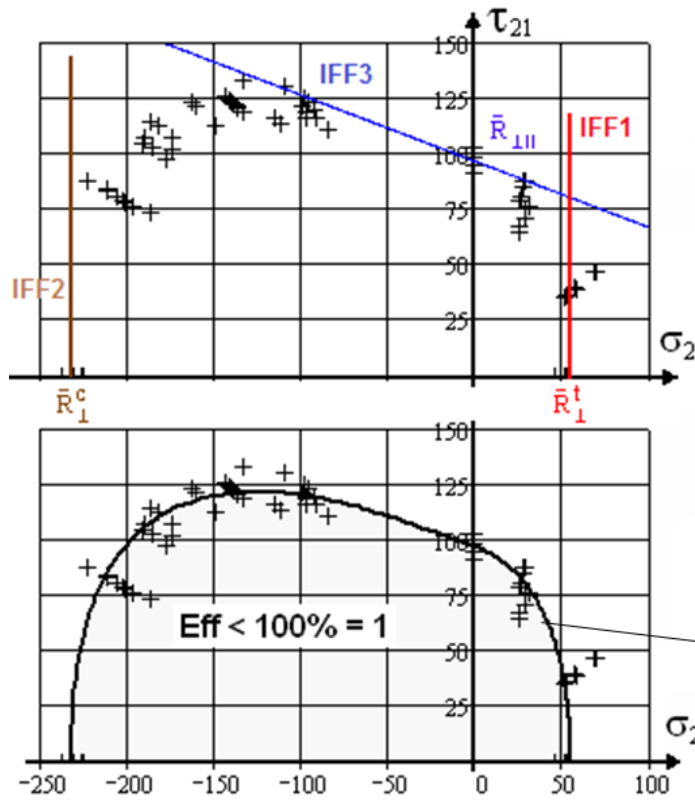


Fig.7-2: Various fracture failure curves linked to UD material

The fracture stress curves exhibit the actions of a shear stress, which is a stress that is composed for  $\tau_{23}$  of a normal shear stress component and a compression shear stress component.

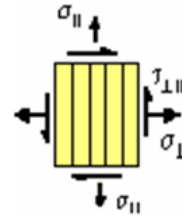
By the way, here, the use of the term ‘stress component’ is correct. Stresses are tensor components or stress vector components.

$I_5$  reflects the different acting of  $\tau_{21}$  and  $\tau_{31}$ , above.



Mapping of course of IFF test data in a pure mode domain by the associated *Mode Failure Condition*.

3 IFF pure modes = straight lines !



$$IFF 1: \frac{\sigma_2}{\bar{R}_{\perp}^t} = 1$$

$$IFF 2: \frac{-\sigma_2}{\bar{R}_{\perp}^c} = 1$$

$$IFF 3 \text{ (2D simplified): } \frac{|\tau_{21}|}{\bar{R}_{\perp\parallel} - \mu_{\perp\parallel} \cdot \sigma_2} = 1$$

$$\tau_{21}(\sigma_2), \check{\sigma}_1 = 0$$

Mapping of course of test data by *Interaction Model*

$$(Eff^{\perp\sigma})^m + (Eff^{\perp\tau})^m + (Eff^{\perp\parallel})^m = 1$$

$$m = 2.5, \mu_{\perp\parallel} = 0.3$$

Fig.7-3: Visualisation of the interaction with a UD-material



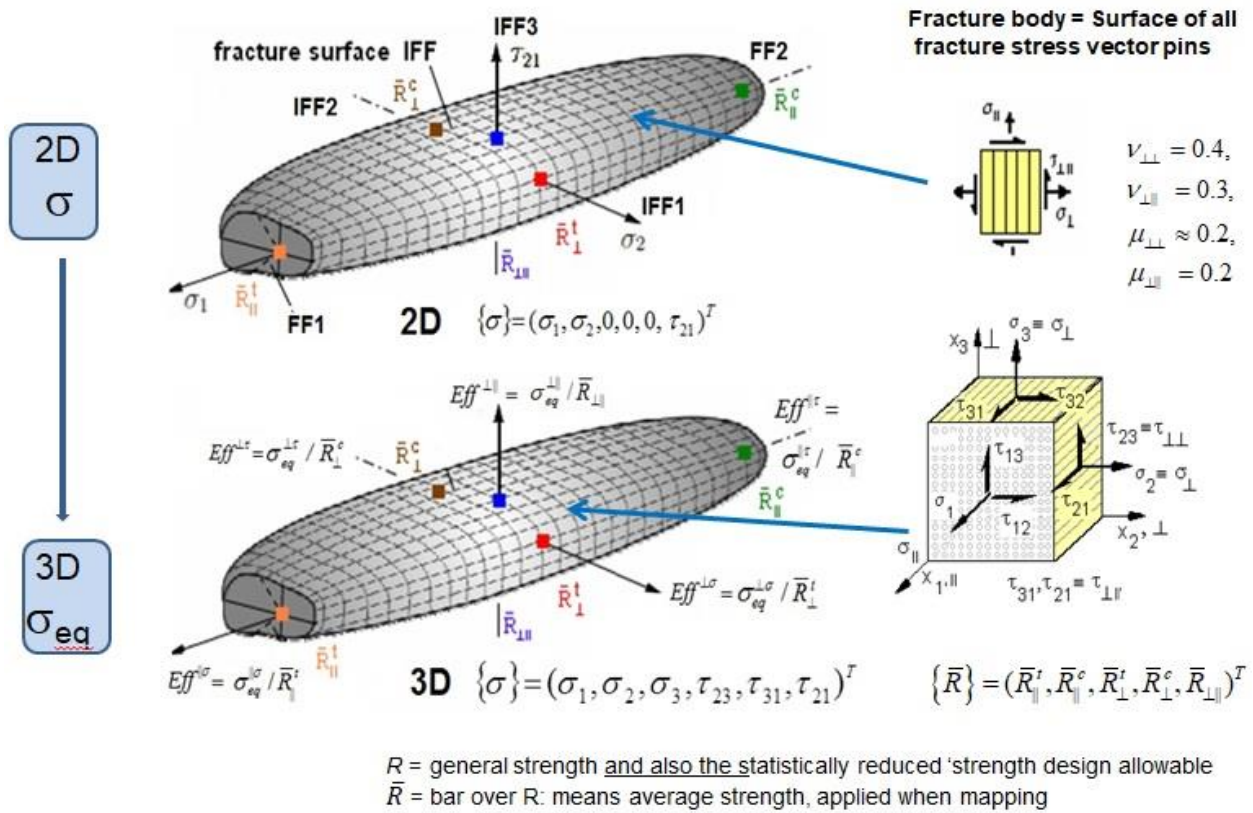


Fig.7-4: From 2D failure body to 3D failure body by replacing stresses by equivalent stresses

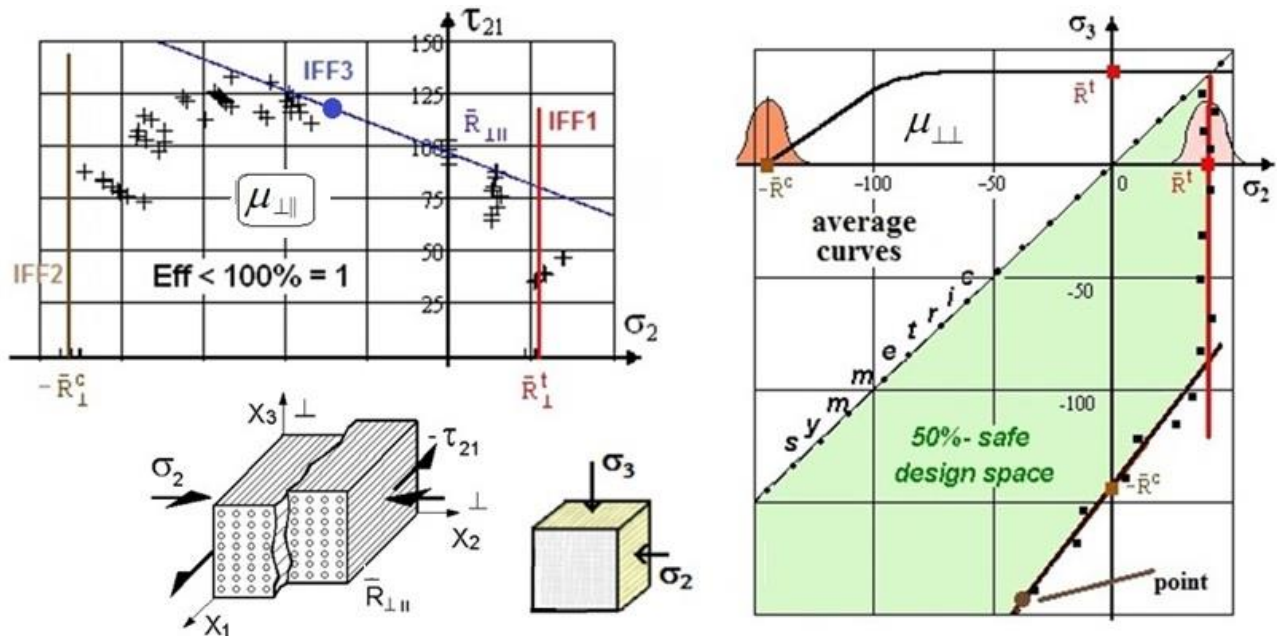


Fig. 7-5: Display of typical fracture test points to estimate the 2 friction parameters  $b$ .  
 When mapping, an average curve is searched, being statistically marked by a bar over:  $R \rightarrow \bar{R}$

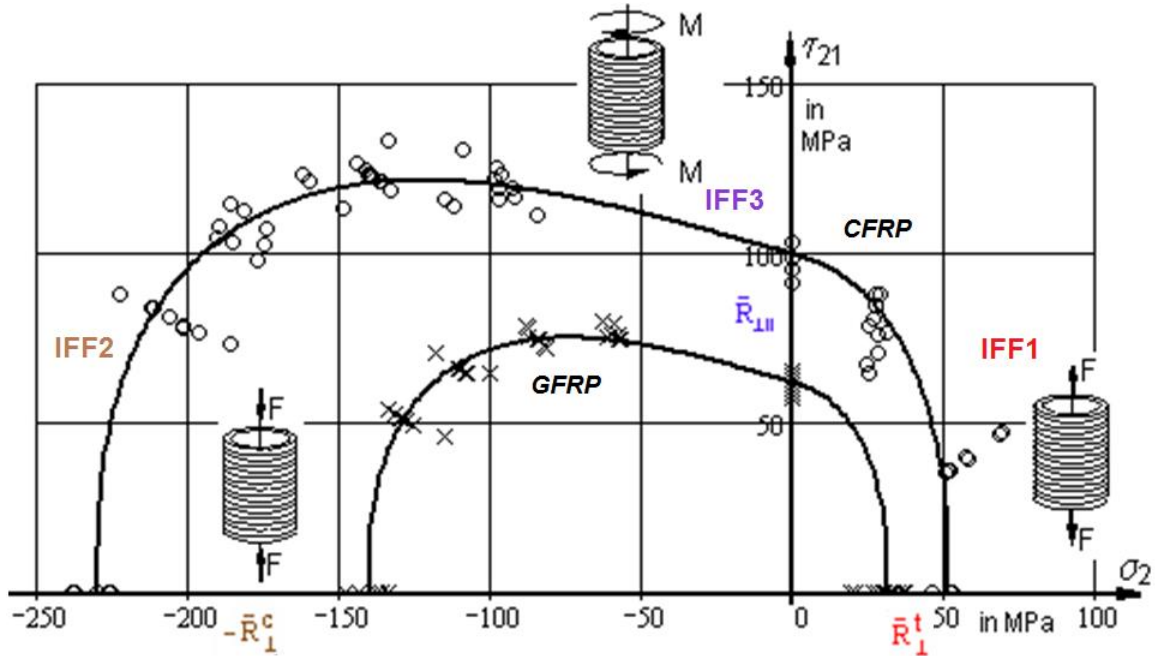


Fig.7-6: Own IFF test results: 2 GFRP, 1 CFRP Test Series

The next figure gives information about ‘Onset-of-yielding’ and how the failure body shrinks under degradation. This degradation is caused by some matrix yielding and diffuse micro-cracking.

‘Onset of (Quasi-)Yielding is difficult to determine. Fig. 7-7 presents a schematic display for the most affected IFF cross-section.

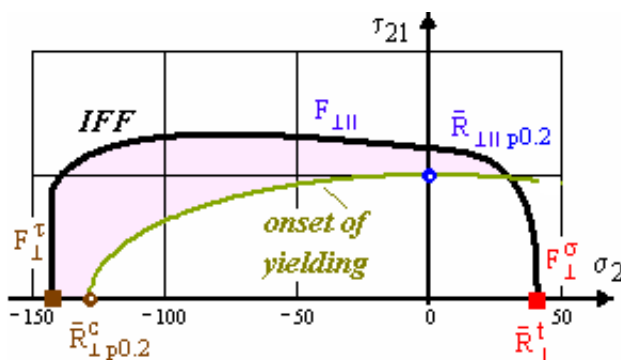


Fig. 7-7: Schematic display of yielding boundaries

$$\frac{I_3}{(\bar{R}_{\perp/0.2}^c)^2} + \frac{I_4}{(\bar{R}_{\perp/0.2}^t)^2} = c_y^2$$

Main sections of the 2D failure body, originally and after shrinking due to a distinct IFF.

The degree of non-linearity in **strain hardening** regime essentially depends on the degrading matrix material. Beyond IFF: Strength and stiffness decay subsequently. This affects the secant IFF moduli. In the post-IFF regime the embedded lamina experiences no sudden death but still has residual strength and stiffness due to in-situ effect. Fig.7-8 shows two cross-sections of the 2D failure body: originally and after shrinking, due to a distinct IFF degradation. Fibers take over load from matrix. Points, marked in figure, are depicted here to highlight effects that are essential for the initial failure load (1, validity of linearity assumption) and for final failure load (2, laterally shrinking failure body).

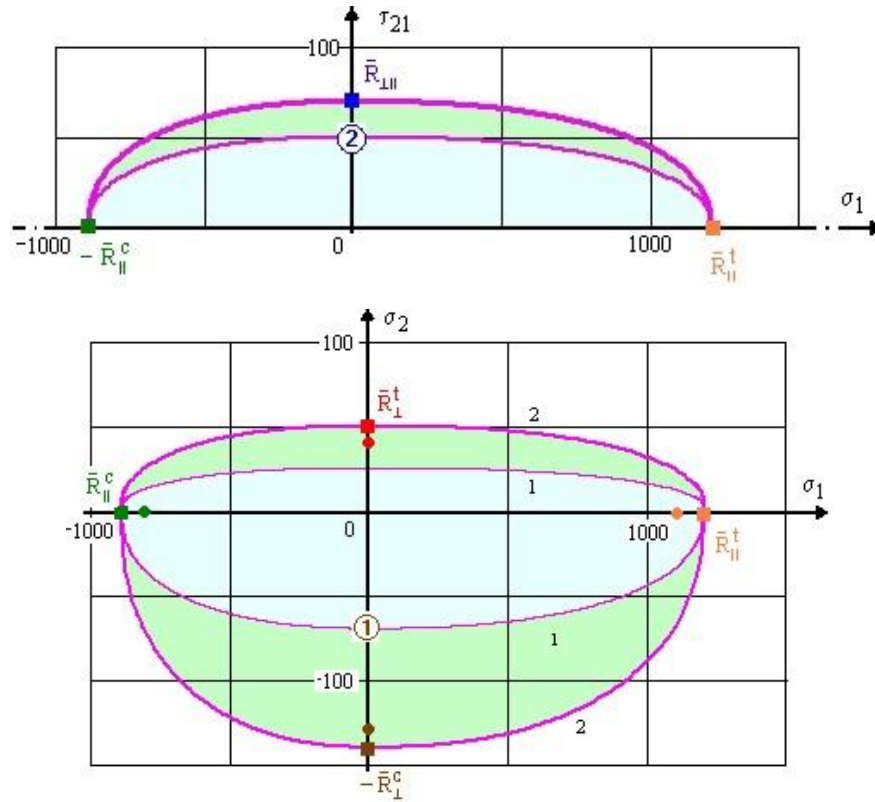
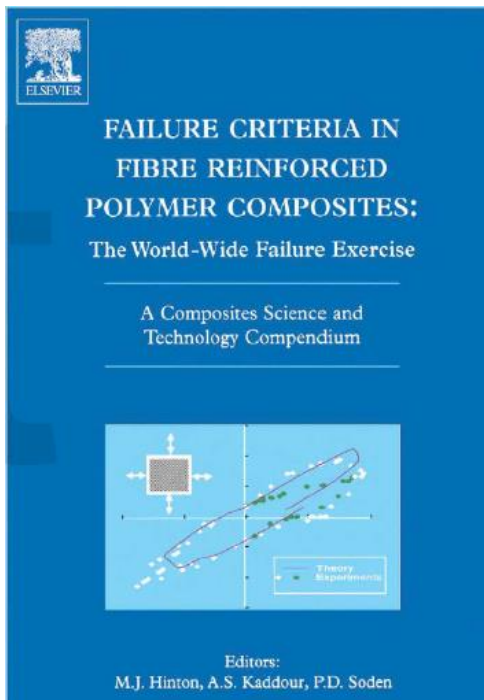


Fig. 7-8: Display of UD material degradation effects under loading

## 7.2 Transversely-isotropic UD-materials, WWFE-I and WWFE-II applications

State of the Art: Static Strength Analysis of the transversely-isotropic UD laminas is best represented by the results of the World-Wide-Failure-Exercises about Static strength criteria for high-performance UD composite parts.



**Organizer:** *QinetiQ, UK*, since 1991

[Hinton, Kaddour, Soden, Smith, Shuguang Li]

**Aim:** (was for the UD materials, only)

*'Testing Predictive Failure Theories for Fiber-Reinforced Polymer Composites to the full!'*

**Method of the World-Wide-Failure-Exercises I,II**

:

Part A: *Blind Predictions on basic strength data*

Part B: *Comparison Theory-Test with (reliable!?)*

*Uni-axial 'Failure Stress Test Data' (= technical, basic strengths) and Multi-axial 'Failure Stress Test Data' (plain test specimens, no notch)*

Thanks to the original UK organizers Mike, Sam and Peter for setting up such a long lasting effortful world-wide exercise.

We contributors know that you could only provide the contributors with test data sets which were available. The quality of them was not known enough well. Hence, the following information shall be given before mapping the courses of test data sets:

- *Part A: Prediction was to made without provision of all needed properties. With strength values alone – in general - a SFC cannot be validated. For compression, however; a friction information must be given.*
- *Part B: Test data sets partly not applicable. Comments on the respective input are given in each Test Case TC.*
- *Validation of lamina SFCs models can be only achieved by lamina 2D- and 3D- test results. 3D-laminate results serve for verification of the laminate design.*

LL:

*Non-accurate test results can barely be mapped by a physically based, test validated SFC. However test-validated SFCs give a possibility to check the goodness of test data.*

At first, what was the meaning of the term ‘Failure’ in the WWFEs?

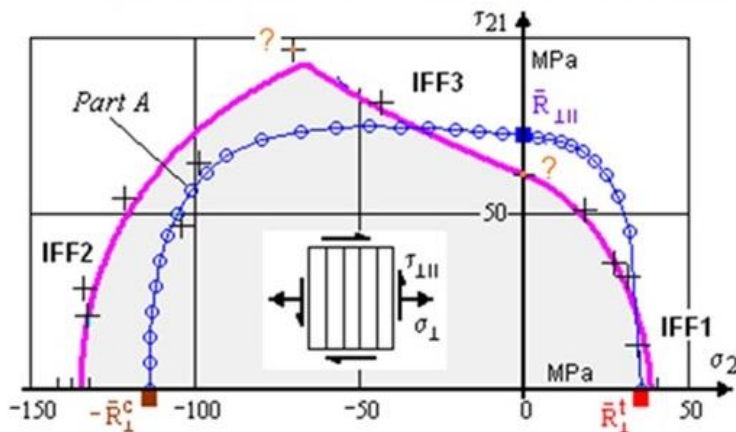
If the structural part does not fulfil its design requirements FF, IFF, leakage, deformation limit, delamination size limit, ...). This was to consider in the Test Cases.

***Depicted and discussed are primarily the essential critical lamina-related TCs of WWFE-I and –II because these serve Model Validation. The laminate-examples serve for Design Verification, ‘only’.***

### WWFE-I, TC1, UD lamina, GFRP, E-glass/LY556 Ep [Test data DLR Stuttgart]

How looks the main cross-section of the IFF body?

**Task:** Determination of fracture failure curve, capturing IFF3, IFF1 and IFF2 by performing a so-called ‘tension-compression-torsion tube test’ campaign



Tube, 90°-filament hoop wound

$$\sigma_1 = \hat{\sigma}_y = \hat{\sigma}_{hoop} = p \cdot r_{int} / t$$

$$\sigma_2 = \hat{\sigma}_{ax} = p \cdot r_{int} / (2 \cdot t) + F_{ax} / (2\pi \cdot r_{int} \cdot t)$$

$$\tau_{21} = M_t / \text{critical cross section area}$$

\*test evaluation based on un-deformed geometry

\*monotonic loading performed in test

$$\{\bar{R}\} = (1140, 570, 35, 135, 72)^T \text{ PartB-change}$$

$$b_{\perp}^f = 1.09 ; b_{\perp||} = 0.13 ; b_{\perp||}^f = 0.4 ; m = 3.1$$

$$\mu_{\perp||} = 0.6 \text{ compared to usual } \mu_{\perp||} = 0.25$$

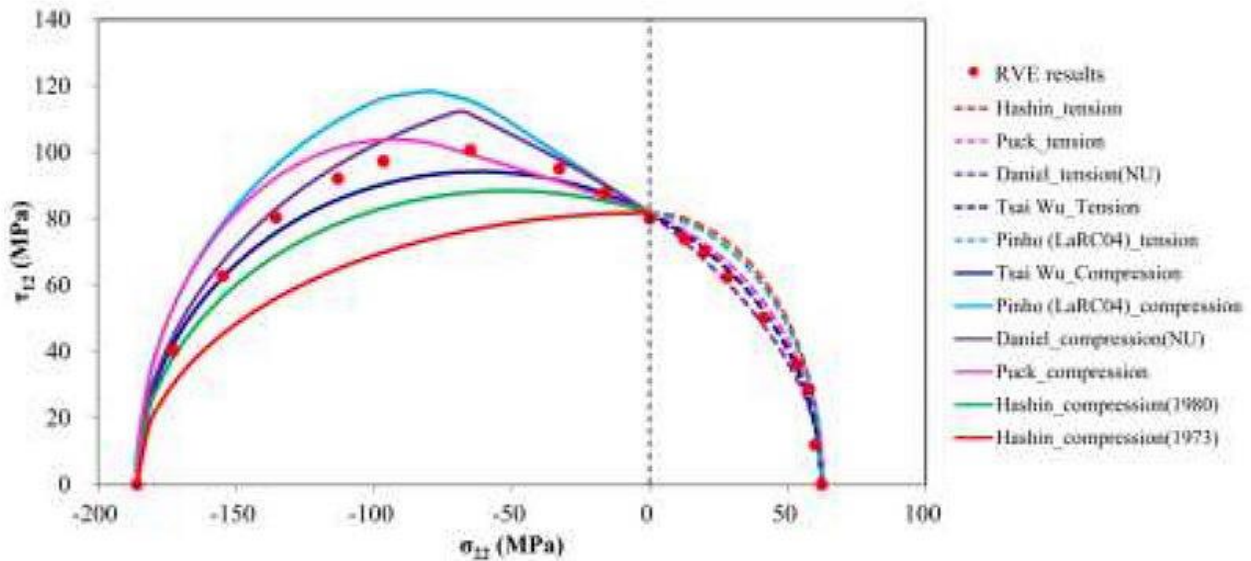
$$\Delta T = -68^\circ\text{C (after curing)}$$

Part A, prediction: Data of elasticity properties, UD strengths  $\bar{R}$  provided, only. No friction value  $\mu$  for IFF3 slope provided! Lowest value for  $\mu$  in Part A assumed (safe side)

Part B: the 3 strength points were altered! Two doubtful (?) failure stress points were provided. Nevertheless, QinetiQ asked to map the course of PartB-test data (magenta curve) despite of the fact that a Poissons ratio  $\mu_{\perp||}$  had to be taken which is much too large, compared to values of own and other test campaigns!

- Before test data evaluation: Check whether a thin tube test specimen ( $r / t > 10$ ), otherwise ‘thick’ formula is to use.
- No reasonable PartA-mapping possible with the provided PartA-information, see blue curve!
- After later discussion with the former test engineer at DLR: “The upper test point must be false!”
  - ▶ TC1 test data set (Part B) is not acceptable for a model validation!

The next figure proves once more, that even false test results are un-intentionally taken for a comparison of theories. **Before performing a comparison one should check in advance the quality of the test results!** For the TC1, the author knew about the test inaccuracy of the two comparison-decisive test points above.

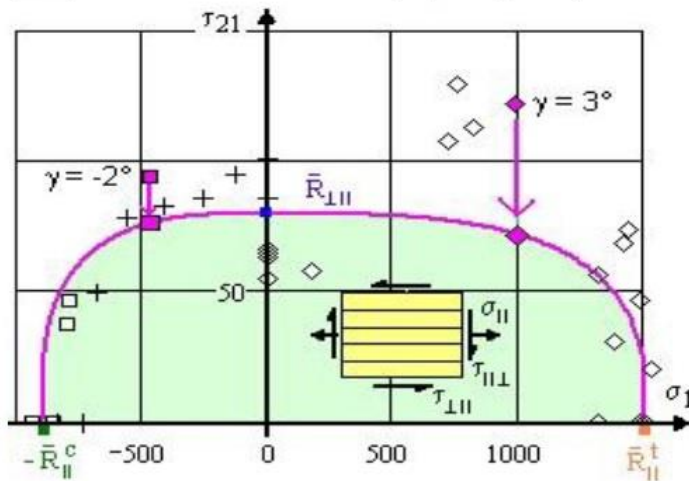


*Failure Criteria of Unidirectional Carbon Fiber Reinforced Polymer Composites Informed by a Computational Micromechanics Model*

[Qingping Suna†, Guowei Zhou, c†, Zhaoxu Mengd†, Haiding Guoa\*, Zhangxing Chene, Haolong Liua, Hongtae Kangf, Sinan Ketend, Xuming. ghd@nuaa.edu.cn]

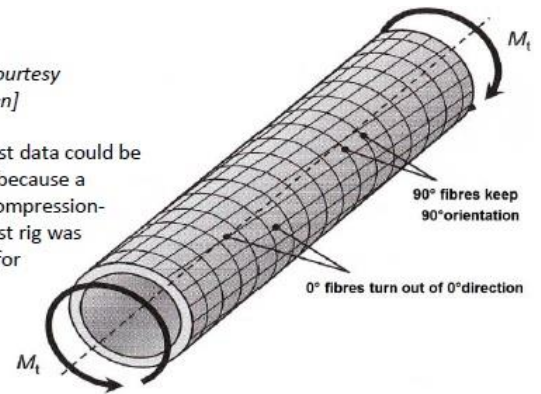
**WWFE-I, TC2, UD lamina, CFRP, T300/BSL914C Ep,  $\tau_{21}^{fr}(\sigma_1)$**

**Task: Determination of IFF curve, capturing IFF3, FF1 and FF2**



[Figure: courtesy IKV Aachen]

Bi-axial test data could be obtained because a tension-compression-torsion test rig was available for tubes



Tube (90°-hoop wound)  $\sigma_1 = \sigma_{hoop}, \sigma_2 = \sigma_{axial}$ ,

$$\{\bar{R}\} = (1500, 900, 27, 200, 80)^T,$$

Part B:  $b_{\perp\parallel} = 0.13; m = 3, \Delta T = -125^\circ\text{C}$  (after curing)

Part A, prediction: Strength data only provided, no friction value (slope)  $\mu$ .

Part B, comparison: Strength data sets were provided, partly from 0°-test specimens (axial fiber direction) and partly from the traditional 90°- tube test specimen! After transformation, the two chosen  $\blacksquare \blacklozenge$ , by executing a *non-linearly CLT-computed* shear strain analysis, these two 0°-points exemplarily could be shifted onto the magenta envelope. The shear strength point (blue) had to be adjusted according to new B information.

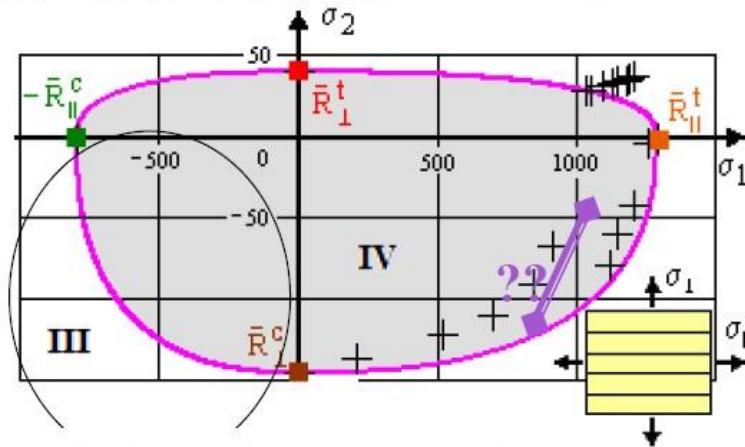
- Data from 0°- tube test specimens  $\diamond$  cannot be used like hoop-wound 90°-tube test specimens, physically non-sense.
- The coordinate system of the 0°-test specimen lamina twists under torsion by  $\gamma$ . Hence, 0°-test data must be transferred into the twisted material coordinate system.
- ▶ TC2 test data set could serve for material model validation after correction by the author and choosing just 90°- wound tubes.

$$\sigma_2 (\bar{\sigma}_1 \equiv \sigma_1)$$

Which is the fracture envelope  $\sigma_2 (\sigma_1)$  ?

**Task:** Mapping in all four quadrants without obtaining sufficient test results

fracture modes: (FF1, FF2, IFF1, IFF2, -)



Tube (90°-hoop filament wound)

$$\sigma_1 = \sigma_{hoop}, \quad \sigma_2 = \sigma_{axial}$$

$$\{\bar{R}\} = (1280, 800, 40, 145, 73)^T$$

(Part A, old IFF3 formula:

$$b_{\perp\parallel} = 0.13, \quad b_{\perp\perp}^r = 0.4, \quad b_{\perp}^r = 1.5, \quad m = 3),$$

Part B:  $b_{\perp\parallel} = 0.13, b_{\perp}^r \rightarrow b_{\perp\perp} = 1.5;$

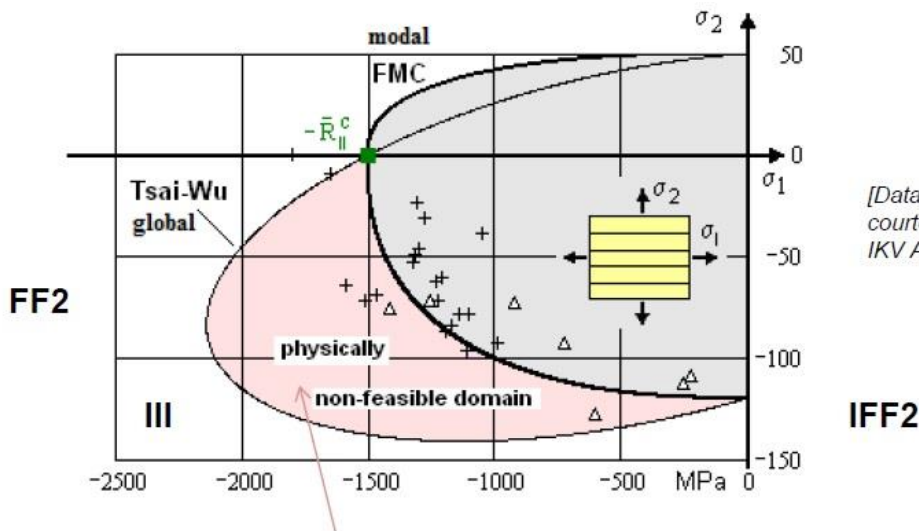
$$m = 3$$

Part A: Data of strength points were provided  $\{\bar{R}\}$ . Remaining necessary frictions  $\mu$  were assumed by the author.

Part B: For the quadrants II and III no multi-axial data sets were provided. Test data in quadrant IV show discrepancy! Real winding angle was  $\pm 85^\circ$  instead of  $90^\circ$  (effect on strength and stiffness was not regarded w.r.t. other missing information and to scatter). IKV, Aachen with Puck, filled the gap in the Tsai-Wu non-feasible domain, of quadrant IV.

- In quadrant IV it seems that two different 'test procedures' have been used obvious in the domain of 1000 MPa.
  - In quadrant I the test data set could be better mapped by a higher  $m$ -value, however this was not done due to the inside oriented scattering data in quadrant IV and that  $m = 3$  well matched the IKV-data set in quadrant III (next slide).
    - The provided TC3 test data set cannot really serve for a SFC material model validation.
- Questions arise w.r.t. quadrant IV: (1) Are different tests used? (2) Was the test data evaluation, regarding the specimen type, performed considering widening of the tube?

### Mapping in the 'Tsai-Wu non-feasible domain' (quadrant III)



[Data, quadrant III: courtesy, Knops, IKV Aachen, 2003]

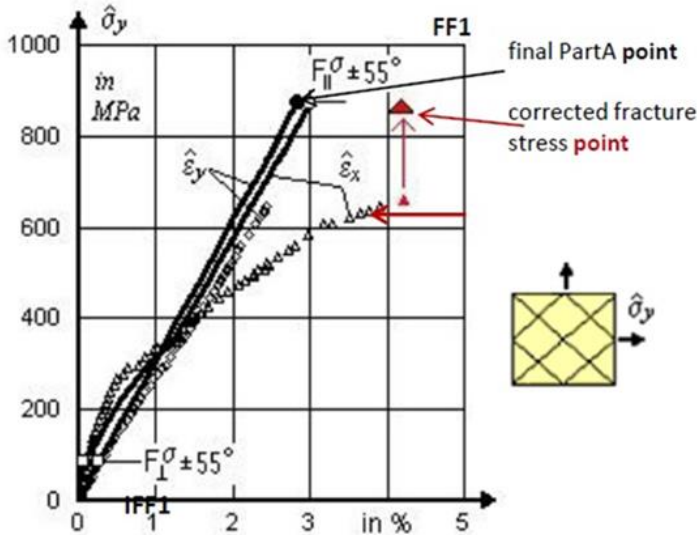
The modal FMC maps correctly, the **global** Tsai-Wu formulation predicts a non-feasible domain!

► TC3 test data set does serve for validation of the SFC model in quadrant III after obtaining the IKV test results.

WWFE-I, TC11, UD, GFRP, E-glass/ MY750 [+55/-55/55/-55],  $\hat{\sigma}_y(\hat{\epsilon}_y)$  and  $\hat{\sigma}_y(\hat{\epsilon}_x)$

Which are the stress-strain curves for  $\hat{\sigma}_y : \hat{\sigma}_x = 2 : 1$  ('pressure vessel, well designed to one single load case 'pressure loading'  $p_{int}$ ) ?

**Task:** Non-linear determination of the tube (waterhose) strains



Tube, filament wound, end-reinforced

Coupon Test Specimen, test data TC 8

$$\{\bar{R}\} = (1280, 800, 40, 145, 73)^T,$$

$$\epsilon_f^{fract} = 2.8\%$$

$$\Delta T = -68^\circ\text{C (after curing)}$$

PartB :

$$b_{\perp\perp} = 1.09 ; b_{\parallel\parallel} = 0.13; m = 3$$

Part A: Data of strength points were provided  $\{R\}$ .

Part B: (1) The evaluated, measured (on outer surface) laminate fracture stresses are about 25% lower than the predicted one. However, due to the end-reinforcement the shape of the tube bulges, becomes a barrel. The radius increases. Bulging will degrade the axial direction more than the hoop direction and probably may change the angle to a slightly higher value according to scissoring. (2) The ratio of the fracture strains is 2:1. The design is fibre-oriented and net theory (matrix stiffness put zero) must be approximately usable at fracture. It is then  $\sigma \sim \epsilon$  and the strain in all directions should be almost the same. (3) The measured hoop strain 4.2 % is higher than the fiber fracture strain 2.8%, but this is for a net theory designed tube at fracture !  
 → What is the meaning of 4.2% ?

*Net theory, increasingly valid after full IFF1 damaging, would show after the curves intersection approximately linearly running curves with about the same strain level. This is not to view. Why? At low stress levels continuum theory gives better results than net theory, of course.*

*The analysis of the bulging of the full barrel requires a FEA, which is not possible for the author. The axial strain at the gauge position is affected by the end constraints more than the hoop strain. The boundaries are too close to the locations of the strain gauges that the readings of the strain gauges are affected by the end conditions. The twofold failure in adjacent 55° layers is subjected to 'joint failure probability' which reduces the IFF load carrying capacity a little. Mind: Such a high straining is usually not permitted in structural applications.*

Laminate quantities have the index roof. The fiber direction angle counts from x (0°) to y (90°).

The critical lamina is the outer lamina that experiences stretching from membrane loading together with bending. Bending comes from the end-reinforced boundaries because these are not so far away from the locations of the strain gauges, so, that barrelling could be really avoided.

As cylindrical widening cannot explain the difference of the curves, the effect must have come from above barrelling. Fracture by 'barrelling (bulging) bending' seems to be the main reason for the difference.

The analysis of the TC11 requires a non-linear FE calculation with an excellent solver to capture the anisotropic stiffness degradation from IFF1 till FF1.

Therefore, TC11 is not so much an exercise for failure criteria but for excellent FE codes.

In addition, 15 years later another nocturnal thought about the discrepancy Prediction ↔ Measurement shall be presented:

\* Designed by using Net Theory:  $\hat{\sigma}_y = \hat{\sigma}_{hoop} = 2 \cdot \hat{\sigma}_{ax}$

Fiber direction angle  $\alpha = \arctan \sqrt{\hat{\sigma}_y / \hat{\sigma}_x} = \arctan \sqrt{2} \rightarrow \alpha^\circ = \alpha \cdot 180^\circ / \pi = 54,75^\circ$ .

\* Measured fracture strains of the bulged laminate tube wall are

On outer surface at fracture  $\{\hat{\varepsilon}_{outer}^{fracture}\} = (+4.2, +2.4, 0)^T \%$ .

Checking the 'scissor effect' = increase of angle  $\hat{\alpha} = \alpha^\circ \cdot \pi / 180^\circ$

$\hat{\alpha}_{final} = \arctan(\tan \hat{\alpha} \cdot (1 + \hat{\varepsilon}_{hoop}^{fracture}) / (1 + \hat{\varepsilon}_{ax}^{fracture})) = 0.97 \rightarrow \alpha_{final}^\circ = \hat{\alpha}_{final} \frac{180^\circ}{\pi} = 55.5^\circ$ .

Result: practically is no scissor effect.

\* Evaluation of measured strain values

Because of the negligible scissor effect, the fiber strain can be calculated by

$$\varepsilon_f^{fr} = \varepsilon_{\parallel}^{fr} = 1 - \sqrt{1.042^2 + 1.024^2} = 0.046 = 4.6\% = 1.64 \cdot 2.8\% \text{ !?}$$

This is 64% higher than the given fiber fracture strength.

It does also not fit to the given (nominal geometry-related?) failure stress  $\hat{\sigma}_{hoop} = 645\text{MPa}$ .

Result: Are there open questions with WFE-I TC11?

The provision of strains, measured on the outer surface, together with the value of the internal pressure would have been clearer. Based on undeformed initial geometry the 'vessel formulas' read:

$$\hat{\sigma}_y = \hat{\sigma}_{hoop} = p \cdot (r_{int} + \Delta r) / t, \quad \hat{\sigma}_x = \hat{\sigma}_{ax} = 0.5 \cdot \hat{\sigma}_{hoop} + F / (2\pi \cdot r_{int} \cdot t) \text{ with } F = 0.$$

*Each interpretation of test results is helpful if it improves understanding.*

*Unfortunately this was not the case with QinetiQ in the WWFEs.*

*LsL:*

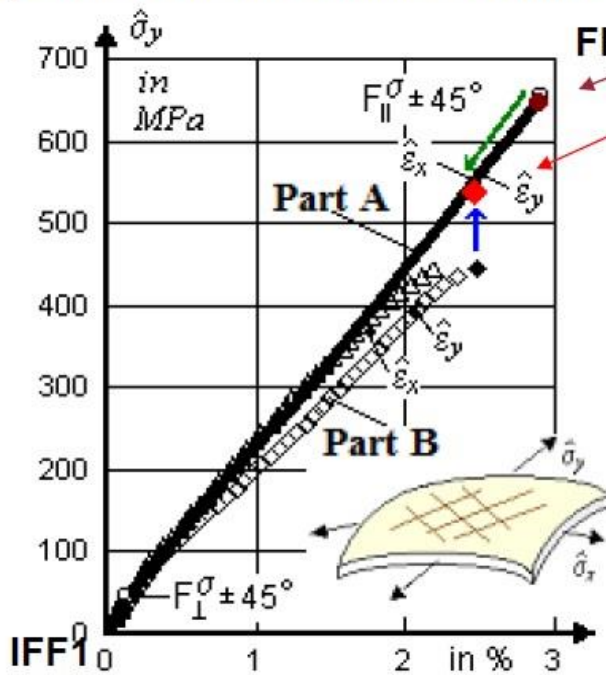
- WWFEs aim: *Testing Predictive Failure Theories for Fiber-Reinforced Polymer Composites to the full !* This includes UD strength criteria and numerical tools.
- User: *Thinks only at a comparison of UD strength criteria!*
- *Tube qualification testing by internal pressure requires a test set-up where the membrane stresses cause the failure.*



WWFE-I, TC13, UD, GFRP, E-glass/MY750/Ep, [45/-45/45/-45]<sub>s</sub>  $\hat{\sigma}_y(\hat{\epsilon}_y)$ ,  $\hat{\sigma}_y(\hat{\epsilon}_x)$

Which are the stress-strain curves for  $\hat{\sigma}_y : \hat{\sigma}_x = 1:1$  ( $p_{int}$  + axial tension) ?

**Task: Non-linear determination of the tube strains**



Final blind PartA prediction point.

PartB test point after the two corrections

Tube, end-constrained

$$\hat{\sigma}_y = \hat{\sigma}_{hoop}$$

$$\{\bar{R}\} = (1280, 800, 40, 145, 73)^T, \Delta T = -68^\circ\text{C (after curing)}$$

$$E_{||} = 45600 \text{ MPa}, \epsilon_f^{fracture} = 2.8\%$$

Using netting theory of this fibre-dominated laminate for a bulging assessment of fracture it follows with the

PartB-information on  $\hat{\epsilon}_{hoop}^{fracture} = 0.022$ ,  $\hat{\epsilon}_{axial}^{fracture} = 0.025$  and

setting  $\sigma_{\perp} = \tau_{\perp||} = 0$  (zero matrix stiffness) the laminate stresses read  $\hat{\sigma}_x = \hat{\sigma}_y = 530 \text{ MPa}$ , delivering lamina stress  $\sigma_{||}^l = 1062 \text{ MPa}$ .

From this a reduction is derivable

$$\hat{\sigma}_y^{reduced} = 660 \text{ MPa} \cdot (1062/1280) = 547 \text{ MPa}.$$

Part A: Data of elasticity properties, UD strengths  $\{R\}$  and  $\epsilon$  were provided. Remaining data assumed.

Part B: No modification of model ! Obvious in the graph is the high fracture load predicted compared to test. Also, non-linearity comes not out. However, bulging with the axially altering widening of the end-constrained tube is reported in experiment. This additional test data information – supported by simple netting analysis – caused to *reduce the computed fracture strain* and to *increase the failure stress* after assessing bulging !

*Fibre-dominated design and laminate behavior*

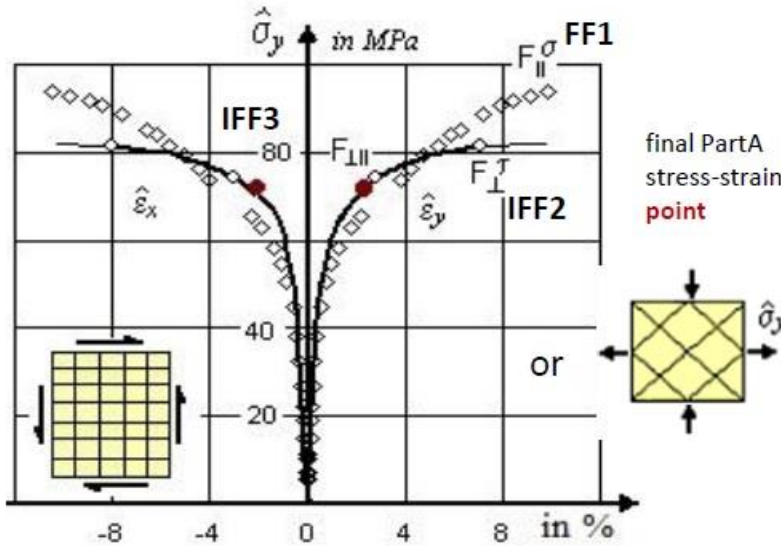
*It is to expect that bulging together with the relatively large deformation will mainly cause that the two test curves do not lie upon another and are shorter than the predicted ones. An interpretation of the PartB-provided strains was helpful. The test fracture points could be raised and the predicted fracture points could be lowered. Bulging must be treated by a FEA program.*

► *After re-evaluation, the TC13 test data set is applicable for the verification of the laminate design. Mapping quality became very good, which proves the used UD material SFC model*

WWFE-I, TC14, UD, GFRP, E glass/ MY750 Ep, [45/-45/45/-45]s,  $\sigma_y(\varepsilon_y)$ ,  $\sigma_x(\varepsilon_x)$

Which are the stress-strain curves for  $\hat{\sigma}_y : \hat{\sigma}_x = 1 : -1$  (means shear, realized by  $p_{int}$  + axial compression) ?

**Task: Non-linear determination of the tube** (using radial stress  $\hat{\sigma}_y = \hat{\sigma}_{hoop} \equiv \hat{\sigma}_{tangent}$  induced by internal pressure  $p_{internal} \cdot \bar{r} / t$  and an axial over-compressed  $\hat{\sigma}_{ax} = \hat{\sigma}_x = F / 2\pi \cdot r \cdot t$ )



$$\{\hat{\sigma}\} = (-\hat{\sigma}_y, \hat{\sigma}_y, 0, 0, 0, 0)^T = (0, 0, 0, 0, 0, \hat{\tau}_{xy})^T$$

Tube, wound  $\rightarrow$  anti-symmetric lay-up

$\hat{\sigma}_y = \hat{\sigma}_{hoop}$ , TC8 data

$$\bar{r} / t = (r_{inn} + t) / t = (50 + 5.9) / 5.9 = 9.5 < 10$$

$$\{\bar{R}\} = (1280, 800, 40, 145, 73)^T$$

$$\Delta T = -68^\circ\text{C (after curing)}, \varepsilon_f^{fracture} = 2.8\%$$

$$\text{Part B: Using } \hat{\varepsilon}_{hoop}^{fracture} = 0.10, \hat{\varepsilon}_{axial}^{fracture} = -0.11$$

$$\hat{\alpha} = 45 \cdot \pi / 180 \text{ the real fracture angle}$$

$$\alpha_{final} = \arctan(\tan \hat{\alpha} \cdot (1 + \hat{\varepsilon}_{hoop}^{fracture}) / (1 + \hat{\varepsilon}_{ax}^{fracture}))$$

$$\Rightarrow 51^\circ \text{ after final scissoring.}$$

Part A: Data of elasticity properties, UD strengths  $\{\bar{R}\}$  and  $\varepsilon_{fracture}$  were provided. Remaining data assumed by author.  
 Part B: „Thick cylinder theory was used in test evaluation. Strains were measured at the inside surface of the tube and provided. Bulging reported. Formula applied for thick cylinder was not provided.”  
 Stiffness of the test curves of this matrix-dominated laminate are smaller from the beginning.  
 Bulging  $\rightarrow$  slight modification Part A to Part B for allowing to compute a higher fracture hoop strain by increasing the maximum shear strain in the computation from 4% to 10%.

Matrix-dominated laminate behaviour is faced.

- (1) Joint failure behavior of adjacent layers acts and causes in test as well an earlier in-plane shear failure as a stiffness loss.
  - (2) The large strain/ bulging deformation behavior cannot be captured by the simple secant modulus non-linearity approach of the author. The author did not trigger his non-linear analysis, FEA is needed with its excellent solvers. The utilized softening curve does not allow for efficient stress-redistribution.
  - (3) The strain-controlled, embedded fibres take over degradation-caused loading, and seem, due to redundancy effects, to still act above the 'weakest link value' level. Mind here my softening curves! Benign IFF2, here.
  - (4) Mind, please: Typical engineering applications are limited to  $< 1.5\%$  operational strain!
- TC14 test data set is applicable for the verification of the laminate design. It proofs the used UD material SFC model.

Two non-funded German engineers won WWFE-I with their failure criteria:

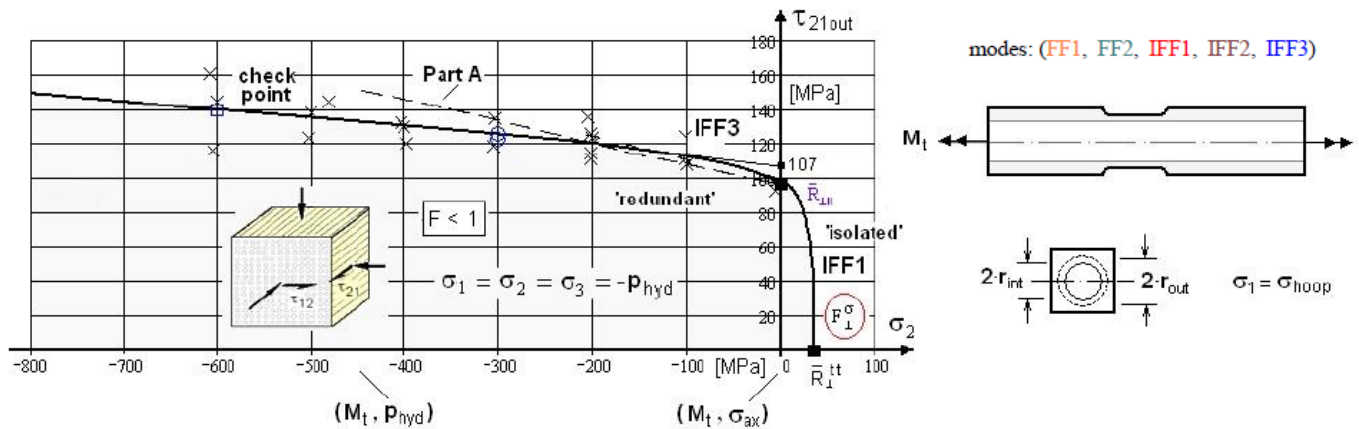
Cuntze with his Failure-Mode-Concept based criteria and

Puck with his Action Plane criteria.

**WWFE-II, TC2, UD lamina, CFRP, T300/PR319Ep,  $\tau_{21}(\sigma_2 = -p_{hyd})$**

Which is the influence of  $p_{hyd}$  on in-plane fracture shear stress or shear stress failure envelope ?

**Task: Non-linear determination of the tube shear failure stress curve under hydrostatic pressure**  $\tau_{21}^{fr}(\sigma_2 = \sigma_1 = \sigma_3 = -p_{hyd})$



Part A: Data of strengths were provided. Remaining necessary data were assumed by author. The prediction of the *average* curves in TC2 and TC3 would have required the provision of an *average* curve however an *upper* stress-strain curve was provided. No information on the acting 2<sup>nd</sup>-Tg effect. It is assumed that  $\tau_{out}$  is the provided shear stress. From the formula  $\tau = 2 \cdot M_T \cdot r / [\pi \cdot r_{out}^4 \cdot (1 - r_{inn}^4 / r_{out}^4)]$  follows  $\tau_{out} \cong 1.4 \cdot \tau_{inn}$

Part B: Barrelling of the specimen was reported. The course of the provided test data does not exhibit the existing 2<sup>nd</sup>-Tg-effect demonstrated by a slope beyond the epoxide-typical '-200 MPa kinking point (hydrostatic pressure). Why? Open failure surface in  $p_{hyd}$ -direction. The data set of the 90° tube is only used but not the 0° tube set, regarding its twisting.

TC2 is fully linked to TC3 and TC4. TC2 and TC3 are average curves. Nevertheless, for Part A an 'upper stress-strain' curve was provided. The use of this curve does not lead to fully linked TCs! With the provided TC4 information of Part B, the author could determine the necessary average curve. Good Mapping was obtained first, after re-evaluation of provided data and the use of the **average stress-strain curve** and by a **novel physical interpretation** of test data, discriminating in modelling near  $\sigma_2 = 0$ , the two domains of 'isolated' and 'embedded (redundant)' failure stress states, if  $\sigma_2 < 0$ ! Having known the average curve in Part A, the predicted curves would not differ from the Part B ones.   
 ► TC2 test data set, - after a new evaluation and interpretation - finally became applicable for SFC model validation.

In TC2 and TC3 included is the modelling of the 2<sup>nd</sup>-Tg-effect for the UD material. Both the figures are also examples for a redundant part (IFF3) and a weakest-link part (IFF2) of a failure curve, which were separately mapped to achieve an accurate mapping.

**WWFE-II, TC2, TC3, TC4: Short derivation of the average stress-strain curve**

Only the derivation of the average curve made it possible to carry out the required mapping. Without this curve, the existing checkpoint in the three graphs would not be hit. This checkpoint  $\gamma_{21} = 0.142 = 14.2\%$ ,  $\tau_{21} = 140$  MPa,  $p_{hyd} = 600$  MPa was intentionally not optimized.

The required curve is a fitting curve through all the fracture points of the shear strain-shear stress Ramberg-Osgood curves (*R-O was the chosen fitting function. All four R-O parameters vary with  $p_{hyd}$  or with  $\sigma_3$* ) according to the formula

$$\gamma_{fr,\sigma_2} = \tau_{fr,\sigma_2} / G_{\sigma_2} + 0.002 \cdot (\tau_{fr,\sigma_2} / R_{\perp 0.2,\sigma_2})^{n_{\sigma_2}}$$

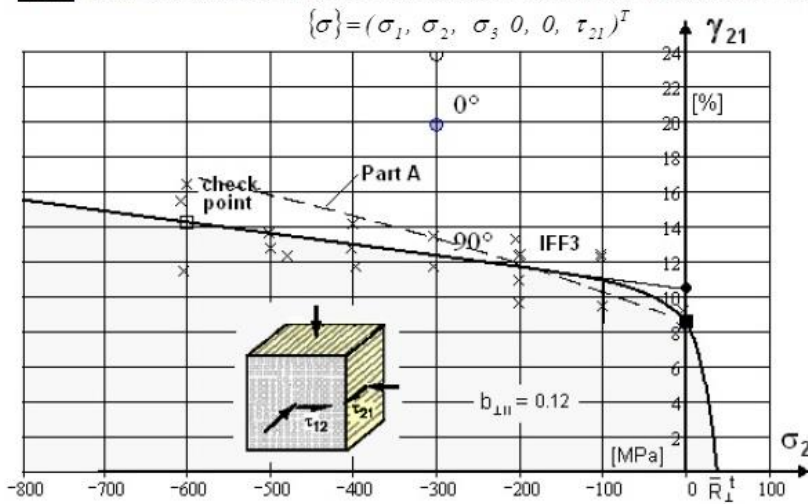
\* The jump in data size at  $p_{hyd} = 0$  can be explained again by the redundancy influence of the be almost straight), between the 'check point' and the above failure strain  $\gamma_{fr}$

$$\gamma_{fr}(\sigma_2) = c_1 + c_2 \cdot \sigma_2 \quad \text{with} \quad c_1 = 0.104, \quad c_2 = -6.33 \cdot 10^{-5}$$

\* The final rounding procedure is performed analogously to TC2 by a correction function, with

$$f_{TC3} = (1 - c_3 / e^{-\sigma_2/c_4}), \quad \text{with} \quad c_3 = 0.173, \quad c_4 = 22$$

**Task: Non-linear determination of one normal stress-shear strain curve of the tube  $\gamma_{21}$  ( $\sigma_2^{fr}$ ,  $\tau_{21}^{fr}$ ) TC3**



**Tube** hoop wound, data for TC2, TC3, TC4

$\sigma_{hoop} = \sigma_1$ ,  $\sigma_{radial} = \sigma_3$ , thick-walled

$\{\bar{R}\} = (1378, 950, 40, 125, 97)^T$  MPa,

$\{\varepsilon_{fracture}\} = (1.07, 0.74, 0.43, 2.8, 8.6)^T$  %,

$\{E\} = (129000, 129000, 5600, 5600, 1330)^T$  MPa

$E_{m0} = 950$  MPa,  $\nu_m = 0.35$ ,  $G_{23} = 1860$  MPa,

$\nu_{\perp\perp} = 0.48$ ,  $\nu_{\perp\parallel} = 0.32$ ,  $m = 2.8$ ,

Check point  $\square$ : ( $\gamma_{21} = 0.142$ ,  $\tau_{21} = 140$ ,  $p_{hyd} = 600$ )

$b_{\perp\perp} = 1.09$ ;  $b_{\perp\parallel} = 0.12$  (in PartA = 0.3),

2<sup>nd</sup> Tg effect could not be considered in Part B,

$\Delta T = -68^\circ\text{C}$  (after curing)

Part A: Data of strengths were provided. Remaining necessary data were assumed by author. The prediction of the *average* curve, task in TC3, would have logically required the provision of an *average* curve (see TC4), however an 'upper' stress-strain curve was provided. No information on the really active 2<sup>nd</sup>-Tg effect. PartA curve with assumed  $b_{\perp\parallel} = 0.3$

Part B: Barrelling of the specimen was reported. The course of the provided test data does not exhibit the existing 2<sup>nd</sup>Tg-effect demonstrated by a slope beyond the epoxide-typical kinking point at  $-200$  MPa hydrostatic pressure. Why? The slope of the curve covers the hidden 2<sup>nd</sup>-Tg effect. Open failure surface in  $p_{hyd}$ -direction.

Two  $0^\circ$ - test specimen data (circles) are shown just for information. These are not used due to the twisting effect.

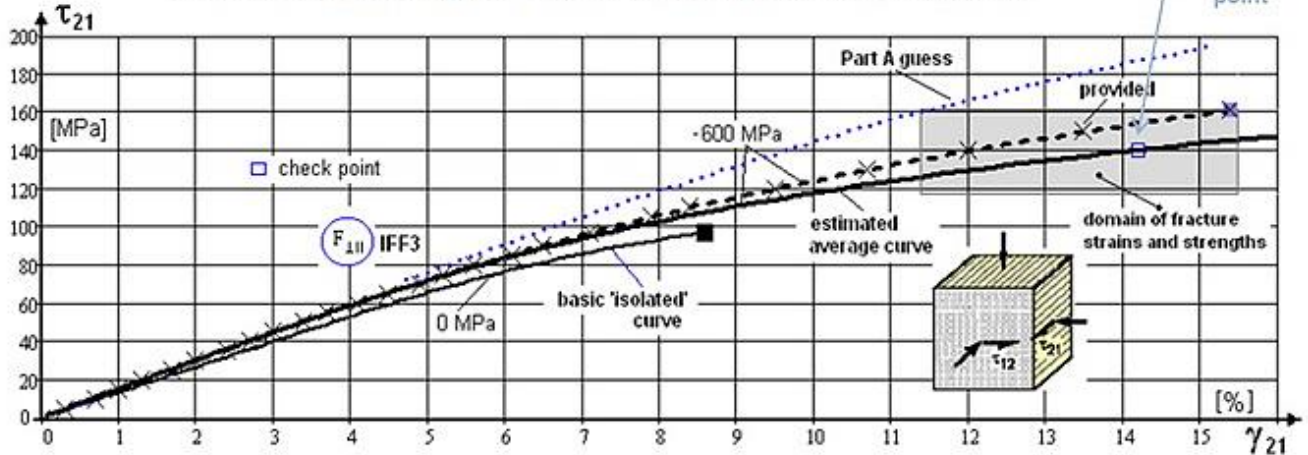
TC2 is fully linked to TC3 and TC4. TC2 and TC3 are *average* curves. The provided 'upper curve' did not lead to fully linked TCs in Part A! Linking succeeded: (1) With the provided TC4 information of Part B the author could determine the necessary average curve. (2) However good mapping of the pretty scattering test data was obtained first, *after a novel physical interpretation* of the course of test data, by discriminating at  $\sigma_2 = 0$  'isolated failure stress states' for  $\sigma_2 > 0$  from the 'embedded (redundant) ones for  $\sigma_2 < 0$ ! This required a separate mapping of the isolated curve part and the embedded curve part with a following interaction work at  $\sigma_2 = 0$ . Then, the TC2-TC3-TC4-Check points were met and proved the quality of the final approach.

► TC2 test data set - after a new evaluation and interpretation - finally became applicable for SFC model validation.

## WWFE-II, TC4, UD lamina, CFRP, T300/PR319Ep

Which is the in-plane transversal stress-shear strain curve for the tri-axial loading  $\sigma_{hyd} = -600$  MPa?

**Task: Non-linear determination of shear stress-shear strain curves of the tube  $\tau_{21}^{fr}(\gamma_{21})$**   
(shear is superimposed on a still acting hydrostatic pressure  $\sigma_{hyd} = -600$  MPa)



Part A: Data of strengths were provided. Remaining necessary data were assumed by the author. For the PartA guess curve (dotted) to be predicted it was assumed.  $\mu_{\perp\parallel} = 0.3$ ,  $\tau_{21} \equiv \tau_{out}$

Part B: Shaded is the area of the PartB-provided shear failure stresses and strains. On basis of this information the required average shear stress-shear strain curve could be estimated. From the shaded area can be seen, that the PartA-provided curve is an 'upper' curve (dashed). Effortful tuning gave the average curve. Change, necessary to the new information:  $b_{\parallel} = 0.3 \rightarrow 0.12$ .

PartA guess is far from the PartB reality according to the non-sufficient input. (1) Assuming a constant shear strain, it can be recognized that the shear failure stress increases with  $p_{hyd}$ . (2) With increasing  $p_{hyd}$  the failure strains increase, too.

► TC4 test data set, after a new evaluation (the provided upper stress-strain curve was not an accurate input for test data mapping. Average properties had to be provided!) and interpretation, finally became applicable for SFC model validation

### WWFE-II, TC3 and WWFE-I, TC2: investigation of 0°-tubes and comparison with 90°-tubes

Just 90°-test specimen data was provided in Part A. For completing the understanding of pressure dependency on the shear behaviour of composites, in Part B additionally, 0°-test specimen data was offered. Already since WWFE-I TC2 was clear that the different stress situations between 0°-tubes and 90° tubes under torsion loading have to be investigated in order to sort out whether the 0° tubes are usable or not.

In the case of only hydrostatic loading a 0° tube initially experiences (*good approach*)

$$\sigma_{hoop} = \sigma_{rad} = \sigma_{ax} = -p_{hyd} \quad \sigma_{hoop} \equiv \sigma_3 = -p_{hyd}, \quad \sigma_1 = \sigma_{ax} = -p_{hyd} \quad \text{and a } 90^\circ \text{ tube a varying } \sigma_{hoop} \equiv \sigma_1 \text{ with } \int \sigma_1(r) \cdot dr = -p_{hyd} \cdot \pi(r_{out}^2 - r_{int}^2), \text{ and } \sigma_{rad} \equiv \sigma_3 = \sigma_2 = -p_{hyd}.$$

This outlines a clearer stress situation for the 0° tube. As far as the angle is small the test results are simpler interpretable than those of the 90° tubes. But this is not anymore true when the larger angles at fracture are encountered. Then, the stresses have to be transformed due to the fact that shearing under torsion loading (see Fig. 5) turns the fibre direction and the lamina coordinate system is not anymore identical with the coordinate system of the tube. The state of stress, applied at significant angles, does not represent lamina stresses (*material coordinate system*) anymore but structural stresses

$$\{\sigma\} = (\sigma_x, \sigma_y, \sigma_z, \tau_{yz}, \tau_{zx}, \tau_{xy})^T \equiv (\sigma_{ax}, \sigma_{hoop}, \sigma_{radial}, 0, 0, \tau_{xy})^T,$$

which have to be transformed into a 3D state of lamina stresses

$$\{\sigma\} = (\sigma_1, \sigma_2, \sigma_3, 0, 0, \tau_{21})^T = (\sigma_{\parallel}, \sigma_{\perp}, \sigma_z, 0, 0, \tau_{\perp\parallel})^T$$

to perform strength verification or data mapping. Otherwise, one would compare apples and oranges if using 90° and 0° data in a mixed way.

In TC2 of WWFE-I, such a transformation has been performed, however there, it was just a simple 2D problem.

Now here, for one 0° test point a transformation is performed by non-linear CLT analysis, via the relationship  $\gamma \cdot L = R_0 \cdot \hat{\varphi}$ , with  $\gamma$  the given shear strain,  $L = 14.24$  mm the gauge length,  $R_0 = 4.57$  mm the outer radius of the tube, and  $\hat{\varphi} = \varphi \cdot (\pi/180^\circ)$  the twist in radians). The following computation, using the relationship  $\{\sigma\} = [T_\sigma]^{-1} \cdot \{\sigma'\} = [T_\varepsilon]^T \cdot \{\sigma'\}$  from [CLT], delivers the real lamina stresses

$$\begin{aligned}\sigma_{\parallel} &= \sigma_x (\cos \varphi)^2 + \sigma_y (\sin \varphi)^2 + 2\tau_{xy} \cos \varphi \sin \varphi, \\ \sigma_{\perp} &= \sigma_x (\sin \varphi)^2 + \sigma_y (\cos \varphi)^2 - 2\tau_{xy} \cos \varphi \sin \varphi, \\ \tau_{\perp\parallel} &= (-\sigma_x + \sigma_y) \cdot \sin \varphi \cdot \cos \varphi + \tau_{xy} \cdot ((\cos \varphi)^2 - (\sin \varphi)^2).\end{aligned}$$

Just to give an impression, it is exemplarily compared one 0°-test point (full circle) with one 90°-test point at  $-300\text{MPa}$ . With above equation and for a simple linear elastic model, taking non-linearity not into account, in contrast to the WWFE-I -TC2, the stresses and stressing efforts

$$\underline{0^\circ \text{ tube:}} \text{ from TC3: } (\sigma_x, \sigma_y, \sigma_z, \tau_{xy})^T = (-300, -300, -300, 123)^T \text{ MPa}, \varphi = 19.8^\circ$$

$$\Rightarrow (\sigma_{\parallel}, \sigma_{\perp}, \sigma_z, \tau_{\perp\parallel})^T = (-222, -378, -300, 95)^T \text{ MPa};$$

$$Eff_o = 0.78 \quad \text{from } Eff^{\parallel r} = 0.005, Eff^{\perp\parallel} = 0.78$$

are determined. This is to be compared to a 90° curve point (average) at  $-300\text{MPa}$

$$\underline{90^\circ \text{ tube:}} \quad (\sigma_{\parallel}, \sigma_{\perp}, \sigma_z, \tau_{\perp\parallel})^T = (-300, -300, -300, 126)^T \text{ MPa};$$

$$Eff_{90} = 1.08 \quad \text{from } Eff^{\parallel r} = 0.114, Eff^{\perp\parallel} = 1.08$$

and characterizes the two very different states of lamina stresses.

### LL:

*A stress point of the 0°-data set cannot be put into a diagram together with 90°-data. Therefore, they are not used in Part B. 90° tube test data can be 2D formulated as  $\sigma(-p_{hyd}, \tau_{\perp\parallel})$  and thereby visualized by a 2D diagram, whereas for the 0° tube a 4D stress state (stresses are different, see above) is to be visualized. In the simple 2D-TC2 of WWFE-I this was still possible. Above coarse comparison further shows that the 0°-tube's twisting generates a reduced shear stress; equilibrium is achieved because the longitudinal fibres take over load. Remember that these 0° tubes were not wound but hot-press moulded.*

**The author learnt:**

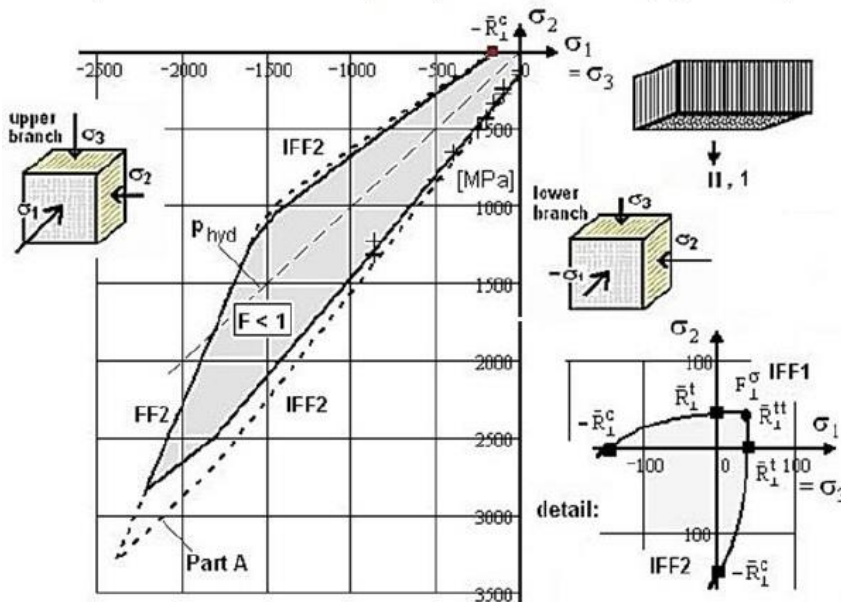
***“Generating reliable 3D test data is a bigger challenge than generating failure criteria !”***

## WWFE-II, TC5, UD, GFRP, E-glass/ MY750 Ep

How much lateral stress  $\sigma_2$  can the UD material sustain if a fibre-parallel stress  $\sigma_1$  acts which is equal to a through-thickness stress  $\sigma_3$ ? Test practice:  $p_{hyd}$  is superimposed by a lateral compressive stress  $\sigma_2^c$  at the  $\sigma_2$ -surfaces.  $\sigma_1$  is the stress acting at the respective coupon surface; the diagonal is the  $p_{hyd}$ -line.  $\{\sigma\} = (\sigma_1 = \sigma_3, \sigma_2, \sigma_3, 0, 0, 0)^T$

**Task: Non-linear determination of the tri-axial fracture failure curve** (cube block)  $\sigma_2^{fr}(\sigma_1 = \sigma_3)$   
(lateral normal stress is super-imposed on a still acting hydrostatic pressure)

modes: (FF1, FF2, IFF1, IFF2, IFF3)



$$\{\bar{R}\} = (1280, 800, 40, 145, 73)^T \text{ MPa,}$$

$$\{\bar{R}_{0.2}^t\} = (-, -, 156, 137, 55)^T \text{ MPa,}$$

$$\{\varepsilon_{fracture}\} = (2.81, -1.75, 0.25, -1.2, 4.0)^T \%$$

$$\{E\} = (-, -, 16200, 16200, 5188)^T \text{ MPa}$$

$$\{n\} = (-, -, 8.5, 7.0, 8.8) \text{ from R-O test data fit}$$

$$\{a\} = (-, -, -0.3, -2.17, -8.0), \text{ softening}$$

$$\{b\} = (-, -, 0.013, 0.21, 0.87), \text{ parameters}$$

$$E_{m0} = 3350 \text{ MPa, } \nu_m = 0.35, G_{m0} = E_{m0} / (2 + 2\nu)$$

$$b_{\perp} = 1.16 \text{ (in PartA 1.21), } b_{\parallel} = 0.2 \text{ (in PartA 0.3)}$$

$$\nu_{\perp} = 0.28; m = 2.8.$$

'2-fold' (bi-axial)  
onset of fracture curve

Part A: Data of strength points provided, remaining necessary properties were assumed by author

Part B: More information became available and the applicability of the provided test data set could be checked.  
Due to missing test data information in the transition zone IFF2-IFF1 no interaction was performed. 2nd Tg effect could not be considered

PartA-prediction was not satisfying, due to missing and partly false input. Considering the lower branch, the test data set had to be re-evaluated by QinetiQ. Good Mapping, after the organizer "QinetiQ" was asked to re-evaluate the lower branch test data! Then, the upper branch is fitting test data from DeTeresa [DeTer99], too, after subtracting his data by  $p_{hyd}$ . Failure curve is closed. ► After re-evaluation, the TC5 test data set became applicable for the validation of the SFC model

**Task:** Determination of the fracture failure curve  $\sigma_{2,fr}(\sigma_1 = \sigma_3)$  in the quadrants III and IV.

- The course of provided test data could be well mapped. The failure curve is closed.
- Assuming that the model pre-requisites remain valid, final failure by kinking (FF2) is possible under  $p_{hyd}$  according to the relationship  $E_{\parallel} \cdot \varepsilon_1 = -p_{hyd} \cdot (1 - 2 \cdot \nu_{12})$ ,  $\nu_{12}$  as larger Poisson's ratio.
- Computation indicates wedge failure IFF2 in quadrant III. Under  $\sigma_3^t$ , IFF1 means final failure.

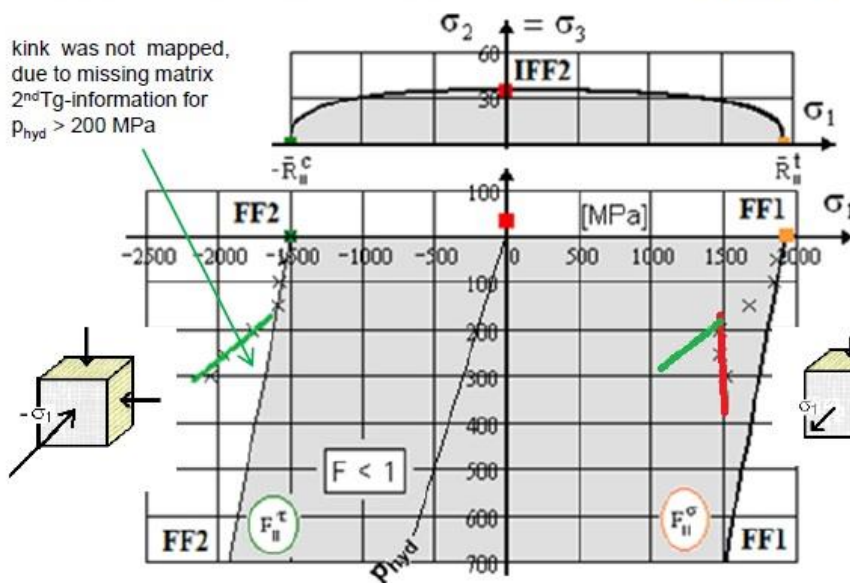
For information: Test data from DeTeresa [24] for the upper branch (2<sup>nd</sup> solution) of the failure curve in quadrant III are lying on the predicted upper branch after being re-evaluated by subtracting  $p_{hyd}$ .

## WWFE-II, TC7, UD, CFRP, A-S-carbon/ Ep 1

How much compressive fibre-parallel stress can the UD material sustain when a lateral compressive stress acts which is equal to a through-thickness stress ( $p_{\text{int}} + \text{axial tension}$ ) ?

**Task:** Non-linear determination of tri-axial failure curves  $\sigma_{\text{1fr}}(\sigma_2 = \sigma_3)$

$$\{\sigma\} = (\sigma_1, \sigma_2, \sigma_3 = \sigma_2, 0, 0, 0)^T$$



**Dogbone** test specimens, [Wronski-Parry] :

$$\{\bar{R}\} = (1990, 1500, 38, 150, 70)^T \text{ MPa,}$$

$$\{\bar{R}_{0.2}^t\} = (-, -, 156, 137, 55)^T \text{ MPa,}$$

$$\{\varepsilon_{\text{fracture}}\} = (2.81, -1.75, 0.25, -1.2, 4.0)^T \%$$

$$\{E\} = (140000, 140000, 10000, 10000, 6000)^T \text{ MPa}$$

$$\{n\} = (-, -, 8.5, 7.0, 8.8) \text{ from R-O fit}$$

$$\{a\} = (-, -, -0.3, -2.17, -8.0),$$

$$\{b\} = (-, -, 0.013, 0.21, 0.87),$$

$$E_{m0} = 3350 \text{ MPa, } \nu_m = 0.35,$$

$$G_{m0} = E_{m0} / (2 + 2\nu)$$

$$b_{\perp\perp} = 1.16 \text{ (in Part A 1.21), } b_{\perp\parallel} = 0.12 ;$$

$$\nu_{\perp\parallel} = 0.30; m = 2.8$$

Part A: Strength data and Poisson's ratio  $\nu$  provided as necessary input, friction values  $\mu(b)$  assumed

Part B: No explanation for different slopes !? Equal slopes would proof the strength capacity reducing 2<sup>nd</sup>Tg-effect, which must act equally in the fourth quadrant. If the two green curves – as data mapping curves – were provided, then the author would have simulated them with his 2<sup>nd</sup>Tg-effect capturing program.

*From physical reasons, the effect of the 2<sup>nd</sup>Tg-effect must cause a similar orientation for both the branches and slopes*  
*No satisfactory mapping is possible in the quadrants III and IV. The course of data points exhibits probable contradictions that cannot be explained by the author. Mapping is sufficient for  $p_{\text{hyd}} < 150$  MPa, only. Idea, concerning a probable error-prone data evaluation: The compressive curve would better match with TC7 data if the  $p_{\text{hyd}}$  value would have been subtracted from  $\sigma_1^c$ . No mapping possible, due to missing 2<sup>nd</sup>Tg information!*  
 ▶ TC7 test data set is not acceptable for SFC model validation.

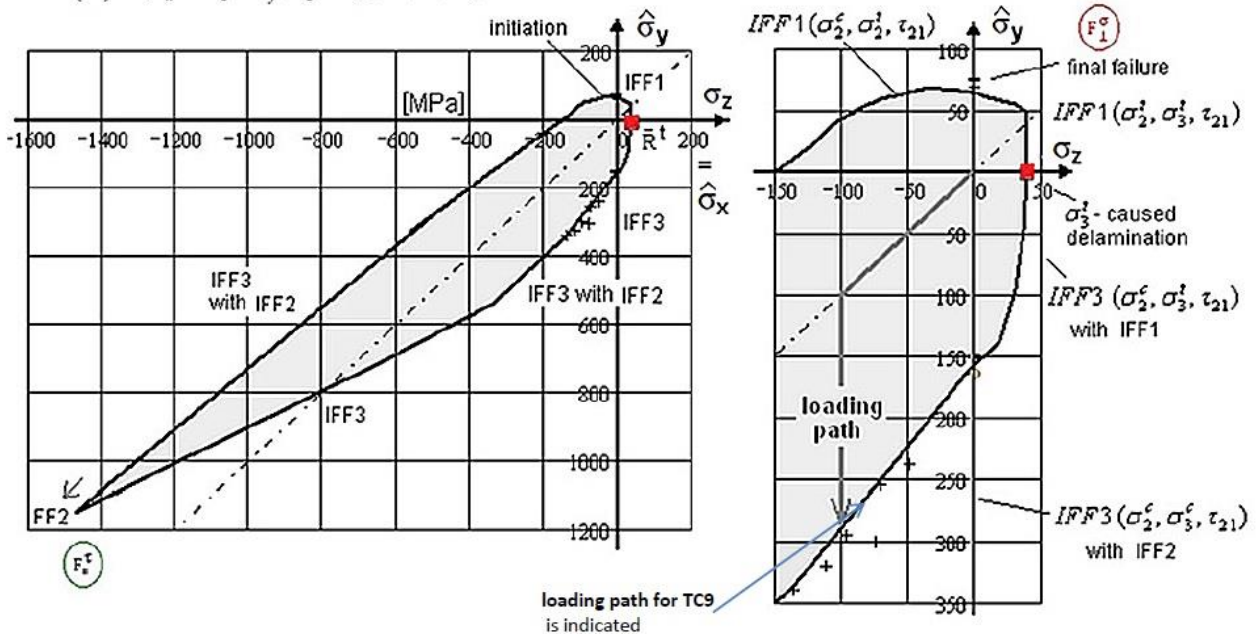


**WWFE-II, TC8, UD, GFRP, E-glass/ MY750Ep, angle-ply [35/-35/35/-35]<sub>s</sub>**

Which is the effect of the applied surface pressure  $\sigma_z = -p$  (through-thickness stress) on the size of the normal section force  $n_y = \hat{\sigma}_y / t$  at fracture, with  $n_x / t = \hat{\sigma}_x = \sigma_z$  and  $t$  as laminate thickness of the filament wound tube.

**Task: Non-linear determination of the average fracture stress  $\hat{\sigma}_y^{fr} (\sigma_z = \hat{\sigma}_x)$**

$$\{\hat{\sigma}\} = (\hat{\sigma}_x = \sigma_z, \hat{\sigma}_y, \sigma_z = -p, 0, 0, 0)^T$$



Part A: Data of strength points  $\{\bar{R}\}$  were provided, only. Remaining necessary data  $\mu$  were assumed by the author

Part B: No SFC and program modification from Part A to Part B. More information now available. Organizers were asked to re-evaluate the provided test data set. Curing stress from effective temperature  $120^\circ - 23^\circ = 97^\circ$  is  $\sigma_2^t = 15$  MPa

**LLs:** After the organizer's re-evaluation of the test data set a good mapping with the SFCs could be achieved  
 ► TC8 test data set is applicable for the verification of the laminate design. Proofs the used UD material SFC models

Data for the upper branch is missing. Data for the quadrants I, II, IV could be not provided in order to have a good basis for the validation. The high values of the 3 test data at the positive y-axis cannot be explained by the

*Citation:* "The test data were taken from [Wronski-Parry] and the test specimens were filament wound tubes".

Data for the upper branch is missing. Data for the quadrants I, II, IV could be not provided in order to have a good basis for the validation. The high values of the 3 test data at the positive y-axis cannot be explained by the author.

The next slide describes test arrangement and stresses.

A re-investigation of the friction parameter  $b_{\perp\perp}$  by some curve 'data fitting' showed that it had to be reduced to 1.16 as for TC5. This value is substantiated by information from WWFE-I. The other friction parameter  $b_{\perp\perp}$  is obtained by mapping the test data provided for quadrant III. Note, that TC5, TC8 and TC9 possess the same material (see respective slide) but belong to different test specimens which will naturally cause some difference in strengths values.

An improved non-linear programming is necessary, especially due to the fact that in the linked TC9 both the failure modes IFF2 and IFF3 have a similar risk to fracture, or - in other words - the

material stressing effort is almost equal for both modes in the envisaged two-fold failure domain. The fibre volume contents for Part B must be increased from the initial 60% up to  $V_f = 67\%$  (“dry” filaments however then possible). This would make a correction necessary so that the TC8 data do not remain the same as for TC5, but, the driving strengths in the *compression* domain might not become better and were kept. An increase of the fibre volume content on the elasticity properties is not considered due to the other uncertainties and that the stress-strain curve would have to be adapted and hardening parameters to be reworked with all its work consequences.

For TC8 and TC9, the analysis followed the mentioned 3D-CLT-MathCad program:

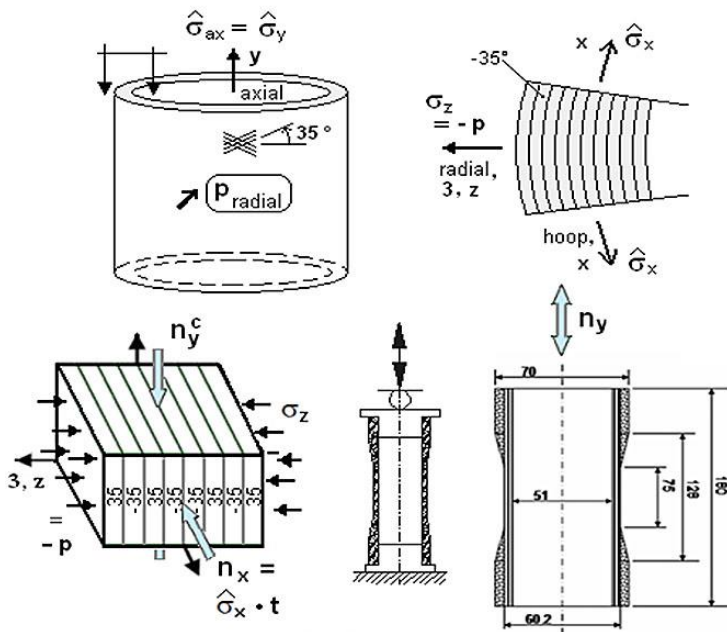
- IFF1 at the positive  $\sigma_z$ -axis belongs to a weakest link value or is an ‘isolated’ value  $\bar{R}_\perp^t$ , initial failure from  $\sigma_3^t$  means final failure. The curing stress has no direct effect, because it acts in the laminate plane.

- At the positive  $\sigma_y$ -axis axis some redundancy governs and the *initial* failure behaviour is more benign. The curing stress has a direct effect. The provided 3 test data belong to *final* failure of this specimen at about  $\bar{\sigma}_y^{final} = 72 \text{ MPa}$ . This value can be explained: IFF1 micro-cracks decrease the stiffness and the fibre angle  $35^\circ = 90^\circ - 55^\circ$  increases. Under non-linear shear loading, more and more load is put onto the fibres until final failure occurs. Mapping of test data is not fully satisfactory in domains (this is valid for TC9, too) where the complicate non-linear treatment of the commonly acting two modes IFF2 and IFF3 (of about the same size of  $\text{Eff}^{\text{mode}}$ ) is located. There, the MathCad program faced numerical problems for some stress combinations and did not converge correctly. With respect to the small data basis was kept 0.2 and not increased to 0.25 for optimum mapping. Birch is considered.

The failure curve is closed.

The complete failure surface consists of piecewise smooth regimes (partial failure surfaces). Each regime represents one failure mode and is governed by one basic strength..

For more information: **Modelling of TC8 test situation**, in short



**Tube** (still thick walled, hoop-wound)

[Wronski - Parry, [20]]:

modes: (FF1, FF2, IFF1, IFF2, IFF3)

$$\{\bar{R}\} = (1280, 800, 40, 145, 73)^T \text{ MPa},$$

$$\{\varepsilon_{fracture}\} = (2.81, 1.75, 0.25, 1.2, 4.0)^T \%$$

$$\{E\} = (-, -, 16200, 16200, 5188)^T \text{ MPa}$$

$$\{n\} = (-, -, 8.5, 7.0, 8.8) \text{ from R-O test data fit}$$

$$\{a\} = (-, -, -0.3, -2.17, -8.0), \text{ softening}$$

$$\{b\} = (-, -, 0.013, 0.21, 0.87), \text{ parameters}$$

$$E_{m0} = 3350 \text{ MPa}, \nu_m = 0.35, G_{m0} = E_{m0} / (2 + 2\nu),$$

$$b_{\perp\perp} = 1.16 \text{ (in PartA 1.21)}, b_{\parallel\parallel} = 0.2 \text{ (in PartA 0.3);}$$

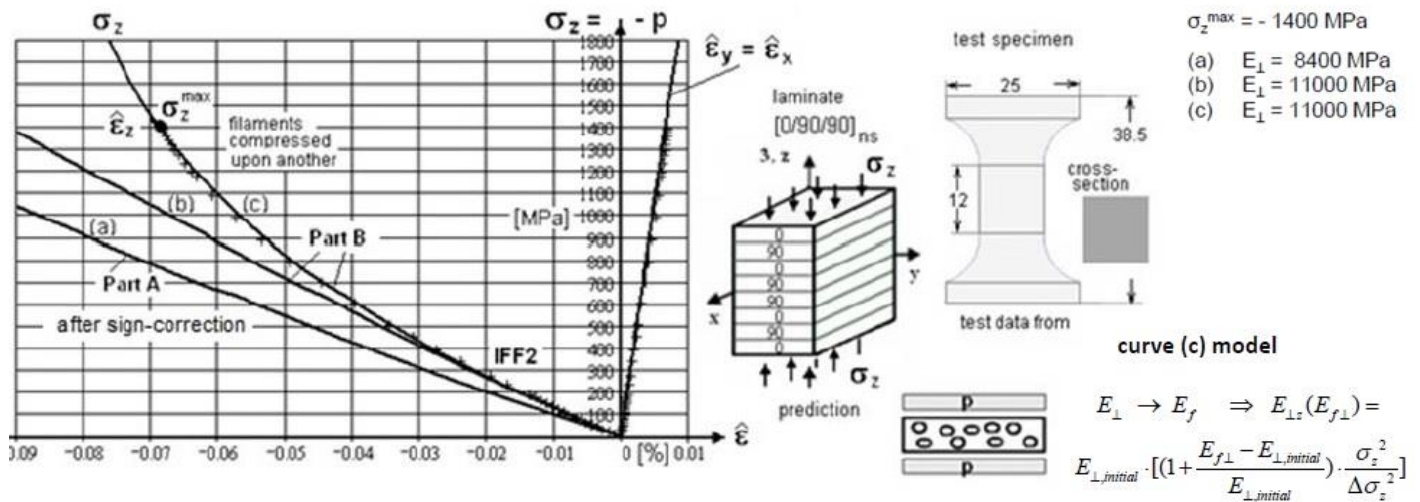
$$\nu_{\perp\parallel} = 0.28; m = 2.8,$$

2<sup>nd</sup> Tg effect could not be considered.

**WWFE-II,TC12, UD, CFRP, IM7/8551-7, cross-ply [0/90/0/90]<sub>ns</sub>, balanced-symmetric**

Which is the effect of the applied surface pressure  $\sigma_z = -p$  (through-thickness compressive stress) on the strains for  $\hat{\sigma}_x = \hat{\sigma}_y = 0$  ?

**Task: Non-linear determination of the 3 average strains as function of  $\sigma_z$ .** The roof denotes a smeared stress



Part A: Data of strength  $\{\bar{R}\}$  were provided. Remaining necessary property  $\mu$  was assumed by the author .

Part B, Modifications from Part A to Part B: (1) Correction of a mistake (*author's curvature of the predicted curve in Part A was wrong, caused by a typing error in the equations coded*), curve (a). (2) Increase of the initial lateral elasticity modulus at origin from of Part A to 11000 MPa in Part B. (3) Consideration of a growing filament contact by a stiffness increase model. Properties TC-10. It is not clear why this TC is marked as a cross-ply but the curve stems from a lay-up that is a quasi-isotropic angle-ply! The given test data set (crosses) stems from a quasi-isotropic laminate [45/0/-45/90]<sub>ns</sub>! More information became available that led to an improved curve (b). Remaining difference was tackled by above assumption and curve (c) model. Then, a good mapping after this necessary physical interpretation of the course of test data could be achieved with curve (c).

The test specimen finally fails structurally, exhibiting a failure mode change. Structural failure cannot be described by a (material) SFC !  
 ► TC12 test data set is not applicable for validation of a SFC model, because a SFC is a material model.

Assumption "Filaments are finally compressed to another which stiffens!".

This is tackled by a model that fits the Part B data-improved curve (b) to (c) as compression-dependent increase of the lateral stiffness filament perpendicular  $E_{f\perp}$ .

Regarding the Test Cases before, it may be concluded:

***Test results can be far away from the reality like a bad theoretical model; theory creates a model of the reality, whereas an experiment is one realisation of the reality.***

### 7.2.2 UD, Novel modelling of Porosity in the quasi-isotropic domain

The effect of friction is reduced by increasing porosity. In order to map this, the author proposes a simple failure function  $F$  that spans from dense to pretty porous materials. The following formulas for the transversely-isotropic UD material are the basis for the curves in Fig.A3-1 below.

\* Failure Function for a dense UD material

$$\begin{aligned} F^{SF} &= [a_{\perp\perp} \cdot I_2 + b_{\perp\perp} \cdot \sqrt{I_4}] / \bar{R}_{\perp}^c = 1 \text{ with } a_{\perp\perp} = b_{\perp\perp} - 1 \text{ after inserting } \bar{R}_{\perp}^c = 104 \text{ MPa} \\ &= [a_{\perp\perp} \cdot (\sigma_2 + \sigma_3) + b_{\perp\perp} \cdot \sqrt{(\sigma_2 - \sigma_3)^2 + 4\tau_{23}^2}] / \bar{R}_{\perp}^c = 1 \\ &= [a_{\perp\perp} \cdot (\sigma_2^p + \sigma_3^p) + b_{\perp\perp} \cdot \sqrt{(\sigma_2^p - \sigma_3^p)^2 + 0^2}] / \bar{R}_{\perp}^c = 1 \leftarrow 2 \text{ structural stresses} \end{aligned}$$

\* Failure Function for a porous UD material (index por, author's simple approach)

$$F_{porosity}^{SF} = \sqrt{a_{\perp\perp por}^2 \cdot I_2^2 + b_{\perp\perp por}^2 \cdot I_4 - a_{\perp\perp por} \cdot I_2} / 2\bar{R}_{\perp}^c = 1.$$

The two curve parameters are determined - as before performed - from insertion of the compressive strength point and from the bi-axial fracture stress point.

In the figure the parallel lines mark that a 'dense' UD material does not shear fracture. This is caused by the axial straining under a bi-axial compression stress state which is impeded by the constraining fibers.

When applying  $a_{\perp\perp por} = 0$ , then parallel lines can be obtained. The parallel lines represent density or zero porosity and exhibit the capability of the simple approach.

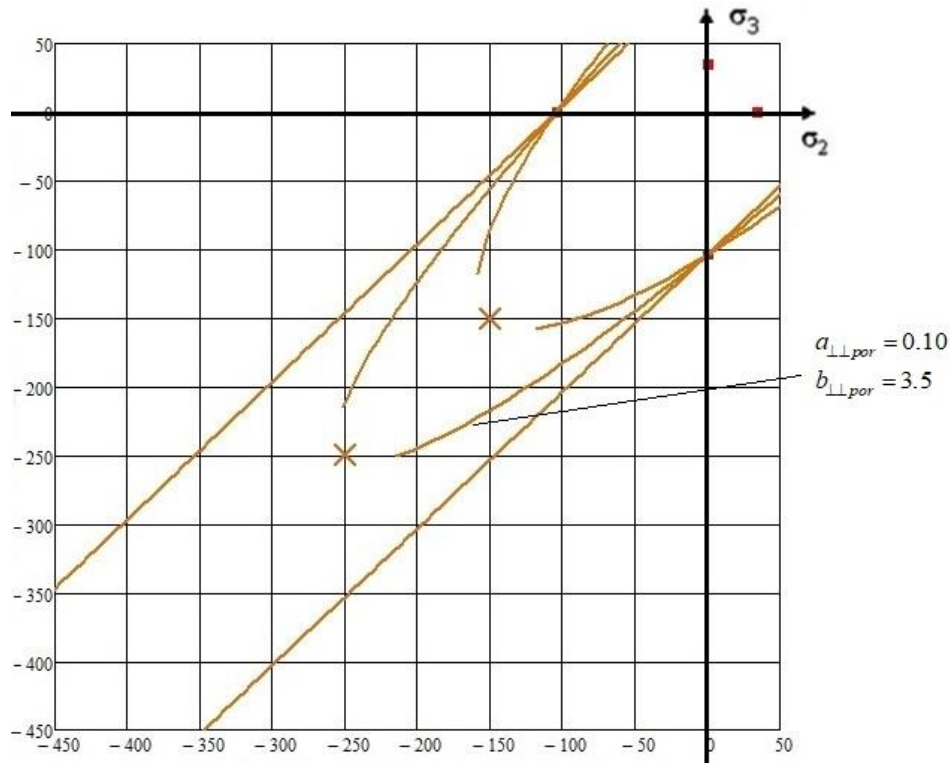


Fig. 7.3-1: Fracture failure curves of UD material regarding two different porosity grades.

$a_{\perp\perp por}$  for 0, 0.10, 0.22 and  $b_{\perp\perp por}$  for 4.0, 3.5, 2.9

Ideal dense materials possess no porosity. A fully porous material may be defined by  $R_{\perp}^{cc} \cong R_{\perp}^c$ . This case can be modelled like foam materials in the quasi-isotropic domain [Cun16a].

**Table: WWFE-provided UD properties**

| Fibre type  | IM7           | T300          | A-S           | S2-glass      | E-Glass      |
|---|---------------|---------------|---------------|---------------|--------------|
| <b>Matrix</b>   | <b>8551-7</b> | <b>PR-319</b> | <b>Epoxy1</b> | <b>Epoxy2</b> | <b>MY750</b> |
| Fibre volume fraction $V_f$ (%)   | 60            | 60            | 60            | 60            | 60           |
| Longitudinal modulus $E_1$ (GPa)  | 165*          | 129           | 140*          | 52            | 45.6         |
| Transverse modulus $E_2$ (GPa)  | 8.4           | 5.6+          | 10            | 19            | 16.2         |
| Through-thickness modulus $E_3$ (GPa)   | 8.4           | 5.6+          | 10            | 19            | 16.2         |
| In-plane shear modulus $G_{12}$ (GPa)   | 5.6*          | 1.33+         | 6*            | 6.7*          | 5.83*        |
| Transverse shear modulus $G_{13}$ (GPa)   | 5.6*          | 1.33+         | 6*            | 6.7*          | 5.83*        |
| Through-thickness shear modulus $G_{23}$ (GPa)  | 2.8           | 1.86          | 3.35          | 6.7           | 5.7          |
| Major Poisson's ratio $\nu_{12}$  | 0.34          | 0.32          | 0.3           | 0.3           | 0.28         |
| Major transverse Poisson's ratio $\nu_{13}$   | 0.34          | 0.32          | 0.3           | 0.3           | 0.28         |
| Through-thickness Poisson's ratio $\nu_{23}$  | 0.5           | 0.5           | 0.49          | 0.42          | 0.4          |
| Longitudinal tensile strength $X_T$ (MPa)   | 2560          | 1378          | 1990          | 1700          | 1280         |
| Longitudinal compressive strength $X_C$ (MPa)   | 1590          | 950           | 1500          | 1150          | 800          |
| Transverse tensile strength $Y_T$ (MPa)   | 73            | 40            | 38            | 63            | 40           |
| Transverse compressive strength $Y_C$ (MPa)   | 185**         | 125**         | 150**         | 180**         | 145**        |
| Through-thickness tensile strength $Z_T$ (MPa)  | 63            | 40            | 38            | 50            | 40           |
| Through-thickness compressive strength $Z_C$ (MPa)                                      | 185**         | 125**         | 150**         | 180**         | 145**        |
| In-plane shear strength $S_{12}$ (MPa)  | 90**          | 97**          | 70**          | 72**          | 73**         |
| Transverse shear strength $S_{13}$ (MPa)  | 90**          | 97**          | 70**          | 72**          | 73**         |
| Through-thickness shear strength $S_{23}$ (MPa)   | 57            | 45            | 50            | 40            | 50           |
| Longitudinal tensile failure strain $\epsilon_{1T}$ (%)                                 | 1.55          | 1.07          | 1.42          | 3.27          | 2.81         |
| Longitudinal compressive failure strain $\epsilon_{1C}$ (%)                             | 1.1           | 0.74          | 1.2           | 2.21          | 1.75         |
| Transverse tensile failure strain $\epsilon_{2T}$ (%)                                   | 0.87          | 0.43          | 0.38          | 0.33          | 0.246        |
| Transverse compressive failure strain $\epsilon_{2C}$ (%)                               | 3.2           | 2.8           | 1.6           | 1.5           | 1.2          |
| Transverse tensile failure strain $\epsilon_{3T}$ (%)                                   | 0.76          | 0.43          | 0.38          | 0.263         | 0.25         |
| Through-thickness compressive failure strain $\epsilon_{3C}$ (%)                        | 3.2           | 2.8           | 1.6           | 1.5           | 1.2          |
| In-plane shear failure strain $\gamma_{12u}$ (%)  | 5             | 8.6           | 3.5           | 4             | 4            |
| Transverse shear failure strain $\gamma_{13u}$ (%)                                      | 5             | 8.6           | 3.5           | 4             | 4            |
| Through-thickness shear failure strain $\gamma_{23u}$ (%)                               | 2.1           | 1.5           | 1.5           | 0.59          | 0.88         |
| Longitudinal thermal coefficient $\alpha_1$ ( $10^{-6}/^\circ\text{C}$ )                | -1            | -1            | -1            | 8.6           | 8.6          |
| Transverse thermal coefficient $\alpha_2$ ( $10^{-6}/^\circ\text{C}$ )                  | 18            | 26            | 26            | 26.4          | 26.4         |
| Through-thickness thermal coefficient $\alpha_3$ ( $10^{-6}/^\circ\text{C}$ )           | 18            | 26            | 26            | 26.4          | 26.4         |
| Energy release rates $G_{IC}$ , $G_{IIC}$ ( $\text{J}/\text{m}^2 = \text{N}/\text{m}$ ) | 200           |               |               |               | 240, 1500    |
| mixed (fracture mechanics) mode to be assumed   |               |               |               |               |              |
| Stress free temperature ( $^\circ\text{C}$ )  | 177           | 120           | 120           | 120           | 120          |
| Test Case   | TC10,11,12    | TC2,3,4       | TC7           | TC6           | TC1,5,8,9    |

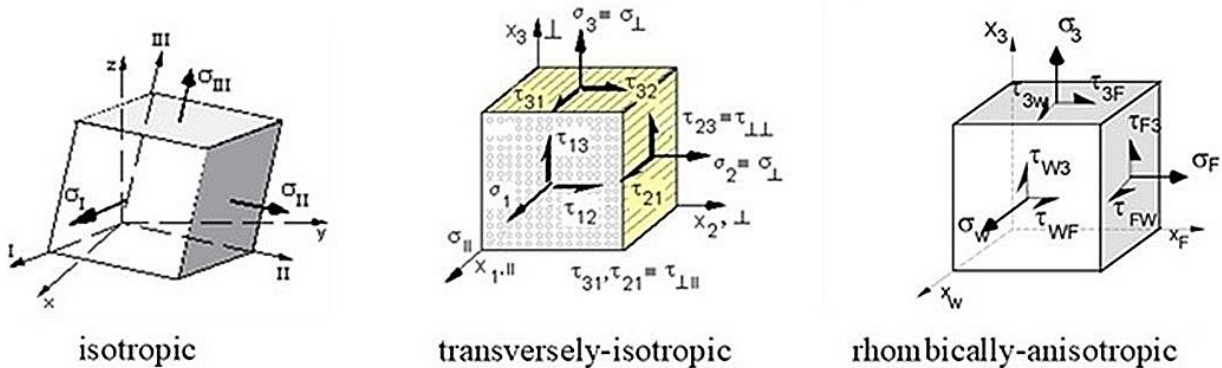
\* Initial modulus. \*\* Nonlinear behaviour and stress strain curves and data points are provided

+ These values are considered to be low, compared with typical data for the same material published somewhere else or quoted by the manufacturers. We have not attempted to change them in order to facilitate a comparison with test data in Part B.

### 7.3 2D-Application to (Technical) Ceramics isotropic, UD and orthotropic fabrics

As reminder, again all stress state figures of the 3 material families are depicted again.

Ceramic (fiber) Matrix Composites CMC represent the applications where ceramic fibers are used for strengthening when facing high temperature



$$\{\sigma\} = (\sigma_x, \sigma_y, \sigma_z, \tau_{yz}, \tau_{xz}, \tau_{xy})^T$$

$$\{\sigma\} = (\sigma_{||}, \sigma_{\perp}, \sigma_3, \tau_{23}, \tau_{13}, \tau_{21})^T$$

$$\{\sigma\} = (\sigma_W, \sigma_F, \sigma_3, \tau_{3F}, \tau_{3W}, \tau_{FW})^T$$

Isotropic:  $\{\bar{R}\} = (\bar{R}^t, \bar{R}^c)^T$  with  $\mu$

Transversely-iso.:  $\{\bar{R}\} = (\bar{R}_{||}^t, \bar{R}_{||}^c, \bar{R}_{\perp}^t, \bar{R}_{\perp}^c, \bar{R}_{\perp||})^T$  with  $\mu_{||}, \mu_{\perp}$

Orthotropic:  $\{\bar{R}\} = (\bar{R}_W^t, \bar{R}_W^c, \bar{R}_F^t, \bar{R}_F^c, \bar{R}_{WF}^t, \bar{R}_3^t, \bar{R}_3^c, \bar{R}_{3F}^t, \bar{R}_{3W}^t)^T$  with  $\mu_{WF}, \mu_{3W}, \mu_{3F}$

#### 7.3.1 Isotropic (monolithic)

Ceramic material is an inorganic, non-metallic oxide, nitride, or carbide material. Monolithic ceramic materials are brittle, hard, strong in compression (if just slightly porous), and weak in tension and in consequence in shearing too. They are applied if wear and high temperature are faced. The material properties are inseparably linked to the manufacturing process steps, consisting of *preparation of the powder* (base material boron nitride, silicon carbide or aluminum oxide) and *shaping* with targeted influence on the microstructures in the final *sintering* process. Decisive for the material properties in the structural component are type, frequency and distribution of flaws.

A common application example is silicon-enriched silicon carbide SiC, which is manufactured under shielding gas from silicon and carbon powder and which is characterized by chemical resistance and corrosion resistance. An example for the reinforcement of a metal with ceramic particles is the hybrid metal-ceramic composite AO-403 [*CeramTec*] that has material parameters of metal alloy 60 vol.-% AlSi9MgMn, ceramic 40 vol.-% Al<sub>2</sub>O<sub>3</sub> density 3.21 g/cm<sup>3</sup>, flexural strength 550 to 620 MPa, tensile strength 380 to 460 MPa, fracture strain  $\approx 0.5\%$ .

The SFCs applicable for isotropic ceramics must capture the porosity. Dependent on the grade of porosity  $\bar{R}^c > \bar{R}^{cc}$  or  $\bar{R}^c < \bar{R}^{cc}$  (very porous, similar to foam). In Fig.7.3-1 as a failure curve example for a differently porous ceramic material is depicted.

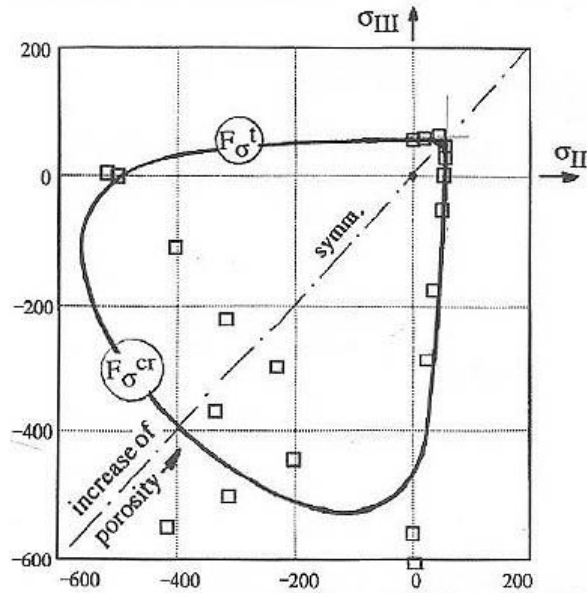
Additive ceramic fabrication will require in future production modelling and SFCs to assess stress states in the structures built up by the distinct ceramic materials such as ZrO<sub>2</sub>, Al<sub>2</sub>O<sub>3</sub>.

Fig.7.3-1: Porous monolithic ceramics  
[Kowaltchuk]

Twofold failure occurrence with UD materials

at  $\sigma_{II} = \sigma_{III}$  (tension cut-off)

$$\{\bar{R}\} = (\bar{R}^t, \bar{R}^c)^T \text{ with } \mu$$



### 7.3.2 UD

For uni-axial and bi-axial reinforcement ceramic filaments are produced and collected in a roving and then embedded in the matrix. Compared to monolithic ceramics, fiber-reinforced ceramic components such as silicon carbide fiber-reinforced silicon carbide (SiC/SiC) reduce brittleness, which means it improves damage tolerance by hindering the spread of cracks in the matrix through the fibers. The ceramic filaments are produced from various polymers, so-called precursors, by pyrolysis. The ceramic fibers are divided into oxide and non-oxide fibers (derived from [Wikipedia]).

Fig.7.3-2 outlines the similarity to FRP material. The same SFCs are to apply as with UD-FRP, regarding the porosity.

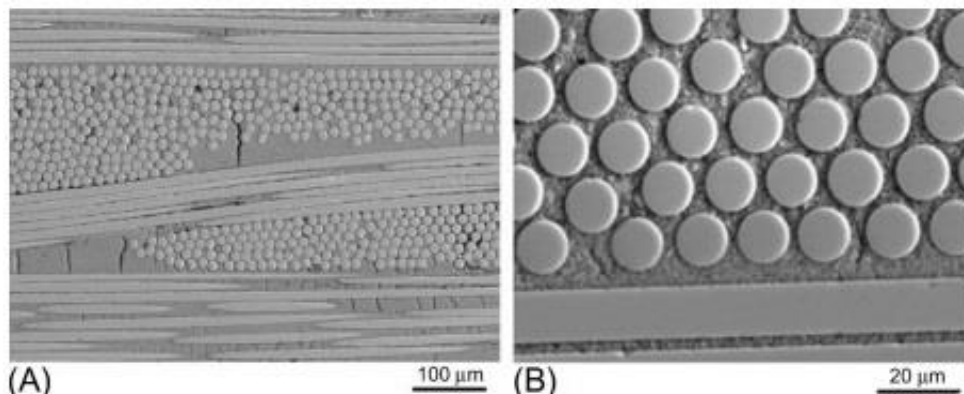


Fig.7.3-2. SEM images of Nextel™ 610/mullite composites with 0/90 fiber orientation, (A) fiber bundles and (B) almost regular and dense packing of fibers within a bundle.

From Simon RA. Progress in processing and performance of porous-matrix oxide/oxide composites. *Int J Appl Ceram Technol* 2005;2:141–9.

Fig.7.3-3 presents an UD example.

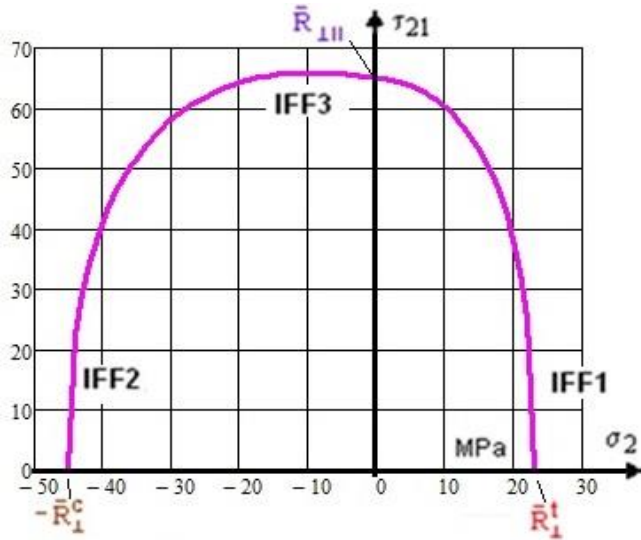


Fig. 7.3-3: UD CMC material, WHIPOX<sup>TM</sup> C/C-SiC, Filament wound tube. Strength provided from [WHIPOX<sup>TM</sup> C/C-SiC, DLR Stuttgart, [Jai20]]. WHIPOX = Wound Highly Porous Oxide Material of the DLR

$$Eff^{\perp\sigma} = [(\sigma_2) + \sqrt{\sigma_2^2}] / 2\bar{R}_1^t = \sigma_{eq}^{\perp\sigma} / \bar{R}_1^t$$

$$Eff^{\perp\tau} = [a_{\perp\perp} \cdot (\sigma_2) + b_{\perp\perp} \sqrt{\sigma_2^2}] / \bar{R}_1^c = \sigma_{eq}^{\perp\tau} / \bar{R}_1^c$$

$$Eff^{\perp\parallel} = \{ [b_{\perp\perp} \cdot I_{23-5} + (\sqrt{b_{\perp\perp}^2 \cdot I_{23-5}^2 + 4 \cdot \bar{R}_{\perp\perp}^2 \cdot (\tau_{21}^2)^2}] / (2 \cdot \bar{R}_{\perp\perp}^3) \}^{0.5}$$

$$I_{23-5} = 2\sigma_2 \cdot \tau_{21}^2, \quad b_{\perp\perp} = a_{\perp\perp} + 1 = 1 / (1 - \mu_{\perp\perp}), \quad b_{\perp\perp} \cong 2 \cdot \mu_{\perp\perp}$$

$$\{\bar{R}\} = (\bar{R}_1^t, \bar{R}_1^c, \bar{R}_1^t, \bar{R}_1^c, \bar{R}_{\perp\perp})^T = (279, 243, 22.5, 45, 65)^T$$

with assumed  $\mu_{\perp\perp} = 0.15, \mu_{\perp\perp} = 0.15$

$$\left( \frac{\sigma_2^t}{\bar{R}_1^t} \right)^m + \left( \frac{-\sigma_2^c}{\bar{R}_1^c} \right)^m + \left( \frac{|\tau_{12}|}{\bar{R}_{\perp\perp} - \mu_{\perp\perp} \cdot \sigma_2^c} \right)^m = 1$$

### 7.3.3 Orthotropic fabric laminas

For a faster understanding the interaction equation, necessary for mapping the course of test data in the transition domains reads:

$$\left( \frac{\sigma_W + |\sigma_W|}{2 \cdot \bar{R}_W^t} \right)^m + \left( \frac{-\sigma_W + |\sigma_W|}{2 \cdot \bar{R}_W^c} \right)^m + \left( \frac{\sigma_F + |\sigma_F|}{2 \cdot \bar{R}_F^t} \right)^m + \left( \frac{-\sigma_F + |\sigma_F|}{2 \cdot \bar{R}_F^c} \right)^m + \left( \frac{|\tau_{WF}|}{\bar{R}_{WF} - \mu_{WF} \cdot \sigma_W} \right)^m$$

$$+ \left( \frac{\sigma_3 + |\sigma_3|}{2 \cdot \bar{R}_3^t} \right)^m + \left( \frac{-\sigma_3 + |\sigma_3|}{2 \cdot \bar{R}_3^c} \right)^m + \left( \frac{|\tau_{3W}|}{\bar{R}_{3W} - \mu_{3W} \sigma_3} \right)^m + \left( \frac{|\tau_{3F}|}{\bar{R}_{3F} - \mu_{3F} \sigma_3} \right)^m = 1.$$

This equation is valid if a mode occurs one-fold. If  $\sigma_F$  is also active then this double mode

contributes by the additional term  $\left( \frac{|\tau_{WF}|}{\bar{R}_{WF} - \mu_{WF} \cdot \sigma_F} \right)^m$ .

Some simple stress states are investigated and visualized in Figs.7.3-4 through -6.

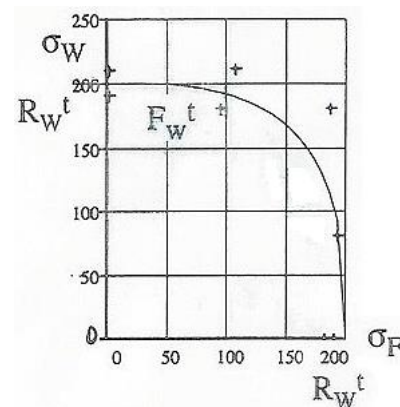
$$\{\bar{R}\} =$$

$$(\bar{R}_W^t, \bar{R}_W^c, \bar{R}_F^t, \bar{R}_F^c, \bar{R}_{WF}, \bar{R}_3^t, \bar{R}_3^c, \bar{R}_{3F}, \bar{R}_{3W})^T$$

$$= (200, -, 195, -, -, -, -, -, -)^T$$

$$\left( \frac{\sigma_W + |\sigma_W|}{2 \cdot \bar{R}_W^t} \right)^m + \left( \frac{-\sigma_W + |\sigma_W|}{2 \cdot \bar{R}_W^c} \right)^m = 1$$

Fig. 7.3-4: C/SiC tube for X38 Body Flap,  $\sigma_W (\sigma_F)$ , RT, MAN,  $m=3$





$$\left(\frac{\sigma_3 + |\sigma_3|}{2 \cdot \bar{R}_3^t}\right)^m + \left(\frac{-\sigma_3 + |\sigma_3|}{2 \cdot \bar{R}_3^c}\right)^m + \left(\frac{|\tau_{3F}|}{\bar{R}_{3F} - \mu_{3F} \sigma_3^c}\right)^m = 1$$

$$\{\bar{R}\} = (\bar{R}_W^t, \bar{R}_W^c, \bar{R}_F^t, \bar{R}_F^c, \bar{R}_{WF}, \bar{R}_3^t, \bar{R}_3^c, \bar{R}_{3F}, \bar{R}_{3W})^T$$

$$\bar{R}_W^t, \bar{R}_W^c, \bar{R}_F^t, \bar{R}_F^c, \bar{R}_{WF}, 3, 99, 7, \bar{R}_{3W})^T$$

with  $\mu_{WF}, \mu_{3W}, \mu_{3F} = 0.3$

Fig. 7.3-5: C/SiC tube,  $\sigma_W(\sigma_F)$ , RT,  $m=3$

[test data from dissertation B. Thielicke on tube test specimens, 1997]

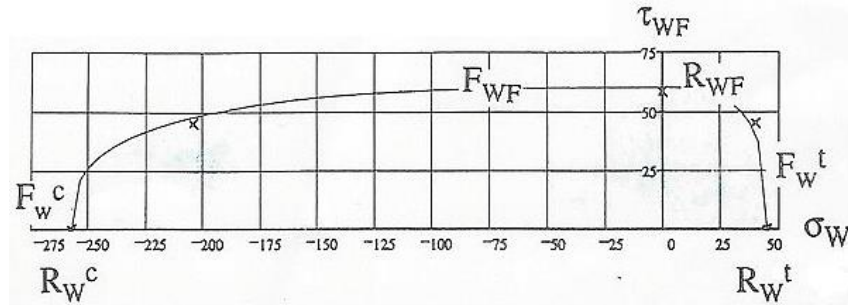
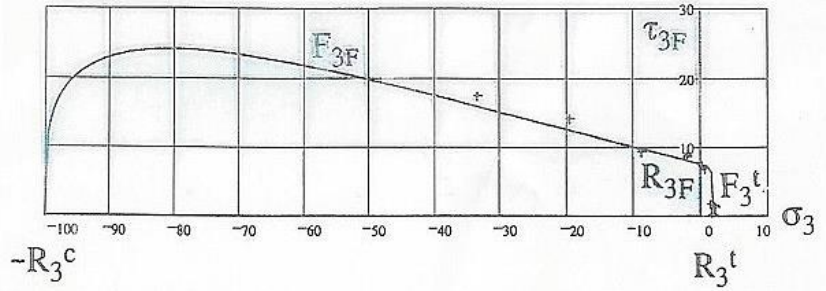


Fig. 7.3-6: C/C-SiC tube,  $\tau_{WF}(\sigma_W)$  fracture curve,  $T=1600^\circ\text{C}$ ,  $m=4$  [Gei97]

$$\{\bar{R}\} = (\bar{R}_W^t, \bar{R}_W^c, \bar{R}_F^t, \bar{R}_F^c, \bar{R}_{WF}, \bar{R}_3^t, \bar{R}_3^c, \bar{R}_{3F}, \bar{R}_{3W})^T = (45, 260, -, -, 59, -, -, -, -)^T$$

Often used as test specimens are coupon test specimen, cut out from a plate under distinct angles. Here one reminder comes in before beginning to map:

**High Fidelity macro-mechanical SFCs must 'onsider' micro-mechanical failure effects caused by the distinct tested specimen.**

For the uni-axial stress states  $\sigma_W^c$  (Stability danger. The same is valid for the Fill direction) and  $\sigma_W^t$  clear fiber failure modes are identified. Under  $\tau_{WF}$ , accompanied by scissoring, matrix failure is faced. This is of minor importance for  $\sigma_W^c, \tau_{WF}$  but essential for  $\sigma_W^t, \tau_{WF}$ , because the increasing  $\sigma_W^t \equiv \sigma_{||}^t$  damages together with the matrix tensile fracture causing tensile component of the shear stress,  $\tau_{WF} \equiv (\sigma_m^c, \sigma_m^t)$ . This leads to an inward dent as logic consequence. Accompanied by a relatively sudden change from a micro-mechanical matrix failure to a macro-mechanical tensile failure of the fabric warp fiber strand under  $\sigma_W^t$  occurs. Sudden changes of failure mode domains take the simple series spring system incorporated in the interaction formula to the limit. An increase of  $m$  cannot work sufficiently well because an inward dent cannot be mapped. A decay function for each of the interacting modes is to employ and is terminated in the other pure domain.

LL: Application limit of the usually and here applied series spring model is given if abrupt changes of a mode are faced.

**Well-understood experiments have to verify the design assumptions made!**

In this context Avula stated in 1987 “Experimental observations and measurements are generally accepted to constitute the backbone of physical sciences and engineering because of the physical insight they offer to the scientist for formulating the theory. Concepts, which are developed from observation, are used as guides for the design of new experiments, which in turn are used for validation of the theory. Thus, experiments and theory have a hand-in-hand relationship.

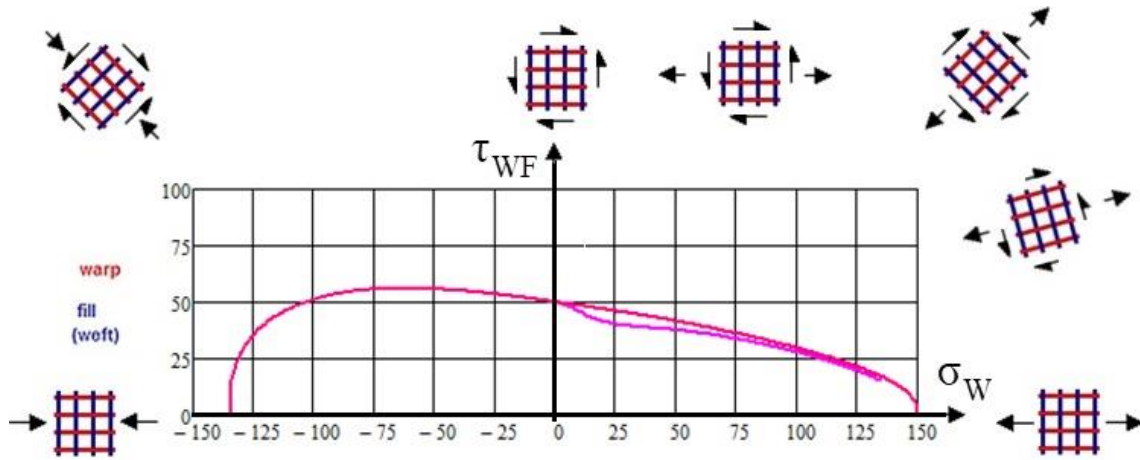


Fig. 7.3-7: Failure curve *with* and *without* mapping of the inward dent.

Plain weave fabric Ceramic Matrix Composite (CMC), defined strength values

In other words: At small tensile warp stresses the danger for matrix (tensile) failure under shear stresses  $\tau_{WF}$  increases through the over-loaded  $\sigma_W^t$ . This lasts until  $\sigma_W^t \equiv \sigma_{||}^t \rightarrow \sigma_{f,W}^{fr}$  and fiber tensile failure stress dominates the failure state. Fig.7.3-7 considers this failure situation.

Fig.7.3-8 finally presents the computation of the two curves above:

Vorgabe  $\tau := 20$

$$\left[ \left( \frac{\sigma + |\sigma|}{2Rt} \right)^m + \left( \frac{-\sigma + |\sigma|}{2Rc} \right)^m + \left( \frac{|\tau|}{RWF - \mu \cdot \sigma} \right)^m \right] = 1$$

$f(\sigma) := \text{Suchen}(\tau)$        $j := 0..Rc + Rt$        $\sigma_j := j - Rc$        $\tau_j := f(\sigma_j)$

Vorgabe  $\tau := 20$

$$\left[ \left[ \frac{\sigma + |\sigma|}{2 \left( Rt \cdot \frac{1}{1 + e^{\frac{c1Wt - \sigma}{c2Wt}}} \right)} \right]^m + \left( \frac{-\sigma + |\sigma|}{2Rc} \right)^m + \left[ \frac{|\tau|}{(RWF - \mu \cdot \sigma) \cdot \frac{1}{1 + e^{\frac{c1WF - \sigma}{c2WF}}}} \right]^m \right] = 1$$

$A(\sigma) := \text{Suchen}(\tau)$        $j := 0..Rc$        $\sigma_j := j$        $\tau_j := A(\sigma_j)$

Fig. 7.3-8: MathCad computation of the Failure curve *with* and *without* mapping of the inward dent

The course in the domain  $\sigma_W^c, \tau_{WF}$  seems to contradict to Fig. 7.3-6, however, the materials are different and the distribution of the provided test points are not comparable.

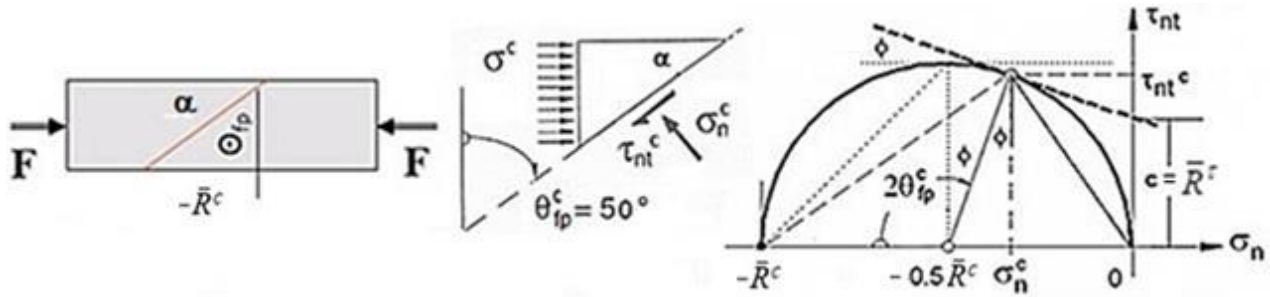
At this place thanks to Prof. Dr.-Ing. Roman Keppeler and Dr.-Ing. Thorsten Steinkopff for the discussions and suggestions on UD and fabric ceramics.

## 8 Mohr Stress Transformation to obtain the dependence Friction Parameter from Friction Value

### 8.1 Dependence of isotropic friction model parameter on friction value $\mu$

#### 8.1.1 General

*Fig.8.1-1* informs about the stress terms and angle terms used in the envisaged uni-axial stress state  $\sigma^c = F / Area$ . These are  $\varphi (\equiv \rho)$  for the slope and  $c (\equiv R^t)$  for the cohesive strength. Further, the fracture plane angle  $\Theta_{fp}$  is displayed on the test specimen together with its complementary angle  $\alpha$ .



*Fig.8.1-1: Shear fracture plane angles in touch point and 'linear' Mohr-Coulomb friction curve.*

*The touch point is  $(\sigma_n^c, \tau_{nt}^c)$*

Mohr fracture stresses act on the fracture plane. Mohr's failure envelope is generally a curved line which most often is approximated by a straight line described by the cohesive strength  $\bar{R}_\tau \equiv c$  and the frictional part, often written as  $\tau_{nt} = c - \sigma_n \cdot \tan(\phi)$  (in civil engineering:  $c + |\sigma_n| \cdot \tan(\phi)$ ).

When dealing with fracture plane angles and Mohr-Coulomb theory some further basic notions should be visualized. In *Fig.8.1-2* an arbitrary spatial fracture plane is shown for an isotropic and a transversely-isotropic material, a fiber-reinforced polymer or a fiber-reinforced concrete matrix.

For practical purposes, it is sufficient to reduce the mathematical variety of possible fracture planes problem by defining a distinct plane. Tests are performed on basis of mathematical stresses where  $\sigma_{III}$  is the most negative stress

- Uni-axial stress states:  $\{\sigma\} = (0, \sigma_{II}, 0)^T$
- Bi-axial stress states:  $\{\sigma\} = (0, \sigma_{II}, \sigma_{III})^T$
- Hydrostatic pressure-linked stress states along Tensile Meridian and Compressive Meridian are  $\{\sigma\} = (\sigma_I, \sigma_{II}, \sigma_{III})^T$  for the cube test specimen and  $\{\sigma\} = (\sigma_\varphi, \sigma_r, \sigma_{ax})^T$  for the cylindrical test specimen.

In mathematical stresses the stress situation under  $p_{hyd}$  in the tests reads:

$$\text{Tensile Meridian: } (\sigma_{ax}^t - p_{hyd}, -p_{hyd}, -p_{hyd}) = (\sigma_I, \sigma_{II}, \sigma_{III}) \rightarrow \sigma_I > \sigma_{II} = \sigma_{III}$$

$$\text{Compressive Meridian: } (-p_{hyd}, -p_{hyd}, \sigma_{ax}^c - p_{hyd}) = (\sigma_I, \sigma_{II}, \sigma_{III}) \rightarrow \sigma_I = \sigma_{II} > \sigma_{III}$$

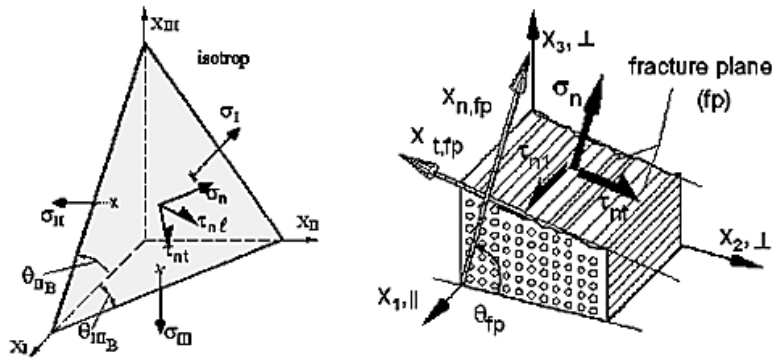


Fig.8.1-2: Mohr stresses of isotropic materials and transversely-isotropic UD materials

### 8.1.2 Pure $F^{SF}$ -based Mohr-Coulomb Fracture Curve and Cohesive Strength Prediction

A Mohr-Coulomb curve is fully linked to the second quadrant of the principal structural stress plane  $\sigma_y(\sigma_x)$  or  $\sigma_{II}(\sigma_{III})$ , respectively. Fig.8.1-3 demonstrates that for this special brittle material at  $\sigma_{III} = > -30$  MPa the  $F^{NF}$  begins to dominate the additional fracture danger portions of  $F^{NF} + F^{SF}$  in the modes' interacting transition zone or, respectively, NF tops SF. The sketch at the right highlights the stress state in the associated test specimen.

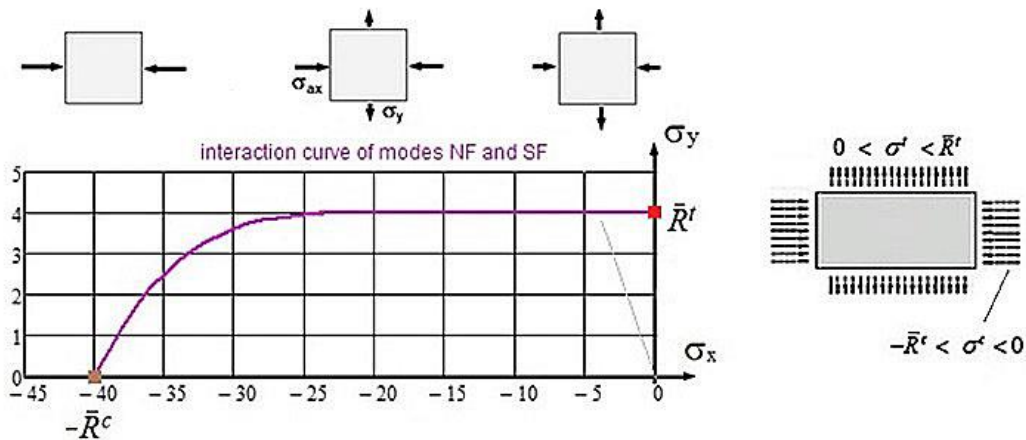
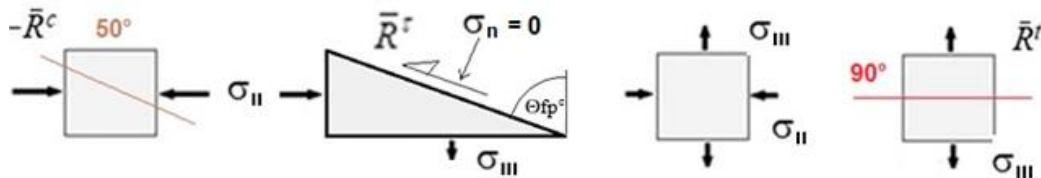


Fig.8.1-3: Schematic visualization of principal structural stress states belonging to the Mohr-Coulomb curve

Physical experience: The fracture plane angle at the compressive strength point (uni-axial, mode SF) is about  $50^\circ$  for brittle materials like Normal Concrete, grey cast iron and is approximately  $70^\circ$  at the cohesive strength point  $(\bar{R}^t, \sigma_n = 0) \equiv (\sigma_{II} = -\bar{R}^t \cdot s/c, \sigma_{III} = \bar{R}^t \cdot c/s)$ , Table 8.1-1,



Span :

$$(\tau_{nt}^c, \sigma_n^c) \rightarrow (\bar{R}^t, 0) \rightarrow (\tau_{nt}, \sigma_n) \rightarrow (0, \sigma_n = \bar{R}^t) \Leftrightarrow (\sigma_{II} = -\bar{R}^c, 0) \rightarrow (\sigma_{II}, \sigma_{III}) \rightarrow (0, \sigma_{III} = \bar{R}^t)$$

Table 8.1-1: Transformation of Cartesian principal stresses into Mohr stresses, addition theorem relations

\* Cartesian coordinate system, isotropic

$$\{\sigma\} = \begin{Bmatrix} \sigma_\ell \\ \sigma_n \\ \sigma_t \\ \tau_{m\ell} \\ \tau_{n\lambda} \\ \tau_{r\lambda} \end{Bmatrix} = \begin{bmatrix} 1 & 0 & 0 & 0 & 0 & 0 \\ 0 & c^2 & s^2 & 2sc & 0 & 0 \\ 0 & s^2 & c^2 & -2sc & 0 & 0 \\ 0 & -sc & sc & (c^2 - s^2) & 0 & 0 \\ 0 & 0 & 0 & 0 & c & -s \\ 0 & 0 & 0 & 0 & s & c \end{bmatrix} \begin{Bmatrix} \sigma_I \\ \sigma_{II} \\ \sigma_{III} \\ 0 \\ 0 \\ 0 \end{Bmatrix}, \quad \varphi = \varphi^\circ \cdot \frac{\pi}{180^\circ}$$

Transformed structural stresses and addition theorems used:  $\tau = 0$

$$s = \sin(\varphi), \quad c = \cos(\varphi), \quad s^2 + c^2 = 1, \quad S^2 + C^2 = 1, \quad C = c^2 - s^2 = 2c^2 - 1, \\ \sigma_n = c^2 \sigma_{II} + s^2 \sigma_{III} = 0.5 \cdot [(C+1) \cdot \sigma_{II} + (1-C) \cdot \sigma_{III}], \quad \sigma_t = s^2 \sigma_{II} + c^2 \sigma_{III} \\ \tau_m = -s \cdot c \cdot \sigma_{II} + s \cdot c \cdot \sigma_{III}, \quad S = 2sc, \quad c^2 = (C+1) \cdot 0.5, \quad s^2 = (1-C) \cdot 0.5 \\ \sigma_n - \sigma_t = C \cdot (\sigma_{II} - \sigma_{III}), \quad \tau_m = -s \cdot c \cdot (\sigma_{II} - \sigma_{III}) = -0.5 \cdot S \cdot (\sigma_{II} - \sigma_{III}) \\ \sigma_n - \sigma_t = c^2 \cdot (\sigma_{II} - \sigma_{III}) - s^2 \cdot (\sigma_{II} - \sigma_{III}) = C \cdot (\sigma_{II} - \sigma_{III}), \quad C = \cos(2\varphi)$$

$$\sigma_n + \sigma_t = \sigma_{II} + \sigma_{III}, \quad \tau_m = -0.5 \cdot S \cdot (\sigma_{II} - \sigma_{III}), \quad S = \sqrt{1 - C^2}$$

The derivation yields the slope in the touch point ( $\sigma_m = 0$ ), index  $c$ :

$$d\sigma_n / d\Theta_{fp} = d(c^2 \cdot \sigma_{II} + s^2 \cdot \sigma_{III}) / d\Theta_{fp} = -2 \cdot s \cdot c \cdot \sigma_{II} = -S^c \cdot \sigma_{II} \\ d\tau_m / d\Theta_{fp} = d(-s \cdot c \cdot \sigma_{II} + s \cdot c \cdot \sigma_{III}) / d\Theta_{fp} = (-c^2 + s^2) \cdot \sigma_{II} = -C^c \cdot \sigma_{II} \\ \Rightarrow \frac{d\tau_m}{d\sigma_n} = -\frac{C^c}{S^c} = \cotan(2\Theta_{fp}). \quad C^c = \cos(2 \cdot \Theta_{fp} \cdot \pi / 180^\circ)$$

\* Cartesian coordinate system, transversely-isotropic UD Material

(1 is fiber direction)

$$\{\sigma\} = \begin{Bmatrix} \sigma_\ell \\ \sigma_n \\ \sigma_t \\ \tau_{m\ell} \\ \tau_{n1} \\ \tau_{r1} \end{Bmatrix} = \begin{bmatrix} 1 & 0 & 0 & 0 & 0 & 0 \\ 0 & c^2 & s^2 & 2sc & 0 & 0 \\ 0 & s^2 & c^2 & -2sc & 0 & 0 \\ 0 & -sc & sc & (c^2 - s^2) & 0 & 0 \\ 0 & 0 & 0 & 0 & c & -s \\ 0 & 0 & 0 & 0 & s & c \end{bmatrix} \begin{Bmatrix} \sigma_1 \\ \sigma_2 \\ \sigma_3 \\ 0 \\ 0 \\ 0 \end{Bmatrix},$$

$$\sigma_n - \sigma_t = c^2 \cdot (\sigma_2 - \sigma_3) - s^2 \cdot (\sigma_2 - \sigma_3) = C \cdot (\sigma_2 - \sigma_3)$$

$$\sigma_n + \sigma_t = \sigma_2 + \sigma_3, \quad \tau_m = -0.5 \cdot S \cdot (\sigma_2 - \sigma_3), \quad S = \sqrt{1 - C^2}$$

Structural stresses:

$$I_1 = \sigma_x + \sigma_y + \sigma_z, \quad I_2 = \sigma_x \cdot \sigma_y + \sigma_y \cdot \sigma_z + \sigma_x \cdot \sigma_z - \tau_{xy}^2 - \tau_{yz}^2 - \tau_{xz}^2$$

$$I_3 = \sigma_x \cdot \sigma_y \cdot \sigma_z + 2\tau_{xy} \cdot \tau_{yz} \cdot \tau_{xz} - \sigma_x \cdot \tau_{yz}^2 - \sigma_y \cdot \tau_{xy}^2 - \sigma_z \cdot \tau_{xz}^2$$

$$6J_2 = (\sigma_y - \sigma_z)^2 + (\sigma_z - \sigma_x)^2 + (\sigma_x - \sigma_y)^2 + 6 \cdot (\tau_{xy}^2 + \tau_{yz}^2 + \tau_{xz}^2)$$

$$27J_3 = 2I_1^3 - 9I_1 \cdot I_2 + 27I_3$$

$$2D: I_1 = \sigma_x + \sigma_y$$

$$6J_2 = (\sigma_y)^2 + (-\sigma_x)^2 + (\sigma_x - \sigma_y)^2 + 6 \cdot \tau_{xy}^2$$

Principal stresses:

$$I_1 = \sigma_I + \sigma_{II} + \sigma_{III} = f(\sigma)$$

$$6J_2 = (\sigma_I - \sigma_{II})^2 + (\sigma_{II} - \sigma_{III})^2 + (\sigma_{III} - \sigma_I)^2 = f(\tau) \quad (\text{'Mises' invariant})$$

$$27J_3 = (2\sigma_I - \sigma_{II} - \sigma_{III}) \cdot (2\sigma_{II} - \sigma_I - \sigma_{III}) \cdot (2\sigma_{III} - \sigma_I - \sigma_{II})$$

$$3 \cdot \sigma_{oct} = \sigma_I + \sigma_{II} + \sigma_{III} = \sigma_\ell + \sigma_n + \sigma_t;$$

$$9 \cdot \tau_{oct}^2 = 6J_2 = 4 \cdot (\tau_m^2 + \tau_t^2 + \tau_{n\lambda}^2)$$

$\tau_{II} = \max \tau(\text{mathematically})$ ,  $\sigma_I, \sigma_{II}, \sigma_{III}$  are principal stresses,

$\sigma_I > \sigma_{II} > \sigma_{III}$  are mathematical stresses (the sign > means more positive)

$$2D: I_1 = \sigma_{II} + \sigma_{III}$$

$$6J_2 = 2 \cdot (\sigma_{II}^2 + \sigma_{III} \cdot \sigma_{III} + \sigma_{III}^2)$$

$$27J_3 = (-\sigma_{II} - \sigma_{III}) \cdot (2\sigma_{II} - \sigma_{III}) \cdot (2\sigma_{III} - \sigma_{II})$$

Mohr stresses: fracture angle measure C

$$I_1 = \sigma_n + \sigma_\lambda + \sigma_t, \quad I_2 = \sigma_n \cdot \sigma_t + \sigma_t \cdot \sigma_\lambda + \sigma_n \cdot \sigma_\lambda - \tau_{n\lambda}^2 - \tau_{m\ell}^2 - \tau_{r1}^2$$

$$I_3 = \sigma_n \cdot \sigma_t \cdot \sigma_\lambda + 2\tau_{m\ell} \cdot \tau_{n\lambda} \cdot \tau_{r1} - \sigma_n \cdot \tau_{n\lambda}^2 - \sigma_\lambda \cdot \tau_{m\ell}^2 - \sigma_t \cdot \tau_{r1}^2$$

$$6J_2 = (\sigma_n - \sigma_t)^2 + (\sigma_t - \sigma_\lambda)^2 + (\sigma_\lambda - \sigma_n)^2 + 6 \cdot (\tau_{m\ell}^2 + \tau_{n\lambda}^2 + \tau_{r1}^2)$$

$$27J_3 = 2I_1^3 - 9I_1 \cdot I_2 + 27I_3$$

$$2D: I_1 = \sigma_n + \sigma_t, \quad I_2 = -\tau_{m\ell}^2 + \sigma_n \cdot \sigma_t, \quad I_3 = 0$$

$$6J_2 = (\sigma_n - \sigma_t)^2 + (\sigma_t)^2 + (-\sigma_n)^2 + 6 \cdot \tau_{m\ell}^2$$

$$27J_3 = 2(\sigma_n + \sigma_t)^3 - 9 \cdot (\sigma_n + \sigma_t) \cdot (\sigma_n \cdot \sigma_t - \tau_{m\ell}^2)$$

According to Mohr's theory the stress  $\sigma_t$  is not effective. It can be eliminated in the 2D case using addition theorems, thus linking structural stresses to Mohr stresses

$\sigma_n - \sigma_t = C \cdot (\sigma_x - \sigma_y)$ ,  $\sigma_t = \sigma_n - C \cdot (\sigma_x - \sigma_y)$ ,  $C = \cos(2 \cdot \Theta_{fp} \cdot \pi / 180^\circ)$

Interpreting structural stresses as mathematical stresses means  $\sigma_x \equiv \sigma_{II}, \sigma_y \equiv \sigma_{III}$ .

### 8.1.3 Finding the relationship friction parameter $c2 \leftrightarrow$ friction value $\mu$

Table 8.1-2: Derivation of the Mohr stresses-transformed FMC-based strength failure conditions

$$F^{SF} = c_{1\Theta}^{SF} \cdot \frac{3J_2 \cdot \Theta^{SF}}{\bar{R}^{c^2}} + c_2^{SF} \cdot \frac{I_1}{\bar{R}^c} = 1 \quad \text{or} \quad Eff^{SF} = \frac{c_{2\Theta}^{SF} \cdot I_1 + \sqrt{(c_{2\Theta}^{SF} \cdot I_1)^2 + 12 \cdot c_{1\Theta}^{SF} \cdot 3J_2 \cdot \Theta^{SF}}}{2 \cdot \bar{R}^c}$$

Inserting compressive strength  $\bar{R}^c$  delivers  $1 + c_{2\Theta}^{SF} = c_{1\Theta}^{SF} \cdot \Theta^{SF}$  with the non-circularity function  $\Theta^{SF} = \sqrt[3]{1 + d^{SF} \cdot \sin(3\theta)} = \sqrt[3]{1 + d^{SF} \cdot 1.5 \cdot \sqrt{3} \cdot J_3 \cdot J_2^{-1.5}}$

which reads  $\Theta = 1$  if  $\bar{R}^{cc} = \bar{R}^c \Leftrightarrow$  rotationally-symmetric

$$\frac{c_{1\Theta}^{SF}}{2\bar{R}^{c^2}} \cdot [(\sigma_n - \sigma_i)^2 + (\sigma_i - \sigma_\lambda)^2 + (\sigma_\lambda - \sigma_n)^2 + 6 \cdot (\tau_{nt}^2 + \tau_{n\lambda}^2 + \tau_{i\lambda}^2)] + c_{2\Theta}^{SF} \cdot \frac{\sigma_n + \sigma_\lambda + \sigma_i}{\bar{R}^c} = 1$$

Derivation of the slope equation in Mohr stresses,  $\sigma_\lambda, \tau_{i\lambda}, \tau_{n\lambda} = 0$

$$\frac{dF^{SF}}{d\sigma_n} = \frac{c_{1\Theta}^{SF}}{2\bar{R}^{c^2}} \cdot [4\sigma_n - 2\sigma_i - 2\sigma_\lambda] + \frac{c_{2\Theta}^{SF}}{\bar{R}^c}; \quad \frac{dF^{SF}}{d\tau_{nt}} = 12 \frac{c_{1\Theta}^{SF}}{2 \cdot \bar{R}^{c^2}} \cdot \tau_{nt}$$

$$\frac{d\tau_{nt}}{d\sigma_n} = -\frac{dF}{d\sigma_n} / \frac{dF}{d\tau_{nt}} \quad (\text{implicit diff.}) = -\left[ \frac{c_{1\Theta}^{SF}}{\bar{R}^{c^2}} \cdot [2\sigma_n - \sigma_i - \sigma_\lambda] + \frac{c_{2\Theta}^{SF}}{\bar{R}^c} \right] / \left[ 6 \frac{c_{1\Theta}^{SF}}{\bar{R}^{c^2}} \cdot \tau_{nt} \right]$$

Transformed structural stresses and addition theorems used:  $\sigma_\lambda = 0$  set

$$S^2 + C^2 = 1, \quad C = c^2 - s^2 = 2c^2 - 1, \quad S = 2sc, \quad c^2 = (C+1) \cdot 0.5, \quad s^2 = (1-C) \cdot 0.5$$

$$\sigma_n - \sigma_i = C \cdot (\sigma_{II} - \sigma_{III}), \quad \tau_{nt} = -s \cdot c \cdot (\sigma_{II} - \sigma_{III}) = -0.5 \cdot S \cdot (\sigma_{II} - \sigma_{III})$$

Transformation relations for equalizing the angle in the touch point,  $\sigma_{II} - \sigma_{III} = \eta$

$$\frac{d\tau_{nt}}{d\sigma_n} = -\left[ \frac{c_{2\Theta}^{SF} \cdot \eta + c_{1\Theta}^{SF} \cdot (2 \cdot c^2 - s^2) \cdot \eta}{6 \cdot c_{1\Theta}^{SF} \cdot (-s \cdot c \cdot \eta)} \right] = -\left[ \frac{c_{2\Theta}^{SF} - c_{1\Theta}^{SF} \left(2 \frac{C+1}{2} - \frac{1-C}{2}\right)}{6 \cdot c_{1\Theta}^{SF} \cdot (-0.5 \cdot S)} \right]$$

Equal slope of curves in touch point:  $\eta$  is multi-axial and cut out

$$\frac{d\tau_{nt}}{d\sigma_n} = \frac{C}{S} = -\left[ \frac{c_{2\Theta}^{SF} - c_{1\Theta}^{SF} \left(C + 1 - \frac{1-C}{2}\right)}{6 \cdot c_{1\Theta}^{SF} \cdot (-0.5 \cdot S)} \right] \quad \text{with} \quad C \Rightarrow C^c = \frac{c_{2\Theta}^{SF} - c_{1\Theta}^{SF}}{-3 \cdot c_{1\Theta}^{SF}}$$

Determination of  $c_{2\Theta}^{SF}$  after inserting  $1 + c_{2\Theta}^{SF} = c_{1\Theta}^{SF}$  for neutral meridian  $\Theta^{SF} = 1$ :

$$C^c = \frac{c_{2\Theta}^{SF} - (1 + c_{2\Theta}^{SF})}{-3 \cdot (1 + c_{2\Theta}^{SF})} = \frac{-1}{-3 \cdot (1 + c_{2\Theta}^{SF})} \Rightarrow c_{2\Theta}^{SF} = \frac{-3 \cdot C^c + 1}{3 \cdot C^c + 1}$$

Mohr, linear fracture condition:  $\tau_{nt} = R^\tau - \mu \cdot \sigma_n$  or  $F = \frac{\tau_{nt}}{R^\tau - \mu \cdot \sigma_n} = 1$

$$\frac{d\tau_{nt}}{d\sigma_n} = -\frac{dF}{d\sigma_n} / \frac{dF}{d\tau_{nt}} = -\frac{\tau_{nt} \cdot \mu}{(R^\tau - \mu \cdot \sigma_n)^2} / \frac{1}{R^\tau - \mu \cdot \sigma_n} = -\frac{\tau_{nt} \cdot \mu}{(R^\tau - \mu \cdot \sigma_n)} = -\mu \equiv \frac{C^c}{S^c}$$

Now, it is possible to sort out the relations between all friction-linked parameters

$$\mu = -\tan \rho = \frac{d\tau_{nt}}{d\sigma_n} = \frac{-C^c}{S^c}, \quad \text{small friction angles} \cong -C^c, \quad \tan \phi \equiv \tan \rho$$

$$c_{2\Theta}^{SF} = \frac{3\mu + 1}{-3\mu + 1} \quad \text{and} \quad \text{if an angle is measured, then} \quad C^c = \cos\left(\frac{2 \cdot \Theta_{fp}^\circ}{180^\circ} \cdot \pi\right).$$

From Fig.4-1 relationships can be derived and from them follows for  $\Theta_{fp}^\circ = 50^\circ$

$$\text{brittle} \quad \Theta_{fp}^\circ = 50^\circ \rightarrow C^c = -0.174, \quad c_{2\Theta}^{SF} = c_2^{SF} = 3.7, \quad \mu = 0.18,$$

$$F^{SF} \text{ bound} \quad \Theta_{fp}^\circ = 45^\circ \rightarrow C^c = 0; \quad \mu = 0, \quad \rho = -\text{atan}(\mu) = 0.$$

In Table 8.1-3 the traditional way of predicting  $\tau_{nt}(\sigma_n)$  and of cohesive strength  $\bar{R}^\tau$  is presented:

Table 8.1-3 : Derivation of Mohr shear curve  $\tau_{nt}(\sigma_n)$  and cohesive strengths from different models

| Rotationally symmetric   | SFCs              | 120°-Rotationally symmetric  |
|--|-------------------|--|
| $F^{SF} = c_1^{SF} \cdot \frac{3J_2 \cdot 1}{\bar{R}^{c2}} + c_2^{SF} \cdot \frac{I_1}{\bar{R}^c} = 1$                   | $\Leftrightarrow$ | $F^{SF} = c_{1\Theta}^{SF} \cdot \frac{3J_2 \cdot \Theta^{SF}}{\bar{R}^{c2}} + c_{2\Theta}^{SF} \cdot \frac{I_1}{\bar{R}^c} = 1$                                     |
| $Eff^{SF} = \frac{c_1^{SF} \cdot I_1 + \sqrt{(c_2^{SF} \cdot I_1)^2 + 12 \cdot c_1^{SF} \cdot 3J_2}}{2 \cdot \bar{R}^c}$ | $\Leftrightarrow$ | $Eff^{SF} = \frac{c_{1\Theta}^{SF} \cdot I_1 + \sqrt{(c_{2\Theta}^{SF} \cdot I_1)^2 + 12 \cdot c_{1\Theta}^{SF} \cdot 3J_2 \cdot (\Theta^{SF})}}{2 \cdot \bar{R}^c}$ |
| $\Theta^{NF} = \sqrt[3]{1 + d^{SF} \cdot (+1)} \equiv \Theta^{TM}$   |                   | $\Theta^{SF} = \sqrt[3]{1 + d^{SF} \cdot (-1)} \equiv \Theta^{CM}$ , $\Theta^{NM} = \sqrt[3]{1 + d^{SF} \cdot (0)} = 1$  |

$\Leftrightarrow$  Determination of friction-related parameters using

\* Information  $c_2(C_{fp}^c)$  assumption  $c_2^{SF} \approx (1 + 3 \cdot \mu) / (1 - 3 \cdot \mu)$  here friction parameter

$$c_1^{SF} = 1 + c_2^{SF}, \quad d^{SF} = 0 \quad \leftarrow \text{inserting } (-\bar{R}^c, 0) \rightarrow c_{1\Theta}^{SF} = 1 + c_{2\Theta}^{SF} \cdot \sqrt[3]{1 + d^{SF} \cdot (-1)}$$

\* Mapping of the course of available test data by a minimum error fit

Simulation process necessary: Numerical tuning to optimally map the course of test data

\* Approximated, by using information on  $\theta_{fp}^c$  or  $\mu$ :  $C^c = \cos(2 \cdot \theta_{fp}^c \cdot \pi / 180) \cong -\mu$ ,

point  $(-\bar{R}^c, 0)$  from compr. meridian test *plus*  $(-\bar{R}^{cc}, -\bar{R}^{cc}, 0)$  from tensile meridian test.

\* The Mohr-Coulomb curve  $\tau_{nt}(\sigma_n)$  depends on the non-circularity function  $\Theta^{SF}$

\* Introducing  $\sigma_\lambda, \tau_{nt}, \tau_{nt} = 0, \quad 1 + c_{2\Theta}^{SF} = c_{1\Theta}^{SF} \cdot \Theta^{SF}$ .

$$\frac{c_{1\Theta}^{SF} \cdot \Theta^{SF}}{2\bar{R}^{c2}} \cdot [(\sigma_n - \sigma_t)^2 + (\sigma_t - 0)^2 + (0 - \sigma_n)^2 + 6 \cdot (\tau_{nt}^2)] + c_{2\Theta}^{SF} \cdot \frac{\sigma_n + 0 + \sigma_t}{\bar{R}^c} = 1.$$

$\Leftrightarrow$  Determination of the  $\tau_{nt}(\sigma_n)$  - curve using addition theorems and inserting  $(-\bar{R}^c, 0)$

$$(\sigma_{II} - \sigma_{III}) = \eta = -\bar{R}^c, \quad \sigma_n - \sigma_t = C \cdot \eta, \quad \tau_{nt} = -s \cdot c \cdot \eta = -0.5 \cdot S \cdot \eta, \quad \sigma_n - C \cdot \eta = \sigma_t$$

$$\frac{c_{1\Theta}^{SF} \cdot \Theta^{SF}}{2\bar{R}^{c2}} \cdot [(C \cdot \eta)^2 + (\sigma_n - C \cdot \eta)^2 + (-\sigma_n)^2 + 6 \cdot (\tau_{nt}^2)] + c_{2\Theta}^{SF} \cdot \frac{\sigma_n + \sigma_n - C \cdot \eta}{\bar{R}^c} = 1$$

$$\tau_{nt}(\sigma_n) = \frac{\sqrt{3 \cdot \sqrt{-c_{1\Theta}^{SF} \cdot \Theta^{SF} \cdot (c_{1\Theta}^{SF} \cdot \Theta^{SF} \cdot [C^2 \cdot \bar{R}^{c2} + C \cdot \bar{R}^c \cdot \sigma_n + \sigma_n^2] - \bar{R}^{c2} + c_{2\Theta}^{SF} \cdot [C \cdot \bar{R}^{c2} + 2 \cdot \bar{R}^c \cdot \sigma_n])}}}{3c_{1\Theta}^{SF} \cdot \Theta^{SF}}$$

$$c_{2\Theta}^{SF} = (3\mu + 1) / (1 - 3\mu), \quad \mu = -\tan \rho \cong -C^c = -\cos(2 \cdot \Theta_{fp}^c \cdot \pi / 180^\circ)$$

**Example:**  $\Theta_{fp}^c = 50^\circ \rightarrow C^c = -0.174, \quad \mu = 0.176 \cong -C^c, \quad d^{SF} = 0.49, \quad \Theta^{SF} = 0.80$

Rotationally-symmetric  $c_2^{SF} = 3.7, \quad c_1^{SF} = 1 + c_2^{SF} = 4.7, \quad C = C^c$

120°-rot.-sym:metric  $c_{2\Theta}^{SF} = c_2^{SF}, \quad c_{1\Theta}^{SF} = 1 + c_{2\Theta}^{SF} \cdot \Theta^{SF} = 5.88, \quad C$  alters with  $\vartheta$

$\Leftrightarrow$  Determination of cohesive shear strengths:

Linear Mohr-Coulomb:  $\bar{R}^\tau = \tau_{nt}^c + \mu \cdot \sigma_n^c, \quad \mu = -(1 - c_2^{SF}) / (-3c_2^{SF} + 3), \quad \bar{R}^\tau = 17 \text{ MPa}$

Rotationally-symmetric: point  $(\tau_{nt} = \bar{R}^\tau, \sigma_n = 0), \quad \bar{R}^\tau = 13.5 \text{ MPa or N/mm}^2$

120°-Rotat.-symm.: point  $(\tau_{nt} = \bar{R}^\tau, \sigma_n = 0), \quad \bar{R}^\tau = 12.5 \text{ MPa}, \quad \delta = -25.1^\circ,$

$$(\bar{R}^\tau, \sigma_n = 0) \equiv (\sigma_{II} = -\bar{R}^\tau \cdot s / c, \sigma_{III} = \bar{R}^\tau \cdot c / s) = (\sigma_{II} = -32 \text{ MPa}, \sigma_{III} = 3.33 \text{ MPa})$$

Geometry:  $d\tau_{nt} / d\sigma_n = \tan \rho = (0.5 \cdot \bar{R}^c - |\sigma_n^c|) / \tau_{nt}^c \rightarrow \tau_{nt}^c = (0.5 \cdot \bar{R}^c - |\sigma_n^c|) / \tan \rho$

$$\tau_{nt}^c = \sqrt{|\sigma_n^c| \cdot (\bar{R}^c - |\sigma_n^c|)} = \left( \frac{(0.5 \cdot \bar{R}^c - |\sigma_n^c|)}{\tan \rho} \right)^2, \quad |\sigma_n^c| = \frac{(\bar{R}^c + \bar{R}^c \cdot \tan^2 \rho) - \bar{R}^c \cdot \tan \rho \cdot \sqrt{1 + \tan^2 \rho}}{2 + 2 \cdot \tan^2 \rho}$$

Touch point coordinates:  $\tau_{nt}^c = 19.7 \text{ MPa}, \quad \sigma_n^c = -16.5 \text{ MPa}.$

Input:  $\bar{R}^t = 4 \text{ MPa}, \quad \bar{R}^c = 40 \text{ MPa (on CM)}, \quad \bar{R}^{cc} = 49 \text{ MPa (on TM)}$ , further point on the CM (or TM) is

required, CM test curve point,  $(I_1 / (\bar{R}^t \cdot \sqrt{3}) = -20, \sqrt{2 \cdot J_2} / \bar{R}^t = 14)$ , usual normalisation by  $\bar{R}^t$ .

As numerical example a material has been chosen above a fracture angle  $\Theta_{fp}^c$  from which follow the friction entities  $\Theta_{fp}^c = 50^\circ \rightarrow C^c = -0.174, \mu = 0.176$ .

Mohr-Coulomb relation:

In order to be able to derive the friction value  $\mu$ , the slope of the linear Mohr envelope at the compressive strength associated point, termed touch point, must be provided.  $\Theta_{fp}^c$  is the fracture angle in the touch point which is linked to the compressive strength, indexed  $^c$ . Viewing Fig.7-1 the relation exists ( $\rho \equiv \phi$ ):  $\mu = -\tan \rho \cong -C^c = -\cos(2 \cdot \Theta_{fp}^c \cdot \pi / 180^\circ)$ .

Table 8.1-4 summarizes the derivation and all relations.

Table 8.1-4: Derivation of relations  $\mu(\Theta_{fp}^c)$  applying the Linear Mohr-Coulomb approach

$$F_{Mohr}^{SF} = \frac{\tau_{nt}}{\bar{R}^\tau - \mu \cdot \sigma_n} = 1 \quad - \text{ compressive SFC, angle } \Theta_{fp}^c \text{ unknown}$$

$$\frac{dF_{Mohr}^{SF}}{d\sigma_n} = \frac{\mu \cdot \tau_{nt}}{(\bar{R}^\tau - \mu \cdot \sigma_n)^2} \quad \text{and} \quad \frac{dF_{Mohr}^{SF}}{d\tau_{nt}} = \frac{1}{\bar{R}^\tau - \mu \cdot \sigma_n}$$

$$\rightarrow \frac{d\tau_{nt}}{d\sigma_n} = \frac{-\mu \cdot \tau_{nt}}{(\bar{R}^\tau - \mu \cdot \sigma_n)^2} / \left( \frac{1}{\bar{R}^\tau - \mu \cdot \sigma_n} \right) = \frac{-\mu \cdot \tau_{nt}}{(\bar{R}^\tau - \mu \cdot \sigma_n)^1} = \frac{-\mu \cdot (\bar{R}^\tau - \mu \cdot \sigma_n)}{(\bar{R}^\tau - \mu \cdot \sigma_n)}$$

$$= -\mu \quad (\text{negative sign due to implicate differentiation}).$$

$$F_{Mohr}^{NF} = \sigma_n / \bar{R}^t = 1 \quad - \text{ tensile SFC, angle } \Theta_{fp}^t = 90^\circ$$

The following chapters show applications where 2D- and 3D-test data sets could be obtained. For providing these test data sets the author is very grateful.

Fig.8.1-4 at first verifies that the Mohr-Coulomb shear curve practically captures the transition zone between the uni-axial border points compressive strength and – if extended – the tensile strength which means it has to capture the interaction between the two modes  $F^{SF}$  and  $F^{NF}$ .

The upper left sketch in Fig.8.1-4 depicts the decomposition of cohesive strength into its normal failure stress components still indicating that the tensile stress will dominate the failure behavior.

The upper right sketch in Fig.8.1-4 depicts three stress states generated between the compressive strength and the cohesive strength point. The lower curves in Fig.8.1-4 present  $\tau_{nt}(\sigma_n)$ -curves including the models Linear Mohr-Coulomb, rotationally-symmetric  $F^{SF}$  and 120°-rotationally-symmetric  $F^{SF}$ .

The differences between the classical rotationally-symmetric model and the 120°-rotationally symmetric model is caused because the 120°-rotationally symmetric model does not stay with the compressive meridian CM which runs through the uni-axial compressive strength point. It reflects that under bi-axial stressing the meridian-marking Lode angle  $\vartheta$  varies from CM via NM ( $\vartheta = 0^\circ$ , due to  $J_3 = 0$  ! This corresponds to the rotationally symmetric model) at the cohesive strength point into the direction of the tensile meridian TM with  $\vartheta = 90^\circ$ .



The results obtained by the three shear stress mode-linked approaches *Linear Mohr-Coulomb*, *Rotationally Symmetric* and the more realistic *120°-Rotationally Symmetric* reveal for the cohesive strength that the ‘extrapolated’ value decreases with the better description but nevertheless stays a little too high as shall be proven.

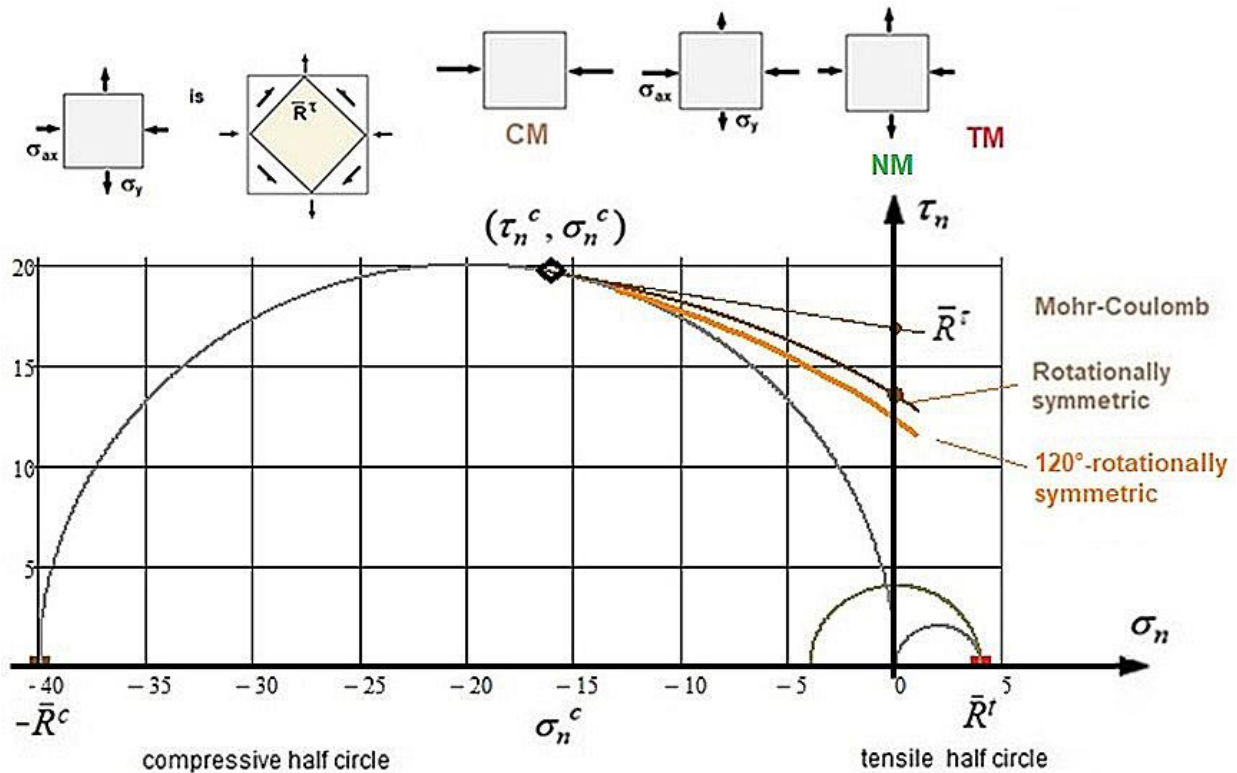


Fig.8.1-4: (upper left) Decomposition of cohesive strength into its normal failure stress components; (upper right) Stress states along the Mohr-Coulomb failure curve; (lower) Mohr stresses- dedicated failure curves  $\tau_{nt}(\sigma_n)$  and cohesive strengths  $\bar{R}^\tau$ . Example  $\Theta_{fp}^c = 50^\circ$  or  $\mu = 0.176$ , CM means compressive meridian, TM tensile meridian, NM neutral meridian

- The failure plane angle  $\Theta_{fp}$  reduces with increasing hydrostatic pressure, which means that the behaviour becomes more ductile. This increase of ‘ductility’, documented by  $\Theta_{fp}$  from about  $50^\circ \rightarrow 45^\circ$ , is witnessed even for marble
- The Mohr stresses  $\tau_{nt}$ ,  $\sigma_n$  grow with  $p_{hyd}$ . Also the driving principal shear stress  $\tau_1 = (\sigma_{II} - \sigma_{III}) / 2$  grows with  $p_{hyd}$
- The additional axial stress from the compression force, that finally leads to fracture failure, equals for the loadings CM and TM.

LL:

- (1) The M-C curve is an interaction curve describing the associated transition zone. For small compressive Mohr stresses  $\sigma_n$  the curves is ruled by NF and his indicate not by SF anymore
- (2) The cohesive fracture stress is a stress that is composed of a normal stress component and a compression stress component. Here, the use of the term ‘stress component’ is to accept ! This indicates the relationship to tension
- (3) Real isotropic materials have deficiencies to the ideal isotropic material. Hence, fracture will occur according to the actual flaw situation. In the case of crack-like flaws so-called wing-

cracks (rock mechanics) occur where the wing crack finally grows into the direction of the acting compression force [Cun20b]

- (4) A physically realistic investigation, performed in structural stresses and including both the modes, tells us that the fracture angle at the cohesive strength point, where  $\sigma_n = 0$ , must approach  $90^\circ$  for really brittle materials like normal concrete..
- (5) The friction value  $\mu$  is a so-called 'physical property'. This practically means: A good average value is sufficient for analysis in design dimensioning where always average values should be used.
- (6) The rotationally-symmetric model corresponds to the Neutral Meridian  $\Theta^{NM}$  ( $\vartheta = 0^\circ$ ).

#### Some Pre-notes on Testing:

- Most of the tri-axial tests are performed on tensile and compressive meridians. These meridians are the opposite lines of an axial cross-section of the fracture failure body, see [Fig.8.1-5](#).
- Looking at the Mohr-Coulomb curve, the angle alters with  $\Theta$  from ( $\vartheta = -30^\circ$ ) via  $\Theta^{NM}$  ( $\vartheta = 0^\circ$ , it represents the rotationally-symmetric model)  $\rightarrow \Theta^{TM}$  ( $\vartheta = +30^\circ$ ). In other words, an essential change is faced with C from  $C^c \approx -0.2$  at  $(\sigma_{II} = -R^c, 0)$  along the bi-axial stress states  $(\sigma_{II}, \sigma_{III})$ .
- Measurement results are 'only' the result of a test agreement defined in a standard, a guideline etc. which serves the comparability of different test investigations and the credibility of the process. The test agreement consists of test facility, test certificate, test specimen and evaluation procedure. This means that we can only speak of 'exact' test results within the frame of the test agreement.
- It must be noted that environment and loading rate affect the results.
- The compressive strength of concrete is determined by a pressure test with specially manufactured test specimens. These are concrete cubes with usually 15 cm edge length (sample cubes) or 30 cm long concrete cylinders with 15 cm diameter (DIN EN 12390-1)
- For the production and storage of test cubes for strength tests, DIN EN 12390-2 applies in addition. The compressed surfaces should be flat and parallel. Otherwise, they must be sanded wet or provided with a thin matching layer.
- 

#### **8.1.4 Fracture Body, Friction Quantities and Mohr-Coulomb Curve of Normal Concrete Invariants, Strength Failure Conditions SFCs and Material data set of Concrete**

For preparing the solution of this task, in the previous chapters still associated sub-tasks have been solved. Nevertheless, at first the full input for the isotropic example Normal Concrete shall be collected in order to pave the way for a shorter performance of the main numerical task presented in [Table 8.1-5](#).

The material input data set for the computation reads:

$$\bar{R}^t = 4 \text{ MPa}, \bar{R}^c = 40 \text{ MPa}, \bar{R}^t = 0.8 \cdot \bar{R}^c \text{ (assumed)}, \bar{R}^{cc} = 51 \text{ MPa}, \bar{R}^{ccc} = 1000 \text{ MPa (set)}$$

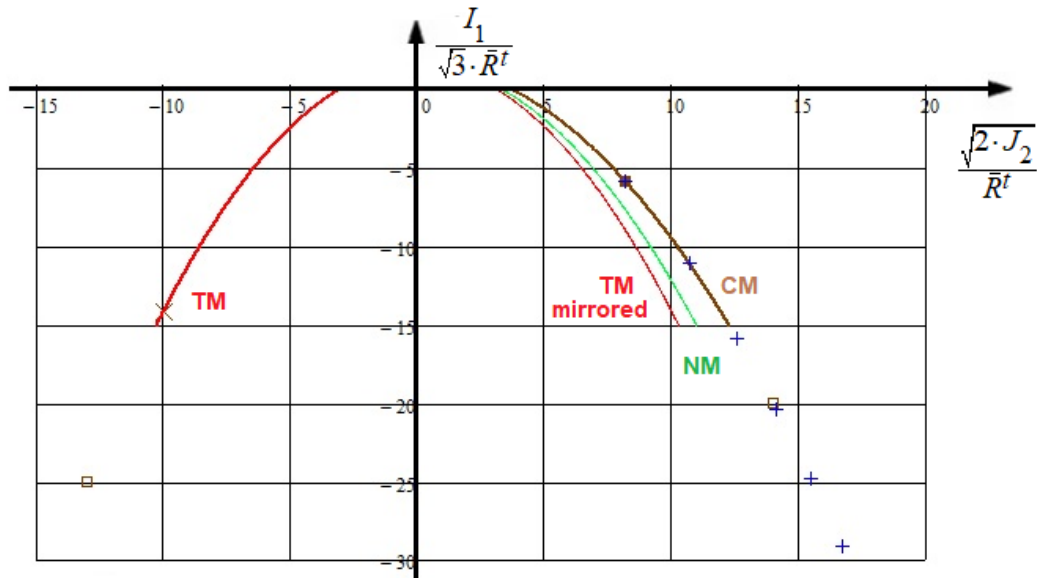
$$120^\circ\text{-rotationally-symmetry parameter: } c_{1\Theta}^{SF} \cdot \Theta^{SF} = 1 + c_{2\Theta}^{SF} \text{ with } c_{2\Theta}^{SF} \text{ as friction parameter}$$

$$\mu = 0.17, \Theta_{fp}^c = 50^\circ, c_{2\Theta}^{SF} = 3.70, c_{1\Theta}^{SF} = 5.88, d^{SF} = 0.49, \Theta^{SF} = \Theta^c = \Theta^{CM} = 0.51.$$

For the interaction exponent  $m = 2.6$  and  $\mu = 0.17$  is set. A smaller  $\mu$  value is more conservative.

As still mentioned the usual tests are run along the tensile meridian and the compressive meridian. This means, that the fracture angle  $\Theta_{fp}$  is meridian-dependent or dependent on the Lode angle  $\vartheta$ , respectively. This situation causes to apply the realistic  $120^\circ$ -rotationally-symmetric model.

The tests are performed by adding an axial load generating  $\sigma_{ax}$  upon a hydrostatic loading  $p_{hyd}$ . In *Fig.8.1-5* the meridian failure curves are depicted and some test points are inserted indicating where the determination of the Mohr quantities  $\tau_{nt}$ ,  $\sigma_n$ ,  $\Theta_{fp}$  has been performed. As coordinates, the Lode-Haigh-Westergaard coordinates are used which equally count in all directions of the 3D stress space.

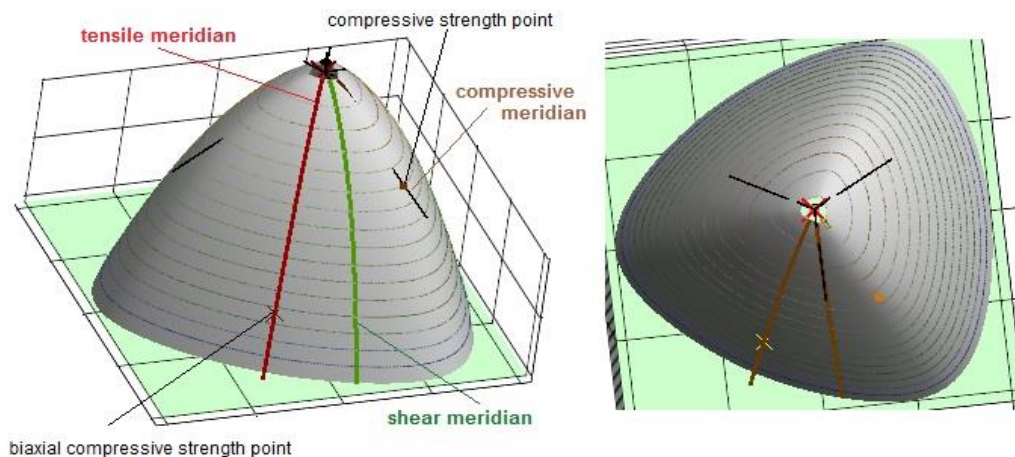


*Fig.8.1-5: Display of all basic meridians of Normal Concrete. The + are the points where the evaluation of  $\tau_{nt}$ ,  $\sigma_n$ ,  $\Theta_{fp}$  was performed.  $p = p_{hyd}$ .  
(Mathcad unfortunately did not draw below -15 !?. An often faced problem)*

The basic three meridians are depicted in *Fig.8.1-5*: Tensile Meridian TM ( $\vartheta = +30^\circ$ ) inside, Neutral Meridian NM ( $0^\circ$ ) and Compressive Meridian CM ( $\vartheta = -30^\circ$ ), outside. Test points lie on the respective meridian, determined by  $\vartheta$ , which means on different distances from the axis for a specific  $I_1 / \sqrt{3} \cdot \bar{R}^t$ . The tensile strength is used for normalization in the case of brittle materials

### 8.1.5 Fracture Failure Body and principal stress plane Cross-section

*Fig.8.1-6* shows the fracture body of the Normal Concrete, see [Cun15].



*Fig.8.1-6: Two views of the 120°-rotationally-symmetric fracture body (hoop cross-section) of the Normal Concrete with the basic three meridians and the two strength points [Cun17]*

The three basic meridians and the two strength points, compressive strength (dot) and bi-axial compressive strength (cross), are indicated.

Table 8.1-5: Input formulas for main task. TM tensile meridian, CM compressive meridian

\* Transformation of Efforts in Mohr stresses-based ones

$$Eff^{NF} = c^{NF} \cdot \frac{\sqrt{4J_2 \cdot \Theta^{NF} - I_1^2 / 3 + I_1}}{2 \cdot \bar{R}^t}, \quad \Theta^{NF} \rightarrow \Theta^{TM} = \sqrt[3]{1 + d^{NF} \cdot (+1)},$$

in this application can be set:  $c^{NF} = \Theta^{NF} = 1$ ,

$$Eff^{NF} = 1 \cdot \frac{\sqrt{4 \cdot [(\sigma_n - \sigma_t)^2 + \sigma_t^2 + (-\sigma_n)^2 + 6 \cdot \tau_{nt}^2] \cdot 1 / 6 - (\sigma_n + \sigma_t) / 3 + (\sigma_n + \sigma_t)}}{2 \cdot \bar{R}^t}.$$

$$Eff^{SF} = \frac{c_{2\Theta}^{SF} \cdot I_1 + \sqrt{(c_{2\Theta}^{SF} \cdot I_1)^2 + 12 \cdot c_{1\Theta}^{SF} \cdot J_2 \cdot \Theta^{SF}}}{2 \cdot \bar{R}^c}, \quad \Theta^{SF} \rightarrow \Theta^{CM} = \sqrt[3]{1 + d^{SF} \cdot (-1)},$$

$$Eff^{SF} = \frac{\sqrt{c_{2\Theta}^{SF2} \cdot (\sigma_n + \sigma_t)^2 + c_{1\Theta}^{SF} \cdot \Theta^{SF} \cdot 2 \cdot [(\sigma_n - \sigma_t)^2 + \sigma_t^2 + (-\sigma_n)^2 + 6 \cdot \tau_{nt}^2]}}{2 \bar{R}^c} + c_{2\Theta}^{SF} \cdot \frac{\sigma_n + \sigma_t}{2 \bar{R}^c}.$$

In contrast to the friction quantities, which are determined in the compressive strength point, where  $\Theta^{SF}$  is the constant above,  $\Theta$  now changes with the Lode angle  $\mathcal{J}$ . This requires  $J_3$  in Mohr stresses) which can be performed when employing the basic form  $27 \cdot J_3 = 2 \cdot I_1^3 - 9 \cdot I_1 \cdot I_2 + 27 \cdot I_3 \cdot I_1^2 \cdot 2 / 27 - I_1$  because the  $I_1, I_2, I_3$  can be displayed in Mohr stresses (Table 3-1). For the present 2D case it reads :

$$I_1 = \sigma_n + \sigma_t, \quad 6J_2 = (\sigma_n - \sigma_t)^2 + \sigma_t^2 + (-\sigma_n)^2 + 6 \cdot \tau_{nt}^2, \quad 27J_3 = 2(\sigma_n + \sigma_t)^3 - 9 \cdot (\sigma_n + \sigma_t) \cdot (\sigma_n \cdot \sigma_t - \tau_{nt}^2)$$

\* Addition theorems considering  $\eta = \sigma_{II} - \sigma_{III}, \quad \sigma_\lambda, \quad \tau_{t\lambda}, \quad \tau_{n\lambda} = 0$

$$\sigma_n - \sigma_t = c^2 \cdot \eta - s^2 \cdot \eta = C \cdot \eta, \quad S = \sqrt{1 - C^2}, \quad C = c^2 - s^2 = 2c^2 - 1 = 1 - 2s^2,$$

$$\sigma_n + \sigma_t = \sigma_{II} + \sigma_{III} = I_1, \quad \tau_{nt} = -0.5 \cdot S \cdot \eta = -0.5 \cdot \sqrt{1 - C^2} \cdot \eta, \quad \sigma_t = \sigma_n - C \cdot \eta.$$

\* Fracture interaction equation  $\equiv$  mathematical equation of the fracture body surface

$$Eff = [(Eff^{NF})^m + (Eff^{SF})^m]^{m^{-1}} \Rightarrow \text{numerically simpler } (Eff^{NF})^m + (Eff^{SF})^m = 1 = 100\% .$$

Fig.8.1-7 displays the course of the measured 2D test data of Normal Concrete, provided by Dr. Silke Scheerer at IfM TU-Dresden (Prof. M. Curbach). It depicts the large scatter of the multi-axial compression tests, which influences the statistically reduced design strength  $R$  significantly. Fig 6-2 is a bias cross-section of the Normal Concrete fracture body which is the shape of the principal stress plane. As coordinates the still mentioned Lode-Haigh-Westergaard coordinates are used which equally count in all directions of the 3D stress space.

The measurement of a realistic fracture angle – based on the usually small-scale test level - is practically not possible. The determination of the curve parameters  $c$  by mapping the course of test data points is the better and practical procedure. Then, the relationship of the curve parameter  $c$  to the friction value  $\mu$  and to the fracture angle  $\Theta_{fp}$  can be derived. These relations are obtained in the *touch point*, pointed out in Fig.8.1-1.

The generation of a realistic Mohr-Coulomb curve requires the determination of the slope *along* the full curve, not a single specific value in the touch *point* only. This slope  $d\tau_{nt}/d\sigma_n$  is linked to the unknown *fracture plane measure*  $C(\Theta_{fp})$ . An equation to determine  $C$  comes from the differentiation of the Mohr stress-transformed interaction equation because both the two modes are activated. This means, instead of the single SF-formulation the SF-NF-coupling *Eff*-formulation is to apply when moving from the structural stress formulation to a Mohr stress one. *Table 6-2* will show the full procedure, later.

Reminder:

The basic assumption of O. Mohr was: “*The strength of a material is determined by the (Mohr) stresses on the fracture plane*”. This means for the here applied linear Mohr-Coulomb (M-C) formulation  $\tau_{nt} = \bar{R}^t - \mu \cdot \sigma_n$ . Herein, the value  $\mu$  is an intrinsic friction property of the material and  $\bar{R}^t$  the so-called cohesion strength. The shear stresses  $\tau_{ix}, \tau_{ni}$  are zero together with the normal stress  $\sigma_x$ . The normal stress  $\sigma_t$  must be accounted for in the investigation but will finally have no influence, which has to be proven when following Mohr and this must be shown.

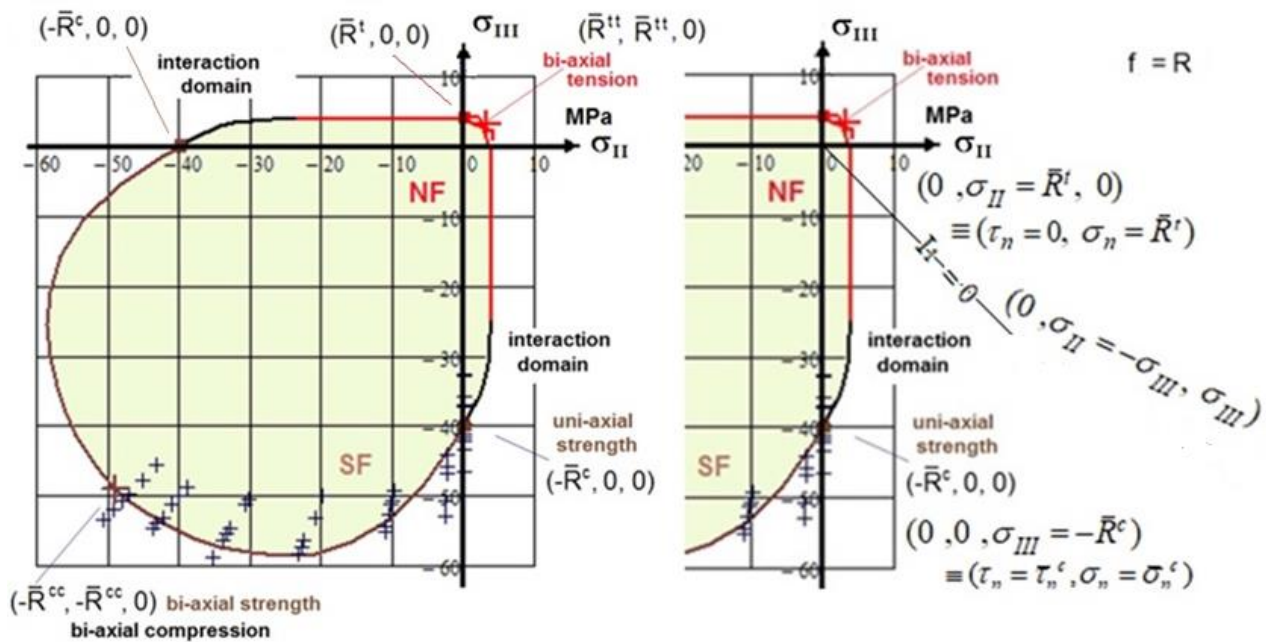


Fig.8.1-7: Bi-axial failure curve of Normal Concrete, 2D-test data set

Fig.8.1-8 displays the 2<sup>nd</sup> quadrant of the bi-axial failure curve formulated in structural stresses and that fully represents the Mohr-Coulomb curve domain. The joint mode situation of the Mohr-Coulomb curve - capturing the transition zone between the pure mode domains NF and SF - requires the application of the interaction equation  $(Eff^{NF})^m + (Eff^{SF})^m = 1$ . It spans over the regime  $0 < \sigma_{III} < \bar{R}^t$  and the Lode angles  $(-30^\circ < \delta < +30^\circ)$ .

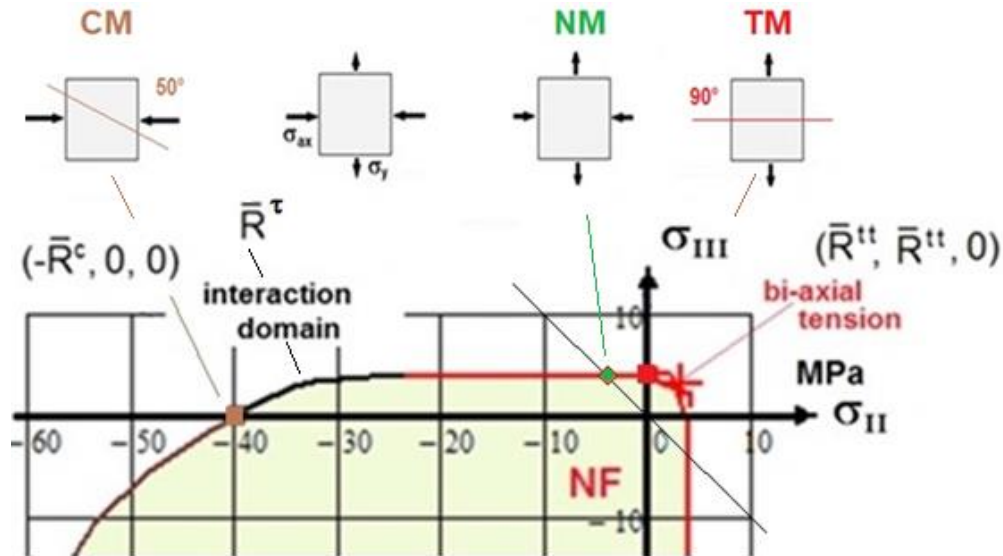


Fig.8.1-8 Second quadrant and associated stress states, transition zone between the 2 mode domains SF, NF

### 8.1.5 Improved Mapping of Failure Stress data with Derivation of a more realistic $\Theta_{fp}^\circ(\vartheta)$

The  $F^{SF}$  curve outlines a local shortcoming of the relatively simple FMC-based SF-formulation. In design-verification the  $Eff^{SF}$  contribution to  $Eff$  is not a problem because the interaction is a conservative procedure. However, when searching a local fracture angle  $\Theta_{fp}^\circ$  a correction should be material-dependently applied to numerically determine a better value for  $\Theta_{fp}^\circ$ .

To sort out a procedure it is helpful to know how the pure mode efforts of the activated modes NF and SF share its influence with  $\sigma_{II}$ . Fig.8.1-9 shows the courses of the efforts  $Eff^{NF}$  ( $= Eff^\circ$ ) and  $Eff^{SF}$  ( $= Eff^\tau$ ) representing the components of the *measured* fracture stress curve.

According to the fact that the compression strength point is located on the compressive meridian and the tensile strength point on the tensile meridian the different Lode angle  $\vartheta$  is to consider in order to achieve an accurate approach when investigating the Mohr-Coulomb curve. This requires to not just consider the rotationally-symmetric  $Eff^{SF}$  but  $Eff^{SF\vartheta}$ , too.

Mathematically-caused,  $Eff^{SF}$ -curve and  $Eff^{SF\vartheta}$ -curve become positive in the pale colored curve part and numerically contribute its effort portion to the total effort (again, no problem for designing). This is physically not accurate and could be by-passed by a query in the numerical process not permitting - after a previous decay - the newly increase. Also one could apply a decay function that - physically logically - keeps  $Eff^{SF}$  zero, like for the UD material in chapter 7.

The shear material stressing effort  $Eff^\tau = Eff^{SF}$  must physically become zero at the tensile strength point  $(0, R^t)$ . This specific shortcoming cannot be by-passed by an increased interaction exponent  $m$ . This is brought about by a correction function that defines the decay of  $Eff^\tau$  and is practically performed by setting  $Eff^\tau = 0$  at  $\sigma_{II} = 0$ . As function was taken an exponential one, namely

$$f_d = 1 / (1 + \exp(\frac{c_{1d} + \sigma_{II}}{c_{2d}})), \text{ with } c_{1d}, c_{2d} \text{ fixed at } (-\bar{R}^c, 0.995), (-0.01, +0.01).$$

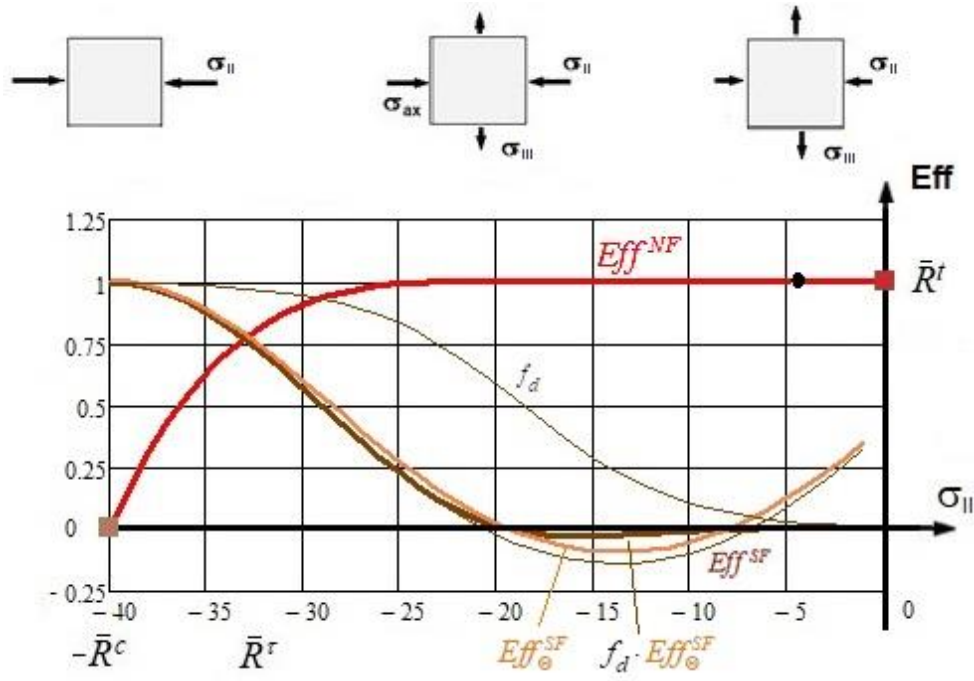


Fig.8.1-9: Visualisation of the course of the pure mode efforts  $Eff^{mode}$  supporting the need to interact them in the case of bi-axial stress states to not exceed  $Eff = 100\%$ .  $c_{1d} = 18.6$ ,  $c_{2d} = 4.04$ .

$$Eff^{NF}, Eff^{SF}, Eff^{SF\Theta}, f_d \cdot Eff^{SF\Theta}$$

The corrected  $Eff^{SF}$ -curve brings the desired improvement and lowers  $\bar{R}^t$  from  $12.5 \rightarrow 11$ .

With the correction above the mandatory locally better  $\Theta_{fp}^\circ$  can be computed and then the envisaged transformation performed.

Note, please: Applying - instead of the present Modal SFC - a so-called Global SFC, which globally maps in a single mathematical equation all test data and modes, a similar difficulty would be found too.

### 8.1.6 Derivation of a realistic Modes-Interaction Considering Mohr-Coulomb Curve $\tau_n(\sigma_n)$

Table 8.1-6 summarizes the relations for the derivation of  $\tau_{nt}(\sigma_n)$  and  $\Theta_{fp}^\circ$  from a given fracture curve  $\sigma_{II}(\sigma_{III})$ . It is to consider the change of the fracture plane angle  $\Theta_{fp}^\circ$  with the Lode angle  $\mathcal{G}$  from  $\Theta_{fp}^\circ$  at  $\mathcal{G} = -30^\circ$  on. The biggest challenge is the necessary differentiation of the interaction equation  $Eff = 1$  within Mathcad. This further produces a giant formula output, that 'generously' can be cut down by using addition theorems and by inserting the given structural stresses input via its invariants  $I_1, J_2, J_3$ .

That is the advantage of invariants:

*They do not depend on the coordinate system. Hence one can switch within one system being here the Mohr-stresses one!*

Fig.8.1-10 displays several failure curves and the course of the altering fracture plane angle  $\Theta_{fp}^\circ$ . Its left part presents the entities in a structural stresses diagram and the right part in a Mohr stresses diagram. This involves the Linear Mohr-Coulomb fracture curve and the real SF-NF interaction curve  $\tau_{nt}(\sigma_n)$ . The 3 Mohr circles are incorporated.

Table 8.1-6: Transformation of a 2D structural stresses-based failure curve into Mohr-Coulomb one

\* **Task:** Known  $\sigma_{II}, \sigma_{III}; \bar{R}^t, \bar{R}^c$ . To determine:  $\sigma_n, \tau_{nt}, \Theta_{fp}^\circ(C)$ ,  $C = \cos(2 \cdot \Theta_{fp}^\circ \cdot \pi / 180^\circ)$

$$\sigma_\lambda, \tau_{t\lambda}, \tau_{n\lambda} = 0. \quad \eta = \sigma_{II} - \sigma_{III}, \quad \sigma_{II} + \sigma_{III} = \sigma_n + \sigma_t = I_1, \quad \sigma_n - \sigma_t = C \cdot \eta,$$

$$\sigma_t = \sigma_n - C \cdot \eta, \quad \sigma_n = 0.5 \cdot [(C+1) \cdot \sigma_{II} + (-C+1) \cdot \sigma_{III}], \quad \tau_{nt} = -0.5 \cdot \sqrt{1-C^2} \cdot \eta.$$

\* **Interaction equation** because 2 modes are activated:  $(Eff^{NF})^m + (Eff^{SF})^m = 100\%$

$$Eff^{NF} = \frac{\sqrt{4 \cdot [(\sigma_n - \sigma_t)^2 + \sigma_t^2 + \sigma_n^2 + 6 \cdot \tau_{nt}^2] / 6 - (\sigma_n + \sigma_t)^2 / 3 + (\sigma_n + \sigma_t)}}{2 \cdot \bar{R}^t},$$

$$\frac{Eff^{SF}}{f_d} = \frac{c_{2\Theta}^{SF} \cdot (\sigma_n + \sigma_t)}{2 \cdot \bar{R}^c} + \frac{\sqrt{(c_{2\Theta}^{SF} \cdot (\sigma_n + \sigma_t))^2 + 2 \cdot c_{1\Theta}^{SF} \cdot \Theta^{SF} [(\sigma_n - \sigma_t)^2 + \sigma_t^2 + \sigma_n^2 + 6 \cdot \tau_{nt}^2]}}{2 \cdot \bar{R}^c}$$

\* **Solution of the task:** equalizing the slopes at each stress state  $\sigma_{II} (\sigma_{III})$

Slope 1: from differentiation of structural stresses-linked Mohr stresses delivers

$$\frac{d\tau_{nt}}{d\sigma_n} = \frac{(s^2 - c^2) \cdot \eta}{-2 \cdot s \cdot c \cdot \eta} = \frac{C}{S} = \frac{C}{\sqrt{1-C^2}}, \quad \text{valid uni-axially and bi-axially}$$

Slope 2: from differentiation of the interaction equation, abbreviation  $\eta_m = 2\sigma_n - C \cdot \eta$

$$Eff^{NF} = \left\{ \sqrt{4 \cdot [(C \cdot \eta)^2 + (\sigma_n - C \cdot \eta)^2 + \sigma_n^2 + 6 \cdot \tau_{nt}^2] / 6 - \eta_m^2 / 3 + \eta_m} \right\} / 2 \cdot \bar{R}^t, \quad \Theta^{NF} = 1$$

$$Eff^{SF} = \left\{ c_{1\Theta}^{SF} \cdot \eta_m + \sqrt{(c_{2\Theta}^{SF2} \cdot \eta_m^2 + 2 \cdot c_{1\Theta}^{SF} \cdot \Theta^{SF} \cdot [(C \cdot \eta)^2 + (\sigma_n - C \cdot \eta)^2 + \sigma_n^2 + 6 \cdot \tau_{nt}^2])} \right\} / 2 \cdot \bar{R}^c$$

$$F = (Eff^{NF})^m + (Eff^{SF})^m \quad \text{with} \quad dF / d\sigma_n \quad \text{and} \quad dF / d\tau_{nt}$$

Equating the 2 equations and replacing Mohr stresses by structural stresses

$$\frac{C}{\sqrt{1-C^2}} = - \frac{dF / d\sigma_n}{dF / d\tau_{nt}} \quad \text{a huge formula for the determination of the fracture angle measure C}$$

$$\Theta^{SF}(\vartheta) = \sqrt[3]{1 + d^{SF} \cdot \sin(3\vartheta)} = \sqrt[3]{1 + d^{SF} \cdot 1.5 \cdot \sqrt{3} \cdot J_3 \cdot J_2^{-1.5}} \quad \text{inserting}$$

$$6J_2 = 2 \cdot (\sigma_{II}^2 - \sigma_{II} \cdot \sigma_{III} + \sigma_{III}^2), \quad 27J_3 = (-\sigma_{II} - \sigma_{III}) \cdot (2\sigma_{II} - \sigma_{III}) \cdot (2\sigma_{III} - \sigma_{II})$$

Implicite solution when determining  $C$  for the bi-axial stress states  $(\sigma_{II}, \sigma_{III})$

$$\sigma_n = (C+1) \cdot 0.5 \cdot \sigma_{II} + (1-C) \cdot 0.5 \cdot \sigma_{III}, \quad \tau_{nt} = -0.5 \cdot \sqrt{1-C^2} \cdot (\sigma_{II} - \sigma_{III})$$

$$a = (12J_2 - I_1^2) / 3, \quad b = \left( (c_{2\Theta}^{SF} \cdot I_1 + \sqrt{d}) / 2\bar{R}^c \right)^{m-1},$$

$$c = 4I_1 \cdot (c_{2\Theta}^{SF2} + c_{1\Theta}^{SF} \cdot \Theta^{SF}), \quad d = c_{2\Theta}^{SF2} \cdot I_1^2 + 2c_{1\Theta}^{SF} \cdot \Theta^{SF} \cdot 6J_2.$$

Vorgabe  $C := -0.1$  and inserting points  $(\sigma_{II}, \sigma_{III})$

$$\frac{C}{\sqrt{1-C^2}} = - \frac{0.5 \cdot \sqrt{a} \cdot [(\bar{R}^t \cdot b \cdot c) / 4] + \bar{R}^c \cdot \sqrt{d} \cdot \left( \frac{2\sigma_n + \sqrt{a} - C \cdot \eta}{2\bar{R}^t} \right)^{m-1} + \bar{R}^t \cdot c_{2\Theta}^{SF} \cdot b \cdot \sqrt{d}}{\tau_{nt} \cdot [\bar{R}^c \cdot \sqrt{d} \cdot \left( \frac{2\sigma_n + \sqrt{a} - C \cdot \eta}{2\bar{R}^t} \right)^{m-1} + 3\sqrt{a} \cdot \bar{R}^t \cdot c_{1\Theta}^{SF} \cdot \Theta^{SF} \cdot b]}$$

Search(C)  $\rightarrow$  equation for the fracture angle measure  $C(\Theta_{fp}^\circ)$  and for  $\sigma_n, \tau_{nt}$

$$C = C(\sigma_{II}, \sigma_{III}) = \cos(2 \cdot \Theta_{fp}), \quad \Theta_{fp} = 0.5 \cdot \arccos C, \quad \Theta_{fp}^\circ = \Theta_{fp} \cdot 180^\circ / \pi,$$

$$\sigma_n = (C+1) \cdot 0.5 \cdot \sigma_{II} + (1-C) \cdot 0.5 \cdot \sigma_{III}, \quad \tau_{nt} = -0.5 \cdot \sqrt{1-C^2} \cdot (\sigma_{II} - \sigma_{III}).$$



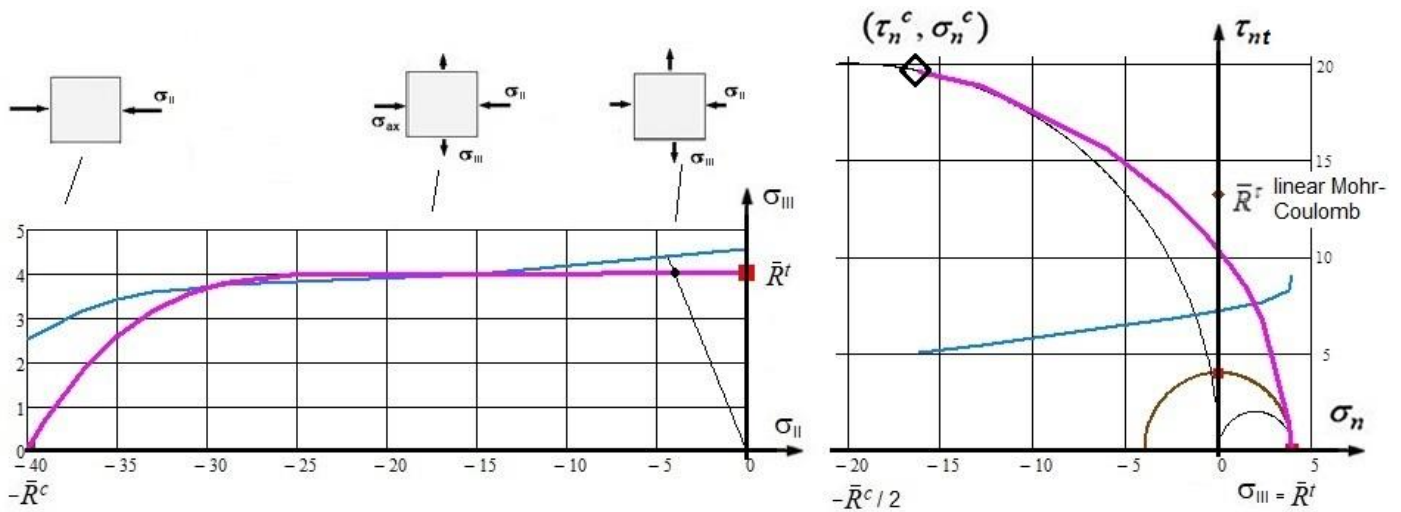


Fig.8.1-10: Joint display of the magenta failure curve in structural stresses (left) and in Mohr stresses (right) with fracture angle increase  $\Theta_{fp}^\circ$ , scaled by twenty (left) and ten (right).

Model: 120°-rotational-symmetric parameters and improved mapping of the measured failure curve by  $f_d$

$$c_{1\Theta}^{SF} \cdot \Theta^{SF} = 1 + c_{2\Theta}^{SF} \text{ with } c_{2\Theta}^{SF} \text{ the friction parameter, } c_{2\Theta}^{SF} = 3.70, c_{1\Theta}^{SF} = 5.88, d^{SF} = 0.49,$$

$$\bar{R}^t = 4 \text{ MPa, } \bar{R}^c = 40 \text{ MPa, } \Theta_{fp}^c = 50.5^\circ, C^c = -0.192, \text{ friction value } \mu = 0.195,$$

$$\bar{R}^\tau = 11 \text{ MPa, } \Theta_{fp}^\circ = 72^\circ, \sigma_{II} = -32 \text{ MPa, } \sigma_{III} = 3.3 \text{ MPa, } \delta = -25^\circ.$$

$$\tau_{nt}^c = 19.6 \text{ MPa, } \sigma_n^c = -16.2 \text{ MPa, } c_{1d} = 18.6, c_{2d} = 4.04, \Theta^{SF} = \Theta^c = \Theta^{CM} = 0.51.$$

The interpretation of the two diagrams in Fig. 8.1-10 leads to the following results:

- ✓ The interaction equation  $Eff$  - representing the surface of the fracture body - in structural stresses can be transferred into Mohr stresses
- ✓ The alteration of the fracture plane angle  $\Theta_{fp}^\circ$  can be computed
- ✓ Complete failure danger is composed of portions  $Eff^{NF}$  and  $Eff^{SF}$ , following the idea of the FMC that NF and SF commonly add its  $Eff$  portions. This leads to the conclusion that the  $\Theta_{fp}^\circ$  is approximately 70° at the cohesive strength point
- ✓ The SF approach could not offer a full accuracy of the fracture plane angle  $\Theta_{fp}^\circ$  and the Mohr-Coulomb curve to be predicted.  $Eff^{SF}$  had to be physically adjusted by a decay function  $f_d$ .
- ✓



Experience  
after solving the very  
challenging task  
of this chapter:

**Challenging  
tasks  
strengthen!**

## 8.2 Dependence of transversely-isotr. friction model parameters on friction values $\mu_{\perp\perp}, \mu_{\parallel\parallel}$

### 8.2.1 Invariants, strength fracture conditions SFCs and fracture body

As with the isotropic materials at first the derivation of the UD-SFCs shall be shortly presented. Therefore invariants and associated stresses used for the transversely-isotropic UD material are collected in *Fig.8.2-1*.

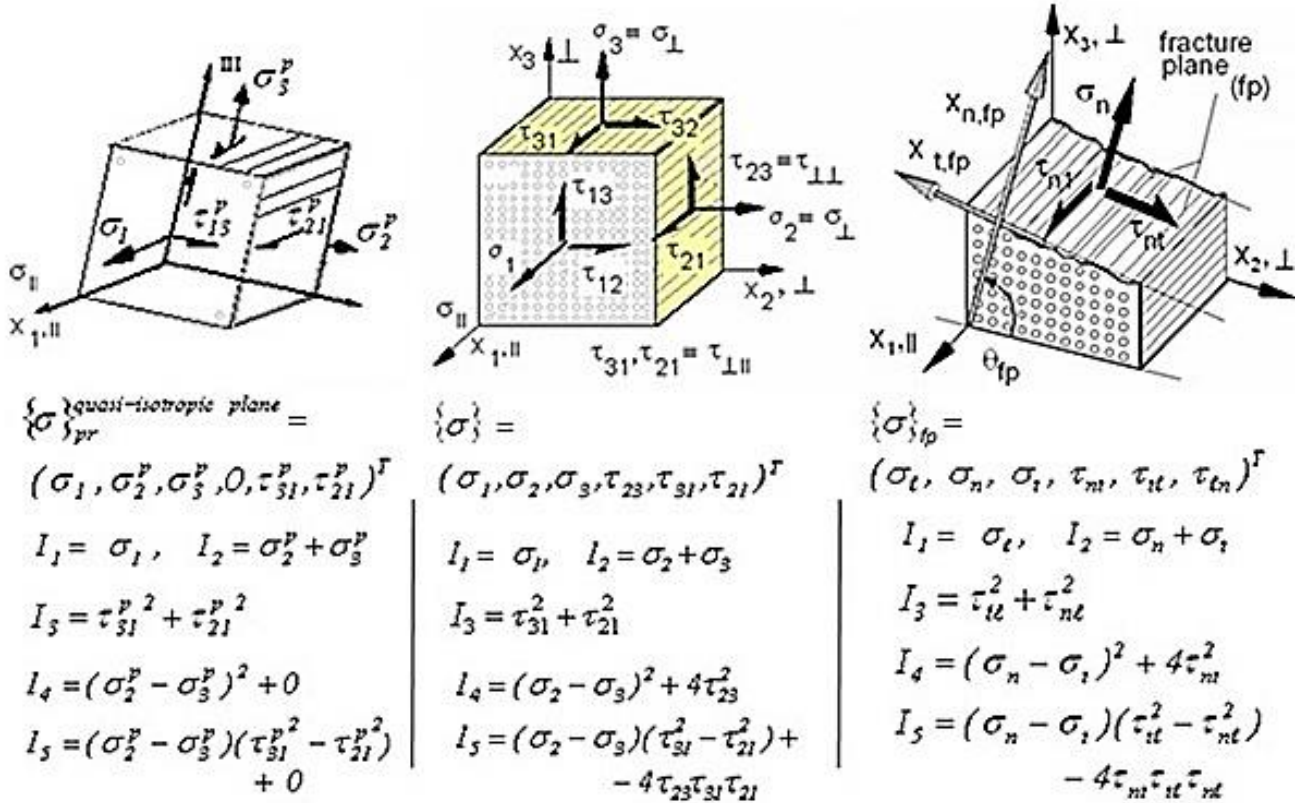


Fig.8.2-1: UD-Invariants and associated stresses (indices  $\ell = 1, p \equiv pr$ )

Repeating the author's invariant-based Failure Mode Concept (FMC) 5 SFCs are to be derived in total. Replacing the UD-invariants by the stresses they are composed of and after simplifications with practical numerical modifications to by-pass probable 3D-solution problems the set of UD-SFCs for fiber-reinforced material, embedded in a matrix (plastic or mortar), is given in *Fig.8.2-2*.

The interaction of the separate five modes, 2 FFs (*Fiber-Failure*) + 3 IFFs (*Inter-Fiber-Failure*), is performed as with the isotropic material, by applying the interaction equation

$$Eff^m = (Eff^{\parallel r})^m + (Eff^{\parallel \sigma})^m + (Eff^{\perp \sigma})^m + (Eff^{\perp r})^m + (Eff^{\perp \parallel})^m = 1.$$

LL:

- (1) Due to mapping experience in the transition zones the interaction exponent is  $2.5 < m < 3$ . This is as for isotropic materials. For reasons of simplicity the same value is applied for all transition zones. The smaller the value is the more the design verification is conservative!
- (2) The Poisson effect is to consider in the macro-mechanical SFCs because bi-axial compression strains the filament without any external  $\sigma_1$ . In *Fig.8.2-2* this fiber constituent failure is considered in FF1.

|      |   |   |
|------|---|---|
| FF1  | $Eff^{\sigma} = \bar{\sigma}_1 / \bar{R}_1^t = \sigma_{eq}^{\sigma} / \bar{R}_1^t,$   | $\bar{\sigma}_1^* \cong \varepsilon_1^t \cdot E_{  }$ filament strains from FEA |
| FF2  | $Eff^{\tau} = -\bar{\sigma}_1 / \bar{R}_1^c = +\sigma_{eq}^{\tau} / \bar{R}_1^c,$   | $\bar{\sigma}_1 \cong \varepsilon_1^c \cdot E_{  }$ <b>2 filament modes</b>     |
| IFF1 | $Eff^{\perp\sigma} = [(\sigma_2 + \sigma_3) + \sqrt{(\sigma_2 - \sigma_3)^2 + 4\tau_{23}^2}] / 2\bar{R}_1^t = \sigma_{eq}^{\perp\sigma} / \bar{R}_1^t$  | Puck's mode A   |
| IFF2 | $Eff^{\perp\tau} = [(\frac{\mu_{\perp\parallel}}{1-\mu_{\perp\parallel}}) \cdot (\sigma_2 + \sigma_3) + \frac{1}{1-\mu_{\perp\parallel}} \sqrt{(\sigma_2 - \sigma_3)^2 + 4\tau_{23}^2}] / \bar{R}_1^c = +\sigma_{eq}^{\perp\tau} / \bar{R}_1^c$   | <b>3 'matrix' modes</b>   |
| IFF3 | $Eff^{\parallel\parallel} = \{[2\mu_{\perp\parallel} \cdot I_{23-5} + (\sqrt{(2\mu_{\perp\parallel})^2 \cdot I_{23-5}^2 + 4 \cdot \bar{R}_{\perp\parallel}^2 \cdot (\tau_{31}^2 + \tau_{21}^2)})] / (2 \cdot \bar{R}_{\perp\parallel}^3)\}^{0.5} = \sigma_{eq}^{\parallel\parallel} / \bar{R}_{\perp\parallel}$ |   |
|      | with $I_{23-5} = 2\sigma_2 \cdot \tau_{21}^2 + 2\sigma_3 \cdot \tau_{31}^2 + 4\tau_{23}\tau_{31}\tau_{21}$ [Cun04, Cun11]   |   |

Modes-Interaction  $Eff^m = (Eff^{\tau})^m + (Eff^{\parallel\sigma})^m + (Eff^{\perp\sigma})^m + (Eff^{\perp\tau})^m + (Eff^{\parallel\parallel})^m$

with influence IFF on FF: = 1 = 100% is 'onset of failure'

with mode-interaction exponent  $2.5 < m < 3$  from mapping test data

Typical friction value data range:  $0.05 < \mu_{\perp\parallel} < 0.3, 0.05 < \mu_{\parallel\perp} < 0.2$

Eff:= material stressing effort (Werkstoffanstrengung), R:= UD strength,  $\sigma_{eq}$ := equivalent stress.  
 Eff:= artificial word, fixed with QinetiQ in 2011, to have an equivalent English term.  
 Poisson effect considered\*: bi-axial compression strains a filament without any  $\sigma_1$   
 t:= tensile, c:= compression, || := parallel to fibre,  $\perp$  := transversal to fibre

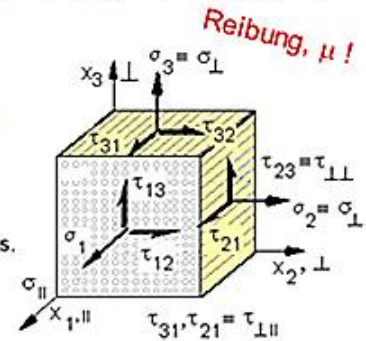


Fig.8.2-2: UD-SFCs for 'Onset of fracture failure', mode interaction, and value ranges [Cun04,12]

Fig.8-3 presents a visualization of the associated fracture body surface. The composite designations follow the guideline VDI 2014, sheet 3 [VDI 06].

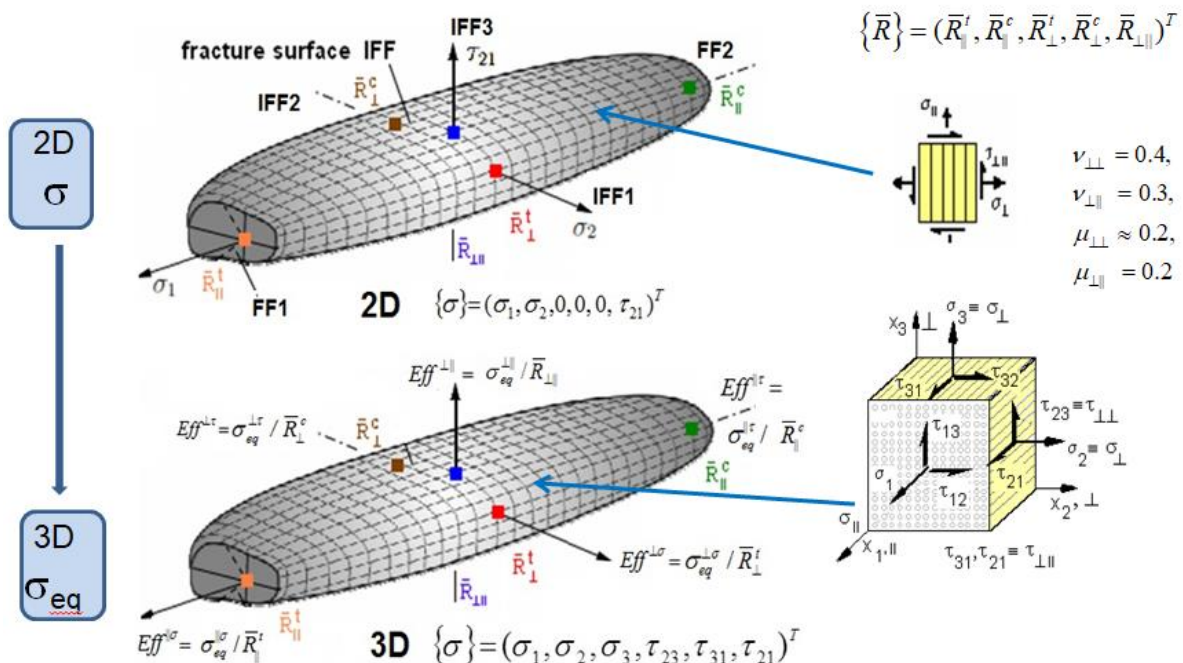


Fig.8.2-3: Fracture body of UD material (lamina, lamella, sheet, tape) for 2D and 3D stress states

The figure above depicts an essential outcome, found by the author after many years:

Taking equivalent stresses instead of lamina stresses  
one can apply the 2D fracture failure body in the 3D case, too!

**NOTES:**

- (1) There are numerous SFCs describing fracture failure of the uni-directionally fiber-reinforced material family. In the World-Wide-Failure-Exercises-I and –II, practically running from 1992 to 2012. R. Cuntze and A. Puck could place their theories at the top. Cuntze participated successfully with his ‘Invariant-based, mode-distinguishing FMC theory’ and Puck with his ‘Mohr-Coulomb-based Action Plane Theory’
- (2) The invariant-based formulation for IFF2 is a pretty simple approach. It is mathematically homogeneous which means that  $F = Eff$ . An approach is always a compromise
- (3) Here, it is - like for the isotropic concrete material- a compromise ‘on the safe reserve factor side’, however, the approach is not accurate enough, if a fracture angle is to determine in cases of not highly brittle materials such as with values below  $R_L^c / R_L^t < 5$ . This is valid for the present UD material.

**8.2.2 Main fracture curves or cross-sections of the fracture body in structural stresses**

The main cross-section of the fracture body is depicted in Fig.8.2-4 with the bare mode mappings (left) together with a demonstration of the goodness of the interaction equation in the transition zone (right).

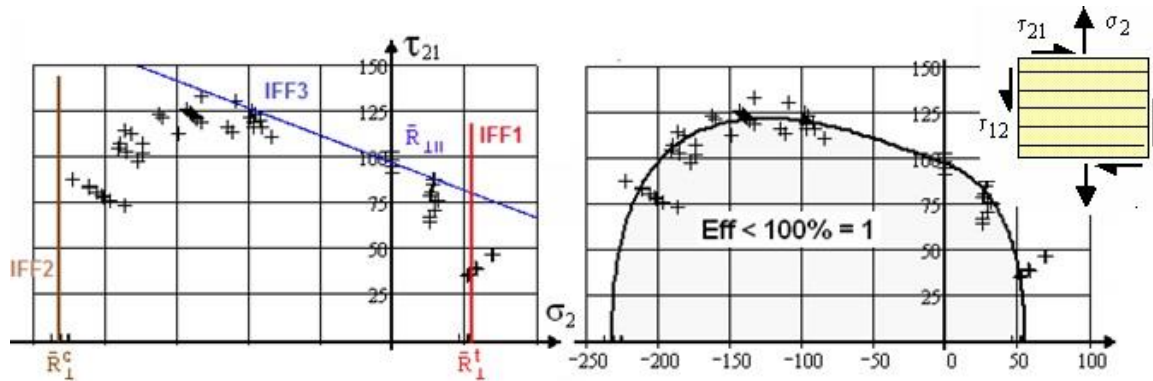


Fig.8.2-4: Interaction, demonstrated in the IFF cross section, CFRP failure curve.

2D stress state within the lamina,  $m=2.7$

In this paper, the first (positive) quadrant is not of interest. Focus here is the Mohr-Coulomb-associated quasi-isotropic plane  $\sigma_2(\sigma_3)$ , displayed in Fig.8.2-5. Applying the shear fracture SFC IFF2 (brown) and computing the interaction curve (magenta) IFF1-IFF2 the failure curves in three quadrants are obtained. The curves are symmetric to the diagonal. For further information in Fig.7.5 a sketch of the classical tension/compression-torsion UD test specimen is included. Also a 3D fracture failure body  $\tau_{21}(\sigma_2, \sigma_3)$  is shown below. One can assume that the interaction curve does not optimally map the usual course of test data (like for isotropic mapping) or – respectively - the mapping quality of IFF2 is not fully sufficient if the alteration of the fracture angle  $\theta_{fp}$  in the transition zone is to determine. This transition zone between a normal fracture mode domain NF and a shear fracture mode domain SF is ruled by interaction and corresponds to the bi-axially stressed Mohr-coulomb curve. This requires both the Eff-modes for the insertion into the interaction

stressed Mohr-coulomb curve. This requires both the Eff-modes for the insertion into the interaction equation.

As before with isotropic materials: The Mohr Envelope is a bi-axial fracture stress curve and the 2<sup>nd</sup> quadrant of  $\sigma_3(\sigma_2)$  is identical to the so-called Mohr envelope or Mohr-Coulomb curve  $\tau_{nt}(\sigma_n)$ , respectively. The interaction curve (magenta) can be dedicated to the basic Mohr-Coulomb curve namely from the compression strength point till the tensile strength point, see Fig.8.2-5.

Like in the isotropic case the bi-axial stress ruled Mohr-Coulomb curve is dominated by two modes, IFF2 (SF) and IFF1 (NF). Therefore, attention must be paid again to the interaction of both these modes in the transition zone in order to finally obtain an ‘accurate’ fracture angle  $\theta_{fp}$ , being the precondition to determine the two Mohr stresses  $\tau_{nt}$ ,  $\sigma_n$  with high fidelity.

Span:  $(\tau_{nt}^c, \sigma_n^c) \rightarrow (\bar{R}_{\perp}^{\tau}, 0) \rightarrow (0, \sigma_n = \bar{R}_{\perp}^t)$  or  $(\sigma_2 = -\bar{R}_{\perp}^c, 0) \rightarrow (\sigma_2, \sigma_3 = -\sigma_2) \rightarrow (0, \sigma_3 = \bar{R}_{\perp}^t)$ .

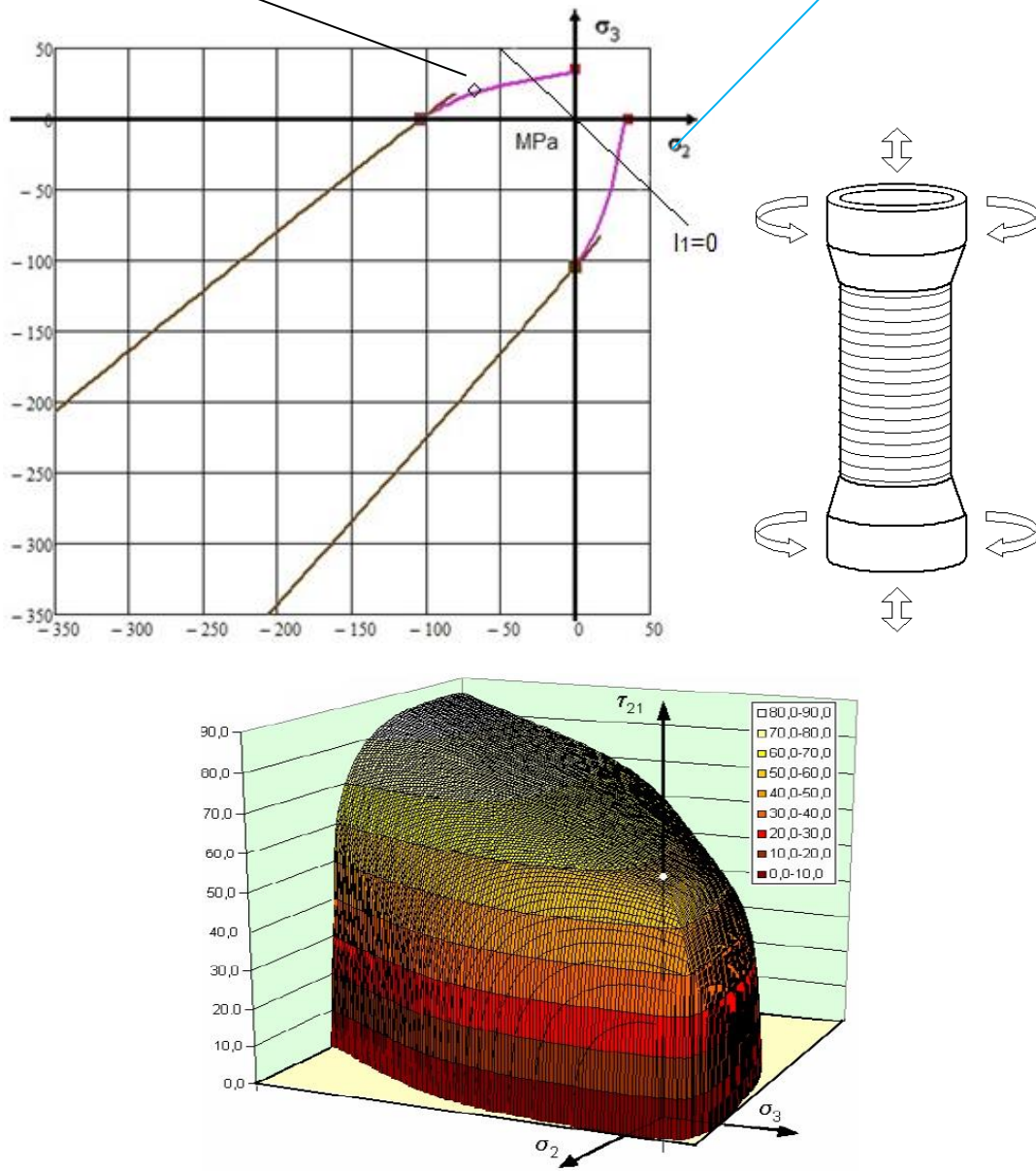
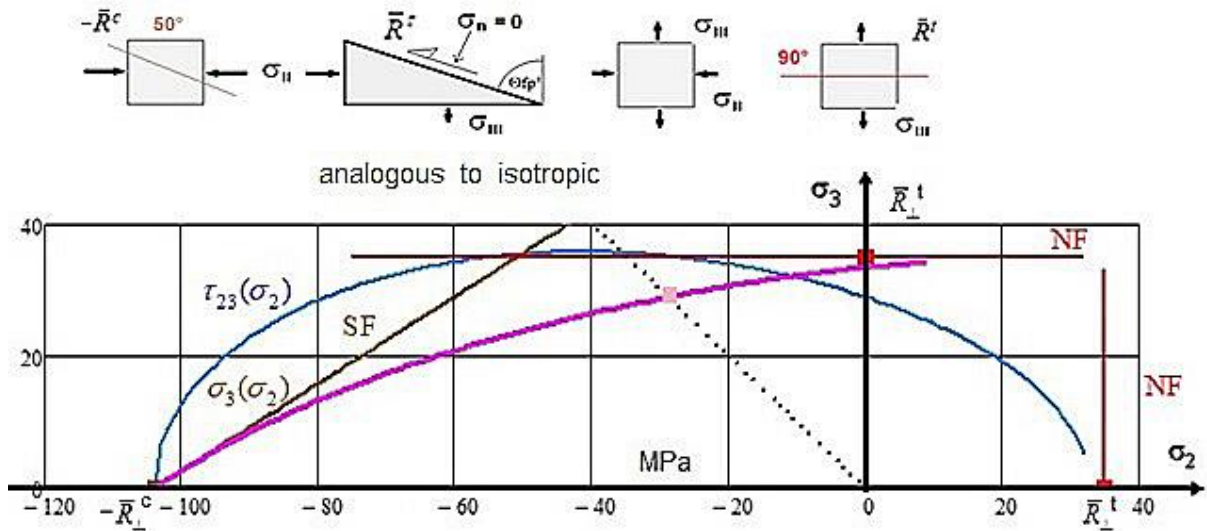


Fig. 8.2-5: The UD fracture stress curves in the quasi-isotropic plane.(right) Scheme of the 90°-wound tension/compression-torsion test specimen, (down) 3D fracture body [figure Cuntze-Sukarie 1997]

In *Fig.8.2-6* the **failure curve** in the second quadrant of *Fig.7-5* is enlarged. For additional information  $\tau_{23}(\sigma_2)$  is included.

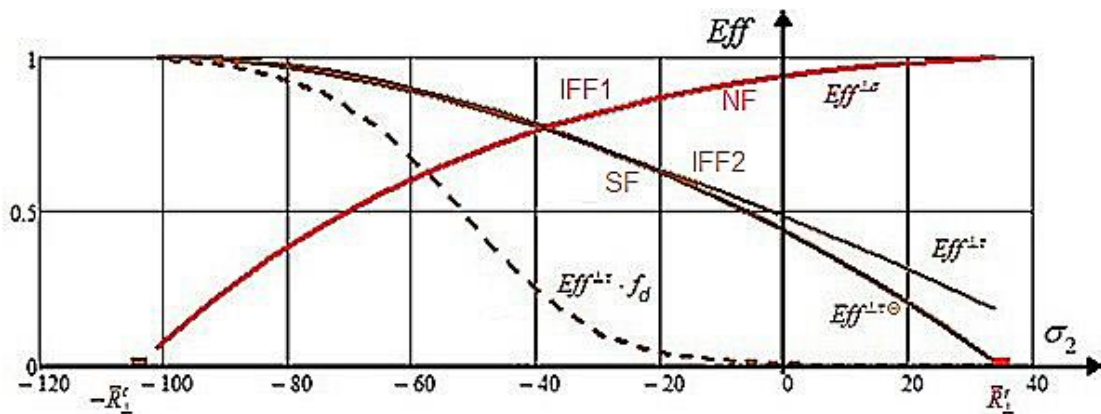


*Fig. 8.2-6, zoom of Fig.7-5 upper, 2<sup>nd</sup> quadrant: (above) Alteration of fracture angles  $\Theta_{fp}^\circ$  allocated to the associated failure stress state  $\sigma_2(\sigma_3)$ , faced in the transition zone.*

*Cohesive point is at the crossing  $\sigma_2 = -\sigma_3$ .*

$$\bar{R}_1^c = 104 \text{ MPa}, \bar{R}_1^t = 35 \text{ MPa}, C_{fp}^c = -0.174, \Theta_{fp}^\circ = 51^\circ, a_{\perp} = 0.26, \mu_{\perp} = 0.18 \cong -C_{fp}^c$$

As with the isotropic material the magenta curve cannot accurately map the course of test data. It shows that with the relatively simple IFF2-FMC approach the shear effort  $Eff^{\perp\tau}$  cannot become zero. This numerical behavior is a shortcoming of the IFF2 approach in the transition zone between the two modes SF and NF. An accurate alteration of the fracture angle  $\Theta_{fp}^\circ$  and of the associated Mohr stresses  $\tau_{nt}, \sigma_n$  is not to achieve with the mathematical course of IFF2 or  $Eff^{\perp\tau}$ , respectively. In this context it is essential how the pure mode efforts of the activated modes IFF1 and IFF2 ( $Eff^{\perp\tau}$ ) share its influence along the  $\sigma_2$ -axis, *Fig.8.2-7*.



*Fig.8.2-7: Course of the two efforts  $Eff^{NF}, Eff^{SF}$  composing the fracture stress curve  $Eff = 1$ .*

$$c_1 = 48.3, c_2 = 10.5$$

$Eff^{d\tau}$  firstly become zero at  $\sigma_2 = \sigma_3 = R^t$ , most often termed bi-axial tensile ‘strength’. This zero point is physically too ‘late’. Again, this is not problematic for design verification but for an accurate transformation of the test curve formulated in structural stresses into a Mohr stress formulation. SF must become physically zero when reaching the pure NF domain. This is brought about by a correction function  $f_d$ , that defines the decay of  $Eff^{d\tau}$  and is practically performed by setting  $Eff^{d\tau} = 0$  at  $\sigma_2 = 0$ . As function for the decay the previously applied exponential one is taken again

$$f_d = 1 / (1 + \exp(\frac{c_{1d} + \sigma_2}{c_{2d}})), \text{ with } c_{1d}, c_{2d} \text{ fixed at } (-\bar{R}_{\perp}^c, 0.995), (-0.01, +0.01).$$

### 8.2.3 Relation of friction parameter $a_{\perp}$ to fracture angle $\Theta_{fp}^c$ and to friction value $\mu_{\perp}$

Again, the measurement of a realistic fracture angle – based on the usually small-scale test level - is practically not possible. The determination of the curve parameters  $a_{\perp}$  and  $b_{\perp}$  by mapping the course of test data points is the practical procedure. Then, the relationship of the curve parameter to the friction value and to the fracture angle can be derived according to [Table 8.2-2](#).

Analogous to the isotropic case the required IFF2-relationships are to derive:

The basic assumption, lying behind all action-plane SFCs (e.g. UD Puck/Hashin) is the *brittle-fracture hypothesis* which goes back to O. Mohr’s “*The strength of a material is determined by the Mohr stresses on the fracture plane*”. This means for the here again applied Linear Mohr-Coulomb (M-C) formulation  $\tau_{nt} = \bar{R}_{\perp}^t - \mu_{\perp} \cdot \sigma_n$ . The friction value  $\mu$  is an intrinsic property of the UD material and  $\bar{R}_{\perp}^t$  the so-called cohesion strength which corresponds to Puck’s fracture plane resistance  $\bar{R}_{\perp}^A$ . In [Puc96]  $\bar{R}_{\perp}^A$  is used as a sixth, model-required ‘strength’ entity.

If IFF occurs in a parallel-to-fibre plane of the UD lamina, the components of the failure stress vector are the normal Mohr stress  $\sigma_n$  and the two Mohr shear stresses  $\tau_{nt}$  and  $\tau_{nl}$ . The shear stress  $\tau_{tl}$  and the normal stress  $\sigma_t$  will have no influence and is to be proven.  $\tau_{nl}$  belongs to IFF 3 and therefore is not of interest in the following investigations.

The transformation of the SFC IFF2 in lamina stresses into a Mohr stresses one works via the addition theorems in [Table 7-1](#). In the equations the bar over is dropped.

LL:

- *The Linear Mohr-Coulomb model can be employed to obtain a sufficiently good relationship for the determination of the friction value  $\mu$  in the compressive stress point  $\sigma_2 = -\bar{R}_{\perp}^c$ .*
- *Establishing the relationship it is assumed that the tangent of the FMC-curve has the same value as that of the straight Linear Mohr envelope curve  $\tau_{nt}(\sigma_n)$  in the touch point with Mohr’s circle, see respective figure*
- *$\sigma_1$  is not relevant. The shear stress  $\tau_{23}$  can be assumed zero because it would anyway vanish after a principal stress transformation. No reduction of generality is caused*
- *The stress  $\sigma_t$  has no influence! It is not representative such as Mohr supposes. Failure responsible are  $\tau_{nt}$  and  $\sigma_n$ , only. But mind: For the differentiation  $\sigma_t$  cannot be simply set zero at the beginning of the derivations but must be considered due to its relation to  $\sigma_n$ .*
- *Above derivation further proves that, if really desired, the fracture plane angle  $\Theta_{fp}^c$  of an UD-material could be determined from the FMC-based SFC formulated in structural stresses*

➤ Viewing Fig.8.2-6 and -7 (indicator  $Eff^{\perp\sigma}$ ) the cohesive strength  $\bar{R}_{\perp}^c$  belongs to the transition zone of the normal fracture mode domain IFF1 and therefore not alone to the shear fracture mode domain IFF2.

#### 8.2.4 Determination of Mohr shear curve, touch point coordinates and guess of cohesive strength

Touch point coordinates  $\tau_{nt}^c, \sigma_n^c$  :

From transformation equations:  $c = \cos(\Theta_{fp}^c) = \cos(\Theta_{fp}^{\circ} \cdot \pi / 180^{\circ})$

$$\sigma_n = c^2 \cdot \sigma_2, \quad \tau_{nt} = -s \cdot c \cdot \sigma_2 \quad \text{and} \quad \Theta_{fp}^{\circ} = 51., \quad \bar{R}_{\perp}^c = 104 \text{ MPa}$$

$$\sigma_n^c = \cos(\Theta_{fp}^c)^2 \cdot (-\bar{R}_{\perp}^c) = -41.3 \text{ MPa}, \quad \tau_{nt}^c = -\sin(\Theta_{fp}^c) \cdot \cos(\Theta_{fp}^c) \cdot (-\bar{R}_{\perp}^c) = 50.9 \text{ MPa}$$

$$\sigma_n^c = 0.5 \cdot (C + 1) \cdot (-\bar{R}_{\perp}^c) = -41.3 \text{ MPa}, \quad \tau_{nt}^c = -0.5 \cdot \sqrt{1 - C} \cdot (-\bar{R}_{\perp}^c) = 50.9 \text{ MPa}$$

( for info  $\sigma_t^c = -62.7 \text{ MPa}$  )

From Mohr circle geometry:

$$\tan \rho = (0.5 \cdot \bar{R}_{\perp}^c - |\sigma_n^c|) / \tau_{nt}^c \quad \text{and} \quad \tan \rho = \tau_{nt}^c / (\bar{R}_{\perp}^c - |\sigma_n^c|) = |\sigma_n^c| / \tau_{nt}^c$$

$$\rightarrow \tau_{nt}^c := \sqrt{|\sigma_n^c| \cdot (\bar{R}_{\perp}^c - |\sigma_n^c|)} = \left( (0.5 \cdot \bar{R}_{\perp}^c - |\sigma_n^c|) / \tan \rho \right)^2$$

$$\rightarrow |\sigma_n^c| = (\bar{R}_{\perp}^c + \bar{R}_{\perp}^c \cdot \tan^2 \rho) - \bar{R}_{\perp}^c \cdot \tan \rho \cdot \sqrt{1 + \tan^2 \rho} / (2 + 2 \cdot \tan^2 \rho)$$

Mohr shear curve  $\tau_{nt}(\sigma_n)$ : based on IFF2, only, is an extrapolation from compressive strength

In the case of brittle materials the Mohr-Coulomb curve is the result of two commonly acting failure modes. Now, neglecting IFF1 (the normal fracture part) and considering just the shear fracture IFF2 leads to the curve in Fig.7-8 according to the relations

$$Eff^{\perp\tau} \equiv F^{IFF2} = [a_{\perp\perp} \cdot (I_2) + b_{\perp\perp} \cdot \sqrt{I_4}] / \bar{R}_{\perp}^c = 1 \quad \text{with} \quad a_{\perp\perp} = b_{\perp\perp} - 1 \quad \text{after inserting} \quad \bar{R}_{\perp}^c$$

$$= [a_{\perp\perp} \cdot (\sigma_n + \sigma_t) + b_{\perp\perp} \cdot \sqrt{(\sigma_n - \sigma_t)^2 + 4\tau_{nt}^2}] / \bar{R}_{\perp}^c = 1$$

$$I_2 = \sigma_n + \sigma_t = \sigma_2 + \sigma_3, \quad \sigma_n - \sigma_t = C \cdot (\sigma_2 - \sigma_3) = C \cdot \eta, \quad \tau_{nt} = -0.5 \cdot \sqrt{1 - C} \cdot \eta$$

In the compression strength point ( $\sigma_2 = -\bar{R}_{\perp}^c, \sigma_3 = 0$ ),  $\eta = -\bar{R}_{\perp}^c$  is obtained  $C \rightarrow C^c$ ,

$$a_{\perp\perp} \cdot (2\sigma_n + C^c \cdot \eta) + b_{\perp\perp} \cdot \sqrt{(C^c \cdot \eta)^2 + 4\tau_{nt}^2} / \bar{R}_{\perp}^c = 1 \quad \Rightarrow \quad \tau_{nt}(\sigma_n, C^c).$$

For a better orientation the four Mohr half-circles are included in Fig.7-8. Both the shear curves Linear Mohr-Coulomb and the FMC-based equation above – due to the definition of the friction value – are linear and equal, because  $C = C^c(\mu_{\perp\perp})$  is constant along  $\sigma_2$ .

The touch point and the cohesive shear strength are depicted in the figure.

Cohesive strength  $\bar{R}_{\perp}^c$  : extrapolation from compressive strength point

\* From the Linear Mohr approach:  $\bar{R}_{\perp}^c = \tau_{nt}^c + \mu \cdot \sigma_n^c \Rightarrow \bar{R}_{\perp}^c = 42 \text{ MPa}.$

\* From the IFF2 equation :  $\tau_{nt}(\sigma_n, C^c)$ :  $\bar{R}_{\perp}^c = \tau_{nt}(\sigma_n = 0) = 42 \text{ MPa}.$

\* General note on prediction of  $\bar{R}_{\perp}^c$  and of A. Puck's  $\bar{R}_{\perp}^A$  :



For the cohesive strength, denoted  $\bar{R}_{\perp}^A$  by Puck, he gave the formula  $R_{\perp\perp}^A = R_{\perp}^c / (2 + 2 \cdot p_{\perp\perp}^c)$  with  $0.25 < p_{\perp\perp}^c < 0.30$  for CFRP. Inserting above set of strength properties  $R_{\perp}^c = 104$  MPa,  $R_{\perp}^t = 35$  MPa into Puck's formula  $R_{\perp\perp}^A$  becomes 41 MPa.

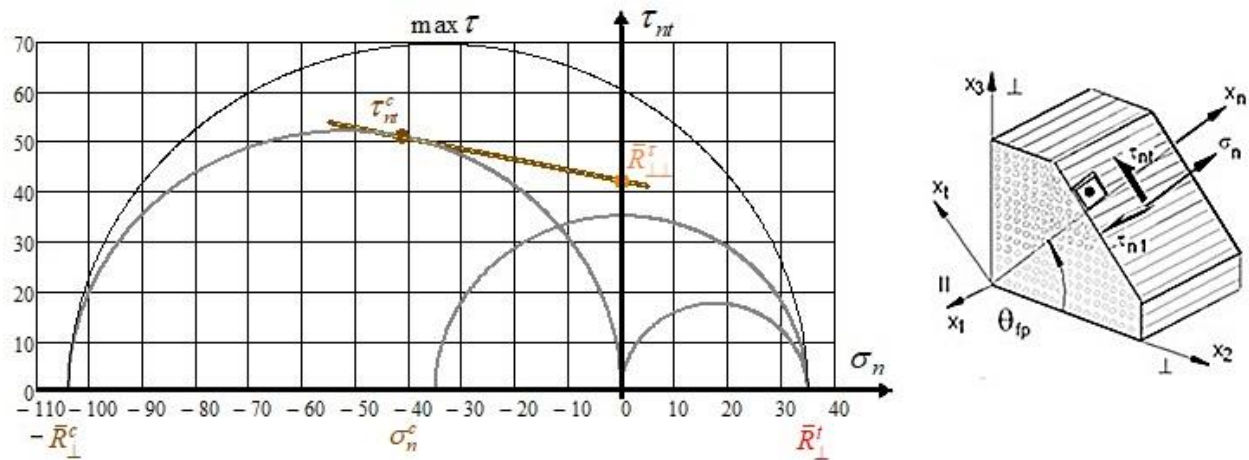


Fig. 8.2-8: Mohr shear curves  $\tau_{nt}(\sigma_n)$  with its special end points and the four Mohr half-circles.

$$\bar{R}_{\perp}^t = 35 \text{ MPa}, \bar{R}_{\perp}^c = 104 \text{ MPa}, \Theta_{fp}^{\circ} = 51^{\circ}, \bar{R}_{\perp\perp}^r = 42 \text{ MPa}, \sigma_n^c = -41.3 \text{ MPa}, \tau_{nt}^c = 50.9 \text{ MPa}$$

$$C_{fp}^c = \cos(2 \cdot \Theta_{fp}^{\circ} \cdot \pi / 180^{\circ}): \mu = -\tan \rho = -C_{fp}^c / S_{fp}^c = -C_{fp}^c / \sqrt{1 - C_{fp}^{c2}} \cong -C_{fp}^c.$$

### 8.2.5 Derivation of the real $\tau_{nt}(\sigma_n)$ and of course of $\Theta_{fp}$ from a measured fracture curve $\sigma_3(\sigma_2)$

In the previous chapters, for isotropic materials the author proved that a transformation from structural stresses to the desired formulations in Mohr stresses is possible. The same is analogously possible for a UD material, where the quasi-isotropic plane has to be investigated in order to determine the lateral cohesive strength.

In Table 8.2-2 all relations necessary for the transformation of a measured fracture curve  $\sigma_3(\sigma_2)$  into a Mohr-Coulomb curve  $\tau_{nt}(\sigma_n)$  are listed. The formulas for the searched entities  $\tau_{nt}$ ,  $\sigma_n$ ,  $\Theta_{fp}^{\circ}$  are presented. These entities are only accurate if the physically necessary correction of the design-practical 'simple' IFF2 (or  $Eff^{\perp r} \equiv Eff^{SF}$ ) is considered by the decay function  $f_d$ . In order to implement  $f_d$  one just has to replace  $a_{\perp\perp}$  by  $f_d \cdot a_{\perp\perp}$  and  $b_{\perp\perp}$  by  $f_d \cdot b_{\perp\perp}$ .

Fig.8.2-11 presents the full range of MathCad-computed Mohr entities:

Upper diagram: Mohr stresses

- straight Linear Mohr Coulomb curve (*extrapolation*)
- IFF2-determined Mohr-Coulomb fracture curve (*IFF2 extrapolation is like Mohr*)
- course of the fracture plane angle  $\Theta_{fp}^{\circ}$  (*bold, decay function corrected*)
- IFF2-IFF1-interacted Mohr-Coulomb fracture curve (*bold, decay function corrected*)

Lower diagram: structural stresses

- course of the fracture plane angle  $\Theta_{fp}^{\circ} / 2$
- IFF2-IFF1- interacted fracture curve (*thin, original IFF2*)
- IFF2-IFF1- interacted fracture curve (*bold, IFF2 decay function corrected, which better maps the course of measured fracture stress data*).

In order to find all relationships in one diagram the Mohr stresses are inserted as functions of the structural stresses and not of  $\sigma_n$ , which is the usual diagram form and was used for the isotropic materials before. The figure further includes the development of the fracture plane angle as function of the structural stress  $\sigma_2$  and the various predicted values for the cohesive strength  $R^\tau$ .

The numerical example stems from a measurement of the fracture plane angle  $\Theta_{fp}^\circ$  in [Cun97].

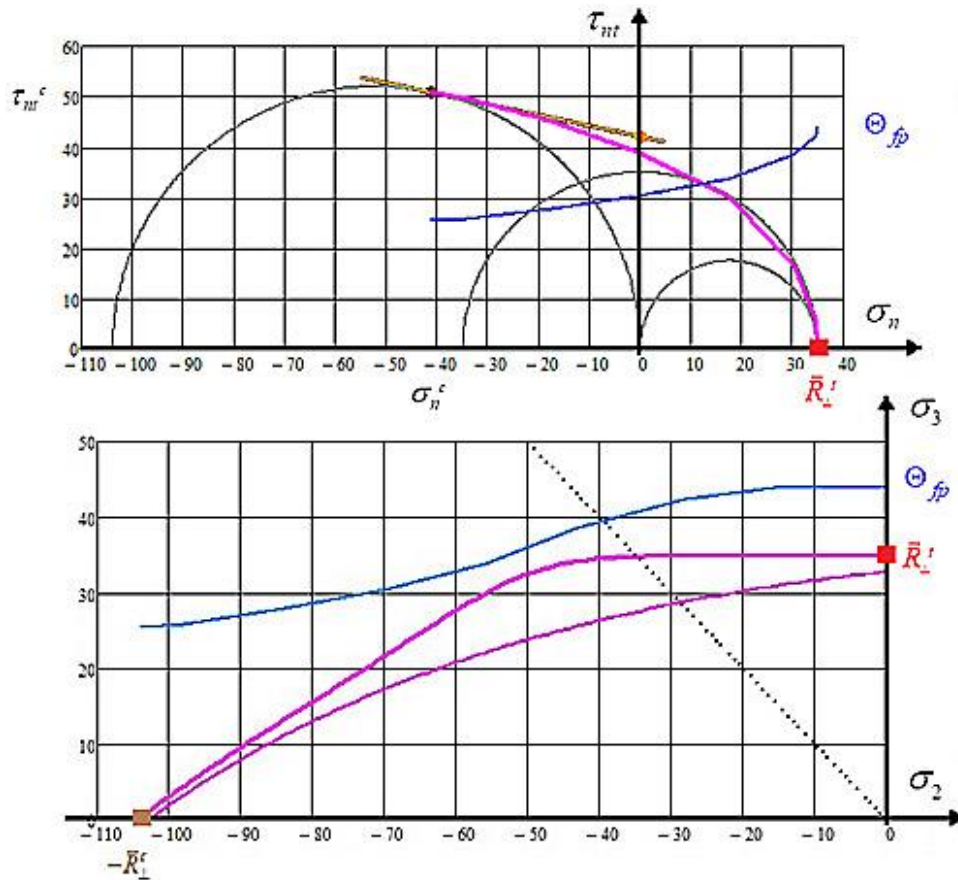


Fig.8.2-11: Joint display of the UD failure curve in Mohr stresses (above) with fracture angle increase  $\Theta_{fp}^\circ$  when approaching  $\bar{R}_\perp^t$  and in structural stresses (below).

Linear:  $\bar{R}_\perp^\tau = 42$  MPa,  $\Theta_{fp}^c = 51^\circ$ , Improved by  $f_d$ :  $\bar{R}_\perp^\tau = 39$  MPa,  $\Theta_{fp}^\circ = 61^\circ$ ,  $\sigma_2 = -70$  MPa,  $\sigma_3 = 22$  MPa.

$\bar{R}_\perp^t = 35$  MPa,  $\bar{R}_\perp^c = 104$  MPa,  $\Theta_{fp}^c = 51.0^\circ$ ,  $C^c = -0.206$ ,  $\mu_\perp = 0.211$ ,  $\tau_{nt}^c = 50.9$  MPa,  $\sigma_n^c = -41.3$  MPa

The interpretation of Fig.8.2-11 leads to the following conclusions:

- ✓ A SFC in structural stresses can be transferred into a Mohr-Coulomb type
- ✓ The alteration of the fracture plane angle  $\Theta_{fp}^\circ$  can be determined, too
- ✓ The idea of the FMC that IFF1 and IFF2 commonly add its *Eff* portions lead to the result that the  $\Theta_{fp}^\circ$  is about  $70^\circ$  at the cohesive strength point  $\bar{R}_\perp^\tau$
- ✓ The simple IFF2 approach cannot offer a full accuracy of the realistically predicted Mohr-Coulomb curve. Just the *physically-based* decay function correction delivers the desired fidelity.

Table 8.2-2: Relationships during derivation of  $\tau_{nt}(\sigma_n)$ ,  $\Theta_{fp}^\circ$  from a measured fracture curve  $\sigma_3(\sigma_2)$

$$\begin{aligned} Eff^{\perp\tau} = Eff^{SF} &= [a_{\perp\perp} \cdot (\sigma_2^p + \sigma_3^p) + b_{\perp\perp} \cdot \sqrt{(\sigma_2^p - \sigma_3^p)^2 + 0^2}] / \bar{R}_\perp^c = 1 \\ &= [a_{\perp\perp} \cdot (\sigma_n + \sigma_t) + b_{\perp\perp} \cdot \sqrt{(\sigma_n - \sigma_t)^2 + 4\tau_{nt}^2}] / \bar{R}_\perp^c = 1 \end{aligned}$$

$$\begin{aligned} Eff^{\perp\sigma} = Eff^{NF} &= (\sigma_2^p + \sigma_3^p) + \sqrt{(\sigma_2^p - \sigma_3^p)^2 + 0^2}] / 2 \cdot \bar{R}_\perp^t = 1 \\ &= [(\sigma_n + \sigma_t) + \sqrt{(\sigma_n - \sigma_t)^2 + 4\tau_{nt}^2}] / 2 \cdot \bar{R}_\perp^t = 1. \end{aligned}$$

Known:  $\sigma_2^p, \sigma_3^p$ . Searched:  $\sigma_n, \tau_{nt}, \Theta_{fp}$  ( $C = \cos(2 \cdot \Theta_{fp}^\circ \cdot \pi / 180^\circ)$ )

Two quantities are known and three are to be determined

Use of addition theorems,  $\sigma_\lambda = 0$ , index  $p$  now dropped

$$\begin{aligned} \sigma_n - \sigma_t &= c^2 \cdot (\sigma_2 - \sigma_3) - s^2 \cdot (\sigma_2 - \sigma_3) = C \cdot (\sigma_2 - \sigma_3), \quad S = \sqrt{1 - C^2} \\ \sigma_t &= \sigma_n - C \cdot (\sigma_2 - \sigma_3), \quad C = c^2 - s^2 = 2c^2 - 1 = 1 - 2s^2, \end{aligned}$$

$$\sigma_n + \sigma_t = \sigma_2 + \sigma_3, \quad \tau_{nt} = -0.5 \cdot S \cdot (\sigma_2 - \sigma_3) = -0.5 \cdot \sqrt{1 - C^2} \cdot (\sigma_2 - \sigma_3)$$

Fracture (interaction) equation  $\equiv$  mathematical equation of the fracture body

$$\begin{aligned} Eff &= [(Eff^{NF})^m + (Eff^{SF})^m]^{m^{-1}} \quad \text{or computationally simpler} \\ (Eff^{NF})^m + (Eff^{SF})^m &= 1 = 100\% \quad \text{total effort.} \end{aligned}$$

Differentiation of structural stresses-linked Mohr stresses delivers

$$\frac{d\tau_{nt}}{d\sigma_n} = \frac{(s^2 - c^2) \cdot (\sigma_2 - \sigma_3)}{-2 \cdot s \cdot c \cdot (\sigma_2 - \sigma_3)} = \frac{C}{S}, \quad \text{valid } uni\text{- and } bi\text{-axial (like isotropic!)}$$

Missing equation from differentiation of the interaction equation,  $\sigma_t$  to insert before,

$$\begin{aligned} \{[(\sigma_n + \sigma_n - C \cdot (\sigma_2 - \sigma_3)) + \sqrt{(\sigma_n - \sigma_n - C \cdot (\sigma_2 - \sigma_3))^2 + 4\tau_{nt}^2}] / 2 \cdot \bar{R}_\perp^t\}^m + \\ + \{[a_{\perp\perp} \cdot (\sigma_n + \sigma_n - C \cdot (\sigma_2 - \sigma_3)) + \\ + b_{\perp\perp} \cdot \sqrt{(\sigma_n - \sigma_n - C \cdot (\sigma_2 - \sigma_3))^2 + 4\tau_{nt}^2}] / \bar{R}_\perp^c\}^m = 1. \end{aligned}$$

$$d[(Eff^{NF})^m + (Eff^{SF})^m] / d\sigma_n =$$

$$\begin{aligned} m \cdot \{2\sigma_n - C \cdot (\sigma_2 - \sigma_3) + \sqrt{(C \cdot (\sigma_2 - \sigma_3))^2 + 4\tau_{nt}^2} / 2\bar{R}_\perp^t\}^{m-1} / \bar{R}_\perp^t + \\ + 2a_{\perp\perp} m \cdot \{a_{\perp\perp} (2\sigma_n - C \cdot (\sigma_2 - \sigma_3)) + b_{\perp\perp} \sqrt{(C \cdot (\sigma_2 - \sigma_3))^2 + 4\tau_{nt}^2} / \bar{R}_\perp^c\}^{m-1} / \bar{R}_\perp^c, \end{aligned}$$

$$[d(Eff^{NF})^m + (Eff^{SF})^m] / d\tau_{nt} =$$

$$\frac{2m \cdot \tau_{nt} \cdot \{2\sigma_n - C \cdot (\sigma_2 - \sigma_3) + \sqrt{(C \cdot (\sigma_2 - \sigma_3))^2 + 4\tau_{nt}^2} / 2\bar{R}_\perp^t\}^{m-1}}{\bar{R}_\perp^t \cdot \sqrt{(C \cdot (\sigma_2 - \sigma_3))^2 + 4\tau_{nt}^2}} +$$

$$+ 4b_{\perp\perp} m \cdot \{a_{\perp\perp} (2\sigma_n - C \cdot (\sigma_2 - \sigma_3)) + b_{\perp\perp} \sqrt{(C \cdot (\sigma_2 - \sigma_3))^2 + 4\tau_{nt}^2} / \bar{R}_\perp^c\}^{m-1} / \bar{R}_\perp^c.$$

Equating the two equations and replacing Mohr stresses by structural stresses

$$\text{via } \sigma_n = (C + 1) \cdot 0.5 \cdot \sigma_2 + (1 - C) \cdot 0.5 \cdot \sigma_3, \quad \tau_{nt} = -0.5 \cdot \sqrt{1 - C^2} \cdot (\sigma_2 - \sigma_3)$$

yields an equation for the fracture angle measure  $C$ ;  $m$  vanishes

$$\frac{C(\sigma_2, \sigma_3)}{\sqrt{1 - C^2}} = - \left[ \frac{m \cdot A}{\bar{R}_\perp^t} + \frac{2 \cdot a_{\perp\perp} \cdot m \cdot B}{\bar{R}_\perp^c} \right] / \left[ \frac{2 \cdot m \cdot A}{\bar{R}_\perp^t \sqrt{(\sigma_2 - \sigma_3)^2}} + \frac{4 \cdot b_{\perp\perp} \cdot m \cdot B \cdot \tau_{nt}}{\bar{R}_\perp^c \sqrt{(\sigma_2 - \sigma_3)^2}} \right]$$

$$A = \left[ \frac{\sigma_2 + \sigma_3 + \sqrt{(\sigma_2 - \sigma_3)^2}}{2 \cdot \bar{R}_\perp^t} \right]^{m-1}, \quad B = \left[ \frac{a_{\perp\perp} \cdot (\sigma_2 + \sigma_3) + b_{\perp\perp} \cdot \sqrt{(\sigma_2 - \sigma_3)^2}}{\bar{R}_\perp^c} \right]^{m-1}$$

and finally  $\Theta_{fp}^\circ$  and the Mohr stresses  $\sigma_n, \tau_{nt}$

$$C = \cos(2 \cdot \Theta_{fp}^\circ), \quad \Theta_{fp} = 0.5 \cdot \arccos C, \quad \Theta_{fp}^\circ = \Theta_{fp} \cdot 180^\circ / \pi, \quad c^2 = (C + 1) \cdot 0.5$$

$$\sigma_n = (C + 1) \cdot 0.5 \cdot \sigma_2 + (1 - C) \cdot 0.5 \cdot \sigma_3, \quad \tau_{nt} = -0.5 \cdot \sqrt{1 - C^2} \cdot (\sigma_2 - \sigma_3).$$

## 9 Miscellaneous

### 9.1 Bridging Shear Fracture $F^{SF}$ and Yield Failure $F^{Mises}$ with view at failure 'planes'

The Failure-Mode-Concept is dedicated to brittle materials ( $R^c / R^t > 3$ ) whereas 'Mises' (Hencky-Mises-Huber, a Modal and Global SFC) describes the yield behavior of ductile materials ( $R_{0.2}^t \approx R_{0.2}^c$ ).

Both the failure conditions shall be used to enlighten the difference between the failure function  $F$  of a SFC and an effort  $Eff$  of both the SFCs. The difference is essential in the elastic domain, where – caused by the design safety factor – most of the structural parts with its critical locations are to be strength-assessed.

Basis is the application of the so-called proportional loading, where all stress states alter proportionally. Difference comes up if  $F$  is not a so-called homogeneous function (see the respective Annex 6). The following table displays all the links:

\* FMC-based Strength Failure Condition  $F^{SF}$  ( non-homogeneous equation)

*Porous*:  $\bar{R}^c > \cong 3 \bar{R}^t$ , rotational symmetry is assumed,  $\Theta_\tau = 1$

$$F^{SF} = c_1^{SF} \cdot \frac{3J_2 \cdot \Theta_\tau}{\bar{R}^{c2}} + c_2^{SF} \cdot \frac{I_1}{\bar{R}^c} = 1 \quad \dots\dots \text{Onset-of-Shear Fracture}$$

or in Eff after applying 'proportional loading'

$$c_1^{SF} \cdot \frac{3J_2 \cdot 1}{\bar{R}^{c2} \cdot Eff^2} + c_2^{SF} \cdot \frac{I_1}{\bar{R}^c \cdot Eff} = 1$$

$$Eff^{SF} = \frac{c_2^{SF} \cdot I_1 + \sqrt{(c_2^{SF} \cdot I_1)^2 + 12 \cdot c_1^{SF} \cdot J_2}}{2 \cdot \bar{R}^c} = 100\% \dots \text{Onset-o- Shear Fracture}$$

Inserting  $(\bar{R}^c, 0)$  delivers  $1 + c_2^{SF} = c_1^{SF} \cdot \Theta_\tau$ ;  $c_2^{SF}$  is friction parameter

For a single failure mode like Onset-of-Shear Fracture  $F^{SF}$  or Onset-of-Yielding  $F^{Mises}$  equivalent stresses can be easily formulated

$$Eff^{SF} = \frac{c_2^{SF} \cdot I_1 + \sqrt{(c_2^{SF} \cdot I_1)^2 + 12 \cdot c_1^{SF} \cdot J_2 \cdot (1)}}{2 \cdot \bar{R}^c} = \sigma_{eq}^{SF} / \bar{R}^c$$

Transition to *Ductile*: (1) Failure angle  $\Theta_{fp}^\circ = 45^\circ$ , (2)  $c_2^{SF} = 0$

$$F^{SF} = 1 \cdot \frac{3J_2 \cdot 1}{\bar{R}^{c2}} + 0 \cdot \frac{I_1}{\bar{R}^c} = \frac{3J_2}{\bar{R}^{c2}} = 1 \rightarrow \frac{\sqrt{3J_2}}{\bar{R}^c \cdot Eff} = 1$$

$$Eff^{SF} = \frac{0 + \sqrt{0 + 12 \cdot 1 \cdot 3J_2}}{2 \cdot \bar{R}^c} = \frac{\sqrt{3J_2}}{\bar{R}^c} = \sigma_{eq}^{SF} / \bar{R}^c, \quad C_{fp} = \cos\left(\frac{2 \cdot \Theta_{fp}^\circ}{180^\circ} \cdot \pi\right),$$

$$\Rightarrow \text{Bound of } F^{SF}, \mu = 0 : c_2^{SF} = \frac{3\mu + 1}{-3\mu + 1} = 1, \quad \mu \cong -C_{fp} = 0, \quad , \quad \Theta_{fp}^\circ = 45^\circ$$

$$\Rightarrow \text{Ductile transfer, } c_2^{SF} = 0 : c_2^{SF} = \frac{3\mu + 1}{-3\mu + 1} = 0, \quad \mu \cong -C_{fp} = \frac{-1}{3}, \quad , \quad \Theta_{fp}^\circ = 35.3^\circ.$$

\* 'Mises' Yield Condition (homogeneous equation,  $F = Eff$ )

*Ductile*:  $\bar{R}_{0.2}^t \cong \bar{R}_{0.2}^c = \bar{R}_{0.2}$  if very ductile

$$F^{Mises} = \frac{\sqrt{3J_2}}{\bar{R}_{0.2}} = 1 \quad \rightarrow \quad \frac{\sqrt{3J_2}}{\bar{R}_{0.2} \cdot Eff} = 1$$

$$Eff^{Mises} = \frac{\sqrt{3J_2}}{\bar{R}_{0.2}} = \sigma_{eq}^{Mises} / \bar{R}_{0.2} .$$

For providing some more information on the differences of  $F^{SF}$ ,  $F^{Mises}$  some features are presented:

Ductile:  $I_1 < 0$ ,  $R_{02}^c$  |  $I_1 > 0$ ,  $R_{02}^t$

In the case of very ductile materials -  $R_{02}^t = R_{02}^c$  – the yield plane angle is caused by the shear stress  $\tau_n$  on the sliding plane (of course  $\sigma_n$  exists from equilibrium condition, too, but is not of influence;  $\tau_{nt} = |\sigma_n| = \sigma_{ax}$ ). The sliding angle is not dependent on the sign of  $I_1$ . It is derived as follows

Derivation of the slope equation in Mohr stresses,  $\sigma_\lambda$ ,  $\tau_{i\lambda}$ ,  $\tau_{n\lambda} = 0$

$$F^{Mises} = \sqrt{\frac{3J_2}{\bar{R}^2}} = \sqrt{\frac{3 \cdot (\sigma_n - \sigma_t)^2 + (\sigma_t - \sigma_\lambda)^2 + (\sigma_\lambda - \sigma_n)^2 + 6 \cdot (\tau_{nt}^2 + \tau_{n1}^2 + \tau_{t1}^2)}{2 \cdot \bar{R}^2}} = 1$$

$$= \sqrt{\frac{3 \cdot (\sigma_n - \sigma_t)^2 + (\sigma_t - 0)^2 + (0 - \sigma_n)^2 + 6 \cdot (\tau_{nt}^2 + 0 + 0)}{2 \cdot \bar{R}^2}} = 1$$

$$\frac{d\tau_{nt}}{d\sigma_n} = - \frac{dF}{d\sigma_n} / \frac{dF}{d\tau_{nt}} \text{ (implicite differentiation)} = - \frac{2 \cdot \sigma_n - \sigma_t}{6 \cdot \tau_{nt}}$$

Transformed structural stresses and addition theorems used:

$$\sigma_n - \sigma_t = C \cdot (\sigma_{II}), \quad \tau_{nt} = -0.5 \cdot S \cdot (\sigma_{II}), \quad \sigma_n = 0.5 \cdot (C + 1) \cdot \sigma_{II}$$

Equal slope of curves in touch point:  $\eta$  is multi-axial and cut out

$$\frac{d\tau_{nt}}{d\sigma_n} = \frac{C}{S} = - \frac{2 \cdot \sigma_n - \sigma_t}{6 \cdot \tau_{nt}} = - \frac{\sigma_n + C \cdot (\sigma_{II})}{6 \cdot (-0.5 \cdot S \cdot \sigma_{II})}$$

$$\frac{C}{S} = - \frac{0.5 \cdot (C + 1) \cdot \sigma_{II} + C \cdot (\sigma_{II})}{6 \cdot -0.5 \cdot S \cdot (\sigma_{II})} \Rightarrow C = \frac{1}{3}$$

For additional information: The cohesive strength corresponding shear stress  $\tau$  reads

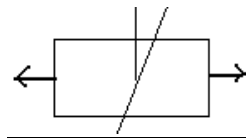
$$\sqrt{\frac{3J_2}{\bar{R}_{02}^2}} = \sqrt{\frac{\sigma_{II}^2 - \sigma_{II} \cdot \sigma_{III} + \sigma_{III}^2}{\bar{R}_{02}^2}} = \sqrt{\frac{\sigma_{II}^2 - \sigma_{II} \cdot (-\sigma_{II}) + (-\sigma_{II})^2}{\bar{R}_{02}^2}} = 1$$

$$\sqrt{\frac{\sigma_{II}^2 - \sigma_{II} \cdot (-\sigma_{II}) + (-\sigma_{II})^2}{\bar{R}_{02}^2}} = 1 \rightarrow \sigma_{II} = \bar{R}_{02} / \sqrt{3} = \tau$$

Brittle:  $-2 \cdot R^{cc}(\text{TM}) < I_1 < -R^c(\text{CM}) < 0$  mode domains |  $I_1 > 0 < R^t(\text{TM}) < 2 \cdot R^{tt}(\text{CM})$

$\Theta_{fp}$  of very brittle materials with  $R^c$  much larger than  $3 \cdot R^t$  is caused by

$$\begin{array}{c|c} (\tau_{nt}, \sigma_n^c) & (\tau_{nt}, \sigma_n^t) \\ \hline > 45^\circ < \Theta_{fp} < 90^\circ, \mu\text{-dependent} & \Theta_{fp} = 90^\circ \text{ at critical plane} \\ \text{cohesive strength } R^t \text{ at } (\tau_{nt}, \sigma_n = 0) \text{ is NF-dominated} & \rightarrow R^t \leq R^t \end{array}$$



## 9.2 Influence of 2D- and 3D-compression stress states on the strength capacity

On the surface of the fracture failure body the material stressing effort is 100%. Located on the surface are the uni-axial failure stress points, termed technical strengths, bi-axial ‘strengths’ and all other multi-axial failure stress points.

Keep in mind: ‘Higher’ multi-axial failure stresses have nothing to do with an increase of strength. In the case of multi-axial compression stress states of dense brittle materials the strength is not increased but the risk of shear fracture becomes smaller indicated by the smaller *Eff*!

### 9.2.1 Isotropic materials (example concrete, UHPC test data, courtesy IfM Dresden)

Test paths: tensile meridian  $\sigma_I = \sigma_{II} > \sigma_{III}$  and compressive meridian  $\sigma_I > \sigma_{II} = \sigma_{III}$ . The test is performed by superimposing an axial stress  $\sigma_{ax}$  to a hydrostatic pressure  $p_{hyd}$ .  $\sigma_{III}$  is the mathematically lowest stress.

|    | Rotational Symmetry Stress States        |               |                     | Eff in % | 120° Symmetry Stress States |               |                     | Eff in % |
|----|--|---------------|---------------------|----------|-----------------------------|---------------|---------------------|----------|
|    | - p                                      | - p           | - p + $\sigma_{ax}$ | 100      | - p                         | - p           | - p + $\sigma_{ax}$ | 100      |
|    | $\sigma_I$                               | $\sigma_{II}$ | $\sigma_{III}$      |          | $\sigma_I$                  | $\sigma_{II}$ | $\sigma_{III}$      |          |
| 1D | 0  | 0             | - $R^c$             | 100      | 0                           | 0             | - $R^c$             | 100      |
| 2D | 0  | 0.25 $R^c$    | - $R^c$             | 72       | 0                           | 0.25 $R^c$    | - $R^c$             | 34       |
|    | 0  | - $R^c$       | - $R^c$             | 60       | 0                           | - $R^c$       | - $R^c$             | 35       |
| 3D | - 0.5 $R^c$                              | - 0.5 $R^c$   | - $R^c$             | 16       | - 0.5 $R^c$                 | - 0.5 $R^c$   | - $R^c$             | 6        |
| 1D | UHPC test result [ <i>Cun17</i> ] in MPa |               |                     |          | 0                           | 0             | -160                | 100      |
| 3D | UHPC test result in MPa                  |               |                     |          | -6                          | -6            | -6 - 224            | 100      |

Conclusions:

(1) *Multiaxial compression lowers Eff.* (2) *2D compression generates a tensile strain in axial direction, which is to be considered in design.* (3) *The physically accurate 120°-rotationally-symmetric model delivers a lower Eff-value for the stress states above.*

### 9.2.2 Transversely-isotropic UD materials (example CFRP)

Here, the difference between a proportionally-stressing derived *Eff* and a driving stress-derived *Eff* is intentionally outlined. The two concepts invite for discussion.

|    | Stress States       |                 | Eff in %   | Eff in %             |
|----|---------------------|-----------------|--|----------------------|
|    | $\sigma_2$          | $\sigma_3$      |  |                      |
| 1D | 0                   | - $R_{\perp}^c$ | 100  | 100                  |
| 2D | - 0.5 $R_{\perp}^c$ | - $R_{\perp}^c$ | 24   | 45                   |
|    | - $R_{\perp}^c$     | - $R_{\perp}^c$ | -52  | 0                    |
|    |                     |                 | $a_{\perp\perp} = 0.26, b_{\perp\perp} = a_{\perp\perp} + 1$ | as = 0.26, bs = 2.52 |
|    |                     |                 | proportional   | driving stress       |

Conclusions:

(1) *Again, multiaxial compression lowers Eff.* (2) *In the case of ‘dense’ UD materials bi-axial compression causes no fracture failure,  $Eff < 0$ .* (3) *2D compression generates a tensile stress because the fibers withstand axial straining. This stress from the constraint situation is usually easily captured by the fiber, on top of the loading stress  $\sigma_I = \sigma_{\parallel}$ .*

The ‘driving stress concept’ leads to higher *Eff*s. About its general value discussion is desired,  $\perp = s$ .

$$\text{Eff2} := \frac{(\sigma_2 + \sigma_3) \cdot \text{ass} + \sqrt{(\sigma_2 - \sigma_3)^2 \cdot \text{bss}}}{\text{Rsc}} \quad \rightarrow \quad \text{Eff2} := \frac{\text{bs} \cdot \sqrt{0.25(\sigma_2 - \sigma_3)^2}}{\text{Rsc} - \text{as} \cdot (\sigma_2 + \sigma_3)}$$

## 9.3 Application of Safety Concepts with Determination of a Reserve Factor

### 9.3.1 General

A Safety Concept implements the necessary reliability into the structural component, to robustly endure uncertain design parameters (variables). Different formats are available to capture the uncertainties of the design parameters:

#### \* Lumped, Deterministic Safety Factor Concept:

Concept, that deterministically accounts for design uncertainties in a lumped manner through enlarging the ‘design limit loads’ by multiplication with a design Factor of Safety *FoS* *j*. This provides an unknown not really deterministically quantifiable ‘safety distance’ between load and load resistance (‘strength’) represented by the required positive Margin of Safety (*MoS* = *RF*-1).

#### \* Partial Safety Factor Concept:

Concept, that semi-probabilistically bridges the deterministic format and the more complicated probabilistic format. A probabilistic format can model each single design parameter’s uncertainty into a stochastic uncertainty described by a probability density function. Accounting for uncertainties informs about the robustness of the design and considers the correlations of the design variables.

In the deterministic formats the worst case scenario is usually applied for loadings considering temperature, moisture, undetected damage. Further, a load is to increase by a ‘Design *FoS*’ and the resistances are to decrease. For strength, statistical distributions are used. If the loading is also based on a statistical distribution, then one speaks about a semi-probabilistic format.

*FoS* capture uncertainties, small inaccuracies, and simplifications in analyses w.r.t. manufacturing process, tolerances, loadings, material properties (strength, elasticity, ..), geometry, strength failure conditions etc. *FoS* *j* or *FoS*  $\gamma$  (*in civil engineering*) do not capture missing accuracies in modeling, analysis, test data generation and test data evaluation! *FoS* are used to counteract the risk of a structural failure or to decrease the chance of failure by capturing the uncertainties of all the given variables outside the control of the designer. Presently, in mechanical engineering the loading is increased by one lumped *FoS* *j*, and in civil engineering the procedure is improved by using several partial Design *FoS*  $\gamma$  for the uncertain stochastic design variables.

Engineers in mechanical and in civil engineering practically want to know “How much can one further increase the loading“? In this context, for the example *ultimate load case* (DUL, ULS, GZT) it is to demonstrate in *strength design verification* that:  $\bar{R}$  (mapping)  $\rightarrow$  *R* (design verification)

Linear analysis is sufficient (presumption):  $\sigma \sim \text{load} \rightarrow RF \equiv f_{RF} = 1 / \text{Eff}$

$$\text{material reserve factor} \quad f_{RF, ult} = \frac{\text{Strength Design Allowable } R}{\text{Stress at } j_{ult} \cdot \text{Design Limit Load}} > 1,$$

Non-linear analysis required:  $\sigma$  not proportional to load

$$\text{reserve factor (load-defined)} \quad RF_{ult} = \frac{\text{Predicted Failure Load at } Eff = 100\%}{j_{ult} \cdot \text{Design Limit Load}} > 1.$$

In other words and terms the question in the engineering disciplines is.

In mechanical engineering: *Is there a sufficient reserve of load-bearing capacity?*

In construction: *Is there a sufficient reserve of reinforcement?*

The load combinations become the design load cases. Since not all loads occur simultaneously at full height and in the worst possible combination, variable loads may be reduced in construction by a combination coefficient  $\Psi$ . Its value depends on the observed limit state

In order to use hidden load carrying reserves, structural analysis is to perform until material failure is reached in the critical location which is indicated for the exhausted material by  $Eff = 100\%$ .

In construction, the material reserve factor  $f_{RF}$  is defined, fully analogous to mechanical engineering and to aerospace by a formulation  $f_{RF} = (f_k / \gamma_m) / (\sigma(G_k) \cdot \gamma_G)$  with the stress level design values (Bemessungswerte)  $f_k \rightarrow f_{ck}$  for instance for concrete (index c) as the characteristic strength and the partial safety factors  $\gamma_{G,static}$  for loading and for material scatter  $\gamma_m \rightarrow \gamma_{c,static}$  (example concrete)

On the loading side - in the ultimate load design case - the usual FoS read:

- Spacecraft DUL [Cun12] : load model factor 1.2 x load factor 1.25 = 1.5, also 1.5!
- Aircraft DUL : lumped load factor  $j_{ult} = 1.5$
- Construction ULS (GZT)  $\equiv$  DUL : partial load factor  $\gamma_{G,static} = 1.35$   
partial material factor concrete  $\gamma_{c,static} = 1.5$ .

On the resistance side: In aerospace for  $R$  so-called *strength design allowables* are applied (see definitions)  $\rightarrow$  A-values and B-values (these higher B-values also allowed for the redundant multi-directional laminates).

\*Unfortunately, still nowadays, instead of the term strength design allowable the not anymore allowed old term 'allowable stress' is used, despite of the fact that

$$\text{Allowable stress} \cdot j \equiv \text{Strength design allowable } R.$$

\*And mind, please (I'm sorry, but unfortunately I must say that again and again):

*A FoS is given for the design dimensioning, and it is not to calculate like the MoS to demonstrate Design Verification!*

### 9.3.2 Two simple Examples for the Determination of a Reserve Factor RF

In the simplest Partial Safety Factor Concept the strength is statistically reduced and all the other uncertainties are included just in a single loading increasing 'Design Factor of Safety' [Cun12].

The material is exhausted if the material stressing effort  $Eff$  reaches 100% which means  $RF = 1$ .

Objective of the material strength analysis in the Design Verification is the determination of the reserve factor  $RF$  in the single critical locations of the structure.  $\bar{R} \rightarrow R$ .

#### **I: Isotropic Material: example Normal Concrete**

The 3D stress state FEA output is automatically to insert into the distinct SFCs. In order to check the accurate working of this a not so practical, however, challenging 3D stress state will be used in



the following  $RF$  calculation beside the checks in the uni-axial and bi-axial strength points. If all of this works, the  $RF$ s will be accurate in the sense of the applied model (hypothesis).

Negativ Effs are a physical nonsense and are to be bypassed in the calculation procedure.

General stress states activate 2 modes NF and SF. Hence, interaction is required to consider both the failure danger portions.

### **\*\*Cuntze's modal SFCs:**

Assumptions: (1) Linear elastic analysis is good enough for this brittle behaving material,  $f_{RF} \equiv RF$ , (2) Residual stresses from manufacturing are zero. (3) Non-symmetric failure body,  $\Theta \neq 1$  (only  $\Theta^{SF}$  considered, because for the NF domain due to the small tensile strength, to consider  $\Theta^{NF}$  is not necessary for this example)

Loading: Stress state  $\{\sigma\} = (\sigma_x, \sigma_y, \sigma_z, \tau_{yz}, \tau_{zx}, \tau_{xy})^T \equiv (\sigma_I, \sigma_{II}, \sigma_{III})^T = (2, -15, -40)^T$

Strength design allowables:

$R^t = 4$ ,  $R^c = 40$ , assumed  $R^{tt} = 0.8 \cdot R^t$ ,  $R^{cc} = 49$ ,  $R^{ttt} = 2.81$  for cap [MPa]

After Awaji-Sato  $\rightarrow$  Weibull-based estimation  $R^{ttt} = R^t / 3^{-M}$  with  $M = \ln(2) / \ln(R^t / R^{tt})$

SFC Model with model parameters:

The modal SFC models

$$Eff^{NF} = c^{NF} \cdot \frac{\sqrt{4J_2 \cdot \Theta^{NF} - I_1^2 / 3 + I_1}}{2 \cdot R^t} = \frac{\sigma_{eq}^{NF}}{R^t} \leftrightarrow Eff^{SF} = \frac{c_{2\Theta}^{SF} \cdot I_1 + \sqrt{(c_{2\Theta}^{SF} \cdot I_1)^2 + 12 \cdot c_{1\Theta}^{SF} \cdot 3J_2 \cdot \Theta^{SF}}}{2 \cdot R^c} = \frac{\sigma_{eq}^{SF}}{R^c}$$

$$\Theta^{NF} = \sqrt[3]{1 + d^{NF} \cdot \sin(3\vartheta)} = \sqrt[3]{1 + d^{NF} \cdot 1.5 \cdot \sqrt{3} \cdot J_3 \cdot J_2^{-1.5}}, \Theta^{SF} = \sqrt[3]{1 + d^{SF} \cdot 1.5 \cdot \sqrt{3} \cdot J_3 \cdot J_2^{-1.5}}$$

Lode angles of failure points given on the meridians:

$$\text{tensile meridian } 30^\circ \rightarrow \Theta^{NF} = \sqrt[3]{1 + d^{SF} \cdot (+1)}; \text{ compr. meridian } -30^\circ \rightarrow \Theta^{SF} = \sqrt[3]{1 + d^{SF} \cdot (-1)}$$

Model parameters

For the diagram  $s_{cap} = -0.85$ . From estimation via fracture angle  $\mu = -Cc/Sc$ ,  $Cc = \cos(2\Theta_{fp}^c \cdot \pi/180^\circ)$ ,

$$Sc = \sqrt{1 - Cc^2}, \text{ the friction parameter } c_{2\Theta}^{SF} = (1+3\mu)/(1-3\mu), c_{1\Theta}^{SF} = (1 + c_{2\Theta}^{SF}) / \sqrt[3]{1 - d^{SF}}$$

Examples:  $\Theta_{fp}^c = 49^\circ \rightarrow c_{2\Theta}^{SF} = 2.46$ ,  $\mu = 0.14$ ;  $\Theta_{fp}^c = 51^\circ \rightarrow c_{2\Theta}^{SF} = 4.52$ ,  $\mu = 0.21$ .

$$Eff = [(Eff^{NF})^m + (Eff^{SF})^m]^{m^{-1}} \rightarrow f_{RF} \equiv RF = 1 / Eff$$

$$Eff = \sqrt[m]{\left(\frac{\sqrt{4J_2 \cdot 1 - I_1^2 / 3 + I_1}}{2 \cdot \bar{R}^t}\right)^m + \left(\frac{c_{2\Theta}^{SF} \cdot I_1 + \sqrt{(c_{2\Theta}^{SF} \cdot I_1)^2 + 12 \cdot c_{1\Theta}^{SF} \cdot 3J_2 \cdot \Theta^{SF}}}{2 \cdot \bar{R}^c}\right)^m}$$

Reserve Factors, 120° rotationally symmetric body: calculation using the Mathcad code

Shape parameters:  $c_2\Theta_{SF} = 3.86$   $c_1\Theta_{SF} = 6.1$   $d_{SF} = 0.493$

Statistically reduced Strengths:

Stress state:  $\sigma_I := 2$   $\sigma_{II} := -15$   $\sigma_{III} := -40$

$mint := 2.7$

$R_t := 4$   $R_c := 40$

$R_{ttt} := 2.81$

$R_{tt} := 0.8 \cdot R_t$   $R_{cc} := 49$

$$I_1 := \sigma_I + \sigma_{II} + \sigma_{III}$$

$$J_2 := \frac{(\sigma_I - \sigma_{II})^2 + (\sigma_{II} - \sigma_{III})^2 + (\sigma_{III} - \sigma_I)^2}{6}$$

$$J_3 := \frac{(2 \cdot \sigma_I - \sigma_{II} - \sigma_{III}) \cdot (2 \cdot \sigma_{II} - \sigma_I - \sigma_{III}) \cdot (2 \cdot \sigma_{III} - \sigma_{II} - \sigma_I)}{27}$$

$$\sqrt{4 \cdot J_2 - \frac{1}{3} \cdot I_1^2} = -I_1 \quad \text{Limit negativ}$$

$$J_{2NF} = \frac{I_{1NF}^2}{3}$$

$$\Theta_{SF} := \sqrt[3]{1 + d_{SF} \cdot 1.5 \cdot 3^{0.5} \cdot J_3 \cdot J_2^{-1.5}}$$

$$\sigma_I := \begin{cases} \sigma_I & \text{if } \sigma_I > 0 \\ 0 & \text{otherwise} \end{cases} \quad \sigma_{II} := \begin{cases} \sigma_{II} & \text{if } \sigma_{II} > 0 \\ 0 & \text{otherwise} \end{cases}$$

$$Eff_{SF} := \frac{\frac{1}{2} \cdot c_2 \Theta_{SF} \cdot I_1 + \frac{1}{2} \cdot (c_2 \Theta_{SF}^2 \cdot I_1^2 + 12 \cdot c_1 \Theta_{SF} \cdot J_2 \cdot \Theta_{SF})^{0.5}}{R_c}$$

$$\sigma_{III} := \begin{cases} \sigma_{III} & \text{if } \sigma_{III} > 0 \\ 0 & \text{otherwise} \end{cases}$$

$$Eff_{SF} = 0.81$$

$$I_{1NF} := \sigma_I + \sigma_{II} + \sigma_{III} \quad J_{2NF} := \frac{(\sigma_I - \sigma_{II})^2 + (\sigma_{II} - \sigma_{III})^2 + (\sigma_{III} - \sigma_I)^2}{6}$$

$$Eff_{NF} := \frac{\sqrt{4 \cdot J_{2NF} - \frac{1}{3} \cdot I_{1NF}^2} + I_{1NF}}{2 R_t}$$

$$Eff_{NF} = 0.5$$

$$Eff := (Eff_{NF}^{mint} + Eff_{SF}^{mint})^{\frac{1}{mint}}$$

$$Eff = 0.89 \quad RF := \frac{1}{Eff} \quad RF = 1.13$$

Estimation of fracture parameter via guess of fracture angle

$$\Theta_{fpc} := 50.5 \quad C_c := \cos\left(2 \cdot \Theta_{fpc} \cdot \frac{\pi}{180}\right) \quad S_c := \left(\sqrt{1 - C_c^2}\right) \quad \mu := -\frac{C_c}{S_c} \quad c_2\Theta_{SF} := \frac{1 + 3 \cdot \mu}{1 - 3 \cdot \mu} \quad c_2\Theta_{SF} = 3.8$$

$$C_c = -0.191 \quad S_c = 0.98 \quad \mu = 0.194$$

$$(\sigma_I, \sigma_{II}, \sigma_{III})^T = (4, 0, 0)^T \Rightarrow Eff = 1.0, RF = 1/Eff = 1$$

$$(\sigma_I, \sigma_{II}, \sigma_{III})^T = (2, 2, 0)^T \Rightarrow Eff = 1.0, RF = 1/Eff = 1$$

$$(\sigma_I, \sigma_{II}, \sigma_{III})^T = (0, 0, -40)^T \Rightarrow Eff = 1.0, RF = 1/Eff = 1$$

$$(\sigma_I, \sigma_{II}, \sigma_{III})^T = (0, -49, -49)^T \Rightarrow Eff = 1, RF = 1/Eff = 1$$

$$(\sigma_I, \sigma_{II}, \sigma_{III})^T = (0, -15, -40)^T \Rightarrow Eff = 0.72, RF = 1/Eff = 1.39$$

$$(\sigma_I, \sigma_{II}, \sigma_{III})^T = (2, -15, -40)^T \Rightarrow Eff = 0.89, RF = 1/Eff = 1.13$$

- Loading could be further monotonically increased by the factor  $RF = f_{RF}$  to reach fracture.
- Mode SF is the slightly higher design driving mode, visualized by  $Eff^{SF}$ .
- 

\*\* For comparison, Drucker-Prager's global SFC, rotationally-symmetric body (cone):

This SFC is often used in civil engineering. It was introduced to deal with the 'plastic' (in-elastic) deformation of soils. It and its many variants have been applied to rock, concrete, polymers, foams, and other pressure-dependent (this means that  $I_1$  is used) construction materials.

$$\frac{\sqrt{J_2} - B \cdot I_1}{A} = 1 \rightarrow Eff = \frac{\sqrt{J_2} - B \cdot I_1}{A} \quad \text{with } B = \frac{\sqrt{J_{2c}} - \sqrt{J_{2t}}}{I_{1c} - I_{1t}}, A = \sqrt{J_{2t}} - B \cdot I_{1t}$$

$$I_{1t} = R_t, I_{1c} = -R_c, \sqrt{J_{2t}} = R_t^3 / 3, \sqrt{J_{2c}} = R_c^3 / 3.$$

For the civil engineers basically the SF domain is of interest.

$$\begin{aligned} (\sigma_I, \sigma_{II}, \sigma_{III})^T &= (4, 0, 0)^T & \Rightarrow Eff = 1.0, RF = 1/Eff = 1 \\ (\sigma_I, \sigma_{II}, \sigma_{III})^T &= (2, 2, 0)^T & \Rightarrow Eff = 1.0, RF = 1/Eff = 1 \\ (\sigma_I, \sigma_{II}, \sigma_{III})^T &= (0, 0, -40)^T & \Rightarrow Eff = 1.0, RF = 1/Eff = 1 \\ (\sigma_I, \sigma_{II}, \sigma_{III})^T &= (0, -49, -49)^T & \Rightarrow Eff = -4.3, RF = 1/Eff = -0.23 \\ (\sigma_I, \sigma_{II}, \sigma_{III})^T &= (0, -15, -40)^T & \Rightarrow Eff = -1.4, RF = 1/Eff = -0.73 \\ (\sigma_I, \sigma_{II}, \sigma_{III})^T &= (2, -15, -40)^T & \Rightarrow Eff = -0.93, RF = 1/Eff = -1.07 \end{aligned}$$

An automatic application of Drucker-Prager's model above is not possible and can be not recommended. Just the uni-axial strength points are captured, bi-axial compressive strength not.

### \*\* Ottosen's global SFC

N.S. Ottosen improved above situation by applying  $\mathcal{J}(J_3)$ , thereby capturing the 120° symmetry with the bi-axial strength point. As with Cuntze's SFC models he includes 4 model parameters  $A, B, K_1, K_2$ . Required test points are:  $\bar{R}^t, \bar{R}^c, \bar{R}^{cc} + 1$  point on compressive meridian.

Ottosen's 4-parameter failure criterion for concrete has the form:

$$A \cdot \frac{J_2}{(\bar{R}^c)^2} + \Lambda(K_1, K_2(\mathcal{J}, J_3)) \cdot \frac{\sqrt{J_2}}{\bar{R}^c} + B \cdot \frac{I_1}{\bar{R}^c} = 1.$$

The Ottosen model was not investigated.

### II: *Transversely-Isotropic UD (sheet) Material:*

The use of the absolute sign avoids the computation of senseless negative  $Eff$ s.

Loading may be increased by the factor  $RF$  until obtaining the fracture failure Limit State at  $Eff = 100\% \equiv RF = 1$

Assumption: Linear elastic problem is valid for the envisaged brittle behaving CFRP

Residual stresses : 0 (effect vanishes with increasing micro-cracking)

Stress state vector :  $\{\sigma\} = (\sigma_1, \sigma_2, \sigma_3, \tau_{23}, \tau_{31}, \tau_{21})^T = (0, -60, 0, 0, 0, 50)^T$

Strengths vector:  $\{R\} = (R_{//}^t, R_{//}^c, R_{\perp}^t, R_{\perp}^c, R_{\perp//})^T = (1050, 725, 32, 112, 79)^T$  MPa or N/mm<sup>2</sup>

estimated from  $\{\bar{R}\} = (1378, 950, 40, 125, 97)^T$

Mode interaction exponent:  $m = 2.7$  and Friction value :  $\mu_{\perp//} = 0.3, (\mu_{\perp\perp} = 0.35)$

$$Eff^{\perp\sigma} = \frac{\sigma_2 - |\sigma_2|^*}{2 \cdot \bar{R}_{\perp}^t} = 0, \quad Eff^{\perp\tau} = \frac{-\sigma_2 + |\sigma_2|}{2 \cdot \bar{R}_{\perp}^c} = 0.60, \quad Eff^{\perp//} = \frac{|\tau_{21}|}{\bar{R}_{\perp//} - \mu_{\perp//} \cdot \sigma_2} = 0.51$$

$$Eff^m = (Eff^{\perp\sigma})^m + (Eff^{\perp\tau})^m + (Eff^{\perp//})^m$$

$$\Rightarrow Eff = 0.72, f_{RF} = 1 / Eff = 1.39, MoS = f_{RF} - 1 = 0.39.$$

#### 9.4 Failure Index $|F|$ versus Material Stressing Effort $Eff$ , Example UD 3D-stress state

The use of  $|F|$  alone is only possible if a ‘global’ SFC is applied. In the case of the physically better mapping ‘modal’ SFCs an interaction of the modes is faced and  $Eff$ s are required to ‘feed’ the interaction equation.

In design, from cyclic loading comes the designation ‘Proportional Loading’ for the increase of the stress state under a loading. As ‘loading’ in general is not proportional to ‘stressing’ the concept as it is applied in the elastic static cases should read ‘proportional stressing’.

Table 9-1: Derivation of  $Eff$ s for the chosen failure function  $F$ ,  $p = pr$

##### Homogeneous mathematical function $F$

\* Concept of proportional loading (stressing): index  $p$  for principal stresses

$$F^{IFF1} = [I_2 + \sqrt{I_4}] / 2\bar{R}_\perp^c = [(\sigma_2^p + \sigma_3^p) + \sqrt{(\sigma_2^p - \sigma_3^p)^2 + 0^2}] / 2\bar{R}_\perp^c$$

$$\rightarrow [(\sigma_2^p + \sigma_3^p) + \sqrt{(\sigma_2^p - \sigma_3^p)^2}] / (2\bar{R}_\perp^c \cdot Eff^{\perp\sigma}) = 1$$

$$Eff^{\perp\sigma} \equiv [(\sigma_2^p + \sigma_3^p) + \sqrt{(\sigma_2^p - \sigma_3^p)^2}] / 2\bar{R}_\perp^c$$

$$F^{IFF2} = [a_{\perp\perp} \cdot I_2 + b_{\perp\perp} \cdot \sqrt{I_4}] / \bar{R}_\perp^c = [a_{\perp\perp} \cdot (\sigma_2^p + \sigma_3^p) + b_{\perp\perp} \cdot \sqrt{(\sigma_2^p - \sigma_3^p)^2}] / \bar{R}_\perp^c$$

$$\rightarrow [a_{\perp\perp} \cdot (\sigma_2^p + \sigma_3^p) + b_{\perp\perp} \cdot \sqrt{(\sigma_2^p - \sigma_3^p)^2}] / (\bar{R}_\perp^c \cdot Eff^{\perp\tau})$$

$$Eff^{\perp\tau} \equiv a_{\perp\perp} \cdot (\sigma_2^p + \sigma_3^p) + b_{\perp\perp} \cdot \sqrt{(\sigma_2^p - \sigma_3^p)^2} / \bar{R}_\perp^c \Rightarrow \text{no difference } |F| \leftrightarrow Eff$$

$$F^{IFF3, 2D} = \tau_{21} / (\bar{R}_{21} - \mu_{\perp\parallel} \cdot \sigma_2) \quad \text{simple 2D formulation}$$

$$\frac{\tau_{21}}{Eff^{IFF3, 2D}} / (\bar{R}_{21} - \mu_{\perp\parallel} \cdot \frac{\sigma_2}{ff^{IFF3, 2D}}) = 1 \rightarrow Eff^{IFF3, 2D} = \frac{\tau_{21} + \mu_{\perp\parallel} \cdot \sigma_2}{\bar{R}_{21}} \quad \text{not permitted}$$

$\Rightarrow Eff$  does not become zero if the driving stress becomes zero

$$\frac{\tau_{21}}{Eff^{IFF3, 2D}} / (\bar{R}_{21} - \mu_{\perp\parallel} \cdot \sigma_2) = 1 \rightarrow Eff^{IFF3, 2D} = \frac{\tau_{21}}{\bar{R}_{21} - \mu_{\perp\parallel} \cdot \sigma_2} \quad \text{permitted}$$

\* Concept of factorizing the driving stress: *invitation for discussion*

$$\rightarrow \left[ \frac{(\sigma_2^p + \sigma_3^p)}{Eff^{\perp\sigma}} + \sqrt{(\sigma_2^p - \sigma_3^p)^2} \right] / 2\bar{R}_\perp^c = 1$$

$$Eff^{\perp\sigma} \equiv (\sigma_2^p + \sigma_3^p) / [2\bar{R}_\perp^c + \sqrt{(\sigma_2^p - \sigma_3^p)^2}] ,$$

$$\rightarrow [a_{\perp\perp} \cdot (\sigma_2^p + \sigma_3^p) + b_{\perp\perp} \cdot \frac{\sqrt{(0.5 \cdot \tau_1)^2}}{Eff^{\perp\tau}}] / \bar{R}_\perp^c = 1, \quad \sigma_2^p - \sigma_3^p = 0.5 \cdot \tau_1$$

$$Eff^{\perp\tau} \equiv b_{\perp\perp} \cdot \sqrt{(\sigma_2^p - \sigma_3^p)^2} / [\bar{R}_\perp^c - a_{\perp\perp} \cdot (\sigma_2^p + \sigma_3^p)] \Rightarrow \text{difference } |F| \leftrightarrow Eff$$

##### Non-homogeneous mathematical function $F$ \* Concept of proportional loading

$$F^{IFF2} = [a_{\perp\perp} \cdot I_2 + b_{\perp\perp} \cdot I_4 / \bar{R}_\perp^c] / \bar{R}_\perp^c$$

$$\rightarrow [a_{\perp\perp} \cdot (\sigma_2^p + \sigma_3^p) + b_{\perp\perp} \cdot (\sigma_2^p - \sigma_3^p)^2 / (\bar{R}_\perp^c \cdot Eff^{\perp\tau})] / (\bar{R}_\perp^c \cdot Eff^{\perp\tau}) = 1$$

$$Eff^{\perp\tau} \equiv a_{\perp\perp} \cdot (\sigma_2^p + \sigma_3^p) + b_{\perp\perp} \cdot \sqrt{(\sigma_2^p - \sigma_3^p)^2} / \bar{R}_\perp^c, \quad \text{difference } |F| \leftrightarrow Eff .$$

Some differences shall be pointed out in the following discriminating the standard “Proportional Loading concept” from a “Failure stress-driven loading” concept. The latter is useful if the SFC does not become zero with the failure driving stress, see Mohr example below.

**LL:** (1) *In the case of a mathematically homogeneous failure function  $E_{ff} = F$ .*

(2) *Stressing is terminated if the driving shear stress or driving tensile stress becomes zero.*

## 9.5 Classical Laminate Theory CLT

### 9.5.1 Theoretical relations

There are two basic theories used to statically design composites: The *Netting Theory* neglecting the matrix loading capability completely and the *Classical Laminate Theory* (CLT) continuum-mechanically considering both the constituents of the composite the fiber and the matrix.

The **2D continuum theory**, applied to laminates, is referred to as Classical Laminate Theory (CLT, *here not cross-laminated timber as in construction*). It includes the so-called Kirchhoffian plate theory and is used to determine the in-plane stresses and in-plane strains in each individual lamina of the laminate. Principally, the procedure is not only valid for UD laminae but for ply, lamella, mat, fiber-grid. Also cross-ply textiles may be treated regarding the stiffness analysis. Decisive is the ‘smearability’. A layer is a physical sub-unit of the laminate, whereas a lamina (ply) is a computational building block in the laminate analysis which might be half of a layer, a double layer or also a single layer of a non-crimped fabric NCF.

A CLT procedure can be used in linear and non-linear analyses. For design verification the CLT-obtained (2D) intra-laminar stresses are inserted into the SFCs to judge whether a FF or an IFF limit state is met or not yet met.

In this context four specifics are regarded:

- The coordinate system with the reference plane (*in literature, unfortunately the direction of the CoS is arbitrarily chosen, however, here the right hand system is applied*)
- The fiber orientation angle  $\alpha$
- The lay-up with the laminate stacking sequence and
- The layer numbering or counting sequence (see sub-chapter 9.5.7).

In the following chapter all these specifics are pointed out.

Modeling the single ply as a solid homogenized material, then *fig1* in [Fig7.5-1](#) displays the UD material cube with the stresses in the UD lamina Coordinate System CoS, also termed material CoS.

The following assumptions are made for the UD lamina material:

- The UD lamina is macroscopically homogeneous. It can be treated as a homogenized (‘smear’) material
- The stress-strain relationship is linear
- The UD lamina is transversely-isotropic. On planes, parallel with the fiber direction  $x_1 \equiv x_{||}$ , it behaves orthotropic and on planes transverse to the fiber direction it behaves quasi-isotropic.

Different notations are used in the FEA programs and manuals.

- Matrix notation:  $\varepsilon_i, \sigma_i$ , indexed  $i = 1, 2, \dots, 6$ ,
- Engineering notation: using so-called engineering strains and stresses  $\sigma, \tau$ , indexed 1, 2, 3.

**LL:**

\*A symbolic, self-explaining indexing, especially of properties, helps to avoid mis-interpretations.

\*In many FEA manuals the normal technical (engineering) stresses and normal strains are doubly indexed.

Forgive the 'upper pedantic' author: What for? It is not tensor-linked anymore and therefore not accurate. Still in 1970 NASA did the differences exactly display in a fiber-reinforced composite 'Glossar'.

In *Table 9.5-1* the 3D compliance matrices  $[S] = [C]^{-1}$  of the three material families were presented. Elasticity matrices  $[C]$  were not fully displayed because of their complexity. The compliance matrix is simpler and used in test data evaluation for the determination of the elasticity 'constants'.

*Table 9.5-1: 2D elasticity matrix [Q] and compliance matrix [S]. 1 ≡ ||, 2 ≡ ⊥*

|  |  |
|--|--|
| <p style="text-align: center;"><b>UD lamina</b></p> $\{\varepsilon\}_k = (\varepsilon_1, \varepsilon_2, \gamma_{21})_k^T = [S]_k \{\sigma\}_k \quad \{\sigma\}_k = (\sigma_1, \sigma_2, \tau_{21})_k^T = [Q]_k \{\varepsilon\}_k$ $\varepsilon_i = S_{ij} \sigma_j \quad \sigma_i = Q_{ij} \varepsilon_j \quad (i, j = 1, 2, 6) \quad \text{i.e. } (\varepsilon_6 \equiv \gamma_{21}, \sigma_6 \equiv \tau_{21})$ $\begin{Bmatrix} \varepsilon_1 \\ \varepsilon_2 \\ \gamma_{21} \end{Bmatrix} = \begin{bmatrix} S_{11} & S_{12} & 0 \\ S_{21} & S_{22} & 0 \\ 0 & 0 & S_{66} \end{bmatrix} \begin{Bmatrix} \sigma_1 \\ \sigma_2 \\ \tau_{21} \end{Bmatrix} \quad \begin{Bmatrix} \sigma_1 \\ \sigma_2 \\ \tau_{21} \end{Bmatrix} = \begin{bmatrix} Q_{11} & Q_{12} & 0 \\ Q_{21} & Q_{22} & 0 \\ 0 & 0 & Q_{66} \end{bmatrix} \begin{Bmatrix} \varepsilon_1 \\ \varepsilon_2 \\ \gamma_{21} \end{Bmatrix}$ <p>Maxwell-Betti <math>v_{\perp\parallel} E_{\perp} = v_{\parallel\perp} E_{\parallel}</math> (material) stiffness matrix</p> $[S] = \begin{bmatrix} \frac{1}{E_{\parallel}} & \frac{-v_{\perp\parallel}}{E_{\parallel}} & 0 \\ \frac{-v_{\perp\parallel}}{E_{\parallel}} & \frac{1}{E_{\perp}} & 0 \\ 0 & 0 & \frac{1}{G_{\perp\parallel}} \end{bmatrix} \quad [Q] = \begin{bmatrix} \frac{E_{\parallel}}{1-v_{\perp\parallel}v_{\parallel\perp}} & \frac{v_{\perp\parallel}E_{\perp}}{1-v_{\perp\parallel}v_{\parallel\perp}} & 0 \\ \frac{v_{\perp\parallel}E_{\parallel}}{1-v_{\perp\parallel}v_{\parallel\perp}} & \frac{E_{\perp}}{1-v_{\perp\parallel}v_{\parallel\perp}} & 0 \\ 0 & 0 & G_{\perp\parallel} \end{bmatrix}$ $[Q] = [S]^{-1}$ $\{\alpha_T\}_k = (\alpha_{T\parallel}, \alpha_{T\perp}, 0)_k^T \quad \{\alpha_M\}_k = (\alpha_{M\parallel}, \alpha_{M\perp}, 0)_k^T$ $\{\varepsilon\}_k = [S]_k \{\sigma\}_k + \{\varepsilon_H\}_k \quad \{\sigma\}_k = [Q]_k \cdot (\{\varepsilon\}_k - \{\varepsilon_H\}_k)$ $\{\varepsilon_H\}_k = \Delta T_k \{\alpha_T\}_k + \Delta M_k \{\alpha_M\}_k$ | <p style="text-align: center;"><b>Fabric lamina</b></p> $\begin{Bmatrix} \varepsilon_W \\ \varepsilon_F \\ \varepsilon_{FW} \end{Bmatrix} = \begin{bmatrix} \frac{1}{E_W} & \frac{-v_{WF}}{E_F} & 0 \\ & \frac{1}{E_F} & 0 \\ \text{(symm.)} & & \frac{1}{G_{FW}} \end{bmatrix} \begin{Bmatrix} \sigma_W \\ \sigma_F \\ \tau_{FW} \end{Bmatrix}$ $v_{FW} E_F = v_{WF} E_W$ <p>Which Poisson's ratio will be the larger depends on the fibre volume contents ratio for warp and fill.</p> <p style="text-align: center;"><b>Mat lamina</b></p> $\begin{Bmatrix} \varepsilon_x \\ \varepsilon_y \\ \varepsilon_{xy} \end{Bmatrix} = \begin{bmatrix} \frac{1}{E} & \frac{-\nu}{E} & 0 \\ & \frac{1}{E} & 0 \\ \text{(symm.)} & & \frac{1}{G} \end{bmatrix} \begin{Bmatrix} \sigma_x \\ \sigma_y \\ \tau_{xy} \end{Bmatrix}$ $G = \frac{E}{2 \cdot (1 + \nu)}$ |
|--|--|

**Rotation of the UD lamina into the laminate**

$$\{\varepsilon'\} = (\varepsilon_x, \varepsilon_y, \gamma_{xy})^T = [T_{\varepsilon}] \cdot \{\varepsilon\} = [S'] \{\sigma'\} + \{\varepsilon_H\}$$

$$\{\sigma'\} = (\sigma_x, \sigma_y, \tau_{xy})^T = [T_{\sigma}] \cdot \{\sigma\} = [Q'] \{\varepsilon'\}$$

$$\{\sigma\}_k = [Q]_k \cdot (\{\varepsilon\}_k - \{\varepsilon_H\}_k)$$

$$s = \sin \alpha, \quad c = \cos \alpha, \quad [T_{\varepsilon}]^{-1} = [T_{\sigma}]^T$$

$$[T_{\sigma}] = \begin{bmatrix} c^2 & s^2 & -2sc \\ s^2 & c^2 & 2sc \\ sc & -sc & (c^2 - s^2) \end{bmatrix} \quad [T_{\varepsilon}] = \begin{bmatrix} c^2 & s^2 & -sc \\ s^2 & c^2 & sc \\ 2sc & -2sc & (c^2 - s^2) \end{bmatrix}$$

$$\{\alpha_T'\} = (\alpha_{Tx'}, \alpha_{Ty'}, \alpha_{Txy'})^T \quad \{\alpha_M'\} = (\alpha_{Mx'}, \alpha_{My'}, \alpha_{Mxy'})^T$$

$$[Q'] = \begin{bmatrix} Q'_{11} & Q'_{12} & Q'_{16} \\ & Q'_{22} & Q'_{26} \\ \text{(symm.)} & & Q'_{66} \end{bmatrix} \begin{Bmatrix} \varepsilon_x \\ \varepsilon_y \\ \gamma_{xy} \end{Bmatrix} \quad \begin{matrix} Q'_{16} \text{ and } Q'_{26} \neq 0! \\ Q'_{11} = Q_{11} c^4 + 2(Q_{12} + 2Q_{66}) s^2 c^2 + Q_{22} s^4 \end{matrix}$$

**Hygrothermal loading**

$$\{\varepsilon_H'\} = [T_{\varepsilon}] \cdot \{\varepsilon_H\} = [T_{\varepsilon}] (\Delta T \{\alpha_T\} + \Delta M \{\alpha_M\}) = \Delta T \{\alpha_T'\} + \Delta M \{\alpha_M'\}$$

$$\{\sigma'\} = [T_{\sigma}] \cdot \{\sigma\} = [T_{\sigma}] \cdot [Q] \cdot (\{\varepsilon\} - \{\varepsilon_H\}) = [Q'] \cdot (\{\varepsilon'\} - \{\varepsilon_H'\})$$

In *Table 9.5-1* the 3D subsets = 2D-Elasticity Stress-Strain Relationships are depicted for the fiber-reinforced materials UD, fabric, mat, necessary for the application of the CLT.

After setting the 3 inter-laminar stresses zero, stress vector and strain vector read (engineering)

$\{\varepsilon\} = (\varepsilon_1, \varepsilon_2, \gamma_{12})^T$ ,  $\{\sigma\} = (\sigma_1, \sigma_2, \tau_{12})^T$  and for the  $k^{\text{th}}$  lamina in the laminate

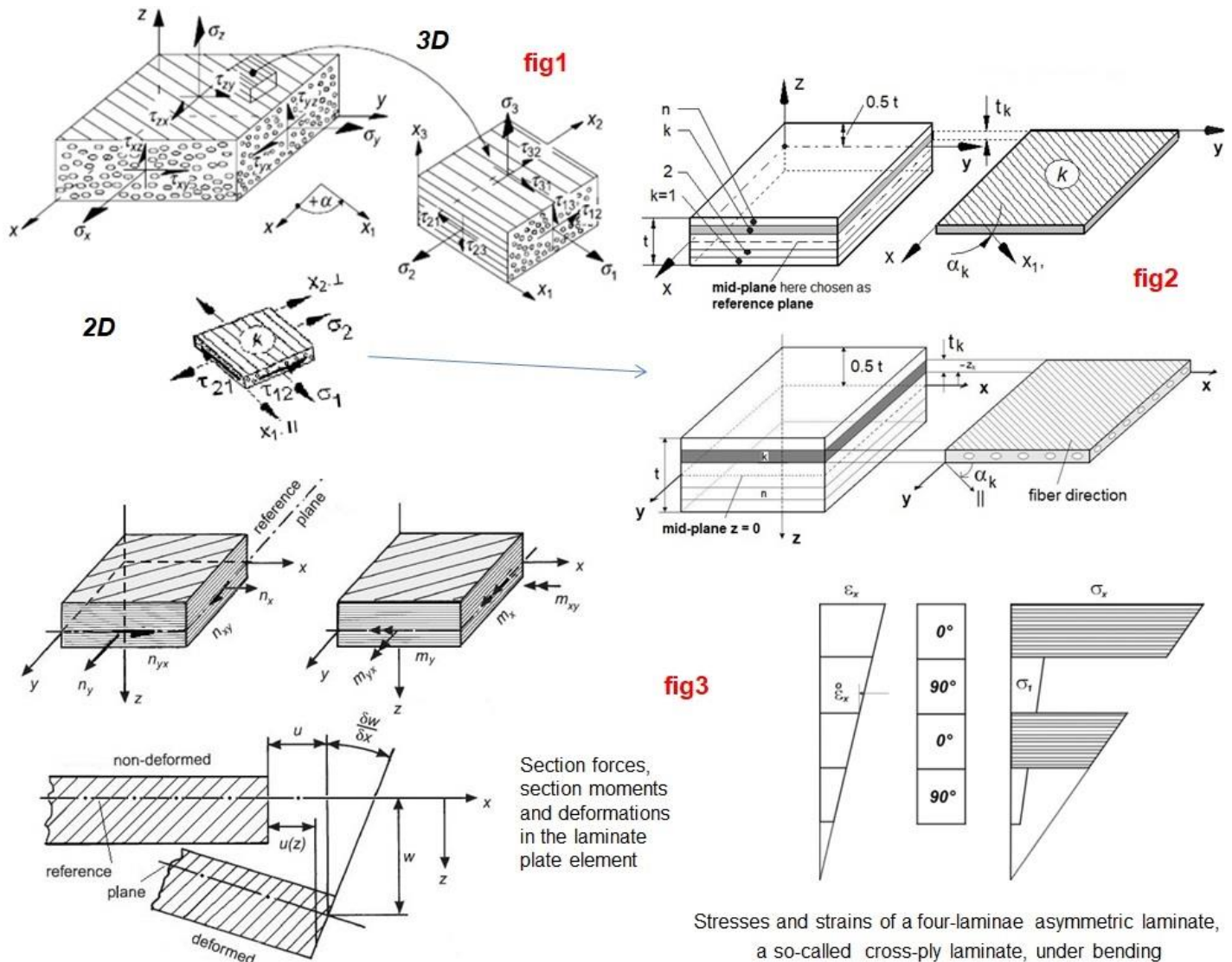
$$\{\varepsilon\}_k = [S]_k \cdot \{\sigma\}_k, \quad \{\sigma\}_k = [Q]_k \cdot \{\varepsilon\}_k \quad \text{with } [Q]_k = [S]_k^{-1}$$

with the in-plane compliance matrix  $[S]$  and  $[Q]$  denoted ‘reduced 3D stiffness matrix’  $[C]$ .

The main axes of the laminate do not generally coincide with those of the lamina. For this reason transformation relationships are required for the rotation from the laminate CoS  $x$  to the lamina (ply)  $x_1 = x_{||}$  with a positively measured  $\alpha_k$  from  $x$  to  $x_1$ . This – here freely chosen rotation, means „What does the off-axis lamina contribute to the laminate?“.

The laminate CoS is used as reference system. Each single lamina quantity is rotated by a positive angle  $\alpha_k$  from laminate CoS to the lamina CoS. Row-normalized indexing is preferred and not the column-normalized one. The relationships above are used for an in-plane stress-strain analysis.

The laminate considered in *Fig.9.5-1* the following is a plane plate with an in-plane (intra-laminar) stress state. It consists of  $n$  UD laminae each having a constant thickness  $t_k$ .



*Fig.9.5-1: Basic entities within CLT*

According to the classical thin plate theory [Kirchhoff-Love] the following pre-requisites must be observed:

- The plate thickness  $t$  is small with respect to other dimensions and the transverse deflection of the mid-plane is small compared to  $t$
- Cross-sections remain planar (Bernoulli hypothesis). This means that the thickness of the plate does not change during a deformation and that the plate is assumed to be rigid to shear stresses
- Straight lines, normal to the reference plane, remain normal.

The CLT-assumptions pre-suppose that all  $n$  laminae fully adhere to each other. Hence, the strain vector  $\{\varepsilon^i\}_k$  at any point of the plate wall at a distance of  $z_k$  from the reference plane can be expressed as  $\{\varepsilon^i\}_k = \{\varepsilon^0\} + z_k \cdot \{\kappa\}$ , where the superscript  $0$  denotes the reference plane, and where  $\{\kappa\}$  represents the curvatures.

$$\{\varepsilon^0\} = \left( \frac{\partial u^0}{\partial x}, \frac{\partial v^0}{\partial y}, \frac{\partial u^0}{\partial y} + \frac{\partial v^0}{\partial x} \right)^T, \quad \{\kappa\} = \left( -\frac{\partial^2 w^0}{\partial x^2}, \frac{\partial v^0}{\partial y}, -2\frac{\partial^2 w^0}{\partial x \cdot \partial y} \right)^T.$$

If advantageous, the geometric mid-plane is selected as reference plane. Above equation may also be used for curved shallow shells.

Strains and curvatures of the reference plane, expressed by the displacements ( $u^0, v^0, w^0$ ) or the slopes  $\varphi$  of the reference plane, respectively, are displayed in [fig.3](#) of [Fig.9.5-1](#).

Counting in  $z$ -direction,  $z_k$  denotes the distance of the more far surface of the  $k$ th layer from the reference plane  $z = 0$  and  $z_{k-1}$  denotes the difference of the surface of the  $k$ th layer less far from the reference plane,  $z_k > z_{k-1}$ . In [fig.2](#) intentionally two different  $z$ -choices are displayed.

**LL:** For avoiding misinterpretations

- ✓ Check always, by applying the Maxwell-Betti formula, that “The smaller  $\nu$  times the larger Young’s modulus  $E_1 = E_{||}$  is equal to the product of the larger  $\nu$  times the smaller Young’s modulus  $E_2 = E_3 = E_{\perp}$ ”. Maxwell-Betti works in the non-linear case, too. One should always take the larger Poisson’s ratio in [S] or [C] because the larger one is the better measurable one.
- ✓ Using symbolic suffixes reduces the danger to use a wrong property as input
- ✓ In common literature different sets of indices are used. Hence, in order to avoid a wrong input of a FEM code’s material card the actual utilization of the suffixes is to be checked. See VDI 2014, sheet 3, and later in sub-chapter 9.5.7 a note on indexing of Poisson’s ratios

The 3 section forces in  $\{n^0\}$  and the 3 section moments in  $\{m\}$  are obtained by summing up all lamina contributions over the laminate thickness  $t$ , see [Table 9.5-2](#). The vectors of the so-called section quantities, the section forces (tractions) and section moments (stress resultants per unit width), are depicted below. If ‘section quantities’ do not act in the chosen reference plane they must be transferred to it.

In [Table 9.5-2](#) [K] is the symmetric stiffness matrix of the laminate and where  $i, j = 1, 2, 6$  (the 6 considers that  $\tau_{12}$  is placed at the sixth position of the contracted 3D stress-strain relation).

The symmetric sub-matrices of [K] are termed extensional (membrane) stiffness matrix [A], coupling stiffness matrix [B] and bending (flexural) stiffness matrix [D], which are yielded by summing up the lamina portions.

- Values for each of the three section forces and section moments in  $\{n^0\}$  and  $\{m\}$  are derived from structural component analysis.



Table 9.5-2: Section quantities-strain relations

$$\begin{aligned} \{n^0\} &= (n_x^0, n_y^0, n_{xy}^0)^T = \int \{\sigma'\} dz = \sum_{k=1}^n \int_{z_{k-1}}^{z_k} \{\sigma'\}_k dz = \Sigma \int [Q']_k \{\epsilon'\}_k dz & \begin{Bmatrix} n^0 \\ m \end{Bmatrix} &= \begin{bmatrix} A & B \\ B & D \end{bmatrix} \cdot \begin{Bmatrix} \epsilon^0 \\ \kappa \end{Bmatrix} = [K] \begin{Bmatrix} \epsilon^0 \\ \kappa \end{Bmatrix} \\ \{m\} &= (m_x, m_y, m_{xy})^T = \int \{\sigma'\} z dz = \Sigma \int \{\sigma'\}_k z dz = \Sigma \int [Q']_k \{\epsilon'\}_k z dz & t_k &= z_k - z_{k-1}, z_{km} = 1/2 (z_k + z_{k-1}) \\ [A] &= \Sigma [Q']_k (z_k - z_{k-1}) = \Sigma [Q']_k t_k & [B] &= 1/2 \Sigma [Q']_k (z_k^2 - z_{k-1}^2) \\ & & &= \Sigma [Q']_k t_k z_{km} & [D] &= 1/3 \Sigma [Q']_k (z_k^3 - z_{k-1}^3) \\ & & & & &= \Sigma [Q']_k (t_k^3/12 + t_k z_{km}^2) \end{aligned}$$

(matrix of in-plane stretching or extensional stiffnesses)      (matrix of (bending-stretching) coupling stiffnesses)      (matrix of the plate or bending stiffnesses)

After integration the laminate stiffness matrix [K] is known.

Considering – beside mechanical loading – hygro-thermal loading (index <sub>H</sub>) delivers

$$\begin{Bmatrix} n^0 \\ m \end{Bmatrix} = [K] \cdot \begin{Bmatrix} \epsilon^0 \\ \kappa \end{Bmatrix} - \begin{Bmatrix} n_H^0 \\ m_H \end{Bmatrix}, \quad \begin{Bmatrix} n_H^0 \\ m_H \end{Bmatrix} = \Sigma (\Delta T_k [Q']_k t_k \{\alpha_T'\}_k + \Delta M_k [Q']_k t_k \{\alpha_M'\}_k) + \Sigma (\Delta T_k [Q']_k (z_k^2 - z_{k-1}^2) \{\alpha_T'\}_k + \Delta M_k [Q']_k (z_k^2 - z_{k-1}^2) \{\alpha_M'\}_k)$$

After calculation of  $\{\epsilon^0\}$  and  $\{\kappa\}$  of the laminate the stresses and strains in the individual laminae can be calculated with  $z = z_k$  or  $z_{k-1}$ , depending on whether the upper or lower lamina boundary is meant. If just membrane forces act, then the section forces can be formulated by smeared laminate stresses  $\hat{\sigma}$ . Dependent on the lay-up (stack) coupling between the sub-matrices is possible which may cause undesired deformations and twisting, see figure below. Units used are:  $MPa \cdot mm$  for  $A_{ij}$ ,  $MPa \cdot mm^2$  for  $B_{ij}$ ,  $MPa \cdot mm^3$  for  $D_{ij}$ . The boundary conditions considering strain and curvature must be known.

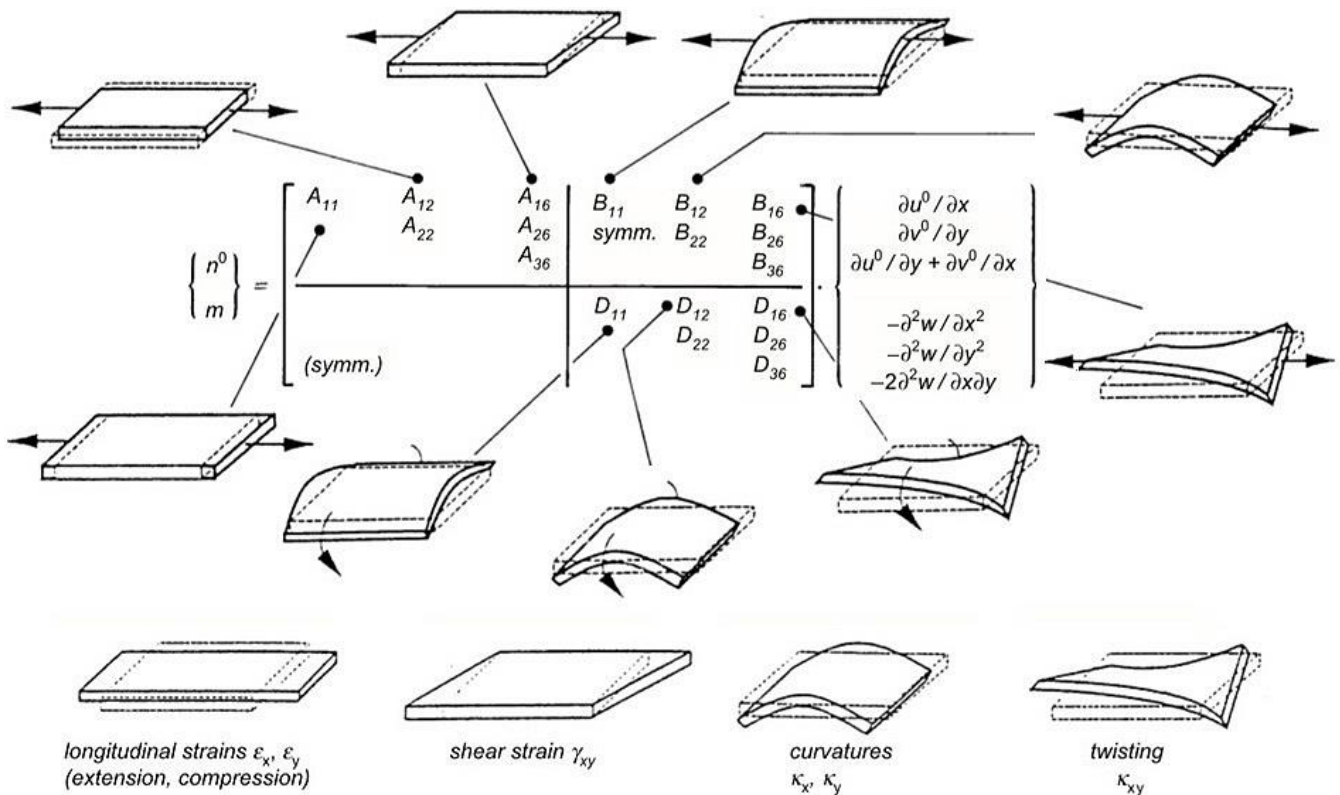


Fig.9.5-2: Effects of the stiffness components in [K]

Finally, Fig.9.5-3 displays the CLT procedure to achieve design verification for the finally chosen laminate design.

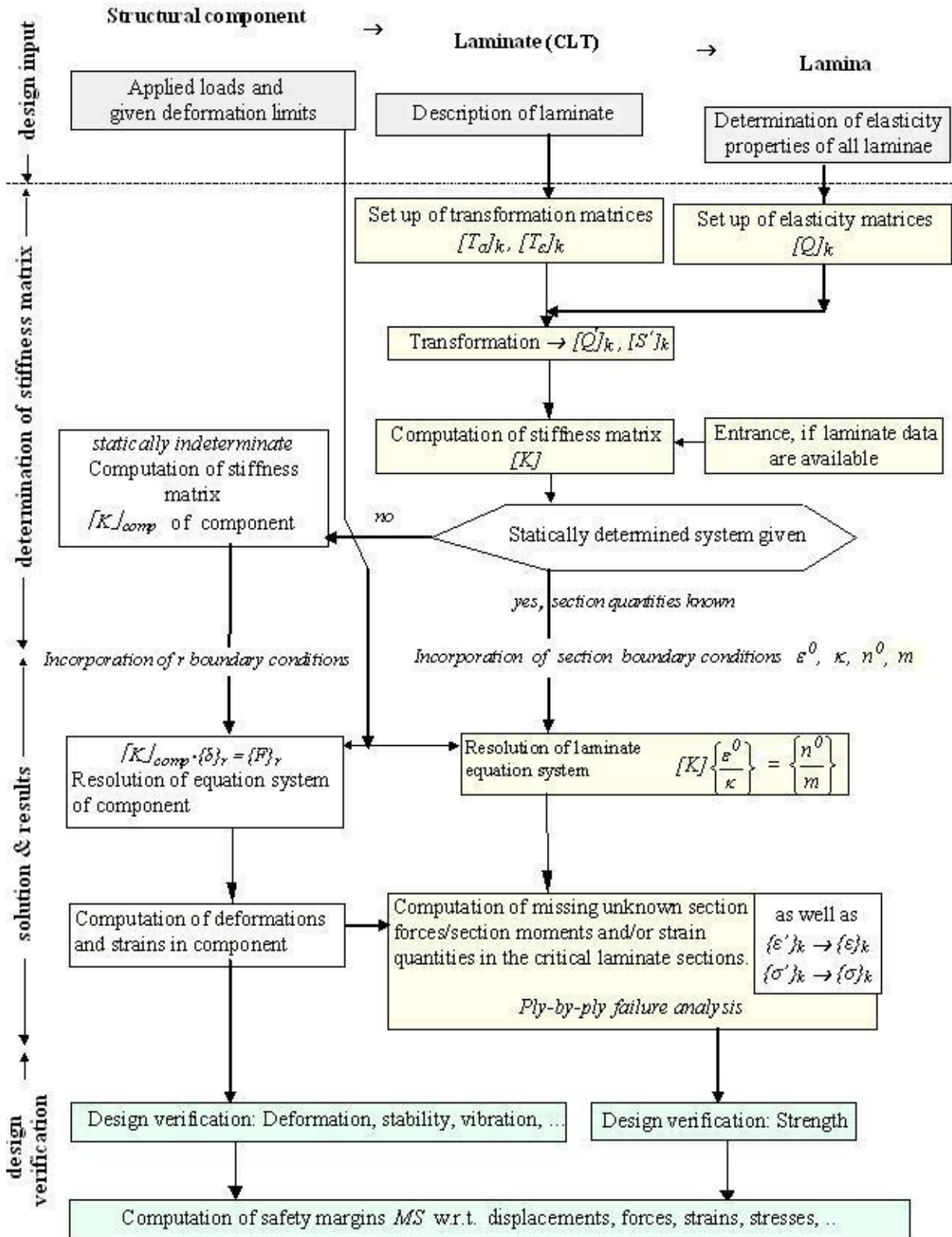


Fig.9.5-3: CLT procedure considering laminate design verification

In a HSB-sheet the 2D-CLT is extended to a 2.5 ELT (Extended LT) in order to avoid the more difficult 3D-computations

### 9.5.2 Some effects in the CLT-analysis of laminates

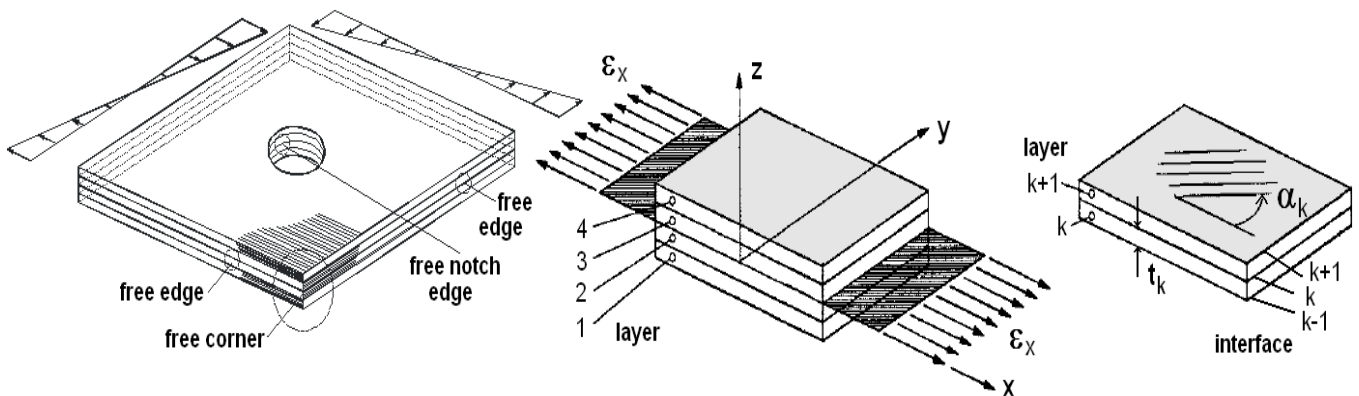
The CLT is based on the assumption of a plane state of stress. However, in the vicinity of laminate joints, at ply drop-offs and at free laminate edges, at curved notches or at straight strips, plates or coupons, a 3D state of stress is faced (next figure). These stress states occur strongly localized with the possible consequence of an undesired premature failure associated by delamination.

Due to its underlying assumptions the CLT cannot capture such a 3D stress situation. However, the CLT is a good approximation in regions remote from the edge because the 3D stress fields at the free edges decay very fast, and in the inner unperturbed laminate regions CLT prevails. Sizing of composite structures can be only reliably performed if the engineer has some knowledge about the nature of the free-edge effect and its implication, still knowing, that the free-edge stress fields are usually confined to an area of the size of about one laminate thickness  $t$ .

Free-edge effects are mainly caused by the (theoretically) abruptly changing elastic properties in the interphase of adjacent laminate layers which results in a mismatch of the stress-strain-relationship and thus in an incompatible deformation behavior. Due to this incompatibility, a pronounced and potentially even singular 3D stress field is encountered at free edges of composite laminates at the interfaces between dissimilar layers which may be of substantial influence concerning the failure behaviour of such structures. This singularity is the result of the 'simple' linear analysis modelling and not a non-linear analysis before 'onset of macro-cracking'. Under a critical edge notch or/and a distinct free edge stress state edge-delaminations can occur which cause an even higher stress singularity (stress intensity) to be treated by means of fracture mechanics.

The delamination effect is important in the assessment of test data from laminate coupons. Generally, the generated inter-laminar stresses (full 3D) decrease if the difference between the orientations of two adjacent layers decreases.

The analysis of free-edge effects is rather difficult. Exact closed-form solutions do not exist, even for the simplest thinkable cases like plane symmetrically laminated specimens under un-iaxial extension as depicted in *Fig.7.5-4*. The analysis of free-edge effects is usually performed by using adequate finite element models that require a distinct mesh refinement in the vicinity of the free edges due to the stress singularities that are encountered at the free edges. However due to the linear treatment the following result is faced: The finer the mesh the higher the singularity or the stress peak, respectively. However, the analyses gives a 'feeling' for the design variant.



*Fig.7.5-4: Sketch of a general plate strip under axial torsion. Edge problems and definitions (courtesy Mittelstedt/Becker)*

The free edge singularity cannot be assessed by strength criteria. However, it is nevertheless advantageous to alleviate the free edge effect of a laminated structural part qualitatively by comparing designs as far as possible despite of the fact that one cannot really quantify the effect.

### 9.5.3 Layer numbering and reference system choice

Non-compatible layer numbering and reference system is an essential problem for the modeller. Also a stress engineer is usually required to follow the manufacturer drawing (a) when building up his FE model. In order to avoid any mistake, the following procedure is suggested for the laminate brick (a):

- Check of ply numbering and of orientation in the manufacturing document/drawing and comparison with the CLT definition
- Check of the loading direction and comparison with the CLT definition
- If different, transformation of layer angles necessary (i.e. complementary angle with a different positive  $\alpha$  counting), layer numbering and loading into the CLT reference system is required by the analysis. The following figures shall visualize this.

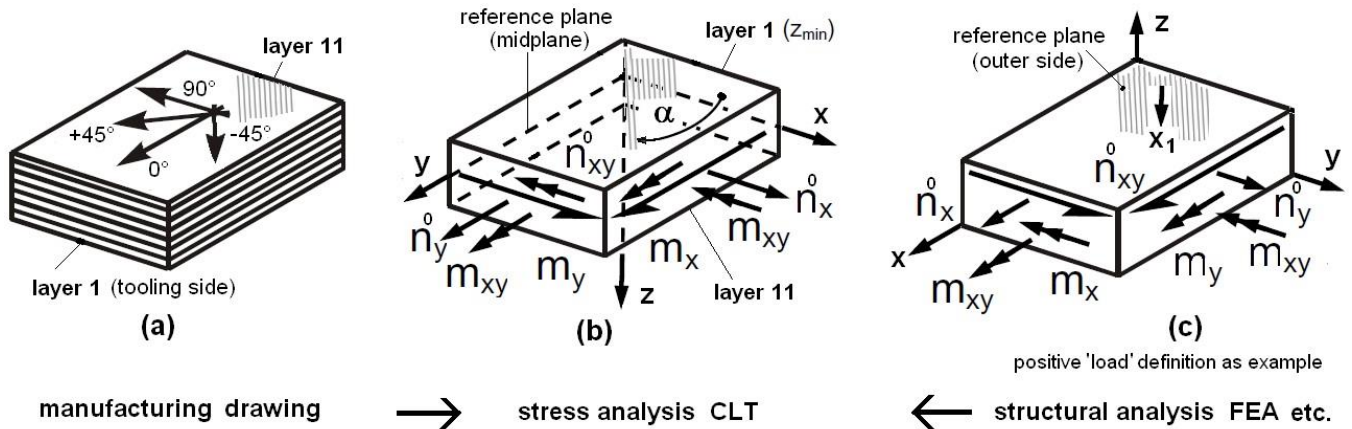


Fig.7.6-1: Layer numbering and reference system

The different worlds, which must be brought together, are now more detailed:

1. Manufacturing world, sketch (a): Given in the manufacturing drawing (a) is a lay-up [45/0/-45/90/0/0/90/-45/0/45/-45] with  $t_k = 0.125\text{mm}$ ,  $t = 1.375\text{mm}$  with the outer surface (top layer) counting 11 with an orientation angle of  $-45^\circ$
2. CLT world, sketch (b): Reference plane = mid-plane = action plane.  $\{n_0\} = (20, 40, 60)^T$  N/mm,  $\{m\} = (40, 15, 35)^T$  N·mm/mm. According to the CoS (b), which is applied in the stress analysis, the numbering and the positively angle-counted ( $x \rightarrow x_1$ ) lay-up is to be transformed into the chosen CoS of (b) obtaining [45/-45/90/45/0/90/90/0/45/90/-45]. The top layer with an orientation angle of  $+45^\circ$  counts 1, because the agreed sequence in writing the layers begins from left [45/0/..] beginning with 1 in positive direction of  $z$
3. Analysis world, FEA, sketch (c): Reference plane is bottom surface (layer 1). Further, the loading is transformed from (b) into (c). Due to the change in direction the forces and moments to be inserted in the analysis read  $\{n^0\} = (40, 20, 60)^T$  N/mm,  $\{m\} = (15 - 40 \cdot t/2, 40 - 20 \cdot t/2, 35 - 60 \cdot t/2)^T = (-12.5, 26.25, 6.25)^T$  with  $\{m\}$  in N·mm/mm,  $z_n = t/2$ . The lay-

up will be denoted in (c) as [-45/90/45/0/90/90/0/45/90/-45/45]. The top layer counts 11 with an orientation angle of  $+45^\circ$  ( $x \rightarrow x_1$ ).

4. Retransformation of the FEA-result into the stress analysis documentation convention, if applicable.

### 9.5.7 Note on indexing Poisson's ratios of UD materials in CLT

The definition of Poisson's ratios is not standardized, see e.g. *Tsai, Composites Design* with  $\nu_{12}$  (formerly). Of course, there is no objective reason for the sequence of indices or to index  $\nu_{21}$  or  $\nu_{12}$ . This might have been the cause for the different use. In the international Aerospace Handbook HSB for instance  $\nu_{12}$  is used for the larger Poisson's ratio to be conform with most of the FE manuals!

In the very early days indexing of Poisson's ratio followed 'location' before 'cause'. This makes more sense and - in addition - follows the convention for the load quantities. This is the reason why, after many discussions and extensive literature work of the VDI-working group, the VDI 2014 guideline still sticks to the 'old' sequencing  $\nu_{21} = -\varepsilon_2/\varepsilon_1$  for the larger Poisson's ratio. This indexing corresponds to a so-called 'column normalization' which allows for a simple interpretation of uni-axial tests.

By the way: Tsai uses now again the 'old' suffix sequencing 'location' before 'cause' for the major Poisson's ratio as we have stuck to in the VDI 2014, opposite to the HSB sheets. How can a provided Poisson's ratio be checked? In order to avoid misuse, each user of a program is asked to perform the Maxwell-Betti check (larger  $\nu \cdot$  smaller E-modulus = smaller  $\nu \cdot$  larger E-modulus) to become sure with the input. This check works for the lamina and the laminate as well.

**LL:** *It should be mentioned that the letter C is used for the spatial or 3D stiffness elasticity matrix and the letter S for the compliance matrix as the inverted formulation of the stiffness matrix. This is just the other way round as the letters say and is unfortunately sometimes mixed- up.*

## 9.6 Material Modelling in Additive Fabrication AF, construction-linked (Bauwesen)

Classification of manufacturing processes: Subtractive manufacturing processes (waste), Formative manufacturing processes and Additive Manufacturing processes (automatically digitized fabrication now) [VDI 2403].

1. In subtractive manufacturing processes, the geometry to be created is created by defining the removal of individual volume regions. Typical representatives of this group of manufacturing processes are machining processes such as turning, drilling or milling. (timber construction etc.)
2. Formative manufacturing refers to the production of geometries by forming in compliance with volume constancy. Formative manufacturing processes are deep drawing, forging or primary forming.
3. Additive fabrication (manufacturing) processes create a geometry by joining together volume elements (so-called "voxels"), such as the standard processes concreting, bracketing, plastering a wall etc.

The two basic digitized additive fabrication processes are:

(1) True 3D printing in construction: Total cross-section including the 'openings' is produced in a powder bed layering process. Layer thickness is usually  $\ll 1$  mm (**powder bed process** FFT for formwork production).

(2) '3D printing' = mortar-strand deposit method: Total cross-section including 'openings' is produced in a 'path tracking operation'. Layer thickness is several mm, depending on the strand thickness. (Extrusion process for walls and other compressed load-bearing structures).

Any material that can be glued, welded or melted can be used in AF (AM). For industrial purposes, metals, plastics, sand and ceramics are common, which are processed appropriately for the respective AF process.

The engineer's desire is to obtain accurate process names however the term **3D print** does not give a clear process information. Therefore some basic definitions are provided:

Printing definition: *Procedure, to apply something by pressure like printing a book*

1. 3a, ISO/ASTM 52900: Automatic digitized fabrication AF (in reality not anymore Manufacturing. AM) is a process of joining materials to make parts from 3D-model CAD data, usually layer upon layer
2. 3b, VDI-Ri-3405, Blatt 3.4, Fused (*geschmolzen*) Deposition Modelling or Fused Layer Modelling: Cold extrusion process, whereby the building material is deposited continuously via a nozzle. Transferred to construction "Extruded deposit of a mortar strand (Mörtel-Strang, -raupe). Is analogous to the so-called polymer-filament strand depositing → **Extruded mortar strand deposit** is clear for the designing engineer.

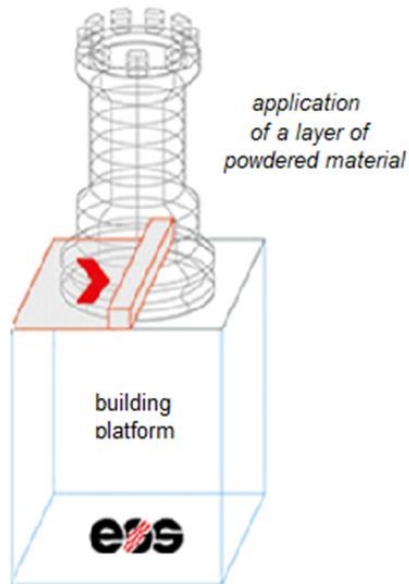
Following RILEM Technical Committee 276 the descriptions below are given:

1. 3a, **Powder-bed binding** (3D-printing. AF process in which particles are selectively joined using a bonding agent, includes binder jetting as sub-class and includes the technique Selective Laser Sintering. *Does pretty well correspond with the printing definition*
2. 3b, Material extrusion with cementitious and polymer agents ('3D-printing' → Mortar strand deposit). *Does not correspond to the printing definition but nevertheless is also used here as meaningless catchphrase "3D-print" confusing by not delivering the necessary knowledge about the actual fabrication process. One should not take the same term 3D-print" for such very different processes*

In construction above two main additive processes above can be also described as follows:

*In both processes, the layer thickness is determined digitally for each structural application.*

1. 3a, the total cross-section, including the 'openings', is produced in a 'layering process'. The layer thickness is usually much smaller than 1mm. Powder bed technique for formwork production with the steps (see *Fig.9.6-1, up left*): \* 3D geometry model or a 3D-scan info for the robot, \* application of a layer of powdered material  $< 1$ mm, \* solidification of the material, repetition by building platform lowering for the next layer, \* loose powder removed, \* complete part.
2. 3b, Mortar strand depositing: The total cross-section, including the 'openings', is produced in a 'path tracking operation'. The layer thickness is several mm, strand thickness-dependent (Extrusion process for walls). *Here, also the path is to define digitally. See Fig.9.6-1 down.*



*Fig.9.6-1: Particle-bed technique (up left), Mortar strand depositing (up, right);  
(below) Peri GmbH 2021, two-story house in Beckum*

Of interest for civil engineering are similar techniques in mechanical engineering:

- Sheet Molding Compound SMC := compound, containing short fibers (CF-SMC, GF-SMC, flächige Pressmasse, Spritzguss)
- Bulk Molding Compound BMC := compound containing short fibers (3D-SMC Pressmasse, Spritzguss)
- Shotcrete (Mörtel-Spritzguss):= process is somehow related to SMC, could be performed with and without short fibers
- (short) Fiber-Reinforced Concrete FRC:= process is somehow related to BMC.

AF-design requires knowledge about the process of the *Fresh Printable Cement-based Materials* (RILEM TC PFC) and the actual local material characteristics, valid for 3a and even more for 3b. Specific topics for mortar strand depositing are:

- 1) Gravitational flow of the deposited strand. The figure excellently depicts the primary problem. Rheology-based production process simulation is required – using computational fluid dynamics CFD - in order to finally achieve Buildability and Shape Stability of the freshly manufactured part.
- 2) Appropriate recipes for the mortar in order to achieve the desired time- and path dependent consolidation
- 3) No dispersion of admixture in print head
- 4) Bypassing the 2 failure modes: (1) material failure (material flows away, because the current yield strength is too low for the mass upon). (2) Structural failure (the erected wall loses its stability).
- 5) Material characterization, time-dependent properties of the fresh mortar after being deposited and further in the build-up process with consolidation
- 6) Introduction of armoring to withstand usual bending of the structural part by short, long and endless fibers (coming up)
- 7) Post-processing (rough surface)
- 8) Quality assurance of mortar, fibers, concrete and fabrication process
- 9) Fabrication process with 'real' reinforcement of components that can be tension-stressed and not only compression-stressed. Possibilities: (1) mortar, (2) concrete and vice versa. Slack armoring and pre-tensioning of structural elements
- 10) Static & cyclic fatigue due to notched layers and surface
- 11) Normative-linked Dimensioning. Special load-bearing capability certificate necessary approval procedure (ZiE).

Combining process analysis with structural analysis is the challenging task.

Extrusion-based processes require a speed, time and cross-section of the strand-depending knowledge of the material flow with a good knowledge about the following solidification of the material strand (see i.e. [Mec21]).\*

For the modelling engineer facing, ‘*Mortar Strand Depositing*’, there are many variants to model:

- Fully isotropic mortar without any steel- and fiber-reinforcement,
- Reinforcement with polymer filament strands or stochastically mixed with short fibers
- Production-directed short fiber reinforcements are anisotropically to model
- Design verification of classical armoring by endless reinforcements remains as before .

## **9.7 Average Properties and Average Stress-strain Curve**

### **9.7.1 Average strength values**

Remind at first, please: *Strengths and strains are derived quantities, which cannot be directly measured. They are by standards ‘commonly agreed definitions’.*

#### Aerospace Engineering

Usually lower bound design values, namely strength design allowables, are published. In order to perform the best prediction of the average structural behavior or to perform a distinct fatigue life and damage tolerance analysis mean (average) values are required.



Not to forget, structural test evaluation on the different test levels also require mean value and mean stress-strain curve. This is not a problem if on structural element ('coupon') level material test may be run. However, it becomes difficult on sub-component and on component level where different material batches are often applied, possibly even from different suppliers.

As in aerospace just lower bound A- and B- strength design values are provided the task given is to estimate from these values the average design values.

As a rough estimation may serve (*a better proposal is going to be published in the HSB*):

$$\text{Mean (average) of basic population } \mu \approx \text{B-value} / (1 - 2 \cdot \text{cov}_\mu) \text{ and}$$

$$\mu \approx \text{A-value} / (1 - 3 \cdot \text{cov}_\mu) \text{ with the coefficient of variation cov.}$$

The table from Airbus below, discussed during several IASB meetings, shows a concept for the various 'Strength Design Values' applied.

| Material Supplier                                   | Customer                                      |   |  |   |
|---|---|---|--|---|
| <b>Manufacture 1</b><br>raw data,<br>T99 / T90 data | In-house tests<br>raw data,<br>T99 / T90 data | Pooling of T data,<br><br>S-value adjustment,<br>Material Procurement | Determination of <b>Strength Design Allowables</b> (A-, B-values) based on statistical rules in MMPDS Hdbk (formerly MIL Hdbk 5) | approval by handbook committee, agency etc. |
| <b>Manufacture 2</b><br>raw data,<br>T99 / T90 data |   |   |  |   |
| <b>Manufacture n</b><br>raw data,<br>T99 / T90 data |   |   |  |   |
|   |   | for design + analysis   | for design verification  |   |

**S-value:** Procurement value

**A-, B-value:** Strength Design Allowables. Statistically defined like T99/T90 –values. Number of different batches is required, on top.

**T99/T90-values:** Material strength allowables. The determination follows the same statistical procedure as with the Strength Design Allowables A, B. However, the data volume and batch requirements are less stringent.  $A > S$ , only allowed if premium selection of material is applied. Normally  $A < S$ .

Fig.9.7-1: 'Strength Design Values' in aerospace

### Construction

The same is required in construction because the so-called characteristic value is – in contrast to other disciplines – not an average value but a still statistically reduced one, the 5% fractile or quantile. A proposal is going to be prepared!

### 9.7.2 Average stress strain curves (hardening branch)

Non-linear stress-strain analysis should use the average strengths  $\{\bar{R}\}$  and the average stress-strain curve and thereby the average stiffness, especially if the structure is statically indeterminate. In this

case, design dimensioning and verification of the chosen design use  $\{\bar{R}\}$  and average stress-strain curve. Otherwise the presented examples WWFE-II, TC2→TC4 could not have been solved ! still mentioned, for the solution of specific tasks an average stress-strain curve is required.

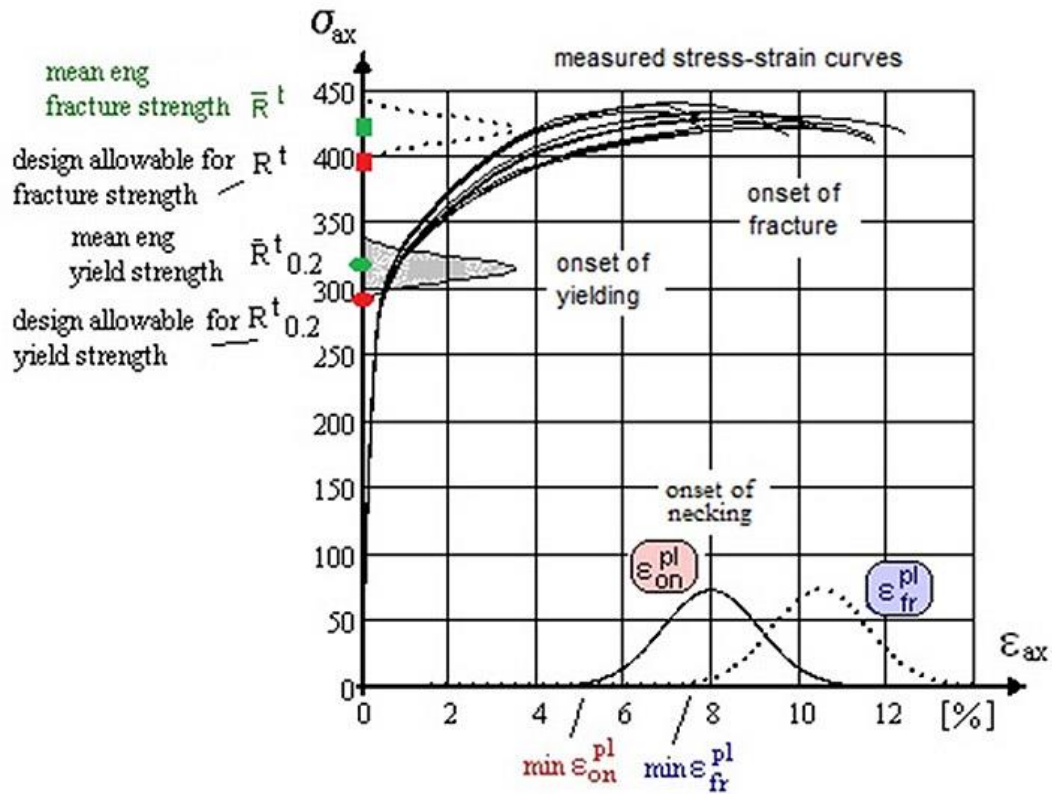


Fig.9.7-2: Average stress–strain curve versus average fracture strain and average strength strength.  
Example aluminum alloy

Fig.9.7-3, at the onset-of-necking the stress must be linked to the reduced area, engineering stress should be replaced by a true stress in analysis.

Total strain curve, mapped with Ramberg-Osgood approach (see also chapter 3.10 for details)

$$\varepsilon = \varepsilon^{el} + \varepsilon^{pl} = \sigma / E_0 + 0.002 (\sigma / \bar{R}_{0.2}^t)^{\bar{n}} \quad \text{with } \bar{n} = \ln(\varepsilon^{pl}(\bar{R}^t)) / \ln(\bar{R}^t / \bar{R}_{0.2}^t).$$

Flow strain curve, defined as plastic part, only:  $\varepsilon^{pl} = 0.002 (\sigma / \bar{R}_{0.2}^t)^{\bar{n}}$ .

$\bar{R}^t$  = ultimate tensile strength (stress at necking),  $\bar{R}_{0.2}^t$  = off-set yield strength (engin. strength)

$\bar{R}_p^t$  = proportional strength →  $\bar{R}_{0.1}^t$  (engineering value)

Another model for the flow curve is the Power law hardening formulation  $\sigma = K \cdot \varepsilon^{se}$

with  $se$  = average strain-hardening exponent,  $K$  = strengthening coefficient.

Permanent strain after constant elongation, then  $eng\sigma \rightarrow true\sigma$ .

The parameter  $n$  can be estimated from the design data  $R_{0.2}^t$ ,  $R^t$ , and  $\varepsilon_{gl}$  ( $= A_{gl}$ , Gleichmaßdehnung).

Fig.9.7-3 visualizes for a ductile metal the different parts of an engineering stress-strain curve . Engineering stress is the ratio of the acting load divided by the (non-deformed) initial area.

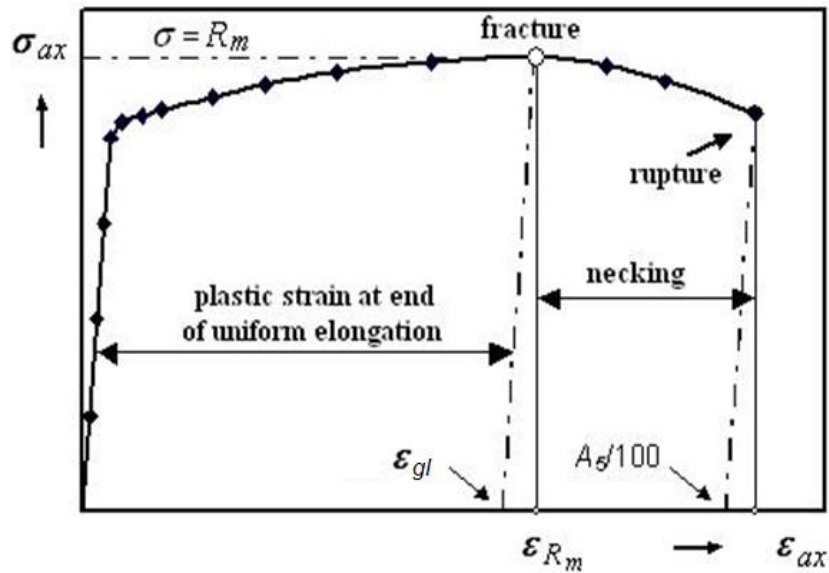


Fig.9.7-3: Typical engineering stress-strain curve of a ductile metal material. End of uniform elongation (Gleichmassdehnung  $\epsilon_{gl}$ )

**LL:**

- (1) For the best possible estimation of the component behavior, the mean stress-strain curve must be taken.
- (2) The average stress-strain curve  $\bar{\sigma}\bar{\epsilon}$  does not necessarily run through the mean points of yield  $(\bar{\sigma} - \bar{\epsilon})_{yield}$  and of fracture  $(\bar{\sigma} - \bar{\epsilon})_{fr}$ .

UD material experiences slight yielding (thermoplastics more than thermosets) from the matrix and a quasi-yielding from micro-damage. Hardening and softening curve part of the full  $\sigma$ - $\epsilon$ -curve is to map. The softening curve is just active in the case of embedded laminas deformation-controlled by the laminate. Ramberg-Osgood can be applied.

Also here the application of average curves in test data mapping is stringent.

## 10 FMC-based Fatigue Life Models, basically displayed for the brittle UD material

Cyclic (fatigue) Life consists of three phases. This means for the example laminate:

Phase I: Increasing damaging in embedded Laminas up to discrete microdamage onset

Determination of accumulating micro-damage (Schädigungen) portions initiated at end of elastic domain and dominated by diffuse micro-cracking + matrix yielding incl. cavitation under 3D tensile stressing, and finally little cracks such as micro-delaminations). Degradation begins with onset of diffuse damaging (strain hardening) until IFF1 or IFF3 occurs.

Phase II: Stable local discrete damage growth in laminate up to delamination

Growth of dominating discrete micro-crack widths incl. micro-delaminations, after onset of discrete damaging. In cyclic loading, degradation is more diffuse than for static loading.

Phase III: Final in-stabile fracture of Laminate initiated by FFs and IFF2 of any lamina and (possible) criticality of the loaded laminate due to the macro-damage delamination.

### 10.1 General and Terms

Methods for the prediction of durability (Dauerhaftigkeit) regarding the lifespan of the structural material and thereby of the component, involves long time static loading which is linked to ‘static Fatigue’ (Dauer-Standfestigkeit) and cyclic fatigue (Dauer-Schwingfestigkeit). The latter is treated here. Fatigue failure occurs if the structural material is cyclically loaded. This provokes design questions and requires a Procedure for Fatigue Life Estimation necessary for design verification:

#### ❖ Design questions

- When does micro-damage start? How can one consider a micro-damage portion?
- How can the single portions be accumulated essential for *fatigue verification*?
- When do the accumulated micro-damage portions build up macro-damage (Schaden)?
- When does such a damage (delamination in case of FRP) become so big to be of a technically critical size?
- How is then the critical damage growth (task for a *damage tolerance verification*) in this second phase of fatigue life in order to determine the part replacement time or the inspection intervals?

#### ❖ Domains of Fatigue Scenarios and Analyses

LCF: high stressing and straining

HCF: intermediate stressing  $10.000 < n < 2.000.000$  (*rotor tubes, bridges, towers, off-shore structures, planes, etc.*)

VHCF: low stress and low strain amplitudes (see SPP1466 Very High Cycle Fatigue)  $> 10^7$  cycles (*centrifuges, wind energy rotor blades, etc.*)

#### ❖ Design requirements

To consider - beside the prediction procedure - environment, material, possible failure modes, statistical basis and accelerated testing for the full design verification.

To ensure that the structure can perform its primary function during its life.

Think maintenance cost throughout life. Avoid premature failures and their costs. Consider in the case of multi-axial stress states whether amplitude and mean stress can be simplified considered as proportional and synchronous.

#### ❖ Input

- Operational (Service) Loading: Load time curves with a counting model like *rain flow*

Time domain: cycle-by-cycle or block-by-block (less computation effort) fatigue analysis

- Frequency domain: operational loading spectra (loss of loading sequence effects) fatigue analysis
  - Safety Concept: Design safety factor Life  $j_{Life} = 3 - 10$  or a project task fixed inspection interval or a replacement time
  - Procedure for the determination of the cyclic-caused micro-damage portions
  - Accumulation model like linear Palmgren-Miner or a more sophisticated non-linear one
  - Haigh Diagram  $\sigma_a(\sigma_m)$ , that represents all available necessary S-N curve information by its ‘Constant Fatigue Life (CFL) curves’
- ❖ **Transfer of operational loadings into stresses  $\sigma_a, \sigma_m$  by using structural analysis, FEA.**

LL:

- The Palmgren-Miner rule cannot account for loading sequence effects, residual stresses, and for stresses below the fatigue limit (life  $\rightarrow \infty$  ?).
- Designing light-weight structures means a reduction of dead mass. Therefore, the ratio ‘variable load / dead load’ reduces, fatigue becomes more decisive and fatigue prediction procedures become also more mandatory in construction industry, for instance!
- In the LCF regime non-linearity causing effects such as creeping, relaxation are to regard.
- Whether the material’s micro-damage driver remains the same from LCF until VHCF must be verified in each given design case.
- Whether a material has an endurance fatigue limit is usually open still regarding its ‘old’ level of  $N = 2 \cdot 10^6$  and further the lack of VHCF tests. However, e.g. CFRP has a high fatigue limit.
- A fatigue failure of brittle reinforcements is not announced by plastic deformations.
- A fatigue-related failure of compressed concrete is announced due to some cracking that is linked to some progressive deformation.

Models and Diagrams used

There are *strain-life* (plastic deformation decisive) and *stress-life* models used. Fig.8-1 displays when the elastic strain amplitude becomes dominant and this is valid for brittle materials.

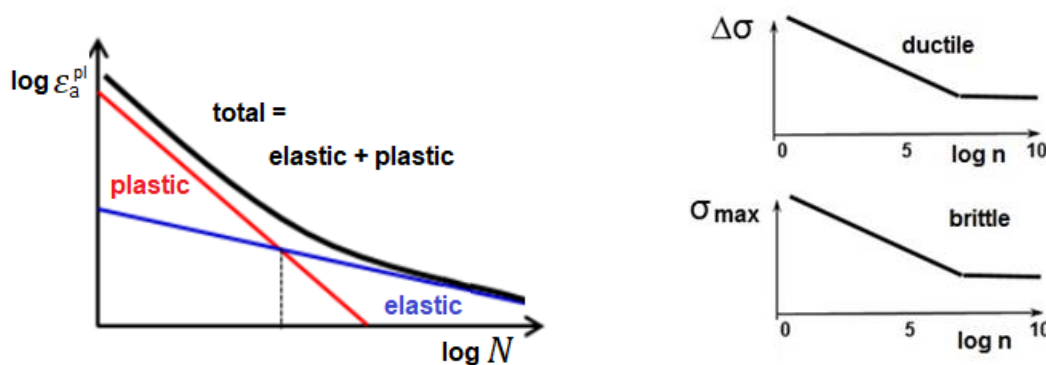


Fig.8-1: Difference of ductile and brittle materials. Plastic strain amplitude  $\epsilon_a^{pl}$

Above two models can be depicted in the Goodman diagram and in a Haigh diagram. The Goodman diagram shows the maximum tolerable stresses of the material  $\sigma_{max}$ . It is commonly used in construction specifically for concrete. The Haigh diagram will be applied here because just to use  $\sigma_a$  or  $\Delta\sigma = 2 \cdot \sigma_a$  is not sufficient in general but  $(\sigma_a, \sigma_m)$  or  $(\sigma_a, R)$ .

For ductile materials *strain-life* (strain-based) models are applied because the single yield mechanism dominates.

With brittle materials micro-damage mechanisms drive fatigue failure and several mechanisms come to act. This asks for a modal approach that captures all modes.

## Fatigue Micro-Damage Drivers of Ductile and Brittle behaving Materials

The are basic differences between ductile and brittle materials:

- Ductile Material Behavior, isotropic materials: mild steel  
*1 micro-damage mechanism acts*  $\equiv$  “*slip band shear yielding*“ drives damaging under tensile, compressive, shear and torsional cyclic stresses: *This single mechanism is the damaging driver. It is described by 1 SFC, a yield failure condition (HMH, ‘Mises’ )!*
- Brittle Behaving Material Behavior, isotropic materials: concrete, grey cast iron,  
*2 micro-damage driving mechanisms act*  $\equiv$  *2 fracture failure modes Normal Fracture failure (NF) and Shear Fracture failure (SF) under compression described by 2 fracture conditions*
- Brittle Behaving Material Behavior, transversely-isotropic materials: UD Materials,  
*5 micro-damage driving Fracture failure mechanisms act*  $\equiv$  *5 fracture failure modes described by 5 SFCs or strength fracture failure conditions.*

### State-of-the-art considering cyclic strength analysis of UD ply-composed laminates

- Experience with to-date composites of fiber-reinforced plastics FRP (fiber-dominated laminates are used in high performance stress applications whereby fiber-dominated means there are 0° plies in all significant loading directions  $\rightarrow$   $> 3$  fiber direction angles) behave brittle, experience early fatigue damage, but show benign fatigue failure behaviour in case of ‘well-designed’ laminates until a final pretty ‘Sudden Death’ occurs.
- No Lifetime Prediction Method is available, applicable to any lamina (lamella) and UD ply-composed laminate. Procedures base on specific laminate lay-ups and therefore test results cannot be generally applied. Embedded ply degradation must be non-linearly considered
- Endurance strength procedures often base – as with metals – on  $\sigma_a, \sigma_m$
- Present Engineering Approach in Mechanical Engineering:  
Up to now as Engineering Approach: Applying a *Static Design Limit Strain* of  $\varepsilon < 0.3\%$  in multi-axial laminate design practically means negligible matrix-micro-cracking. Design experience proved: No IFF-caused fatigue danger of a laminate is given  
Future: *Design Limit Strain* shall be increased beyond  $\varepsilon \approx 0.5\%$  (EU-project: MAAXIMUS to better exploit UD-materials). Then, dependent on the matrix, *first filament breaks may change the early diffuse matrix micro-cracking to a discrete and more critical localized one.*
- Present Engineering Approach in Civil Engineering for FRP materials and its semi-finished products such as a pultruded rod, a strand cut-out of a fiber-grid, lamella (tape) etc. In the case of a ‘not predominantly static loading’ (nicht vorwiegend ruhende Belastung) the required fatigue life must be demonstrated by measured S-N curves, loading spectrum and a hypothesis for the accumulation of the micro-damages are required. Bounds are set by the required minimum micro-crack width of the Serviceability Limit State SLS (GZG) and deformation restrictions for instance for bridge bending.

Considering the high-performance UD lamina-composed laminates the classical fatigue tests are performed on laminates. The idea of the author-founded Germany-wide group BeNa (in 2010) however is to base fatigue life prediction ‘embedded lamina-wise’ in order to be more general in future fatigue life design and to save test costs and time. Associated test specimens shall capture the interface effect of the lamina embedded in the laminate.

### Constant amplitude loading and variable amplitude loading:

Cyclic loadings are most often given by an operational loading spectrum with its automatic loss of the stress-time relationship.

The lifetime increasing variable amplitude loading (operational fatigue life curve, after Gaßner) of the structure in operation or service is displayed together with the harsher constant amplitude loading. A loading spectrum-representing block-loading stands for a more realistic fatigue life estimation. Good information about the loading spectrum pays off.

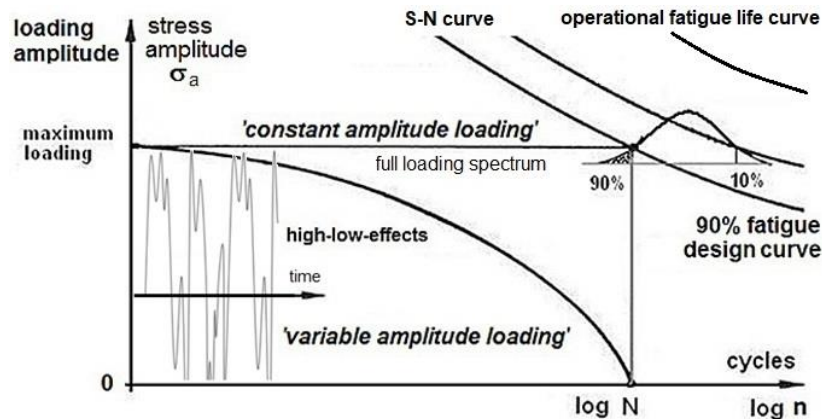


Fig.8-2: Display of constant amplitude loading and load history-linked variable amplitude loading

Brittle behavior:  $\sigma_{max}$  (Oberspannung) or  $\sigma_{min}$  or its mixture is responsible for micro-damage.

### Proportional and non-proportional stressing (loading)

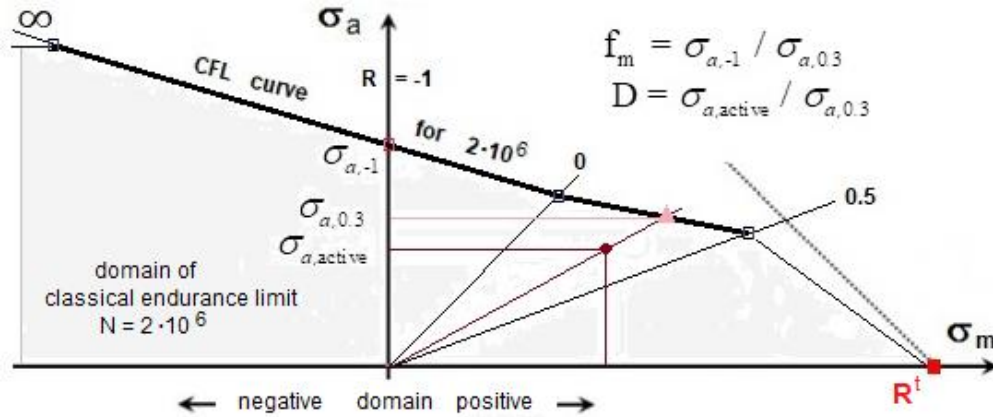
Compared to proportional stressing non-proportional stressing (e.g. 90° out-of-phase) may lead to a significant life reduction. Due to the time-dependent, differently oriented stress states the growing flaws have a better chance for coalescence viewing slip bands in ductile materials under strain-controlled fatigue testing or viewing micro-cracks in brittle materials.

### Mean stress sensitivity

Not fully ductile isotropic materials show an influence of the mean stress on the fatigue strength depending on the tensile strength and the material. Mean stresses in the tensile range ( $\sigma_m > 0$  MPa) lead to a lower permanently sustainable amplitude, whereas compressive mean stresses ( $\sigma_m < 0$  MPa) increase the permanently sustainable amplitude or in other words: Tensile mean stress lowers the fatigue strength and compressive mean stress increases the fatigue strength. How strongly the material reacts to mean stresses is described by the so-called mean stress sensitivity, the relationship between the mean stress and the permanently sustainable amplitude. Mean stress sensitivity  $M$  is captured by a correction function  $f_m$  (not topic here because brittle materials are basically addressed). The following sketch informs about the relationships.

The more brittle the material the more mean stress influence acts. This is why micro-damage is not anymore caused by yielding (1 strength failure mode,  $\sigma_{eq}^{Mises}$ ) alone but by micro-cracking that is caused by many fracture strength failure modes. Brittle materials like the transversely-isotropic UD material with its five fracture failure modes possess a strong mean stress sensitivity. That requires a

failure mode-linked treatment which cannot be captured by a mean stress correction as performed with not fully ductile materials.



Ductile behavior :  $M \rightarrow 0$ , amplitude stress  $\sigma_a$  is responsible for **yielding** (slipping is damaging)  
 Brittle behavior :  $\sigma_{max}$  (Oberspannung) or  $\sigma_{min}$  or its mixture is responsible for **micro-damage**

In the Haigh diagram in [Fig.8-3](#) (here test example UD material, 2 fiber failure modes) the huge effect of the mean stress sensitivity of brittle materials is demonstrated very clearly.

#### Determination of Micro-Damage Portions, FF1-linked example

In service an outstanding number of up and downs is given as varying stress input ([Fig.8-2](#)). Counting methods help to reduce the number of turning points in this time-domain provided course of the stress in order to achieve a set of simple stress reversals. This allows the application of Miner's rule in order to estimate the fatigue life under complex loading. The rain-flow counting method from Endo-Matsuishi, 1968, is the most often used method. Stress amplitude and mean stress may be collected in a Markov matrix, see [Fig.8-3](#). A distinct stress state with the largest stresses  $\sigma_{max}$  and  $\sigma_{min}$  possesses the stress ratio  $R = \sigma_{min} / \sigma_{max}$ . Analogous to the ductile material case where a complex stress state is captured by an equivalent stress  $\sigma_{eq}^{Mises}$  it may be assumed that for anisotropic materials the same is valid for each single strength failure mode, if equivalent stresses are available such as with the FMC-based SFCs of the author. A change from  $\sigma_{max}$  to  $\sigma_{eq^2max}$  will simplify the analyses.

## 10.2 S-N curve (Woehlerkurve) and Haigh-Diagram

### 8.2.1 Modelling of S-N curves and choice of an appropriate S-N curve

S-N curves can be modelled linearly, non-linearly in semi-log, log-log diagrams. Possible mapping formulations are non-linear curves such as from the Weibull-model and the Wearout-model [[VDI 2014](#)] or linear models in the log-log diagram. Below, five S-N curve mapping models are investigated and displayed.

As still mentioned, for brittle behaving materials it is physically reasonable to use the strength (average value, bar over) as maximum stress  $\sigma_{max}$  at  $n = N = 1$ . This advantageously reduces the number of free parameters by one. (Mind: In literature like the HSB the strength at origin is not taken in order to get more freedom for a better mapping in the domain of highest interest, LCF).

The choice of the S-N model mainly depends on the fact whether an endurance limit for VHCF is given, that should be mapped or not. Such a limit should exist for the example FF1 of CFRP



(thermoset polymer at least), the course of test data [M. Kawai] is mapped. The following conclusions can be drawn considering the desire “minimum number of free parameters”, just as many as physically required in the given work case.

In the HCF-regime ( $10^3$  through  $2 \cdot 10^6$ , the course of test data is mapped by: Lin-log curves (model 1 and 2 work very well and model 2 approximately may consider an endurance limit in the VHCF regime) and Log-log curves. The models 1, 2 show highest mapping capability due to the higher number of free parameters. The simple model 5 may work sufficiently well in appropriate courses of test data.

Considering the stochastic nature of the problem, it seems to be sufficient for many engineering applications to apply model 5. Here, the models 1 and 5 are applied.

- 1) 3 free parameter-Weibull + strength

$$\sigma_{max}(N) = c1 + \frac{\bar{R} - c1}{e^{\left(\frac{\log(N)}{c3}\right)^{c2}}}$$

- 2) 2 free parameter-Weibull + strength

$$\sigma_{max}(N) = \frac{\bar{R}}{e^{\left(\frac{\log(N)}{c3}\right)^{c2}}}$$

- 3) 2 free parameter + strength point, Sendecky, Wear-out Model

$$\sigma_{max}(N) = \bar{R} \cdot \left(\frac{1 - c1}{N - c1}\right)^{c2}$$

- 4) 2 free parameter + strength point

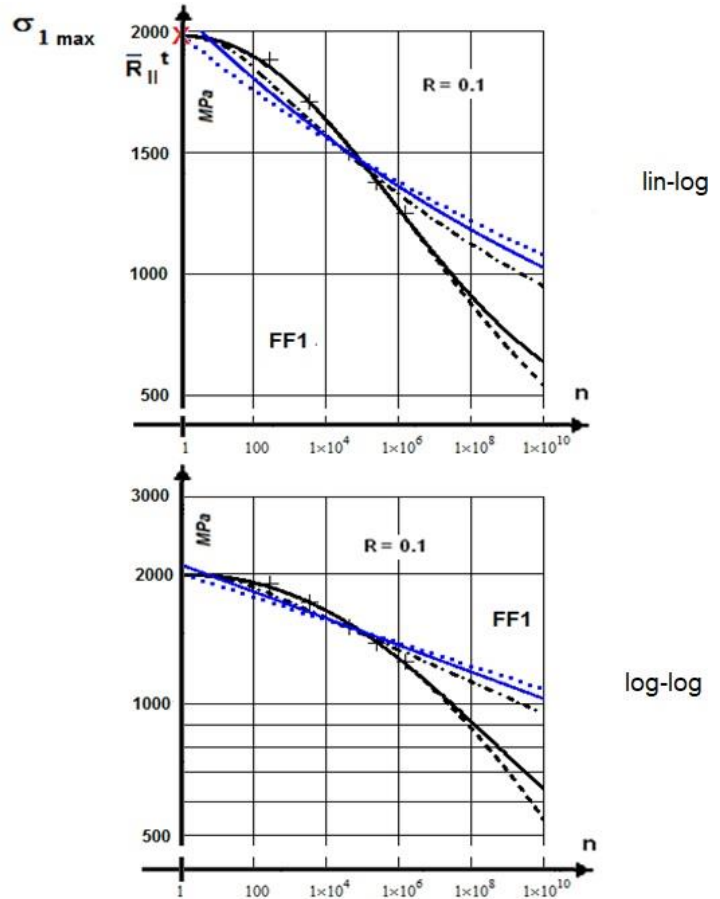
$$\sigma_{max}(N) = c1 \cdot \bar{R} \cdot N^{c2}$$

- 5) 1 free parameter + strength point

$$\sigma_{max}(N) = \bar{R} \cdot N^{c1}$$

is straight line in log-log diagram

$$\log \sigma_{max}(N) = \log \bar{R} + c1 \cdot \log N$$



The choice of the mapping function determines the extrapolation  $n > 2 \cdot 10^6$ ! Lack of data: Haibach-correction by halving the angle for  $n > 2 \cdot 10^6$  or other estimation methods.

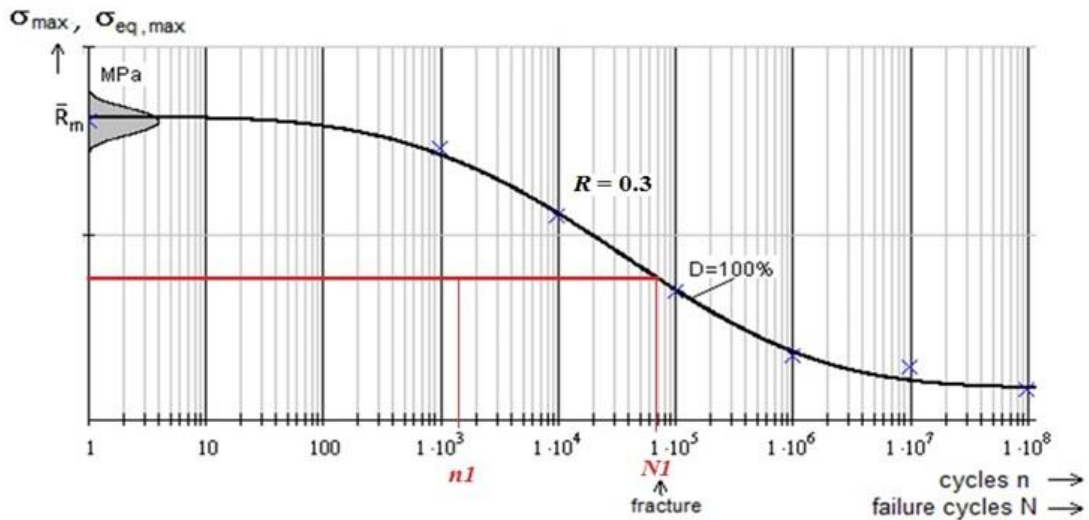
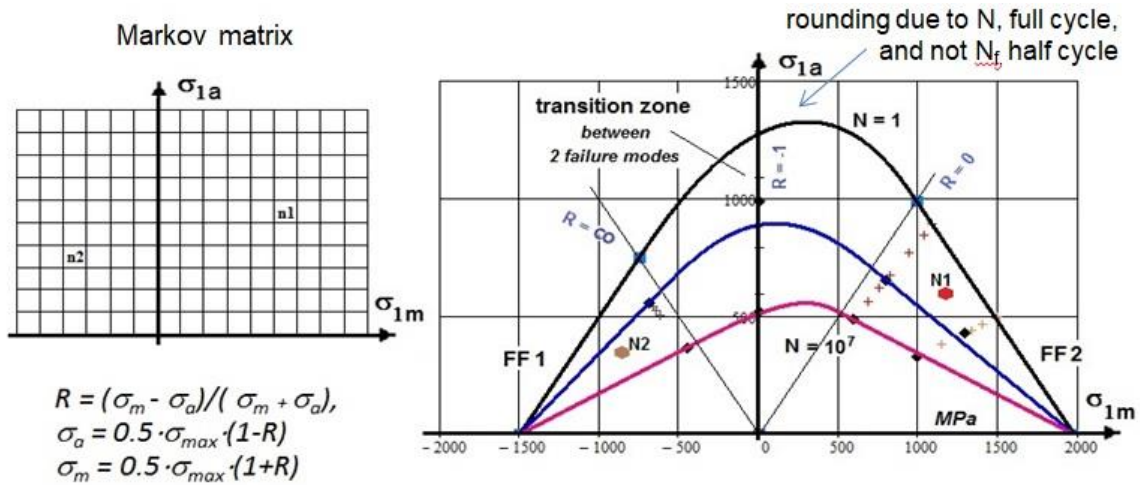
In the VHCF domain, similar to  $da/dN$  ( $\Delta K_0$ ) in fracture mechanics, micromechanically different damage may occur in comparison to the macro-mechanical technical crack domain. Such a change of the destructive mechanism may require the mapping of two distributions. For simplification, Model 1 – still used in the HSB as 4 parameter model – might be sufficient to map both test data domains.

### 8.2.1 General information on Markov Matrix, S-N curve and Haigh diagram

Fig.8-3 collects a Markov matrix, a Haigh diagram with 3 CFL curve examples, a S-N curve and the computation of a S-N curve, with curve parameter determination example performed by Mathcad. The so-called S-N (Stress-failure cycle N) curve is a constant amplitude curve, see bottom

picture. Unfortunately in practice, the S-N curve is linked also to the letter R. The reason for this is that **R** is now the Ratio of  $\sigma_{\min}/\sigma_{\max}$ . The average strengths are kept bias **R**.

For the design, S-N curves are to formulate. There are practically two possibilities to present them: (1) using in the case of ductile materials the stress amplitude  $\sigma_a(R,N)$ , also termed alternating stress, and (2) using in the case of brittle materials the maximum or upper stress  $\sigma_{\max}(R,N)$ , usually termed *fatigue strength*. The latter is physically simpler to understand by the stress man than the amplitude.



$v := \text{länge}(Y01) - 3$      $F(X01, c101, c301, c401) := c101 + \frac{Rpt - c101}{e^{\left(\frac{\log(X01)}{c301}\right)^{c401}}}$

$v = 5$

$R = 0.1$      $i := 0..v$

$SSE(c101, c301, c401) := \sum_i (Y01_i - F(X01_i, c101, c301, c401))^2$

Parameter - Ausgangsschätzung     $c101 := 20$      $c301 := 5$      $c401 := 2$

Vorgabe     $SSE(c101, c301, c401) = 0$

$\begin{pmatrix} c101 \\ c301 \\ c401 \end{pmatrix} := \text{Minfehl}(c101, c301, c401)$

$c101 = 347.4$      $c301 = 7.77$      $c401 = 2.16$

$Y01 = \begin{pmatrix} 1980 \\ 1883 \\ 1710 \\ 1498 \\ 1378 \\ 1251 \\ 0 \\ 0 \end{pmatrix}$      $X01 = \begin{pmatrix} 1 \\ 261 \\ 3306 \\ 41860 \\ 245000 \\ 1494000 \\ 0 \\ 0 \end{pmatrix}$

$\sigma_{01}(n) := \left[ c101 + \frac{Rpt - c101}{e^{\left(\frac{\log(n)}{c301}\right)^{c401}}} \right]$

Fig.8-3:Markov matrix, Haigh diagram, S-N curve with computation example

Namely, a decaying S-N curve is interpretable like a decaying ‘static’ strength after a micro-damage process with  $n$  cycles. Thereby, the static material stressing effort  $Eff$  (Werkstoffanstrengung,  $N_f = 1$ ) is replaced by the accumulated cyclic micro-damage sum  $D(N)$ . Applied here is the classical 3-parameter Weibull curve. Hence, in the case of brittle behaving materials the strength value  $\bar{R}^t = \sigma_{max}$  ( $n = N = 1$ ) is preferably used as origin in the tension domain and anchor point of the S-N curve and in the compression domain  $-\bar{R}^c = \sigma_{min}$  ( $n = N = 1$ ).

\* The following part-figures present a FF-linked example to visualize the next step of the process the determination of micro-damage portions: There are two stress states indicated in the Markov matrix and the Haigh diagram. Exemplarily, just for  $n_1$  the necessary associated S-N curve is provided. For the first of the two marked loading cycles  $n(\sigma_{1a}, \sigma_{1m})$  the calculation delivers  $D_{||1} = n_1/N_1$  for the FF1 mode and for the second  $D_{||2} = n_2/N_2$  for the FF2 mode-linked stress state.

\* The Haigh diagram in Fig.8-3 shows the maximum tolerable stress (loading) amplitudes of the material  $\sigma_a(\sigma_m)$ . Again, one can see the huge effect of the mean stress sensitivity very clearly.

Fig 8.4 visualizes the transfer from the load-driven increase of the material stressing effort  $Eff$  via 100% to the cycle-driven material micro-damage sum  $D = 100\%$  of the S-N curve.

If static failure  $\rightarrow \max\sigma = \bar{R}_{static}$ ,  $Eff = 1$  and if cyclic failure  $\max\sigma = \bar{R}_{cyclic}$ ,  $D = 1$ .

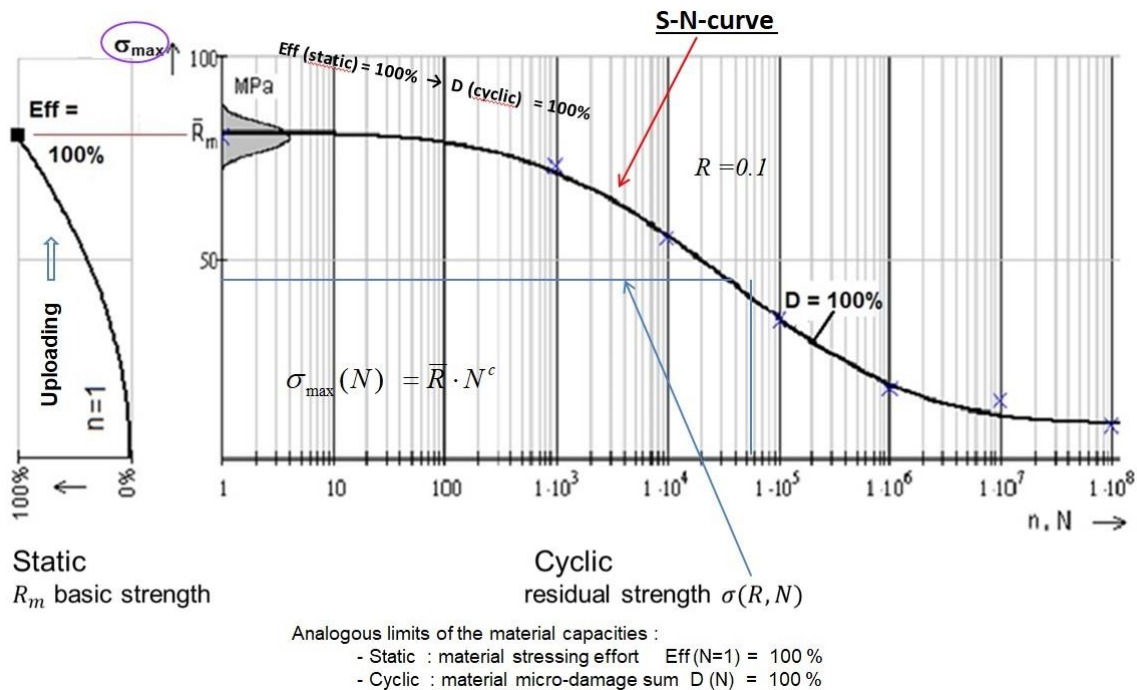


Fig.8-4: Eff versus D

Certain materials have an endurance limit which represents a stress level below which the material does not fail and can be cycled infinitely. If the applied stress level is below the endurance limit of the material is said to have an infinite life. This might have been acceptable in some cases for the old HCF-level of 10<sup>6</sup> cycles, however needs to be checked for VHCF because the failure mechanism might be not fully the same as for HCF.

As within static strength design the average S-N curve cannot be applied in fatigue life design verification, a statistically reduced curve is to determine as design curve.

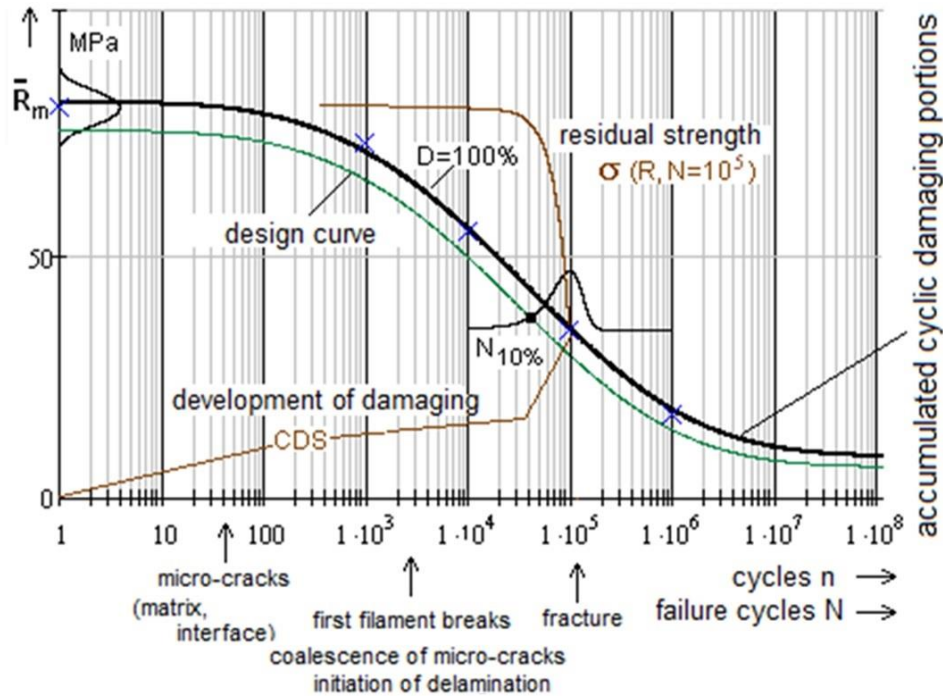


Fig.8-5: Fatigue average curve and design curve. CDS is ‘characteristic damage state’ of lamina

### 10.3 FMC-based Fatigue Life Estimation Model

#### 8.3.1 Idea of an Automatic Establishment of Constant Fatigue Life Curves $\sigma_a(\sigma_m, N = \text{constant})$

In aircraft industry, for a design-necessary interpolation to achieve constant fatigue life (CFL) curves much effort is spent to map them piece-by-piece by straight lines, see for instance the respecting sheets on metals in the HSB (Hickethier H.: *Interpolation and Extrapolation of S-N data*). Regarding curved CFLs, the dissertation of C. Hahne [Hah15] is highly recommended. Therefore, an automatic possibility to generate CLFs is highly desired in order to avoid difficult interpolations between the constant life curves. A reliable procedure helps to save test costs and development time. Here, for the multiple failure mode ‘suffering’ brittle materials an automatic establishment of the non-pieewise straight Constant Fatigue Life Curves (CFL) in Haigh Diagrams is searched – generally applicable to brittle isotropic (including compressed concrete) and UD-materials.

#### Detailed ideas of the author for achieving these CFL curves

- Measurement of only a minimum number of S-N curves
- Finding a physically-based model to predict other S-N curves, required for fatigue analysis, on basis of a Master S-N curve of each mode
- Presumption: An appropriate Master S-N curve for each failure mode domain compression (SF) and tension (NF) is available
- In order to map the test data in the transition domain, where the modes interact (*most problematic region in the Haigh diagram*) a practicable mode domain decay function is looked for to regard the opposite decay of the modes.

In order to achieve this, a reliable Assumption is needed:

*“If the failure mechanism of a mode cyclically remains the same as in the static case, then the fatigue micro-damage-driving failure parameters are the same and the applicability of static SFCs is allowed for quantifying micro-damage portions“.*

### 8.3.2 Modal Dedication of Kawai's Modified Fatigue Strength Ratio $\Psi$ , applied for example UD

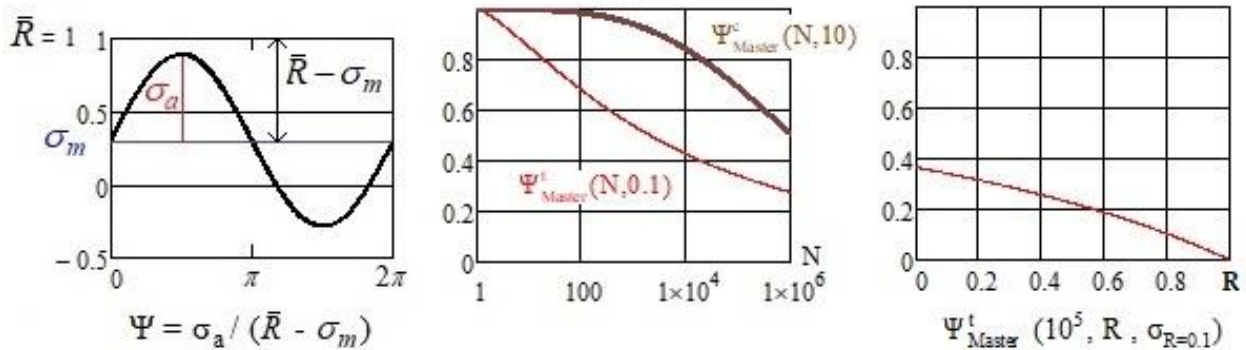
#### Ideas of Kawai and Cuntze

- Kawai's Fatigue Strength Ratio  $\Psi$ : Normalization of the fatigue strength  $\sigma_{max}(N)$  by a static strength  $\psi = \sigma_{static} / \bar{R} = 1$  ( $\equiv Eff$ ) such referring to  $Eff$  (see also Fig.8-4,  $Eff \rightarrow D$ )
- Kawai's Modified Fatigue Strength Ratio  $\Psi$ : Reformulation in order to get the stress ratio  $R$  into the static concept  $\psi = (\sigma_a + \sigma_m) / \bar{R} = 1$

$$\Rightarrow 1 = (\sigma_a + \sigma_m) / \bar{R} \Rightarrow \sigma_a / (\bar{R} - \sigma_m) = \Psi \equiv \text{cyclic part / 'static' part .}$$

Each measured S-N-curve is normalized by its static strength and the 'bulk' of S-N curves (hopefully is more than one S-N curve measured within the domains and in the transition zone) then fitted to obtain the Master curve. Kawai used all R-curves to obtain  $\Psi(R_{fit})$ , independent of the inherent failure mode). Whether it practically makes sense to determine a Master curve by fitting all curves is to check: tension ( $R=0.1, 0.5$ , compression ( $R=10$ ) and of the transition zone  $R = -1, R_{trans}$ .

For visualization of  $\Psi$  see the following pictures



- The author remains with the FMC and sticks to mode domain separation in the following. *He tracks a mode-dedication of Kawai's Modified Fatigue Strength Ratio  $\Psi$ . This requires - as usual in FMC application - to tackle the transition zone between the modes separately.*

Thanks to Masamichi Kawai for inform me about his paper [Kaw04] because former work of the author was performed using physically not adequate ideas.

*Due to missing test data the author could not investigate whether Kawai's global fitting  $\Psi(R_{fit})$  of all S-N curves enables to predict a desired more or less reliable S-N curve in the transition zone.*

All formulations, necessary for the author's mode-dedicated variant, shall be put together in Table 8-1.

As material example a UD material with the modes FF1 and FF2 is stressed.

In the context of the UD material choice:

Fatigue pre-dimensioning of 'well-designed' (*optimal fiber directions and minimum amount of fiber reinforcement for all load cases*), high-performance UD lamina (ply)-composed laminates just by single lamina-dedicated, mode-representative Master ('basic') S-N curves, derived from sub-lamina test specimens, which capture the embedding (in-situ) effects, and on S-N data from automatically derivable (curved) Constant-Fatigue-Life curves or thereof numerically constructed Haigh Diagrams, respectively.

Table 8-1: Determination of S-N curves on basis of Kawai's  $\Psi$  model with Master S-N curve

\* Formulas to provide

$$\sigma_{max} = \Delta\sigma / (1-R) \equiv 2 \cdot \sigma_a / (1-R) \quad \text{with} \quad \Delta\sigma = \text{stress range, } \sigma_a \text{ is positive}$$

$$R = (\sigma_m - \sigma_a) / (\sigma_m + \sigma_a), \quad \sigma_a = \sigma_m \cdot (1-R) / (1+R)$$

$R = -1$ , fully reversed alternating stress.  $R = 0$ ,  $R = 100 (\infty)$ , swelling stress.

$$\bar{R}^t = \sigma_{max} (n = N = 1), \quad \bar{R}^c = \sigma_{min} (n = N = 1)$$

$$\sigma_a = 0.5 \cdot \sigma_{max} \cdot (1-R), \quad \sigma_m = 0.5 \cdot \sigma_{max} \cdot (1+R); \quad \sigma_a = -0.5 \cdot \sigma_{min} \cdot (1-1/R), \quad \sigma_m = \sigma_{min} \cdot (1-0.5 \cdot (1-1/R))$$

Choice of problem-adequate mapping function and individually mapping of course of test data

$$\sigma_{max}(N) = c1 + \frac{\bar{R} - c1}{e^{\left(\frac{\log(N)}{c3}\right)^{c2}}}, \quad \sigma_{min}(N) = c1 + \frac{-\bar{R} - c1}{e^{\left(\frac{\log(N)}{c3}\right)^{c2}}} = c1 + (-\bar{R} - c1) \cdot \exp\left(\frac{\log(N)}{c3}\right)^{c2}.$$

\* Mode dedicated Application of Kawai's model  $\psi = \sigma / \bar{R}$ ;  $\psi, \Psi$  positive

Static failure occurs at  $\sigma_{max} = \bar{R}^t = \sigma_a + \sigma_m$  and  $\sigma_{min} = -\bar{R}^c = -\sigma_a + \sigma_m$ .

$$\sigma_{max} = \bar{R}^t = \sigma_a + \sigma_m \rightarrow \sigma_a = \bar{R}^t - \sigma_m \rightarrow 1 = \sigma_a / (\bar{R}^t - \sigma_m) \equiv \text{cyclic / 'static'}$$

Kawai's cyclic danger intensity to fail ( $N > 1$ )

$$\Psi_{Master}^t = \frac{\sigma_a}{\bar{R}^t - \sigma_m} \quad \text{and} \quad \Psi_{Master}^c = \frac{\sigma_a}{\bar{R}^c + \sigma_m} = \frac{-0.5 \cdot \sigma_{min} \cdot (1-1/R)}{\bar{R}^c + \sigma_{min} \cdot (1-0.5 \cdot (1-1/R))}$$

Above relations are reformulated in order to bring the stress ratio R into the model

$$\Psi_{Master}^t(\sigma_{max}^{Master}, R) = 0.5 \cdot \sigma_{max}^{Master} \cdot (1-R) / (\bar{R}^t - 0.5 \cdot \sigma_{max}^{Master} \cdot (1+R)) \quad \text{and after resolution}$$

$$\sigma_{max}^{Master}(R, N) = 2 \cdot \bar{R}^t \cdot \Psi_{Master}^t / (\Psi_{Master}^t - R + R \cdot \Psi_{Master}^t + 1), \quad 0 < R < 1$$

$$\Psi_{Master}^c(\sigma_{min}^{Master}, R) = \sigma_{min}^{Master} \cdot (1-R) / [2 \cdot R \cdot \bar{R}^c + \sigma_{min}^{Master} \cdot (1+R)] \quad \text{and after resolution}$$

$$\sigma_{min}^{Master}(R, N) = -2 \cdot \bar{R}^c \cdot \Psi_{Master}^c / (\Psi_{Master}^c + R + R \cdot \Psi_{Master}^c - 1), \quad 1 < R < 100 (\infty).$$

Mode Master S-N curves and S-N curves to be predicted have the same origin at  $\bar{R}^t, \bar{R}^c$ .

Cuntze does not fit the bunch of all available S-N curves, only mode-associated ones.

For  $n > 1$  Eff is replaced by D and static strength by cyclic strength, see Fig.8 - 4.

\* Test input of available Master curves (usually just the following ones)

$$\sigma_{max}^{Master}(N, R = 0.1) \rightarrow = \sigma_{R=0.1} = c_1^{NF} + (\bar{R}^t - c_1^{NF}) / \exp\left(\frac{\log(N)}{c_1^{NF}}\right)^{c_2^{NF}} = \bar{R}^t \cdot \Psi_{Master}^t$$

$$\sigma_{min}^{Master}(N, R = 10) \rightarrow = \sigma_{R=10} = c_1^{SF} + (-\bar{R}^c - c_1^{SF}) / \exp\left(\frac{\log(N)}{c_1^{SF}}\right)^{c_2^{SF}} = -\bar{R}^c \cdot \Psi_{Master}^c.$$

\* Transfer into the boundary S-N-curves  $R = 0$  and  $R = 100 (\cong \infty)$

$$\sigma_{R=0}(N, R) = 2 \cdot \bar{R}^t \cdot \Psi_{Master}^t / (\Psi_{Master}^t - R + R \cdot \Psi_{Master}^t + 1), \quad R = 0$$

$$\sigma_{R=100}(N, R) = -2 \cdot \bar{R}^c \cdot \Psi_{Master}^c / (\Psi_{Master}^c + R + R \cdot \Psi_{Master}^c - 1), \quad R = 100$$

and replacing  $\Psi$  finally follows

$$\sigma_{R=0}(N, R) = (2 \cdot c_1^{NF} + (\bar{R}^t - c_1^{NF}) / \exp\left(\frac{\log(N)}{c_1^{NF}}\right)^{c_2^{NF}}) / (\Psi_{Master}^t - R + R \cdot \Psi_{Master}^t + 1)$$

$$\sigma_{R=100}(N, R) = (2 \cdot c_1^{SF} + (-\bar{R}^c - c_1^{SF}) / \exp\left(\frac{\log(N)}{c_1^{SF}}\right)^{c_2^{SF}}) / (\Psi_{Master}^c + R + R \cdot \Psi_{Master}^c - 1)$$

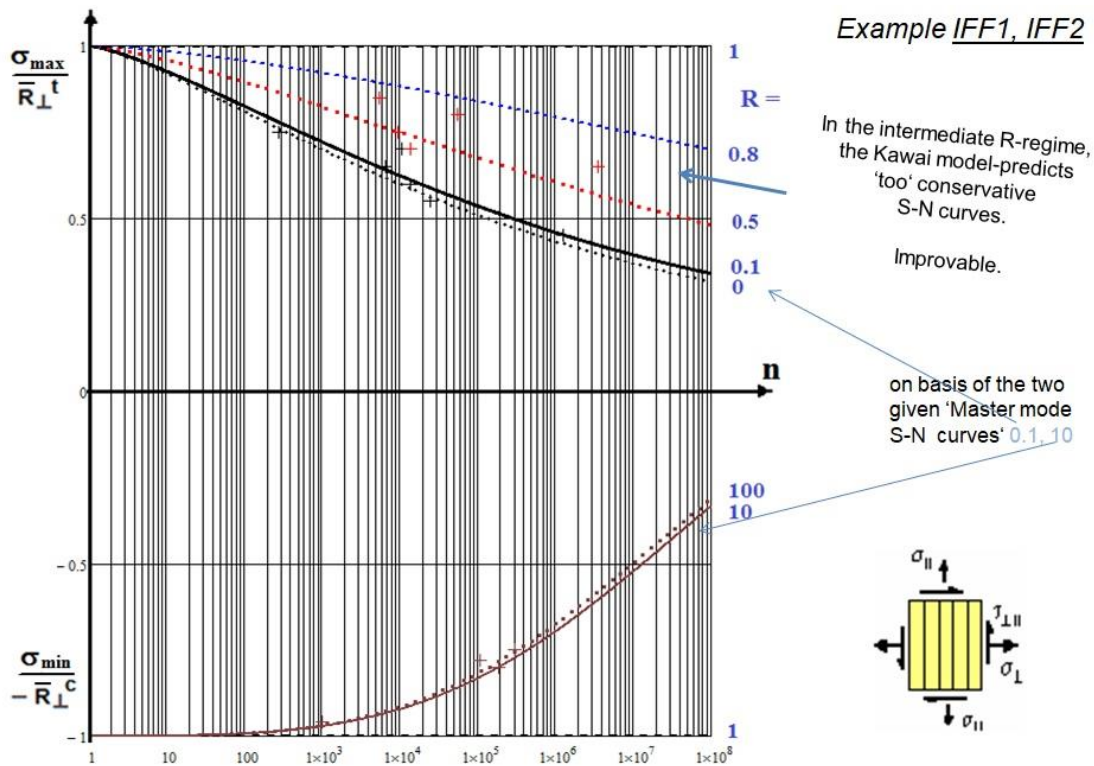
The same procedure is valid for all other S-N curves to be predicted.

Justification check: To prove the general applicability of the ‘mode-dedicated Kawai model-predicted S-N curves’, the curves in *Fig.8-6* have been numerically derived.

The application results for IFF demonstrate:

- Limit Curves  $R = 1, 0$  and  $100 (\infty), 1$  could be generated
- The question, whether the intermediate curves between the limit curves are good enough, can be only responded by further test results and associated modelling research work
- The question, whether Kawai’s global fit of all available S-N curves is satisfactory could be not supported due to lack of test data. Kawai’s model would make it possible to also predict the S-N curves in the transition zone  $\infty > R > 0$ .

*Fig.8-6* shows the Master S-N curves and the predicted S-N curves. With respect to the FMC mode domain view  $R = -1$  is not depicted in *Fig.8-6*.



*Fig.8-6: Mode-dedicated Kawai model-derived S-N curves. + R=0.5 test data, +R=0.1 test data.*

→ Kawai’s model looks very promising.

### 8.3.3 Constant Fatigue Life CFL curves in the Transition Domain

There is no problem to establish Haigh diagrams for FF and IFF3 due to the fact: The strength values are of similar size in each case. The static interaction formula was relatively sufficient. However for a Haigh Diagram for really brittle materials, indicated by a  $R_{trans}$  very different to  $-1$ , a solution procedure has to be looked for. Chosen was a mode-linked exponentially decaying function  $f_d$ , that practically ends where the other pure mode begins to reign.

Table 8-2 informs about the steps for the example IFF1-IFF2.

Table 8-2: Mode decay function  $f_d$  for tension and compression domain in the Haigh diagram

$$Eff = [(Eff^{NF})^m + (Eff^{SF})^m]^{m^{-1}} = 100\%$$

formulated in amplitude and mean stresses this reads

$$\left( \frac{-(\sigma_{2m} - \sigma_{2a}) + |\sigma_{2m} - \sigma_{2a}|}{2 \cdot \bar{R}_\perp^c \cdot f_d} \right)^m + \left( \frac{\sigma_{2m} + \sigma_{2a} + |\sigma_{2m} + \sigma_{2a}|}{2 \cdot \bar{R}_\perp^t \cdot f_d} \right)^m = 1$$

delivering the CFL curve for  $N = 1$  cycle,  $f_d = 1$ , activating both NF with SF.

To obtain a CFL curve for higher  $N$  and larger ratios  $R_{trans} = -\bar{R}^c / \bar{R}^t$  above interaction formula, working in the transition zone, is engineering-like to adjust because the action of a mode ends where the other mode begins. Chosen is an exponential decay function  $f_d$  that decays from the end of the pure SF mode at  $R = \infty$  ( $R=10$  possible) down to zero at the beginning of the pure NF mode at  $R = 0$  ( $R=0.1$  possible) and vice versa

$$\rightarrow f_d = 1 / [1 + \exp(\frac{c_1 + \sigma_m}{c_2})].$$

Fig.8-7 visualizes the effect of the formulas above. Bounds are given by the S-N lines for  $R = \infty : \sigma_a = -\sigma_m$  ;  $R = 0 : \sigma_a = \sigma_m$ .

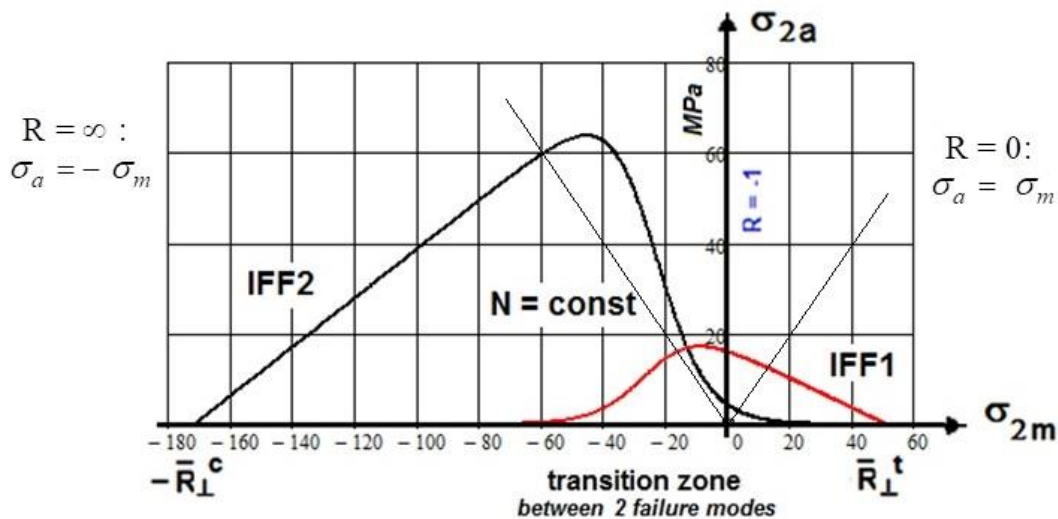


Fig.8-7: Effect of the decay function in the transition zone  $-\infty < R < 0$

For fully ductile materials no transition zone between 2 modes exists, because just one single mode reigns, namely ‘Yielding’.



Table 8-3: Numerical derivation of the parameters of the decay function  $f_d = 1/[1 + \exp(\frac{c_1 + \sigma_m}{c_2})]$

Vorgabe  $\underline{c1sSF} := -20$   $\underline{c2sSF} := -5$   $0.998 = \frac{1}{1 + e^{\frac{c1sSF - \sigma m105}{c2sSF}}}$   $0.01 = \frac{1}{1 + e^{\frac{c1sSF + \sigma m015}{c2sSF}}}$

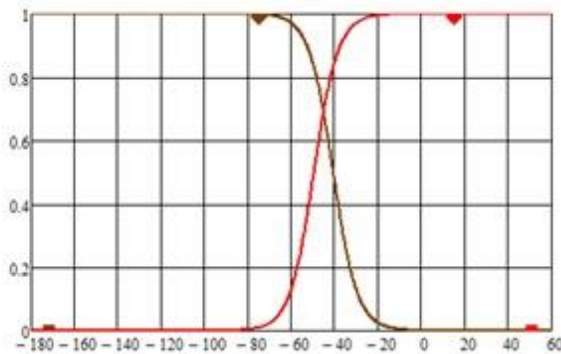
$AsSF := \text{Suchen}(c1sSF, c2sSF)$   $AsSF = \begin{pmatrix} -40.55 \\ -5.553 \end{pmatrix}$   $\underline{c1sSF} := AsSF_0$   $\underline{c2sSF} := AsSF_1$   
 $c1sSF = -40.55$   $c2sSF = -5.553$

Vorgabe  $\underline{c1sNF} := -20$   $\underline{c2sNF} := 5$   $0.01 = \frac{1}{1 + e^{\frac{c1sNF - \sigma m105}{c2sNF}}}$   $0.998 = \frac{1}{1 + e^{\frac{c1sNF + \sigma m015}{c2sNF}}}$

$AsNF := \text{Suchen}(c1sNF, c2sNF)$   $AsNF = \begin{pmatrix} -49.532 \\ 5.553 \end{pmatrix}$   $\underline{c1sNF} := AsNF_0$   $\underline{c2sNF} := AsNF_1$   
 $c1sNF = -49.532$   $c2sNF = 5.553$

$$fsNFa(\sigma m) := \frac{1}{1 + e^{\frac{c1sNF - \sigma m}{c2sNF}}}$$

$$fsSFa(\sigma m) := \frac{1}{1 + e^{\frac{c1sSF - \sigma m}{c2sSF}}}$$

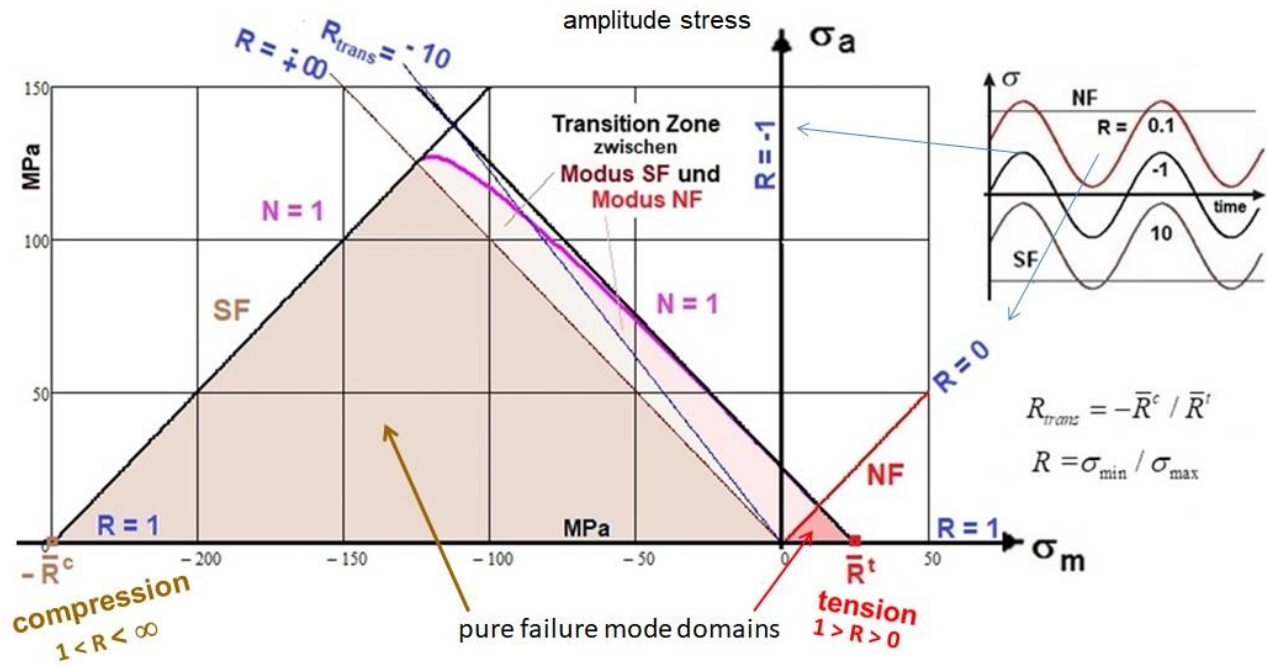


The quality of the approach for the transition zone is practically checked by “How good is the test data course along the stress ratio  $R_{trans}$  line mapped?”.

### 8.3.4 CFL curve application of the decay function $f_d$ in the Haigh-Diagram

At first Fig.8-8 shall schematically show the pure domains and the transition zone.

The figure is also applicable for brittle isotropic material like concrete.



NF = Normal Fracture, SF = Shear Fracture, N = fracture cycle number

Fig.8-8: Scheme for understanding a Haigh-Diagram of a Brittle Isotropic Material  
Up right: alternating stress states of 3 R curves

In Fig.8-9 two CFL-curves are displayed, the static envelope  $N=1$  and a curve for  $N=10^7$ . The pure mode domains are colored and the transition zone is separated by  $R_{trans}$  into two influence parts. The course of the R-value is depicted by the bold dark blue lines. For  $N = 1$  the static procedure is applicable using the strength failure envelope represented by the interaction formula. In the negative domain lie the SF-determined S-N-curves, in the positive domain the NF determined ones. In the transition zone 2 modes are principally activated which shows either a more SF- or a more NF-determined interaction visualized by the two pale colors.

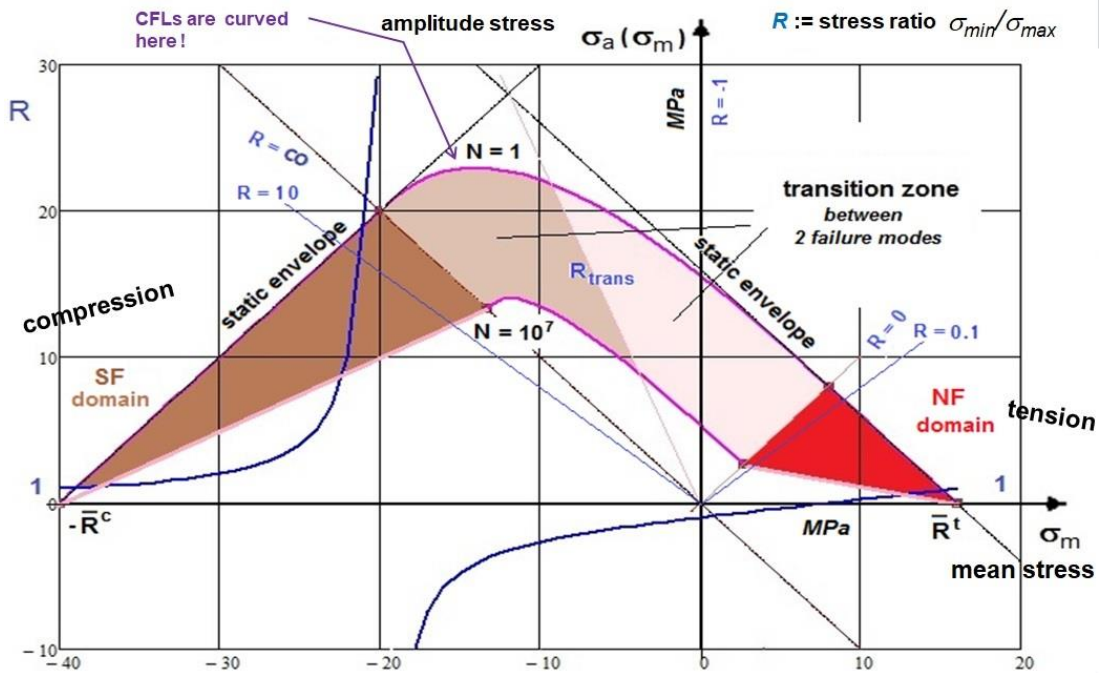


Fig.8-9: Scheme of pure mode domains, course of R and transition zone parts

**Mind:** The CFL curve  $N=1$  is curved at top because 2 modes act in the case of brittle materials. This is in contrast to uniaxial static loading, depicted by the straight static envelopes.  $N \neq N_f$ . One cycle damage is the sum of 2 damage portions!

Fig.8-10 gives a feeling how the ‘rich bulk’ of tested S-N curves usually looks.

It further shows how the mapped curve is running in the higher VHCF regime. There is no fidelity given when using extrapolated values far off the tested range.

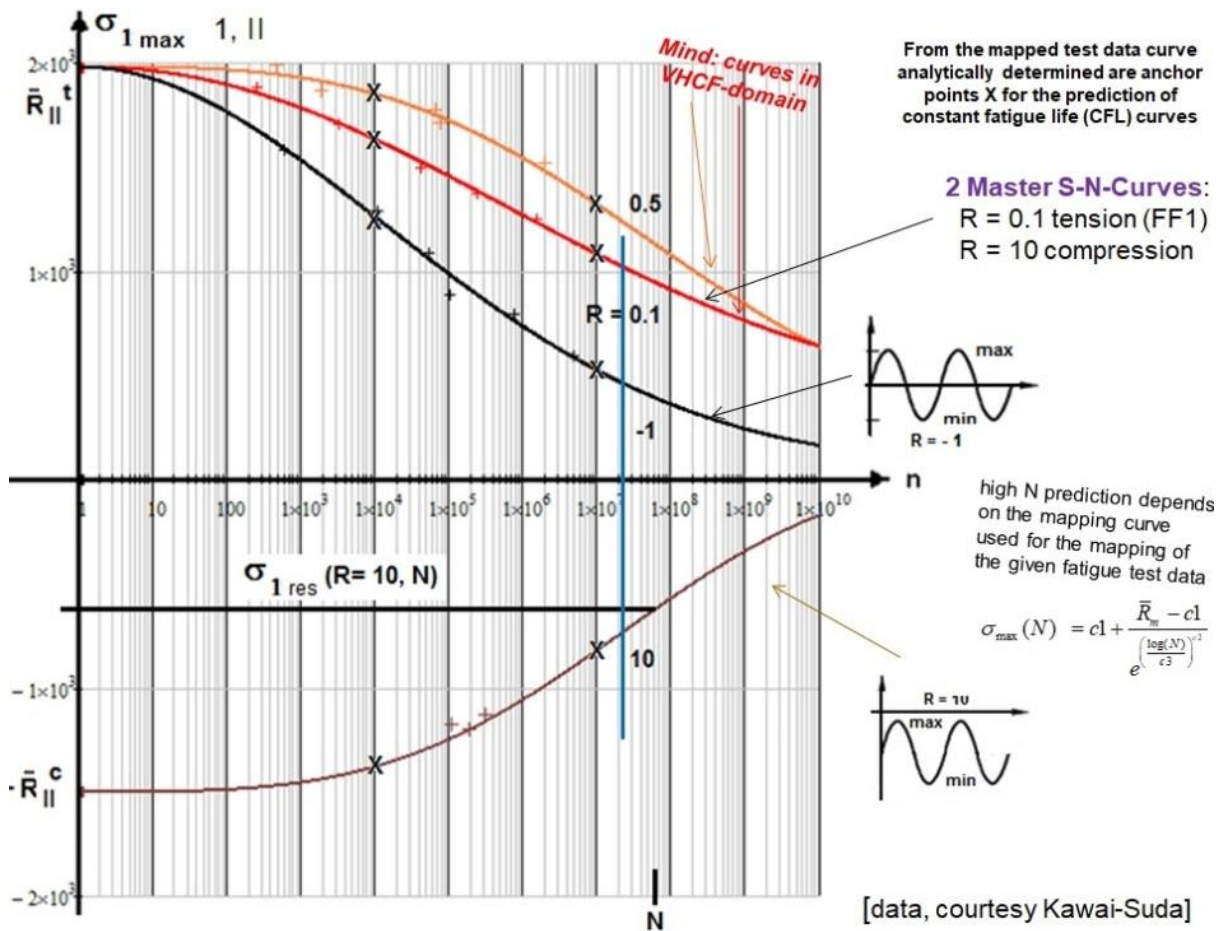


Fig.8-10, Test example UD: Individually lin-log mapped FF1-FF2-linked S-N curves

The bold blue vertical fatigue strength functions  $\sigma_{\max}^5(R, 10^5)$ ,  $\sigma_{\min}^5(R, 10^5)$  replace the static strengths.

#### 10.4 Some examples of S-N curves ‘feeding’ Haigh-Diagrams, FF and IFF

At first the author likes to thank Dr.-Ing. Clemens Hahne, AUDI, for his valuable UD test results making the generation of the following figures possible and thereby the application of the author’s CFL model. The reader is invited to read the content-rich and imaginative dissertation [Hah15] and this not only for comparison of the different CFL modeling ideas of Hahne and Cuntze.

Fig.8-11 presents failure mode-linked CFL curves  $\sigma_a(\sigma_m, N = \text{constant})$ . The computed ‘S-N curve X-points’ are mapping fixed points (anchors) for the CFL curves to be predicted. The blue curve is for  $N = 10^5$ .

The used S-N test curves are still given in the previous figure, Fig.8-10.

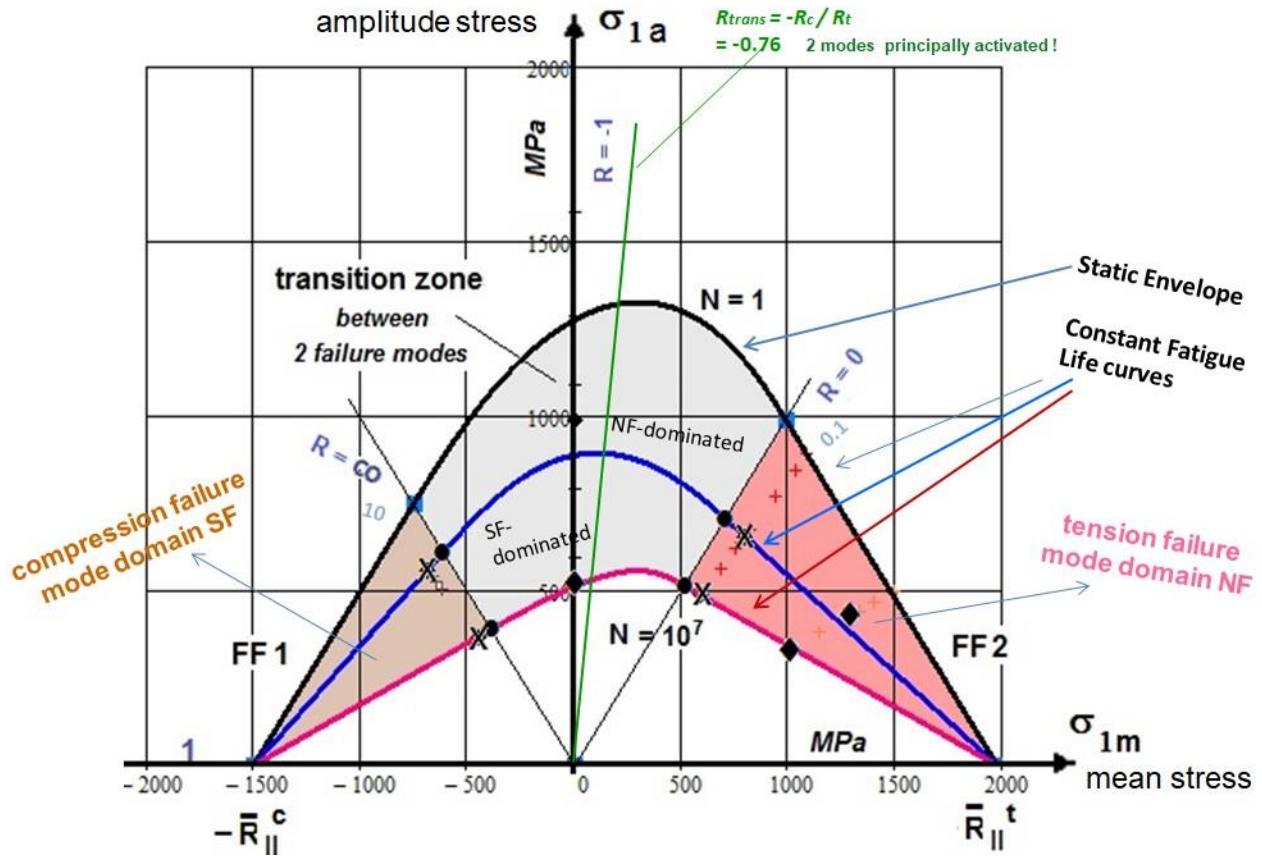


Fig.8-11: Rigorous Interpretation of the Haigh diagram for the UD example FF1-FF2 displaying failure mode domains and transition zone. Test data [Hah14]. CFRP/EP,  $\bar{R}_{\parallel}^t = 1980$ ,  $\bar{R}_{\parallel}^c = 1500$ ,  $\bar{R}_{\perp}^t = 51$ ,  $\bar{R}_{\perp}^c = 172$ ,  $\bar{R}_{\perp\parallel} = 71$  [MPa].

Fig.8-12 presents two mapped IFF3 S-N curves.

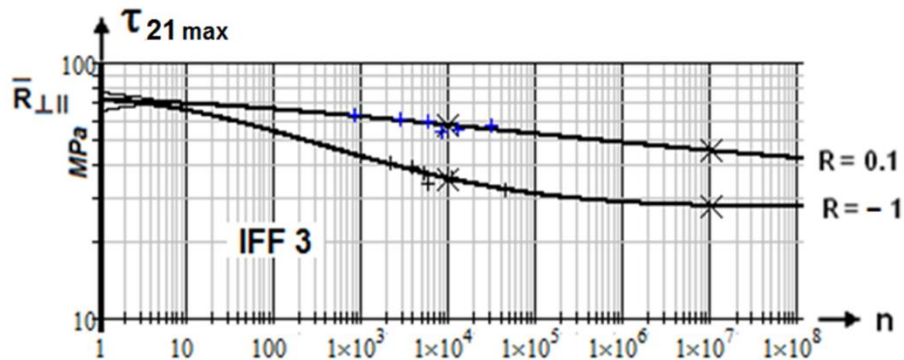


Fig.8-12: Log-log IFF3-linked S-N curves [data, courtesy C. Hahne]

Fig.8-13 depicts the CFL curves derived. Obvious is the symmetry and that the two-fold mode effect flattens the curve at  $\sigma_m=0$ .

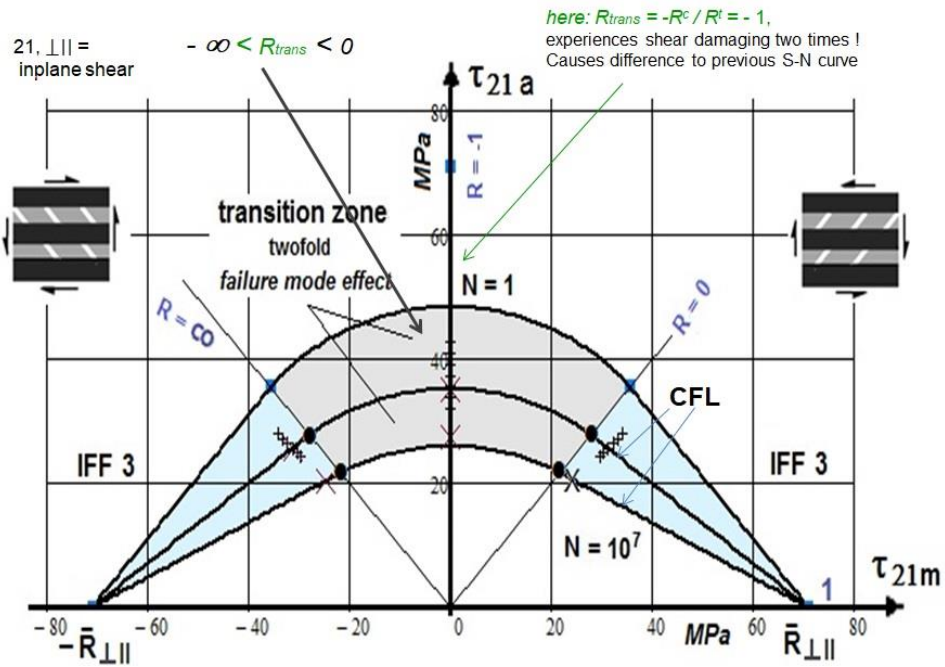


Fig.8-13: IFF3 UD Haigh diagram, Display of a two-fold mode effect ( $a :=$  amplitude,  $m :=$  mean,  $N :=$  number of fracture cycles,  $\bar{R} :=$  strength and  $R := \sigma_{min}/\sigma_{max}$ ). Test data CF/EP, courtesy [Hah15]

In Fig.8-14 mapped IFF S-N-curves are presented.

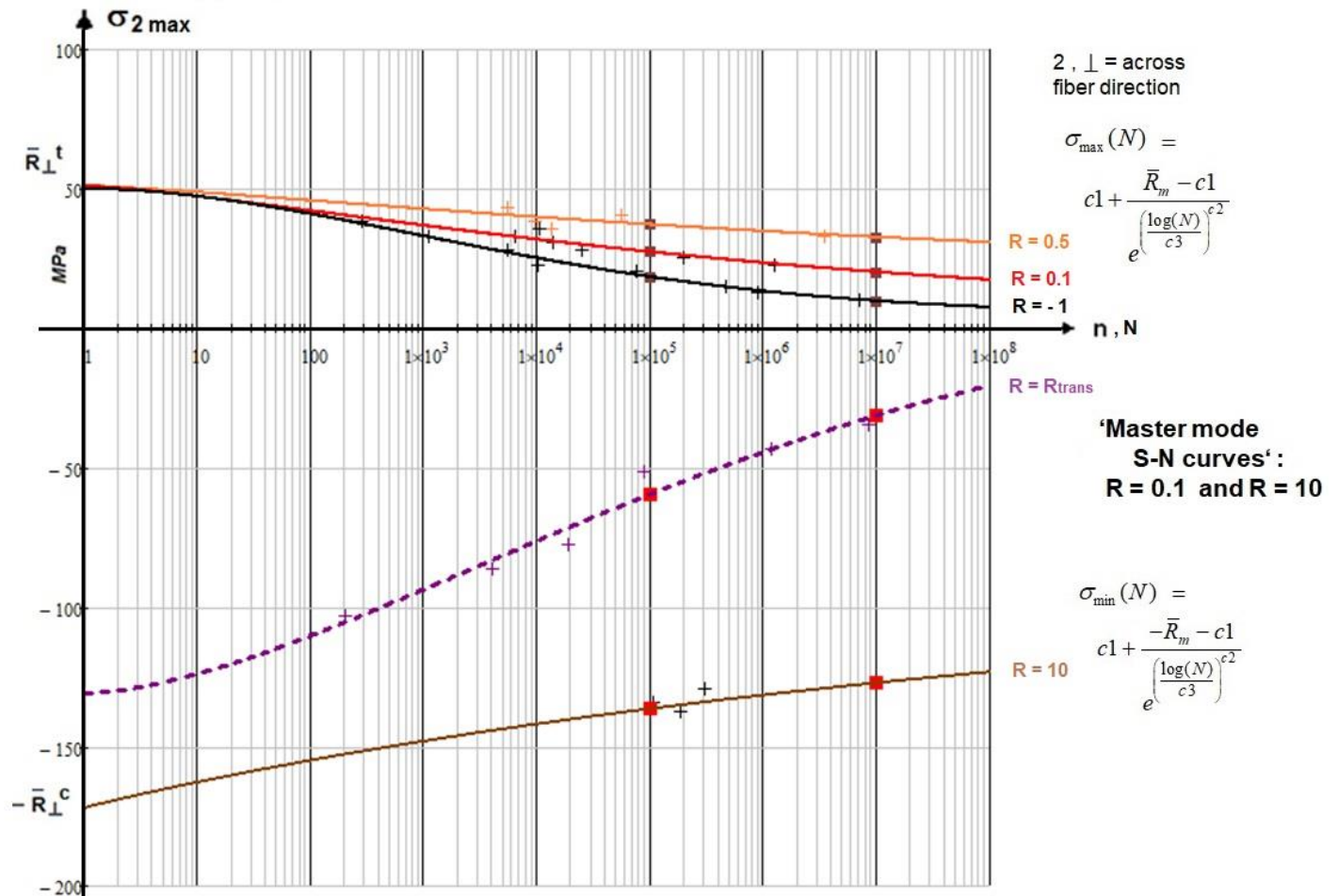


Fig.8-14: Mapped lin-log IFF1-IFF2-linked S-N curves [test data, courtesy C. Hahne]

Of interest are the S-N curves in the transition zone  $R_{trans}$  and  $R = -1$  which have other origin values than the strengths of the modes.

From the various curves the  $R_{trans}$  curve is novel.

Its origin was not given and had to be determined before mapping. Applied was the static interaction curve,  $N = 1$ , because points on the boundary must fulfill the static equilibrium:

$$R_{trans} = -\bar{R}_\perp^c / \bar{R}_\perp^t = -3.4 : \left( \frac{\sigma_{2fr}}{\bar{R}_\perp^t} \right)^m + \left( \frac{\sigma_{2fr} \cdot R_{trans}}{\bar{R}_\perp^c} \right)^m = 1 \rightarrow \sigma_{2fr} = -131 \text{ MPa},$$

$$R = -1 : \left( \frac{\sigma_{2fr}}{\bar{R}_\perp^t} \right)^m + \left( \frac{\sigma_{2fr} \cdot R}{\bar{R}_\perp^c} \right)^m = 1 \rightarrow \sigma_{2fr} = 50.1 \text{ MPa}.$$

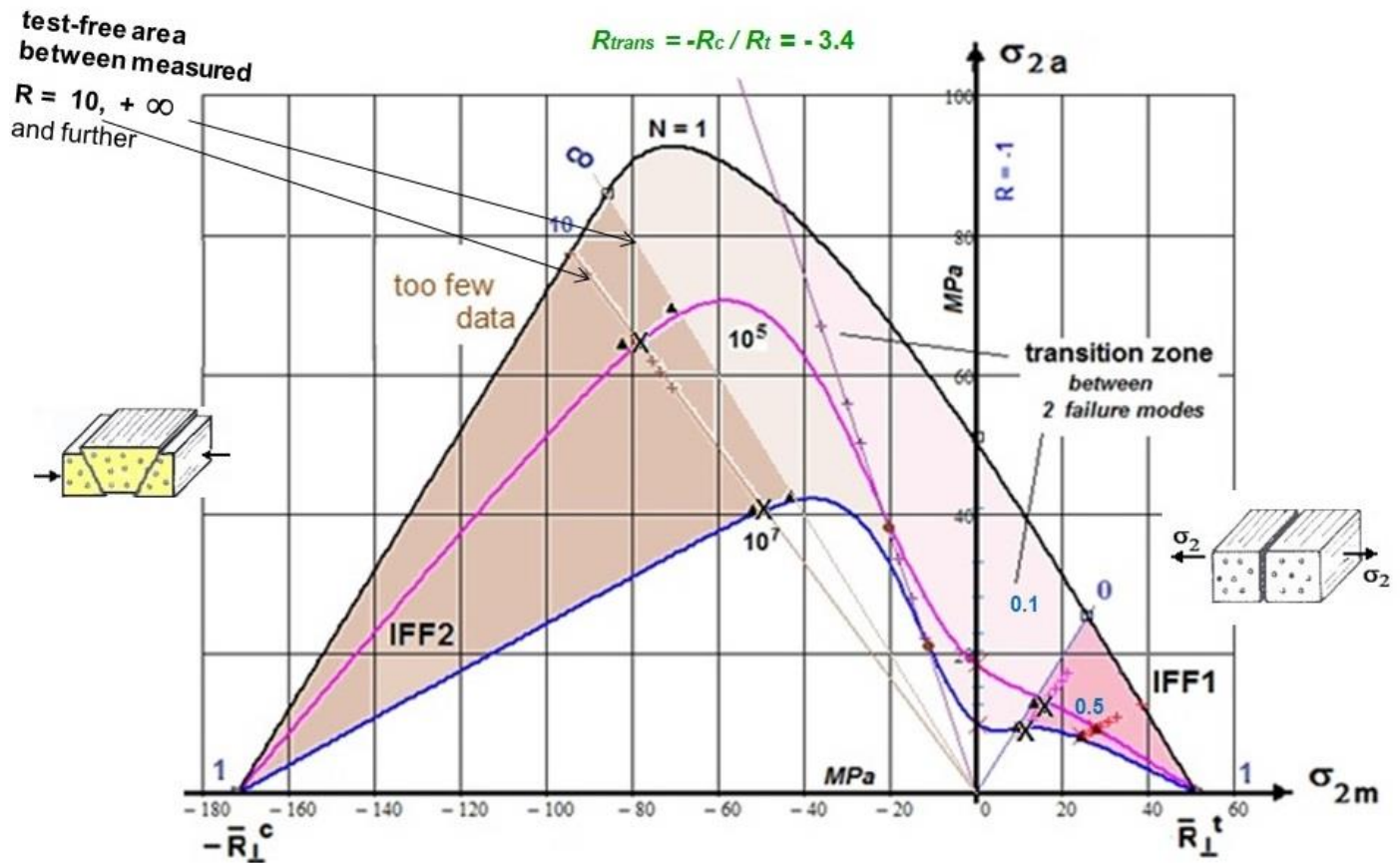


Fig.8-15: IFF1- IFF2 UD Haigh diagram (similar for UD, lamella and concrete) displaying the failure mode domains, transition zone [data courtesy C. Hahne]

### 10.5 Procedure for deriving CFL curve estimates and associated Steps

The author proposes his procedure in [Table 8-4](#) for deriving CFL curve estimates on basis of one Master S-N curve of each mode.

As example serves UD material stressed in the modes IFF1 and IFF2.

If static failure  $\rightarrow \max \sigma = \bar{R}_{static}$ ,  $Eff = 1$  and if cyclic failure  $\max \sigma = \bar{R}_{cyclic}$ ,  $D = 1$ .

[Table 8-5](#) presents the associated steps to generate a CFL curve.

Table 8-4: Estimation of a CFL curve  $\sigma_{2a}$  ( $\sigma_m \equiv \sigma_{2m}$ ,  $N = \text{const}$ ) for IFF,  $N = 10^5$  cycles

### S-N curves in the two Mode Domains IFF1, IFF2

- \* From FMC reasons - in contradiction to Kawai - a strict mode separation is to apply.
- \* S-N curves are generally given for domains IFF1, IFF2 and sometimes  $R = -1$ ,  $R_{\text{trans}}$ . Available Master curves are usually just the standard ones  $R = 0.1$  (IFF1),  $R = 10$  (IFF2)
- \* Computation of the CFL curve parameters for the 2 domains (example  $N = 10^5$ , indexed 5)

$$\sigma_{\text{max},5}^{\text{Master}}(10^5, R=0.1) = \sigma_{R=0.1}(10^5, R=0.1) = c_1^{\text{NF}} + (\bar{R}^t - c_1^{\text{NF}}) / \exp\left(\frac{\log(10^5)}{c_1^{\text{NF}}}\right)^{c_2^{\text{NF}}} = \bar{R}^t \cdot \Psi_{\text{Master}}^{t,5}$$

$$\sigma_{\text{min},5}^{\text{Master}}(10^5, R=10) = \sigma_{R=10}(10^5, R=0.1) = c_1^{\text{SF}} + (\bar{R}^c - c_1^{\text{SF}}) / \exp\left(\frac{\log(10^5)}{c_1^{\text{SF}}}\right)^{c_2^{\text{SF}}} = -\bar{R}^c \cdot \Psi_{\text{Master}}^{c,5}$$

- \* The fatigue strengths  $\sigma_{\text{max}}^5(R, 10^5)$ ,  $\sigma_{\text{min}}^5(R, 10^5)$  replace static strengths

$$\sigma_{\text{max}}^5(R) = 2 \cdot \bar{R}^t \cdot \Psi_{\text{Master}}^{t,5} / (\Psi_{\text{Master}}^{t,5} - R + R \cdot \Psi_{\text{Master}}^{t,5} + 1), \quad 0 < R < 1$$

$$\sigma_{\text{min}}^5(R) = -2 \cdot \bar{R}^c \cdot \Psi_{\text{Master}}^{c,5} / (\Psi_{\text{Master}}^{c,5} + R + R \cdot \Psi_{\text{Master}}^{c,5} - 1), \quad 1 < R < 100 (\infty).$$

$$\text{with } R = (\sigma_m - \sigma_{2a,5}) / (\sigma_m + \sigma_{2a,5}).$$

### CFL curves $\sigma_{\text{max}}^5(R, 10^5)$ within the 2 IFF domains $\bar{R} \rightarrow \sigma^5(R)$

$$\frac{-(\sigma_{2m} - \sigma_{2a}) + |\sigma_{2m} - \sigma_{2a}|}{2 \cdot \bar{R}_\perp^c} = 1 \quad \text{and} \quad \frac{\sigma_{2m} + \sigma_{2a} + |\sigma_{2m} + \sigma_{2a}|}{2 \cdot \bar{R}_\perp^t} = 1 \quad \text{static}$$

$$\frac{-(\sigma_{2m} - \sigma_{2a}) + |\sigma_{2m} - \sigma_{2a}|}{2 \cdot \sigma_{\text{min}}^5(R)} = 1 \quad \text{and} \quad \frac{\sigma_{2m} + \sigma_{2a} + |\sigma_{2m} + \sigma_{2a}|}{2 \cdot \sigma_{\text{max}}^5(R)} = 1 \quad \text{cyclic.}$$

### Modelling in the Transition Zone between the mode domains

- \* The transition zone where both the modes interact requires the interaction equation

$$\text{Eff} = [(\text{Eff}^{\text{NF}})^m + (\text{Eff}^{\text{SF}})^m]^{m^{-1}} = 100\% = 1.$$

Formulated in CFL coordinates  $\sigma_a$  and  $\sigma_m$  the static interaction equation reads

$$\left(\frac{-(\sigma_{2m} - \sigma_{2a}) + |\sigma_{2m} - \sigma_{2a}|}{2 \cdot \bar{R}_\perp^c}\right)^m + \left(\frac{\sigma_{2m} + \sigma_{2a} + |\sigma_{2m} + \sigma_{2a}|}{2 \cdot \bar{R}_\perp^t}\right)^m = 1 \quad \text{static curve, } n=2N_f.$$

- \* For the  $N = n = 1$  cycle with  $n = 2 \cdot N_f$ : Static interaction equation delivers a curve which still runs through the full Haigh diagram.

### CFL curves in the full Haigh diagram

- \* To obtain a CFL curve for higher  $N$  and larger ratios  $R_{\text{trans}} = -\bar{R}^c / \bar{R}^t$  the two opposite mode decays in the transition zone are to adjust by  $f_d = 1 / [1 + \exp((c_1 + \sigma_m) / c_2)]$ .
- \* Inserting  $R = (\sigma_m - \sigma_{2a,5}) / (\sigma_m + \sigma_{2a,5})$  for  $\sigma_m \rightarrow \sigma_{2m}$  as running variable the CFL curve  $\sigma_{2a}(\sigma_{2m}, N = \text{const})$  is to determine by solving the complicate implicit equation for  $\sigma_{2a}$  below

$$\left(\frac{-(\sigma_{2m} - \sigma_{2a,5}) + |\sigma_{2m} - \sigma_{2a,5}|}{2 \cdot \sigma_{\text{max}}^5(R) / (1 + e^{-\frac{c_{1SF} + \sigma_{2m}}{c_{2SF}}})}\right)^m + \left(\frac{(\sigma_{2m} + \sigma_{2a,5}) + |\sigma_{2m} + \sigma_{2a,5}|}{2 \cdot \sigma_{\text{max}}^5(R) \cdot (1 + e^{-\frac{c_{1NF} + \sigma_{2m}}{c_{2NF}}})}\right)^m = 1.$$

Table 8-5: Steps to generate a CFL curve. IFF,  $N=10^5$  cycles, via 'side lines' of the Haigh diagram

1 Choice of the distinct CFL (example  $N = 10^5$ )

2 Determination of the 2 Master curves

Assumption: usual test curves  $R=0.1$  (NF),  $R=10$  (SF) are sufficient instead of  $R=0$ ,  $R=1000 \cong \infty$

$$\sigma_{max}^{Master}(N, R = 0.1) \rightarrow = \sigma_{R=0.1} = c_1^{NF} + (\bar{R}^t - c_1^{NF}) / \exp\left(\frac{\log(N)}{c_1^{NF}}\right) c_2^{NF}$$

$$\sigma_{min}^{Master}(N, R = 10) \rightarrow = \sigma_{R=10} = c_1^{SF} + (-\bar{R}^c - c_1^{SF}) / \exp\left(\frac{\log(N)}{c_1^{SF}}\right) c_2^{SF} .$$

3 Assumption: Straight asymptotic side lines in the 2 mode domains  $\sigma_a(\sigma_m) = c_1 + c_2 \cdot \sigma_m$

2 strength points are given and 2 mean  $\sigma_a(\sigma_m, N)$  of  $R=0.1$  and  $R=10$  are to compute as a fixed point of each side line

4 Computation of the fixed points in the domains NF, SF (n MPa)

$$\sigma_{R=0.1}^{100000} = 27.3 \rightarrow \sigma_{a R=0.1}^{100000} = 0.5 \cdot \sigma_{R=0.1}^{100000} \cdot (1-0.1) = 12.3, \quad \sigma_{m R=0.1}^{100000} = \sigma_{R=0.1}^{100000} - \sigma_{a R=0.1}^{100000} = 15.0,$$

$$\sigma_{R=10}^{100000} = -136.5 \rightarrow \sigma_{a R=10}^{100000} = -0.5 \cdot \sigma_{R=10}^{100000} \cdot (1-1/10) = 61.4, \quad \sigma_{m R=10}^{100000} = \sigma_{R=10}^{100000} + \sigma_{a R=10}^{100000} = -75.$$

5 Function for the decay of mode influences  $\sigma_a(\sigma_m)$  over the transition zone

Parameters sets from the strength point and a fixed point  $f_d = 1 / [1 + \exp((c_1 + \sigma_m)/c_2)]$ .

$$f_d(\text{SF}): (\sigma_a, \sigma_m, N, R=10) \rightarrow 0.99 \text{ with } (\sigma_a, \sigma_m, N, R=0.1) \rightarrow 0.01 ;$$

$$f_d(\text{NF}): (\sigma_a, \sigma_m, N, R=10) \rightarrow 0.01 \text{ with } (\sigma_a, \sigma_m, N, R=0.1) \rightarrow 0.99.$$

6 'Static' envelope curve: Solving the interaction equation for  $\sigma_a(\sigma_m, N = 1)$

$$\left( \frac{-(\sigma_{2m} - \sigma_{2a}) + |\sigma_{2m} - \sigma_{2a}|}{2 \cdot \bar{R}_\perp^c} \right)^m + \left( \frac{\sigma_{2m} + \sigma_{2a} + |\sigma_{2m} + \sigma_{2a}|}{2 \cdot \bar{R}_\perp^t} \right)^m = 1 \rightarrow \sigma_{2a}(\sigma_{2m}, \bar{R}_\perp^c, \bar{R}_\perp^t).$$

7 Asymptotic side line approach for the decaying curves  $\sigma_a(\sigma_m, N > 1)$

$$[\sigma_{2a}(\sigma_{2m}, N)]^m = (c_{1SF} + c_{2SF} \cdot \sigma_{2m})^m + (c_{1NF} + c_{2NF} \cdot \sigma_{2m})^m$$

Work case  $N = 10^5$  cycles,  $m = 2.5$

$$c_{1SF} = 0.63 = c_{2SF}, \quad c_{1NF} = 0.34 = -c_{2NF}; \quad c_{1SF5} = -40.6, \quad c_{2SF5} = -5.56, \quad c_{1NF5} = -49.5, \quad c_{2NF5} = 5.55$$

$$\sigma_{2a}(\sigma_{2m}, N=10^5, c_i) = \left[ \left( \frac{c_{1SF} + c_{2SF} \cdot \sigma_{2m}}{1 + \exp\left(\frac{c_{1SF5} + \sigma_{2m}}{c_{2SF5}}\right)} \right)^m + \left( \frac{c_{1NF} + c_{2NF} \cdot \sigma_{2m}}{1 + \exp\left(\frac{c_{1NF5} + \sigma_{2m}}{c_{2NF5}}\right)} \right)^m \right]^{1/m} .$$

## 10.6 Check of the FMC-driven Idea to Split the Operational Loading mode-wise

The failure mode thinking of the FMC forces to think about the idea "A loading  $R = -1$  can be split into 2 swelling loadings", see [Fig.8-16](#).



A separation is performed due to the activated inherent different failure modes. For a UD material the fully reversed alternating S-N curve  $R = -1$  is split into its mode portions associated to the tensile and compressive domain.

The FMC principally permits predictions in the transition zone from pure domains information  $\sigma_{R=0}, \sigma_{R=\infty}$ . Hence, in *Table 8-3* an attempt was made to estimate the fatigue life of the fully (mode) reversed  $R = -1$  from the ‘Basic or Master’ S-N curves of the 2 modes.

Question was: “Is the sum of micro-damage  $D$  on basis of 2 strengths and 2 Master S-N curves the same as for  $R = -1$ ?”.

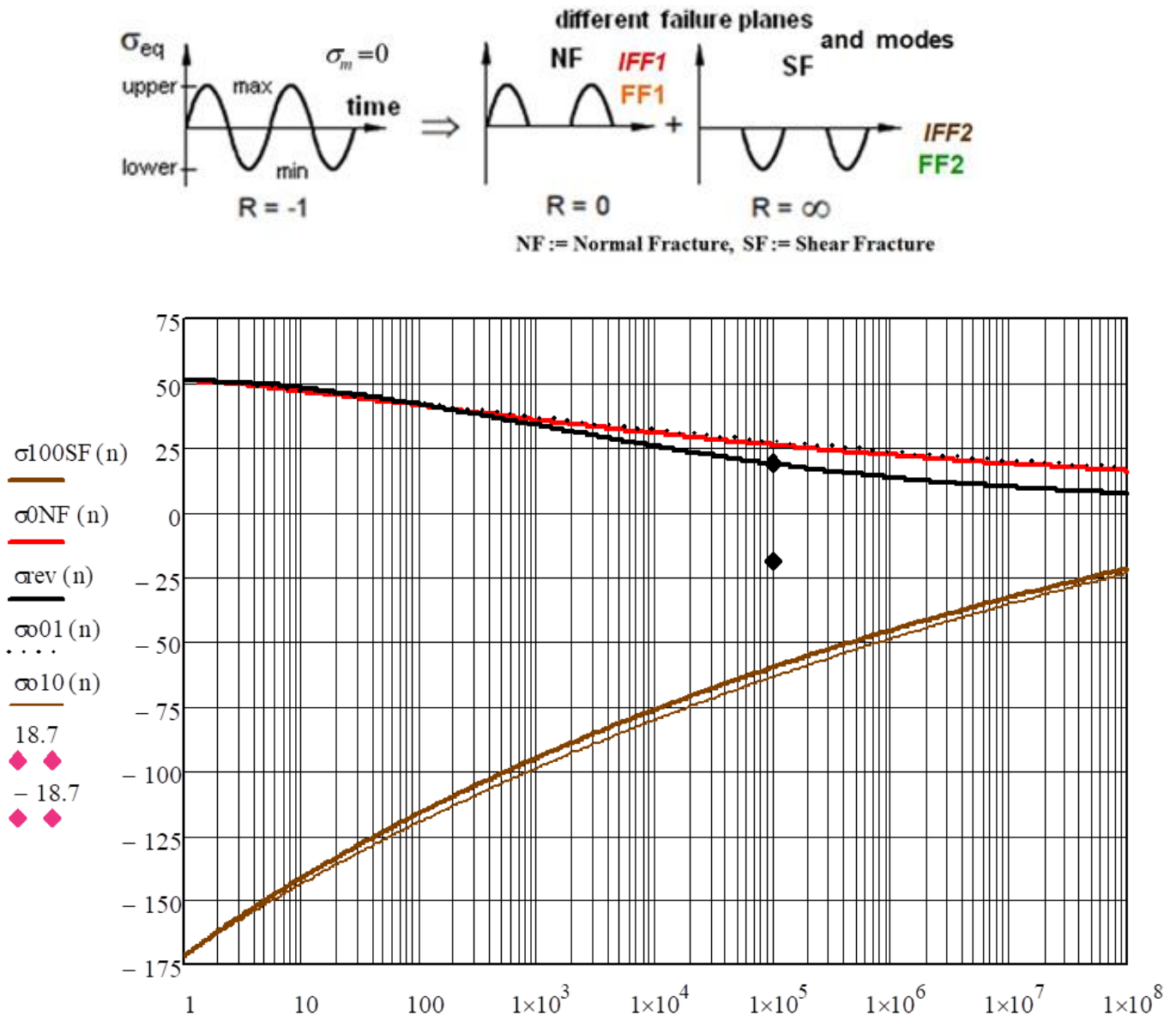


Fig.8-16: (up) IFF mode-wise modeling of loading cycles (example  $R = -1$ ) for high-performance ‘fiber-dominated designed’ UD laminas-composed laminates. (down) S-N curves used,  $\sigma_{rev} \equiv \sigma_{R = -1}$

The results in *Table 8.3* demonstrate that the FMC-fed hope “In the case of brittle materials fatigue treatment may become simpler by mode-wise load splitting” was not fulfilled. The micro-damage

process depends on the alteration effects and in the transition zone the scatter of test data is larger than in the pure domains.

This reminds the author of his former (1968-1970), colleague Wolf Elber † when Wolf worked on his crack-closure concept for metallic materials. Here, one must think about the closure and opening of flaws in brittle materials.

Table 8-3: Numerical example and idea check.  $\bar{R}_{\parallel}^t = 1980$ ,  $\bar{R}_{\parallel}^c = 1500$ ,  $\bar{R}_{\perp}^t = 51$ ,  $\bar{R}_{\perp}^c = 172$ ,  $\bar{R}_{\perp\parallel} = 71$  [MPa].  
From mapping of S-N test curves:  $c_1^{SF} = 87$ ,  $c_1^{SF} = 9.47$ ,  $c_3^{SF} = 0.96$ ;  $c_1^{NF} = 7.1$ ,  $c_2^{NF} = 6.05$ ,  $c_3^{NF} = 1.34$  and for reversed alternating stress  $c_1^{rev} = 5.0$ ,  $c_2^{rev} = 4.5$ ,  $c_3^{rev} = 1.84$

Example with Idea 'Mode Separation of Loading R = - 1' ( $\sigma_m = 0$ )

R = - 1 reversed alternating stress → split into the 2 swelling parts R = 0 and 100 (∞).

Fatigue Life prediction: Estimation for R= -1 on basis of  $\sigma_{R=0}$ ,  $\sigma_{R=\infty}$

The FMC *should* permit predictions in the transition zone from pure domain information, only

\* From testing as Master S-N curves are available

$$\sigma_{max}^{Master}(N, R = 0.1) = \sigma_{R=0.1} = c_1^{NF} + (\bar{R}^t - c_1^{NF}) / \exp\left(\frac{\log(N)}{c_1^{NF}}\right)^{c_2^{NF}}$$

$$\sigma_{min}^{Master}(N, R = 10) = \sigma_{R=10} = c_1^{SF} + (-\bar{R}^c - c_1^{SF}) / \exp\left(\frac{\log(N)}{c_1^{SF}}\right)^{c_2^{SF}} .$$

\* Determination of  $\Psi$  (defined positiv)

$$\Psi_{Master}^t = \frac{0.5 \cdot (1 - R) \cdot \sigma_{max}^{Master}}{\bar{R}^t - 0.5 \cdot (1 + R) \cdot \sigma_{max}^{Master}} \quad \text{and} \quad \Psi_{Master}^c = \frac{(1 - R) \cdot \sigma_{min}^{Master}}{(1 + R) \cdot \sigma_{min}^{Master} + 2 \cdot R \cdot \bar{R}^c} .$$

\* Transfer to boundary SNs as the mode-Basic S-N-curves R = 0 and R = 100 ( $\cong \infty$ ) using

$$\sigma_{R=0}(N^{NF} = 0, R) = 2 \cdot c_1^{NF} + (\bar{R}^t - c_1^{NF}) / \exp\left(\frac{\log(N^{NF})}{c_1^{NF}}\right)^{c_2^{NF}} / (\Psi_{Master}^t - R + R \cdot \Psi_{Master}^t + 1)$$

$$\sigma_{R=100}(N^{SF} = 100, R) = 2 \cdot c_1^{SF} + (-\bar{R}^c - c_1^{SF}) / \exp\left(\frac{\log(N^{SF})}{c_1^{SF}}\right)^{c_2^{SF}} \sqrt{(\Psi_{Master}^c + R + R \cdot \Psi_{Master}^c - 1)}$$

Application: Work case  $10^5$  cycles (indexed by<sup>5</sup>, stresses in MPa, N and n in cycles)

IFF1-IFF2: Test data Hahne, Fig.8-15,  $\sigma_{2a} = 18.7$  MPa  $\cong 100\%$  computed from mapping  $SN_{R=-1}$

\* Given: R = -1, n = N =  $10^5$ ,  $\sigma_{2a} = 18.7$ ,  $\sigma_{2m} = 0$ , D = 100 %.

$$\sigma_{R=0}(N^{NF*}, R=0) = 18.7 \rightarrow N^{NF*} = 2 \cdot 10^9 ; \sigma_{R=100}(N^{SF*}, R=100) = -18.7 \rightarrow N^{SF*} = 2 \cdot 10^{11}$$

\* Estimation of micro-damage portions and of  $D = n / N^{NF*} + n / N^{SF*}$

$$\Rightarrow R = -1, n = N = 10^5 \text{ cycles, } \sigma_{2a} = 18.7, D = 100 \%, \text{ failure.}$$

$$\Rightarrow \text{Split into 2 modes: } D < 1 \% \rightarrow \text{FMC-Idea: not applicable.}$$

LL: Compute a realistic example before trusting a hope. A close view at Fig.8-16 would have revealed the reality.

## 10.7 Estimation of the Amplitude and Comparison with the Measured Value

The data set of the example before is further used for a prediction example.

Estimation of maximum  $\sigma_{2a}$  using Constant Fatigue Life curve:  $R = -1$ ,  $m = 2.5$

$$c_{1SF} = 0.63 = c_{2SF}, \quad c_{1NF} = 0.34 = -c_{2NF}; \quad c_{1SF5} = -40.6, \quad c_{2SF5} = -5.56, \quad c_{1NF5} = -49.5, \quad c_{2NF5} = 5.55$$

$$\sigma_{2a}(\sigma_{2m}, N=10^5, c_i) = \left[ \left( \frac{c_{1SF} + c_{2SF} \cdot \sigma_{2m}}{1 + \exp\left(\frac{c_{1SF5} + \sigma_{2m}}{c_{2SF5}}\right)} \right)^m + \left( \frac{c_{1NF} + c_{2NF} \cdot \sigma_{2m}}{1 + \exp\left(\frac{c_{1NF5} + \sigma_{2m}}{c_{2NF5}}\right)} \right)^m \right]^{1/m}$$

$$\rightarrow \sigma_{2a} = 17.4 \text{ MPa} < 18.7 \text{ MPa} \quad \text{from measurement.}$$

Result:

Micro-damage portion  $D = 100\%$  is still reached at a lower amplitude stress  $\Rightarrow$  conservative.

## 10.8 Steps of the FMC-based Fatigue Life Estimation Procedure

The steps of the fatigue life estimation procedure are depicted in the following figures. **Step 1** is searching measured S-N curves. Fig.8-17 presents a measured S-N-curve that serves as master S-N curve. This S-N curve can be mapped by a straight line in a log-log diagram.

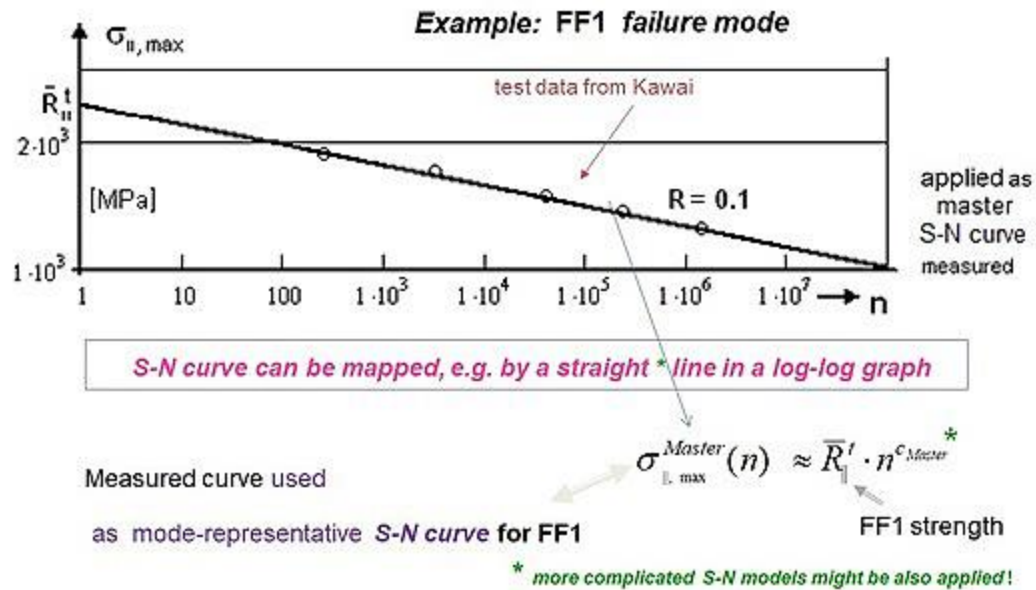
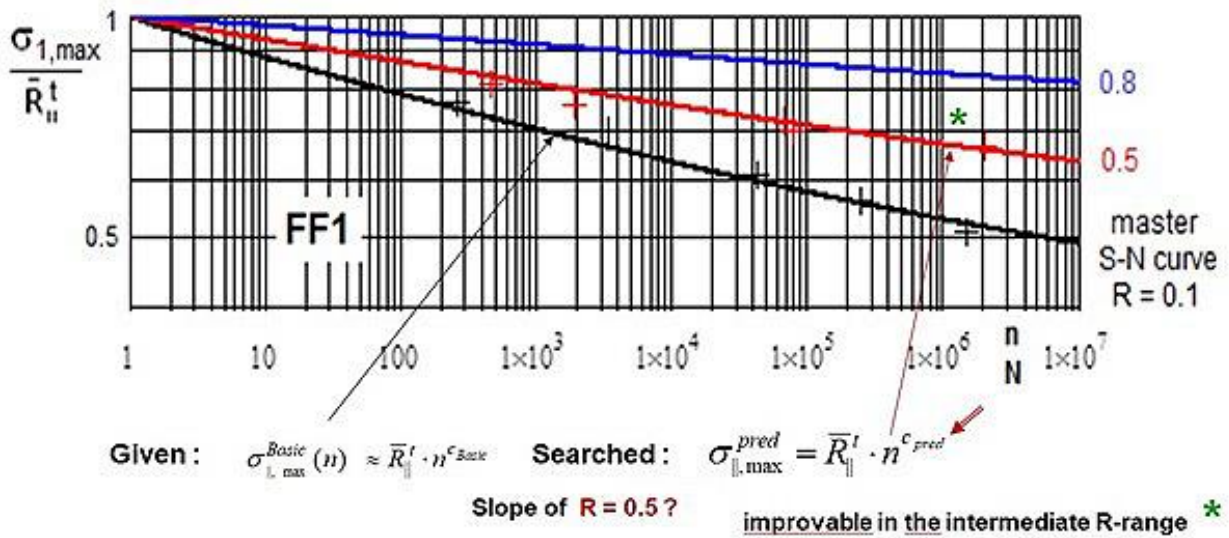


Fig.8-17: Mapping of UD S-N data and mode-representative Master S-N curve, FF1 here

In the case of variable amplitude loading several S-N curves are needed. This will be performed for the tension domain in Fig.8-18 by application of Kawai's model however a mode-wise application.

Statistical analyses have shown that the fatigue life estimation using the linear accumulation method of Palmgren-Miner tends to be too optimistic, Fig.8-19. However a satisfactory reason could not yet found. One explanation is the right use of the right SFC. A more severe explanation is the loss of the loading sequence which is different for ductile and brittle materials. This is to consider in the design by the application of Relative Miner with a  $D_{feasible} < 100\%$ .

Fig.8-20 finally shall briefly give the fatigue life estimation procedure for the example laminate.



*Application of Kawai's 'Modified Fatigue Strength Ratio'*

Fig.8-18: Prediction of other needed FF1 S-N curves from Master mode S-N curve and Cuntze's mode-dedicated Kawai model ( $\Psi$  curve)

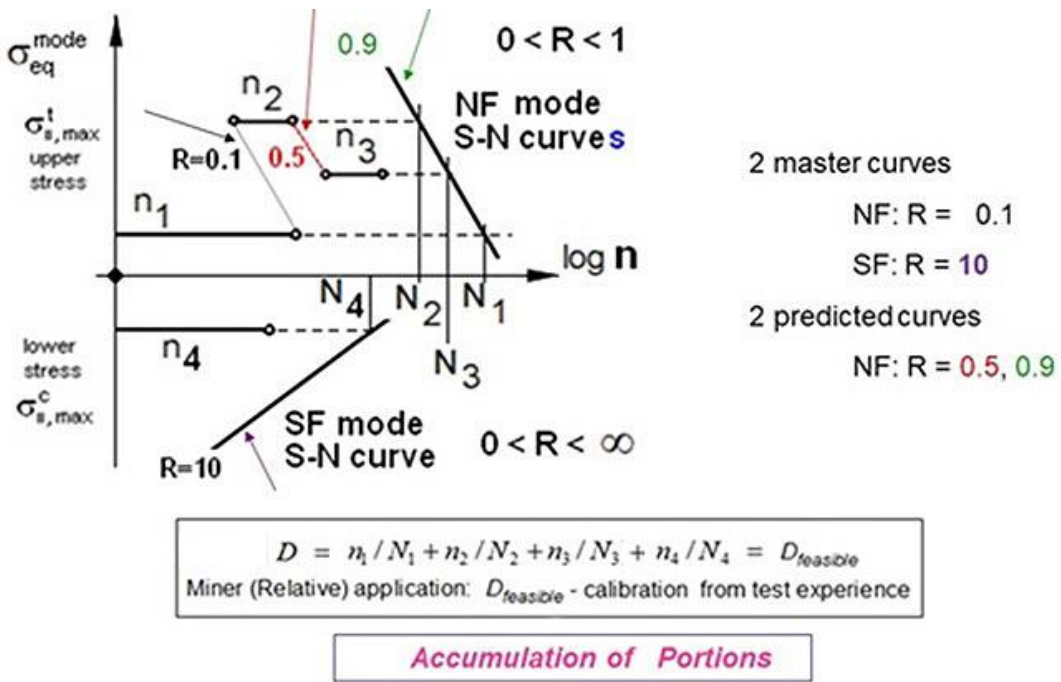


Fig.8-19: Lifetime Prediction (estimation) Method. Schematic application for a simple example, 4 blocks.  $D_{feasible}$  from test experience

Due to the lack of test data regarding ductile and slightly brittle metals the author he could not apply the CFL generation method above for this type of materials.

Everything in the world is terminated by **chance** and **fatigue**. *Heinrich Heine*

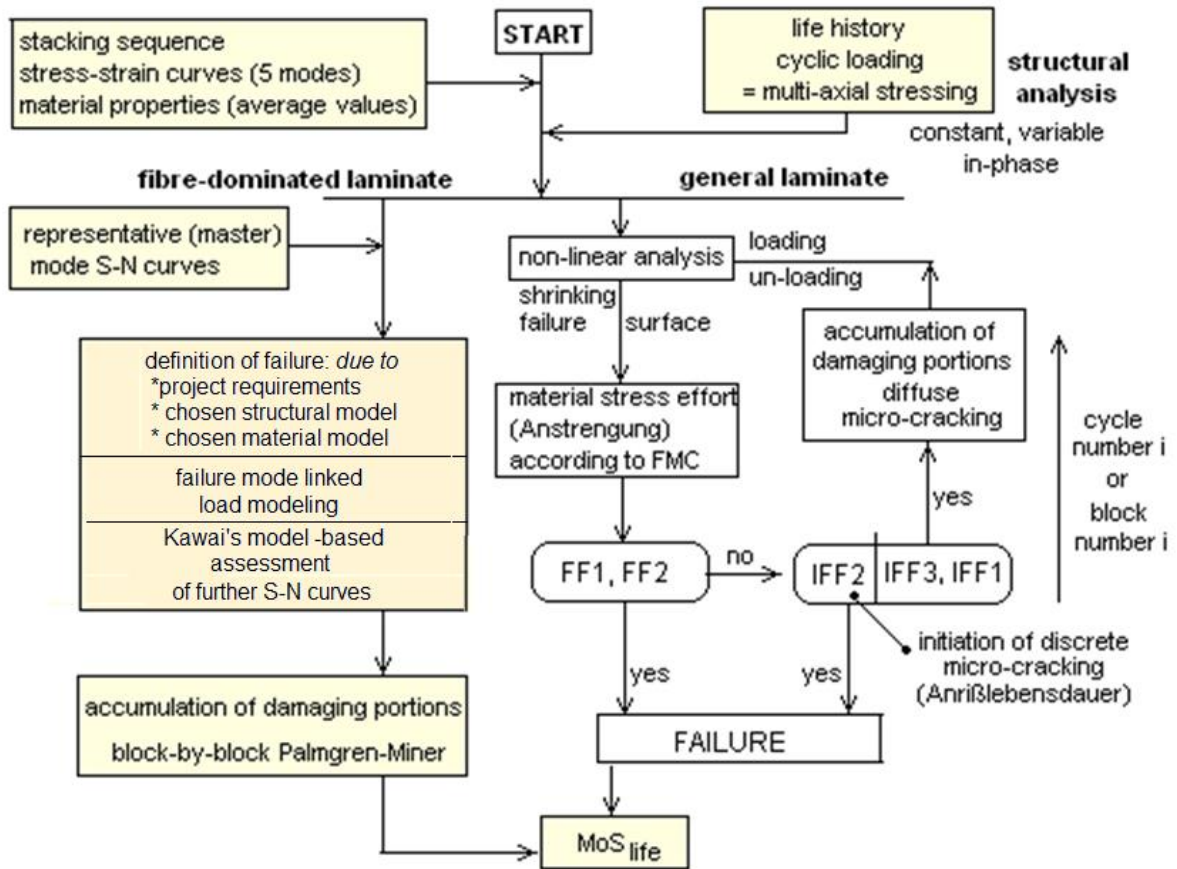


Fig.8-20: Non-linear estimation of a laminate's fatigue life

After having had some pushing new ideas one should not think to be at the top, but just an intermediate High Fidelity level is reached. The next figure enables to get a feeling how the author feels regarding the High Fidelity level reached for 3D SFCs situation and with his Fatigue modelling.



*After a tough ascent - considering the fatigue life estimation idea - the arrival at the 'top'.*

*"Is it really the top? No. It goes even higher".*

*A High Fidelity level is not fully reached with the given models according to missing test data.*

# 11 Conclusions, Literature and Terms

## 11.1 Conclusions

### 11.1.1 Failure-Mode-Concept, considering the investigated 3 Material Families

- Formulation basis: Does the material element experience a volume change, a shape change and friction. Then, following Beltrami's statement, a successful demonstration of the advantageous use of the 'physics-based' invariants  $I_1$  and  $J_2$  for the very different materials Normal Concrete, Ultra-High-Performance-Concrete, PMMA [Cun20b] and foam [Cunββ] could be presented. For UD material the same happened
- FMC-based SFCs are simple but describe physics of each single failure mechanism pretty well. Delivers a combined formulation of independent modal failure modes, without the well-known shortcomings of global SFC formulations, which mathematically combine independent failure modes
- The determination of model parameters is to perform by mapping in each pure failure domain and of the interaction exponent  $m$  by determination in the transition zone between the modes
- Direct use of the friction value  $\mu$  in the SFC - *instead of using a friction model parameter* - better matches with the engineer's thinking
- The use of the entity  $Eff$  excellently supports 'understanding the multi-axial strength capacity of materials'
- Clear equivalent stresses can be calculated for the presented Modal SFCs. Unfortunately, equivalent stresses are differently defined. For instance V. Kolupaev in his Springer book 'Equivalent Stress Concept for Limit State Analysis' [Kol17] and other authors define equivalent stress for Global SFCs. One question comes up here: Which strength does one refer to the determined equivalent stress?
- Fracture stresses are acting stresses divided by the stress effort  $Eff$  in order to fulfil the failure condition  $F = I$
- A usual SFC just describes a 1-fold occurring failure mode (mechanism)
- A multi-fold occurrence of a failure with its joint probabilistic effects must be additionally considered in the formulas
- A SFC can be validated, principally, by 3D test data sets, only. If just 2D test data is available, then the 2D-reduced 3D-SFC is applied. Then, the required High-Fidelity is not fully achieved. This means that the necessary 3D mapping quality is not fully proven
- A test series of an isotropic material along a tensile meridian (it delivers  $R^t$ ,  $R^{cc}$ ) or along a compressive meridian (delivers  $R^c$ ,  $R^{tt}$ ) alone is not sufficient, on both the meridians tests must be performed. For a general 3D-mapping at least multi-axial failure stress states ( $R^{tt}$ ,  $R^{cc}$ ) are required which generate two-fold failure modes. Then the significant inherent 120°-symmetry of brittle isotropic materials can be mapped
- When creating an SFC,  $Eff^{mode}$  must become zero if the driving stress  $\tau$  in the case of SF and  $\sigma^t$  in the case of NF becomes zero
- Rounding-off, by employing an interaction equation in the transition zone of adjacent modal failure curves (2D) or of partial failure surfaces is leading to a pseudo-global failure curve or surface. In other words, again a 'single surface failure description' is achieved, however, without the well-known shortcomings of Global SFCs.
- The FMC does not build on a material but on the material's solid deformation behavior!

- Efficient concept, that improves prediction + simplifies design verification, applicable to brittle and ductile, dense and porous, isotropic, transversely-isotropic and orthotropic materials if clear failure modes can be identified and the material element can be well homogenized.

### 11.1.2 Structural Mechanics Building: presumption ‘homogeneous material’

The author believes that the investigations prove a generic number of 2 for isotropic and of 5 for transversely-isotropic materials. Orthotropic ‘materials’ are practically still of structural nature and require a ‘material’-dedicated special treatment.

Intension of this investigation was to demonstrate, as far as test data was available, that material symmetry might be a sound basis for obtaining a more ‘closed’ building in mechanics desired by the author since about 30 years.

The following results can be now provided supporting the existence of a generic number 2 for isotropic materials:

- *Assessment of critical multi-axial stress states:* The formulations of invariant-based isotropic strength failure conditions (criteria) SFC just need 2 invariants. Due to the fact that a stress state may activate a multi-fold fracture failure type NF or SF the original rotational symmetric fracture body becomes 120°-symmetric. This is tackled by employing the invariant  $J_3$ .
- *Failure type Normal Yielding NY:* It could be test data-based shown that this 2<sup>nd</sup> yield type exists in parallel to Shear Yielding SY. Considering the concave failure surface Drucker’s stability postulate is to discuss
- *Existence of SIF  $K_{IIcr}^c$ :* The author also tried to pave the way for a 2<sup>nd</sup> ‘basic’ SIF  $K_{IIcr}^c$  in parallel to  $K_{Icr}^t \equiv K_{Ic}$ , where the self-explaining suffix <sub>cr</sub> must (unfortunately) replace the classical <sub>c</sub> and where <sup>t</sup> denotes tensile and <sup>c</sup> compression in order to not confuse readers with two c as indices. The term ‘basic’ is given to  $K_{Icr}^t$  and  $K_{IIcr}^c$  because the original fracture stress state-induced flaw inclination angle remains ‘stable’ under further loading and no turning crack under tension or a wing (secondary) crack under compression is activated. The SIF  $K_{IIcr}$  and  $K_{IIIcr}$  are necessary (friction-free crack surface) for crack-turning Mixed Mode Fracture investigations. The basic SIFs  $K_{Icr}^t$  (see Table 4-2) and  $K_{IIcr}^c$  show equilibrium,

Material symmetry seems to have told the author:

*In the case of isotropic materials – capturing ductile and brittle - for the material’s entities a generic (basic) number of 2 is inherent. This is valid for modes, invariants, yield strengths, fracture strengths, fracture mechanical SIFs, fatigue modes and more.*

*In the transversely-isotropic case the number is 5.*

Does this not simplify the engineer’s situation and lead to a ‘closed macro-mechanical building’?

One might think: “*Material macro-mechanics seems to possess a mathematical order*”.

### 11.1.3 Generation of the Mohr-Coulomb failure curve

1. Proof, that the structural stresses-formulated fracture curve  $\sigma_2$  ( $\sigma_3$ ) can be transferred into a Mohr-Coulomb one  $\tau_{nt}$  ( $\sigma_n$ )
2. Demonstration that a dependence of the shear fracture plane angle  $\Theta_{ip}^\circ$  with growing hydrostatic compressive stress is given, as far as SF is the primary failure mode. The angle

decreases which looks like becoming more ductile. Failure occurs in that plane where the driving shear stress  $\tau$  or equivalently where  $Eff^{SF}$  is maximum

3. The interaction formula maps the course of test data in the mode transition zone. For very brittle materials the mapping quality of  $F^\tau$  and IFF2 is sufficient for design verification as it is conservative. For an accurate determination of the altering fracture plane angle  $\Theta_{fp}^\circ$  both the SFCs had to made more ‘physically correct’ by the chosen degradation function  $f_d$
4. The huge effort spent for the generation of  $\Theta_{fp}^\circ$  and the Mohr-Coulomb failure curve paid off for the isotropic and for the UD material as well. For the isotropic material the effort was even higher because  $\Theta_{fp}^\circ$  also alters with the meridian-marking Lode angle  $\vartheta$  caused by the 120°-rotational symmetry which impacts  $\tau_{nt}(\sigma_n)$
5. The determination of the cohesive strength  $\bar{R}^\tau$ , by considering the SF-mode only from touch point information  $(\tau_{nt}^c, \sigma_n^c)$ , is just an *extrapolation*, because in the case of brittle materials  $\bar{R}^\tau$  is usually located in the transition domain NF-SF. Hence, a realistic cohesive strength can be not predicted by properties just belonging to the SF mode if the NF mode is activated, too. An interaction of the modes is mandatory. At least for Normal Concrete data sets were available and shall outline this by the following predictions:  
 $\bar{R}^c = 40$  MPa,  $\bar{R}^c = 4$  MPa,  $\mu = 0.19$ 
  - Linear Mohr-Coulomb, single mode SF:  $\bar{R}^\tau = \tau_{nt}^c + \mu \cdot \sigma_n^c = \tau_{nt}^c + \mu \cdot \sigma_n^c = 17$  MPa
  - FMC-extrapolation, single mode SF, rot-symm:  $\Theta^{CM} = \Theta^c = \text{constant} \rightarrow \bar{R}^\tau = 13.5$  MPa
  - FMC-extrapolation, single mode SF, 120°-model:  $\bar{R}^\tau = 12.5$  MPa
  - FMC, interaction SF-NF, 120°-model, considering  $f_d$ :  $\bar{R}^\tau = 11$  MPa .

### 9.1.4 Fatigue

Chapter 8 provides a novel life time prediction way:

- A continuous determination of *constant fatigue life* curves CFL  $\sigma_a(\sigma_m, N = \text{const.})$  in the Haigh diagram  $\sigma_a(\sigma_m)$  on basis of the FMC-based static SFCs with interaction equation to capture the transition zone between the modes and on basis of available SN test curves depicted as fatigue (reserve) strength  $\sigma_{res}(R, N)$ . The chosen fitting function practically is the 4 parameter Weibull curve model (*strength point with three curve parameters*).
- Mapping in the transition zone became possible because the author used a decay function which terminates the influence of the SF (compression) part in the Haigh diagram when the NF part begins at  $R=0$  and vice versa for NF. Essential is that the FMC-based static SFCs are equivalent stress curves  $\sigma_{min,eq}(R, N)$  and  $\sigma_{max,eq}(R, N)$  of a mode like the Mises equivalent stress in the case of ductile materials to capture multi-axial stress states
- The author’s mode-dedication of Kawai’s Modified Fatigue Strength Ratio  $\Psi$  optimizes Kawai’s idea to firstly determine a strength-normalized master SN curve for each mode. Other necessary SN curves, necessary for the verification of the usually faced variable amplitude operational loading, can then be derived from this Master curve. Also the boundary mode SN curves  $R=0$  and  $R=+\infty$  ( $\cong 100$ ) may then be determined and could be used as basic SN curves.

*Here one may add:*

***Theory is the Quintessence of all Practical Experience.*** [August Föppl]  
*Engineering scientist for mechanics and  
 head of the materials testing office for mechanical engineering in Munich.*



And, from the author

Validated isotropic 3D SFCs enable to predict the 120°-symmetric fracture failure body and further they enable to 'judge' the provided 3D fracture stress states for physical plausibility.

### 11.1.5 Some specific material conclusions

#### Isotropic material

- Shear fracture emerges orthogonally to that plane, where the maximum effort  $E_{ff}^{SF}$  stresses the solid. Mechanically, this is as well given in the uniaxial compression case in the axial cross-section of the fracture body as in the bi-axial compression stress case
- With the 'isotropic' invariant  $J_3$  the bi-axial strength capacity of isotropic brittle materials is captured. This bi-axial strength capacity ( $\sigma_{fr}$ ,  $\sigma_{fr}$ ) is  $\neq$  the uni-axial strength  $R$  in the compressive domain and in the tensile stress domain, too. For dense materials is valid  $R^{cc} \equiv \sigma_{fr}^{cc} > R^c$ , and for porous materials  $\sigma_{fr}^{cc} < R^c$ . Under bi-axial tension for brittle and porous materials holds  $\sigma_{fr}^{tt} < R^t$ .  $J_3$  can be employed in each case
- Due to the Poisson effect, bi-axial compression leads to an axial tensile straining  $\varepsilon_3 = -2 \nu \cdot \sigma^c / E$
- The 120°-located dents of the isotropic fracture failure body, are the probabilistic result of a 2-fold acting of the same failure mode and can be mapped by  $J_3$
- Porous Concrete Stone: the fracture body is 120° rotational symmetric, fully non-circular and the dents - in contrast to Normal Concrete - are oppositely located in the  $I_1 < 0$  domain to those in the  $I_1 > 0$  domain. Any high 3D-compression state is possible for compression-condensed porous materials, however, the material cannot be used further due to crushing
- Concrete: The Poisson effect, generated by a Poisson ratio  $\nu$  (estimation, for  $\nu > 0.2$ ), may cause tensile failure under 2D compression, because concrete fractures under an internal axial tensile straining
- UHPC: Due to redundancy effects ('healing' of the fracture inducing flaws) the non-circularity of the failure body will reduce with increasing  $p_{hyd}$ . For the pretty flawless UHPC - in comparison to Normal Concrete - this effect still holds. Under much higher hydrostatic loading stresses a volume reduction effect occurs.

#### Transversely-isotropic UD material

- For UD materials the failure curve denting bi-axial strength capacity  $R^t > R^{tt} = (\sigma_{fr}^{tt}, \sigma_{fr}^{tt})$  could be captured (analogous to  $J_3$ ) by an additional part in IFF1, if required by the given special task
- Due to the Poisson effect, bi-axial compression leads to a tensile straining  $\varepsilon_3 = \varepsilon_1$  captured by a tensile stress of the axially placed fibers. Hence, under hydrostatic pressure  $p_{hyd}$  'dense' UD materials will fiber-fracture due to  $\varepsilon_{||} \cdot E_{||} = R'_{||}$  at about thousands of MPa. Mind: UD lamina may even fracture under a 3D compression stress state
- Ply, Lamella, Sheet in construction: The fracture body is the well-known flattened 'cigar' of UD materials.  
Concrete: The Poisson effect, generated by a Poisson ratio  $\nu$  (estimation, for  $\nu > 0.2$ ), may cause tensile failure under 2D compression, because concrete fractures under an internal axial tensile straining.

#### Ceramic materials group: isotropic, transversely-isotropic, orthotropic

- For ceramic materials test data sets are practically merely available in literature. The author could only provide some graphs.

### 11.1.6 Some remarks considering fidelity in Engineering Design, Analysis, Simulation and Test

For a successful, faster and low-risk design development, a meaningful interaction of the above design topics: design, analysis, simulation and test is mandatory. This will help industry to reduce costs, time to market and by-passes the re-design process in case of small design changes. At any stage of the design development, product decisions must rely more and more on virtual tests based on reliable and robust structural analysis processes attached to realistic simulations. Time-consuming and costly physical tests can be commonly better run due to cross-fertilization of both the disciplines. A simulation-driven design development reduces - due to the virtual test possibilities by investigating multiple design options - later very costly bad design decisions in the early design phase. Further, a minimum number of material and structural tests can be focused. Response is given to “Which physical tests are stringent necessary?” Uncertainty in design is turned into a more robust design. (*Basically from NAFEMS information sheets: The author was a long-time member of the NAFEMS composite WG*).

In the case of critical structural tasks the engineer must have system knowledge about the product, its physics behind and the right tools to solve the task. Therefore, the author cannot see – considering the engineer’s responsibility to design reliable structures – a general change for the often proclaimed ‘Democratization of design, analysis and manufacture’. For him this might lead to the use of black boxes for not enough well experienced designing engineers. I think Ian Symington, NAFEMS, makes the democratization idea, basically for less critical applications - more realistic by saying: “*The users have to be educated so that they understand the limitations of the method they are using and also educated so that they are aware of their own limitations!*”

Virtual testing creates new responsibility for the engineer to guarantee the required confidence level by building confidence for taking decisions in design verification and product certification. Therefore SFCs are mandatory to reduce failure risk. Physical testing on material level becomes more important to obtain really 3D-validated SFC models that can demonstrate their predictive capability. Further confidence will be given if a clearly structured and reliable ‘Macro-mechanics building’ is given indicating which verifications must be performed and which provides the hear focused reliable 3D SFCs.

Above procedure requires High Fidelity. In this context shall be reminded:

- Concerning the material models used: Usual assumption for the models is an ideally homogeneous material.
- Input in Structural Analysis: - The best prediction of the typical behaviour of the structure is performed with typical values = average values, - In the later design verification, *dependent on the project requirements*, the average, the upper or the lower value of the respective property is to use
- Be similarly certain, reliable in the design with applied equations, properties, etc.!

### 11.1.7 Concerns from the Miscellaneous Chapter

- Determination of the interesting failure angle relations bridging  $F^{SF}$  and  $F^{Mises}$
- Successful evaluation of the not very appropriate ARCAN test data to quantify  $\mu_{\perp\perp}$
- Creation of a relatively simple novel model  $IFF2^{porosity}$  for a porous UD material in the quasi-isotropic domain
- Visualization of the influence of 2D- and 3D-compression stress states on the strength capacity by the material stressing effort  $E_{ff}$  and proving that all the failure stress states are

located on the failure surface  $Eff = 100\%$ . *The technical strength is not increased. One might only call this ‘increase of strength capacity’*

- Determination of a Reserve Factor by application of a Safety Concept
- For mathematically homogeneous and non-homogeneous SFCs the difference of Failure Index  $|F|$  and material stressing effort  $Eff$  has been outlined. In this context the concept of ‘proportional loading’ and the concept idea of ‘driving stress’ were presented. This Annex invites for discussion regarding linear and non-linear stress analyses.

### 11.1.8 Lessons Learned LL from the application of the SFCs

- It is advantageous from physical and from modelling reasons not to employ ‘global’ SFCs
- The challenge is not so much the establishment of a SFC but the convincing test data-based visualization of its associated fracture failure body and in this context for isotropic materials the display of the failure curve in the principal stress plane as a bias cross-section of the failure body. In the case of brittle isotropic materials, heavy effort causes the depiction of the different meridian curves as the axial cross-sections of the failure body with inward and outward dents along the axis of the 120°-symmetric isotropic failure body
- The use of the entity  $Eff$  excellently supports to understand a multi-axial strength capacity of a material (see Annex 5), visualized on some displayed failure bodies
- It is too discriminate bi-axial fracture stress state and (uni-axial) strength, defined as technical strength in engineering. Just for practical reasons the term bi-axial strength ( $R^t$ ,  $R^c$ ) is used for marking the bi-axial fracture stress state. In this context mind: Under multi-axial compression states the (material) strength is not increased but the risk of shear fracture failure is decreased, indicated by an  $Eff^{SF} < 1$ , see Annex 4.  $Eff = 1$  represents the outward dent of the failure surface, also
- An estimation of the cohesive strength value  $\tau_{nt}$  ( $\sigma_n = 0$ ) by using just  $Eff^{SF} = 1$  is an extrapolation and leads to higher values dependent on the specific model applied
- ‘Touch point’: It’s coordinates ( $\tau_{nt}^c$ ,  $\sigma_n^c$ ) in Mohr stresses correspond to the compressive strength point ( $R^c$ , 0) in structural stresses. Of-course, friction quantities, which are determined in the Mohr-Coulomb touch point, remain the same for the rotationally-symmetric model and for the 120°-rotationally-symmetric mode,  $c_{2\theta}^{SF} = c_2^{SF}$ ,  $\mu$ ,  $C^c$  of the isotropic material
- Multi-axial compression works as quasi-plasticizer
- Due to the redundancy effect (‘healing’ that causes increasing load carrying ability) found with concrete and grey-cast iron under bi-axial compression – in contrast to foam and concrete stones – the dent in the negative  $I_1$ -domain is oriented outward, opposite to the tensile domain
- Flaw distribution effect: Activation of the critical fracture plane depends on the spatial distribution and orientation of the flaws
- Hoop Planes = deviatoric planes =  $\pi$ -planes are convex. Meridian Planes are **not convex** at max  $I_1$  (tension) and for UHPC in the high hydrostatic domain
- The applicability of a SFC ends (example UD) when the driving mode stress  $\sigma^t$  (IFF1) or  $\tau$  (IFF2) becomes zero and the associate  $Eff$  becomes negative. Therefore, the traditional use to just apply the so-called ‘Proportional Loading (stressing)’ concept in order to derive  $Eff$  from F must be checked whether the condition above is fulfilled or not (see Annex 6)
- Limits of the applicability of the (material-linked) SFCs: Structural failure may occur which cannot be described by a SFC because it is not a material failure anymore (UD examples: instability of a tube test specimen under compression; filament-upon-filament compression within an ultra-highly compressed stack, as in Test Case 12 of WWFE-II, sub-chapter 5.7)
- A physically based strength model possesses a minimum number of model parameters. After proven demonstrations of a good mapping of the courses of accurate test data (‘goodness of fit’)

such a model is able to even sort out false test data.results of a successful qualification of a model (i.e. material model).



It would be nice if the engineering disciplines mechanical engineering and civil engineering (construction) were as close to using terms as river horse and crocodile show here !

**Sambia,**  
**surprising picture :**  
**Cuntze 2011**

> 4 m

**To proceed, we must improve the interdisciplinary work, for instance  
Mechanical Engineering with Civil Engineering.**

## 11.2 Literature

- [Arg73] Argo A S: *Physical basis of distortional and dilatational plastic flow in glassy polymers*. J. Macromol. Sci. Phys B8 (1973), 573-596
- [Awa78] Awaji H and Sato S: *A Statistical Theory for the Fracture of Brittle Solids under Multiaxial Stresses*. Int. J. of Fracture 14 (1978), R 13-16
- [Bec94] Becker W. and Kress,G: *Stiffness Reduction in Laminate Coupons due to the Free-edge Effect*. Comp.Science and Technology 52 (1994), 109-115
- [Bil11] Bilisik K: *Advances in Modern Woven Fabrics Technology*. Edited by Savvas Vassiliadis, ISBN 978-953-307-337-8, 252 pages
- [Bir38] Birch R.: *The Effect of Pressure Upon the Elastic Parameters of Isotropic Solids, according to Murnaaghan's Theory of Finite Strains*. Journal of Applied Physics 9 (4), 279-288.
- [Boe0?] Böhm, R.:
- [Boer89] de Boer, R. and Dresenkamp, H.T.: *Constitutive Equations for concrete in failure state*. J. Eng. 115 (8), 1989, 1591-1608
- [Boe85] *Boehler, J.P.*: Failure criteria for glass-fiber reinforced composites under confining pressure. J. Struct. Mechanics 13, 371-393
- [Boe87] Boehler J P : *Introduction to the invariant formulation of anisotropic constitutive equations*. 1987. In: Boehler J.P. (Ed.) *Applications of Tensor Functions in Solid Mechanics*. CISM Course no. 292. Springer-Verlag. In addition a personal note from J. Boehler on UD invariants which were later applied by the author in his FMC
- [Bre79] Breuer H und Stabenow J: *Schädigungskriterien glasiger Polymere im Hinblick auf deren Schlagzähmodifizierung*. Die Angewandte Makromolekulare Chemie 78 (1979), 45-65. SF-shape is SY-shape
- [Bri52] Bridgeman P.W.: *Studies in Large Plastic Flow and Fracture*. McGraw-Hill, New York, 1952
- [Bro18] Brocks W: *Plasticity and Fracture*. Springer, Series Solid Mechanics, Applications.
- [Bus06] Busse G , Kröplin B-. and Wittel F K: *Damage and its Evolution in Fiber-Composite Materials: Simulation and Non-Destructive Evaluation*. SFB 381, Stuttgart, ISBN 3-930681-90-3
- [Che11] Cherif Ch: *Textile Werkstoffe für den Leichtbau*. Springer-Verlag, 2011

- [Che13] Cherif, editor: *Leichtbau mit Textilverstärkung für Serienanwendungen: Bindermaterialien – Textile Preforms – Verbundbauteile; Buch zum DFG-AiF-Clustervorhaben – Leichtbau und Textilien*. Verlag Wissenschaftliche Skripten, 2013, ISBN 978-3-942267-81-6
- [Chr98] Christensen R M: *The Numbers of Elastic Properties and Failure Parameters for Fibre Composites*. Transactions of the ASME, Vol. 120 (1998), 110-113
- [Cun87] Cuntze R: *Failure Path Analysis of Multi-layered Fibre Reinforced Plastic Components with the Reliability Calculation Programme FRPREL*. ESA/ESTEC conference Noordwijk, Oct. 1987
- [Cun93] Cuntze R: *Deterministic and Probabilistic Prediction of the Distribution of Inter-Fibre Failure Test Data of Pre-strained CFRP Tubes composed of Thin Layers and loaded by radial pressure*. Wollongong, *Advanced Composites '93*, 579-585. *The Minerals, Metals & Materials Society*, 1993
- [Cun96a] *Bruchtypbezogene Auswertung mehrachsiger Bruchtestdaten und Anwendung im Festigkeitsnachweis sowie daraus ableitbare Schwingfestigkeits- und Bruchmechanik-Aspekte*. DGLR-Kongreß 1996, Dresden. Band 3
- [Cun96b] Fracture-type strength criteria , formulated by invariants which consider the material symmetries of the isotropic(anisotropic material. Conference on Spacecraft Structures, Materials & Mechanical Testing, 27-29 March 1996, ESA SP-386 pp 399-409
- [Cun97] Cuntze R: Evaluation of Multi-axial Test Data of UD laminae by so-called “Fracture-type Strength criteria” and by supporting probabilistic means, ICCM 1997, 14 pages\*
- [Cun98a] Cuntze R: *Strength Prediction for Multi-axially Loaded CMC-Materials*. 3rd European Workshop on thermal Protection Systems. ESA-ESTEC: Noordwijk, March 1998, WP P141
- [Cun98b] Cuntze R: *Application of 3D-strength criteria, based on the so-called "Failure Mode Concept", to multi-axial test data of sandwich foam, concrete, epoxy, CFRP-UD lamina, CMC-Fabric Lamina*. ICCE/5, Las Vegas, July 1998 (presentation)
- [Cun98c] Cuntze R and Sukarie G.: *Effective Dimensioning of 3D-stressed UD-laminae on Basis of Fracture-type Strength Criteria*. *Int. conf. on Mechanics of Composite Materials*. Riga, April 20-23, 1998. *Conference handbook*, presentation
- [Cun98d] Cuntze R: *The Failure Mode Concept- a new comprehensive 3D-strength Analysis Concept for any Brittle and Ductile behaving Material*. European Conference on Spacecraft and Structures, Materials and Mechanical Testing. ESA-CNES-DGLR-DLR, Braunschweig, Nov.4-6 1998
- [Cun99] Progressive Failure of 3D-stressed Laminates: Multiple Non-linearity treated by the Failure Mode Concept (FMC). DURACOSYS99, Brussels, July 1999. Balkema, Rotterdam, 2000
- [Cun00a] *Static Design and Strength 'Proof of Design' of Pressure Vessels, built from Ductile or Brittle Materials*. Problems of the North; Yakutsk 2000
- [Cun00b] *Are there Cost Drivers in the Structural Analysis of the ARIANE 5-Development?* Noordwijk, 29. Nov./1. Dec. 2000.
- [Cun01] *Assessment of Load- and Strain-controlled States of Stress in 'hot Spots' -On the way to an Industrial Approach for Gurson Materials*. 3rd European Conference on Launcher Technology. CNES, DLR, ESA-ESTEC, ISU: Strasbourg, Dec. 11-14, 2001.
- [Cun02] Cuntze R. and Memhard D.: *Evaluation of the Tension Rod Test for Ductile Material Behaviour - Key item for the establishment of a procedure to assess strain-controlled 'hot spots'*. European Conf. on Spacecraft Structures, Materials and Mechanical Testing; ESA-CNES-DGLR-DLR, Toulouse 2002, Conference handbook
- [Cun04] Cuntze R.: *Should we consider Matrix Yielding when investigating the Deformation Behaviour?* 9<sup>th</sup> European-Japanese Symposium on Composite Materials.. Technical University of Hamburg –Harburg, May 2014

- [Cun04a] Cuntze R and Freund A: *The predictive capability of failure-mode-concept-based strength criteria for multidirectional laminates*. WWFE-I, Part A. Comp. Science Technology 2004 , pp 343-377
- [Cun04b] Cuntze R: *The Predictive Capability of Failure Mode Concept-based Strength Criteria for Multidirectional Laminates*. WWFE-I, Part B. Comp. Science and Technology 64 (2004), 487-516
- [Cun05] Cuntze R: *Is a costly Re-design really justified if slightly negative margins are encountered? Konstruktion*, März 2005, 77-82 and April 2005, 93-98 (reliability treatment of the problem)\*
- [Cun05] Cuntze R: *Efficient 3D and 2D failure conditions for UD laminae and their applications within the verification of the laminate design*. Comp. Sci and Technology 66 (2006), 1081-1096
- [Cun08] Cuntze R.: *Strength Failure Conditions of the Various Structural Materials: Is there some Common Basis existing?*. SDHM, vol.074, no.1, pp.1-19, 2008
- [Cun12] Cuntze R: *The predictive capability of Failure Mode Concept-based Strength Conditions for Laminates composed of UD Laminae under Static Tri-axial Stress States*. WWFE-II, Part A . Journal of Composite Materials 46 (2012), 2563-2594
- [Cun13] Cuntze R: *Comparison between Experimental and Theoretical Results using Cuntze's Failure Mode Concept model for Composites under Tri-axial Loadings - Part B of the WWFE-II*. Journal of Composite Materials, Vol.47 (2013), 893-924
- [Cun13b] Cuntze R.: *Tackling Uncertainties in Design – uncertain design parameters, safety concept, modelling and analysis*. Verbundwerkstoffe, GDM, 18. Symposium, Chemnitz 30.3. – 1.4. 2011
- [Cun14] Cuntze R: *The Fracture Failure Surface of Foams, derived on basis of the author's Failure Mode Concept*. PPT presentation, Carbon Composites e.V. (CCeV), meeting of the working group 'Engineering', July 11, 2014\*
- [Cun14b] Cuntze R: *The WWFEs I and II for UD Materials – valuable attempts to validate failure theories on basis of more or less applicable test data*. In Conference Handbook SSMET 2014:= Europ. Conf. on Spacecraft Structures, Materials and Environmental Testing. Braunschweig, 1- 4 April 2014, 8 pages
- [Cun14c] HSB 01501-01: *Essential Topics in the Determination of a Reliable Reserve Factor*. IASB, Issue A, 2014 (Cuntze author) TIB Hannover, 20 pages,
- [Cun15a] Cuntze R: *Static & Fatigue Failure of UD-Ply-laminated Parts – a personal view and more*. ESI Group, Composites Expert Seminar, Uni-Stuttgart, January 2015, 27-28, keynote presentation\*
- [Cun15b] Cuntze, R: *Reliable Strength Design Verification - fundamentals, requirements and some hints*. 3rd. Int. Conf. on Buckling and Postbuckling Behaviour of Composite Laminated Shell Structures, DESICOS 2015, Braunschweig, March 26 ~27, Extended Abstract, Conf. Handbook, 8 pages
- [Cun15c] Cuntze R: *Basis Document, Update ComPoLyX Manual chapter Cuntze and Relationship of Cuntze's UD friction parameters b with Mohr's friction coefficients*. CCeV website, May 4, 2015 \*
- [Cun16a] Cuntze R: *Fracture failure surface of the foam Rohacell 71G*. 3. NAFEMS Regionalkonferenz, 25.-27. April, 2016. Berechnung und Simulation, 35 slides \*
- [Cun16b] Cuntze R: *Introduction to the Workshop - from Design Dimensioning via Design Verification to Product Certification*. Experience Composites 16 (EC16), September 21 – 23, 2016, Augsburg. Extended Abstract in the Symposium Abstracts. 10 pages\*
- [Cun16c] Cuntze R: *Progress reached, in Static Design and Lifetime Estimation?* Mechanik-Kolloquium, TU-Darmstadt, December 21, 2016 (UD and isotropic materials, Extended Presentation, 150 slides) \*
- [Cun17] Cuntze R: *Fracture Failure Bodies of Porous Concrete Stone (isotropic foam-like), Normal Concrete, Ultra-High-Performance-Concrete and of the Lamella (sheet) - generated on basis of Cuntze's Failure-Mode-Concept (FMC)*. NWC 2017, June 11-14 Stockholm. Extended Abstract, Symposium Handbook, 13 pages \*

- [Cun19a] Cuntze R: presentation in the author's working group CU AG "Engineering" on *3D-Festigkeitsbedingungen für spröde Werkstoffe isotrop, transversal-isotrope UD-Schicht und orthotropes Gewebe - ermittelt auf Basis des Failure-Mode-Concepts (FMC) von Cuntze*. June 25, 2019 Basel (English slides) \*
- [Cun19c] Cuntze R: *Technical terms for composite components in civil engineering and mechanical engineering*. Fachbegriffe mit Erklärung und Definition. In: *Fachbegriffe für Kompositbauteile – Technical terms for composite parts*. Springer Vieweg, Wiesbaden, 2019, 171 pages \*
- [Cun20a] Cuntze R: Einführungsvortrag des Autors als Leiter der AG „Bemessung und Nachweis“ zum CU-Thementag „*Richtlinien, bauaufsichtliche Zulassungen und Bauartgenehmigungen für die potentiellen Anwender Architekten, Tragwerksplaner und Bauherrn*“. Zoom conference, 19. Nov. 2020. 40 slides (English and German) \*
- [Cun20b] Cuntze R: *Normal Yielding NY and Compression-induced Critical Stress Intensity Factor  $K_{IIcr}^c$  - Missing Links in an Isotropic 'Closed' Macro-Mechanics Building*. 30 pages \*
- [Cun21] Cuntze R: *Strength capacity of bi-axially compressed UD strands at turning points of rotor blade loops and of hangers of network arch bridges*. CU-AG "Engineering", May 20. \*
- [Cun21b] Cuntze R: *The Mohr Coulomb Fracture Failure Curve  $\tau_m(\sigma_n)$  and Associated Topics*. June 21, pp 59 \*
- [DeTer99] De Teresa S.J.: *Failure of a composite lamina under three-dimensional stresses*. UCRL-JC-135664
- [DeTer04] DeTeresa S J, Dennis C, Freeman O C, and Groves S E: *The Effects of Through-thickness Compression on the Interlaminar Shear Response of Laminated Fibre Composites*. J. Compos Mater, V 38, No. 8, pp681-697, 2004
- [Dru52] Drucker D C and Prager W: *Soil mechanics and plastic analysis for limit design*. Quarterly of Applied Mathematics, 1952, vol. 10, no. 2, pp. 157–165
- [Ern07] Ernst G., Vogler M, Hühne C. and Rolfes R.: *Multi-scale Simulation for Stiffnesses and Strengths of Textile Composites*. NAFEMS Seminar, Simulating Composite Materials and Structures. Bad Kissingen, Nov. 2007
- [Fla82] Flaggs D L and Kural, MH: *Experimental Determination of the In Situ Transverse Lamina Strength in Graphite Epoxy Laminates*. J. Comp. Mat. Vol 16 (1982), 103-116
- [Gai19] Gaier C and Dannbauer H: *Eine Software-basierte Methode zur Betriebsfestigkeitsanalyse von Strukturbauteilen aus CFK*. Engineering Center Steyr, Magna, J. Maier, G. Pinter, Montanuniversität Leoben
- [Gei97] Geiwitz W, Theuer A and Ahrends F J: *Experimentelle Bestimmung eines Versagenskriteriums für faserverstärkte Keramik*. Tagungband "Verbundwerkstoffe und Werkstoffverbunde", Kaiserslautern september 1997
- [Ger94] Germanovich JN, Dyskin AV. *A model of brittle failure for material with cracks in uniaxial loading*. Mechanics of Solids 1988;23(2):111-123
- [Gie94] Gierlinski j t & Smith M (WS Atkins, UK); Thoft-Cristensen P (CSR Denmark); Santos J L T (IST Portugal); Cuntze R (MAN) & Gollwitzer S (RCP), Germany: *Reliability-based Design of structural components*. Proc. Symp. On Advanced Materials for Lightweight Structures at ESTEC Noordwijk, March 1994, ESA –WPP-070, pp 121 -125
- [Gol66] Goldenblat, I.I., Kopnov, V.A.: *Strength of Glass-Reinforced Plastics in the complex stress state*. Polymer Mechanics of Mechanical Polimerov, Vol. 1 1966, 54-59
- [Gri20] Griffith, A.A.: *The phenomena of Rupture and Flow in Solids*. Phil. Trans. Roy. Soc., London, A221 (1920), S. 163-198

- [Gur77] Gurson A L: *Continuum Theory of Ductile Rupture by Void Nucleation and Growth. Part 1: Yield criteria and flow rules for porous ductile media*. J.Eng. Mater. Techn.99 (1977), 2-15
- [Fla82] Flaggs D L and Kural M H: *Experimental Determination of the In Situ Transverse Lamina Strength in Graphite Epoxy Laminates*. J. Comp. Mat. Vol 16 (1982), S. 103-116
- [Gri21] Griffith, A.A.: *The phenomena of rupture and flow in solids*. Philosophical Transactions of the Royal Society of London, 1921, A 221: 163–198
- [Gur77] Gurson A L: *Continuum Theory of Ductile Rupture by Void Nucleation and Growth. Part 1: Yield criteria and flow rules for porous ductile media*. J. Eng. Mater. Techn.99 (1977), 2-15
- [Hah15] Hahne C: *Zur Festigkeitsbewertung von Strukturbauteilen aus Kohlenstofffaser-Kunststoff-Verbunden unter PKW-Betriebslasten*. Shaker Verlag, Dissertation 2015, TU-Darmstadt, Schriftenreihe Konstruktiver Leichtbau mit Faser-Kunststoff-Verbunden, Herausgeber Prof. Dr.-Ing Helmut Schürmann
- [Har93b] Hart-Smith L J: *An Inherent Fallacy in Composite Interaction Failure Curves*. Designers Corner, Composites 24 (1993), 523-524 [Has80] Hashin Z: *Failure Criteria for Unidirectional Fibre Composites*. J. of Appl. Mech. 47 (1980), 329-334
- [Has80] Hashin Z: *Failure Criteria for Unidirectional Fibre Composites*. J. of Appl. Mech. 47 (1980), 329-334
- [Hin04] Hinton M J, Soden, P D and Kaddour A S: *Failure criteria of fibre reinforced polymer composites*. The World-Wide Failure Exercise. Elsevier, 2004, ISBN 0-08-044475-X, 700 pages
- [Hop95] Hoppel C.R.R., Bogetti T.A. and Gillespie J.W.jr.: *Literature review – Effects of hydrostatic pressure on the Mechanical Behaviour of Composite Materials*. J. of Thermoplastic Composite Materials 8 (1995), 375-409
- [Hoek14] Hoek E and Martin C D: *Fracture initiation and propagation in intact rock - A review*. Journal of Rock Mechanics and Geotechnical Engineering 6 (2014) 287-300
- [Hol19] Holschemacherk (editor) et al.: *Entwurfs-und Berechnungstafeln für Bauingenieure*. 8.Auflage, Beuth Verlag GmbH
- [HSB] German Aeronautical Technical Handbook ‘*Handbuch für Strukturberechnung*’, issued by Industrie-Ausschuss-Struktur-Berechnungsunterlagen. TIB Hannover
- [Irw57] Irwin, G: *Analysis of stresses and strains near the end of a crack traversing a plate*. Journal of Applied Mechanics 24 (1957), 361–364.
- [Kad13] Kaddour A and Hinton M: *Maturity of 3D failure criteria for fibre-reinforced composites: Comparison between theories and experiments*. Part B of WWFE-II, J. Compos. Mater. 47 (6-7) (2013) 925–966.
- [Kaw04] Kawai M: *A phenomenological model for off-axis fatigue behaviour of uni-directional polymer matrix composites under different stress ratios*. Composites Part A 35 (2004), 955-963
- [Kaw88] Kawagoe M and Kitagawa M: *On criteria for craze initiation in glassy polymers*. J. of Materials Science 23 (1988), 3927-3932
- [Kno03] Knops M.: *Sukzessives Bruchgeschehen in Faserverbundlaminaten*. Diss. 2003. Aachen, Institut für Kunststoffverarbeitung
- [Kol12] Kolupaev V A, Bolchoun A and Altenbach H: *Unified Representation and Evaluation of the Strength Hypotheses*. 2012
- [Kol17] Kolupaev V A: Equivalent stress concept for limit state analysis. Springer, Vol 86 in Advanced Structured Materials
- [Kow83] Kowaltschuk B.I. and Giginjak F.F.: .....in Russian, Kiew, Naikowa Dumka 1983



- [Kup73] Kupfer H: *Das Verhalten des Betons unter mehrachsiger Kurzzeitbelastung unter besonderer Berücksichtigung der zweiachsigen Beanspruchung*. In Deutscher Ausschuss für Stahlbeton, Band 229, 1973
- [Laf 12] Laffan M.J., Pinho S.T., Robinson P., McMillan A.J., *Translaminar fracture toughness testing of composites: A review*, Polymer Testing (31) 2012, 481-489.
- [Laf 12] Laffan M. J., Pinho S. T., Robinson P., Iannucci L., McMillan A. J., *Measurement of the fracture toughness associated with the longitudinal fibre compressive failure mode of laminated composites*, Composites Part A: Applied science and manufacturing (43) 2012, 1930-1938.
- [Lan19] Hengxing Lan, Junhui Chen & Renato Macciotta: *Universal confined tensile strength of intact rock*. Scientific Reports | (2019) 9:6170 | <https://doi.org/10.1038/s41598-019-42698-6>
- [Leg02] Leguillon D: *Strength or Toughness? –A criterion for crack onset at a notch*. Europ. J. of Mechanics A/Solids 21 (2002), 61 – 72 end. ist. d. sci. lett., Cl. mat. nat.18, 705-714 (1885)
- [Lem08] Lemnitzer L, Eckfeld L, Lindorf A and Curbach M (IfM TU Dresden): *Bi-axial tensile strength of concrete - Answers from statistics*. In: Walraven, J. C.; Stoelhorst, D. (Hrsg.): Tailor made concrete structures. New solutions for our society. Amsterdam, The Netherlands: CRC Press / Balkema, 2008, S. 1101-1102
- [Liu14] Liu J, Zhu Z and Wang B: *The fracture characteristic of three collinear cracks under true tri-axial compression*. The scientific World Journal, V 2014, article ID459025, 5 pages
- [Lod26] Lode Walter.: *Versuche über den Einfluß der mittleren Hauptspannung auf das Fließen der Metalle Eisen, Kupfer und Nickel*. Z Phys 36:913–939 66.1926
- [Mas94] Masters, J.: *Fractography of Modern Engineering Materials*. Composites and Metals. 2<sup>nd</sup> volume. ASTM STP1203,1994
- [Mat75] Matsushige K, Radcliffe S V and Baer E: *The mechanical behavior of polystyrene under pressure*. J. of Material Science 10 (1975), 833-845
- [Mathcad 13 and 15]: *PTC mathematical program*, used by the author
- [Mat95] Matzenmiller A, Lubliner J and Taylor R L .: *A constitutive model for anisotropic damage in fiber-composites*. Mechanics of Materials 20 (1995), 125-152
- [Mat07] Matzenmiller A and Koester B.: *Consistently Linearized Constitutive Equations of Micro-mechanical Models for Fibre Composites with Evolving Damage*. Int. Solids and Structures 44 (2007), 2244-2268
- Mec21] Mechtcherine V: *Klassifizierverfahren digitalerFertigungsvefafahren im Betonbau*. March 2012. Cu Bau AG. 4. Thementag (lead by the author) ‚Automatisierte Fertigung im Bauwesen inklusive Serielles Bauen‘.
- [Mel77] Melville PH: *Fracture mechanics of brittle materials in compression*. Int. J. Frac.13, 532-534 (cited in Liu 14)
- [MIL17] MIL-HDBK 17 “*Polymer Matrix Composites*”: Vol I “Guidelines for Characterization of Structural Materials”; Vol II “Material Properties”; Vol. III "Utilization of Data". Dep. of Defence (DOD), Technomic Publishing USA
- [Moh00] Mohr O.: *Welche Umstände bedingen die Elastizitätsgrenze und den Bruch eines Materials?* Civilingenieur XXXIV (1900), 1524-1530, 1572-1577
- [Mul67] Mulhern J F, Rogers T G and Spencer A J M: *A Continuum Model for Fiber-Reinforced Plastic Materials*. Proceedings of the Royal So ciety, Series A, Vol. 301,1967, p. 473
- Mur09] Murthy A R, Ch, Palani G S and Iyer N: *State-of-the-art review on fracture analysis of concrete structural components*. Sadhana Vol.34, Part 2, April 2004, 345-367

- [Nem90] Nemeth, N.N., Manderscheid, J.M. and Gyekenyesi, J.P.: *CARES (Ceramic Analysis and Reliability Evaluation of Structures) users and Programmers Manual*. NASA Technical Paper 2916, August 1990
- [Ott77] Ottosen N S: *A failure criterion for concrete*. Journal of the Engineering Mechanics. ASCE, 103(EM4):527–535, August 1977
- [Oro68] Orowan E: *Fracture and strength of solids*. Reports on Progress in Physics XII, 1948, 185–232
- [Pae96] Pae K D: *Influence of Hydrostatic Pressure on the Mechanical Behaviour and Properties of Unidirectional, Laminated, Graphitefibre/Epoxy matrix Thick Composites*. Composites Part B 27B (1996), 599-611
- [Pag81] Page A W : *The biaxial compressive strength of brick masonry*. Proc. Inst.Civil Engrs.; 71(2) (1981), pp. 893–906.
- [Pag83] Page A W: *The strength of brick masonry under biaxial tension–compression*. International Journal of masonry constructions; 3 (1), (1983),pp. 26-31.
- [Pap96] Papa E : *A unilateral damage model for masonry based on a homogenization procedure*. Wiley online library, Volume1, Issue4, October 1996. Pages 349-366
- [Pau61] Paul, B.: *A Modification of the Coulomb Mohr Theory of Fracture*. J. of Appl. Mech. (1961), 259-268
- [Pet15] Petersen E, Cuntze R and Huehne C: *Experimental Determination of Material Parameters in Cuntze’s Failure-Mode-Concept-based UD Strength Failure Conditions*. Submitted to Composite Science and Technology 134, (2016), 12-25 \*
- [Pin06] Pinho S T, Robinson P, Iannucci L, *Fracture toughness of the tensile and compressive fibre failure modes in laminated composites*, Composites Science and Technology 66 (2006), 2069–2079.
- [Pha03] Phan A V, Napier J A L , Gray L J and Kaplan T: *Stress intensity factor analysis of friction sliding at discontinuity interfaces and junctions*. Computational Mechanics 32 (2003), 392 -400
- [Puc96]Puck A: *Festigkeitsanalyse von Faser-Matrix-Laminaten - Modelle für die Praxis*. Carl Hanser Verlag München
- [Puc02] Puck A and Schürmann H: *Failure Analysis of FRP Laminates by Means of Physically-based Phenomenological Models*. Composites Science and Technology 62 (2002), 1633-1662
- [Puc02b] Puck A, Knops M and Kopp J: *Guidelines for the determination of the parameters in Puck’s action plane strength criterion*. Comp. Science and Technology 62 (3) (2002) 371–378
- [Rac87] Rackwitz R and Cuntze R: *System Reliability Aspects in Composite Structures*. Eng. Opt. 11 (1987), 69-76
- [Ric68] Rice, J.R.: *A path independent integral and the approximate analysis of strain concentration by notches and cracks*. Journal of Applied Mechanics 35 (1968), 379–386
- [Ric13] Richard H., Eberlein A. and Schirmeisen N-H.: *Experiments on Cracks under Spatial Loading*. 13<sup>th</sup> Int. Conf. on Fracture, Beijing June 16-21 2013
- [Ren38] Rendulic, L.: *Eine Betrachtung zur Frage der plastischen Grenzzustände*. Der Bauingenieur, 19 (1938), 159-164
- [Rou87] Rousselier, G.: *Ductile fracture models and their potential in local approach of fracture*. Nucl. Eng. Design. 105: 97-111, 1987.
- [Ric69] Rice, J.R. and Tracey, D.M.: *On the Ductile Enlargements of Voids in Triaxial Stress Fields*. J. Mech. Phys. Solids (17), 1969, pp. 201-217
- [Roh14] Rohwer K.: *Predicting Fiber Composite Damage and Failure*. Journal of Composite Materials, published online 26 Sept. 2014 (online version of this article can be found at: <http://jcm.sagepub.com/content/early/2014/09/26/0021998314553885>) (on Carbon Connected, CCeV)
- [Sch06] Schürmann H.: *Konstruieren mit Faser-Kunststoff-Verbunden*. Springer-Verlag 2005

- [Ste97] Steglich, D. and Brocks, W.: *Micromechanical Modelling of the Behaviour of Ductile Materials including Particles*. Comp. Mat. Science 9 (1997), 7-17
- [Ste73] Sternstein S S and Myers F A: *Yielding of glassy polymers in the second quadrant of principal stress space*. J. Macromol. Sci, Phys. B 8 (1973), 539-571
- [Tal94] Ralreja, R. (Hrsg.): *Damage Mechanics of Composite Materials*. Elsevier, Amsterdam/ London/New York/Tokyo 1994
- [Tay02] Taylor D.: *The Theory of Critical Distances - a new perspective in fracture mechanics*. Elsevier, Oxford, UK, 2000
- [The96] Theuer, A.: *Experimentelle Untersuchungen zum thermomechanischen Verhalten von Faserkeramik*. Dissertation. Univ. Stuttgart, 1996
- [Thi07] Thielicke B: *Die Ermittlung der interlaminaeren Scherfestigkeit von kohlenstoff-faserverstärkten Kohlenstoffen mit dem Druckscherversuch im Temperaturbereich zwischen Raumtemperatur und 2000°C*. Dissertation, Uni Karlsruhe, 1997
- [Tsa71] Tsai S W and Wu E M: *A General Theory of Strength for An-isotropic Materials*. Journal Comp. Materials 5 (1971), 58-80
- [Tsa15] Tsai S W and Melo J D : *Composite Materials design and Testing (unlocking mystery with invariants)*. ISBN 978-0-9860845-1-5
- [Tve81] Tvergaard, V.: *Influence of Voids on Shear Band Instabilities under Plane Strain Conditions*. Int. J. Fracture 17 (1981) 389-407
- [Kaw88] Kawagoe M and Kitagawa M: *On criteria for craze initiation in glassy polymers*. J. of Materials Science 23 (1988), 3927-3932
- [Vas10] Vassilopoulos A P: *Methods for fatigue life prediction of composite materials and bonded composite joints*. Composite Construction Laboratory Lausanne
- [VDI97] Cuntze R, Deska R, Szelinski B, Jeltsch-Fricker R, Meckbach S, Huybrechts D, Kopp J, Kroll L, Gollwitzer S, and Rackwitz R: *Neue Bruchkriterien und Festigkeitsnachweise für unidirektionalen Faserkunststoffverbund unter mehrachsiger Beanspruchung –Modellbildung und Experimente –*. VDI-Fortschrittbericht, Reihe 5, Nr. 506 (1997), 250 pages. (*New fracture criteria (Puck's criteria) and Strength 'Proof of Design' for Uni-directional FRPs subjected to Multi-axial States of Stress –model development and experiments-*. In German) \* BMBF-Vorhaben 03N8002 (A. Puck, adviser 1995)
- [VDI2014] VDI 2014: German Guideline, Sheet 3 *Development of Fibre-Reinforced Plastic Components, Analysis*. Beuth Verlag, 2006. (in German and English, author was convenor)
- [Wei15] Weißgräber P, Leguillon D and Becker W: *A review of Finite Fracture Mechanics: crack initiation at singular and non-singular stress raisers*. Arch. Appl. Mech. DOI 10.1007/s00419-015-1091-7, Springer-Verlag Berlin Heidelberg 2015
- [You15] Strength criterion for rocks under compressive-tensile stresses and its application.. J. of Rock Mechanics and Geotechnical Engineering 7 (2015) , 434-439
- [Yu02] Yu M: *Advances in Strength Theories for Materials under Complex Stress States in the 20th Century*. Appl. Mech. Rev, vol 55, no3, May 2002
- [ZTL80] Dornier, Fokker, MBB, DLR: *Investigations of Fracture Criteria for Laminae* (in German). 1975-1980, Grant from Ministry of Defence, BMVg, Koblenz



\*<https://www.carbon-connected.de/Group/CCeV.Fachinformationen/Dokumente/Documents/Index/10381>

### Some guidelines considering fiber-reinforcement in mechanical and civil engineering (construction):

[VDI 2014] VDI 2014: German Guideline, Sheet 3 “*Development of Fiber-Reinforced Plastic Components, Analysis*”. Beuth-Verlag, 2006 (in German and English. Cuntze was convenor and contributor. This guideline was initiated, driven and edited primarily by construction engineers!)

[BÜV10] “*Tragende Kunststoffbauteile im Bauwesen [TKB] - Entwurf, Bemessung und Konstruktion*“ . Upcoming update of the Bau-Überwachungsverein: BÜV-Arbeitskreis „Tragende Kunststoff-bauteile im Bauwesen“ aufgestellte Entwurf. Formelzeichen sind der DIN EN 1990BÜV-Empfehlung Stand 08 / 2010 (re-worked presently)

[D36] DAfStb UA: *Nichtmetallische nm Bewehrung: (Entwurf, in Bearbeitung). DAfStb-Richtlinie “Betonbauteile mit nichtmetallischer Bewehrung“*. Anwendungsbereich dieser DAfStb-Richtlinie. Dieses Dokument gilt für den Entwurf, die Berechnung und die Bemessung von Hoch- und Ingenieurbauten aus Beton, die mit nichtmetallischen Bewehrungselementen bewehrt sind. Bewehrungselemente sind dabei in der Regel Stäbe und bi-axiale Gitter.

[FKM] Richtlinie „*Rechnerischer Festigkeitsnachweis für Maschinenbauteile*“., Standard für einen statischen und zyklischen Festigkeitsnachweis vom Forschungskuratorium Maschinenbau (FKM) entwickelt

### Some further works of the author: MAN-Technisches Informationszentrum Augsburg NT, MT etc

1. Dissertation, TH Hannover 1968, ***Ermittlung von Eigenfrequenzen dünner, schiefwinkliger isotroper Platten***. ZAMM 49 (1969)
2. ***Ermittlung transversaler Eigenfrequenzen dünner Rechteckscheiben und Vergleich mit der Näherung von Timoshenko***. Acta Mechanica (1969)
3. ***Theoretische Ermittlung der dreidimensionalen Spannungsverteilung in Radialverdichterrädern***. DLR-FB-70-16 (1970)
4. ***Der Einfluß von Eigengewicht und elastischer Einspannung auf die Biegeeigenfrequenzen eines schlanken Stabes von linear veränderlicher Dicke***. Der Bauingenieur (1971)
5. Meinke, Celep, Cuntze: ***Eigenverhalten und Umwuchteinflüsse eines zweigliedrigen Rotors mit elastischem Gelenk***. MAN-NT 71 (1971)
6. Meinke P und Cuntze R: ***Bewegungsgleichungen eines starren zweigliedrigen Sickenrotors***. NT 6/71
7. ***Reduktion der Randstörungen von Rotationsschalen durch gezielte Formgebung des Randauflagerung***. NT 25/71
8. ***Vergleich faserverstärkter und fasergewickelter Behälter mit Metallbehältern***. MAN-FB-72002 (1972)
9. Cuntze R und Celep Z: ***Freie Bewegungen 2- und 3-stöckiger Rotoren***. NT 39/71
10. Kreft, Wolf, Cuntze: ***Investigation of Fibres and Composites Applicable to the Design of High Pressure Vessels for Satellites***. ESTEC Contract No. 1485/7111, ESRO-Bericht (1972)
11. ***Festigkeitsqualifikation der G2-Zentrifuge zur Urananreicherung***. NT 20/72
12. ***Eine Bemerkung zur Anwendung des Finite-Element-Verfahrens in der Strukturmechanik***. Die Konstruktion (1973)
13. ***Gehäuse-Auslegungsstudie zur Definition eines Standard-Feststoff-Apogäumsmotors***. NT 11/74
14. MAN-Beitrag zur Entwicklungsstudie „CFK-Bauteile für Spacelab“. NT 30/74

15. *Compendium über Auslegung von Bauteilen aus Faserverbundwerkstoff (design of structures built from FRP)*. M.A.N.-Neue Technologie (1975), 600 Seiten. Eigendruck MAN
16. Cuntze R und Thiele H-M: *Vorstudie über Möglichkeiten einer experimentellen und rechnerischen Lebensdauerbestimmung eines Nutzfahrzeugs und seiner Strukturteile*. NT 9/77
17. *Schwierigkeiten bei der Ermittlung von genauen Spannungen und Verformungen an Rotationsschalen aus Faserverbundwerkstoffen*. Strukturmechaniktagung 1.6./2.6.1977 in Ottobrunn über Probleme der Festigkeitsforschung im Flugzeugbau und Bauingenieurwesen. Sonderheft der DFVLR (1977).
18. 12. Cuntze R and Zaun J: *Calculation of the Natural Frequencies of the braced GROWIAN tower with dead head mass* (1978). KFA-Jül. Spez-28, Jan.79. ISSN 0343-7639
19. *Entwurf und Festigkeitsanalysen fließgedrückter Rohre*. NT 29/78
20. Habilitationsschrift, TU München, 1978: *Grundlagen für die Berechnung von Rotationsschalen aus Faserverbundwerkstoff*
21. ROTTSCHWIMM 32- *Einsatz eines 5 t schweren Energiespeicherrades bei einem Schwimmkran – Auslegung und bruchmechanischer Nachweis*. NT 4/82 (viele Jahre in Betrieb)
22. Cuntze R. und Eder J: *Einfluß von Schubelastizität auf Drehträgeit und Biegeeigenfrequenz gleichförmig massebelegter Einfeldbalken*. Die Konstruktion 35 (1983), H.5, S 183-186
23. *Der Einfluß von Schubelastizität und Drehträgeit auf die kritischen Drehzahlen gleichförmig massebelegter, einfeldriger Wellen*. Ing.-Archiv (1984)
24. Cuntze R und Wein J: *Strukturauslegung und -nachweis in Einbindung leistungsfähiger Pre- und Postprozessorsysteme*. DGLR-Fachauschuß "Festigkeit und Bauweisen". Neubiberg, 5.7.1984. Tagungshandbuch
25. *Probleme bei der Übertragung eines Zwischenfaserbruchkriteriums von einem UD-Probekörper auf einen Mehrschichtenverbund*. DGLR-Symposium "Entwicklung und Anwendung von CFK-Strukturen". TU, Berlin. 8./9.11.1984
26. *CAE-Einsatz beim Projekt ARIANE. Ein Anwenderbericht*. CAE-Journal, Heft 6 (1984), 24-31
27. Cuntze R and Löbel G.: *Evaluation of Stress Strain Test Results for Effective Use in Computational Analysis and Adequate Statistical Quantities*. ICOSSAR 85, 4th Intern. Conf. on Structural Safety and Reliability. Kobe, Japan
28. *Bruchverhalten von kohlenstofffaserverstärkten Kunststofflaminaten. - Theor. Untersuchungen - Bericht: MAN-NT 44/83 (20.12.84)*. BMFT-Forschungsvorhaben 01ZA 029-/K/NT/NTS 1022
29. *Strukturberechnung. Teil der Bauteilentwicklung - ein Überblick*. Konferenzbericht der Tagung Mechanik und Industrie. IGLS, Österreich. 26./27. Februar 1985. Herausgeber: Institut für Mechanik, Universität Innsbruck. Springer, Wien 1986
30. Cuntze R und Hajek M.: *Eigenfrequenz eines angerissenen Kragträgers*. Ing. Arch. 55 (1985), S. 237-241
31. Crostack H.A., Nolte F., Zeilinger H. und Cuntze R.: *Untersuchung des Schädigungsablaufes in kohlenstoff-faserverstärkten Kunststoffen*. Zeitschrift für Werkstofftechnik 16 (1985) 366-372
32. Rackwitz, R. and Cuntze, R.: *Formulations of Reliability-oriented Optimization with Application*. NATO Advanced Study Institute. Conference on Computer Aided Optimal Design, Troia, Portugal. June 29-July 11, 1986. Springer
33. Cuntze R and Grimmelt M: *Influence of the Variation of Structural Properties on the Probability of a Composite Plate to meet a Target Eigenfrequency*. EUROMECH Coll. 219, Sept. 23-25, 1986, Kassel
34. Cuntze R und Schuelein R.: *Einsatz der Bruchmechanik bei der Entwicklung von Struktur-Bauteilen aus Faserkunststoffverbund (FKV)*. Vortragsveranstaltung "Bruchmechanik bei Verbundwerkstoffen" bei der Dechema. Frankfurt, 19.02.1987
35. Rackwitz R and Cuntze R: *System Reliability Aspects in Composite Structures*. Eng.' Opt., 1987, Vol. 11, pp. 69-76
36. Cuntze R: *Failure Path Analysis of Multilayered Fibre Reinforced Plastic Components with the Reliability Calculation Programme FRPREL*. Noordwijk, Oct. 1987
37. Cuntze R: *Influence of the Stochastic Behaviour of Design Parameters on the First Ply Failure (FPF) in Pressurized CFRP-Tubes*. ESA/ESTEC, Noordwijk, March 1988
38. Scharringhausen J. and Cuntze,R: *FEM-Calculations on the Domes of Fibre Reinforced Plastic Cases for Solid Propellant Motors*. ESA/ESTEC Workshop, Noordwijk, March 23-25, 1988

39. Cuntze R and Zaun J: *Delamination Optimization of Hoop-Wound Composite Fly-wheels*. ICCM 7, Beijing, August 1 - 4, 1989
40. Cuntze R and Schuelein R: *Werkstoffdatenbanken im industriellen Einsatz (material data banks in industrial use) - aus der Sicht eines Anwenders*. MAN Technologie GmbH, München. Bericht und Vortrag MAN-intern (Febr. 23, 1989). Fachgespräch bzgl. MAN Werkstoff-Informationssystem
41. Grimmelt M and Cuntze R: *Probabilistic Prediction of Structural Test Results as a Tool for the Performance Estimation in Composite Structures Design*
42. . VDI-Bericht 771 (1989), 191-200
43. Dr. med. Stock W und Dr.-Ing. Cuntze R: *Computergestützte biomechanische Untersuchungen zur Knochen-transplantation*. Vortrag, BMFT Seminar. Hamburg, 1988
44. Cuntze R und Schuelein R: *Werkstoffdatenbank: Qualitätswerkzeug für die Entwicklung zuverlässiger Bauteile*. VMPA-Tagung "Qualität und Zuverlässigkeit durch Materialprüfung", München, April 1990
45. *Auslegung, Nachweis und Zuverlässigkeitsoptimierung von Faserkunststoffverbund-Bauteilen*. Fachtagung "Rechnereinsatz beim Konstruieren von Kunststoff-Formteilen". Süddeutsches Kunststoffzentrum, Mannheim, Mai 1990
46. Cuntze R: *Influence of the Stochastic Behaviour of Design Parameters on the First Ply Failure (FPF) in Pressurized CFRP-Tubes*. ESA/ESTEC, Noordwijk, March 1988
47. *Structural Design, Optimization and Reliability Justification - a comparative survey related to the example: Axially compressed strut*. GAMM/IFIP-Workshop "Stochastic Optimization", Neubiberg, May 1990 (not published)
48. Cuntze R. and Heibel R: *Increasing the Limit of Usability of CFRP Tubes by Built-in Stresses*. X. Int. Herman F. Mark-Symposium. Wien, 1991
49. *Prediction of the Distribution of Inter-Fibre-Failure Test Data of Radial Loaded, Pre-strained CFRP Tubes composed of Thin Layers*. 5th Workshop "Composite-Forschung in der Mechanik", Paderborn, October 1992
50. Gollwitzer S, Cuntze R, Grimmelt M and Zwerev A.: *Structural Reliability Applications in Aerospace Engineering*. ICOSSAR 93, Innsbruck, 1993
51. *Deterministic and Probabilistic Prediction of the Distribution of Inter-Fibre-Failure Test Data of Pre-strained CFRP Tubes composed of Thin layers and loaded by radial pressure*. Wollongong, Advanced Composites '93. The Minerals, Metals & Materials Society, 1993
52. *Evaluation and Application of a New Physically Based 2D/3D-Inter-Fibre-Fracture (IFF) Strength Criterion*. Proceedings of International Symposium on Advanced Materials for Lightweight Structures, Noordwijk, März 1994, ESTEC, 133-139
53. Gierlinski, Smith, Thoft-Christensen, Santos, Cuntze, Gollwitzer: *Reliability-based Design of Structural Components*. Proceeding of the int. Symp. on Advanced Materials for Light weight structures, ESTEC, Noordwijk, March 1994 (ESA-WPP-070), 121-125
54. *"Quick Design", Entwurfsregeln und Normen zur Strukturberechnung*. Kolloquium "Ausgewählte Probleme der Strukturmechanik", 11.5.95, zu Ehren von Dr.-Ing. B. Geier. IB 131-95-13, DLR-Braunschweig
55. *Festigkeitskriterien für Werkstoffe aus Faserkunststoffverbund (FKV)*. Symposium "Berechnungen von Faserverbundstrukturen unter Anwendung numerischer Verfahren". München, Techn. Uni, 13/14. März 1996
56. *"Fracture-type Strength Criteria" formulated by Invariants which consider the Material Symmetries of the Isotropic/Anisotropic Material used*. Conf. on Spacecraft Structures, Materials and Mechanical Testing. ESA-CNES-DARA: Noordwijk, 27-29 March 1996, pp. 399-409
57. *Zum verbesserten Festigkeitsnachweis von FKV-Bauteilen*. Werkstoffwoche 96, Stuttgart 28.- 31. Mai 1996. Projektberichterstattung
58. *Bruchtypbezogene Auswertung mehrachsiger Bruchtestdaten und Anwendung im Festigkeitsnachweis sowie daraus ableitbare Schwingfestigkeits- und Bruchmechanikaspekte*. DGLR-Kongreß 1996 Dresden. Kongreß-Band
59. *Evaluation of Multiaxial Test Data of UD-laminae by so-called "Fracture-type Strength Criteria" and by supporting Probabilistic Means*. ICCM-11, Gold Coast, 1997
60. Cuntze R et.al.: *Neue Bruchkriterien und Festigkeitsnachweise für unidirektionalen Faserkunststoffverbund unter mehrachsiger Beanspruchung - Modellbildung und Experimente*. VDI-Fortschrittbericht, Reihe 5, Nr. 506 (1997), 250 pages. [New fracture criteria (Puck's criteria)]

- and Strength 'proof of Design' for Unidirectional FRPs subjected to Multi-axial States -model development and experiments-, in German]
61. *Stand von Auslegung und Nachweis von Bauteilen aus Faserkunststoffverbund nebst einigen Ausblicken*. Plenarvortrag, DGM-Tagung "Verbundwerkstoffe und Werkstoffverbunde", Kaiserslautern, Sept. 1997
  62. *Strength Prediction for Multi-axially Loaded CMC-Materials*. 3rd European Workshop on Thermal Protection Systems. Conf. on Spacecraft Structures, Materials and Mech. Testing. ESA-ESTEC: Noordwijk, March 1998, WP P141
  63. *Application of 3D-strength criteria, based on the so-called "Failure Mode Concept", to multi-axial test data of sandwich foam, concrete, epoxy, CFRP-UD lamina, CMC-Fabric Lamina*. ICCE/5, Las Vegas, July 1998 (presentation)
  64. *The Failure Mode Concept - a new comprehensive 3D-strength Analysis Concept for Any Brittle and Ductile behaving Material*. Europ. Conf. on Spacecraft Structures, Materials and Mechanical Testing. ESA-CNES-DGLR-DLR; Braunschweig, Nov. 1998, ESA SP-428, 269-287
  65. *Progressive Failure of 3D-stressed Laminates: Multiple Non-linearity treated by the Failure Mode Concept (FMC)*. DURACOSYS99, Brussels, July 1999. Balkema, Rotterdam, 2000
  66. *Static Design and Strength 'Proof of Design' of Pressure Vessels, built from Ductile or Brittle Materials*. Problems of the North; Yakutsk 2000
  67. *Are there Cost Drivers in the Structural Analysis of the ARIANE 5-Development?* Noordwijk, 29. Nov./1. Dec. 2000
  68. *Assessment of Load- and Strain-controlled States of Stress in 'hot Spots' - on the way to an Industrial Approach for Gurson Materials*. 3rd European Conference on Launcher Technology. CNES, DLR, ESA-ESTEC, ISU: Strasbourg, Dec. 11-14, 2001
  69. Huybrechts D, Cuntze R., Druwen S, and Lutz G.: *VDI-Richtlinie 2014, Blatt3, Berechnungen*. SAMPE 2002.
  70. Cuntze R: *Non-linear Failure Analysis of FRP Laminates composed of UD Laminae – a comparison of the author's predictions with test results within the Failure Exercise in the UK*. 3rd Int. Conf. on Fracture and Damage Materials; Paderborn, September 2-4, 2003

### 11.3 Basic Terms and Definitions

As the body text should be applicable for engineers in mechanical, civil and geotechnical engineering basic terms must be provided for a common understanding:

Action: loading applied in design

Brittle material behavior: materials with about  $R^c / R^t > 3$

Cross sections of the fracture failure body (surface): (1) convex  $\pi$ -plane  $\equiv$  plane  $I_1 = \text{constant} \equiv$  hoop plane, deviatoric plane. (2) meridian planes (tensile, compressive, shear), may be not convex at  $I_1 \rightarrow \max I_1$

Cohesive model: traction-separation law describing distinct non-linear separation process of the material (is neither an elasticity-dedicated nor a plasticity-dedicated model)

Cohesive strength: maximum tensile stress  $\sigma^t$  ( $\equiv$  separation strength  $R^t$ ) of bonding between surfaces or of tensile stressed particles building a material. However, in rock and soil mechanics cohesive strength is 'differently' defined as the inherent shear strength  $R^t = \tau_{nt}$  of a plane, where the normal compressive Mohr stress  $\sigma_n^c = 0$  on the about  $\Theta_{ip} \approx 70^\circ$  bias shear fracture plane and whereby the cohesive strength value  $R^t$  is extrapolated from compression point-associated quantities. This seems to be not accurate because  $R^t$  is an brittle-dependent entity of the transition zone between shear fracture mode SF and Normal Fracture mode NF.  $\rightarrow$  *Difference* between the terms in the technical disciplines

Composite material versus material composite (2 structural composite types): Composite Material (*Verbundwerkstoff*) combination of constituent materials, different in composition. Material Composite (*Werkstoffverbund*) structural-mechanically a composite 'construction of different materials (a not

smearable ‘conglomerate’ such as i.e. carbon mat-reinforced concrete which is not a ‘composite material’ despite it is usually termed so)

Connection versus joints: connection is (uncountable) the act of connecting while joint is the structural point where two components of a structure join.

Condition versus criterion:  $F = 1$  versus  $F < = > 1$

Confining pressure: lithostatic pressure in geo-mechanics, the pressure forced on a layer of soil or rock by the heaviness of the overlying substance. Corresponds to a hydrostatic pressure  $p_{hyd}$

Confining stress: usually stress  $\sigma_z$  caused by  $p_{hyd}$  at level  $z$

Damage (Beschädigung): physical harm, which captures in English as well *micro-damage*  $D$  (Schädigung) as the *macro-damage* (Schaden) crack, delamination

Damage (Schaden): sum of the accumulated damaging or an impact failure that is judged to be critical. Then, Damage Tolerance Analysis is used to predict the growth of the damage under further cyclic loading or static failure under Design Ultimate Load

Defect (should not be used for legal reasons): *flaw, manufacturing imperfection*

Design verification: determination of the reserve factor  $RF$  on basis of a statistically reduced strength failure body, spanned by its strengths

Durability verification (Dauerhaftigkeitsnachweis): *ability to withstand wear, pressure, or damage. In construction to have considered the design rules, execution of construction work, concrete cover etc*

Effective stress: stress that considers a reduced load-carrying cross-section  $\sigma_{eff} = \sigma / (1 - D)$

(mode !) Equivalent stress  $\sigma_{eq}^{mode}$ : mode-dedicated equivalent stress. The highest mode equivalent stress gives the designer a possibility where to turn the design screw. (a) equivalent (gleichwertig) to the stress state, as performed in  $\sigma_{eq}^{Mises}$ , and (b) comparable (vergleichbar) to the value of the strength  $R$  which dominates one single failure mode or failure type, respectively

Failure: state of inability of an item to perform a required function in its limit state, also loss of a function under stated component part conditions → A situation when a structural part does not fulfil its functional requirements such as the failure modes Onset-of-Yielding, brittle fracture (NF, SF, Crushing Fracture CrF), Fiber-Failure FF, Inter-Fiber-Failure IFF (matrix failure), leakage, abrasive wear, deformation limit (tube widening), fretting corrosion, delamination size limit, frequency bound, or heat flow etc. *A failure is a project-defined ‘defect’ or limit state.* For each failure mode a Limit State with  $F =$  Limit State Function or Failure Function is to formulate. A specific mark for failure exemplarily is: A second loading, under a distinct failure mode (here SF), cannot be sustained anymore, like a slightly porous UltraHighPerformanceConcrete UHPC compression test specimen after a crushing test under  $p_{hyd} = 1000$  MPa where the first loading of the crumbles might have been still further increased, densification enables it)

(Strength) Failure Condition (SFC):  $F = 1 = 100\% \leftarrow Eff$

Failure Mode Concept FMC : invariant, failure mode-based general concept to generate strength failure conditions for single failure modes (‘modal’ formulation in contrast to failure modes-linking ‘global’ concepts) for materials that can be homogenized (smeared). The applicability of a SFC ends if homogenization as pre-requisite of modeling is violated and no longer valid

Failure criterion:  $F > = < 1$

Failure initiation (onset) : event that initiates a certain defined failure

Failure function  $F$  : mathematical description of the failure  $F = 1$  (limit state function (Grenzzustand)  $\hat{G} = F - 1$



Failure mode: Failure mode is a commonly used generic term for the types of failures, is a name for a potential way a system may fail (in design verification usually a project- associated failure)

Failure surface: graphical representation of a failure condition  $F = 1$  (envelope that contains the non-failed domain  $F < 1$  or the non-failure body, respectively)

Failure surface and failure body: the surface of the strength failure body is the shape defined by

$$F = 1 \text{ or } Eff = 1 = 100\%$$

Failure initiation (onset) : event that initiates a certain defined failure

Failure mechanism : underlying phenomenon that determines the mode of failure

Failure type: Normal Fracture NF, Shear Fracture SF under compression, Crushing Fracture CrF, Normal Yielding NY, Shear Yielding SY, Fiber Failure FF, Inter-Fiber-Failure IFF etc

Filament: endless single fibre

Flaw: local discontinuity in a structural material. Example: Scratch, notch, crack, void or pores in case of metallic and homogeneous non-metallic material; delamination or porosity in case of composite material. (due to legal reasons one should avoid the term defect)

Flaw versus micro-crack: a micro-crack is a sharp flaw (Ungänze), grade of singularity is decisive

Fracture: separation of a whole into parts

Fracture ‘plane’ angle  $\Theta_{fp}^\circ$ : average value of the scattering fracture plane that is seldom a plane. A tensile stress causes an angle perpendicular to the stress direction of  $90^\circ$ . This definition matches with the  $90^\circ$ -wound UD tensile-compression-torsion test specimen

Fracture (failure) body: Surface of the tips of all fracture (failure stress) vectors. Fracture is the failure of brittle materials

Fracture toughness  $K_{cr}$ : ability of a material to withstand a loading in the presence of a sharp crack  $\equiv$  critical stress intensity factor. Usually just indexed c, but this is still the much older index for compression)

Friction: here, material internal behaviour (often not clearly termed pressure-dependent material behaviour)

Friction: slope of the Mohr-Coulomb failure curve (Mohr failure envelope) defined after the ratio of the derivation shear stress  $d\tau_{nt}$  to normal stress  $d\sigma_n$  at failure in the so-called touch point. The ratio  $d\tau_{nt} / d\sigma_n$  is termed internal friction value  $\mu$

(strain or work) Hardening (Verfestigung): strengthening of a material during increasing deformation

Homogeneous: descriptive form for a material of uniform condition

Hydrostatic failure point (top cap or bottom closure of failure body): statistically estimated tri-axial failure point (failure behaviour acts three-fold). Note of the author: “Such a point cannot be calculated from a ‘one-fold failure condition’ as it is unfortunately sometimes executed

Hydrostatic pressure: absolute value of hydrostatic compression test (hydrostatic stresses have signs!)

Inelastic: behavior, that captures both yield and micro-damage

Inelastic potential versus yield potential (plastic): *inelastic*  $\rightarrow$  micro-damage, brittle, fracture modes, friction occurs and is indicated by the paraboloid-shaped SFCs (*an inelastic potential shall be not termed yield potential*); *plastic*  $\rightarrow$  metal plasticity, ductile, yield mode, frictionless sliding indicated by the cylinder shape of ‘Mises’, yield potential

Initial failure: ‘practical’ onset of degradation. Note: E.g., initial failure is usually indicated by the occurrence of a distinct knee in the stress-strain curves of a laminate, and this is determined by the first IFF mode of failure

Interaction: process of a combined action of stresses, or loadings, or failure modes. Interaction occurs between strength failure modes FF and IFF, NF and SF, between different stability modes, however also between stability failure modes and strength failure modes. It is a common triggering

Invariant: combination of stresses or strains. Its value does not change when altering the coordinate system. The stresses in the invariants may be powered (exponents may be 2 or 3 or 4) or not powered (1). Invariants are advantageous when formulating the usually desired scalar failure conditions. Such material-associated invariants are utilized for isotropic and composite materials.  $I_1/3$  is often termed hydrostatic stress  $\sigma_{hyd}$

Isotropic material: material with identical properties in all directions

Lamina, ply: computational element of the laminate. Lamina in mechanical engineering becomes a lamella in the construction industry and then serves as a semi-finished product for the so-called upgrading of bridges, ceilings and silos!

Laminate: stack of laminae

Layer: physical lamina or physical ply

Length scales: Micro: length scale where usually damaging and fracture occurs ( $> 1 \mu\text{m}$ ). Micro: length scale where usually damaging and fracture occurs ( $> 1 \mu\text{m}$ ). Macro: desired engineering length scale for composites modeling. However, ( $> 1\text{mm}$ ) strength criteria formulations must consider that fracture occurs at micro-scale. Meso: per definitionem no length scale. Is used and defined on very different length scales – as an intermediate scale - in order to mark a specific meso-model level (one should use the term meso- model and not meso-scale)

Mapping of a course of test data: average test data fit

Material: ‘homogenized‘ (macro-)model of the envisaged complex solid or heterogeneous material combination which principally may be a metal, a lamina or further a laminate stack analyzed with effective properties. Homogenizing (smearing) simplifies modelling

Material behavior: *brittle* behavior can be characterized with the complete loss of tensile strength capacity at first fracture,  $R^t$ . Quasi-brittle behavior shows - after reaching  $R^t$  - a slight strain hardening followed by a gradual decay of tensile strength capacity during a strain softening domain. Thereby *Eff* remains 100%. *Ductile* behavior is accompanied by a gradual increase of tensile stress (strain hardening), and after reaching  $R^t$  a strain softening domain follows

Material Stressing Effort (Werkstoffanstrengung, nicht Werkstoffausnutzung) Eff: artificial technical term created – as compromise - together with QinetiQ, UK, during the World-Wide-Failure-Exercises (since 1991) in order to obtain an English expression for the German term Werkstoff-Anstrengung. Note: In non-linear analysis the computation must run up to a theoretical fracture loading at  $\text{Eff} = 100\%$  in order to determine the required RF. Definition as  $\text{Eff}^{mode} = \sigma_{eq} / R$  with  $\max \text{Eff} = 100\%$  is reached at  $F = 1 = 100\%$ . The total Material stressing effort  $\text{Eff} = f(\text{Eff modes})$  represents as interaction equation – capturing the damaging portions of all activated modes - the mathematical equation of the surface of the fracture (failure) body. Just for 100%  $F = \text{Eff}$ .

Mathematical stresses: structural stresses used as mathematical stresses means  $\sigma_I > \sigma_{II} > \sigma_{III}$

Meridian: axial cross-section of the failure body. Tensile meridian mathematically defined as  $\sigma_I > \sigma_{II} = \sigma_{III}$ , compressive meridian defined as  $\sigma_I = \sigma_{II} > \sigma_{III}$ . These meridians are those meridians where tests are usually performed along. The shear meridian is the neutral meridian, where  $\sigma_{II} = -\sigma_{III} \rightarrow \text{shear} \dots\dots$ . Tensile meridian involves strength point  $R^t$ , means  $p_{hyd} + \text{axial tension}$ . Compressive meridian: involves strength point  $R^c$ , means  $p_{hyd} + \text{axial compression}$

Micro-mechanical formulas and properties: formulations determined by micro-mechanical properties.

Micro-mechanical properties can be used on the macro-mechanical engineering level only together with the equations they have been determined with!! (*In the WWFE i.e. not accurately performed*)

Mixed Strength (fracture) Failure: several different failure modes may be activated by the acting stress state. The *interaction* of both the activated fracture mode types Normal Fracture NF with Shear Fracture SF under compression increases the danger to fail! Hence, the associated fracture test data are so-called joint-probabilistic results of several acting modes (2, if isotropic)

Mixed (fracture) Failure: Different failure modes are activated by the acting stress state (example: isotropic Normal Fracture NF + Shear Fracture SF under compression). Interaction of fracture modes increases the danger to fail! Associated test data are 'joint-probabilistic' results

'Modal' versus 'Global' SFCs: Modal means that only a test data set of one failure mode domain is mapped whereas global (examples Drucker-Prager isotropic, Tsai UD) means that mapping is performed over several mode domains

Mortar: material composed of one or more inorganic binders, aggregates, water and admixtures

Multi-fold (fracture) Failure Mode: The acting stress state with maximally equal orthogonal stresses activates the same mode multi-fold. Hence, the associated fracture test data are so-called joint-probabilistic results of a multi-fold acting mode! Usually, SFCs consider just one single failure mode (mechanism) and do not capture the bi-axial effect of  $\sigma_I = \sigma_{II}$  or hydrostatic tensile or compressive failure stress states. This must be considered by an additional term in the SFC!

Multi-fold (fracture) Failure Mode: The acting stress state with equal orthogonal stresses activates the same mode multi-fold (example isotropic  $\sigma_I = \sigma_{II}$ ,  $\sigma_I = \sigma_{II} = \sigma_{III}$ ,  $\rightarrow \sigma_{hyd}$ , 3-fold); example transversely-isotropic UD  $\sigma_2 = \sigma_3$ , 2-fold). A multi-fold fracture mode:

- increases the danger to fail !  $R^t > R^{tt}$  (weakest-link effect),  $I_I > 0$
- increases the danger to fail !  $R^t > R^{tt}$  (weakest-link effect),  $I_I < 0$ , porous
- decreases the danger to fail !  $R^{tt} > R^t$  (redundancy effect),  $I_I < 0$ , dense

Onset-of-delamination: the laminate, composed of several UD-plyes may experience inter-laminar fracture failure caused by inter-laminar stresses, preferably  $\sigma_3$ , or further by 3D states of stress from notching the surface of the next ply

Pre-form: uncompleted part after preliminary shaping (semi-finished product)

Prepreg: ready to mold or cure material in sheet form which may be tow, tape, cloth, or mat

Pressure independent material: elastic-plastic material in which plasticity exhibits only in the deviatoric stress-strain response, whereas the volumetric stress-strain response is linear-elastic and is independent of the deviatoric response

Probability: likelihood that failure occurs

Proportional loading: often assumed loading procedure applied to stresses here. How the material stressing effort  $Eff$  is derived from the failure function  $F$ . In the case of a non-homogeneous function  $F$  the associated values are only equal for the failure state  $F = 1 \equiv Eff = 100\%$

Reserve factor: ratio of a 'resistance value' and a so-called 'action value'.  $RF > 1$  permits a further increase of loading. This is terminated by  $Eff = 100\%$  'material stressing effort' (Werkstoffanstrengung) in the last critical Hot Spot, when no more stress redistribution in the structural component is possible...predicted failure load / (design factor of safety x Design Limit Load). If linear analysis is permitted the material reserve factor  $f_{RF} = \text{strength} / \text{Design Stress}$  will correspond to  $RF$ . A value higher than 1 would permit a loading increase. For brittle behaving materials, the main load case is Design Ultimate Load

Risk: probability of loss of personnel capability, loss of system, or damage to or loss of equipment or property. Risk (criticality) level = severity of the failure times its probability of occurrence

Semi-finished product: products which are further processed to become more finished products

Shrinking: chemical shrinking (Schwinden), physical shrinking due to deformation mismatch

Sizing: generic term for compounds which are applied to yarns to bind the fiber together and stiffen the yarn to provide abrasion-resistance during weaving. Starch, gelatin, oil, wax, and man-made polymers such as polyvinyl alcohol, polystyrene, polyacrylic acid, and polyacetates are employed

(test) Specimen: piece or portion of a sample or other material taken to be tested. Specimens normally are prepared to conform with the applicable test method

Stochastic design parameter (uncertain basis variable): design parameter which is uncertain (before realization) and random (after realization)

Servicability (Gebrauchstauglichkeit): conditions under which a building is still considered useful. Should these limit states be exceeded, a structure that may still be structurally strength sound would nevertheless be considered unfit. Serviceability limit state design of structures includes factors such as durability, overall stability, fire resistance, deflection, cracking, excessive vibration. After [Wikipedia]

Severity: consequence of a failure

(strain) Softening (Entfestigung): degradation of strength with increasing strain (phenomenon observed in damaged quasi-brittle materials, including fiber-reinforced composites and concrete)

Spalling: process of surface failure in which spall is shed where spall are flakes broken from a larger solid body

Splitting (longitudinal): failure mechanism, resulting from compression loading that creates cracks parallel to the compression load axis generated by perpendicular tensile stresses acting at internal flaw tips which are usually combined with so-called wing cracks

Strain approach: approach, if limiting strains are used in design. Not advantageous in case of brittle materials where on top residual stresses have to be considered

Strand (Strang): bundle of rovings, mortar ‘caterpillar’

Strength  $R$  (resistance): in engineering linked to a uni-axial fracture stress. fracture tensile stress  $\sigma^t \equiv$  ultimate tensile strength  $R^t$ , ultimate compressive strength  $R^c$ . In test data mapping, in order to validate a strength criterion model the average failure curve or average failure body, respectively surface, is searched. Therefore, the task ‘average test data fit’ is tackled by applying average strength values  $R$ . In design verification, when determining an  $RF$  a statistically reduced surface (shrunk failure body) is used applying a strength value marked  $R$  (1) Characteristic strength: in mechanical engineering the typical average strength, in civil engineering a reduced (5% fractile) average strength value! (2) Design strength: a statistically reduced average strength.  $R$  = general strength and also the statistically reduced ‘strength design allowable.  $\bar{R}$  (bar over the  $R$ ) means *average* strength and is to apply when mapping, like here

Strength designations:  $R$  is strength, in general, and also the statistically-reduced value.  $\bar{R}$  denotes the average strength which is used when mapping a course of test data points. In construction, still most often: letter  $R \rightarrow f$ . Think ‘**Terms 4 Future**’

Strength Failure Condition (SFC): mathematical formulation of the strength failure surface, that takes the mathematical form  $F = 1$ , a tool to assess a ‘multi-axial failure stress state’ in a critical material location of the structural component. The usually macro-mechanical SFC should consider, that failure usually occurs at a lower than the macro-mechanic level, micromechanically, such as the matrix in a macro-mechanically described UD SFC

Stress: component of the stress tensor defined as the force divided by the area of cross-section (stress tensor component but not stress component)

Stress vector: vector which incorporates mechanical stresses from external and internal loads + hygro-thermal stresses due to environment + residual stresses from manufacture

Structural stability (Standicherheit): *condition of safely transferring static and cyclic loads as impact loadings on the building like self weight of the building and live load on the building (the resistance offered by a structure to undesirable movement like sliding, collapsing and over turning is called stability. Stability depends upon the support conditions and arrangements of structural members)*

Tape: prepreg fabricated in widths up to 12 inches wide for carbon and 3 inches for boron. Cross stitched carbon tapes up to 60 inches wide are available commercially in some cases

Tendon: prestressing element, comprising tensioned elements like bars, strands that apply compression to the surrounding concrete

Test: experiment, performed physically or virtually by realistic digital simulations

Tension cut-off: limit of the failure body, mathematically defined by

$$\{\sigma\} < (\sigma_I = \bar{R}^t, \sigma_{II} = \bar{R}^t, \sigma_{III} = \bar{R}^t)^T$$

Test procedures regarding loading: Load-controlled → The stress in a structure is determined by the load and the cross section area, the load has to be transferred through. This stress does not depend on the deformation. Strain (deformation)-controlled → The stress in embedded lamina (ply) depends on the adjacent layers

Thermoplastic: plastic that repeatedly can be softened by heating and hardened by cooling through a temperature range characteristic of the plastic, and when in the softened stage, can be shaped by flow into articles by molding or extrusion

Thermoset: plastic that is substantially infusible and insoluble after having been cured by heat or other means

Tow: untwisted bundle of continuous filaments. Commonly used in referring to man-made fibers, particularly carbon and graphite fibers, in the composites industry. Heavy tow, e.g. a roving of > 48 k (thousand) filaments

Transversely-isotropic: descriptive term for a material exhibiting a special case of orthotropy in which properties are identical in two orthotropic dimensions, but not the third; having identical properties in both transverse directions but not the longitudinal direction

Tri-axiality factor: defined as  $TrF = p_{hyd} / \sigma_{eq}^{Mises} = (I_1/3) / \sqrt{3}J_2$ .

(model) Validation (validus = strong, kräftig, wirksam): ‘qualification’ of a created model by well mapping physical test results with the model

(design) Verification (from Latin, veritas facere): fulfillment of a set of design requirement data. Proof, that the product fulfils the product requirements data, defined in the performance requirements specification (= Pflichtenheft). *Note: Performed by a computation and/or a physical experiment such as a structural test like a girder, bent under loading.*

Weaves or Woven fabrics: types are plain (Leinwandgewebe), twill (Köpergewebe), satin (Atlasgewebe). The weave may be UD, tri-axial plain, near-net shape, polar or a spacer weave (Abstandsgewebe), 3D

Yarn: assembly of twisted or practically un-twisted (rovings) filaments (in yarns) suitable in textile fabrication (from fiber via yarn to fabric)

Yield strength: distinct stress linked to yielding. As it is difficult to determine a precise onset-of-yield point, in general, one should discriminate from practical engineering reasons the proportional (tensile)

limit  $R_p$  ( $\equiv f_y$ ) and  $R_{p0.2}$  ( $\equiv R_{0.2}$ ), where the offset yield point is taken as the stress at which 0.2% plastic deformation remains (*in English literature  $R_{p0.2}$  is termed proof stress*)

120°-symmetry of the isotropic failure body: wording according to the equality of the 3 principal stresses each ‘perturbation’ of the rotational failure body exists 3 times

*BsF*: basalt fiber (*BF is Bor Fiber!*)

*C*: fracture angle measure  $C = 1/3$  with  $\Theta_{fp}^\circ = 35^\circ$  (very ductile);  $C = 0$ ,  $\mu = 0$  with  $\Theta_{fp}^\circ = 45^\circ$  (bound of  $F^{SF}$ );  $C = -1$  with  $\Theta_{fp}^\circ = 90^\circ$  (very brittle, tension)

*d*: non-circularity parameter of the hoop cross-section of the failure body which is here a fracture failure body or also termed  $\pi$ -plane shape parameter

*F*: force

*f*: strength (*Festigkeit*) in *civil engineering* (in the context of the development of partial safety factor concept in Germany about 1985 it was going to become replaced by *R* and this the more viewing the future EuroCodes) → one should not wait and replace *f* by *R* to become clearer. The tensile strength of a non-metallic<sub>nm</sub> reinforcement  $f_{nm,k}$  is defined as a characteristic value (index <sub>k</sub>).

*f*: index of pure fiber. Could be applied for a non-cured fiber-matrix strand (roving, tow).

*k*: thousand filaments

*K*: critical stress intensity factor (SIF) or fracture toughness

*LL*: lesson learned (learnt)

*m*: index of a matrix

*nm*: non-metallic

*G*: shear elasticity modulus

$\mathcal{G}$ : critical energy release rate  $\mathcal{G} =$  rate at which energy is transformed as a material undergoes fracture, expressed as the decrease in total potential energy per increase in fracture surface area

$\mathcal{G}$ : design limit state (*Grenzzustand*).  $\mathcal{G} = F - 1 = 0$

*p*: load from payload per area

*r*: recycling (not with capital letter as in Recycled Concrete = RC used in civil engineering. This is in contradiction to the generally used term Reinforced Concrete RC and to recycled Carbon Fiber rCF in EN 206-01)

*R*: index Reinforced, letter for strength

$\bar{R}$  bias: average strength used when mapping test data

*R*: straight letter: stress ratio  $\min \sigma / \max \sigma$

*q*: total load per area

*Q*; *q* cross-section loading: lateral or transversal force; lateral force per width

$\rho$ : density of a material

$\rho$  or  $\phi$ : slope of Mohr-Coulomb curve (Mohr envelope)

$\Theta_{fp}^\circ$ : angle of the fracture ‘plane’

$\Theta$ : non-circularity function

$\mu$ : friction value (practically is  $0 < \mu < 0.3$ ) and in statistics mean value of the basic population

$\mu, \sigma$  : mean value, standard deviation of the Normal Distribution of the (basic) statistical population ( $m, s$  of the sample)

$\nu$ : Poisson's ratio (low 3D compressive stress state):  $\nu$  for isotropic and  $\nu_{\perp\parallel}, \nu_{\perp\perp}$  for the transversely-isotropic UD-material.  $\nu_{\perp\parallel}$  is the major Poisson's ratio (in civil engineering sometimes  $\mu$  is used).  $\nu$  grows with compression with ductile and dense brittle materials

$\sigma_1, \sigma_2, \tau_{21}$ : intra-laminar stresses of the lamina (ply) in lamina COS ( $\tau_{12}$  is not driving shear stress)

$\sigma_3, \tau_{32}, \tau_{31}$ : inter-laminar stresses of the lamina (ply)

$\sigma_{oct}, \tau_{oct}$  : octahedral stresses.  $\sigma_{oct} = I_1/3, \tau_{oct} = \sqrt{J_2/3}$

$\xi, \rho$  : Lode-Haigh-Westergaard coordinates  $\xi = \sqrt{3} \cdot \sigma_{oct}, \rho = \sqrt{3} \cdot \tau_{oct}$

AFP: Automated Fiber Placement

AFPP: Automated Fiber Patch Placement

ATL: Automated Tape Laying

CLT: Classical Laminate Theory

CoS: Coordinate System

FRC: fiber-reinforced concrete (mineral matrix). However most often still understood as 'long steel fiber-reinforced concrete' which disturbs a general use of this term. Sometimes unfortunately used as abbreviation for fiber reinforced composite

FRM: fiber-reinforced metal

FRP: fiber-reinforced plastic (polymer matrix)

sFRC,  $\ell$  FRC: short, long fiber reinforced concrete or mortar

FVF: Fiber Volume Fraction  $V_f$

HSB: Handbuch für StrukturBerechnung (German aerospace handbook)

LsL: Lessons Learned (lernt)

NAFEMS: National Agency for Finite Element Methods and Standards (an independent, not-for-profit organization)

PDM: Project Data Management

RILEM. Reunion Internationale des Laboratoires et Experts des Materiaux

HPTL: HPTL Carbon GmbH

SLS: limit state of serviceability (*GZG Grenz-Zustand der Gebrauchstauglichkeit*)

ULS: Ultimate Limit State (*GZT Grenz-Zustand der Tragfähigkeit*)  $\equiv$  Design Ultimate Load DUL

WWFE: World-Wide-Failure-Exercise on 2D- and 3D-strength of UD materials

'3D'-fabrics: usually fabrics with fibers in 3 directions of the plane

3D-fabric: fabrics with spatially oriented fibers (real 3D-textile, a 3D-'material' if it can be homogenized)

Note:

Establishing a glossar becomes more difficult by the fact that some terms have evolved away from the original definition and further by the fact that, for example, the letter C has long been used for

composite and carbon, concrete, ceramics and compressive as well. Such a problem is not new, as the quotations below show: "Unfortunately, we have used these words in so different ways that we no longer clearly understand each other when we say them" [A. Donabedian, 1982] or even much older "A general system of signs and symbols is of high importance for a logically consistent universal language for scientific use!" attributed to Gottfried Wilhelm Leibniz, 1700.

### **Acknowledgement:**

This non-funded work above all addresses the static strength – just one part of the author’s working life in industry – with the intension to transfer theory into engineering application.

This ‘single authored’ work includes: \*Idea finding, \*idea exploitation to generate the FMC-theory, \*text writing of this document, \*extensive numerical analyses with rendering of results like fracture bodies using the programs Mathcad 13 and 15, \*typing of formulas, \*difficult visualizations of the calculation results, sketches, diagrams etc. All these works have been performed by the author himself.

Many thanks are given to those who believed in my work [*W. Becker*] and had some discussions with me on several topics [*W. Brocks, A. Freund, B. Szelinski*]. It includes the WWFE organizers within the performance of WWFE-I and –II from 1999 through 2013 especially *Sam (Kaddour)* and peers of my WWFE-contributions.

To my wife Maria:

*“My heartfelt thanks for allowing me to devote so much time of ‘our time together’ to my time-consuming hobby”.*

### *Dedication:*

*To all the people who have led me to a wide variety of technical fields during my almost 55-year working life. This was challenging but also difficult and at the same time beautiful.*

*Never giving up was the motto.*

Much Experience is required in Design!

But what is experience?

Experience is not what happens to you;  
it’s what you do with what happens to you.

*Aldous Huxley*

### **In future Intended short Supplements for Completion**

(In a following issue some Annexes will be added out of the author’s remaining practical fields

Design dimensioning thoughts about ductile metals,  
Procedure on Performing Design Verification in Stability,  
Multi-scale modelling and Continuum Damage Method,  
Vibration, Rotor Dynamics,  
Filament winding theory and Structural reliability.





This textbook is a glossary designed to provide a broad overview of terms used in several disciplines. The focus is on highly stressed components made of fiber composites, i.e. fibers - primarily carbon fibers - with polymer matrix (epoxy, thermoplastic) and concrete matrix (carbon concrete with the technical textile reinforcement grid or with the rod). The wide range of applications includes pipes and containers, rotor blades, pedestrian bridges, textile building envelopes, prefabricated garages, pre-stressed panels, spatial supporting structures made of all possible combinations of a fiber with a matrix, up to a carbon reinforcement of rusty reinforced concrete bridges and waterproof foundations. Several engineering groups are therefore to be connected conceptually with each other.

The author critically deals with some terms and comments on and visualizes them for a better understanding where it seems necessary to him. It is a work to stimulate constructive discussion, which should connect specialist disciplines and help to avoid mistakes and misunderstandings in the development process by "speaking the same language". This project is made more difficult because some terms have evolved away from the original definition. Thus, terms and their definitions are the central subject of the glossary. This includes abbreviations and indexing as well as an overview of the classification scheme for component-reinforcing fiber composites. Above all, the dimensioning engineer is addressed.

The Glossar includes a scheme that collects notions and abbreviations in fiber-reinforced composites.


*In the notation, self-explaining symbols are used if a property is addressed. A lamina, defined to be the calculation unit, may consist of several physical layers or plies (pre-pregs). **Green** means applied abbreviations.*

|   |                              |                 |  |                                   |  |   |                                 |  |  |     |                           |
|---|------------------------------|-----------------|--|-----------------------------------|--|---|---------------------------------|--|--|-----|---------------------------|
| isotropic   | Normal-Concrete              | Concrete matrix | water + cement (CEM I, CEM III) + aggregate (sand, gravel) + possibly additives, such as super-plasticiser, retarder |                                   |  |   | max. grain > 4 mm <sup>1)</sup> | Fiber Reinforced Concrete<br>GFRC<br>CFRC<br>PPFRC<br>PBOFRC | F(R)C  |     |                           |
|   | Fine <sup>1)</sup> Concrete  |                 |  |                                   |  |   | max. grain < 4 mm               |  |  |     |                           |
| anisotropic   | CRC<br>or CC<br>GFC<br>or GC | FRC             | <b>grid-type reinforcing structures</b>  |                                   |  |   |                                 |  | Fiber Composite Materials  | FCM |                           |
|   |                              |                 | <b>Fiber-Concrete-Composite FCC</b>  |                                   |  |   |                                 |  |  |     |                           |
|   |                              |                 | <b>UDRC</b>  |                                   | <b>Textile-Reinforced Concrete TRC</b> |   |                                 |  |  |     |                           |
|   |                              |                 | rope bar   | rebar grid                        | R-, Q-grid                             |   | embroidered sandwich            | non-woven (randomly oriented, oriented)                      |  |     | short fiber<br>long fiber |
|   |                              |                 | <b>1D</b>  | <b>2D</b> Reinforcement Alignment |  | <b>2D</b>                               | <b>2D – 3D</b>                  |  |  |     | <b>2D – 3D</b>            |
| semi-finished products for reinforcements (endless fiber, long fiber) |                              |                 |  |                                   |  |   | for matrix improvement          |  |  |     |                           |
| isotropic   | Thermosets<br>Thermoplastics | FRP             | UD ply lamella strips  | NCF lamella sheet                 | fabric                                 | non-woven (randomly oriented, oriented) | SMC, BMC                        | FP   |  |     |                           |
|   |                              |                 |  |                                   |  |   |                                 |  | <b>Fiber-Polymer-Composite FPC</b><br><i>closed reinforcing structures</i> |     |                           |
|   |                              |                 | Resin Systems:<br>thermosets, thermoplastics, with catalysts etc.  |                                   |  |   |                                 |  |  |     |                           |

Figure: First Attempt to structure the various composites in Civil Engineering (2019)

Often, the term concrete is used instead of mortar when the component is structurally reinforced.

## Contributions of the author to Handbooks, Guidelines

|   |                          |                                |
|---|--------------------------|--------------------------------|
| <b>HSB</b><br>HANDBUCH STRUKTUR<br>BERECHNUNG   | General description      | Issue E Year 2018              |
|   |                          | Page 1 of 21                   |
| <p>Luftfahrt-Technisches Handbuch (LTH)</p> <h1>HSB</h1> <h2>HANDBUCH STRUKTUR<br/>BERECHNUNG</h2> <p>Fundamentals and Methods<br/>for<br/>Aeronautical Design and Analyses</p> <p>issued by</p>  <p>INDUSTRIE-<br/>AUSSCHUSS-<br/>STRUKTUR-<br/>BERECHNUNGSUNTERLAGEN</p> |                          |                                |
| Prepared:<br>Dr. M. Schagerl  | Checked:<br>Dr. M. Magin | Date:<br>22.11.2018 IASB / IVW |

22.11.2018, 12:05 page 1 of 21  
 Source: File: ~\www\lth\proceed\www\gl\lth\BIB\BIBSCH1-lyc-1-1-1.k4

© Industrie Ausschuss Struktur Berechnungsunterlagen (IASB) - All rights reserved. Confidential and proprietary document

Digitally signed by Michael Magin  
 Date: 2020.10.20 00:13:05 CEST

*Co- reworker and Co-translator of the handbook into English (2004)  
 and contributor 1972-2015*

VEREIN  
DEUTSCHER  
INGENIEURE

Entwicklung von Bauteilen  
aus Faser-Kunststoff-Verbund  
Berechnungen  
Development of FRP components  
(fibre reinforced plastics)  
Analysis

VDI 2014

Blatt 3 / Part 3

Ausg. deutsch/englisch  
Issue German/English

Frühere Ausgabe: 04.97 Entwurf, deutsch  
Former edition: 04.97 Draft, in German only

Zu beziehen durch / Available at Beuth Verlag GmbH, 10772 Berlin - Alle Rechte vorbehalten / All rights reserved © Verein Deutscher Ingenieure e.V., Düsseldorf 2006

Die deutsche Version dieser Richtlinie ist verbindlich.

No guarantee can be given with respect to the English translation. The German version of this guideline shall be taken as authoritative.

| Inhalt  | Seite     | Contents   | Page      |
|---|-----------|--|-----------|
| Vorbemerkung . . . . .  | 3         | Preliminary note . . . . .   | 3         |
| <b>1 Anwendungsbereich . . . . .</b>  | <b>3</b>  | <b>1 Scope . . . . .</b>   | <b>3</b>  |
| <b>2 Abkürzungen, Begriffe, Symbole, Indizierung . . . . .</b>                      | <b>4</b>  | <b>2 Abbreviations, terminology, symbols, superscripts and subscripts . . . . .</b>      | <b>4</b>  |
| <b>3 Berechnungsablauf . . . . .</b>  | <b>12</b> | <b>3 Analytical procedure . . . . .</b>  | <b>12</b> |
| 3.1 Allgemeines . . . . .   | 12        | 3.1 General comments . . . . .   | 12        |
| 3.2 Auslegungsphilosophie . . . . .   | 14        | 3.2 Design philosophy . . . . .  | 14        |
| 3.3 Berechnungsprogramme . . . . .  | 15        | 3.3 Computer programs . . . . .  | 15        |
| <b>4 Modellierung der Schicht . . . . .</b>   | <b>16</b> | <b>4 Modelling the lamina . . . . .</b>  | <b>16</b> |
| 4.1 Allgemeines . . . . .   | 16        | 4.1 General comments . . . . .   | 16        |
| 4.2 Eben beanspruchte Schicht . . . . .   | 18        | 4.2 Two-dimensionally loaded lamina . . . . .  | 18        |
| 4.2.1 UD-Schicht (faserparalleles KOS) . . . . .                                    | 18        | 4.2.1 UD lamina (parallel-to-fibre COS) . . . . .  | 18        |
| 4.2.2 G-Schicht und M-Schicht . . . . .   | 20        | 4.2.2 WF lamina and M lamina . . . . .   | 20        |
| 4.2.3 Drehung der UD-Schicht in das Laminat-KOS . . . . .                           | 21        | 4.2.3 Rotation of the UD lamina into the laminate . . . . .                              | 21        |
| 4.2.4 Berücksichtigung der Schubspannungen aus Querkraft bei UD-Schichten . . . . . | 22        | 4.2.4 Inclusion of shear stresses from transverse forces in case of UD laminae . . . . . | 22        |
| 4.3 Räumlich beanspruchte Schichten . . . . .                                       | 23        | 4.3 Laminae subject to three-dimensional loading . . . . .                               | 23        |
| 4.3.1 Mechanische Beanspruchung (faserparalleles KOS) . . . . .                     | 23        | 4.3.1 Mechanical loading (parallel-to-fibre COS) . . . . .                               | 23        |
| 4.3.2 Mechanische Beanspruchung einer UD-Schicht (gedrehtes KOS) . . . . .          | 25        | 4.3.2 Mechanical loading of a UD lamina (rotated COS) . . . . .                          | 25        |
| 4.4 Einfluss von Beanspruchungsarten/-dauer . . . . .                               | 26        | 4.4 Influence of loading type and duration . . . . .                                     | 26        |
| 4.4.1 Kurzzeitbeanspruchung . . . . .   | 26        | 4.4.1 Short-term load . . . . .  | 26        |
| 4.4.2 Ruhende Langzeitbeanspruchung . . . . .                                       | 26        | 4.4.2 Long-term static load . . . . .  | 26        |
| 4.4.3 Schwingbeanspruchung . . . . .  | 30        | 4.4.3 Cyclic load . . . . .  | 30        |
| 4.4.4 Stoßbeanspruchung . . . . .   | 31        | 4.4.4 Impact load . . . . .  | 31        |
| 4.5 Festigkeitskriterien . . . . .  | 31        | 4.5 Strength criteria . . . . .  | 31        |
| 4.5.1 Allgemeines . . . . .   | 32        | 4.5.1 General comments . . . . .   | 32        |
| 4.5.2 Bruchbedingungen für UD-Schichten . . . . .                                   | 36        | 4.5.2 Fracture conditions for UD lamina . . . . .  | 36        |
| 4.5.3 G-Schicht . . . . .   | 44        | 4.5.3 WF lamina . . . . .  | 44        |
| 4.5.4 M-Schicht . . . . .   | 45        | 4.5.4 M lamina . . . . .   | 45        |
| 4.5.5 Einzusetzende Festigkeitswerte . . . . .                                      | 46        | 4.5.5 Strength values to be used . . . . .   | 46        |
| 4.6 Anwendung von Berechnungsprogrammen . . . . .                                   | 46        | 4.6 Application of calculation programs . . . . .  | 46        |
| 4.6.1 UD-Schicht . . . . .  | 46        | 4.6.1 UD lamina . . . . .  | 46        |
| 4.6.2 G-Schicht . . . . .   | 48        | 4.6.2 WF lamina . . . . .  | 48        |

VDI-Gesellschaft Kunststofftechnik

VDI-Handbuch Kunststofftechnik  
VDI-Handbuch Konstruktion

Vervielfältigung – auch für innerbetriebliche Zwecke – nicht gestattet / Reproduction – even for internal use – not permitted

|   | Seite |
|---|-------|
| <b>5 Modellierung des Laminates</b> . . . . .   | 48    |
| 5.1 Ermittlung von Spannungen und Verformungen . . . . .  | 49    |
| 5.1.1 Netztheorie . . . . .   | 49    |
| 5.1.2 Klassische Laminattheorie (CLT) . . . . .   | 55    |
| 5.1.3 Interlaminare Spannungen (ILS) . . . . .  | 61    |
| 5.1.4 Berücksichtigung der Verzerrung aus Schubspannungen durch Querkraft . . . . .   | 68    |
| 5.1.5 Behandlung von Kerben . . . . .   | 69    |
| 5.2 Schichtenweise Bruchanalyse . . . . .   | 72    |
| 5.2.1 Grundsätzliche Betrachtungen . . . . .  | 72    |
| 5.2.2 Nichtlineare Spannungsanalyse vor dem ZFB . . . . .   | 73    |
| 5.2.3 Kontinuierliche Modulabminderung (Degradation) nach dem ZFB . . . . .   | 77    |
| 5.2.4 Auswirkung von FB . . . . .   | 81    |
| 5.2.5 Vereinfachungen und selektive Nachprüfung . . . . .   | 81    |
| 5.2.6 Maßnahmen zur zielgerichteten Verbesserung von Laminaten . . . . .  | 82    |
| 5.3 Anwendung der schichtenweisen Bruchanalyse für verschiedene Beanspruchungsarten . . . . .   | 83    |
| 5.3.1 Kurzzeitbeanspruchung . . . . .   | 83    |
| 5.3.2 Langzeitbeanspruchung . . . . .   | 83    |
| 5.4 Schwingbeanspruchte Laminat . . . . .   | 89    |
| 5.4.1 Schädigungsvorgänge . . . . .   | 89    |
| 5.4.2 Darstellung von Schwingfestigkeitsergebnissen . . . . .   | 92    |
| 5.4.3 Bauteilbelastungsgeschichte . . . . .   | 96    |
| 5.4.4 Methoden der Schwingfestigkeitsanalyse . . . . .  | 97    |
| 5.4.5 Auslegungshinweise . . . . .  | 99    |
| 5.5 Anwendung von Berechnungsprogrammen . . . . .   | 100   |
| 5.5.1 Laminat-Analyseprogramme . . . . .  | 100   |
| 5.5.2 FEM . . . . .   | 101   |
| 5.5.3 Berechnung von Anstrengung und „Streckungsfaktor der lastbedingten Spannungen“ bei gleichzeitig wirkenden Eigenspannungen . . . . . | 102   |
| <b>6 Bauteilberechnung</b> . . . . .  | 105   |
| 6.1 Allgemeines . . . . .   | 105   |
| 6.2 Stabilitätsberechnungen . . . . .   | 107   |
| 6.2.1 Knicken von Stäben . . . . .  | 109   |
| 6.2.2 Beulung ebener Platten . . . . .  | 110   |
| 6.2.3 Beulung zylindrisch gekrümmter Flächenträger . . . . .  | 113   |
| 6.2.4 Anmerkungen . . . . .   | 120   |
| 6.2.5 Berechnungen mit FEM . . . . .  | 122   |
| 6.3 Verbindungen und Krafteinleitungen . . . . .  | 122   |
| 6.3.1 Klebverbindungen . . . . .  | 123   |
| 6.3.2 Bolzenverbindungen . . . . .  | 128   |
| 6.3.3 Schlaufenanschlüsse . . . . .   | 129   |
| Schrifttum . . . . .  | 131   |
| <b>Anhang</b> . . . . .   | 134   |

|   | Page |
|---|------|
| <b>5 Modelling the laminate</b> . . . . .   | 48   |
| 5.1 Determining stresses and strains . . . . .  | 49   |
| 5.1.1 Netting theory . . . . .  | 49   |
| 5.1.2 Classical laminate theory (CLT) . . . . .   | 55   |
| 5.1.3 Interlaminar stresses (ILS) . . . . .   | 61   |
| 5.1.4 Taking into account the strains arising from shear stresses due to transverse forces . . . . .  | 68   |
| 5.1.5 Treatment of notches . . . . .  | 69   |
| 5.2 Lamina-by-lamina fracture analysis . . . . .  | 72   |
| 5.2.1 Fundamental aspects . . . . .   | 72   |
| 5.2.2 Non-linear stress analysis before IFF . . . . .   | 73   |
| 5.2.3 Continuous modulus reduction (degradation) after IFF . . . . .  | 77   |
| 5.2.4 Effect of FF . . . . .  | 81   |
| 5.2.5 Simplification and selective reviews . . . . .  | 81   |
| 5.2.6 Making specific improvements of laminates . . . . .   | 82   |
| 5.3 Application of lamina-by-lamina fracture analysis for different types of loading . . . . .  | 83   |
| 5.3.1 Short term loading . . . . .  | 83   |
| 5.3.2 Long term loading . . . . .   | 83   |
| 5.4 Cyclically loaded laminates . . . . .   | 89   |
| 5.4.1 Fracture processes . . . . .  | 89   |
| 5.4.2 Presentation of fatigue strength results . . . . .  | 92   |
| 5.4.3 Component loading history . . . . .   | 96   |
| 5.4.4 Methods of fatigue strength analysis . . . . .  | 97   |
| 5.4.5 Advices for design . . . . .  | 99   |
| 5.5 Application of calculation programs . . . . .   | 100  |
| 5.5.1 Laminate analysis programs . . . . .  | 100  |
| 5.5.2 FEM . . . . .   | 101  |
| 5.5.3 Calculating of stress exposure and “stretch factor of the load-determined stresses” with simultaneous by acting residual stresses . . . . . | 102  |
| <b>6 Analysis of FRP components</b> . . . . .   | 105  |
| 6.1 General comments . . . . .  | 105  |
| 6.2 Stability analyses . . . . .  | 107  |
| 6.2.1 Buckling of struts . . . . .  | 109  |
| 6.2.2 Buckling of flat plates . . . . .   | 110  |
| 6.2.3 Buckling of cylindrically curved plates and shells . . . . .  | 113  |
| 6.2.4 Comments . . . . .  | 120  |
| 6.2.5 Finite element analyses . . . . .   | 122  |
| 6.3 Joints . . . . .  | 122  |
| 6.3.1 Bonded joints . . . . .   | 123  |
| 6.3.2 Mechanically fastened joints . . . . .  | 128  |
| 6.3.3 Loop joints . . . . .   | 129  |
| Bibliography . . . . .  | 131  |
| <b>Annex</b> . . . . .  | 134  |

*Editor (2006) and contributor since 1980!*



## Space engineering

### Buckling of structures

ECSS Secretariat  
ESA-ESTEC  
Requirements & Standards Division  
Noordwijk, The Netherlands

This Handbook has been authored and agreed upon by:

J. Arboez, TU Delft  
C. Bisagni, Politecnico di Milano  
A. Calvi, ESA-ESTEC (Convenor)  
E. Carrera, Politecnico di Torino  
R. Cuntze, formerly MAN-Technologie  
R. Degenhardt, DLR Braunschweig and PFH Göttingen  
N. Gualtieri, Thales Alenia Space  
H. Haller, Intales  
N. Impollonia, Università di Catania  
M. Jacquesson, CNES  
E. Jansen, TU Delft  
H.R. Meyer-Piening, ETH Zuerich  
H. Oery, RWTH Aachen  
A. Rittweger, Astrium EADS  
R. Rolfes, Leibniz Universitaet Hannover  
G. Schullerer, MT Aerospace  
G. Turzo, CNES  
T. Weller, Technion, Haifa  
J. Wijker, Dutch Space

The valuable contributions of the following persons are acknowledged:

C. Huehne, DLR Braunschweig; D. Petry, Astrium EADS;  
H. G. Reimerdes, RWTH Aachen; K. Rohwer, DLR Braunschweig;  
R. Zimmermann, DLR Braunschweig.

The ECSS-E-HB-32-24 has been prepared by merging the volunteer contributions of the authors. Comments concerning the technical content of this handbook will be welcomed by the European Cooperation for Space Standardization, Noordwijk, the Netherlands, [www.ecss.nl](http://www.ecss.nl).

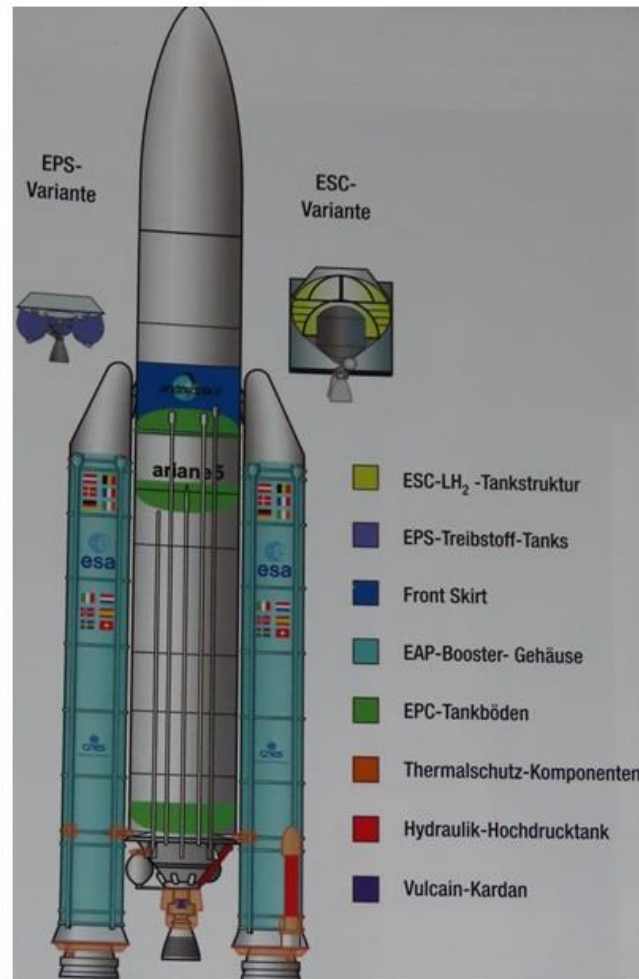
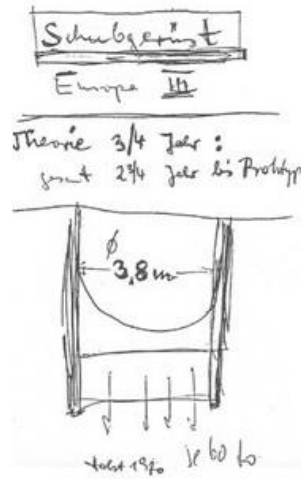
*Author was organizer of the WG, convener and contributor*

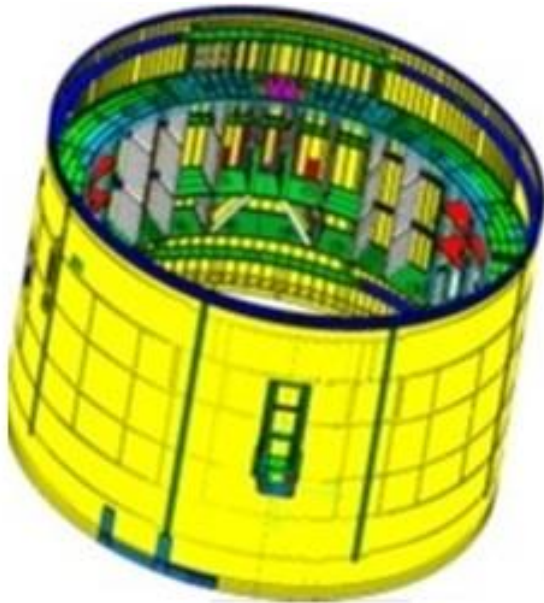
## Founder and organizer of Working Groups at Composites United e.V.

- Engineering, *aerospace, mechanical engineering*
- Composites Fatigue, *aerospace, mechanical engineering*
- Design Dimensioning and Design Verification, *civil engineering*
- Automated fabrication in construction including serial production (*3D-Printing in civil engineerin)g*)

# Projects involved: Memories of working at MAN

The slip of paper below was the start of my work at MAN-Neue Technologie in 1970 regarding the development of the **Ariane launcher family**:  
**"Make a design proposal for an offer, please"** (Thrust structure).

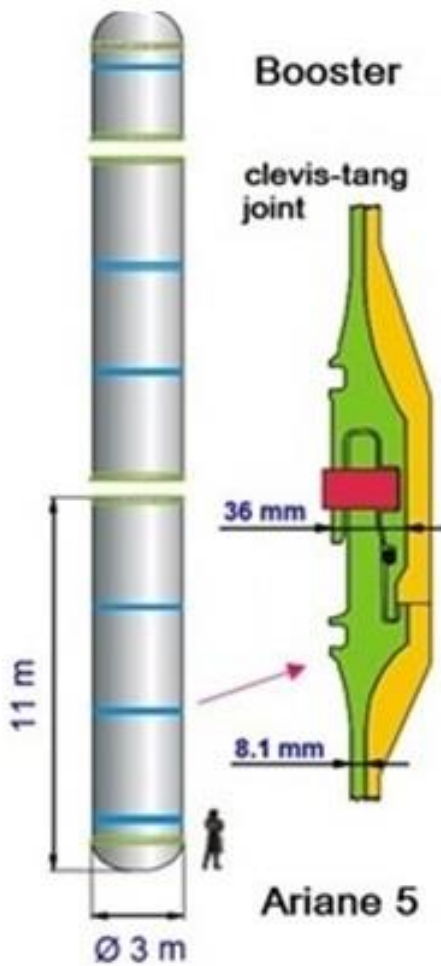




Front Skirt Ariane 5



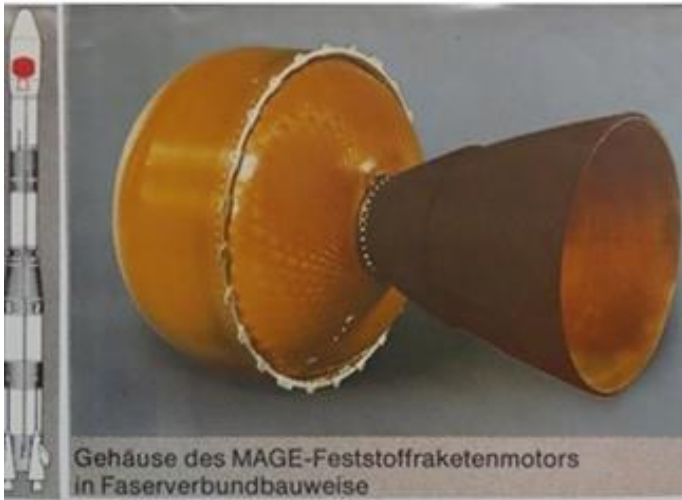
Tank-in-tank system  
unconventional  
'nested' tank



A502 no structural failure







### Apogee motors and pressure vessels

| Tanktyp            | GAM-Hochdruck-<br>tank (Bild 1) | GAT-Hochdruck-<br>tank (Bild 2) |
|--------------------|---------------------------------|---------------------------------|
| Volumen            | 183 l                           | 520 l                           |
| Operationsdruck    | 230 bar                         | 450 bar                         |
| Mindest-Berstdruck | 460 bar                         | 900 bar                         |
| Durchmesser        | 400 mm                          | 400 mm                          |
| Länge              | 1700 mm                         | 4400 mm                         |
| Masse              | 59 kg                           | 200 kg                          |

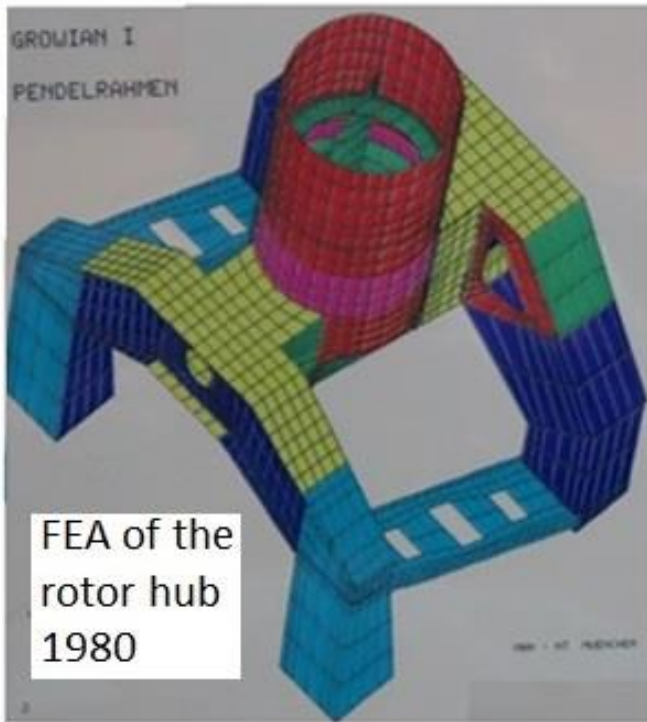


3 MWe

GROWIAN tested at IABG, 1980, GFRP shell



L = 50 m



FEA of the rotor hub 1980



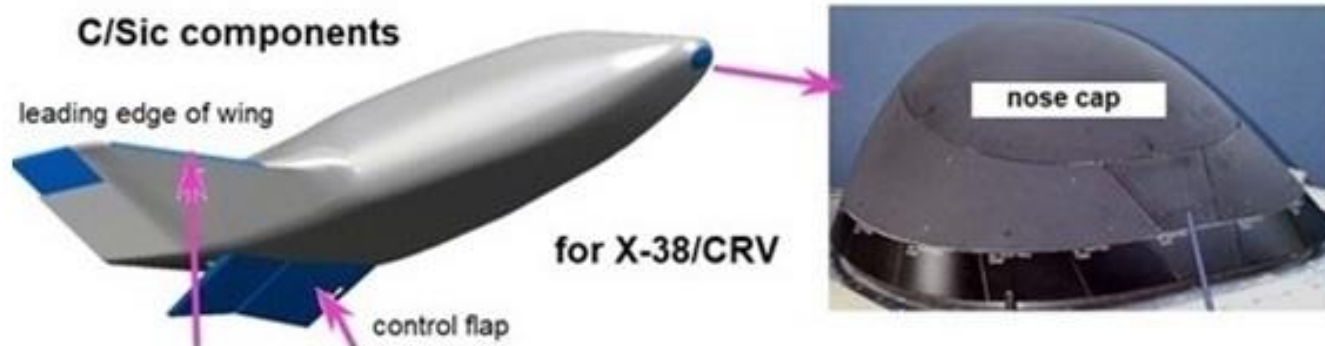
Aeroman

Test specimen  
Development of a  
Braided CFRP hip shaft



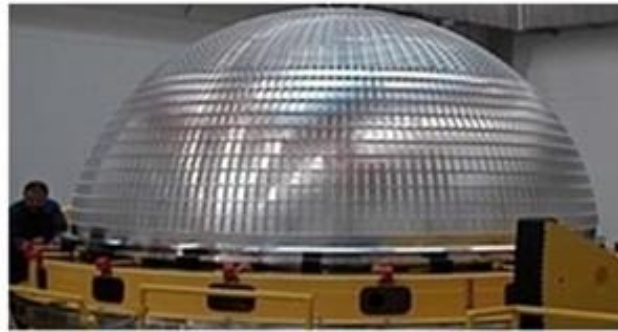


*NIESYTO design, S. Guisard,*





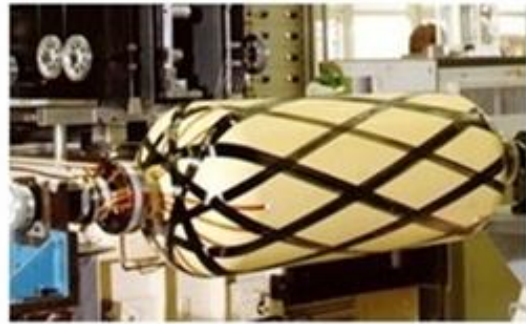
CFRP Booster section



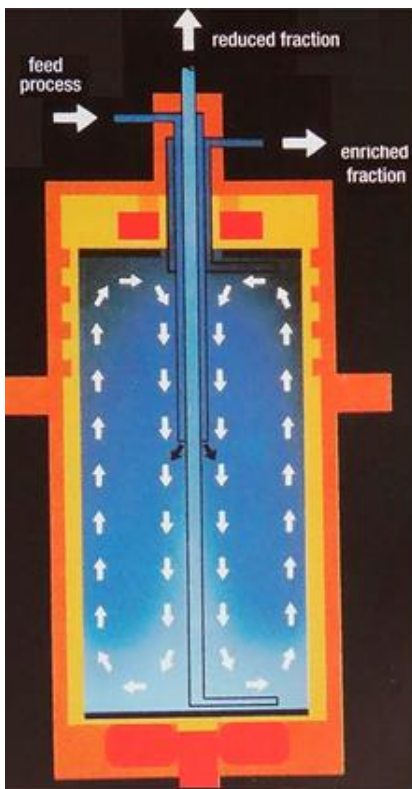
Liquid H<sub>2</sub>-tank dome for Ariane 5



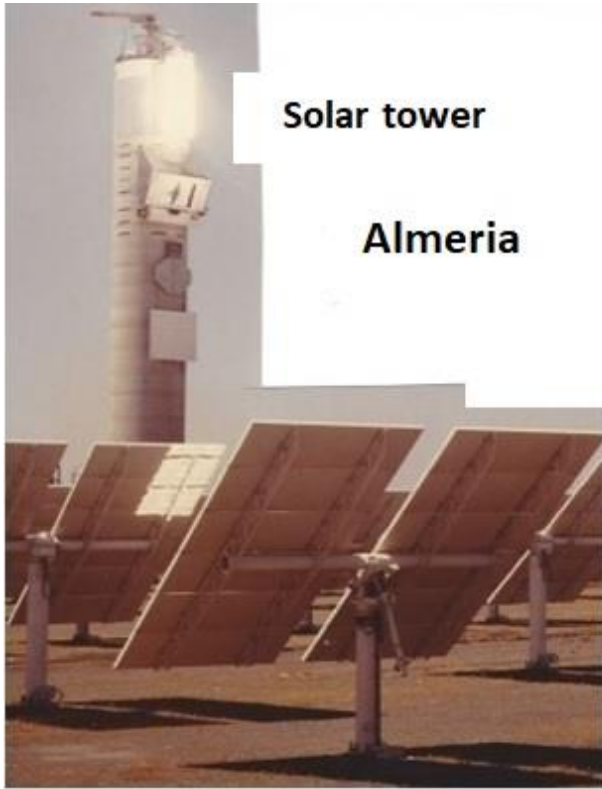
Apogee motor



Filament winding of a pressure vessel

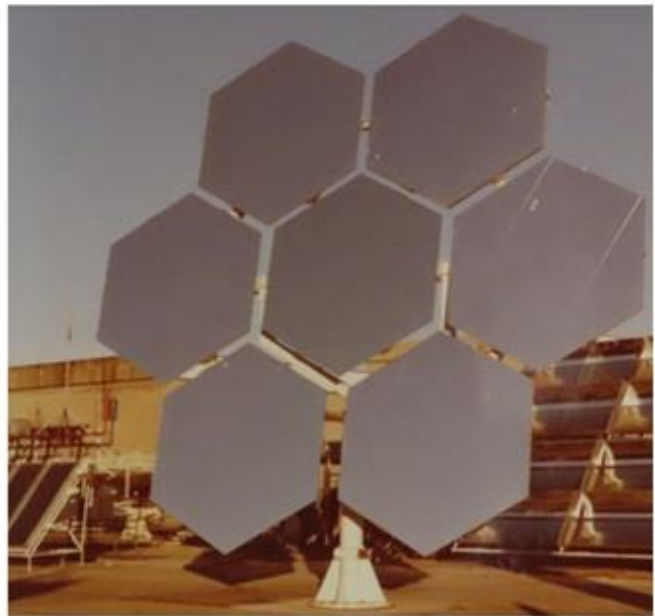


Uranium enrichment in Gas-Ultra-Centrifuges (metal, CFRP). Separation of U<sup>235</sup> from U<sup>238</sup>



**Solar tower**

**Almeria**



**Solar field**



## Working as Civil Engineer



5<sup>th</sup> German  
'climbing garden'

rock material

steel reinforced  
concrete

Designed,  
concrete casted,  
one side masoned with  
rock stones from the alps  
*by the author*



*Structural engineering, armouring plans, pile foundation*



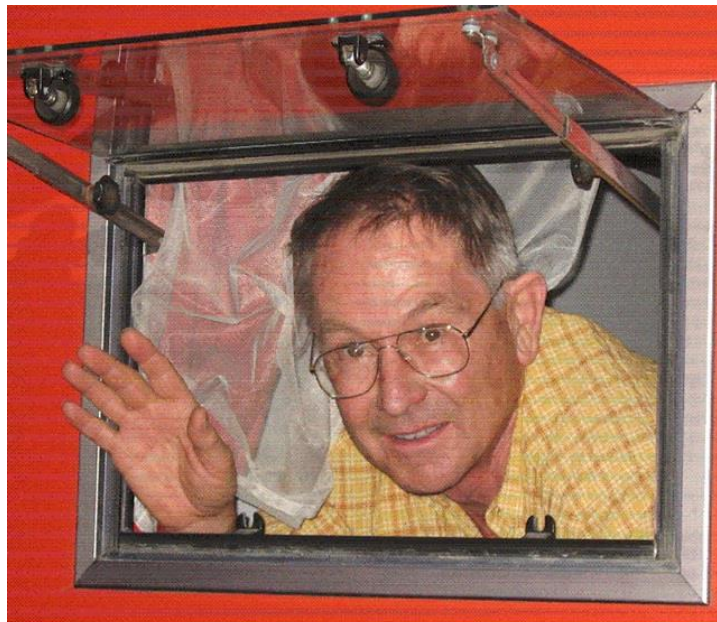
**At least one medium high peak has been reached with the effort used for this document.**

*Since the porters with the equipment were missing, we had to take spare clothes.  
Take what you have. In the WWFE, the author also had no FE program available.*

**However, much is possible if a goal is pursued !**

**The relative narrowness of a ROTEL sleeping cabin helped the author  
to explore the wide world.**

**A good basic engineering education helped him to widely explore the world of engineering.**



Cabin: 80cm x 80cm x 210cm